UNIVERSITY OF SOUTHAMPTON

FACULTY OF ENGINEERING, SCIENCE
AND MATHEMATICS

National Oceanography Centre, Southampton
School of Ocean and Earth Science

Particle Fluxes in the North-East Atlantic and Southern Ocean

By

Ian Salter

Thesis for the degree of Doctor of Philosophy

September 2007

Graduate School of the
National Oceanography Centre, Southampton

This PhD dissertation by

Ian Salter

has been produced under the supervision of the following persons

Supervisors:

Dr. Richard S. Lampitt

Prof. Alan E.S. Kemp

Chair of Advisory Panel:

Dr Rachel A. Mills

"*Begin at the beginning and go on till you come to the end; then stop*". (Lewis Carrol)

DECLARATION OF AUTHORSHIP

- I, **Ian Salter**, declare that the thesis entitled **Particle fluxes in the North East Atlantic and Southern Ocean** and the work presented in it are my own. I confirm that:

- This work was done wholly or mainly while in candidature for a research degree at this University

- Where any part of this thesis has been previously submitted for a degree or any other qualification at this University or any other institution, this has been clearly stated;

- Where I have consulted the published work of others, this is always clearly attributed;

- Where I have quoted from the work of others, the source is always given. With the exception of such quotations, this thesis is entirely my own work;

- I have acknowledged all main sources of help;

- Where the thesis is based on work done by myself jointly with others, I have made clear exactly what was done by others and what I have contributed myself;

- Parts of this work have been published as:
  Salter, I., Lampitt, R., Sanders, R., Poulton, A., Kemp, A., Boorman, B., Saw, K., Pearce, R. "Estimating carbon, silica, and diatom export from a naturally fertilised phytoplankton bloom in the Southern Ocean using PELAGRA: A novel drifting sediment trap." Deep-Sea Research II, In Press.

Signed:……

Date:……

ACKNOWLEDGMENTS

My sincere thanks go to my supervisor Dr. Richard Lampitt for giving me the initial opportunity, and subsequent freedom and support to explore my own ideas. I would also like to thank my co-supervisor, Prof. Alan Kemp who has been a great help, particularly during the long write-up.

I would like to thank my Mum and Dad for the sacrifices that they have made to provide me with the opportunities that they did not have, and always supporting me in every decision I have ever made. I would like to thank my brother for always being on the other end of the phone when I needed him, despite being at the other end of the world, and also my sister, Louise for her support and greeting cards.

There are many people at the National Oceanography Centre who deserve my thanks. I would particularly like to acknowledge the support of Richard Sanders, Martha Gledhill, and Peter Statham. I would also like to thank Raymond Pollard for organising and implementing the excellent CROZEX programme which I am very proud to have been involved with.

And lastly, but by no means least, I would like to thank Maria to whom I dedicate this work. I would probably have to write another thesis of equal length to ever fully acknowledge the support and patience that she has shown towards me throughout this journey; it simply would not have been possible without her.

UNIVERSITY OF SOUTHAMPTON

ABSTRACT

FACULTY OF ENGINEERING, SCIENCE, AND MATHEMATICS
SCHOOL OF OCEAN AND EARTH SCIENCE

Doctor of Philosophy

PARTICLE FLUXES IN THE NORTH-EAST ATLANTIC AND SOUTHEN OCEAN

Ian Salter

Concerns regarding the climatic implications of the increase in atmospheric CO_2 concentrations throughout the anthropocene have provided the impetus to obtain a mechanistic understanding of oceanic processes and their role in regulating atmospheric pCO_2. One important mechanism is the functioning of the biological pump which partitions carbon between the atmosphere and ocean reservoirs over relevant time scales. Current uncertainties revolve around the accuracy of upper ocean particle flux measurements, and the effect of iron and ballast minerals on the strength and efficiency of the biological carbon pump. This study documents the design and deployment of a neutrally buoyant sediment trap (PELAGRA). In the north-east Atlantic organic carbon fluxes were measured using this new technology and compared to indirect estimates of export based on ^{234}Th and nutrient budgets. The vertical fluxes of ^{234}Th into the traps were less than those estimated from the ^{234}Th water column budget, which is interpreted to be the result of previous export events removing ^{234}Th from the water column and the lateral advection of gradients of total ^{234}Th/^{238}U disequilibria confounding the Eulerian budgeting approach adopted. Successful simultaneous deployments in July 2006 at different depths provided a direct measurement of the attenuation of flux with depth, which at 1.8 is substantially greater than the canonical value of 0.856. PELAGRA deployments in the Southern Ocean were conducted as part of the CROZEX project, which examined the role of iron supply on bloom dynamics and subsequent export. Using a mass balance approach to account for the seasonal depletion of dissolved silica acid in surface waters and Si fluxes from the euphotic zone, potential surface export$_{(100m)}$ of organic carbon from +Fe bloom area was estimated to be in the order of 11-15 g C m^{-2}, which is higher than previous estimates obtained from artificial fertilisation experiments. The issue of temporal decoupling between production and export processes was addressed by employing retrospective estimates of production. Particle export efficiency in the +Fe region to the north of the plateau (25-70%) was higher than similar estimates in the –Fe region (11-20%). Diatom size was well correlated with a range of calculated export ratios$_{(100m)}$. The main diatoms involved in the export from the surface were *E. Antarctica* in the +Fe region and *F. kerguelensis* in the –Fe region. E. Antarctica fluxes also dominated deep-water (3000m) diatom fluxes in the +Fe region, and its importance is attributed to the regions proximity to the Crozet Islands, where resting spores and dissolved iron are advected into the bloom area during the winter. Deep-water carbon fluxes measured to the south of the plateau. Deep-water carbon fluxes measured south of the plateau (0.09 g C m^{-2} yr^{-1}) are consistent with previous measurements in a similar environment. In the +Fe region to the north, deep water fluxes were 0.4 g C m^{-2} yr^{-1} indicating that natural iron fertilisation can increase the strength of the biological carbon pump by a factor of 4. Comparison of fluxes with satellite-derived productivity also suggests that the efficiency of the biological pump in transferring organic carbon to the deep-ocean is increased by a factor of 3 in the presence of iron. The flux and composition of amino acids, in relation to the dominant mineral phases that comprised the particulate flux in the NE Atlantic and the Southern Ocean was also examined. The fraction of carbon that could be accounted for by the total hydrolysable amino acids varied very little (20-30%) with sample composition. Protein amino acids were used to quantify the degradation state of the settling particulate material. Specific amino acids seem to infer diatomaceous rather than calcareous as the dominant organic matter source. Multiple linear regression analysis reveals that mineral fluxes can only explain a very small amount of the variability in amino acid composition, which does not support previous hypotheses that relate mineral fluxes and organic carbon fluxes through the differential protective capacity of various mineral phases.

List of Contents

List of Figures

List of Tables

1. INTRODUCTION

1.1 Background

Since the beginning of the industrial period in the late 18th century, humankind has emitted about 244 ± 20 Pg C (Sabine *et al*., 2004) into the atmosphere mainly as a result of fossil-fuel burning, but also because of changes in land-use practices e.g. deforestation. Approximately two thirds of this, 165 Pg C, has remained in the atmosphere increasing the atmospheric CO_2 concentration from a pre-industrial value (~1800) of 281 ± 2ppm (Indermuhle *et al*., 1999) to a present day value (1994) of 359 ± 0.4ppm (e.g. Keeling *et al*., 1995). Such increases in the concentration of carbon dioxide and other gases in the atmosphere alter the radiative forcing globally by decreasing the long-wave radiative flux leaving the troposphere leading to climatic effects (Boyd and Doney, 2003). A synthesis of many observational studies indicates that the global average surface temperature has increased by approximately 0.6°C in the 20th century (IPCC, 2001), and there is also strong evidence that the oceans are exhibiting a warming trend (Levitus et al, 2000). Recent estimates suggest that the ocean inventory of anthropogenic CO_2 is 118 ± 19 Pg, and that the terrestrial biosphere has acted as a net source of 39 ± 28 Pg C for the period between 1800 and 1994 (Sabine *et al*., 2004). Without this oceanic uptake, atmospheric CO_2 would be about 55ppm higher today than currently observed levels. The present rate of change in atmospheric CO_2 is without precedent, necessitating the development of a mechanistic understanding in the processes controlling climate change (IPCC, 2001).

In addition to contemporary changes in atmospheric CO_2, there is evidence of substantial climate change from the geological past, with, for example, glacial core records showing large variations in temperature and greenhouse gas concentrations associated with glacial/interglacial oscillations over the last 400,000 years (e.g. the Vostok core record; Petit, *et al*., 1999). The ultimate pacing of these glacial cycles is statistically linked to cyclic changes in the orbital parameters of the Earth, with characteristic frequencies of 100, 41, and 23 kyr (Hays *et al*., 1974). These orbitally driven variations in the seasonal and spatial distribution of solar radiation incident on

the Earth's surface, known as "Milankovitch cycles", are thought to be fundamental drivers of glacial/interglacial oscillations. However, the direct energy budget affects of the orbital variations are insufficient to drive the large amplitude of glacial cycles that are observed, and orbital variations alone do not provide an obvious cause of the rapid climate transitions evident in paleoclimatic and paleoceanographic records (Sigman and Boyle, 2000). It is apparent that both positive and negative feedbacks within the Earths' climate systems operate to amplify and suppress orbital forcing to produce glacial cycles. The modern carbon cycle provides the basis for discerning the processes that may play an important role in glacial/interglacial CO_2 changes and predicting the Earth's response to contemporary elevations of atmospheric CO_2.

During the last glacial maximum (LGM), the terrestrial reservoir would have acted as source of carbon to the ocean/atmosphere system. Reconstructions of biome distributions for the glacial world coupled with information about carbon storage by different biomes (Adams *et al*., 1990; Crowley, 1995), along with independent estimates based on $^{13}C/^{12}C$ ratios of benthic foraminifera (Duplessy *et al*., 1988; Bird *et al*., 1994) imply between 300 and 700 Pg C were redistributed from the terrestrial to the ocean/atmosphere reservoir. A transfer of 500 Pg C is equivalent to an increase in atmospheric pCO_2 by around 45 ppm (Sigman and Boyle, 2000). Although a portion of this would have been buffered by the ocean carbon reservoir, terrestrial carbon represented a source, not a sink of CO_2 to the atmosphere during the LGM. Oceanic processes must thus account for the observed 80-100ppm drawdown, as well as the additional 10-45ppm resulting from decreased terrestrial carbon storage during glacial periods compared with interglacial periods.

A large number of oceanic processes and earth-system feedbacks have been proposed to explain the observed amplitude, rate and phasing of atmospheric CO_2 change during glacial/interglacial cycles:

1) Changes in the temperature and salinity of sea-water and their effect on the solubility of CO_2 (Fairbanks, 1989; Guilderson *et al*., 1994;; Sigman and Boyle, 2000).

2) Changes in ocean alkalinity from increased weathering of carbonate and decreased coral reef growth (Archer and Maier-Reimer, 1994; Sigman and Boyle, 2000).

3) Changes in phosphate and nitrate supply to the low-latitude oceans (McElroy, 1983; Sigman *et al*., 1998; Gruber and Sarmiento, 1997; Ganeshram *et al*., 1995; Altabet *et al*., 1995; Falkowski, 1997; Haug *et al*., 1998)

4) Changes in Southern Ocean ventilation of CO_2 rich deep-waters through increased ice-cover (Stephens and Keeling, 2000) and surface-water stratification (Francois *et al*., 1997)

5) Changes in the ratio of $CaCO_3$ exported relative to organic carbon (Archer and Maier-Reimer, 1994)

6) Changes in the preformed nutrient concentrations of Southern Ocean mode waters (Sigman and Boyle, 2000; Brzezinski *et al*., 2002; Matsumoto *et al*., 2002)

7) Increased efficiency of the marine production and subsequent export through iron fertilisation of HNLC regions (Broecker, 1982; Martin, 1990; Jickells *et al*., 2005; Kohfeld *et al*., 2005)

Clearly these processes are inextricably linked by a very complex network of positive and negative feedbacks. This thesis focuses on the operation of the biological carbon pump, which is primarily associated with the final point mentioned above, but obviously influences a number of the other processes listed.

1.2 The "biological carbon pump"

In the euphotic zone, using light as a substrate, phytoplankton convert dissolved inorganic carbon (DIC) into particulate organic carbon (POC) through the process of photosynthesis. The majority of this particulate organic carbon is respired back to DIC in the surface ocean by bacteria and other heterotrophs (e.g. Azam, 1998; Sherr and Sherr 1996; Rivkin and Legendre, 2001). A fraction of the POC sinks out of the euphotic zone (2-20%; Buesseler *et al*., 1998) through the gravitational settling of particles, and is termed export production. Export production acts to "pump" DIC from the surface ocean to the deep-ocean. The removal of DIC reduces the concentration of pCO_2 in surface waters and drives a net flux from the atmosphere to

the ocean in order to re-establish the equilibrium between the two reservoirs, subsequently lowering the concentration of atmospheric carbon dioxide (e.g. Fig 1.1). A further fraction of the POC is remineralised below the euphotic zone (Nagata *et al*., 2000; Harris *et al*., 2001) generating a depth gradient of DIC in the ocean. As deep-ocean waters are not in contact with the atmosphere they can be considered as "climatically-inactive" until they return to the surface ocean. The timescale of overturning circulation in the world's oceans is 1500 years and so these processes are relevant with respect to the anthropogenic influence on atmospheric CO_2 concentrations and climate. A further fraction of sinking POC reaches ocean sediments, about 90% of which is remineralised at the sediment-water interface and within the sedimentary column and a very small fraction is buried in the sediment.

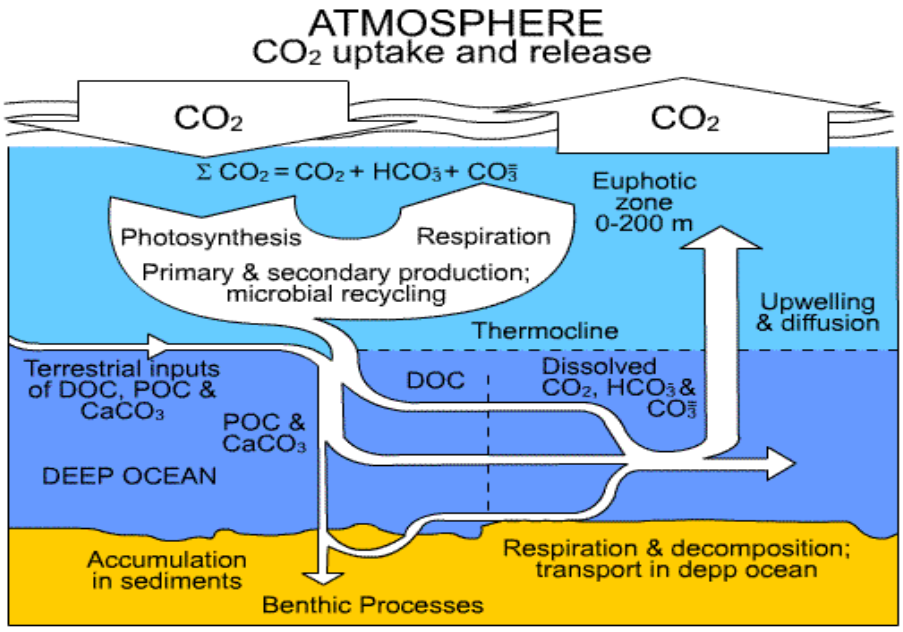

Figure 1.1 Diagram showing the biological pump, carbon dioxide from the atmosphere diffuses into the ocean where it is utilized by photosynthetic algae. A portion of this primary production is remineralised in the euphotic zone, and some of the organic matter sinks to depth where the inorganic nutrients are regenerated. (Source http://www.sd-commission.gov.uk/panel-sd/position/co2/1.gif).

1.3 Present uncertainties in our knowledge

In the modern day ocean, the biological pump transfers around 5 – 15 GT C yr^{-1} to the deep ocean (Falkowski *et al*., 1998), which is large in comparison to the 6 GT C yr^{-1} of anthropogenic CO_2 emissions to the atmosphere. The identification of the factors controlling the downward export of biogenic particles has received considerable attention over the last few decades (Treguer *et al*., 2003). During the last decade there have been considerable advances in biogeochemical studies, including increased temporal and spatial coverage of both the surface and deep-ocean, with much of this undertaken in a co-ordinated way via the Joint Global Ocean Flux Study (JGOFS). The recent review of Boyd and Trull (2007) provides an excellent synthesis of the current understanding of particle export in oceanic waters. A few of the present uncertainties that are addressed in this thesis are outlined below.

1.3.1 Vertical Attenuation of sinking particle fluxes in the sub-surface ocean

The exponential decrease of carbon flux with depth is reasonably well documented (e.g. Martin *et al*., 1987; Berelson, 2001; Lutz *et al*., 2002). Quantitative expressions for POC flux attenuation with depth are well defined by a power-law expression of the form $F(z) = F(z_0 * (z/z_0)^{-b}$, where F(z) is the flux of carbon at depth z, z_0 defines the reference depth of the surface layer export flux $F(z_0)$, and *b* characterises the flux attenuation with depth. Martin *et al*. (1987) suggested $b \approx 0.858 \pm 0.1$ for the open ocean based on a composite of limited observations from the Pacific Ocean, and this formulation has since been widely adopted in global biogeochemical models (e.g. Doney *et al*., 2004). The value of "*b*" essentially parameterises the level of remineralisation of POC flux, and since the amount of flux that sinks below the maximum extent of winter mixing (i.e. the ventilation depth) determines the sequestration efficiency of the biological pump, it is crucial that this value is accurately constrained. However, most evaluations of "b" have been based on decreases in fluxes to moored sediment traps at depths of 1000-4000m, where

decreases in POC fluxes with depth are relatively small. "b" values have also been inferred from comparison of deep fluxes with outputs from surface ocean production or export models (e.g. Lampitt and Antia, 1997; Antia *et al*., 2001; Berelson, 2001; Lutz *et al*., 2002).

There have been few direct determinations of flux in the surface (i.e. 0-100m) and sub-surface (i.e. 100-1000m) where attenuation is strongest, as accurate sampling in this region is difficult to achieve. Under- and over-trapping resulting from hydrodynamic effects has been revealed from laboratory and field studies of trap behaviour (Gardner, 2000) and radionuclide budgets (Buesseler, 1991; Scholten *et al*, 2001; Yu *et al*., 2001). The development of neutrally buoyant sediment traps (Buesseler *et al*., 2000; Valdes and Price, 2000; Stanley *et al*., 2004) offer promising approaches to minimise these hydrodynamic problems. It remains to be seen whether present estimates of downward export in the subsurface ocean need to be significantly revised, although a very recent study indicate this may be the case (e.g. Buesseler *et al*., 2007).

1.3.2 The ballast –theory

There is extensive literature on most of the processes known to affect the efficiency of the biological carbon pump. These are often inter-related processes and typically include aggregation and disaggregation of organic rich aggregates (e.g. Fowler and Knauer, 1986; Alldredge and Silver, 1988; Banse, 1990; Jackson and Burd 1998), microbial activities (Simon *et al*., 2002; Bidle and Azam, 1999) grazing and faecal pellet production (e.g. Turner, 2002), community size structure (e.g. Boyd and Newton, 1995, Boyd and Newton, 1999), and the role of suspended ballast minerals (Ittekkot, 1993; Armstrong *et al*., 2002; Francois *et al*., 2002; Klaas and Archer, 2002; Passow, 2004). Based on correlations from global syntheses of deep-sea sediment trap material (e.g. Armstrong *et al*., 2002; Francois *et al*., 2002; Klaas and Archer, 2002), the hypothesis has emerged that mineral fluxes (i.e. opal, calcite, and lithogenic) control POC fluxes to the deep ocean. This is in contrast with the idea

that aggregation in surface waters drives the sedimentation of POC, and that the flux of POC controls the mineral flux by sinking aggregates scavenging suspended minerals too small to sink on their own (Honjo, 1982; Passow, 2004). Conceptually one could imagine that mineral fluxes promote POC fluxes by increasing the density of sinking particles (Ittekkot and Haake, 1990; Hamm, 2002, Passow and De La Rocha, 2006), and/or by protecting organic matter from remineralisation through physical and chemical association with mineral phases (Kiel *et al*., 1994; Mayer, 1999; Hedges *et al*., 2000; Ingalls *et al*., 2003; 2006). To date empirical evidence for these explanations has not been provided and it is a source of intense debate (e.g. Passow and De La Rocha, 2006).

1.3.3 Impact of iron on carbon export

The hypothesis that high nutrient low chlorophyll (HNLC) areas of the global ocean are limited by the availability of the micronutrient iron (e.g. Martin, 1990) has stimulated much scientific attention. Numerous artificial fertilisation experiments have demonstrated that the addition of iron causes an increase in phytoplankton biomass and CO_2 drawdown (synthesised by De Baar *et al*, 2005). However, proving the strength and efficiency of the biological carbon pump is enhanced under iron-replete conditions (e.g. during the LGM; Martin, 1990; Petit *et al*., 1999) is much more equivocal. This is largely attributed to the time and space scales of artificial fertilisation experiments (e.g. Pollard *et al*., 2007). It has become apparent that assessing the biological pump under iron-replete conditions should be conducted in natural settings (Blain, 2002; Blain *et al*., 2007; Pollard *et al*., 2007). Understanding whether the strength and efficiency of the biological carbon pump increases after iron addition has crucial implications in explaining glacial/interglacial CO_2 cycles and for the purposeful addition of iron as a climate mitigation strategy (e.g. www.planktos.com).

1.4 The Crozet Natural Iron Bloom and Export Experiment (CROZEX)

The Southern Ocean is the largest HNLC region of the global ocean, yet there are areas within the Southern Ocean where there are annual phytoplankton blooms, and the logical hypothesis is that these are supported by a natural source of iron, most likely supplied from local islands or shallow sediments (De Baar *et al*., 1995; Blain *et* al., 2001; Moore and Abbott, 2002; Holeton *et al*., 2005). CROZEX was an extensive multidisciplinary research project to target such an area in order to constrain the physical oceanography of the region (Pollard *et al*., 2007; Read *et al*., 2007; Venables *et al*., 2007) test the iron supply hypothesis (Charette *et al*., 2007; Planquette *et al*., 2007) describe the physiological and taxonomical response (Moore *et al*., 2007a,b) and community structure (Poulton *et al*., 2007) of the resultant phytoplankton bloom (Lucas *et al*., 2007; Seeyave *et al*., 2007) and its effect on local nutrient (Sanders *et al*., 2007) and carbon dioxide (Bakker *et al*., 2007) drawdown. The response of mesozooplankton (Fielding *et al*., 2007) and bacterial (Zubkov *et al*., 2007) communities were assessed in addition to a suite of export measurements (Morris *et al*., 2007; Salter *et al*., 2007; Sanders *et al*., 2007; Lucas *et al*., 2007; Marsh *et al*., 2007) to inform the hypothesis that pCO_2 was lowered during glacial times due to increased iron supply and efficiency of the biological pump (Watson *et al*., 2000; Sarmiento *et al*., 2004)

1.5 Study Areas

The sediment trap samples analysed for this thesis were collected in the Indian-Sector of the Southern Ocean and the North-East Atlantic Ocean.

1.5.1 North-East Atlantic: PAP

The Porcupine Abyssal Plain (PAP) is located at 49°N 16.5°W in the Sub-Polar regime of the North-East Atlantic as defined by Dutkiewicz *et al*., (2001). The PAP site lies to the south of the main stream of the North Atlantic Current and is subject to return flows coming from the west and northwest. Nutrient concentrations are

controlled by both horizontal and vertical transport processes although convective nitrate fluxes dominate the supply to the euphotic zone (Williams *et al*., 2000). Deep-winter mixed layers (>250m) (Levy *et al*., 2005) are formed by surface convection in response to a surface buoyancy loss or wind stirring (Marshall and Schott, 1999; Williams and Follows, 2003). Photosynthesis is light-limited during winter such that chlorophyll values are very low (Levy *et al*., 2005). The well-documented spring bloom (e.g. Ducklow and Harris, 1993) is characterised by an abrupt increase in chlorophyll in response to a rapid shoaling of the mixed layer, which allows phytoplankton to remain within the sunlit region and enable net growth (Sverdrup, 1953). These characteristics are reflected in deep-water particle flux profiles (Honjo and Manganini, 1993; Lampitt *et al*., 2001) which along with the underlying sediments are dominated by calcite (e.g. Broerse *et al*., 2000)

1.5.2 Southern Ocean: Crozet Islands

The dominant physical control on biogeochemical distributions in the Southern Ocean is the banded structure of the Antarctic Circumpolar Current (ACC) (Pollard *et al*., 2002). The Crozet Islands are located north of the Polar Front (PF) and south of the Sub-Antarctic Front (SAF) and are thus within the boundaries of the Polar Frontal Zone (PFZ). Within the PFZ, macronutrients, including orthosilicic acid (silicate), are present at non-limiting concentrations, despite this phytoplankton biomass and productivity are much lower than expected (Read *et* al., 2000) and the area is thus characterised as high nutrient low chlorophyll (HNLC). The enhanced chlorophyll observed to the north of the Crozet Island-system (Venables *et* al., 2007) is consistent with an iron supply from the islands (Planquette *et al*., 2007) and weak circulation north of the plateau (Pollard *et al*., 2007). The physical hydrography to the north of the plateau creates an area with a sufficiently long residence time, of order 60 days (Pollard *et al*., 2007) for iron-rich water to accumulate throughout the winter (Planquette *et al*., 2007) to support the requirements of the local phytoplankton population (Lucas *et al*., 2007). In contrast the area to the south of the plateau is mainly fed by waters from the south and west (Pollard *et al*., 2007) which have had

little interaction with the iron-rich sediments of the Crozet Islands resulting in surface chlorophyll concentrations of 0.2-0.5 mg m^{-3} that are close to "background" PFZ values (Venables *et al*., 2007), compared to 1.5-8 mg m^{-3} to the north. There is also a less favourable light climate to the south of the plateau as the mixed layer decreases by 11 m per degree on average, resulting in winter MLDs in the range of 100-250 m compared to 75-100 m in the north. The gradient in the MLD, together with the latitudinal gradient in photosynthetically active radiation (PAR) explains the observed spatial progression of the bloom (Venables *et al*., 2007). Particulate flux in the Southern Ocean mainly consists of diatoms, and this reflects the high-SiO_2 composition of the underlying sediments (Marsh *et al*., 2007).

1.6 Objectives

- To set-up and validate methods for the analysis of organic carbon, biogenic silica and total hydrolysable amino acids in particulate material.
- To describe the development and deployment of a neutrally buoyant sediment trap (PELAGRA) for measuring upper-ocean particle fluxes.
- To compare carbon fluxes obtained by PELAGRA in the North-East Atlantic with indirect estimates of particle export from ^{234}Th and nutrient budgeting approaches.
- To deploy numerous PELAGRA traps simultaneously at multiple sampling depths to describe the attenuation of carbon flux with depth in the upper ocean (100-500m).
- To deploy PELAGRA in the contrasting productivity regimes of the Crozet Plateau as part of the CROZEX project, to constrain the magnitude, composition, and variability of upper ocean particle export.
- To examine sediment trap material recovered from deep-moored sediment traps (>2000m) deployed north and south of the Crozet Plateau as part of the CROZEX project. Analyse the samples for their major biogenic constituents and the species composition of sedimenting particles. Assess the biogeochemical processes responsible for any differences observed.

- To create annual budgets of carbon flux and compare them with the overlying productivity regimes to test the hypothesis that iron fertilisation of HNLC areas increases the strength and efficiency of the biological carbon pump.
- To extend the long time-series analysis of deep-water particle flux at the PAP site in the North-East Atlantic.
- To measure the amino acid composition of sediment trap samples from the two contrasting biogeochemical regimes of the North-East Atlantic and the Southern Ocean. Use the amino acid spectra to quantify the degradation of organic carbon in relation to the prevailing biogenic mineral phases to test the recently proposed ballast hypothesis.

1.7 Structure of Thesis

The rationale for the development of a novel drifting sediment trap (PELAGRA) is discussed in **Chapter 2**. Estimates of upper ocean carbon export obtained from the deployment of PELAGRA in the North-East Atlantic are discussed in the context of alternative methods of export quantification. **Chapter 3** presents results obtained from PELAGRA when deployed in the Indian sector of the Southern Ocean. The results are explained and synthesised within the context of a natural iron fertilisation experiment (CROZEX). **Chapter 4** presents results obtained from the deployment of deep-moored sediment traps in the vicinity of the Crozet Plateau. The chapter focuses on deep-water particle fluxes in response to iron fertilisation and the implications for the iron-hypothesis with reference to both glacial/interglacial CO_2 cycling and recently proposed climate mitigation strategies involving purposeful fertilisation of the World's Oceans. **Chapter 5** presents a multi-year particle flux dataset from the Porcupine Abyssal Plain in the NE Atlantic. The analysis of amino acids and comparison with the biogenic composition of sedimenting particles facilitates an assessment of the "ballast hypothesis" in mediating organic carbon fluxes to the deep ocean. **Chapter 6** provides a synthesis of the conclusions from the

four results chapters and highlights directions for future research. **Appendices 1-3** document the information regarding the set-up and validation of the various methods used throughout this study. **Appendix 4** summarises the deployment schedules for the deep-moored sediment traps analysed. **Appendix 5** provides an additional analysis on the deep-carbon fluxes measured in the North-East Atlantic and compares these to annual estimates of productivity and meteorological variables to ascertain the temporal variability in the export efficiency. **Appendix 6** summarise mass balance equations and propagated errors for the calculation of lithogenic fluxes by difference. **Appendices 7 and 8** summarise the raw data obtained from the PELAGRA deployments. **Appendices 9-11** summarise the raw data from the carbon, silica, and amino acid measurements carried out on sediment trap samples.

1.8 Publications

1. Lampitt, R., Boorman, B., Brown, L., Lucas, M., **Salter, I**., Sanders, R., Saw, K., Seeyave, S., Thomalla, S., Turnewitsch, R. "Particle export from the euphotic zone: Estimates using a novel drifting sediment trap, ^{234}Th and new Production" Deep-Sea Research I, Accepted (2008)

2. Salter, I., Lampitt, R., Sanders, R., Poulton, A., Kemp, A., Boorman, B., Saw, K., Pearce, R. "Estimating carbon, silica, and diatom export from a naturally fertilised phytoplankton bloom in the Southern Ocean using PELAGRA: A novel drifting sediment trap." Deep-Sea Research II, 54, 18-20, 2233-2259, 2007

3. Marsh, R., Mills, R., **Salter, I**., Green, D., Taylor, S. "Controls on sediment geochemistry in the Crozet Region." Deep-Sea Research II, 54, 18-20, 2260-2274, 2007

4. Planquette, H., Statham, P., Fones, G., Charette, M., Moore, M., **Salter, I**., Nedelec, F., Taylor, S., French, M., Baker, A., Mahowald, N., Jickells, T. "Dissolved iron in the vicinity of the Crozet Plateau." Deep-Sea Research II, 54, 18-20, 1999-2019, 2007

5. Charette, M., Gonneea, M., Morris, P., Statham, P., Fones, G., Planquette, H., **Salter, I.**, Garabato, A. "Radium isotopes as tracers of iron sources fuelling a Southern Ocean phytoplankton bloom". Deep-Sea Research II, 54, 18-20, 1989-1998, 2007

6. Kemp, A., Pearce, R., Grigorov, I., Rance, J., Lange, C., Quilty, P., **Salter, I**. "Production of giant marine diatoms and their export at oceanic frontal zones: Implications for Si and C flux from stratified oceans." Global Biogeochemical Cycles 20 (4): Art. No. GB4S04 OCT 13 2006

7. Pollard, R., **Salter I**., Richard J. Sanders, R., Lucas, M., Mills, R., Moore C., Statham, P., Allen, J., Baker, A., Baker, D., Charette, M., Fielding, S., Fones, G., French, M., Hickman, A., Holland, R., Hughes, A., Jickells, T., Lampitt, R., Morris, P., Nédélec, F., Nielsdóttir, M., Planquette, H., Popova, E., Poulton, A., Read, J., Seeyave, S., Smith, T., Stinchombe, M., Talor, S., Thomalla, S., Venables, H., Williamson, R., Zubkov, M. "Natural Iron fertilisation enhances deep-water carbon flux in Southern Ocean" **Submitted to Nature**.

8. Lampitt, R., **Salter I**., Johns, D. "Radiolarian as major exporters of organic carbon" **Submitted to Global Biogeochemical Cycles**.

9. Lampitt, R., **Salter I**., Cuevas B.A., Hartman S., Larkin K., Pebody C " Long-term variability of downward particle flux in the deep Northeast Atlantic: causes and trends" **Submitted to Deep-Sea Research II**

DATA

The analysis of PELAGRA and SAPS samples for organic carbon and nitrogen were carried out by the author, a summary of which can be found in Appendix 7. Thorium measurements were carried out by Robert Turnewitsch (NOC) and Sandy Thomalla (NOC/UCT). Primary productivity and new production measurements were carried out by Mike Lucas and Sophie Seeyave (NOC/UCT) and nitrogen uptake studies by Stuart Painter (NOC).

2. Particle export from the euphotic zone: Estimates using a novel drifting sediment trap, ^{234}Th and new production

Abstract

The first results obtained using a novel free drifting neutrally buoyant sediment trap; PELAGRA are described. The trap uses an APEX float to maintain its location at a predetermined depth or density horizon and is designed to be deployed in the depth range 100-600m for periods of up to a week. PELAGRA was deployed into a well characterised region of the NE Atlantic over the Porcupine Abyssal Plain (PAP) during the summers of 2003, 2004, 2005 and 2006 in post-bloom conditions. In parallel, measurements were made of total and new primary production and particle export based on ^{234}Th deficits in the upper water column. Samples of sinking material from PELAGRA were recovered almost uncontaminated by "swimmers". The material collected by the trap differed from that obtained using water bottles and an *in-situ* filtration system indicating selective export of centric diatoms. Fluxes of ^{234}Th into the traps were consistently less than that calculated from the deficit of this isotope in the upper water column, implying that export events had occurred prior to the deployments. Fluxes of organic carbon into the PELAGRA traps were similar to those expected from measurements of new production in the upper mixed layer. During 2006 simultaneous PELAGRA deployments at depths of 150 and 250m provided a direct measurement of the decrease in flux with depth. This decrease was substantially more than that predicted by the often-used "Martin equation" and yielded a "*b* value" of 1.7. Using this value it seems that in the Northeast Atlantic about 14% of the total production reaches a depth of 150m during the post bloom period under nutrient limitation.

2.1 Introduction

The downward flux of particulate material out of the upper mixed layer of the ocean has a major effect on biogeochemical processes in the oceans and on the earth system as a whole. Loss of this material affects the chemical inventory of the upper ocean and is the principal means by which deep-ocean biological communities are sustained. This flux necessarily decreases with depth as the material is remineralised or dissolves and it is widely accepted that the rate of decrease in flux diminishes with depth such that in the deep water column (eg >2000m) the rate of decrease with depth is slight. Several models have been developed to describe this change in flux with depth (review by Antia, *et al*., 2001) and although these have a seductive mathematical simplicity, the uncertainties in their predictive abilities in the upper ocean are very large. This is particularly unfortunate as the depth at which the material is remineralised or dissolves determines the time before it is once again able to contribute to surface ocean processes. For instance CO_2 released affects air sea fluxes within a year if remineralised above the depth of winter mixing (200 - 800m depending on location) but if below that depth, the carbon is sequestered for hundreds of years. A clear understanding of the rates of change in flux with depth and the factors that control this is obviously of very great importance in ocean biogeochemistry and biology.

There are several means by which export flux can be estimated but almost all of these are indirect methods such as those based on budgets of nutrients (Eppley and Peterson, 1979; Sanders *et al*., 2005; Schlitzer, *et al*., 2002), of oxygen (Jenkins 1982), of radioisotopes such as thorium-234 (^{234}Th) (e.g. Buesseler *et al*., 2006), or by synthesising numerous biological rate processes (Boyd *et al*., 1999). Numerous models have been developed to reflect the processes of export and the remineralisation of material as it sinks (e.g. Laws *et al*., 2000; Dunne *et al*., 2005; Howard *et al*., 2006) although validation of such models presents serious challenges due to the high levels of uncertainty associated with the supporting data. The only direct method uses the particle interceptor or sediment trap (see review Buesseler *et*

al., 2007). Such devices appear to give good data in the deep ocean when compared to fluxes of conservative tracers such as ^{230}Th or aluminium or when compared to the rate processes on the seafloor, such as oxygen consumption (Scholten *et al*., 2001; Lampitt *et al*., 1995; 2000). However, in the upper ocean two major problems confound attempts to obtain reliable data. Firstly the rate of sinking of the particulate material is low in comparison to the rates of water movement expected at the mouth of the trap (2.1.1 Hydrodynamics). Secondly planktonic organisms (2.2.2 Swimmers) are attracted to the traps and swim into them causing contamination of the collected material by their carcasses and probably modification of the material before they die through ingestion, defecation, moulting etc). Additionally, material collected in near surface traps is subjected to substantial dissolution even if properly treated with preservative (Antia, 2005). Only sediment traps can provide direct estimates of the magnitude of export flux and how this changes with depth or information on the physical, biological and chemical nature of sedimenting particles and it is therefore of considerable importance to establish a means by which the problems of the method can be overcome.

2.1.1 Hydrodynamics

The majority of open ocean data on downward flux in the upper 1000m have been obtained using drifting traps that are attached to a surface float (e.g. Knauer *et al*., 1979; Nodder and Waite, 2001; Lutz *et al*., 2002). While the sinking rates of the particles contributing most to flux are likely to be 0.01-0.1cm/sec, the water movements relative to the trap are likely to be 10-100 times larger due to the action of internal waves, upwelling, current shear, wind effects on surface floats and turbulent flow. It seems very unlikely with such a large discrepancy between the flow speed and that of the sinking particles, that the measured flux will approximate the real flux. In spite of this, there are examples where fluxes into drifting surface tethered traps have been in good agreement with estimates based on budgets of ^{234}Th (Coppola *et al*., 2002). Indeed this work was carried out in an area of considerable complexity in the Barents Sea.

2.1.2 Swimmers

Zooplankton and nekton are attracted to any subsurface structure presumably because of the enhanced probability of encountering food. Their means of locating food sources have been addressed experimentally for many years (Bainbridge, 1953; Kiorboe and Visser, 1999; Jackson and Kiorboe, 2004) and although they can favourable environments by vertical and horizontal migration, the probability of an organism locating the trap is improved if it moves through the water. A reduction of water flow relative to the trap and associated mooring lines is thus likely to reduce swimmer contamination considerably.

2.1.3 Neutrally Buoyant Traps

One solution to avoid both of these problems is to use a sediment trap that follows the motion of the surrounding water. This can be achieved using a neutrally buoyant trap with compressibility close to that of seawater and high drag. These are the requirements for all Lagrangian floats although none perform perfectly (D'Asaro *et al*., 1996). Such ambitions were first addressed in the 1970's (Staresinic *et al*., 1978, 1982) and more recently have been developed into the much more sophisticated Neutrally Buoyant Sediment Traps (NBST) which have made major progress in addressing these problems (Valdes and Price, 2000; Buesseler *et al*., 2000; 2007). The NBST has been shown to attract far fewer swimmers than traps deployed attached to a surface float and comparisons have been made with samples collected using surface tethered traps: Some components were represented more strongly in NBST while others were more prevalent in surface tethered traps (Buesseler *et al*., 2000, Stanley *et al*., 2004) and the reasons for these differences are hard to determine at present.

This study was carried out at the Porcupine Abyssal Plain time series site (PAP) in the Northeast Atlantic (49˚N 16.5˚W) where deep ocean fluxes have been measured since 1989 along with a variety of other variables (Lampitt *et al*., 2001; Körtzinger *et al*., submitted). The objective of this paper is to describe another novel free-drifting

sediment trap PELAGRA (**P**article **E**xport measurement using a **Lagra**ngian trap) and to present the first reliable direct measurements of export flux and its attenuation with depth in the Northeast Atlantic. This paper also provides estimates of export using budgets of ^{234}Th and ^{15}N new production. The design of PELAGRA differs in some significant ways from the NBST but both designs now provide a basis for reliable measurements of downward flux in this most crucial part of the water column.

2.2 Methods

2.2.1 The PELAGRA trap

The traps were designed around commercially available APEX floats from the Webb Research Corporation, USA (Figure 2.1). These are platforms with active buoyancy control to maintain the instrument at a level of constant pressure or density. They are primarily used in the international ARGO program to measure deep ocean currents and many floats are currently in use world-wide. They comprise a 165mm diameter x 1.3m long aluminium pressure case, rated to 2000m water depth, which houses control electronics, batteries and a hydraulic pump. The pump is used to adjust the density of the vehicle by changing the volume of an external oil-filled bladder situated at the base. A CTD module is fitted at the top with an ARGOS satellite antenna. Two types of float have been procured for this project: an 'isobaric' version which is configured to descend to a pre-determined pressure surface and maintain it within a range of +/-10 dbar of the target pressure and an 'isopycnal' version which descends to a pre-determined density surface and maintains it to within +/- 0.01 sigma-theta of the target density.

Both versions of float operate in a similar manner (Figure 2.2). Deployment takes place after verification of the ARGOS satellite transmissions and after the oil bladder has deflated to its "park position". The trap then descends to the specified pressure or density surface assisted by a depressor weight of about 1kg which is jettisoned at a

depth of 100m. After a predetermined period the float begins a 'fast adjust' period and measures the pressure or sigma-theta at 5-minute intervals. If any two consecutive samples are outside of the target range, the oil bladder is adjusted accordingly by 1cc increments (equivalent to ~ 1g buoyancy change). Once the target conditions have been satisfied, the 'equilibrium period' commences. During this period, the float will drift in a near-Lagrangian manner adjusting its buoyancy by +/- 1g only if any two consecutive 1.5-hour measurements are out of range. The 'equilibrium period' ends after a predetermined time interval at which point the oil bladder inflates to full buoyancy and the float ascends to the surface. Simultaneously, a stainless steel abort weight of 2kg is jettisoned from the base of the trap enhancing ascent rate and freeboard at the surface. The abort weight is suspended from a timer activated anodic 'burn-wire' release. This self-contained unit incorporates a pressure switch that bypasses the timer circuit and drops the abort weight should the float inadvertently descend beyond its safe working depth of 600m.

CTD data are acquired by the Apex float when each buoyancy adjustment is made as well as at predetermined depths during the final ascent. Data loggers are attached to PELAGRA to provide a record of ambient conditions in terms of pressure and sometimes conductivity at intervals of 10 or 20 seconds (Richard Brancker DR-1050 depth/pressure and Idronaut Ocean Seven 304 CTD). Once on the surface ARGOS transmissions begin and continue for a maximum of 255 hours. As well as the CTD data and various float parameters, latitude and longitude are transmitted to enable location and recovery. A Gonio receiver facilitates precise location once the ship is within about 4km of the trap. Newer versions of PELAGRA also have a GPS beacon that transmits positional data to the ship on reaching the surface.

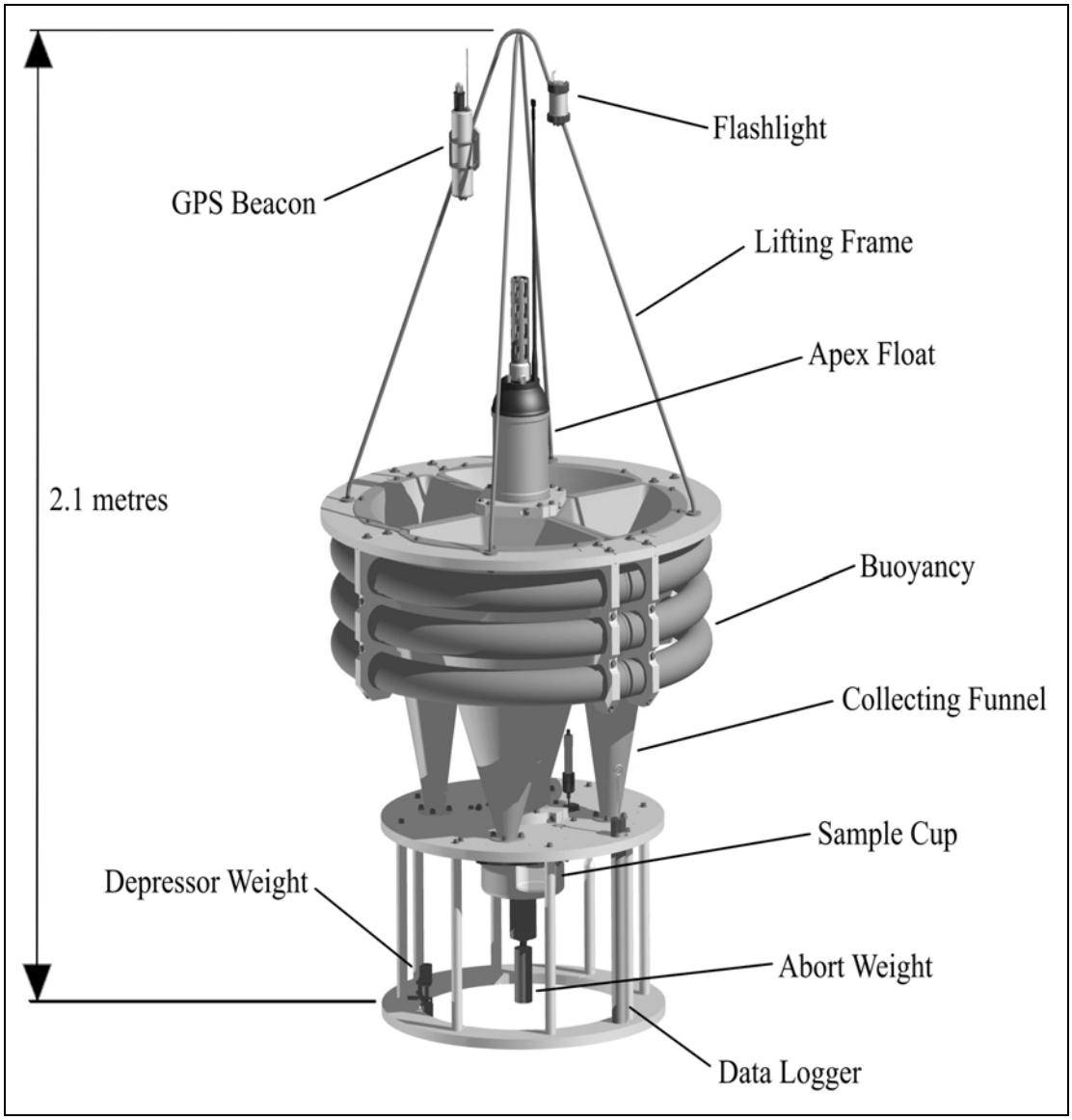

Fig. 2.1. General arrangement of PELAGRA

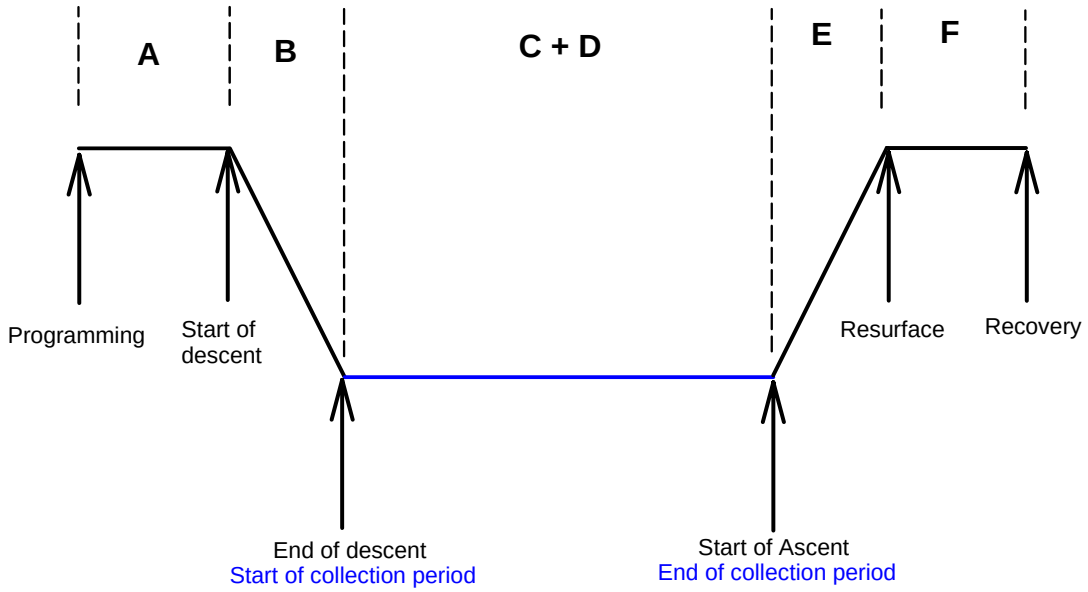

Fig. 2.2 Deployment schematic for PELAGRA

2.2.1.1 Sediment trap components

Figure 2.1 shows an assembled trap module. Four un-baffled collecting funnels are arranged around the APEX float and offer a total collecting area of approximately 0.46m^2 (0.115m^2 per funnel). They are not symmetrical (side angles 7.6˚ to 19˚ to the vertical) and are manufactured from glass fibre reinforced polyester (GFRP) the inner surface of which is finished smooth to allow particles to travel down unhindered. A 500ml polycarbonate sample container is located at the base of each funnel and this is sealed at the end of the deployment period at the same time as the oil bladder inflates and the abort weight is jettisoned.

The hardware described above adds an extra 54.5kg mass to the PELAGRA, which is equivalent to 10.7 kg weight in seawater. Additional buoyancy of 13.8kg is incorporated to counter this consisting of six semi-toroids manufactured from rolled aluminium alloy tubes. The toroidal configuration distributes the buoyancy laterally and keeps the centre of buoyancy high. The fully assembled PELAGRA trap weighs

approximately 122kg in air with net buoyancy in seawater of 3.2kg. This provides a margin for inclusion of additional sensors, or can be countered with ballast.

2.2.1.2 Compressibility and coefficient of thermal expansion

All materials, including seawater, are compressible when subject to hydrostatic pressure. Similarly most materials have a positive coefficient of thermal expansion, i.e. their volume will increase as temperature increases. If an object has compressibility and a coefficient of thermal expansion greater than seawater, then its rate of buoyancy loss with increased depth and reduction in temperature will be greater than that of the water. Clearly such a system is unstable. The ideal solution is to match the characteristics of the trap with those of the seawater; this is technically very difficult to achieve. The practical solution, to produce stability in a stratified body of water, is to ensure that the compressibility and thermal coefficients of the submersed object are less than those of the seawater. Although some individual materials used for PELAGRA, notably polypropylene, have a compressibility and coefficient of thermal expansion greater than those of seawater, the net values for the whole assembly are less. Vertical motions induced by internal waves will cause a net buoyancy change due to the difference in compressibility of PELAGRA and seawater. The resulting acceleration force will cause PELAGRA to deviate from the ideal Lagrangian trajectory. The ability of the APEX buoyancy engine to compensate adequately for this has yet to be determined.

2.2.1.3 Ballasting

Careful ballasting is necessary for successful operation of PELAGRA at an intended depth or density surface; a 1g ballasting error gives rise to approximately 3m of depth error. The APEX buoyancy engine is able to provide +/-118cc (equivalent to +/-115g) of buoyancy adjustment. Prior to each cruise the traps are weighed in air using an industrial platform scale with a precision of 10g and then immersed in a freshwater tank for ballasting. Stainless steel ballast is added gradually until the traps are

completely submerged and judged to be neutrally buoyant. Prior to deployment at sea a CTD cast is made and the additional ballast required is added. Nevertheless a short deployment of a few hours is made at the start of each cruise in order to refine this ballast calculation.

2.2.1.4 Measurements during cruises

Data were obtained during four cruises to the Porcupine Abyssal Plain observatory site (approx 49°N 16.5°W). These cruises were in July 2003, June 2004, July 2005 and June-July 2006 (Table 2.1). In addition to deployments of PELAGRA, a variety of other biogeochemical properties were measured including total primary production (^{14}C), new production (^{15}N) and export flux estimated from the budget of ^{234}Th (e.g. Buesseler et al 1992; Thomalla et al. 2006).

2.2.2 Nutrients

Samples were taken at predetermined light depths and frozen for subsequent nitrate +nitrite ($NO_3^- + NO_2^-$), hereafter nitrate, ammonium (NH_4^+), urea, silicic acid ($SiOH_4$), hereafter silicate and soluble reactive phosphorus, hereafter phosphate (PO_4^{3-}) analyses ashore. Water was collected from the CTD rosette sampler into 10L polyethylene carboys then decanted into 20ml Diluvial containers, and frozen immediately at –20˚C. Samples were also collected directly from each Niskin bottle to a depth of 200m. Urea was determined manually following the diacetylmonoxime thiosemicarbazide method of (Mulvenna & Savidge, 1992) adapted to room temperature using longer reaction times (Goeyens *et al*., 1998). Ammonium was measured using the fluorometric method of Holmes *et al*., (1999). Samples from beginning (Ro) and end (Rt) of the ammonium regeneration experiment were also taken to assess ammonium re-cycling (see section on nutrient uptake measurements). Nitrate, phosphate and silicate samples were analysed using a Skalar San Plus autoanalyser (Sanders & Jickells, 2000).

2.2.3 Primary Production (^{14}C)

Primary production incubations were undertaken on seawater samples collected from pre-dawn 500m CTD casts using the ^{14}C radionuclide labelling technique (Joint & Pomroy, 1986) over 10h in on-deck incubations. Seawater was collected from 10L Niskin bottles into 2L black polyethylene bottles using silicon tubing, from light depths corresponding to 97, 55, 33, 14, 1 and 0.1% incident irradiance (2003, 2004) or 97, 55, 33, 14, 4.5 and 1% (2005, 2006). For each light depth, 4 seawater samples (3 light and 1 dark bottle) were inoculated with 10 µCi $NaH^{14}CO_3$ (100µL stock solution) in 60ml acid-rinsed polycarbonate bottles. A further 4 samples (including 1 dark) were inoculated for size- fractionated measurements of primary production. 5 replicates of total activity standards were prepared in Carbosorb (CO_2 trapping agent). Incubations were performed for approximately 10h in an on-deck incubator cooled by subsurface seawater from the shipboard supply. Light levels correspond to the illumination at the depths from which the samples were collected using neutral density filters (Lee Misty Blue [061] and Neutral Density Grey [210 ND]).

At the end of the experiment, samples were filtered under vacuum onto 25mm diameter, 0.2µm polycarbonate Millipore filters. Filters were rinsed with filtered seawater and acid-fumed under a fume hood for 45min-1h to expel any unfixed ^{14}C and remove calcite, then placed in 5mL Hi-Safe (Packard) scintillation cocktail. Particulate activity was measured at NOC on a Wallac 1220 Quantulus liquid scintillation counter.

2.2.4 New and regenerated production (^{15}N)

Water was collected at the same depths as the primary productivity samples into darkened 10L polyethylene carboys. Three 2L samples were decanted into rinsed polycarbonate bottles and inoculated with 100µL from stock solutions of ^{15}N-labelled potassium nitrate $K^{15}NO_3$, ammonium chloride $^{15}NH_4Cl$ and urea $CO(^{15}NH_2)_2$. The volume of ^{15}N spike in each case was adjusted to represent approximately 10% of the

ambient substrate concentration. The bottles were incubated for ~10 hours alongside the primary production experiments, then filtered onto 25 mm pre-combusted GF/F filters. After filtration, the filters were stored at –20˚C to await analysis by isotope mass spectrometry ashore. At NOC, they were dried (50ºC, overnight) and pelletted into tin capsules, then analysed on a GV Instruments IsoPrime stable isotope mass spectrometer coupled with a EuroVector Euro EA elemental analyser.

Ammonium regeneration experiments were conducted in 2005 simultaneously with the ammonium uptake experiments, to correct the NH_4^+ uptake rates for NH_4^+ re-cycling. A fourth 2L bottle was spiked with 100µL of $^{15}NH_4Cl$ as for the uptake experiments, but was immediately filtered through a 25mm ashed Whatman GF/F filter to collect 900ml filtrate (T_0). Exactly 1mL of a 10mM NH_4Cl solution was added to each bottle as a "carrier" prior to freezing the samples at –20°C. At the end of the incubation period, a further 900mL of filtrate was recovered from the NH_4^+ uptake filtration to measure ^{15}N isotopic dilution by excreted NH_4^+, and the same procedure was carried out as for T_0. At NOC, the aqueous NH_4^+ was recovered onto GF/F filters by diffusion. MgO was added to the thawed samples to increase the pH to ~9 and a pre-combusted 25mm GF/F filter acidified with 20µL H_2SO_4 was suspended from the inside of each bottle cap to retain the diffused NH_4 (Probyn, 1987). The isotopic composition of the NH_4 trapped on the filters was measured by mass spectrometry to provide a measure of aqueous enrichment at the start (R_0) and at the end of the experiment (R_t). The average aqueous enrichment R over the time course of the incubation was then calculated based on the assumption that R decreases exponentially over time [Equation 2.1(Glibert *et al*., 1982)]:

$$R_G = R_0 / \ln(R_0/R_t)\,(1-R_t/R_0) \qquad \textbf{(2.1)}$$

This corrected value of aqueous enrichment (R_G) was then substituted for R in the calculation of uptake [Equation 2.2(Dugdale & Wilkerson, 1986)]:

$$\rho = \frac{r\ PON}{R\ T} \qquad \textbf{(2.2)}$$

where ρ is uptake (μmol L^{-1} h^{-1}), r is particulate enrichment (At%), PON is particulate organic nitrogen (μmol L^{-1}), R is aqueous enrichment (At%) and T is incubation length (h).

2.2.5 Export flux of particulate organic carbon (POC) based on ^{234}Th budget

This approach was first introduced by Tsunogai and Minagawa (1976) and has been routinely used since the work of Buesseler *et al*., (1992). ^{234}Th is a highly particle-reactive radionuclide. It has a short half life of $t_{1/2} = 24.1$ d (decay constant: $\lambda_{Th} = \ln 2/t_{1/2} = 0.02876$ d^{-1}; mean life: $\tau = 1/\lambda_{Th} = 34.8$ d) and reflects quasi-integratively processes of particle dynamics that occur on a time scale of 3-4 weeks before sampling. ^{234}Th is produced by radioactive decay of its very long-lived (half life: 4.468 x 10^9 y) and chemically conservative parent ^{238}U. The distribution of ^{234}Th does not seem to be significantly controlled by processes other than radioactive decay, net adsorption onto particulate material, and particulate matter settling. Depending on the relative magnitudes of transport and reaction processes, scavenged particle-associated ^{234}Th can settle from or decay in a given parcel of water. If the scavenging rate of ^{234}Th onto particles and the rate of ^{234}Th export on settling particles from a given layer of the water column is high in comparison to ^{234}Th production by ^{238}U decay, a radioactive disequilibrium occurs, i.e., the radioactivity of ^{234}Th is less than the ^{238}U radioactivity. The vertical distribution of total (particulate + dissolved) ^{234}Th relative to the parent nuclide ^{238}U can therefore provide information on the export flux of ^{234}Th (and other particle-associated chemical constituents) from a given parcel of water.

The analytical procedures of this study are very similar to the ones used by Turnewitsch and Springer (2001), Thomalla *et al*., (2006) and Morris *et al*., (2007) and are based on Rutgers van der Loeff and Moore (1999) and Rutgers van der Loeff *et al*., (2006). To obtain vertical profiles of total ^{234}Th 10 L samples were collected

with the CTD rosette sampler from 8 - 10 depths to around 1000m with finer resolution near the surface where radioactive disequilibrium between ^{234}Th and ^{238}U is expected. In most cases the sampling depths in the surface 70m were determined by the light depths used for productivity incubations.

Dissolved ^{234}Th ($^{234}Th_d$) was co-precipitated from 7 L (cruise Poseidon 300) or 10 L (other cruises) of unfiltered seawater by formation of MnO_2. To form MnO_2, 375 µL of 25% NH_3 solution, 250 µL of $KMnO_4$ solution (60 g L^{-1}) and 100 µL of $MnCl_2 \cdot 4H_2O$ solution (400 g L^{-1}) were added successively to each sample. The precipitating MnO_2 particles were allowed to grow for at least 8 hours. Afterwards the MnO_2 suspension and the natural particles were collected simultaneously on 142 mm-diameter polycarbonate filters with 1.0 µm nominal pore width by filtration at ~ 400 mbar overpressure. A second precipitation was conducted on selected samples to determine the initial extraction efficiency, which was 100 %. This outcome agrees with findings reported by Rutgers van der Loeff and Moore (1999) and Turnewitsch and Springer (2001). Volumes of filtered water were determined with volumetric flasks and graduated cylinders.

All filters were air-dried, folded in a reproducible way and wrapped in Mylar foil. The radioactivity from these sample packages was counted non-destructively in a Risø GM-25-5 low-level beta multicounter. Samples were typically counted three times over at least ~ 150 days (~ 6 ^{234}Th half-lives) after sampling to follow the decay of ^{234}Th, check for contamination and determine background activities. In open ocean samples the background originates from radionuclides (eg ^{210}Pb, ^{40}K) whose half lives are very long in comparison to the ^{234}Th half life. The background activities after ~ > 150 days after sampling can therefore be assumed to be constant.

As the reported activities are expressed as activity per volume, activities were also corrected for the pressure-related volume change between the in-situ sampling depth and the ship-board environment. All uncertainties are reported as plus/minus one

standard deviation (± 1SD) and have been propagated considering uncertainties in pressure, temperature, salinity, density, differences between detectors, counts per minute (cpm), estimate of the activity at the time of sampling, counting efficiency, volume of filtered sample water, and ^{238}U activity. Samples were also corrected for minimal ^{234}Th ingrowth from ^{238}U decay during the short time between sampling and filtration. The ^{238}U activity was calculated from salinity according to Chen *et al*., (1986). The overall counting efficiency for the filter packages was determined assuming radioactive ^{234}Th/^{238}U equilibrium for samples that were taken in the ocean interior (between ~ 500 m depth and ~ 1500 metres above bottom (m.a.b)). The precision of the method was tested by analysing replicate samples from the interior ocean and was found to be typically ± 3 - 4%.

2.2.5.1 Thorium-234 scavenging model

The activity balance of total ^{234}Th at a given site can be described under Eulerian assumptions by equation (2.3):

$$\frac{\partial A_t}{\partial t} = \left(A_U - A_t\right)\lambda_{Th} - P + V \qquad \textbf{(2.3)}$$

where $\partial A_t / \partial t$ (dpm m^{-3}d^{-1}) is the temporal rate of change in total ^{234}Th activity [A_t (dpm m^{-3})], A_U is the uranium activity (dpm m^{-3}), λ_{Th} is the decay constant for ^{234}Th (0.02876 d^{-1}), P is the net loss of ^{234}Th on sinking particles (dpm m^{-3}d^{-1}), and V is the sum of advective and turbulent diffusive terms (dpm m^{-3}d^{-1}).

On each cruise the PAP site was sampled at least twice for total ^{234}Th. However, in terms of the time between consecutive sampling the time span was too short to derive information on possible non-steady states on a time scale of a few weeks, the relevant time scale for the ^{234}Th tracer. Because of this lack of information on temporal variability we have to resort to a steady-state model where $\partial A_t/\partial t = 0$. Given the absence of major upwelling or downwelling systems it seems safe to assume that net vertical advection does not play an important role in the PAP region. Given typical vertical A_t gradients and vertical turbulent diffusivities at or and near the pycnocline a

significant net turbulent diffusive upward transport of ^{234}Th into the surface ocean also seems to be unlikely. Because of these lines of reasoning and due to a lack of information on horizontal ^{234}Th variability, net horizontal advection and turbulent diffusion are assumed to also be negligible so that $V = 0$. Hence, Equation (2.3) simplifies to a one-dimensional (vertical) steady-state (Equation 2.4):

$$P = (A_U - A_t)\,\lambda_{Th} \qquad \textbf{(2.4)}$$

To calculate the ^{234}Th flux from the surface into the deep ocean the activity profile of total ^{234}Th is integrated from the sea surface down to the depth, z, where radioactive equilibrium was reached (Equation 2.5):

$$P = \int_0^z (A_U - A_t)\,dz \qquad \textbf{(2.5)}$$

In the discussion the validity of some of the assumptions that go into this equation will be assessed in more detail. Uncertainties of export fluxes were propagated taking into account uncertainties in total ^{234}Th activities, ^{238}U activities and sampled water depth.

2.2.5.2 Derivation of particulate organic carbon (POC) export from ^{234}Th export estimates

In order to derive the downward flux of particulate organic carbon (POC) from the surface ocean the export flux of ^{234}Th, P, is multiplied by the ratio of POC to ^{234}Th on large and rapidly settling particles (Buesseler *et al*., 2006). This ratio is affected by collection method, depth, season and type of particle with a very wide range of 1 to >100 μmol dpm^{-1} (Buesseler *et al*., 2006). Currently it is considered that the two best ways of determining this ratio are based on analyses of material collected using either sediment traps or *in situ* pumps with coarse filters of about 50μm mesh size. This reflects the widely held view that downward flux is dominated by particles of this size.

2.2.6 Stand Alone Pumping System (SAPS)

Material was collected by filtering 692 – 3098 L of sea water through a 293mm (cruise Poseidon 300) or 143mm diameter (other cruises) 70µm (cruise Poseidon 300) or 50µm (other cruises) nylon mesh using battery operated SAPS. Once on board the samples on the mesh were re-suspended using "^{234}Th-free" seawater (the filtrate after MnO_2 precipitation and filtration) and split using a Fulsom splitter. One split of the sample was filtered onto 142mm 0.8µm polycarbonate filters for ^{234}Th analyses. The other split of the sample was filtered onto pre-combusted and pre-weighed 25mm GFF filters and stored frozen in Petri dishes for subsequent POC analysis (see below). After filtration the ^{234}Th samples were processed in the same way as the bottle-derived total ^{234}Th samples (section 2.2.5).

2.2.7 PELAGRA samples

As with the SAPS material samples were resuspended and split. Here the samples were split into 8 aliquots of equal volume (62.5ml) using a Fulsom or McClane splitter (replication error <3%). One split was collected on 142mm 0.8µm polycarbonate filters for ^{234}Th analysis. After filtration the ^{234}Th samples were processed in the same way as the bottle-derived total ^{234}Th samples (see above). For POC and particulate organic nitrogen (PON) aliquots were filtered onto pre-combusted (450°C, 12 hrs), pre-weighed 25mm GF/F filters (nominal pore size – 0.7µm), and dried for 48 hours at 60°C. The samples and filters were fumigated with concentrated sulphurous acid in a vacuum dessicator for 48 hours (Verardo *et al*., 1990), and then dried at 60°C for a further 48 hours. The filters were subsequently placed onto pre-combusted (450°C, 12hrs) tin-foil discs (elemental microanalysis). POC and PON were measured using a Carlo-Erba NA-1500 elemental analyzer, after standardization with acetanilide. The relative standard deviation (RSD) of the measurements was <13% for both POC and PON).

2.3 Results

2.3.1 Nutrients and Primary Production

Figure 2.3 shows that on each of the cruises during which PELAGRA was deployed at the PAP site, the surface layer (to 30m) was strongly depleted in nitrate, silicate and phosphate. Winter values at PAP are typically: nitrate = 10 mmol m^{-3}, silicate = 3 mmol m^{-3}, phosphate 1 mmol m^{-3} (Hartman, personal communication).

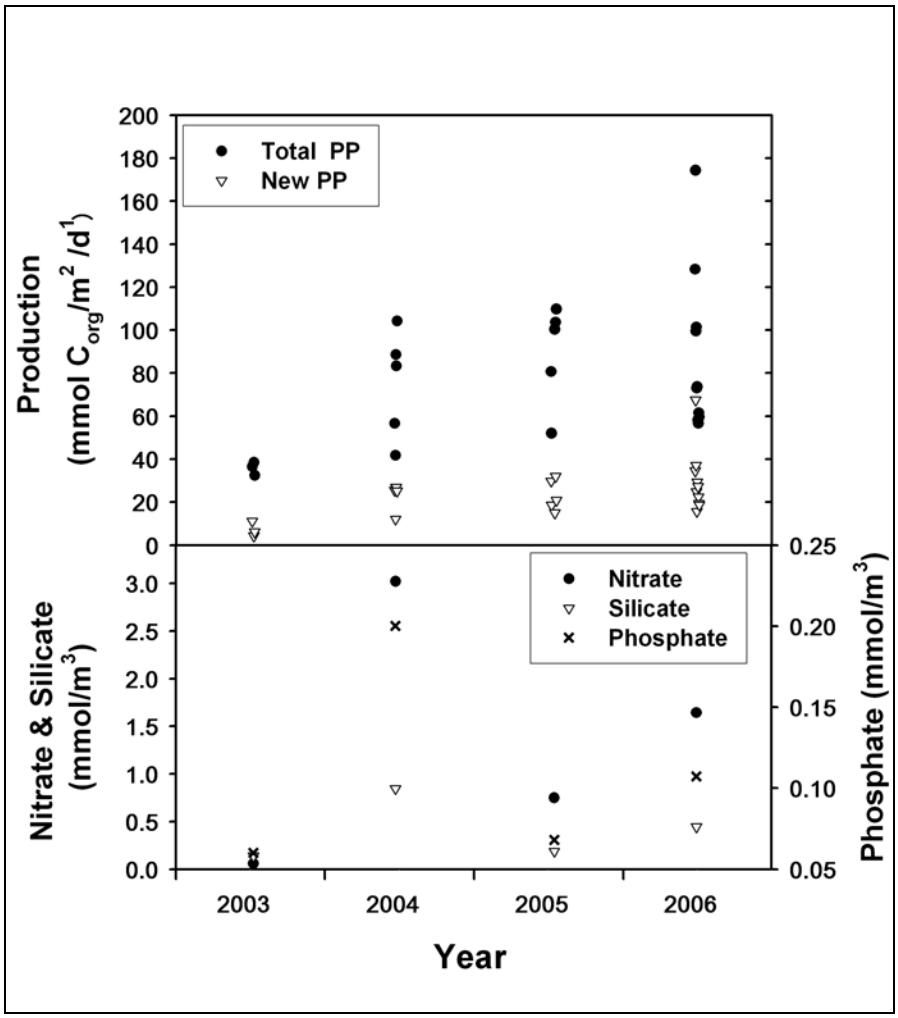

Figure 2.3 Primary production over the top 100m and average nutrient concentration over the top 30m at the PAP site.

Substantial variability in primary production was observed with integrated total production in the range 32-174 mmol m^{-2} d^{-1} and f ratios in the range 0.11-0.47 giving new production in the range 4.3-67.5 mmol m^{-2} d^{-1}. These are similar to values previously published from the site where total production was in the range 38-213 mmol m^{-2} d^{-1} (measured during spring and summer) and 12-276 mmol m^{-2} d^{-1} (modelled over an entire annual cycle) (Lampitt *et al*., 2001).

2.3.2 Trap performance

Figure 2.4 shows depth / time plots of the PELAGRA traps from the onboard pressure sensors. Clearly the trap behaviour was not always as anticipated although technical developments and operational experience have led to significant improvements in performance since 2003. A critical but somewhat subjective derivative from these graphs is the time during which the trap is assumed to be collecting material and furthermore the nominal depth of collection. For these deployments the trap cups were open from before deployment until the moment the abort weight dropped prior to ascent (From 2007 onwards, sample cups have an opening and closing mechanism). The simultaneous deployments in 2006 were remarkable in that they were deployed within 100m of each other and recovered only 2.8 km apart after nearly 4 days drifting.

Table 2.1. PELAGRA deployment details

Date	Cruise	Station	Sampling depth (m)	Duration (Hrs)
12-13th July 2003	Poseidon 300	429	380	3
24-25th June 2004	Charles Darwin 158	56522	175	7
18-20th July 2005	Discovery 296	15716#2	120	32
1-6th July 2006	Discovery 306	183004	150	66
1-6th July 2006	Discovery 306	183003	250	87

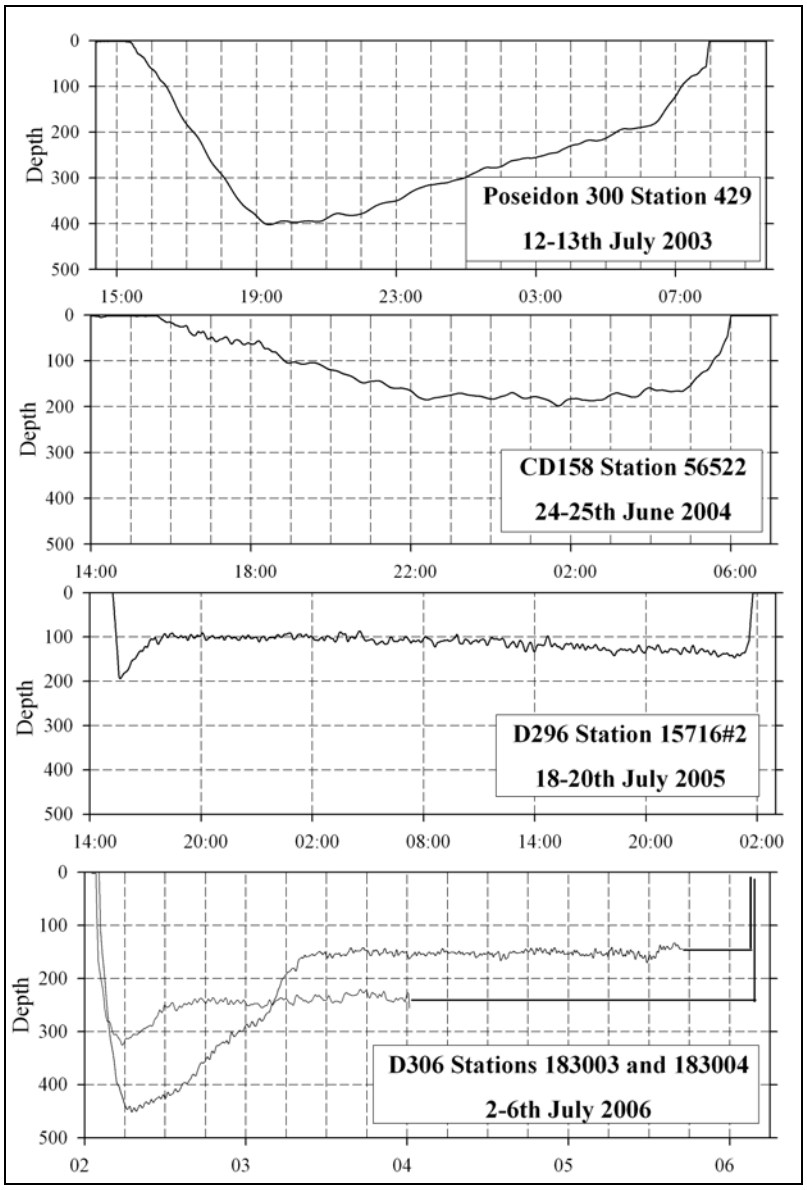

Fig. 2.4. Time / depth plots for all deployments. Note that the grids are at 1 hour intervals in the upper two graphs and 6 hour intervals in the lower two. The horizontal lines on the bottom graph are extrapolations necessitated by failures of the depth sensors.

2.3.3 ^{234}Thorium budgets

Figure 2.5 shows profiles of ^{234}Th activity at the study site from all four years. A large depletion was observed in the upper waters during all cruises leading to estimates of ^{234}Th export in the range 806-2431 dpm/m^2/d (Figure 2.6) at the equilibrium depths which were in the range 54-202m. The absence of outliers and the similarity in the profiles between years is unusual and reflects methodological consistency and the fact that all the cruises took place during similar post bloom oligotrophic conditions.

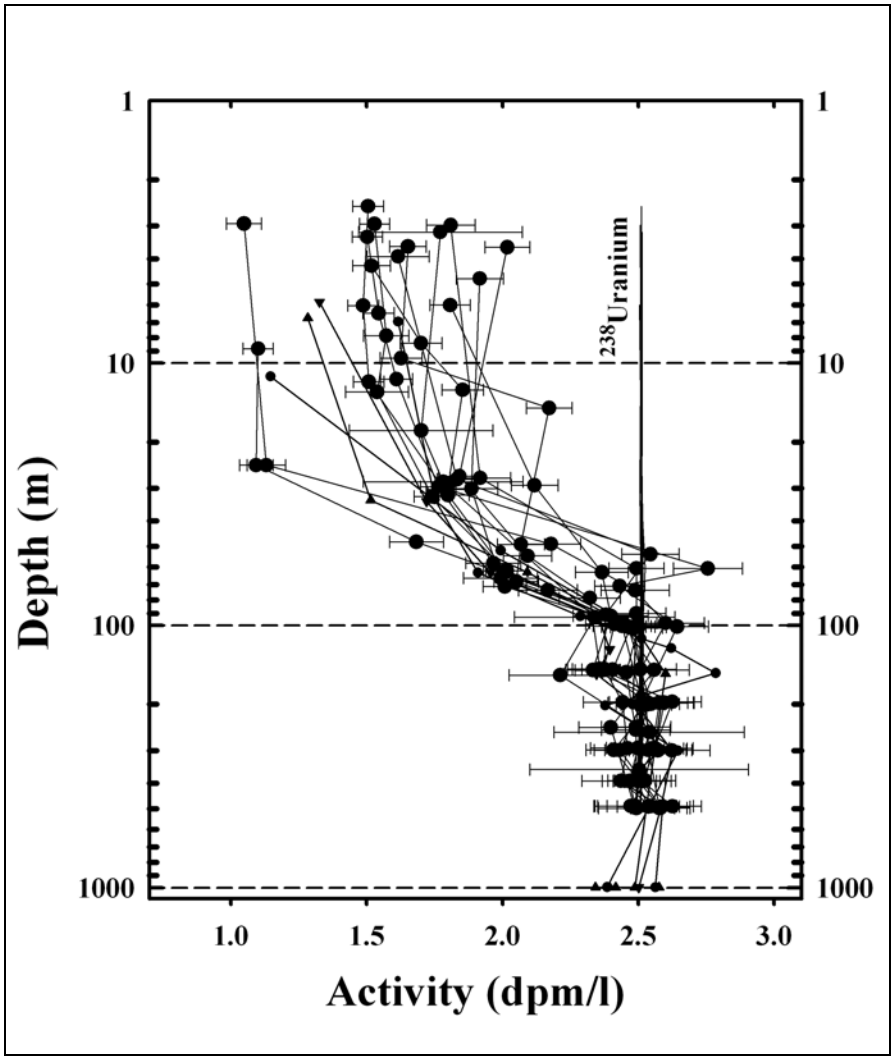

Figure 2.5 Profiles of activity of total ^{234}Th and ^{238}U at the PAP site 2003-2006.

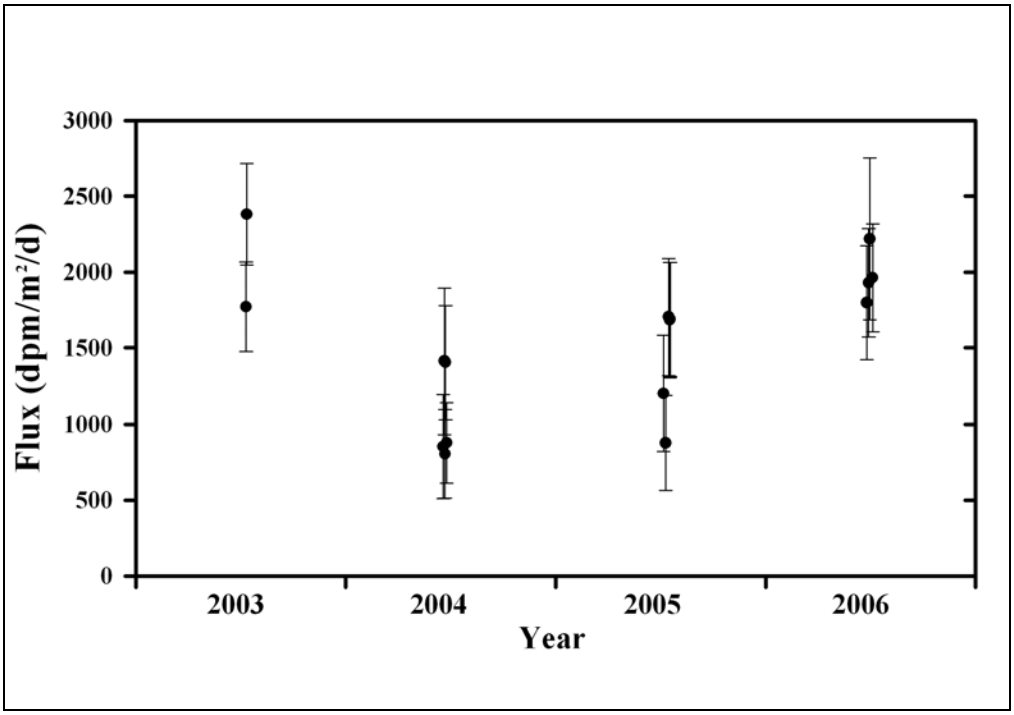

Figure 2.6 Downward flux of ^{234}Th through the depth where equilibrium with ^{238}U was reached (range 54-202m). Error bars are ± 1σ and have been propagated considering uncertainties in pressure, temperature, salinity, density, differences between detectors, counts per minute (cpm), estimate of the activity at the time of sampling, counting efficiency, volume of filtered sample water, and ^{238}U activity.

2.3.4 Composition of settling material

One of the major advantages of the trapping method for examining export processes is that a sample of the settling material is obtained and can be subsequently analysed for its chemical composition and microscopically. In terms of the chemical composition (Figure 2.7), the PELAGRA samples were in general similar to those collected by SAPS with a C:N ratio of about 6.5, about 5-9% organic carbon and 1% nitrogen. Measurement of POC:PIC ratios in PELAGRA samples was unreliable due to small sample size and the occurrence of occasional large calcifying organisms such as foraminifera. SAPS samples had POC:PIC ratios in the range 6.9 to 7.5. There is a much closer agreement between the PELAGRA and SAPS samples in terms of carbon and nitrogen than for ^{234}Th where the Corg:^{234}Th ratio varied widely (Figure 2.12).

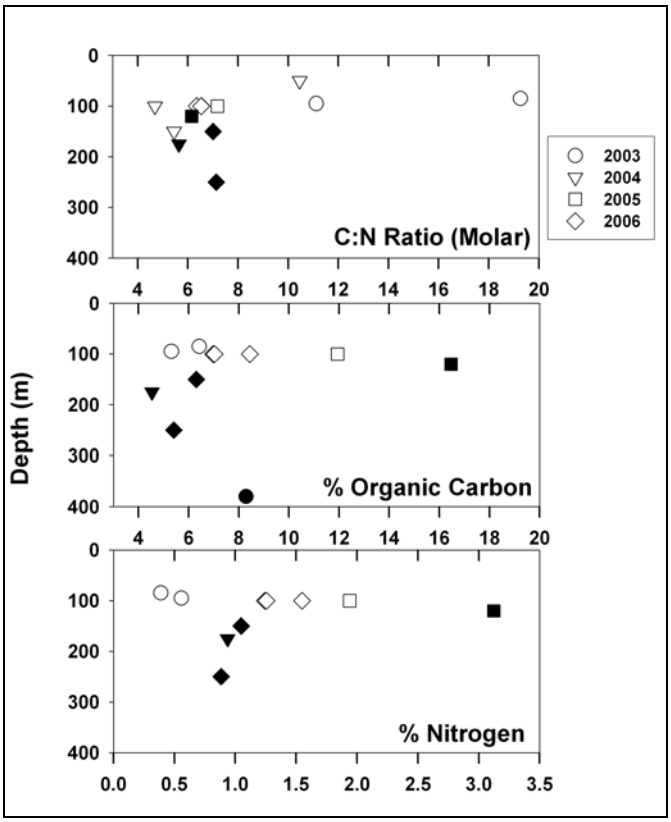

Figure 2.7 Composition of the material collected using SAPS (open symbols) and PELAGRA (closed symbols). Percentages are as a percent of dry material.

In 2006, analysis was carried out on the phytoplankton species composition in the water column from water bottles, in the SAPS and in the PELAGRA samples (Fig. 2.8). While the bottle-derived biomass comprised a mixture of diatoms, dinoflagellates and flagellates, the SAPS samples contained only diatoms and dinoflagellates and the PELAGRA samples only diatoms. Diatom specimens in PELAGRA were almost entirely large centric diatoms: *Actinocyclus sp.* and *Coscinodiscus sp* (83% of biomass) and *Rhizosolenia styliformis* (3%) but also with a contribution from the pennate diatom *Navicula spp* (possibly *N. directa*) (13%). Both PELAGRA samples (150m and 250m) were almost identical in composition and appeared to contain substantial quantities of mucoid material similar to transparent exopolymer particles (TEP) which was also a characteristic of the SAPS samples.

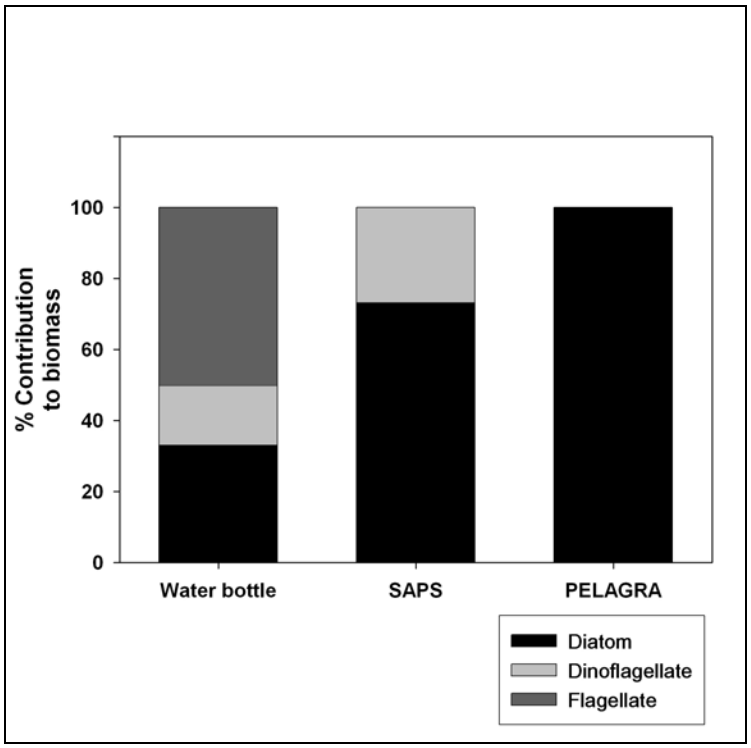

Fig. 2.8 Contribution of various phytoplankton taxa to the biomass of identifiable cells collected by bottles, SAPS and PELAGRA in summer 2006.

2.4 Discussion

The object of this chapter is to describe the function of the new PELAGRA trap, to compare the measurements of downward flux using this device with estimates based on the distribution of ^{234}Th and with measurements of new production and finally and most importantly to provide the first reliable direct measurements of shallow export flux in the Atlantic and its attenuation with depth.

2.4.1 The PELAGRA trap

PELAGRA has shown itself to be a reliable instrument. It is still in the process of development the most important being a radically different closure mechanism which now moves each sample cup under the collecting funnel and removes them at

predetermined times. The great advantage of this is that the funnels are free flowing during deployment and thus any debris from the ship is not included in the final samples. Furthermore samples are now only collected when the trap is expected to have reached its equilibrium pressure or water density. Other improvements include incorporation of a GPS beacon and flash light to aid recovery. The depth-time profiles of the traps (Fig 2.4) show that the performance of such instruments is far more complex than expected and modelling studies of the trap behaviour have so far not provided reliable descriptions and thus a degree of subjectivity is required to determine the required ballast. Nevertheless the simultaneous deployments in July 2006 were a major achievement and have provided the first direct and reliable measurements of export flux and its attenuation with depth in the Atlantic.

2.4.2 Comparison of flux estimates

The relevant time scales of the three key measurements (^{234}Th, New Production and PELAGRA) are different and as such, disagreement between the methods does not necessarily indicate that one is subject to artefacts or incorrect assumptions any more than another. New production reflects the instantaneous synthesis of material based on nitrate uptake which, when averaged over an annual cycle, should be close to the export flux assuming nitrogen fixation and nitrification are negligible. This has recently been fundamentally challenged with the conclusion that nitrifying bacteria convert large quantities of upper ocean ammonium to nitrate which should therefore be properly characterised as a contribution to regenerated production. Failure to account for this will cause a substantial overestimate of new production and hence on the estimate of export fluxes (Yool *et al*., 2007). The ^{234}Th budget reflects the export processes that have occurred over the previous several weeks in a non-linear manner (mean life of ^{234}Th: 34.8 days). Finally the PELAGRA traps collect material that has been synthesised over the previous weeks but the measurement is of the instantaneous export flux at the time of the deployment. It is almost certain that when examining the conditions in the upper mixed layer "today's particles may not be characteristic of yesterday's flux" (Buesseler *et al*., 2006) and it would be surprising in an

environment with such large spatial and temporal variability if the three methods gave similar interpretations of the export process.

Before considering the ways in which ^{234}Th flux can be used to estimate the flux of POC it is worthwhile making a simple comparison of flux using the same unit of ^{234}Th. This avoids the additional step of conversion of ^{234}Th to organic carbon and the associated uncertainties in this conversion. To date there have been no direct comparisons between integrated ^{234}Th losses from the water column with ^{234}Th fluxes into neutrally buoyant traps. There is some evidence (in the form of ^{234}Th/^{238}U activity ratios >1) of release of ^{234}Th from particles to solution below the depth where equilibrium is first reached. Our measurements are of total ^{234}Th activity (dissolved plus particulate) and a more useful comparator with the flux into the PELAGRA traps is the integrated loss of isotope from the water column above the trap (not just above the equilibrium depth). This can then be compared with the flux of ^{234}Th measured by

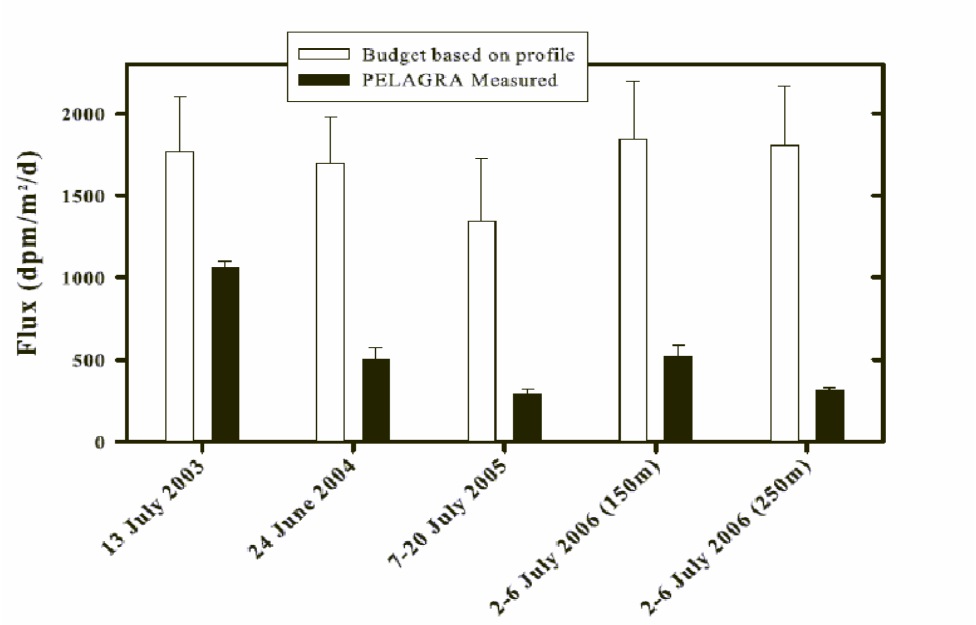

Figure 2.9. Downward flux of ^{234}Th at the deployment depth of the trap determined from the integrated depletion to the trap depth and from the measured flux into the trap.

the trap.

Figure 2.9 demonstrates that there is substantially less ^{234}Th flux into the traps than would be expected if the system is in steady state and if the traps are collecting with 100% efficiency

The traps provide measurements of ^{234}Th flux between 18 and 57 % of the estimates based on ^{234}Th profiles. The two possible explanations are that either the traps are inefficiently collecting the settling material or that during each of the occupations of the station there had been significant flux prior to occupation which had depleted upper water column ^{234}Th, the sinking material having already left the euphotic zone before deployment of the PELAGRA traps. In spite of the fact that the satellite images give little evidence of a phytoplankton bloom, the nutrient profiles demonstrate conclusively that substantial production had taken place prior to arrival at the site. Furthermore on all cruises significant subsurface chlorophyll maxima were present which would not be evident from the satellite but nevertheless would strip out ^{234}Th from the water column. Additionally the trend in productivity on all occasions decreased during occupation of the site. During 2006, which is the best data set (Fig 2.10), the levels of production prior to trap deployment were substantially higher and are likely to have stripped out significant quantities of ^{234}Th from the upper water column prior to trap deployment. Similarly the integrated water column POC declined substantially between 25th June and 1st July just prior to the trap deployment. As with all such Eulerian time series measurements may be heavily influenced by advective processes at the sampling location.

Because of the lack of information on the ^{234}Th history of the sampled water during the weeks before sampling a steady state model for calculation of the ^{234}Th flux has been used. However, it has been shown that these overestimate fluxes during times of declining bloom conditions (Buesseler *et al*., 1992; Savoye *et al*., 2006) and therefore a number of simulations have been computed to determine if the measured fluxes are compatible with conjectured but reasonable conditions prior to arrival at the site.

^{234}Th fluxes for a range of time scales and under different original ^{234}Th activities have been calculated using the non-steady state (NSS) Equation (2.6):

$$P = \lambda_{Th}\left[\frac{A_U(1-e^{-\lambda_{Th}t}) + A_{t1}e^{-\lambda_{Th}t} - A_{t2}}{1-e^{-\lambda_{Th}t}}\right] \quad \textbf{(2.6)}$$

where P is the net loss of ^{234}Th, $t2$ is the time of sampling, $t1$ is the assumed time when the NSS situation started and t is the time between $t1$ and $t2$. A_{t1} and A_{t2} are the total ^{234}Th activities at times $t1$ and $t2$, respectively (cf. Buesseler *et al*., 1992, Savoye *et al*., 2006). The average total ^{234}Th and ^{238}U activities in the topmost 150m of the water column at $t2$ are taken to be those measured during the 2006 cruise: 2.11 dpm L^{-1} and 2.51 dpm L^{-1}, respectively

The six different simulations adopt average total ^{234}Th activities at $t1$ in the upper 150m from 1.5 – 2.0 dpm L^{-1} with t in the range 10 – 35 d. For simplicity, complete mixing of the top 150m is assumed such that A_U, A_{t1} and A_{t2} can be expressed as inventories (dpm m^{-2}) in this layer. The results of the simulations (Fig 2.11) show that the fluxes measured using PELAGRA in 2006 (~400 dpm m^{-2} d^{-1}) and estimated from the assumed steady-state water column deficit (~1700 dpm m^{-2} d^{-1}) could both have been generated by conditions 24 days earlier in which the average activity of ^{234}Th was 1.8 dpm L^{-1} (dashed line in Figure 2.11). Alternatively if the NSS situation started 35 d before sampling, A_{t1} would have been ~ 1.6 dpm L^{-1}. Such values are perfectly reasonable, based on observations of ^{234}Th deficits observed elsewhere (e.g. Morris *et al*., 2007) The conclusion using these modest assumptions about the conditions at the site up to ~ 35 days prior to the PELAGRA deployments is that the difference between the PELAGRA and ^{234}Th budget estimates (
Figure 2.9) can easily be reconciled with each other by using a non-steady state model and do not imply that the sediment trap was collecting with low efficiency.

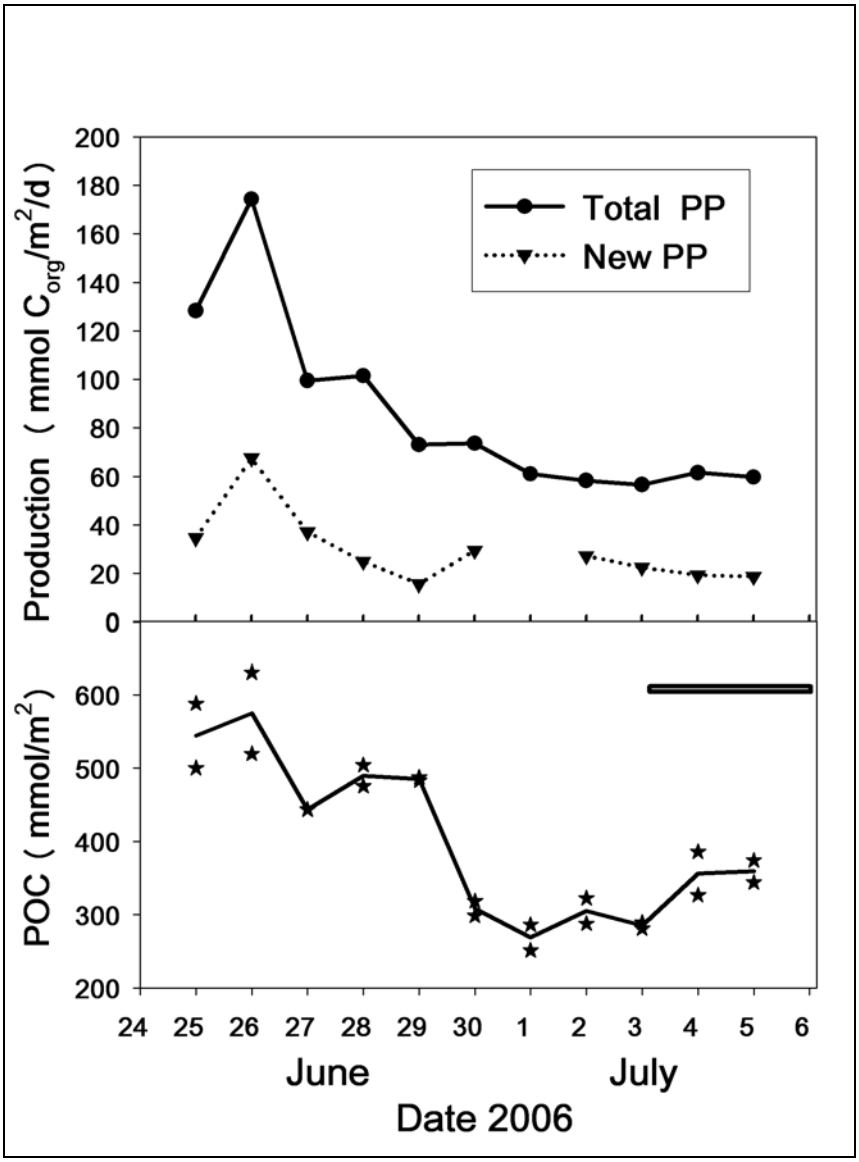

Figure 2.10. Trend in integrated total & new primary production (top) and POC (bottom) in 2006 at PAP. The horizontal bar indicates the time of the PELAGRA trap deployments.

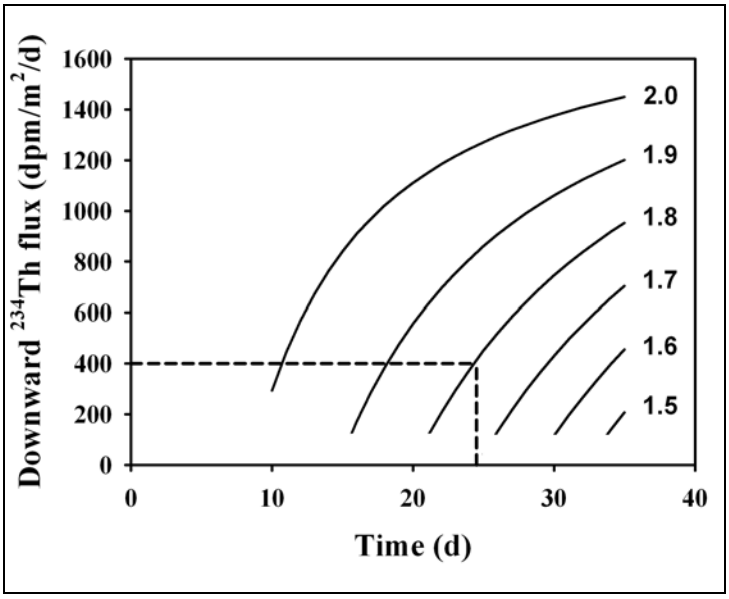

Figure 2.11 Export flux of ^{234}Th from the upper 150m of the water column under non-steady state conditions using simulations of six alternative starting activity levels (from 1.5 to 2.0 dpm m^{-2}) on the assumed time interval between the start of the NSS situation and sampling (between 10 and 35 days). ^{234}Th fluxes determined by PELAGRA on the 2006 cruise were about 400 dpm m^{-2}d^{-1}.

In order to derive fluxes of POC from the profile-derived ^{234}Th flux data, large sinking particulate material is analysed for both properties, the ratio derived and multiplied with the ^{234}Th flux estimate. Literature values for the POC/^{234}Th ratio vary from 1 to > 100µmol/dpm and depend on collection method, season, depth and geographical location (review by Buesseler et al 2006). The SAPS as used in this study recover particles greater than 50 µm which are often assumed to constitute the bulk of the sinking particles and are used to calculate POC flux from ^{234}Th deficiency. Analysis of these particles yielded a POC/ ^{234}Th ratio in the range 2.1 to 53.2µmol dpm^{-1} (Figure 2.12). An alternative means of deriving the POC/ ^{234}Th ratio is to analyze the material collected in the PELAGRA traps (Figure 2.12) which ranges from 1.8 to 24.8µmol dpm^{-1}; there is considerable scatter in the data with no clear relationship between the two methods. All that can be said is that within a method the values for each cruise have little variation. This is of little help in

determining the method to be adopted in order to convert profile-derived ^{234}Th flux to units of POC which are of more widespread interest and use.

Between the cruises and deployments the volume filtered by the SAPS ranged from 692 L to 3098 L and filter holders with different diameters (142 and 293 mm) were used. For GF/F filters there is growing evidence that the amount of organic carbon collected depends not only on the volume filtered and the true POC concentration in seawater but also on the amount of OC adsorbing to the filter and elusive processes such as washout of collected material from the filter holder during pump retrieval (Moran *et al*., 1999; Gardner *et al*., 2003; Liu *et al*., 2005; Turnewitsch *et al*., 2007). The chemical composition of the SAPS collected material also seems to be influenced by the filtered volume (Turnewitsch *et al*., 2007). In this study 50 µm or 70 µm nylon mesh was used instead of 0.7 µm GF/F filters. However, it is conceivable that filtration using nylon mesh is affected by aforementioned parameters and processes in a similar way as filtration using GF/F. Therefore, the use of different filter holders and volumes in this study may also have had an impact on the POC / ^{234}Th ratios. With this in mind the ratios measured from material collected in the traps have been used, but as with all such measurements, the uncertainties should always be considered during any interpretation.

Certain aspects need to be considered when comparing estimates of carbon export flux made by the various approaches: new production, ^{234}Th and PELAGRA. The values of ammonium uptake were not corrected for remineralisation, since ammonium regeneration was only measured in 2005. The new production values presented (Figure 2.10, Figure 2.13) are therefore likely to be overestimates. In 2005 the mean f-ratio for all stations was 0.19 (±0.09) when corrected for NH_4 regeneration, versus 0.25 (±0.10) uncorrected, i.e the average overestimate was 37%. An alternative method to calculate carbon flux using ^{15}N measurements, which avoids taking NH_4 uptake into consideration, is to scale nitrate uptake with the Redfield

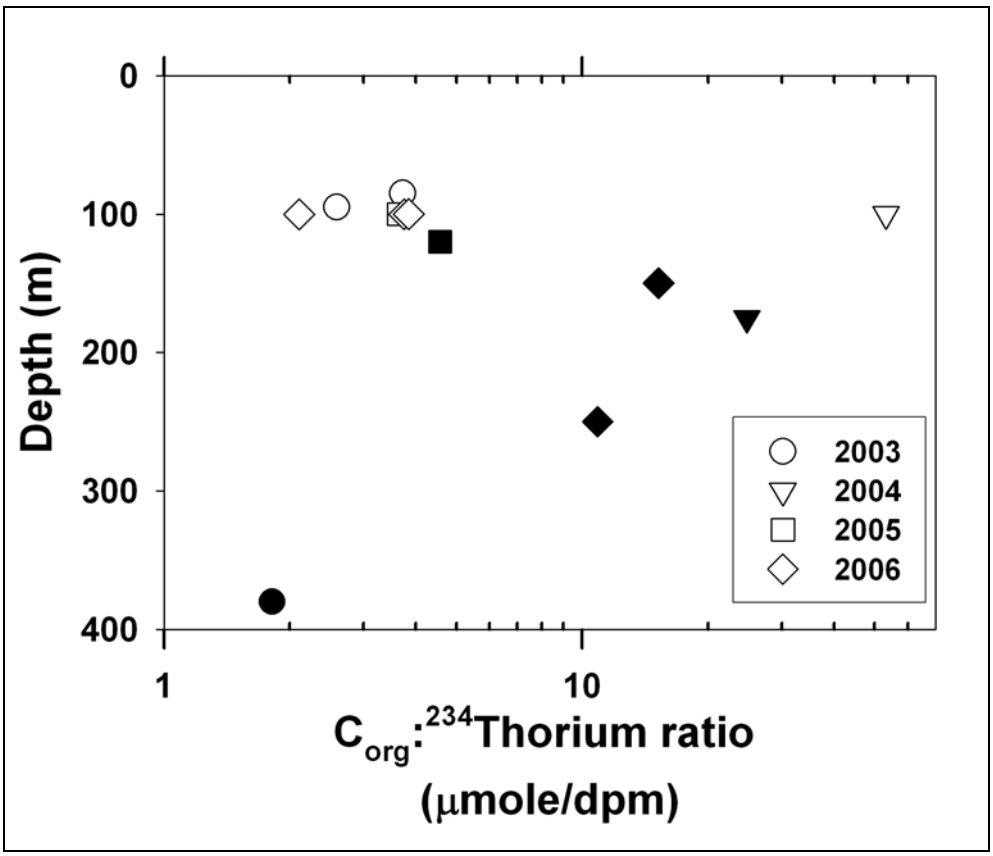

Figure 2.12 The ratio of particulate organic carbon to ^{234}Th determined in samples from SAPS (open symbols) and from the PELAGRA (closed symbols).

Ratio. This lead to estimates of new production in 2005 of 28.9 mmol C m^{-2} d^{-1} whereas new production based on the f-ratio (uncorrected for NH_4^+ regeneration) was 23.2 mmol C m^{-2} d^{-1}. Therefore this method introduced once again an average overestimate of 24%. However, in 2003 the difference between the two methods was much greater (a factor of 7 on average) due to high NO_3^- uptake rates relative to total production. It would appear that in this case using the Redfield ratio to scale NO_3^- uptake would not have been a valid approach. In 2006, only the latter method was applied as no NH_4^+ or urea uptake measurements were made. The new production values obtained were comparable to those obtained the previous year using the same method (29.7 and 28.9 mmol C m^{-2} d^{-1}, respectively), thus it is likely that this value is only overestimated by ~24%.

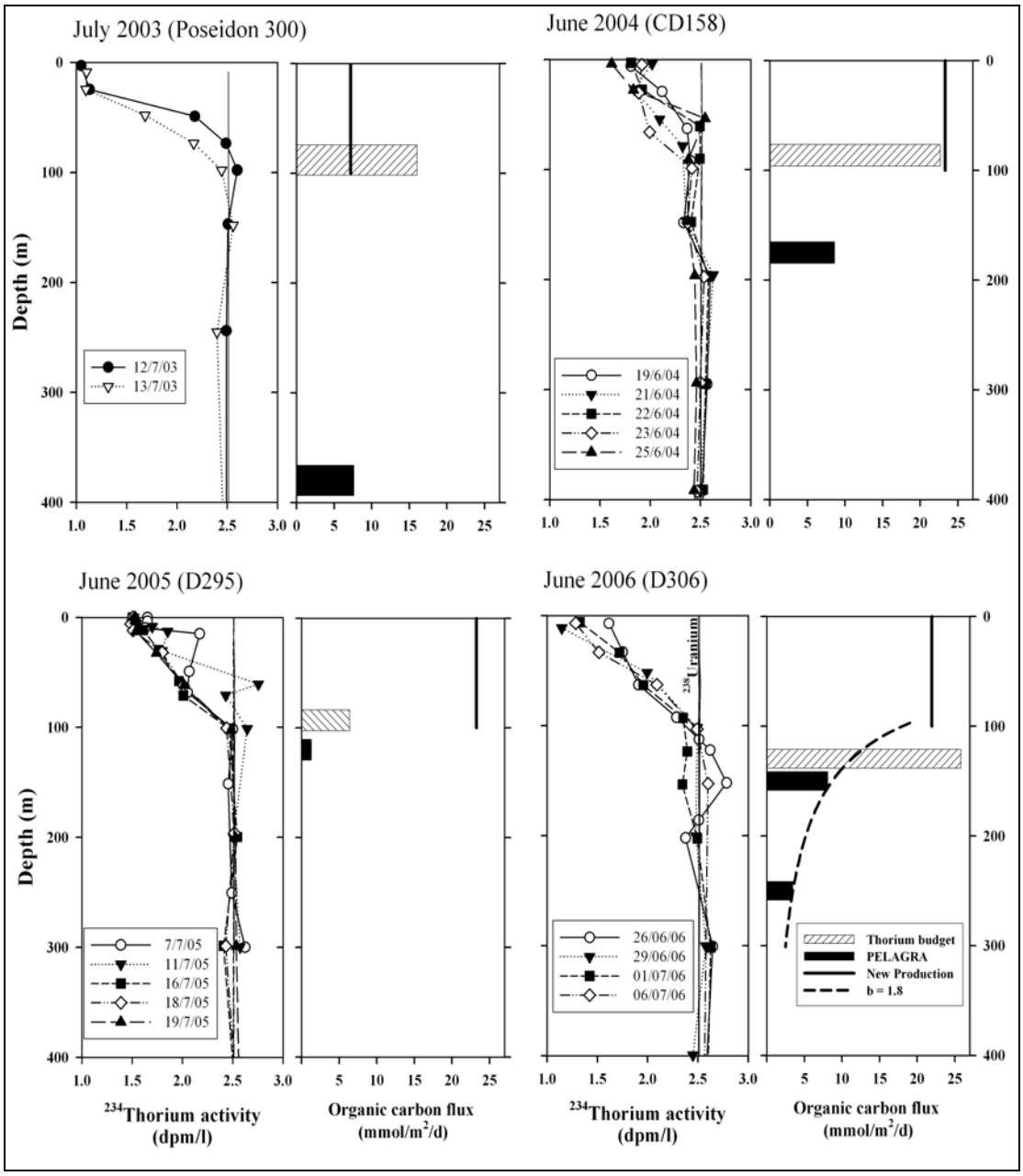

Figure 2.13 For each of 4 years, vertical profiles of ^{234}Th and ^{238}U (left hand panels) and downward flux of POC (right hand panels). These were derived from ^{234}Th budgets down to the equilibrium depth, from new primary production to the 0.1% light level during PELAGRA deployments and measured by PELAGRA traps. Conversion of ^{234}Th to POC flux was based on the ratio derived from trap collected material. The Martin-regression for the 2006 PELAGRA data is extrapolated to the 0.1% light depth (see text and equation 5) (Dashed line).

Thus it seems likely that if the system were operating at equilibrium over some timescale with the diffusive flux of nitrate across the thermocline being exactly balanced by the export of particulate matter from this region then the vertical carbon flux at the base of the mixed layer was 7.2-23.3 mmol C m^{-2} d^{-1} using the f-ratio and 28.9-29.7 mmol C m^{-2} d^{-1} (discarding the suspiciously high value in 2003) using NO_3 uptake only. To convert the observed depletions of ^{234}Th to carbon drawdown it is necessary to multiply the steady-state ^{234}Th export estimate by the POC/^{234}Th ratio and achieve a POC flux at the base of the mixed layer flux. On two of the cruises this differs greatly from that inferred from the ^{15}N uptake (Figure 2.13). In order to understand the reason for this discrepancy it is necessary to understand the timescales over which the two measurements are working. Due to its dependence on the radioactive decay process the ^{234}Th technique integrates removal of particles from the upper mixed layer over some unknown period, often assumed to be similar to the ^{234}Th mean life of 34.8 d. In contrast ^{15}N export estimates are operating over timescales that are more similar to those made using the PELAGRA trap. Moreover, as shown above, the steady-state estimates are likely to overestimate the true flux because of the post-bloom situation during sampling.

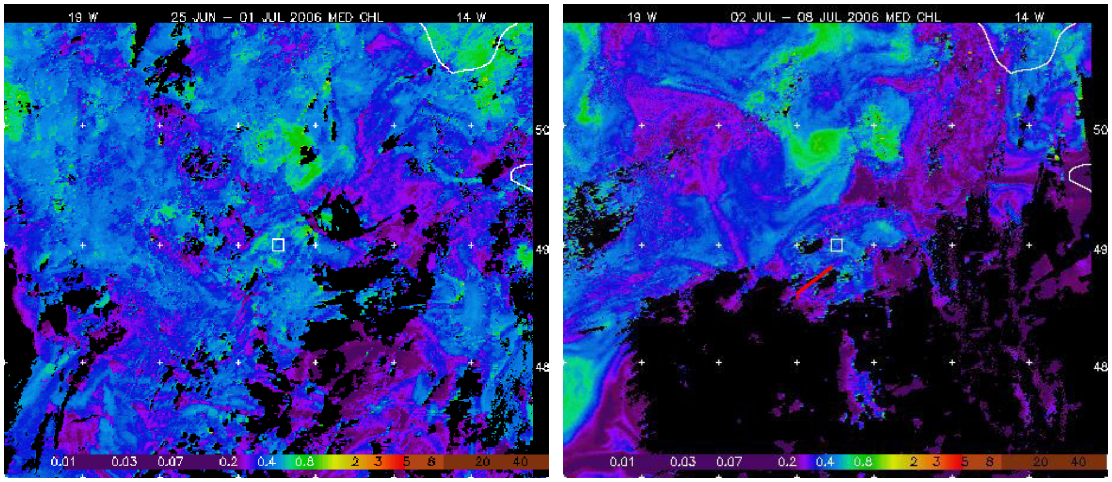

Figure 2.14 Chlorophyll distribution 25th June-1st July and 2-8th July 2006 (µg/l) The trajectory of the traps is indicated by the red line on the right hand chart with the traps moving in a SW direction.

Another possible bias of the ^{234}Th export estimates derives from the potential impact of lateral advection of horizontal ^{234}Th gradients through the sampling site. In Figure 2.14, the two plots of remotely sensed chlorophyll fluorescence covering the time of ^{234}Th and PELAGRA sampling in 2006 show horizontal variability on scales of (1 - 10 km). This variability is less than the variability normally seen in blooms at PAP but it could still be reflected in local particle and, hence, ^{234}Th distribution and dynamics. If such gradients pass through a study site they clearly affect the local (Eulerian) ^{234}Th budget. Therefore, the assumption of a negligible V in Equation 2.3 might not be entirely justified and might have contributed to the differences we see between the various approaches used to estimate POC export. It seems safe to conclude that different time scales of the various approaches used to estimate POC export and inherent differences between Eulerian versus Lagrangian techniques are the main reasons for the range of results of export estimates in this study.

2.4.3 Organic carbon flux and attenuation

The downward flux of organic carbon varied between 1.8 and 8.6 mmol m^{-2} d^{-1} depending on the depth the traps were finally adjusted to. As can be seen from Figure 2.13, the relationship of these values to those of new production is not consistent with values that are surprisingly large in 2003 and 2004. They were very similar to the new production estimates in spite of the fact that the traps were substantially below the euphotic zone. In 2005 the measured export at 120m was only 20% of the new production in the immediately overlying water column. In 2006, which were the longest deployments the measured export was entirely consistent with the overlying new production and the fitted Martin-regression extrapolated to 100m agrees well with the new production estimate (see below). Three potential reasons for this disparity in agreement are firstly that as mentioned previously the relevant time scales of the two measurements are different. Secondly the calculation of an f ratio may have been biased by the presence of nitrifiers as recently discussed by Yool *et al*., (2007) who conclude that more direct measurements of export flux are required rather than an assumption that export can be calculated from new production. Thirdly, the

duration of the PELAGRA deployments was variable and on some occasions the period of stability of the trap was very short in comparison to the total duration of the deployment. It is not possible to determine the level of flux into the trap during times of instability although it is assumed this to be zero. During 2006 the traps were stable for most of the deployment period and the conclusion is that future deployments should not be carried out for a period of less than 2 days.

A key calculation is the attenuation of flux with depth represented by equation 2.7

$$F_{(z)} = F_{(Zo)} (z/z_o)^{-b} \quad \textbf{(2.7)}$$

where $F_{(z)}$ is the measured flux at depth z and $F_{(zo)}$ is the flux at a near surface depth (i.e. 100m; Martin *et al*., 1987) which in the original paper was deemed to be 0.86. The samples on which this was based were heavily contaminated with swimmers and were derived from samples collected in various locations and at different times. Nevertheless, this value is widely used and the concept is of considerable importance as it facilitates a normalisation procedure for comparative purposes (e.g. Lampitt and Antia, 1997) and is used to parameterise global biogeochemical models (e.g. Doney *et al*., 2004). In this study a value of 1.7 was determined, which is substantially higher than that originally reported by Martin *et al*., (1987) and implies that at least at this time and place the attenuation in flux with depth is higher than expected. The only comparable data made with neutrally buoyant traps are from the Pacific as part of the VERTIGO program (Buesseler *et al*., 2007). Using the NBST, b-values of 0.5 and 1.3 were found respectively for stations K2 in the mesotrophic Northeast Pacific and ALOHA in the oligotrophic central Pacific near Hawaii. The very surprising aspect of this work is that even when the absolute flux levels changed at K2 during the period of occupation (by a factor of 3), the b-value remained constant and distinct from that at ALOHA where flux did not change. This was inferred to have been due to the contrasting characteristics of the two sites and to depend on such factors as the food web structure both of the producers and consumers of sinking particles. There are not enough data from the PAP site to comment on whether the b-value of 1.7 is in some way a defining characteristic of the site but it certainly demonstrates that the

decrease in flux with depth can occur much more rapidly than previously thought and in this case PAP seemed more similar to the oligotrophic ALOHA station.

Table 2.2 Downward carbon flux measured directly by PELAGRA and extrapolated to 150m (approximate 0.1% light level) and to 100m.

Date	Sampling depth (m)	Flux measured (mmol/m^2/d)	Flux at 150m depth using b=1.7 (mmol/m^2/d)	Flux at 100m depth using b=1.7 (mmol/m^2/d)	New production (mmol/m^2/d)	Export ratio (% of total PP exported to 150m)
12-13th July 2003	380	7.6	37.0	73.8	7.2	103.4
24-25th June 2004	175	8.6	11.1	13.9	23.3	14.8
18-20th July 2005	120	1.3	0.9	1.8	23.2	1.0
1-6th July 2006	150	8.1	8.1	16.1	22.0	**13.7**
1-6th July 2006	250	3.5	"	16.4	"	"

Extrapolating the data to 150m depth using b=1.7 (Table 2.2) gives export values much less than the model estimation by Laws *et al*., (2000) who calculated an annual average export of about 30 mmol/m^2/d in the region. The export measurements from this study are similar to fluxes at 150m depth measured using surface tethered traps during the JGOFS North Atlantic Bloom Experiment close to PAP (Range 7-13 mmol/m^2/d) (Martin *et al*., 1993). This is surprising as the JGOFS material was probably heavily contaminated with swimmers as well as suffering from hydrodynamic biases and taking place at a different time of year (18-31st May). One might conclude that the JGOFS data approximated reality as a result of a combination of opposing errors and biases. Values obtained by Goutx *et al*., (2005) also using surface tethered traps to the South of PAP were very much lower (range: 0.5-1.6mmol/m^2/d) but the comparison is not particularly pertinent bearing in mind the different technique and the significant distant further south where fluxes are likely to be lower (38-45˚N). The measurements in this study are however close to that

predicted from the 1D model previously used at PAP (Lampitt *et al*., 2001) with maximum values of 19 mmol m^{-2} d^{-1} and an annual average of 3.2 mmol m^{-2} d^{-1}. The proportion of total primary production reaching 150m (export ratio) during the most successful deployment at PAP (2006) indicated a similar proportion of the productivity as was exported at both K2 and ALOHA. In these Pacific sites export was 11-21% of PP while at PAP the figure was 13.7% (Table 2.2)

2.5 Conclusions

The design and deployment of a free drifting buoyancy-controlled sediment trap, PELAGRA during post-bloom periods in the Northeast Atlantic is described. Substantial technical challenges have been resolved and it is believed that this will provide a stream of high quality data on the export of material from the upper ocean and how this is attenuated with depth.

The vertical fluxes of ^{234}Th into the traps were less than those estimated from the upper water column budget of the isotope and we interpret this as a consequence of previous export events that had stripped ^{234}Th from the water column. Alternatively, lateral advection of gradients of total ^{234}Th/^{238}U disequilibria may have confounded the Eulerian budgeting approach we adopted. In order to understand the relationship between estimates of flux based on ^{234}Th budgets and those based on direct measurements by PELAGRA, longer periods of observation are required and preferably during times of both increasing and decreasing productivity.

Organic carbon fluxes measured by the traps are compatible with estimates of new production although the time scales of observation are clearly different and therefore unlikely to agree well. Two highly successful simultaneous deployments in July 2006 by traps at different depths provide a direct measurement of the attenuation in flux with depth and a measure of the Martin b-value of 1.7 which is substantially greater than the canonical value of 0.86. This agrees well with estimates of new production in the overlying water column. In common with comparable observations in the Pacific

(Buesseler *et al*., 2007), it would seem that there are major geographical variations in the rate of attenuation of flux with depth and that these must be incorporated into global biogeochemical models as soon as the number of observations increases.

3. Estimating Carbon, Silica and Diatom Export from a Naturally Fertilised Phytoplankton Bloom in the Southern Ocean using PELAGRA: a novel drifting sediment trap

Reproduced with permission from Elsevier Science from Deep-Sea Research. Minor textual modifications have been made.

Abstract

During the austral summer of 2004 – 2005, a large multi-disciplinary research cruise investigated the development and fate of a naturally iron-fertilised phytoplankton bloom in the Southern Ocean (Crozet Plateau). As part of this extensive process study, a neutrally buoyant sediment trap (PELAGRA) was deployed to constrain the magnitude, composition and variability of upper ocean particle export. In the productive regime north of the plateau we observed depth-normalised (100m) organic carbon fluxes between 11 and 320 mg C m^{-2} d^{-1}, and in the HNLC control region to the south similarly normalised fluxes between 28 and 46 mg C m^{-2} d^{-1}. Mass balance calculations indicate that the high levels of carbon export north of the plateau would need to be maintained for at least 30 days in order to account for estimated seasonal depletion of dissolved silicic acid in surface waters. This would imply the flux of organic carbon is 11-15 g C m^{-2} for the period of the bloom north of the plateau. A range of export ratios (proportion of surface production lost to downward flux) were calculated using both contemporaneous and retrospective estimates of integrated production, and these highlight the temporal decoupling between production and export. Calculated export ratios were at their highest north of the plateau and correlate strongly with the selective export of large, heavily silicified diatoms, particularly *Eucampia antarctica*, relative to the surface community structure. By normalising the molar elemental ratios measured in the exported particles to the molar elemental ratios of the upper ocean particle field we also observed a strong decoupling of Si:C and Si:N. This suggests that the decoupling of the global silica and carbon cycles that is well known as a defining feature of the Southern Ocean has its origins in the upper ocean.

3.1 Introduction

Oceanic regions characterised by perennially high macronutrient levels yet low and constant levels of phytoplankton stocks have been a paradox long recorded by oceanographers as reviewed by Boyd, (2002). As early as the mid-1930's iron supply was suggested as a potential explanation for these so-called high nitrate-low chlorophyll (HNLC) regions (Hart, 1934). Martin (1990) linked increase in iron supply to an enhancement in primary production and subsequent carbon sequestration in HNLC waters during both the present day and the geological past. Morel *et al*., (1991) provided a detailed framework linking iron supply, food-web structure, and macronutrient concentrations to explain low phytoplankton stocks in HNLC regions. The hypotheses led to a suite of *in-situ* iron fertilisation experiments in major HNLC regions; IronEx-1 (Martin *et al.,* 1994) and Iron Ex-2 (Coale *et al*., 1996) in the equatorial Pacific, SERIES (Boyd *et al*., 2004) in the north-east Pacific, SEEDS (Tsuda *et al*., 2003) in the north-west Pacific, and in the Southern Ocean, SOIREE (Boyd *et al*., 2000), EisenEX (Gervais *et al*., 2002), SOFeX (Coale *et al*., 2004), and EIFEX (Hoffmann *et al*., 2006).

The mesoscale perturbation experiments listed above provide strong evidence that iron fertilisation of HNLC regions can cause an increase in primary production (Gall *et al*., 2001a), a significant increase in photosynthetic quantum efficiency (Kolber *et al*., 1994; Behrenfeld *et al*., 1996), an increase in chlorophyll a concentrations (Gervais *et al*., 2002), phytoplankton community shifts (Cavender-Bares *et al*., 1999; Gall *et al*., 2001b), strong nutrient drawdown (Cooper *et al*., 1996; Frew *et al*., 2001), and a decrease in the fugacity of carbon dioxide (Cooper *et al*., 1996; Bakker *et al*., 2001). However, export fluxes from iron enrichment experiments tend to be small or negligible and difficult to quantify during the time course (12-24 days) of the experiments (De Baar *et al*., 2005).

During the 13-day observation period of SOIREE, no measurable changes in POC flux were observed using either the ^{234}Th method (Charette and Buesseler, 2000) or 2- to 3-day shallow sediment trap deployments (Nodder *et al*., 2001). Over the 22 days of EisenEx ^{234}Th activity showed no differences between inside and outside of the fertilised

patch (Buesseler *et al*., 2004). Iron enrichment had a measurable impact on ^{234}Th derived POC export from the southern (high Si) SOFeX patch (Buesseler *et al*., 2004), the magnitude of the flux increase was small relative to that of natural blooms in the region (Buesseler *et al*., 2001). Although thorium based estimates from the northern (low Si) SOFeX patch showed no difference in POC export (Buesseler *et al*, 2004), data obtained from an autonomous float to measure particle abundances (Bishop *et al*., 2004) suggested an increase in POC flux ranging from 2 fold to 6-fold depending on which assumptions are followed. Perhaps the most convincing evidence to date is the enhancement (2-3 fold) of carbon fluxes measured by sediment traps 25 days after iron enrichment in the SubArctic Pacific (Boyd *et al*, 2004).

The main problems influencing export measurements from iron-fertilisation experiments are the period of observation and lateral advection of the iron-infused patch. Generally, there is a time-lag on the order of 20-30 days between the onset of phytoplankton growth and the subsequent export of POC out of the surface ocean (Buesseler *et al*., 2004). When factoring in the multiple additions of iron that characterise such experiments, it is unsurprising that export observations are equivocal. Also, in all of the iron enrichment studies undertaken so far, lateral mixing tends to dilute the initial patch (e.g. see Fig. 15 of De Baar *et al*., 2005). These factors cause the experiment to behave like a chemostat (Boyd *et al*., 2000), the exchange with surrounding HNLC waters can entrain macronutrients and allow the bloom to continue whilst there is sufficient iron (Abraham *et al*., 2000). More importantly for export observations, this stirring effect also mixes phytoplankton out of the patch. This slows down the rate at which phytoplankton cells reach the critical concentration for aggregation i.e. C_{cr} (Jackson, 1990; Jackson *et al*, 2005), and delays sedimentation of the bloom. It may be possible to avoid some of these problems by conducting similar studies in Southern Ocean blooms that are seeded by natural sources of iron.

There are several ways in which Southern Ocean HNLC regions can receive a natural source of iron which promotes enhanced phytoplankton biomass and growth, mixing with iron rich water masses such as the Polar Front jet (De Baar *et al*., 1995), melting of

sea-ice (Sedwick and Di Tullio, 1997), or the "island mass effect" (Martin *et al*., 1994; Blain *et al*., 2001). Composite satellite images of the Southern Ocean show that island systems such as South Georgia (Korb *et al*., 2004), the Crozet Plateau (Venables *et al*., *this issue*), and the Kerguelen Plateau (Blain *et al*., 2001) have higher phytoplankton biomass associated with these topographical features in comparison to the surrounding HNLC water.

The aim of this study was to analyse particulate export from a naturally fertilised iron bloom in the Southern Ocean using PELAGRA (Chapter 2). Samples were analysed for the chemical composition of major biogenic components and for diatom species composition. Data is compared from seven PELAGRA deployments, five from the productive regime north of the plateau and two from the HNLC area to the south. Flux parameters are related to upper ocean measurements during the Crozex project to elucidate the controls on the magnitude and variability of upper-ocean particle flux from an iron-stimulated bloom.

3.2 Study Area

The Crozet Islands form part of a larger plateau that is located in 4200m of water in the Southern Ocean at 46°S, 52°E (Fig. 3.1). The archipelago is situated in the northern part of the Indian-sector of the Southern Ocean and is thus within the boundaries of the Polar Frontal Zone (PFZ). Circulation patterns in the region are affected by local topography, the Antarctic Circumpolar Current (ACC), and zonal wind fields. The Sub-Antarctic Front (SAF), a major branch of the ACC, flows eastwards to the south of Del Cano Rise and is then deflected northwards into the Crozet Basin, before turning eastward and combining with the Agulhas Return Current and the Sub-Tropical Front, creating an S-bend feature (Pollard and Read, 2001);(Fig. 3.2). South of this S-bend and north of the plateau itself mean circulation is weak, allowing dissolved iron from the land or sediments of the Crozet plateau to accumulate throughout the winter in the PFZ between Crozet and the SAF. With excess macronutrients present in the HNLC waters this, facilitates an annual

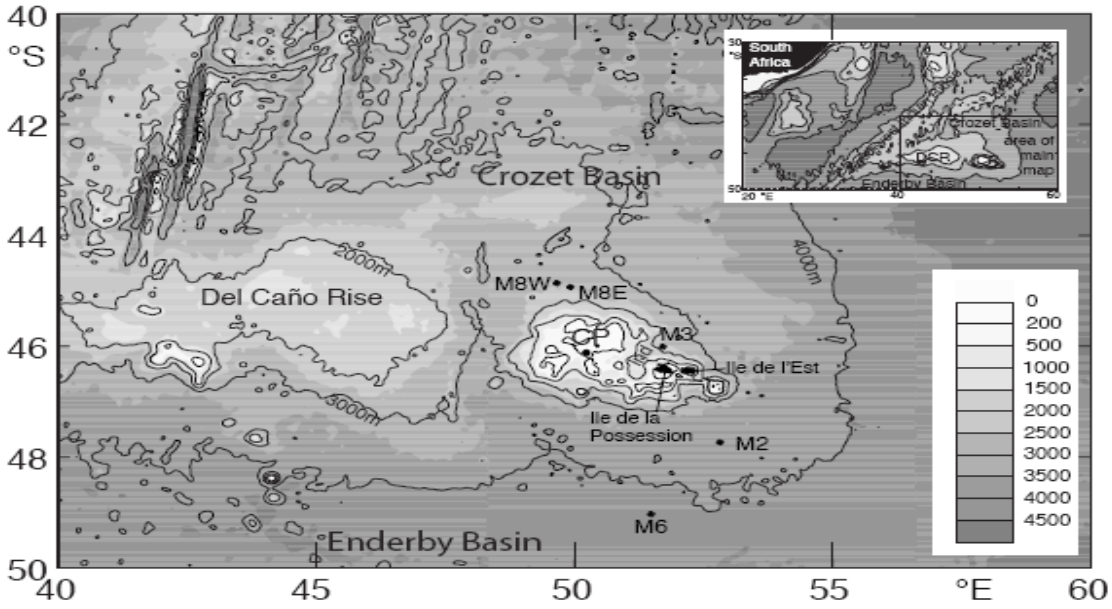

Fig. 3.1 Bathymetry of the CROZEX survey area between 40-50°S and 40-60°E. The inset shows the location of the area relative to South Africa and the Southwest Indian Ridge. CP is the Crozet Plateau. Black filled circles mark the seven deployment locations of PELAGRA, M3 (M3.3, M3.7, and M3.8), M8E, M8W, M6, and M2.

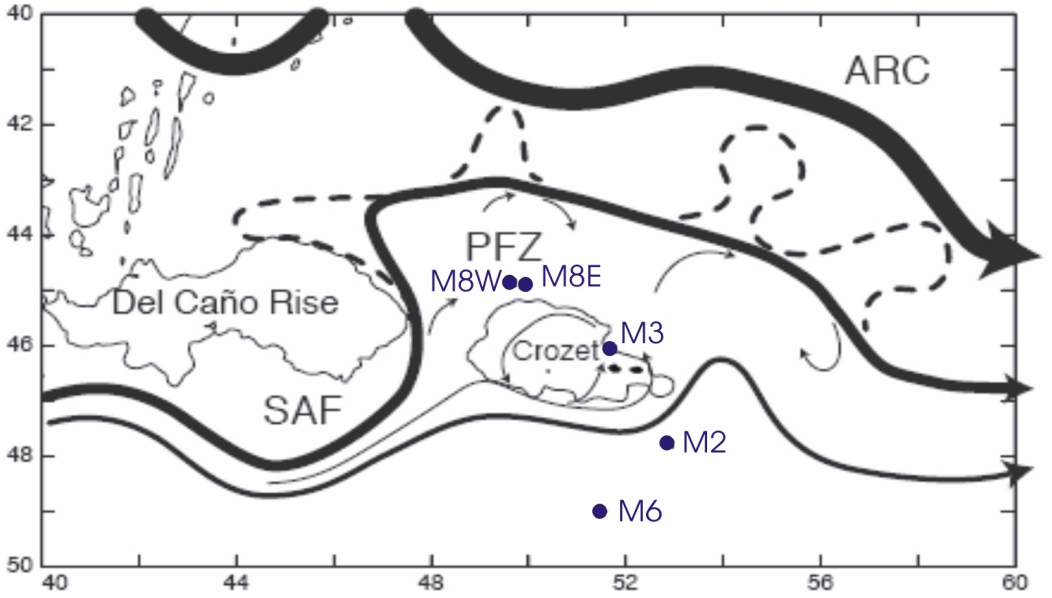

Fig. 3.2 Map of CROZEX survey area showing deployment locations and the main features of local hydrography. The thick black line marks the Agulhas Return Current (ARC), the bold solid line is the SubAntarctic Front (SAF), with dashed lines between them marking transient propagating eddies. The thin arrows represent the very weak circulation in the polar frontal zone. Modified from Pollard *et al.*, (2007).

bloom (September – January) to the north of the plateau as shown by composite satellite imagery (see Venables *et al*., 2007).

3.3 Materials and Methods

3.3.1 PELAGRA

PELAGRA was deployed successfully seven times as part of the CROZEX project on cruises D285 (3rd November 2004 – 10th December 2004) and D286 (13th December 2004 – 21st January 2005). Five of these deployments took place in the productive regime north of the Crozet Plateau (M3.3, M3.7, M3.8, M8E and M8W) and two in the HNLC "control" waters to the south (M2 and M6), (Table 3.1). Prior to each PELAGRA deployment, hydrographic CTD profiles were studied to ascertain the temperature and in-situ density profiles of the deployment area; this information was used to calculate the additional mass required to affect the neutral buoyancy of the trap at a specified depth (see Chapter 2). The sample cups were filled with 500mL of hyper-saline preservative solution to prevent the dissolution and/or resuspension of particles during the deployment period. The preservative solution was made by mixing 19L of hyper-saline seawater with 1L of formaldehyde (AnalR® grade, VWR International) buffered to pH 8.6 with sodium tetraborate. The seawater was made hyper-saline by adding 100g of sodium chloride to 19L pre-filtered (0.4μm) seawater.

3.3.2 Swimmers

Prior to chemical analysis of the particulate samples, swimmers were removed from the sample with plastic forceps under a strong dissecting microscope. Swimmers are defined as the zooplankton that have entered the sample cups alive and intact, and therefore do not represent the passive flux from the surface ocean (Michaels *et al*, 1990). Although swimmers were not enumerated to species level, 82-96% of all organisms removed from the traps were classified as either calanoid or cyclopoid copepods. Using Equation 3.1 (Razouls, 1985) which relates total body length to dry weight for *Drepanopus pectinatus,* a species commonly encountered in the study area

Table 3.1 Shows the date, location, and physical and chemical parameters characterising the PELAGRA deployment locations.

Station	Date dd/mm/yyyy	Station Number	Latitude deg. south	Longitude deg. east	Wind mixed layer depth (m)	Surface $Si(OH)_4$ µmol l^{-1}	Surface NO_3^{-2} µmol l^{-1}	Temperature °C
M2	20/11/2004	15504	47.80	52.86	149	15.6	24.0	3.4
M6	21/11/2004	15507	49.00	51.49	207	18.5	22.9	2.7
M8E	30/11/2004	15532	44.92	49.91	75	2.9	22.2	5.9
M8W	02/12/2004	15538	44.87	49.64	53	0.2	18.0	5.7
M3.3	25/11/2004	15518	46.07	51.77	167	7.7	21.8	4.5
M3.7	10/01/2005	15619	46.03	51.87	45	1.2	20.9	5.7
M3.8	12/01/2005	15628	46.04	51.96	49	0.2	18.0	6.2

(Fielding *et al.*, 2007), the contribution of swimmers to total mass flux was calculated for each deployment. Generally swimmers represented between 15-20% of total mass flux, with the exception of M6 where they accounted for around 40%, and M8E and M8W were much lower at 1 and 0.3% respectively. There were no obvious patterns in relation to deployment times when considering *diel* migrations of zooplankton.

$$\text{Log DW} = 3.064\log\text{TL} - 8.169 \quad \textbf{(3.1)}$$

where, DW is dry weight in μg and TL is total length in um.

3.3.3 Chemical Analyses

3.3.3.1 Sample splitting and total mass flux

The 500mL samples were split into 8 aliquots of equal volume (62.5mL) using a McLane splitter (replication error <3% for this methodology; Lampitt, pers. obs.). Total mass flux was determined gravimetrically following filtration onto pre-weighed cellulose nitrate filters (0.45µm pore size, 47mm diameter). Filtration of sub-sample was followed by rinsing with 0.56 M ammonium formate solution (pH 7) to remove salt and excess formalin. Samples were oven dried at 60°C until a constant weight was obtained.

3.3.3.2 POC/PON

In order to reduce errors associated with sample heterogeneity aliquots were combined where possible. For particulate organic carbon (POC) and particulate organic nitrogen (PON) aliquots were filtered onto pre-combusted (450°C, 12 hrs), pre-weighed 25mm GF/F filters (nominal pore size – 0.7µm), and dried for 48 hours at 60°C. Based on a modified version of the of Verado *et al.* (1990), samples and filters were fumigated with concentrated sulphurous acid in a vacuum desiccator for 48 hours, and then dried at 60°C for a further 48 hours. The filters were subsequently placed onto pre-combusted (450°C, 12hrs) tin-foil discs (Elemental Microanalysis) according to Hilton *et al*. (1986). POC and PON were measured using a Carlo-Erba NA-1500 elemental analyzer, after standardization with acetanilide. Relative standard deviation (RSD) of analytical

replicates was <13% (n = 3) for both POC and PON. Procedural blanks for C and N demonstrated that sample contamination was negligible (<1%).

3.3.3.3 Biogenic opal

Opal was determined using a wet chemical technique modified from Mortlock and Froelich, (1989). Aliquots were filtered onto pre-weighed 25 mm polycarbonate filters (pore size - 0.45μm) and dried at 60°C for 24 hours. Particulate opal was dissolved by treatment with 0.2M sodium hydroxide for 3hrs at 110°C. The extract was separated from the residue via centrifugation (3,000 rpm, 15 mins) and the sediment residue was rinsed with ultra-pure water, and dried overnight (60°C). A second sodium hydroxide digestion was used to confirm the removal of all particulate silica in the samples, and the residues were also checked under a scanning electron microscope (SEM) to verify the complete dissolution of siliceous frustules. The dissolved silicate was converted to the silico-molybdate complex (Strickland and Parsons, 1968) and the absorbance read at 812 nm with a Hitachi U-2000 spectrophotometer. Biogenic opal was calculated assuming 10% water content of silicon dioxide, a value typically reported for marine diatoms (Mortlock and Froelich, 1989). RSD of replicate silicon measurements was <10% (n = 3).

3.3.4 Phytoplankton analyses

3.3.4.1 SEM imaging

Prior to examination under the SEM, aliqouts were gently filtered onto 25mm polycarbonate filters (pore size – 0.45μm). The filters were sliced into quarters and mounted onto 25 mm aluminium SEM stubs layered with an adhesive carbon coating. The samples were subsequently coated with 20 nm gold using a Hummer VI-A gold sputter coater. Imaging and analysis was undertaken using a Leo 1450VP Scanning electron microscope. Backscatter electron images were obtained with operating conditions using a voltage of 20 kV with a nominal probe current of 500 pA, and a working distance of 19 mm.

3.3.5 Data from other sources

3.3.5.1 Phytoplankton cell counts – surface assemblage and trap assemblage

Water samples were collected from 2 depths during predawn deployment of a Seabird 911+ CTD and 24-bottle rosette. Sampling depths were selected based on the vertical density, temperature and fluorescence profiles. Water samples for phytoplankton enumeration were preserved in 100 mL brown bottles with 2% acidic Lugol's solution. For both water and sediment trap samples, sub-samples were settled in 10 mL settling chambers (Hydro-Bios) for ~10-12 hrs and examined using a Leitz inverted microscope. Large and numerically rare taxa were counted during full examination of the settling chamber at high magnification (x10), while small and numerically dominant taxa were counted on 1-2 transects of the chamber (x10, x20) or from cumulative counts from several (5-10) fields of view (x40). Diatoms and dinoflagellates were identified to genera or species following Priddle and Fryxell (1985) and Tomas (1997), with unidentified taxa (e.g. ciliates) grouped according to cell size (Poulton *et al.*, 2007).

3.3.5.2 Upper ocean particulates

Analysis of the upper ocean particle field was achieved by filtering sea-water samples (0-500 m) using a CTD system mounted on either a stainless steel or titanium rosette sampler. For this study samples were integrated to the base of the euphotic zone, defined here as where the light level is 1% of surface incident irradiance. For stations M8E, M8W, M3.7 and M3.8 this corresponds to a depth of 60m, whereas at stations M2, M6, and M3.3 it was 80m. Samples were taken from depth intervals of 5, 10, 20, 40, 60, and 80m.

For measurements of POC and PON, 1 – 4.2 litres of sea-water were filtered onto pre-combusted (450°C, 12 hrs) Whatman GF/F glass fibre filters. The filters were stored at -20°C, fumed with sulphurous acid and analysed using a Thermo Finnigan Flash EA1112 Elemental Analyser. RSD between replicate POC measurements was ~13%. Biogenic silica measurements were made on 1 litre seawater samples filtered onto 0.4µm polycarbonate filters, stored at -20°C, digested in 0.2M sodium hydroxide and

neutralised with 0.1M hydrochloric acid. Dissolved silicon concentrations were analysed as described above.

3.3.5.3 Primary production

Primary production measurements were carried out using the ^{14}C radionuclide labelling technique over 24h simulated *in situ*, on-deck incubations. The measurements were made at 6 depths for 3 size fractions (>2µm, 2-20µm and >20µm). Seawater samples were collected from pre-dawn titanium CTD casts. Subsamples were drawn directly into acid-washed, 2L polycarbonate bottles (Nalgene) in Ziploc bags to avoid contamination. For each light depth, triplicate 60mL samples and a dark sample were inoculated under a Class 100 laminar flow hood with ~10 µCi $NaH^{14}CO_3$. The same procedure was carried out for each of the size fractions. Total activity standards were prepared in Carbosorb CO_2 trapping agent (Packard). Incubations were run for a 24 hour period in on-deck Perspex tubes covered with neutral density (Lee: Misty Blue [061] and Neutral Density Grey [210 ND]) filters which reconstructed water column light attenuation (i.e. 97, 55, 33, 14, 4.5 and 1% incoming irradiance) and removed red light. Incubators were cooled by a constant flow of surface seawater.

At the end of the experiment, samples were filtered under vacuum onto 25mm diameter, 0.2 µm (Whatman), 2µm and 20µm (Poretics) polycarbonate filters. Filters were first rinsed with filtered seawater, then transferred to a fume hood for rinsing with a few mL of 0.5% HCl solution made up in artificial sea-water prior to acid fuming for several hours to expel any remaining unfixed inorganic ^{14}C. The filters were then placed in 5 mL Optiphase Hi-Safe 3 scintillation cocktail (Packard) and counted on-board on a Tri-Carb 3100 TR liquid scintillation counter. Total CO_2 concentrations measured from the associated stainless steel casts were used for the calculation of production (Seeyave *et al.*, 2007).

3.3.5.4 Remote-sensing data

The remotely-sensed chlorophyll data used in this chapter is the merged SeaWIFS/MODIS product which is a composite of the two chl-a estimates. MODIS

derived chl-concentrations (Feldman and McClain, 2006a) were processed using the standard OC3v1.1 algorithm. SeaWIFs derived chl-a concentrations (Feldman and McClain, 2006b) were processed using the standard OC4v5.1 algorithm. For each of the 810 *in situ* chl-a measurements collected during the cruises, the value from the corresponding individual pixel of the ocean colour image of the day of collection was recorded, if the pixel was cloud free. This resulted in 224 pairs of *in situ* and satellite data for the merged SeaWIFS/MODIS product. The least squares regression fits, with 95% confidence intervals are shown equations 3.2 and 3.3

$$CHL_{merged} = 0.12_{\pm 0.04} + (0.38_{\pm 0.03}) * CHL_{in\ situ},\ r^2 = 0.78 \quad \textbf{(3.2)}$$

$$CHL_{in\ situ} = -0.08_{\pm 0.08} + (2.05_{\pm 0.15}) * CHL_{merged} \quad \textbf{(3.3)}$$

The remotely-sensed chlorophyll data was corrected using these relationships (Venables *et al.*, 2007)

3.4 Results

3.4.1 Deployment profiles

The deployment profiles of PELAGRA are presented in Fig. 3.3. The success of a deployment is quantified by calculating the mean deviation of the float away from the average depth it occupied during its deployment. Based on this parameter the deployments were generally successful, particularly at M2 (122.9 ± 3.5m), M6 (108.5 ± 18.5m), M8E (232.2 ± 11.1m), M8W (248.2 ± 5.7m), and M3.3 (157.2 ± 14.5m). For the two deployments at M3.7 (86.9 ± 54.5m) and M3.8 (99.8 ± 36.0m), the float experienced a quite a large deviation from the average depth. For stations M3.7 and M3.8 the notion of calculating an average depth seems a little inappropriate based on the deployment profiles. It is necessary to define a depth horizon for the flux measurements in order to enable a full comparison of the data set, however it is noted that the depths used for stations M3.7 and M3.8 are poorly constrained.

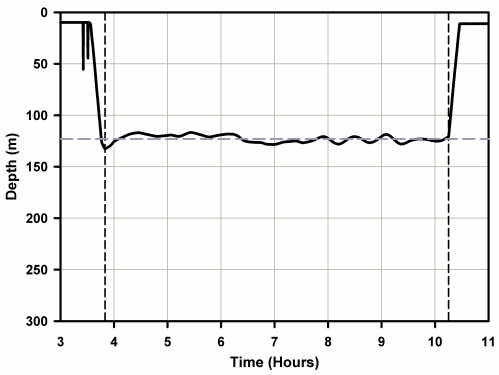

Figure 3a – M2 deployment

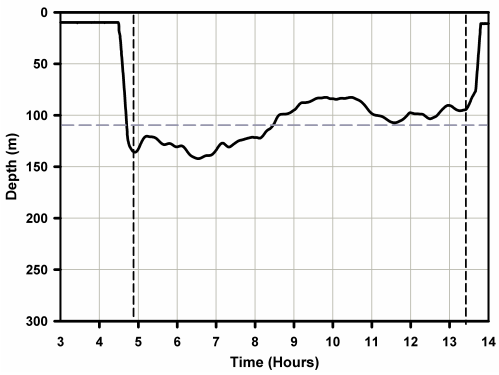

Figure 3b – M6 deployment

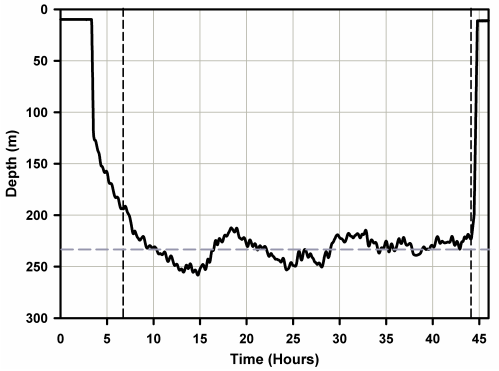

Figure 3c – M8E deployment

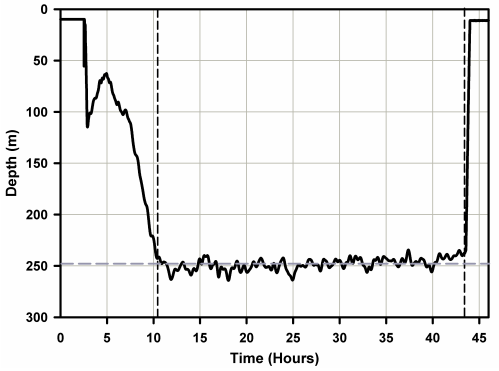

Figure 3d – M8W deployment

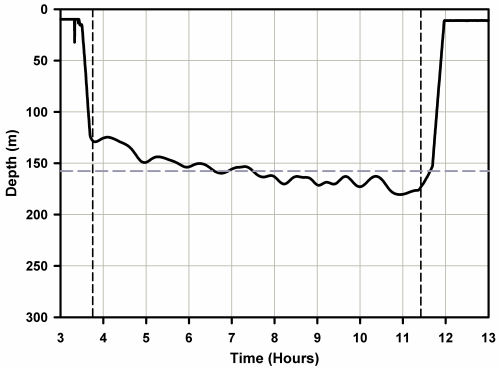

Figure 3e – M3.3 deployment

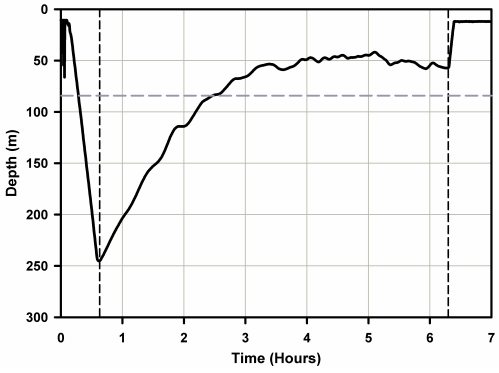

Figure 3f – M3.7 deployment

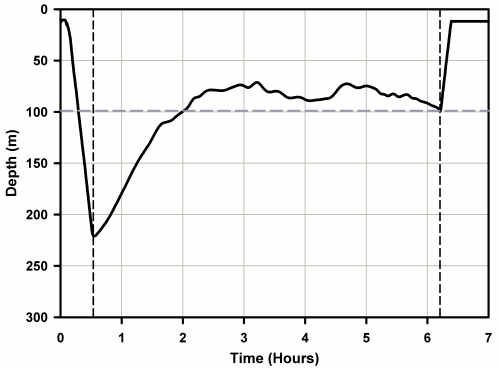

Figure 3g – M3.8 deployment

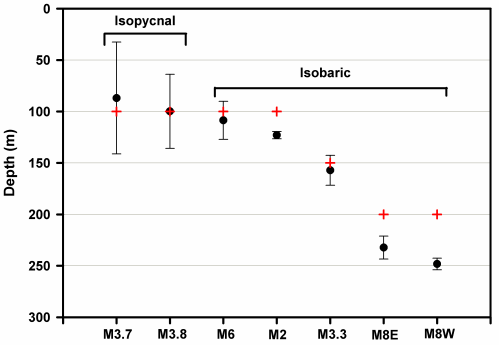

Figure 3h

Fig. 3.3 Panels 3a-3g shows the depth profiles as a function of time for each of the deployments. The vertical black dashed lines mark the start and end of the collection period and are used to determine the length of the deployments for flux calculations. The start and end of the deployments are set when the vertical movement of the trap over a 1 hour period is <1cm s^{-1}. The horizontal grey dashed line shows the average depth of the deployment calculated from the start and end of the pre-defined collection period. Panel 3f shows the average depth of each deployment (black circles) with error bars. Red crosses mark the target depths.

Fig. 3h summarises the average depths and associated standard deviations of the PELAGRA deployments in comparison to the target depths. In most instances the average depth of the traps closely approximates the target depth, with the largest differences occurring for the deep deployments at M8E and M8W. Although these deployments were programmed to descend to 200m the average depth is 232m at M8E and 248m at M8W. These discrepancies represent imperfections in the ballasting algorithm described in Chapter 2. In many ways the absolute depth of the deployment is of less concern than the depth range the trap occupies over the period of the deployment. Fig. 3h suggests that the error on the calculated average depth is generally larger at shallower depths, with the notable exception of M2. This inference is however compromised by the fact that the two shallowest deployments, M3.7 and M3.8, were made with the isopycnal version of PELAGRA (Chapter 2)

The differences in deployment depths and durations complicate the interpretation of the results. There is no reason to doubt that the hydrodynamic performance of the traps retards collection efficiency in the early stages of the deployment. However, it is less certain that diel cycles in particle production and export, if they exist in this region, do not influence our observations for the shorter deployments. Furthermore, slight differences in deployment profiles, for example the slow rise to an average depth for M3.7 and M3.8, may affect the sampling efficiency of the trap. Unfortunately there is no way to distinguish the variation in flux parameters from different intervals of the deployment period. Consequently this must be regarded as a potential uncertainty associated with the measurements.

3.4.2 Primary productivity

Primary productivity measurements are discussed for the PELAGRA deployment stations presented in this chapter. Primary production was measured in 3 size classes (<2 µm, 2-20 µm, >20 µm) using the ^{14}C technique (Seeyave *et al*., 2007), and integrated to the 1% irradiance level. A range of total integrated production was observed from 0.14 – 2.2 g C m^{-2} d^{-1}, with the highest values recorded at M3.7 and M3.8. The size distribution of primary production also varied (Fig. 3.4), with 54 and 55% of the production occurring in the >20µm size class at stations M8W and M6, respectively. However, at station M3.7, where the largest total integrated production (2.2 g C m^{-2} d^{-1}) was observed, the >20µm size class contributed only 19%, and production was dominated by the 2-20µm fraction (70%).

3.4.3 Biogenic fluxes

Total mass flux and the fluxes of the major biogenic components are shown in Table 3.2 for each of the deployments. There was large variability in the total mass flux ranging from 0.09 – 2.7 g m^{-2} d^{-1}, with the lowest value recorded at the southern station, M2 and the largest value at M8W, north of the plateau. The particle flux at M8W was an order of magnitude greater (2.7 g m^{-2} d^{-1}) than at the other six stations (0.09 – 0.67 g m^{-2} d^{-1}). Excluding M8W the mean flux of organic carbon was 25.6 mg C m^{-2} d^{-1} (range 11.5 – 43.3 mg C m^{-2} d^{-1}), whereas including M8W increases the mean flux two-fold to 50.7 mg C m^{-2} d^{-1}. Similarly, the mean flux of organic nitrogen was 4.6 mg N m^{-2} d^{-1} (2.3 – 6.3 mg N m^{-2} d^{-1}) excluding M8W and was 8.5 mg N m^{-2} d^{-1} including M8W. Finally, the mean flux of biogenic opal (expressed as BSi) was 122.9 mg BSi m^{-2} d^{-1} (17.1 - 429 mg BSi m^{-2} d^{-1}) and with M8W the mean flux increases three-fold to 349.7 mg BSi m^{-2} d^{-1}. Correlations between bulk mass flux and major biogenic elements were statistically significant ($P<0.01$). For organic carbon and total mass flux, $r^2 = 0.97$ ($n = 7$), for organic nitrogen and total mass flux, $r^2 = 0.97$ ($n = 7$), and for biogenic opal and mass flux, $r^2 = 0.99$ ($n = 7$).

Table 3.2 Deployment information for each of the seven PELAGRA deployments
*Average depth of trap during deployment; see Fig. 3.3
** This value is actually given by Mass Flux – [(POC FLUX * 2) + Biogenic opal flux]. This value is assumed to approximate the calcite component of the particulate flux since SEM imaging indicates the contribution of lithogenic material to be negligible.
***Deployment extended into a second day

Site	Deployment Date *dd/mm/yyyy*	Deployment Length *(days)*	Deployment Depth* *(m)*	Collection Period *Local (hh:mm)*	Mass Flux *(mg m^{-2} d^{-1})*	Organic Carbon Flux *(mg m^{-2} d^{-1})*	Organic Nitrogen Flux *(mg m^{-2} d^{-1})*	Biogenic Opal Flux *(mg m^{-2} d^{-1})*	Caclite Flux** *(mg m^{-2} d^{-1})*
M2	20/11/2004	0.271	123	03:30 - 09:30	91.8	23.6	4.9	23.1	21.5
M6	21/11/2004	0.358	109	00:30 - 09:30	263.7	43.3	6.3	50.4	126.7
M8E	30/112004	1.540	232	23:30 - 13:30***	673.5	30.7	7.0	429.0	183.1
M8W	02/12/2004	1.388	248	02:00 - 11:00***	2740.6	201.3	32.0	1710.3	627.6
M3.3	24/11/2004	0.321	157	06:30 - 14:30	325.1	23.8	3.7	181.5	95.9
M3.7	10/01/2005	0.237	87	21:50 - 03:50	132.9	20.6	3.3	17.1	74.6
M3.8	12/01/2005	0.235	100	22:45 - 04:45	110.3	11.5	2.3	36.6	50.9

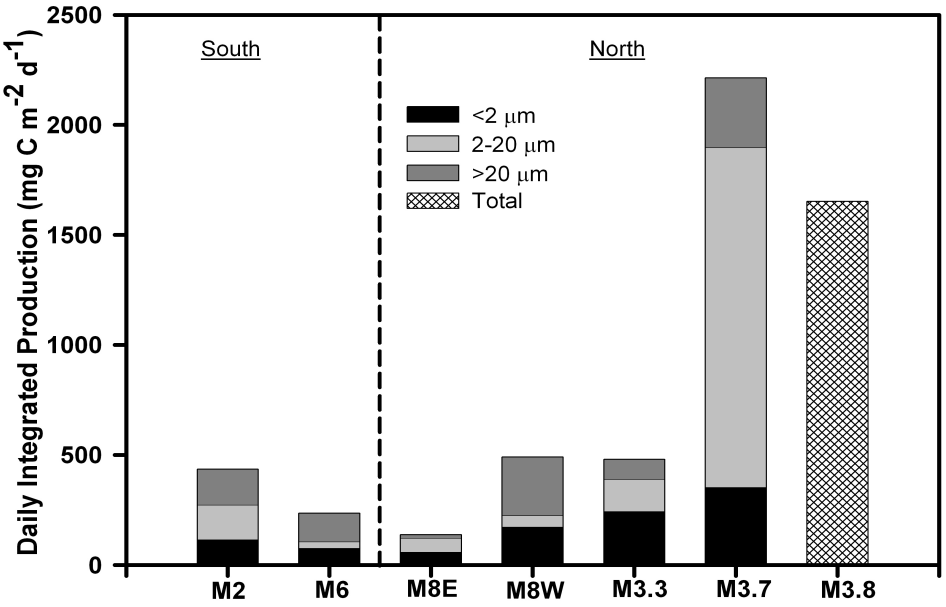

Fig. 3.4 Total integrated primary production for each of the seven stations where there was a PELAGRA deployment. Production measurements were made for three size classes, <2μm, 2-20μm, >20μm, no size fraction data is available for station M3.8. Total integrated production is calculated by performing a trapezoidal integration to the 1% irradiance level (Seeyave *et al*, 2007).

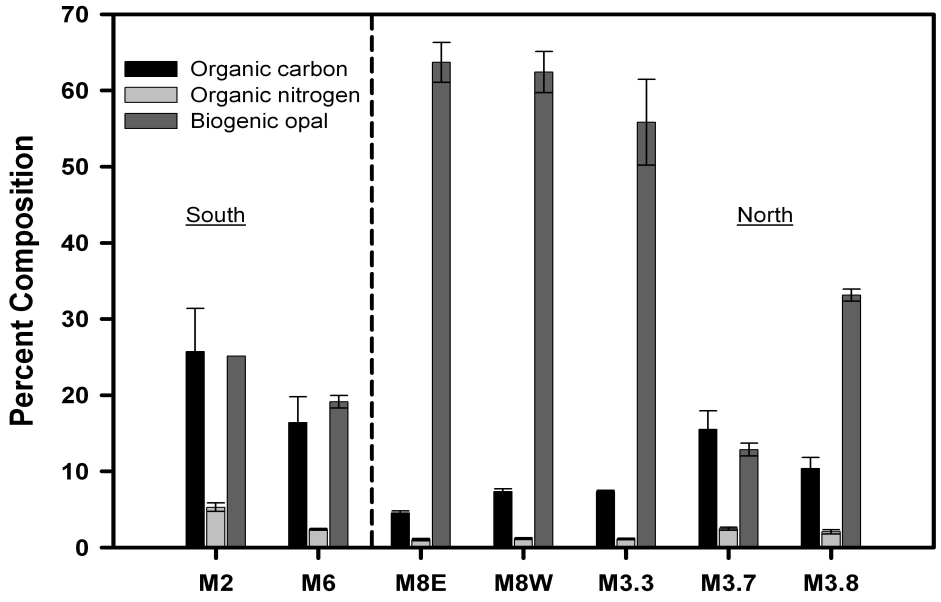

Fig. 3.5 Percentage composition by mass of the major biogenic components of the sediment trap material caught at each station.

Whilst it is useful to express particle flux data as rates, this can be difficult when attempting to compare stations as the fluxes are biased by the magnitude of bulk mass flux. It is therefore useful to assess the flux by its percentage composition. Fig. 3.5 shows the biogenic composition of the exported material at each of the seven stations. Average compositions from stations M3.3, M8E, and M8W, all north of the plateau; contain 60.6 ± 3.4 % biogenic opal, 6.4 ± 1.6 % organic carbon, and 1.1 ± 0.06% organic nitrogen (here ± values represent the standard deviation of the mean calculated from grouping stations with similar compositions). Stations south of the plateau, M2 and M6, have markedly different compositions, biogenic opal comprised 22.1 ± 4.3%, organic carbon 21.1% ± 6.6%, and organic nitrogen 3.8% ± 2.0%. Stations of lowest flux, M3.7 and M3.8, do not appear to relate well to each other, or fit into either of the two groups described above, but the biogenic composition most resembles the southern stations M2 and M6.

3.4.4 Molar elemental ratios

Similar groupings between the sites were also observed in the molar elemental ratios of exported material (Fig. 3.6). M8E, M8W, and M3.3 all have Si:N ratios in excess of 10, with a mean of 11.5 ± 1.2, and Si:C ratios that were greater than 1.3 with a mean of 1.8 ± 0.6. M2, M6, and M3.7 also group together when comparing their elemental ratios, Si:N ratios are lower with a mean of 1.3 ± 0.3, and Si:C ratios of 0.2 ± 0.03 (Fig. 3.6). The molar ratios calculated at M3.8 were not characteristic of either of the two groups described above, with a Si:N ratio of 3.3 and Si:C of 0.6.

Depth-integrated ratios were calculated for the particle field "above" the trap over the upper 60m (depths used for integration were 5, 10, 20, 40 and 60m) (Fig. 3.7). A depth integral of 60m was selected because for the majority of the stations (M8E, M8W, M3.7, M3.8) this depth represented the base of the euphotic zone (light level 1% of surface incident irradiance). For stations (M2, M6, M3.4) the base of the euphotic zone was 80m, but productivity occurring between 60m and 80m accounted for relatively minor fractions of total water-column productivity (6, 10 and 3%, respectively) and thus 60m was used for these stations also. There is much greater consistency between the

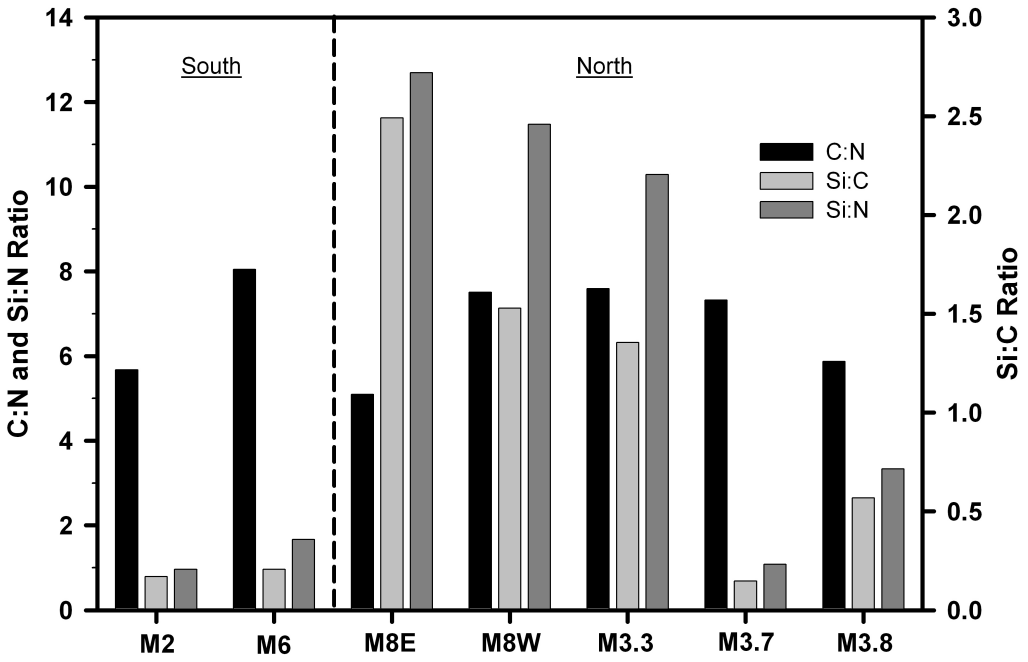

Fig. 3.6 C:N, Si:C, and Si:N molar elemental ratios for exported particles at each station

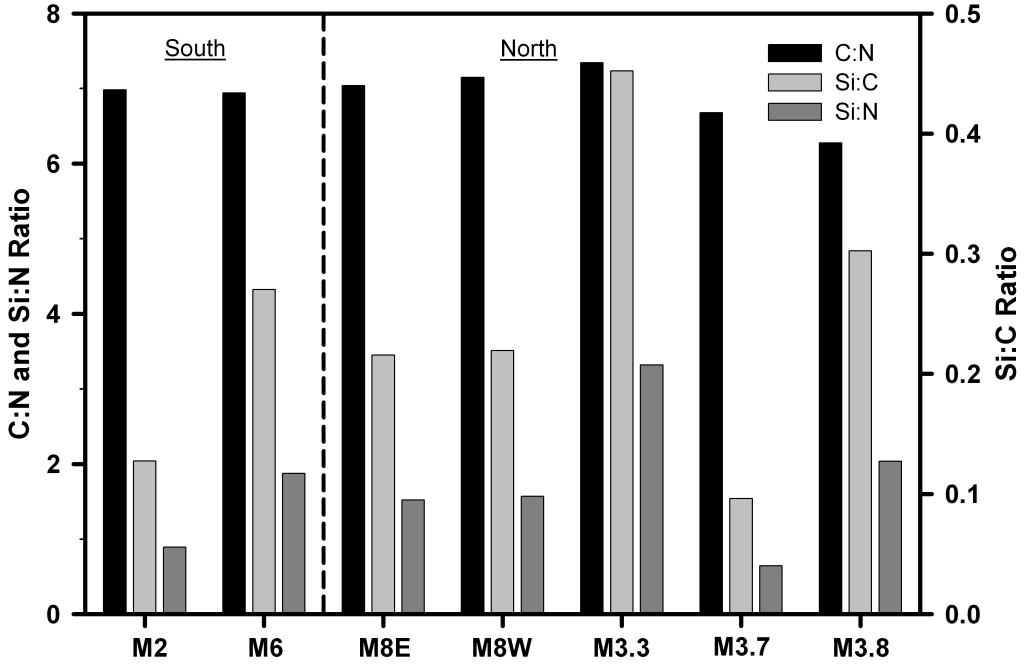

Fig. 3.7 C:N, Si:C, and Si:N molar elemental ratios for particulates in the upper water column. Depths used for vertical integration are 5, 10, 20, 40, and 60m.

upper ocean particle fields than for the exported particles. The C:N ratio ranges from 6.7 - 7.3 with an average of 7.0 ± 0.23. By comparison the Si:C ratio exhibits more variability between the stations, ranging from 0.10 at M3-2 to 0.45 at M3.3 with a mean of 0.24 ± 0.12. The patterns in the Si:N ratio are identical to those in the Si:C due to the low variation of the C:N ratio.

3.4.5 Phytoplankton composition

Exported material from south of the Plateau (M2 and M6) in the oligotrophic control area contained a small fraction of centric diatoms in the 40μm size range (plate I-1), 2% at M2 and 4% at M6 (table 3.3). The presence of *Eucampia antarctica* was also detected at M2 (plate I-2) contributing 9% of the total diatom count. The diatoms in exported material south of the plateau consisted primarily of pennate diatoms, such as *Fragilariopsis kerguelensis* and *Thalissionema nitzschoides*, which made up 34% and 55%, respectively at M2 and 29% and 66% respectively at M6. Plate I-3 shows a chain of *F. kerguelensis* typically found in these assemblages and plate I-4 demonstrates how *F. kerguelensis* and *T. nitzschoides* become entangled with organic material to form marine aggregates that promote the export of both biogenic opal and organic carbon from the upper ocean (Alldredge and Silver, 1988; Jackson, 1990).

Plates I-5 to I-8 highlight the differences in exported material between M8E and M8W, despite chemical analysis revealing both samples contained ~60% biogenic opal (Fig. 3.5). Cell counts suggested that *T. nitzschoides* dominates the export at M8E, accounting for 80% of cell numbers, whilst *E. antarctica* accounted for only 16%. Plate I-5 demonstrates the large number of *E. antarctica* frustules present in the M8E export assemblage, and shows that the cell counts are numerically dominated by small species such as *T. nitzschoides*. Plate I-6 highlights the difference in silicification levels between the two diatoms, *E. antarctica* and *T. nitzschoides*, with the latter being much less robust and appearing almost transparent compared to *E. antarctica*. M8W was comprised almost exclusively (92%) of *E. antarctica*, whilst SEM images (plate I-7,8)

Table 3.3 Percentage contributions of individual diatom species and genus', calculated from cell abundances measured in sediment trap material. *Denotes the unit cells mL^{-1}.

Station	M2	M6	M8E	M8W	M3.3	M3.7	M3.8
Centric							
Chaetoceros resting spores	-	-	0.13		-	-	
Centric 20 um	-	-	0.22	0.02	-	-	
Centric 40 um	2.21	4.29	0.00	0.03	-	-	0.58
Centric 100 um	0.13	0.09	-	-	-	-	-
Corethron crophilium	0.23	0.02	0.03	0.08	-	-	0.01
Dactyliosolen antarticus	-	-	0.68	0.14	-	-	-
Eucampia antarctica	8.65	0.72	16.27	91.78	-	0.21	0.33
Rhizolsolenia spp	0.05	0.05	-	-	-	-	-
					-		
Pennate					-		
Thalassionema nitzschoides	54.84	28.47	79.95	-	-	91.52	97.26
Fragilariopsis kerquelensis	33.86	66.37	1.99	7.95	-	8.21	1.82
Pseudonitzschia spp.	0.03	-	0.73	-	-	0.06	-
Tintinnids*	11.2	13.8	-	-	-	46.9	2.6

Table 3.4 Percentage contributions of functional groups calculated from cell abundances measured in sediment trap material.

Site	Centric diatoms	Pennate diatoms	Dinoflagellates	Ciliates	Phaeocystis colonies	Phaeocystis cells	Flagellates
M2	11.12	87.48	0.33	1.02	0.00	0.00	0.05
M6	5.10	93.79	0.08	0.93	-	-	0.09
M8E	11.95	60.29	0.11	0.09	0.01	0.77	26.79
M8W	91.80	8.20	-	-	-	-	-
M3.3	-	-	-	-	-	-	-
M3.7	0.00	94.94	0.45	4.57	0.00	0.00	0.03
M3.8	0.01	99.76	0.07	0.15	0.00	0.00	0.00

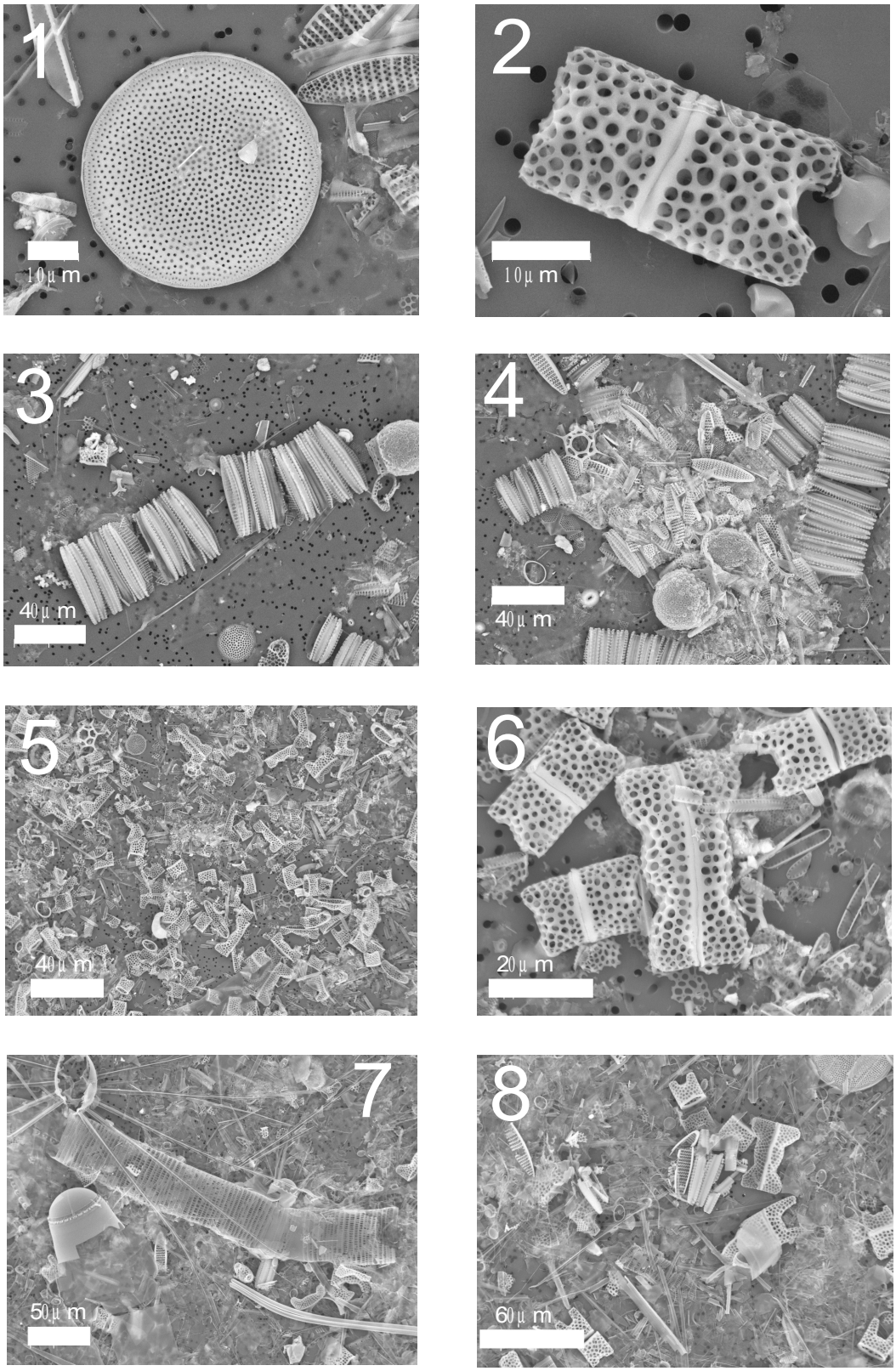

Plate I

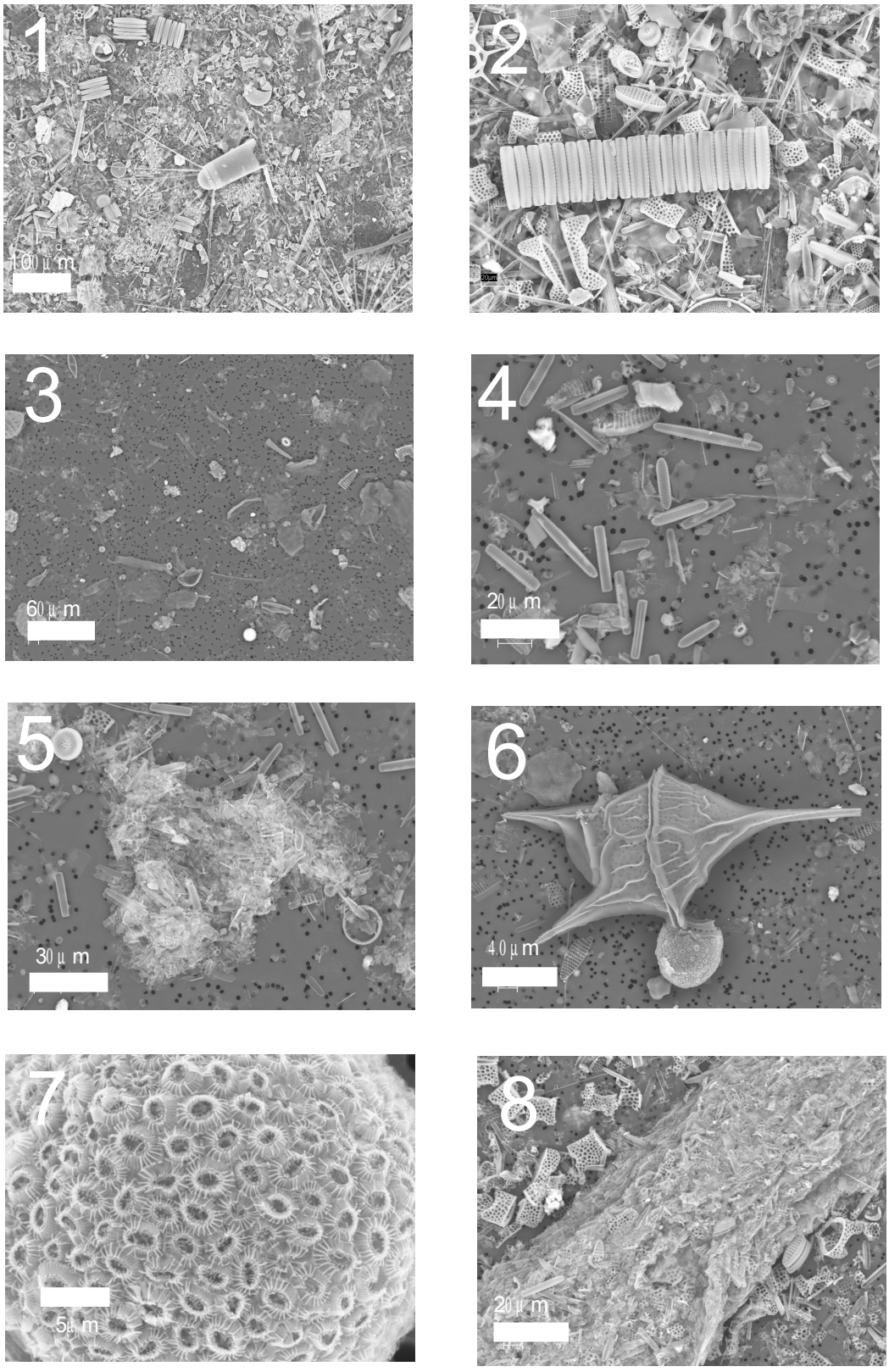

Plate II

Plate I

1. M2 – Centric diatom approximately 40µm in diameter and *F. kerguelensis* frustules in top right corner
2. M2 – *E. antarctica* approximately 20µm in length, frustules connected by girdle.
3. M6 – Details chains of *F. kerguelensis* commonly found in samples to the south of the plateau, also presence of tintinnids and *T. nitzschoides* along with unidentified fragments of larger diatom frustules.
4. M6 – Detail of a marine aggregate composed primarily of *F. kerguelensis* but also featuring tinitinnid loricae and silicoflagellates, showing the adhesive role of organic matter.
5. M8E – Broad view of the assemblage highlighting the export composition is dominated by *E. antarctica* and *T. nitzschoides*. Also demonstrates the broad range of frustule dimensions observed in *E. antarctica*.
6. M8E – View of *E. antarctica* and *T. nitzschoides* displaying the different levels of silicification between these two species, E. antarctica is large, robust and very heavily silicified compared to T. nitzschoides which appears almost transparent.
7. M8W – details more diverse species composition of the export assemblage, *D. antarcticus* in centre of image with a long cylindrical cell approximately 250µm in length. Also present is *C. criophilum*, with the characteristic spiny setae clearly visible. The setae are heavily silicified and easily detach from the main frustule, setae ubiquitous in imaging of this sample.
8. M8W – Fragmented frustules of *E. antarctica* and *F. kerguelensis*. Can also observe large number of girdle bands and spiny setae from *C. criophilum*.

Plate II

1. M3.3- Highlights similarities in composition between this sample and M8W, presence of *C. criophilium* is visible in centre of image, with *F. kerguelensis* and *E. antarctica* also visible.
2. M3.3- Shows a chain of *F. kerguelensis* present in sample, containing 21 cells and 140µm in length.
3. M3.7 - Demonstrates the sparse presence of diatoms in this sample, mainly *T. nitzschoides* but also some fragments of *E. anatarctica* and *F. kerguelensis*.
4. M3.8 – Plate shows the increased abundance of T. nitzschoides caught in sediment trap compared to M3.7.
5. M3.8 - *T. nitzschoides* entangled in a marine aggregate
6. M2 – Dinoflagellate *C. lineatum* and a tintinnid
7. M3.7 Close view of tintinnid shows agglutination of coccoliths to organic loricae. It is still unclear whether the coccoliths are actively accreted through consumption of coccolithophores, or whether the agglutination is passive from suspended coccoliths in water column. Represent an important part of calcite flux and have also been recorded in deep sediment traps from AESOPS (Grigorov, Pers. Comms.).
8 – Fecal pellet containing fragments of diatoms; can identify *E. antarctica*, *T. nitzschoides*, and *F. kerguelensis* embedded into pellet.

demonstrates the presence of large heavily silicified diatoms like *Corethron criophilium* and *Dactyliosolen antarcticus.* There are no light microscopy counts available for M3.3, however SEM imaging revealed a remarkable consistency between this station and M8W, with the presence of *C. criophilium* (Plate II-1), *D. antarcticus*, and *E. antarctica*. The difference appears to be the presence of *F. kerguelensis* (Plate II-2) chains, which although were not clearly visible from M8W did account for 8% of total diatom cells. At both M3.7 and M3.8 *T. nitzschoides* dominated the export assemblage, accounting for 92% and 97%, respectively. Despite the likeness of these two samples Plates II-3 and II-4 highlight the elevated numbers of *T. nitzschoides* cells at M3.8 compared to M3.7, and Plate II-5 shows how these frustules form marine aggregates.

Aside from diatoms a number of other plankton functional groups contributed to the particle export assemblage, although at much lower numbers. Overall diatoms accounted for between 72 – 100% of the export assemblage (Table 3.4) with a mean of 94% ± 10%. M8E was unique as it contained a few *Phaeocystis* sp. cells and colonies in the particle flux (Table 3.4). Dinoflagellates (Plate II-6) were also present in the exported material from all stations, but never accounted for more than 0.5% of cell numbers.

SEM imaging (Plate II-6) also revealed the ubiquitous presence of tintinnids in the particle flux assemblages (Table 3.4). These planktonic ciliate protists were most abundant at stations M3.7>M6>M2>M3.8 (47>14>11>3 cells mL^{-1}), where calcite was a more significant component of the flux measurements (Table 3.2), Plate II-7 clearly shows the agglutination of individual coccoliths to the organic loricae. The role that this organism plays in calcite flux in the ocean is largely un-quantified. The presence of coccoliths in such numbers itself suggests that we may have underestimated the significance of calcite production in the Southern Ocean (see Bakker *et al*., 2007). Anomalously high reflection in some of the satellite data (Read *et al*, 2007) was observed during the cruise and this may have been caused by the presence of suspended coccoliths. Analysis of the SEM images suggests that fecal pellets were a rare

component of exported material, although occasionally observed (Plate II-8). Whilst numerous phyto-detrital aggregates (Plates I-4 and II-5) were detected, it is difficult to know for certain if information about particle-type is lost / affected during sample handling.

3.5 Discussion

3.5.1 What is the magnitude of POC Flux and what are the export ratios?

As discussed in section 3.4.1 the PELAGRA deployments were conducted at different depths, complicating the interpretation of the flux data. In order to compare the regional differences observed in the magnitude of organic carbon flux at each station the data have been normalised to 100m using a remineralisation co-efficient following equation 3.4:

$$\mathbf{Corg_{(100m)} = Corg(z) / (Z/100)^{-b}} \quad \mathbf{(3.4)}$$

where, $Corg_{(100m)}$ is the flux of organic carbon at 100m, Corg(z) is the flux of organic carbon at sampling depth Z, and Z is the sampling depth, and b is remineralisation co-efficient

The remineralisation co-efficient normally used in this type of flux normalisation is an empirically-derived one based on flux data from the subtropical-temperate NE Pacific (15-35 ºN) (Martin *et al*., 1987). However, despite its common usage in models to describe flux attenuation across regions and globally this is a normalising procedure which has no observational validity at this site or in similar environments. In addition, one may question how appropriate it is to use a single normalisation factor for flux measurements north and south of the plateau where ecosystem structure and functioning is clearly disparate. Recently, using similar neutrally buoyant sediment traps, Buesseler *et al*. (2007) quantified the flux attenuation in two contrasting environments. Station ALOHA is an oligotrophic regime dominated by picophytoplankton and low seasonality, with relatively low rates of primary production and POC flux at the base of the euphotic zone (Karl *et al*., 1996). In contrast K2 is characterised by high nutrient

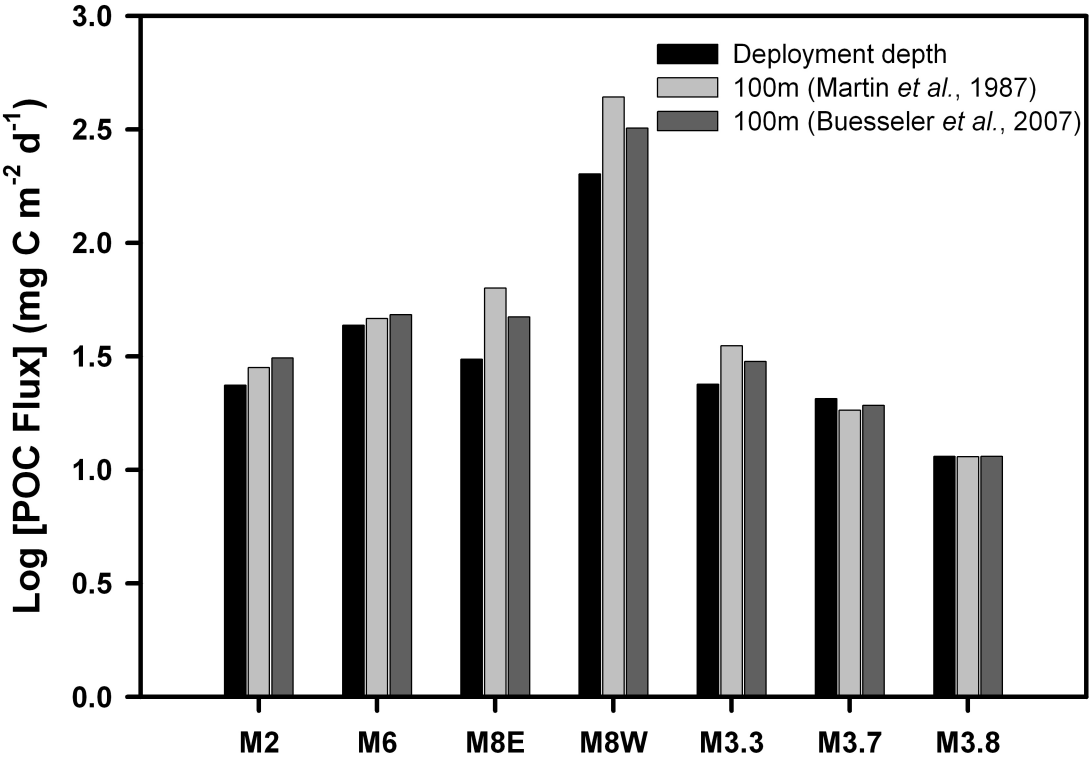

Fig. 3.8 Black bars show POC flux measured at the deployment depth (Fig. 3.3; table 3.2), light grey bars are POC flux normalised to 100m using equation 3.4 and Martin *et al*. (1987) remineralisation co-efficient (b = 0.86). Dark grey bars are POC flux normalised to 100m using equation 3.4 and Buesseler *et al*. (2007) remineralisation co-efficients (b_1 = 1.33; b_2 = 0.51). For the Buesseler *et al*. (2007) normalisation b_1 is empirically derived from station ALOHA and is applied to the southern HNLC stations M2 and M6, b_2 is empirically derived from station K2 and is applied to the northern productive stations M3.3, M3.7, M3.8, M8E, and M8W. POC flux on y-axis is a logarithmic scale.

conditions, resulting in more seasonality in algal stocks, production, and export (Honda *et al*., 2006).

Fig. 3.8 shows the POC flux measured at the deployment depth, and normalised to 100m using the Martin exponent and Buesseler's exponents. When using the Buesseler normalisation the remineralisation co-efficient for the oligotrophic regime (ALOHA) is applied to the HNLC stations south of the plateau, and the remineralisation co-efficient

for the productive regime (K2) is used for stations north of the plateau. Applying the Martin-exponent under-predicts POC flux at the southern stations and over-predicts POC flux at the northern stations compared to using Buesseler's regime-specific remineralisation co-efficients. This discrepancy is most significant for the deep deployments north of the plateau at M8E, M8W and M3.3; using the Martin exponent overestimates POC flux at 100m by 25, 27, and 15% respectively. At stations M3.7 and M3.8 north of the plateau the difference between the two normalisations is small since the deployment depths were close to 100m and thus the affect of the normalisation procedure is negligible. Based on these differences it seems more appropriate to use Buesseler's remineralisation co-efficients that have been derived in environments similar to the contrasting regimes of the CROZEX study area.

The flux of organic carbon (normalised to 100m) was largest, 320 mg C m^{-2} d^{-1}, at M8W north of the plateau. South of the plateau organic carbon fluxes ranged from 31 - 48 mg C m^{-2} d^{-1}. The flux of POC at M8W was an order of magnitude greater than the POC fluxes from all other PELAGRA deployments in the region. Using a pre-bloom silicate concentration 15 μM (Sanders *et al*, 2007) and silicate concentrations at the time of the M8W PELAGRA deployment (0.2 μM) integrated to a depth of 60m, it is calculated that there is a net removal of 869.9 mmol m^{-2} of silicate from the upper mixed layer for the bloom period. The PELAGRA deployment at M8W recorded a silica flux of 25 mmol m^{-2} $d^{-1}$and thus accounts for 3% of the net silica removal. It is therefore suggested that this level of export could, and would need to be sustained for a period of 34 days in order to close the silicate budget.

Based on these calculations, the flux of POC from the bloom at M8W is tentatively calculated to be ~11 g C m^{-2}. This value is similar to the 6-9 g C m^{-2} estimated from the SOIREE bloom using 100 m-normalised POC fluxes (Nodder *et al*, 2001) integrated over a 30-45 day period. However, the POC flux estimated from SOIREE used the Martin curve to normalise the fluxes to 100m. As previously mentioned, this may lead to an over-estimation of normalised POC flux when compared to using a remineralisation co-efficient from a similar environment. Substitution of the Martin-

normalised POC flux at M8W into the silica budget calculation described above increases the CROZEX estimate to ~15g C m^{-2}, almost double the SOIREE estimate. This range of 11-15 g C m^{-2} d^{-1} is slightly higher than the POC flux estimate of 9-14 g C calculated by Bishop *et al* (2004) during SOFeX. The SERIES experiment in the Sub-Arctic Pacific measured a 2-3 increase in POC flux after iron fertilisation (Boyd *et al*, 2004), estimated to represent 5 g C m^{-2} over the 25-day observation period. Data from M8W, which we consider to be our best estimate of carbon export from the bloom area, is generally higher than previous estimates obtained from mesoscale enrichment experiments. Whilst one must consider these estimates with caution, it is tempting to speculate that the difference could be related to methodical approach. The sudden perturbation of iron addition into a light replete, iron-depleted environment mean that phytoplankton community structure, grazing levels, and resulting carbon flux may not be comparable to those found in natural iron fertilisation systems, which have much longer timescales and where light limitation is lifted from iron replete surface waters.

With values for both total integrated production and organic carbon flux one can calculate the export ratio (Murray *et al*., 1989), defined as the proportion of total primary production that is exported; here export ratios are expressed as their equivalent percentages (i.e. 0.1 ≡ 10%). In Fig. 3.9, the export ratio is presented as the percentage of primary production that is exported to the deployment depth (Table 3.2). The highest export ratios were recorded north of the plateau at M8E and M8W (22% and 41%), respectively, despite these also being the deepest deployments. Since most deployments were at different depths, the results calculated for the export ratio are hard to compare due to the remineralisation of particles between the bottom of the euphotic zone and the trap depth. The export ratios have therefore also been calculated using depth-normalised carbon flux data (see equation 3.4 above) and will be referred to as e-$ratio_{(100m)}$.

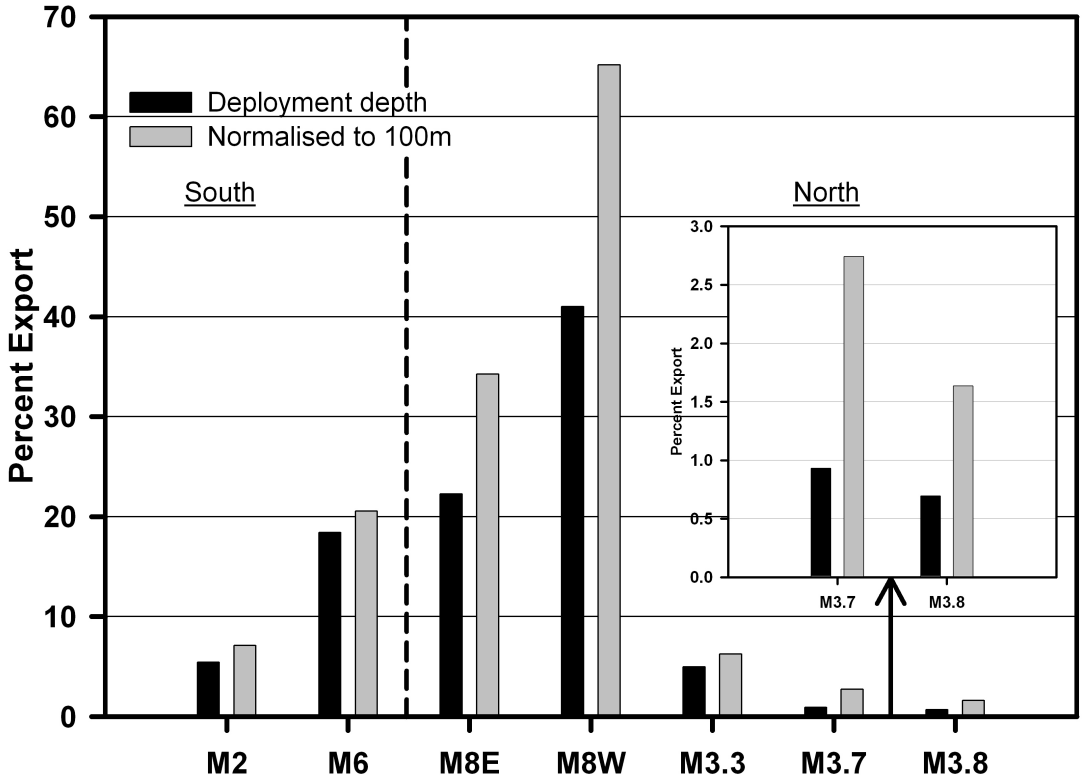

Fig. 3.9 Export ratios calculated for each deployment station using *in situ* ^{14}C production estimates (Fig. 3.4). Black bars are export ratios calculated using carbon flux data measured at deployment depth, grey bars are export ratios calculated using depth-normalised (100m; Fig. 3.8) carbon flux data.

After normalisation to 100m the largest e-ratios calculated occurred north of the islands at M8E and M8W, (34 and 65%, respectively). South of the islands e-ratios$_{(100m)}$ were comparatively low, 7% at M2 and 20% at M6, and are much more consistent with global data sets (Buesseler, 1998 The export ratios$_{(100m)}$ calculated at M8W and M8E are extraordinarily high; these values could represent the temporal decoupling of production and export. The temporal decoupling of production and export is difficult to resolve as there are only discrete measurements of biomass with very coarse resolution available to aid the interpretation of flux data. However, using surface chlorophyll data obtained from remote sensing (Venables *et* al, 2007) and an empirically derived relationship between surface chlorophyll and integrated production (Seeyave *et* al, 2007), it is

possible to estimate the temporal progression of integrated production at each deployment location (Fig. 3.10a-e). An *a priori* knowledge of aggregate sinking rates would allow one to diagnose the temporal origin of exported particles and the associated integrated production. Calculating an export ratio based on a retrospective estimate of production seems to be a more logical approach than simply using contemporaneous production measurements.

In order to try and eliminate the artefact of temporal decoupling from the export ratio calculations the approach described above was followed. Based on assumed sinking velocities (W_S) of 20, 50, and 100 m d^{-1} production at each of the deployment locations (see Fig. 3.10f as an example) has been estimated retrospectively. The export ratio is then calculated based on these production estimates and is plotted alongside existing data in Fig. 3.11. The export ratio at M8W ranges from 33-72% depending on which sinking rate is selected, and is probably the most severely affected by the issue of decoupling, followed by M8E which has values ranging from 7-15%. The e-ratios$_{(100m)}$ south of the plateau appear to be largely unaffected by the production estimate, ranging from 10.4-10.6% at M2 and 17.5-18.2% at M6. This is because the integrated production in the days preceding the PELAGRA deployments at these stations does not vary greatly, and thus the issue of temporal decoupling at these southern stations can be viewed as redundant. Despite these considerations the e-ratio$_{(100m)}$ is much higher at M8W than at all other stations regardless of the production estimate used.

Station M3 provides the opportunity to assess temporal variations of flux parameters in addition to the spatial considerations described above. Satellite-derived production at M3 initially peaked at ~1600 mg C m^{-2} d^{-1} in early November (Fig. 3.10c) and dropped to baseline values of around 400 - 500 mg C m^{-2} d^{-1}. This persisted until early January where mesoscale eddy activity initiated a secondary peak in productivity (Fig. 3.10). The first PELAGRA deployment at this station, M3.3, succeeded the first productivity peak by approximately 30 days, with calculated export ratios $_{(100m)}$ ranging from 6.3-7.9% (Fig. 3.11). Species composition of the export assemblage (Plates II-1+2) suggests this represents the remnants of the flux event resulting from this

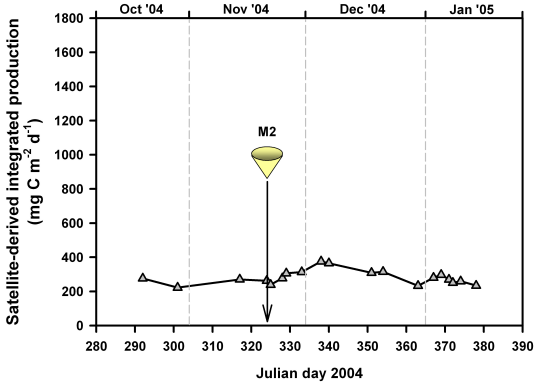

Figure 3.10a –

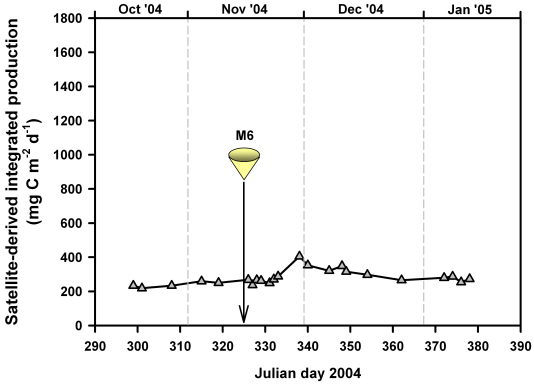

Figure 3.10b –

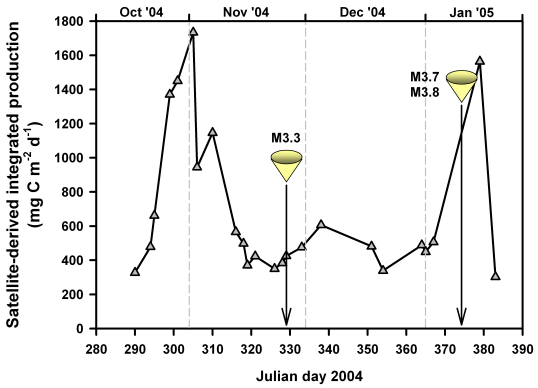

Figure 3.10c –

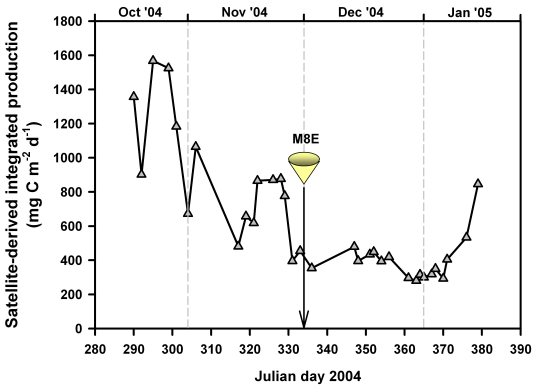

Figure 3.10d –

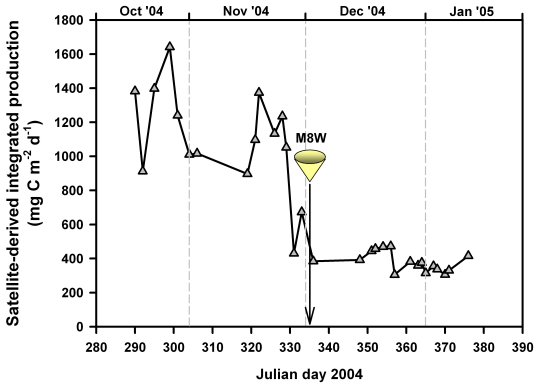

Figure 3.10e –

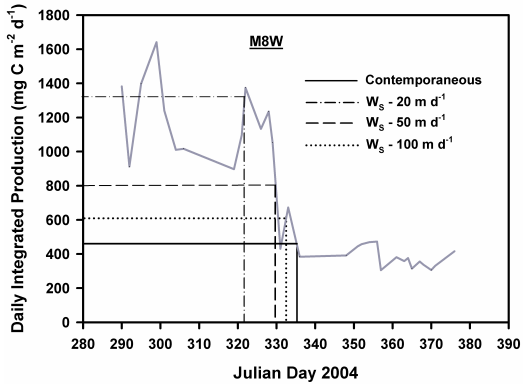

Figure

Fig. 3.10 Panels a-e show satellite-derived integrated production as a function of time, arrows and trap icon indicate time of PELAGRA deployment. Satellite-derived integrated production is calculated using satellite-derived surface chlorophyll and *in situ* ^{14}C integrated production data; conversion is based on the empirical observations of Seeyave *et al*., 2007. Panel f shows how retrospective estimates of production are calculated using M8W as an example. Solid black line represents the PELAGRA deployment date and thus the contemporaneous estimate of integrated production based on satellite data. Hatched lines demonstrate how retrospective estimates of production are calculated based on assumed sinking speeds of 20 m d^{-1} (dash-dot), 50 m d^{-1} (dash), or 100 m d^{-1} (dotted) and the average deployment depth, which was ~250m for the example shown.

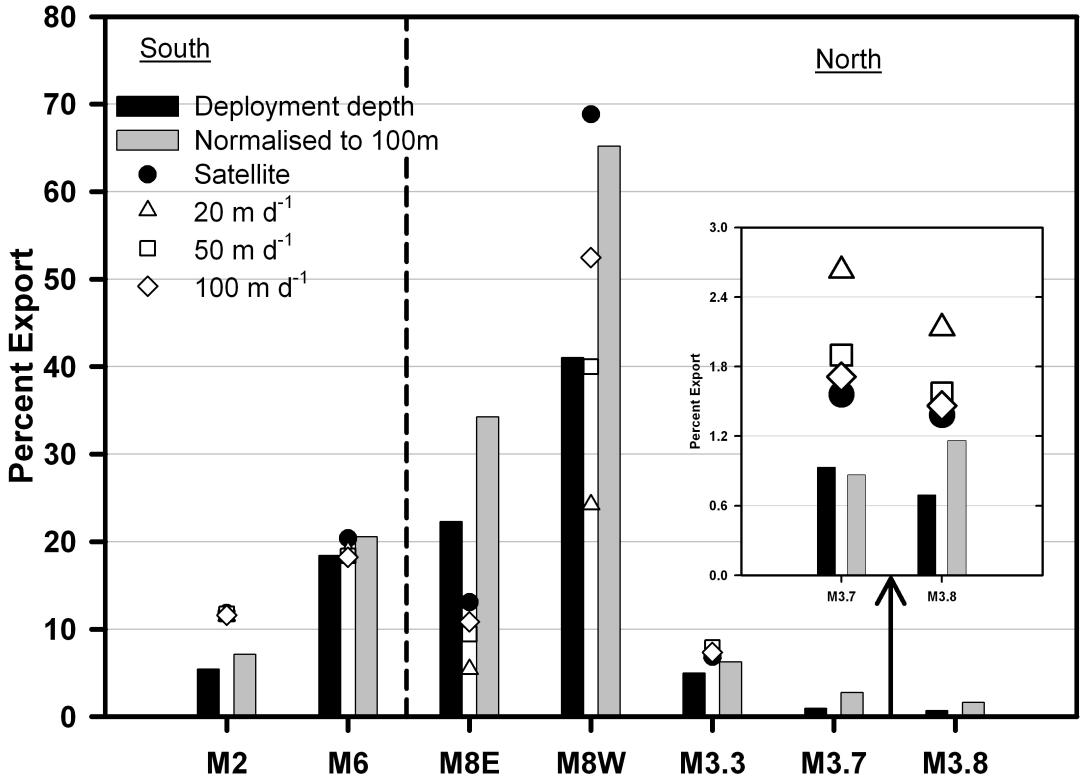

Fig. 3.11 Export ratios calculated for each deployment station. Black bars are export ratios calculated using *in-situ* ^{14}C production estimates (Seeyave *et al*., 2007) and organic carbon flux measured at the deployment depth. Grey bars are export ratios calculated using *in-situ* ^{14}C production estimates and depth-normalized (100m) organic carbon flux (equation 3.4). Filled black circles are export ratios calculated using depth-normalized carbon flux (100m) and satellite-derived integrated production. Open symbols are export ratios calculated using depth-normalized carbon flux (100m) and retrospective estimates (satellite-derived) of integrated production based on sinking speeds of 20 m d^{-1} (triangles), 50 m d^{-1} (squares), and 100 m d^{-1} (diamonds).

production maximum. In contrast deployments M3.7 and M3.8 preceded the secondary peak in productivity by 4 and 2 days respectively, with calculated export ratios ranging from 0.9-2.7%, associated with the presence of small, lightly silicified *T. nitzschoides* cells.

It is possible that the relatively short deployment periods of PELAGRA at M3.7 and M3.8 (Table 3.2) may have resulted in a low probability of any large, episodic flux events being sampled. However, the similarity of results between the two deployments, which were separated by only 2 days, lends confidence to the observations of a low flux

regime. Low autotrophic growth rates (Moore *et al*, 2007), elevated abundance of microzooplankton (Poulton *et al*, unpublished data), low mesozooplankton grazing rates (Fielding *et al*, 2007) and dominance of small pennate diatoms (Table 5.6) support the plausibility of a low-export system at these stations. In contrast low relative bacterial abundance (Zubkov *et al*, 2007), high *f*-ratios (Lucas *et al*, 2007) and C:N ratios close to Redfield stoichiometry in trap material (Fig. 3.6) and upper ocean particulate material (Fig. 3.7) do not fully infer a recycling system.

3.5.2 What drives the variability in the export ratio?

The large regional variability in export observed around the Crozet Plateau from PELAGRA is more complicated than a picture of high values north of the plateau versus low values south, as indicated from new production estimates (Sanders *et al*., 2007). It was hypothesised that the magnitude of the carbon flux was related to nutrient exhaustion in the upper ocean and the cell size of the dominant diatom species present. Although, there was no significant correlation between any surface parameter and the export ratio$_{(100m)}$ (Table 3.5), there was a statistically significant positive correlation between mean diatom cell biovolume (i.e. cell size) of the diatoms found in the trap and the export ratio $_{(100m)}$ (r^2 = 0.72, P<0.02, n = 6). This relationship was found to be statistically significant with export ratios calculated using retrospective estimates of production based on assumed sinking speeds of 20, 50 and 100 m d^{-1} (Table 3.5). This observation corroborates the inference of Trull and Armand (2001) who proposed the selective export of large diatoms from the SOIREE bloom based on $\delta^{13}C$ data.

Previous studies (Legendre and LeFèvre, 1989; Boyd and Newton, 1999; Dunne *et al*., 2005) have highlighted the importance of community structure and grazing in controlling upper ocean carbon fluxes, but correlations between size-fractionated primary production data (Fig. 3.4) or zooplankton grazing measurements (Fielding *et al*., 2007) and export ratio$_{(100m)}$ estimates were not significant (Table 3.5). Although these statistics are based on a limited number of observations (n = 7), they suggest that

Table 3.5 Pearson correlation coefficients between surface/trap parameters and calculated export ratios. E-ratio (100m) uses production measured *in*-situ with C^{14} technique (Seeyave *et al*, 2007). Satellite uses contemporaneous production estimated from remote sensing data. Ws uses satellite production estimates as a function of sinking speed (see section 3.5.1)

***Significant at 99% confidence level**

****Significant at 98% confidence level**

*****Significant at 95% confidence interval**

Calculated using Pearson product-moment correlation and t-values

[1] Nitrate and silicate concentrations reported are taken from 5m depth at all stations.

[2] Mixed layer depth calculated from $>2^0$C change in temperature gradient measured from local CTD casts.

[3] Surface particulate data taken from filtered CTD casts at 5m

[4] Mean diatom volume - surf calculated from taxonomical cell counts and site-specific derived cell dimensions from SEM images.

[5] Particulate data taken from filtered sediment trap material (see methods)

[6] Percent primary production grazed by meso-zooplankton (Fielding *et al*, 2007)

[7] Mean diatom volume – trap derived from cell counts from trap deployment and site specific cell dimensions

[8] *Phaeocystis* cell abundance calculated from surface (5m) cell count.

Surface Parameter	Nitrate concentration [1]	Silicate concentration [1]	Mixed Layer Depth [2]	Particulate organic carbon [3]	Particulate organic nitrogen [3]	Partiuclate Biogenic silica [3]	Particulate calcite [3]	Mean Diatom Volume - Surf [4]
E-ratio (100m)	0.04	0.04	0.05	0.11	0.07	0.01	0.01	0.08
Satellite	0.00	0.01	0.20	0.06	0.05	0.00	0.01	0.02
Ws 20 m d^{-1}	0.01	0.13	0.51	0.25	0.25	0.00	0.20	0.08
Ws 50 m d^{-1}	0.00	0.00	0.32	0.14	0.12	0.00	0.07	0.00
Ws 100 m d^{-1}	0.00	0.00	0.24	0.09	0.07	0.00	0.03	0.00

Trap Parameter	Particulate organic carbon [5]	Particulate organic nitrogen [5]	Particulate biogenic silica [5]	Particulate calcite [5]	% PP grazed [6]	Mean diatom volume - trap [7]	Mean Phaeo volume - surf [8]
E-ratio (100m)	0.20	0.19	0.42	0.27	0.04	**0.74***	0.74
Satellite	0.06	0.07	0.23	0.23	0.02	**0.94***	**0.95****
Ws 20 m d^{-1}	0.01	0.00	0.04	0.16	0.04	**0.80****	0.53
Ws 50 m d^{-1}	0.02	0.04	0.20	0.25	0.02	**0.95***	**0.90*****
Ws 100 m d^{-1}	0.05	0.06	0.22	0.25	0.02	**0.96***	**0.95*****

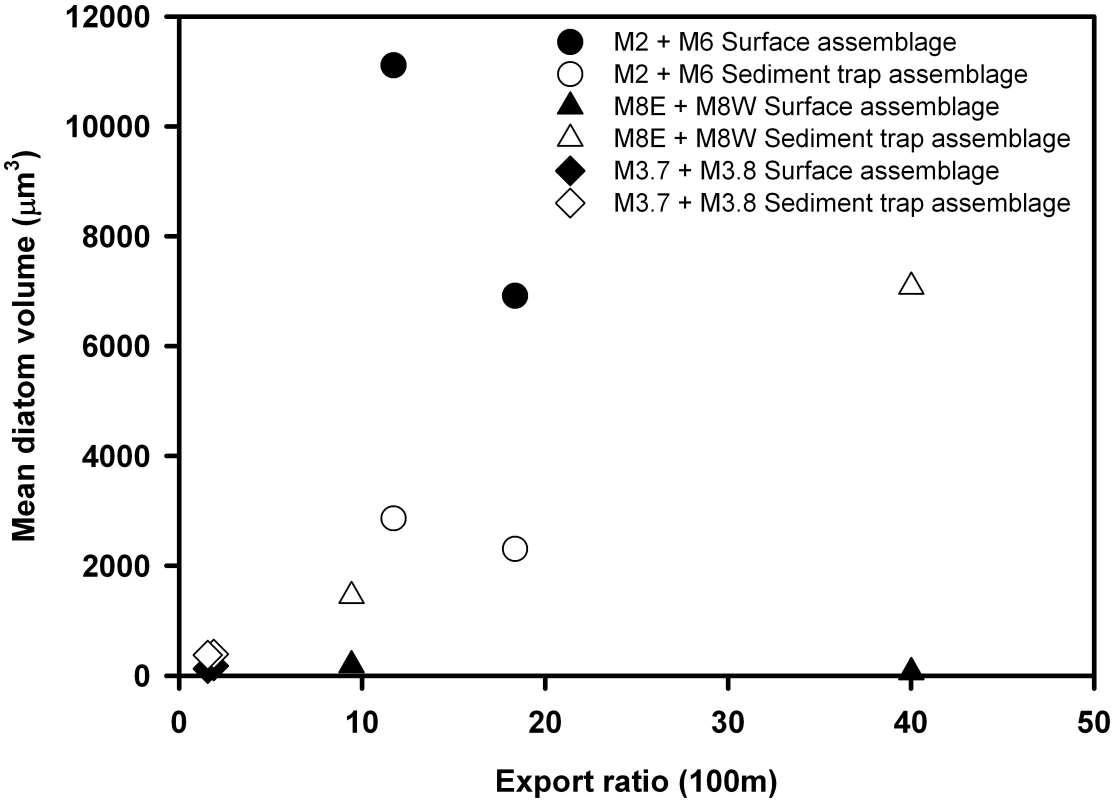

Fig. 3.12 Depth-normalized export ratios (100m) calculated using equation 3.4 against mean diatom size. Carbon-flux has been normalized to 100m using data from Buesseler *et* al., (2007), integrated production has been derived from satellite data based on an assumed sinking velocity of 50 m d^{-1}. Filled symbols represent mean diatom volume of surface assemblage (5m) and clear symbols the mean diatom volume calculated from trap material. Circles are M2 and M6 south of the plateau, triangles are north of the plateau at M8E and M8W, and diamonds are M3.7 and M3.8

large diatoms are an important factor controlling the magnitude and variability of export ratios $_{(100m)}$ in the region. This result is not completely unexpected since intuitively a high concentration of large diatoms is likely to lead to high aggregation rates and therefore high fluxes. It is also feasible that the formation of iron hydroxides in the bloom area could enhance sinking fluxes as observed in the Subantarctic waters southeast of New Zealand (Frew *et al*., 2006), but there is no data to support this hypothesis. Despite large diatoms being found south of the plateau (Fig. 3.12) the trap

material was not enriched with these large diatom species. Conversely, north of the plateau, large diatom species seem to sink preferentially relative to the surface assemblage as they are enriched in the trap material (Fig. 3.11). The next section assesses the export composition of trap material relative to the surface community, and the factors that may control the selective export processes observed.

3.5.3 Can selective export processes be explained in a regional context?

Stations M2 and M6 were intended to be representative of the HNLC areas within the vicinity of the Crozet Plateau. The exported particles at M2 and M6 shared very similar Si:C molar ratios (Fig. 3.6) consistent with the similarities between these two control sites demonstrated by other properties. The diatom cells exported at M6 were dominated by *F. kerguelensis,* 66% of exported diatom frustules. Exported particles at M2 also contained *F. kerguelensis* frustules, but to a smaller extent (34%), and were mainly dominated by *T. nitzschoides* (55% of the exported diatom frustules). In general, the particles exported south of the plateau appear to be enriched in *F. kerguelensis* relative to the surface community which at M2 made up 14%, and 13% at M6 of the surface community (Table 3.6).

The dominance of *T. nitzschioides*, *Pseudo-nitzschia* spp. together with *Chaetoceros* species and *F. kerguelensis* in the surface (5m) samples is consistent with other studies of summer diatom floras in the region of the Polar Front in the Indian Sector of the Southern Ocean (Kopczynska et al., 1998). The almost complete absence of *Pseudo-nitzschia* spp. from the PELAGRA samples is not surprising. This delicate and lightly silicified diatom rarely contributes to flux due to dissolution and/ or grazing (Abrantes and Moita, 1999; Lange et al., 1994), and probably also low aggregation and sinking rates of smaller diatoms, compared to larger species. Thus the increase in relative abundance of *T. nitzschioides* is to be expected although the greater proportional increase in *F. kerguelensis* may result from enhanced abundances of this species at depths greater than 5m in the surface mixed layer. During the SOIREE experiment aggregates captured by sediment traps after iron enrichment were enriched in *F.*

kerguelensis relative to measured water column abundances (Waite and Nodder, 2001). The large diatoms *C. criophilium* and *D. antarcticus* that were present in the surface community (Poulton *et al*., 2007) were not found in PELAGRA samples south of the plateau. Based on this we must conclude that these organisms were not dominant in export processes at this locality, however previous work in the Southern Ocean has demonstrated that *C. criophilum* can play a significant role in bloom sedimentation (Crawford, 1995).

The species composition of the export assemblage was different at M8E and M8W; cell counts (Table 3.3) revealed that 91% of the diatom cells exported at M8W was of a single species, *E. antarctica*, with smaller contributions (8%) from *F. kerguelensis, D. antarcticus* and *C. criophilium* at M8W. The community structure of the diatom population at 10m (Table 3.6) showed that *E. antarctica* makes up <1% of diatom cells and *F. kerguelensis* ~4% (see also Poulton *et al*., 2007). This result demonstrates that there is selective export of not only one functional group, i.e. diatoms, but just one or two key species within that group. The architecture of heavily silicified diatom shells offer mechanical protection (Hamm *et al*., 2003) against grazing thus enriching the export of these species and facilitating their accumulation in Southern Ocean diatom oozes (Verity and Smetacek, 1996).

The situation at M8E was somewhat different; *T. nitzschoides* accounted for 80% of the exported diatom cells, and *E. antarctica* for only 16% (Table 3.3). However, the surface community structure at the time of sampling contained fewer *E. antarctica* cells (Table 3.6), and thus the export was again enriched with *E. antarctica*. Moore *et al*. (2007) reported that *E. antarctica* responded most favourably to Fe-addition experiments, and results from the sediment trap shows it is a major exporter of both POC and biogenic silica from iron-fertilised regions, implying that it plays a key role in the biogeochemical cycling of POC and silica in this study area. Previous laboratory experiments and mesoscale enrichment experiments in the Southern Ocean (e.g. Gall *et al*, 2001*a*) have also noted the response of heavily silicified diatoms to iron addition, particularly

Table 3.6 Percentage contributions of individual diatom species to the surface assemblage (5m) from each station calculated from absolute cell abundance. Number in brackets is the proportion of the species' frustules that were observed to be empty, no brackets indicates 100% of frustules contained cellular material.

Station	M2	M6	M8E	M8W	M3.3	M3.7	M3.8
Centric diatoms							
Small Chaetoceros sp.	0.65	-	-	-	-	6.61	16.35
Chaetoceros "peruvianum"	-	0.84	-	1.52	0.17	-	-
Chaetoceros 'mitra' / debilis	1.18	2.35	-	24.24	3.61	-	-
Chaetoceros curvitus	-	2.01	-	-	-	-	-
Chaetoceros debilis	-	-	-	-	-	-	-
Chaetoceros resting spores	-	-	-	-	-	-	-
Centric 20 um	11.19 (32.55)	12.39 (4.05)	1.12 (16.67)	2.12 (21.43)	3.66 (21.88)	6.93 (1.16)	21.61 (0.54)
Centric 40 um	-	1.68 (0)	-	-	-	-	-
Corethron crophilium	2.09	1.01 (20.0)	-	1.21	0.74 (18.18)	-	-
Dactyliosolen antarcticus	0.92	1.34	-	-	0.11	-	-
Eucampia antarctica	-	-	-	0.91 (83.33)	0.46 (25.0)	-	-
Guinardia spp.	1.18	0.34	-	3.18	0.40	0.04	-
Leptocylindricus spp.	1.31	0.84	-	1.82	0.11	-	-
Rhizolsolenia spp.	-	0.17	-	-	-	-	-
Proboscia alata	-	-	-	0.15	-	-	-
Pennate diatoms							
Cylindrotheca closterium	2.35	1.01	-	5.30	1.26	0.14	0.23
"Thalassionema nitzschoides"	35.42 (38.40)	44.89 (39.93)	93.68 (14.09)	24.70 (24.54)	51.40 (23.27)	60.35 (9.89)	47.65 (34.56)
Fragilariopsis kerquelensis	14.51	13.07	0.74	3.94	4.12	0.48 (12.50)	1.40 (20.83)
Thalassiothrix antarctica	-	-	-	-	0.23	-	-
Pseudo-nitzschia spp.	28.50 (0.92)	16.42	4.46	29.85	33.60	22.42	5.85
Small pennates	-	1.17	-	-	-	3.02	6.89
Manginea spp (M. rigida)	-	-	-	0.15	0.06	-	0.01
Haslea trompii	0.65	0.50	-	0.91	0.06	-	-

F. kerguelensis. The importance of *E. antarctica* in the CROZEX study area may be related to the formation of winter resting spores that are advected from the shallow topography of the Crozet Plateau, along with dissolved Fe, northwards into the bloom area. Subsequently, when light limitation is relieved, *E. antarctica* may possess an ecological advantage over other heavily silicified diatoms. Significantly the presence of *E. antarctica*, usually associated with ice marginal zones has also been documented near other Southern Ocean Islands in the vicinity of the Polar Front (e.g. (Froneman et al., 1997).

Vertically integrated production at M3.7 and M3.8 (Fig 3.4) was an order of magnitude higher than all the other stations, the bloom probably being at its peak with a small vertical loss term. *T. nitzschoides* was the diatom species dominating the export, accounting for 92% of the diatom export assemblage at M3.7, relative to 54% in the surface community, and 97% at M3.8, relative to 48% in the surface. At these stations there did not seem to be the selective export of large diatoms and this is associated with very small calculated export ratios$_{(100m)}$ of 1%. At station M3.7, ~10% of the *T. nitzschoides* cells in the surface were present as empty frustules, whereas at station M3.8 this proportion had increased to ~35%. This suggests that the small vertical loss term measured at M3.7 and M3.8 is probably dictated by individual cell deaths and slow gravitational settling potentially caused by self-shading or low cell concentrations (Jackson, 1990; Kiorboe *et al*., 1990) rather than the formation of marine aggregates.

North of the plateau at M8E and M8W there seems to be selective export of large diatom species, whereas south of the plateau the large diatoms present in the water column were not exported. These phytoplankton community differences between north and south of the plateau are likely to be reflected in the characteristics of export flux with south HNLC waters dominated by small picophytoplankton and pennate diatoms due to the iron-limited conditions, resulting in lower export rates. Fv/Fm values, an indication of physiological stress, were much lower at stations M2 and M6 (Moore *et al*, 2007) relative to the other stations, suggesting that the cells were suffering from nutrient limitation, possibly Fe. The presence of *Phaeocystis* sp. in the upper water column may have a

significant effect on the magnitude of export from a diatom bloom, as observed by comparing stations M8E and M8W north of the plateau. *Phaeocystis sp.* cell abundance at M8W was an order of magnitude higher than M8E, 1.2 x 10^6 and 2.4 x 10^5 cells l^{-1}, respectively. There is also a strong linear correlation (r^2 0.74, n = 7, $P<0.05$) between *Phaeocystis sp.* cell abundance and the export $ratio_{(100m)}$ suggesting it plays a role in regulating export, possibly through the production of transparent exopolymer particles (TEP) (Mari *et al*., 2005), which have been demonstrated to be important mediators for the formation of large marine aggregates (Passow *et al*., 2001; Passow, 2002). Whilst previous studies (Wassman, 1994; DiTullio *et al*, 2000) have documented the direct involvement of *Phaeocystis* sp in rapid flux events, possibly related to iron supply, our sediment trap observations do not suggest this to be the case around the Crozet Plateau. It remains unclear why we detected a small contribution of *Phaeocystis* cells in the M8E deployment compared to zero at M8W, despite the increased cell abundance at the surface. Based on a strong power-law correlation (r^2 0.74) between *Phaeocystis* sp. and $Si(OH)_4$ concentrations, it is suggested the observed correlation between export $ratio_{(100m)}$ and *Phaeocystis* sp. cell abundance is an artefact caused by Si depletion, which induces export, and the subsequent community shift to *Phaeocystis* sp., rather than the organism having a direct role in the export process.

3.5.4 What are the biogeochemical implications?

Silica fluxes dominate the annual input of particulate material to the deep Southern Ocean as mirrored by the extensive accumulation of opaline sediments (De Master, 1981). Previous laboratory cultures (Takeda, 1998) and field observations (Hutchins and Bruland, 1998) have demonstrated that iron-replete cells take up less silica per unit carbon. Thus, the observation of low Si : C ratios in trap materials are occasionally interpreted as evidence of carbon export from a bloom where the previously iron-replete cells began to senesce and aggregate (Nodder and Waite, 2001). However, these ratios are likely skewed by the selective export of large species, empty frustules, and the presence of carbon-rich functional groups such as *Phaeocystis*, dinoflagellates etc.

Conversely, high Si:C ratios may not be accurately viewed as the sedimentation of iron-deplete diatoms either.

Rather than exclusively commenting on the magnitude of Si:C ratios, one can express their deviation away from the integrated (upper 60m) elemental molar ratios of the suspended particulate field, thus minimising any regional community structure biases. Si:C and Si:N ratios in sinking material at M8E, M8W, and M3.3 were all depleted relative to the overlying particle field (Fig. 3.13) compared to the remainder of the stations. As all the PELAGRA deployments occupied different depths, one has to use remineralisation co-efficients derived from empirical observations (Martin *et al*., 1987; Buesseler *et al*., 2007) to calculate organic carbon flux at 100m albeit with large uncertainties. Normalising Si measurements is even more difficult owing to the complicated dissolution kinetics (Van Cappellen *et al*., 2002). The departure of Si:C and Si:N ratios in sediment trap particles away from the ratios in suspended particulates displays an increase in both variables with depth (Fig. 3.14). The observed decoupling of silica and organic material suggests that downward POC flux from iron fertilised diatom blooms is preferentially remineralised relative to silica, as has been inferred from other studies (Nodder and Waite, 2001). These conclusions are consolidated upon inspection of the dissolved nutrient profiles of silicate and nitrate, at M8W for example these values are much lower (Si:N = 0.065) than they are at M2 and M6 (Si:N = 0.82). Our study suggests that the decoupling of the global silica and carbon cycles that is well known as a defining feature of the Southern Ocean (Nelson *et al*, 2002; Sarmiento *et al*, 2004) has its origins in the upper ocean.

It has been suggested recently (Matsumoto *et al*., 2002) that during glacial periods an increase in aeolian iron supply induces the preferential uptake of nitrate relative to silicate in Southern Ocean diatoms, as demonstrated by incubation experiments (Takeda, 1998). The resulting excess silicic acid in Subantarctic Mode Waters is advected northward by Ekman transport and allows low-latitude diatom production at the expense of calcifying organisms. Models suggest that the export of diatoms over calcifying organisms in low-latitude environments can cause a drawdown of atmospheric CO_2 in

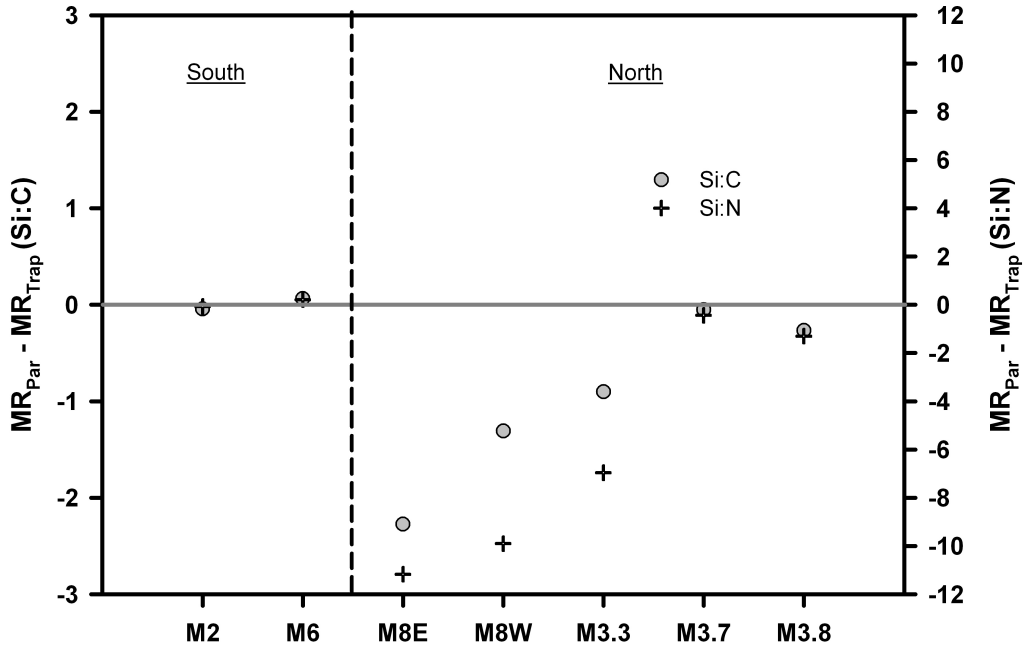

Fig. 3.13 MR_{Par} is the molar ratio of the suspended particulate phase integrated over the upper 60m using depths of 5, 10, 20, 40, and 60m. MR_{Trap} is the measured molar ratios of exported particles captured in PELAGRA. The difference between these molar elemental ratios is plotted as the deviation away from zero which is marked with a dark grey horizontal line.

the order of 70ppm, which accounts for glacial / interglacial atmospheric CO_2 cycles (Archer *et al*., 2000). The silicic acid leakage hypothesis (Matsumoto *et al*., 2002; Sarmiento *et al*., 2004) described above is dependant on the reduction of Si:N ratios in Fe-replete diatoms. The central question to the silicic acid leakage hypothesis is what governs the Si:N values in Southern Ocean waters advected north? If it is the Si:N uptake ratio of 1 by marine diatoms as suggested by culture experiments (Hutchins and Bruland, 1998., Takeda, 1998) then this would allow excess silicic acid to reach low-latitudes. However, data from this study clearly show that diatom export from Fe-fertilised blooms experiences selective regeneration of nitrate over silica as a function of depth relative to the ambient particle field (Fig. 3.14), thus increasing the Si : N ratio of diatoms and consequently lowering the potential excess silicic acid in Subantarctic surface waters predicted from this hypothesis.

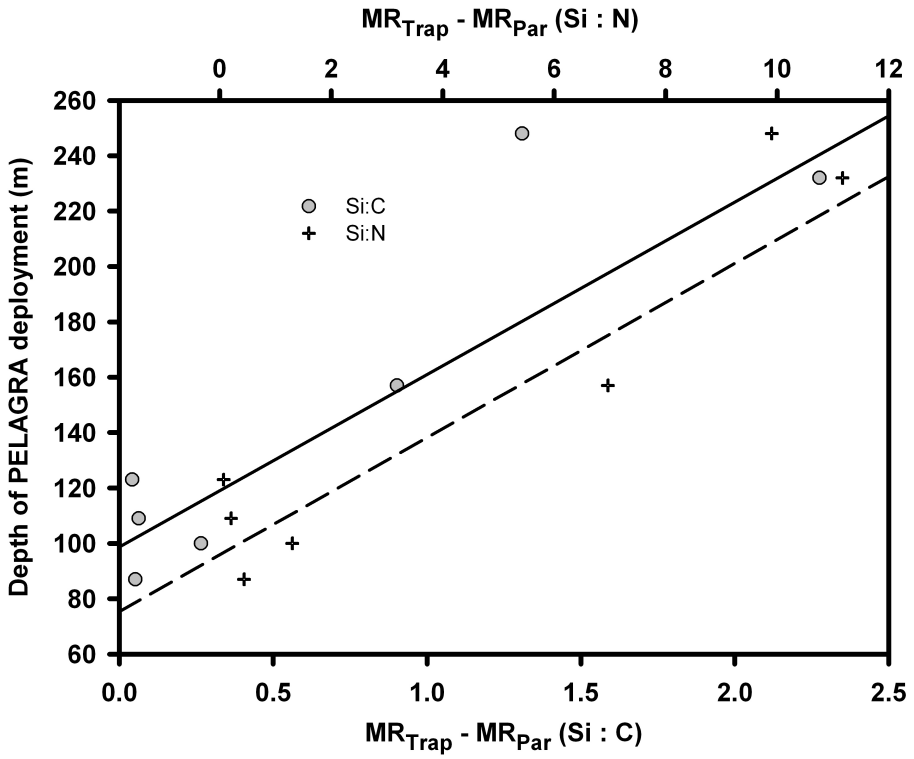

Fig. 3.14 MR_{Par} is the molar ratio of the suspended particulate phase integrated over the upper 60m using depths of 5, 10, 20, 40, and 60m. MR_{Trap} is the measured molar ratios of exported particles captured in PELAGRA. The difference between these molar elemental ratios is plotted as a function of depth. . Grey circles and black regression line for Si:C ($y = 0.0117x - 1.0713$; $r^2 = 0.80$, $n = 7$, $P<0.02$) and black crosses and dashed regression line for Si:N ($y = 0.0715x - 6.4986$, $r^2 = 0.90$, $n = 7$, $P<0.02$)

In the deep-sea the correlation between opal fluxes and organic carbon fluxes is not as strong as the correlation observed between organic carbon and calcium carbonate fluxes (Francois *et al*., 2002; Klaas and Archer, 2002), despite opal fluxes previously being implicated as crucial vectors for POC flux (Ragueneau *et al*., 1994; Buesseler, 1998). It has been suggested from these data (Klaas and Archer, 2002) that calcium carbonate is the primary mineral responsible for the sedimentation of POC. It has also been shown that areas of high organic matter flux are characterised by high Si:C ratios with a high fraction of production exported. The further decoupling of Si:C ratios during downward particle transport (this study; Nelson *et al*, 2002) shows how this can lead to low and variable correlation co-efficients in deep-sea sediment trap material.

3.6 Conclusions

It is difficult to ascertain accurately the detailed processes of carbon export from single point measurements. The comparison of normalised carbon fluxes to contemporaneous measurements of production is often undertaken in many studies. This generally produces over- and under-estimates of export ratios which can only be sensibly interpreted within the context of temporal decoupling between production and export processes. In this study satellite-derived chlorophyll data and empirical observations between *in-situ* chlorophyll and integrated production have been used to generate retrospective estimates of production. Using assumed particle sinking velocities this approach provides a range of export ratios for comparison, and decoupling, as one would expect, was more prevalent in the productive regime north of the plateau.

It was important to normalise organic carbon fluxes to a nominal depth to enable full comparison of the data set. Instead of normalising fluxes by a single factor based on an empirical relationship that has no observational validity in the study area, this study had the benefit of employing normalising factors from similar environments derived from recently published work. Comparison of these two techniques reveal that the traditionally-used Martin curve may under- and over-estimated normalised fluxes at southern and northern stations respectively.

The measured and depth-normalised organic carbon flux at M8W north of the plateau was an order of magnitude larger than fluxes from all other stations. Based on observed production profiles this deployment seems to represent the best estimate of export from the fertilised region north of the plateau. Using a simple mass balance approach to account for seasonal depletion of dissolved silicic acid in surface waters and Si fluxes from the euphotic zone, potential export of organic carbon from the bloom area was estimated to be in the order of 11-15 g C m^{-2}. This is higher than previous estimates obtained from mesoscale perturbation experiments and may reflect fundamental differences in methodical approach.

Diatom size correlates well with a range of calculated export ratios$_{(100m)}$ demonstrating the significant role of large diatoms in export from a naturally fertilised bloom. The main diatoms involved in export from the surface are medium-large centric diatoms, particularly *E. antarctica*; although to the south of the plateau the heavily silicified pennate *F. kerguelensis* was most important, reflecting the regional differences in community structure and its effect on the magnitude of carbon export. Si:C and Si:N ratios of the particles normalised to the overlying particle field increase proportionally with depth, highlighting the preferential remineralisation of carbon and nitrogen over silica has its origins in the surface ocean.

It appears that events or regions of high surface export are characterised by a decoupling of production and export and these events are under-sampled and poorly represented in models. The following chapter will focus on the analysis of deep-sea sediment trap material recovered from the CROZEX study region.

Data

The data presented in Chapter 4 includes:

- Organic carbon measurements
- Total carbon measurements
- Biogenic silica measurements
- Sediment trap current speeds
- Diatom taxonomy of sediment trap samples
- Satellite-derived chlorophyll

The picking and splitting of all sediment trap samples was carried out by the author
All biogenic silica measurements and organic carbon data was measured by the author.
Total carbon samples were prepared by the author but analysed on the elemental analyser at the University of Liverpool (UOL) due to equipment failure at the National Oceanography Centre, Southampton (NOCS). The agreement between total carbon measured at NOCS and UOL is presented in Appendix 1. Sediment trap current speeds were downloaded from the current meters by Jane Read (NOCS) and processed by the author. Diatom taxonomy samples were prepared by the author and counted by Alex Poulton, this was to maintain consistency within the CROZEX project. Satellite data was downloaded from SeaWifs by Hugh Venables (NOCS), validated according to Venables *et al*., (2007) and processed by the author.

4. DEEP WATER PARTICLE FLUX FROM A NATURAL IRON FERTILISATION EXPERIMENT

Abstract

The CROZet natural iron bloom and export EXperiment (CROZEX) examined the development and fate of a naturally-occurring phytoplankton bloom in the vicinity of the Crozet Plateau in the Indian Sector of the Southern Ocean. Peak chlorophyll concentrations within the naturally iron-fertilised regions north of the plateau were 4mg Chl m^{-2}, an order of magnitude higher than the 0.5mg Chl m^{-2} observed in the high-nutrient low chlorophyll (HNLC) "control" region located to the south. As part of the project, six deep-moored sediment traps were deployed both north and south of the Crozet Island system to elucidate geochemical and biological differences in deep-water (2000-3000m) particle fluxes. Current meters moored directly beneath the Parflux traps indicate that current speeds averaged over 30 minute intervals rarely exceeded 10 cm s^{-1}. Flux profiles of the major biogenic components, organic carbon, biogenic opal, and calcium carbonate exhibited a high degree of seasonality, with much of the year characterised by negligible fluxes. The annual flux of organic carbon north of the plateau was 0.42g C m^{-2} yr^{-1} compared to 0.087 g C m^{-2} yr^{-1} measured to the South. Annual fluxes of all components were larger north of the Crozet Plateau. Fluxes were dominated by biogenic silica which accounted for 35-80% by mass. Taxonomical analysis of the sediment trap material revealed that whilst *Fragilariopsis kerguelensis* dominated the sedimenting diatom assemblage south of the plateau, the centric diatom, *Eucampia antarctica* was important to the north. The ≈4-fold increase in annual carbon flux is the first evidence to demonstrate that the supply of iron to an otherwise HNLC system increases the export of carbon to the deep-ocean. Comparison of deep-water carbon fluxes with satellite-derived productivity imply that the fraction of surface production reaching 3000m is 3-times higher in the iron-replete north than the HNLC south, providing strong evidence that the presence of iron enhances the efficiency of the biological carbon pump.

4.1. Introduction

Recent modelling studies indicate that the Southern Ocean plays an important role in the global carbon cycle and the uptake of anthropogenic CO_2 (Sarmiento *et al*., 1998; 2000; Caldeira and Duffy, 2000), and global syntheses of pCO_2 datasets suggest that it could account for more than half of the global ocean CO_2 uptake (Takahashi *et al*., 2002). The Southern Ocean is subject to a strong upwelling of deep-water characterised by high concentrations of phosphate, nitrate, silicate and DIC. This area could thus act as a net source of CO_2 since the high carbon concentrations in the upwelled water would outgas CO_2 to the atmosphere. Crucially, biological activity and subsequent export from the surface ocean causes a drawdown of dissolved nutrients and carbon which lowers the partial pressure of CO_2 in the surface water and thus affects its exchange with the atmosphere. It is clear from modelling studies (e.g. Takahashi *et al*., 2002) that the magnitude of this downward particle flux is sufficiently large to generate a net air-sea flux of CO_2. Despite the direction of this flux the Southern Ocean contains a large repository of unused macronutrients that are associated with generally low levels of primary production and it is a high nutrient low chlorophyll (HNLC) region. A more complete utilisation of the available macronutrients could potentially increase downward carbon flux and thus the air-sea flux of CO_2 with important consequences for global carbon cycling and future climate change scenarios.

The importance of iron (Martin *et al*., 1990; de Baar *et al*., 1995), light (Mitchell *et al*., 1991) and grazing (Morel *et al*., 1994; Smetacek *et al*., 2004) in controlling phytoplankton processes in the HNLC Southern Ocean is well established, with artificial fertilisation experiments demonstrating that iron availability can exert a primary control on the proliferation of phytoplankton biomass (e.g. Boyd *et al*., 2000; Coale *et al*., 2004; Hoffmann *et al*., 2006). Artificial fertilisation experiments in the Southern Ocean and other HNLC regions have however experienced difficulties in providing strong evidence for an associated increase in downward carbon flux (e.g. de Baar *et al*., 2005). There has been some indication from SOFeX (Coale *et al*.,

2004) of an increase in shallow-water carbon fluxes from ^{234}Th measurements (Buessler *et al*., 2004) and an autonomous drifter package (Bishop *et al*., 2004). The methodical limitations presented by mesoscale enrichment experiments have provided the impetus to study carbon flux from naturally iron-fertilised phytoplankton blooms associated with island-systems in the Southern Ocean (Blain *et al*., 2007; Pollard *et al*., 2007). Results from a study at the Kerguelen Plateau suggest that shallow-water carbon fluxes determined from ^{234}Th measurements are significantly higher in the island-influenced bloom area relative to a HNLC control site (Blain *et al*., 2007).

4.1.2 Study Focus

Deep-water particle fluxes resulting from an iron-fertilised bloom of either artificial or natural origins have not hitherto been examined. Although some evidence (Bishop *et al*., 2004; Buesseler *et al*., 2004; Blain *et al*., 2007; Chapter 3) indicates an increase in shallow-water (100-250m) carbon fluxes, the inferences that can be drawn from these are limited since intense remineralisation of carbon at depths between 100 and 1000m is well documented (e.g. Martin *et* al., 1987; Schlitzer, 2002; Buesseler *et al*., 2007). The sequestration of CO_2 into the deep-ocean by the biological pump is central to hypotheses linking particle fluxes and climate change in both the modern day ocean and geological past (Martin 1990; Moore *et al*., 2000). The analysis of deep (>2000m) sediment trap material collected beneath the iron-fertilised bloom north of the Crozet Plateau and HNLC control areas to the South can address some of these issues.

The results from the deep-sediment traps will attempt to build on the results obtained from the short shallow deployments of PELAGRA discussed in Chapter 3. In particular the following questions will be addressed:

1. Does natural iron fertilisation increase the strength of the biological carbon pump in the PFZ of the Southern Ocean?

2. Does natural iron fertilisation affect elemental stoichiometry of exported particles and if so what are the biogeochemical implications?
3. Does natural iron fertilisation affect the species composition of diatom fluxes?
4. Do the sediment trap results support the second tenet of Martin's iron hypothesis that iron supply increases the efficiency of the biological carbon pump?

4.2. Regional oceanography and experimental design

The Crozet islands form part of a larger plateau that is located in 4200m of water in the Southern Ocean at 46^{o}S, 52^{o}E. The archipelago is situated in the northern part of the Indian-sector of the Southern Ocean and is thus within the boundaries of the Polar Frontal Zone (PFZ). Circulation patterns in the region are affected by local topography, the Antarctic Circumpolar Current (ACC), and zonal wind fields, (Pollard *et al*., 2007). The SubAntarctic Front (SAF), a major branch of the ACC, flows eastwards to the south of Del Cano Rise and is then deflected northwards into the Crozet basin, before turning eastward and combining with the Agulhas Return Current and the SubTropical Front, creating an S-bend feature (Pollard and Read, 2001) (Figure 4.1). South of this S-bend and north of the plateau itself mean circulation is weak, allowing dissolved iron from the land or sediments of the Crozet plateau to accumulate throughout the winter in the PFZ between Crozet and the SAF. With excess macronutrients present in the HNLC waters, this facilitates an annual bloom to north of the plateau; as shown from composite satellite imagery (Venables *et al*., 2007).

During the austral summer of 2004-2005 six McLane sediment traps (21 cup) were deployed at four strategic stations; M2 (2000m), M5(2000 and 3000m), M6 (2000 and 3000m), and M10 (2000m), Fig. 4.1 shows the location of these moorings in relation to the plateau. Stations M2 and M6 were located south of the plateau in the HNLC "control" region, M5 and M10 were to the north-east and north of the plateau underneath the annually occurring enhanced surface chlorophyll feature. The moorings deployed at M2 and M10 were type A, and had just one sediment trap at 2000m water depth, moorings at M5 and M6 were type B with two traps at approximately 2000m and 3000m.

The configuration of type A and type B moorings are shown in Appendix 4. All the sediment trap moorings were recovered on the Benthic Crozet cruise which took place in December 05- January 06 (RRS Discovery. 300)

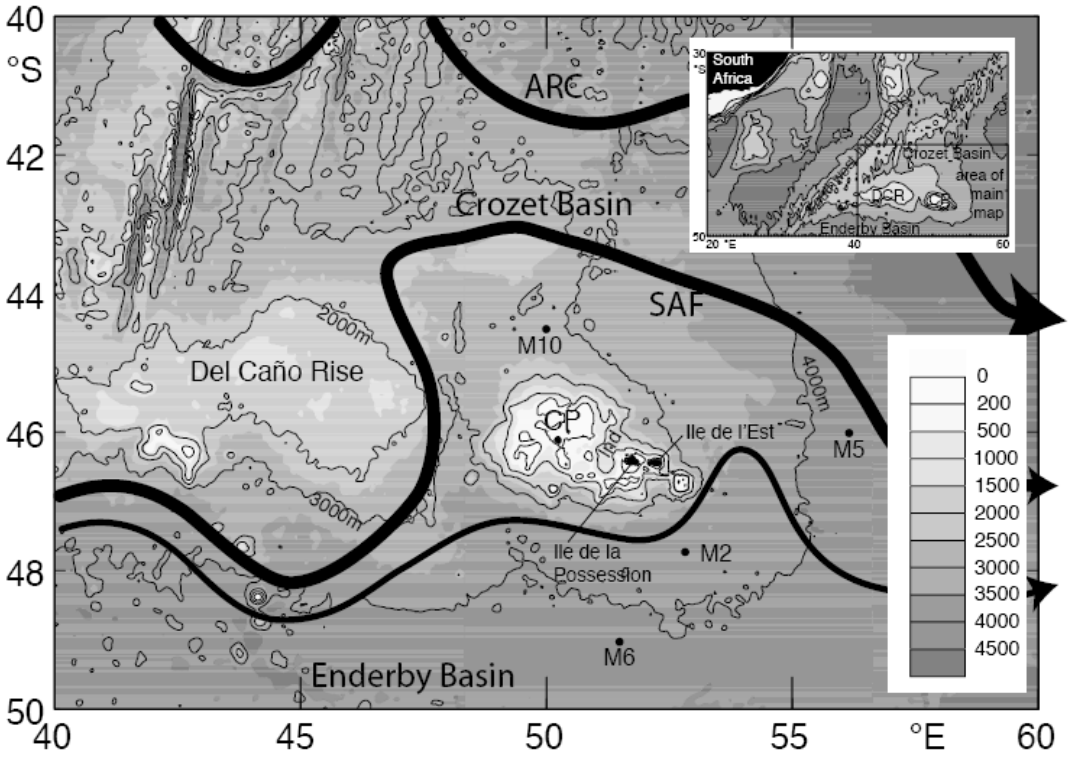

Figure 4.1 Map of study area showing sediment trap deployment locations and the main features of local bathymetry and hydrography. The thick black lines mark the Agulhas Return Current (ARC), and the SubAntarctic Front (SAF). The thin black line at the bottom of the graphic delineates the HNLC and productive waters. Modified from Pollard *et al*. (2007).

4.3 Methods

4.3.1 Sediment traps

All traps were large funnels (0.5 m^2 surface area) with a baffle at the top and a narrow opening at the bottom through which the particles fall into individual cups (McLane, INC. Parflux 21 cup). Deployment schedules were programmed with a sampling

resolution that reflected anticipated periods of high and low flux, full details of which can be found in Appendix 4. The 250 mL sample cups were filled with a preservative solution. The preservative solution was prepared by adding 100 g of analytical grade NaCL to 19 L of unfiltered deep (>2000m) seawater from the trap deployment location. 1 L of formaldehyde (AnalR® grade, VWR international) was buffered to pH 8.6 with sodium tetraborate and added to the 19 L of hyper-saline seawater, and the solution left to stand for a period of 1 day.

4.3.2 Swimmers and fish debris

Prior to chemical analysis of the particulate samples swimmers were removed from the sample with plastic forceps under a dissecting microscope (x50). Swimmers are defined as the zooplankton that have entered the sample cups alive and intact, and therefore do not represent the passive flux from the surface ocean (Michaels *et al*., 1990). The number of swimmers removed from samples was very low and thus removed without enumeration. Numerous samples were heavily contaminated with fish debris and scales. All of the large debris and scales were removed from the samples with plastic forceps under a dissecting microscope (x50). A significant number of cups contained very few particles as indicated by the volume flux (Appendix 4) and as such are treated as zero fluxes in subsequent figures and tables.

4.3.3 Sample splitting and total mass flux

The 250mL samples were split into 8 equal aliquots of equal volume using a rotary splitter (replication error <3% for this methodology; Lampitt, pers. obs.) Depending on sample mass, 1-5 these eighths were filtered onto cellulose nitrate filters (47mm, 0.45µm pore size) and the filtrate from 1 aliquot stored in a clean LDPE bottle (60 mL). The samples and filters were subsequently rinsed with a 0.56 M ammonium formate solution (pH 7) to remove excess sea-salt and formalin. The sample was carefully removed with a metal spatula as a wet cake of material and transferred to pre-combusted (450^{o}C; 12 hours) glass vials and frozen at -20^{o}C. Frozen samples were freeze-dried over night and homogenised to a fine powder using the flat end of a

metal spatula. This material was used to weigh samples for the determination of particulate organic carbon (POC), total carbon (TC) and biogenic silica (BSi). Total mass flux was determined gravimetrically following the filtration of a $1/8^{th}$ aliquot onto a pre-weighed cellulose nitrate filter (47mm diameter, 0.45 µM pore size). The filter was rinsed with 0.56M ammonium formate (pH 7) to remove salt and excess formalin and dried at 60°C until a constant weight was achieved.

4.3.4 Chemical analyses

TC was determined using a Carlo-Erba NA-1500 elemental analyser following standardisation with acetanilide. 2-4mg of freeze-dried samples were weighed into pre-combusted (550°C; 12 hours) silver cups which were formed into small capsules with metal spatulas. POC was determined using the same procedure on acidified samples. A 15µl aliquot of 20% HCl was added to the sample in order to remove calcium carbonate. After each aliquot was added the acid was evaporated by gently heating on a hot plate (<60°C). The procedure was repeated until all carbonates were removed as shown by the absence of any effervescence upon addition of the acid, and then two more additions of acid were performed to ensure complete removal of inorganic carbon. Samples were subsequently rinsed with a 40 µl aliquot of ultra-pure water and dried on a hotplate at <60°C. This procedure was repeated five times and the samples were then dried overnight at 50°C. Care was taken to note any sample loss from silver cups and samples discarded if this was the case.

Biogenic silica was determined using a wet chemical technique modified from Mortlock and Froelich, (1989). Samples (3-5 mg) were weighed into clean polypropylene tubes. Particulate opal was converted into dissolved silicon by treatment with 0.2M sodium hydroxide for 3 hours at 100°C. The extract was separated from the residue via centrifugation and the sediment residue was rinsed with ultrapure water and dried overnight (60°C). The dissolved silicate was converted to the silico-molybdate complex (Strickland and Parsons, 1968) and the absorbance read at 812 nm with a Hitachi U-2000 spectrophotometer. Full details of these methods, including set-up and validation may be found in Appendices 1 and 2.

4.3.5 Phytoplankton analyses

A 1/8th split of each sediment trap sample was designated for phytoplankton taxonomy. The volume of the split was recorded prior to removal of any material. The 1/8th aliquot was shaken thoroughly to re-suspend the particulate slurry and 1-3mL removed with a modified pipette tip and transferred to a 60mL LDPE bottle containing 19mL of clean preservative solution. The pipette tip was rinsed with a known volume of clean preservative solution to remove any material adhering to the interior surfaces. The standard pipette tip (5mL) had the bottom 1cm removed to increase the diameter of the tip aperture and thus minimise selective removal of certain particle sizes. Sub-samples were settled in 10 mL settling chambers (Hydro-Bios) for ~10-12 hrs and examined using a Leitz inverted microscope. Large and numerically rare taxa were counted during full examination of the settling chamber at high magnification (x10), while small and numerically dominant taxa were counted on 1-2 transects of the chamber (x10, x20) or from cumulative counts from several (5-10) fields of view (x40). Diatoms were identified to genera or species following Priddle and Fryxell (1985) and Tomas (1997), more details can be found in Poulton *et al*. (2007).

4.3.6 Remote-sensing data

The remotely-sensed chlorophyll data used in this chapter is the merged SeaWIFS/MODIS product which is a composite of the two chl-a estimates. MODIS derived chl-concentrations (Feldman and McClain, 2006a) were processed using the standard OC3v1.1 algorithm. SeaWIFs derived chl-a concentrations (Feldman and McClain, 2006b) were processed using the standard OC4v5.1 algorithm. For each of the 810 *in situ* chl-a measurements collected during the cruises, the value from the corresponding individual pixel of the ocean colour image of the day of collection was recorded, if the pixel was cloud free. This resulted in 224 pairs of *in situ* and satellite data for the merged SeaWIFS/MODIS product. The least squares regression fits, with 95% confidence intervals are shown equations 4.1 and 4.2

$$CHL_{merged} = 0.12_{\pm 0.04} + (0.38_{\pm 0.03}) * CHL_{in\ situ},\ r^2 = 0.78 \quad \textbf{(4.1)}$$

$$CHL_{in\ situ} = -0.08_{\pm 0.08} + (2.05_{\pm 0.15}) * CHL_{merged} \quad \textbf{(4.2)}$$

The remotely-sensed chlorophyll data was corrected using these relationships (Venables *et al.*, 2007)

4.4. Results

4.4.1 Current speeds, trapping efficiencies and particle trajectories

The time-series of current profiles documented by the Aanderaa current meters deployed directly beneath the sediment traps (Appendix 4) are presented for each sediment trap in Fig 4.2. Table 4.1 summarises the mean current speed and maximum current speed for the relevant time period of each deployment. The effect of current speeds on trapping efficiency is only considered for the period(s) of the deployment in which particle flux was measured (see Fig 4.2). For all deployment locations and depths average current speeds were <5 cm s^{-1}, with occasional short excursions to higher velocities. Present understanding of the behaviour of particles under turbulent conditions is inadequate to correct for current-induced biases. Consequently current-meter data can only be used qualitatively to assess the general integrity of a sample set (Yu *et al.*, 2001). Based on a large-scale inter-comparison experiment conducted in the Panama Basin (Honjo *et al.*, 1992), samples collected when current velocities are <10 cm s^{-1} are considered reliable with higher current velocities incurring increasing levels of doubt (Honjo, 1996). Elegant studies using ^{230}Th and ^{231}Pa appear to support this notion and indicate that in quiescent deep-sea environments, with current speeds similar to those observed here, calculated trapping efficiencies are close to 1 (e.g. Bacon *et al.*, 1985; Yu *et al.*, 2001). Based on the current understanding it is thus suggested that trap collection variations present only a minor aspect of the observed flux variations.

Table 4.1 A summary of the mean and maximum current speeds for each sediment trap. The data presented is only considered for the relevant time period of the deployment, see Fig. 4.2 for more details.

Site and Trap Designations	Latitude ° S	Longitude ° E	Bottom Depth m	Trap depth Below Surface m	Mean Current Speed cm s^{-1}	Max. Current Speed cm s^{-1}
North						
M10 (2000m)	44.5	50.0	2965	2000	4.5 ± 2.6	14.5
M5 (2000m)	46.0	56.1	4277	2001	5.0 ± 2.4	12.6
M5 (3000m)	46.0	56.1	4277	3195	4.6 ± 2.4	18.8
South						
M2 (2000m)	47.8	52.9	3856	1973	4.0 ± 2.4	15.5
M6 (2000m)	49.0	51.5	4221	2007	3.5 ± 2.4	14.6
M6 (3000m)	49.0	51.5	4221	3160	4.0 ± 2.7	16.9

4.4.2 Satellite chlorophyll

The bloom around the Crozet Plateau started in September 2004 with enhanced chlorophyll features appearing initially to the north of the plateau (Fig. 4.3). In October the bloom area increased and spread south and south-east towards the two main islands. At this stage a strong contrast existed between high chlorophyll values in the bloom to the north of the plateau compared to the low chlorophyll values observed to the south. The values to the south show little difference from those upstream to the west, suggesting that waters in the south experience a negligible effect from the island system. The bloom is bound to the west and the north by low chlorophyll concentrations in the Sub-Antarctic front (SAF) and this separates it from increased levels further north associated with the Sub-Tropical Front and Agulhas Return Current. Between late November and early December the chlorophyll levels reduce rapidly and collapse back towards the plateau. In January and February chlorophyll levels increase again but are constrained over and to the edge of the plateau.

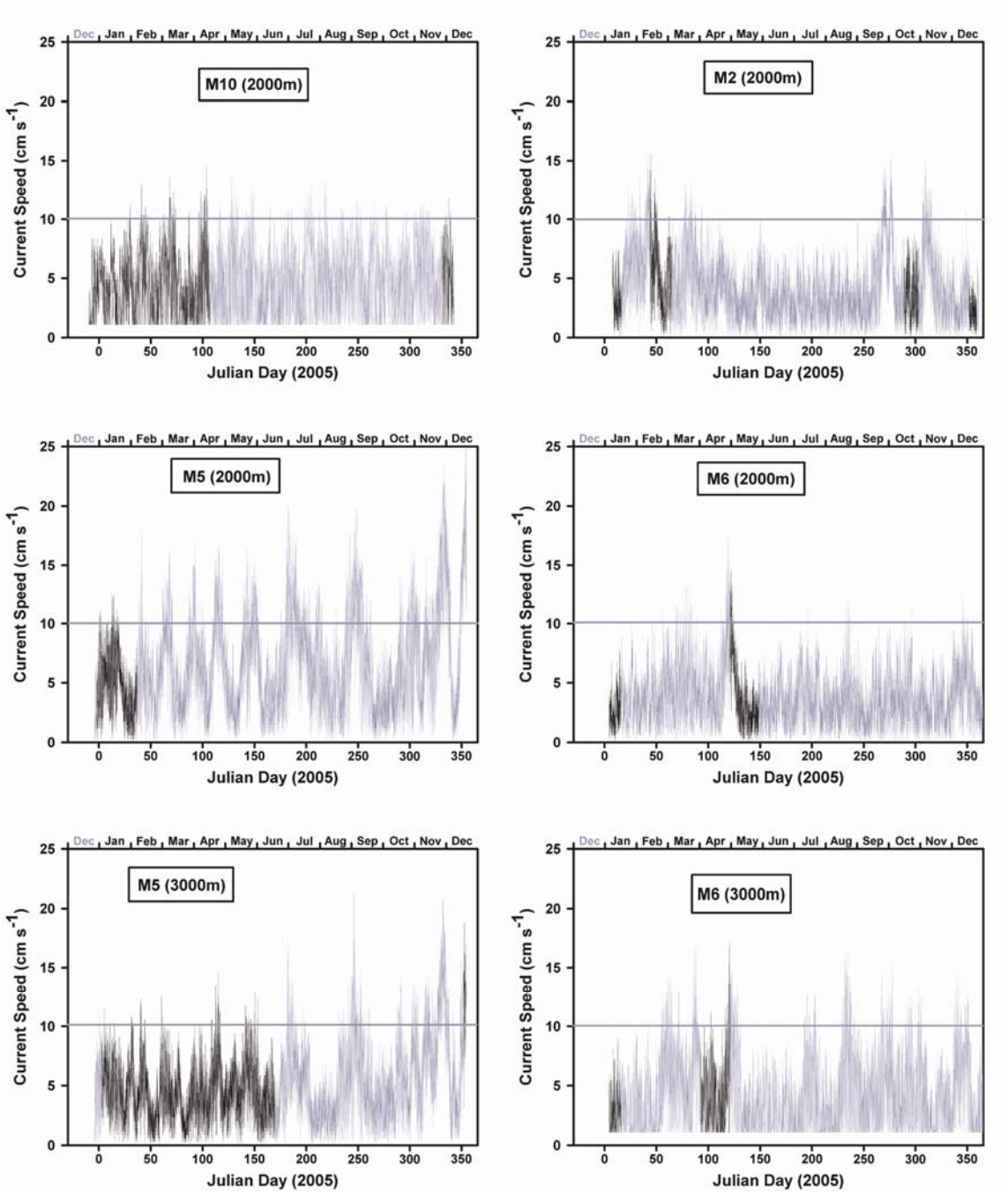

Figure 4.2 Current velocities at 30 minute intervals for each sediment trap deployment. Black lines indicate current velocities for the periods occupied by sediment trap sampling intervals in which downward particle flux was measured. Summary data presented in Table 4.1 is based on this data. Grey horizontal line denotes the threshold of 10 cm s^{-1}, see text for discussion.

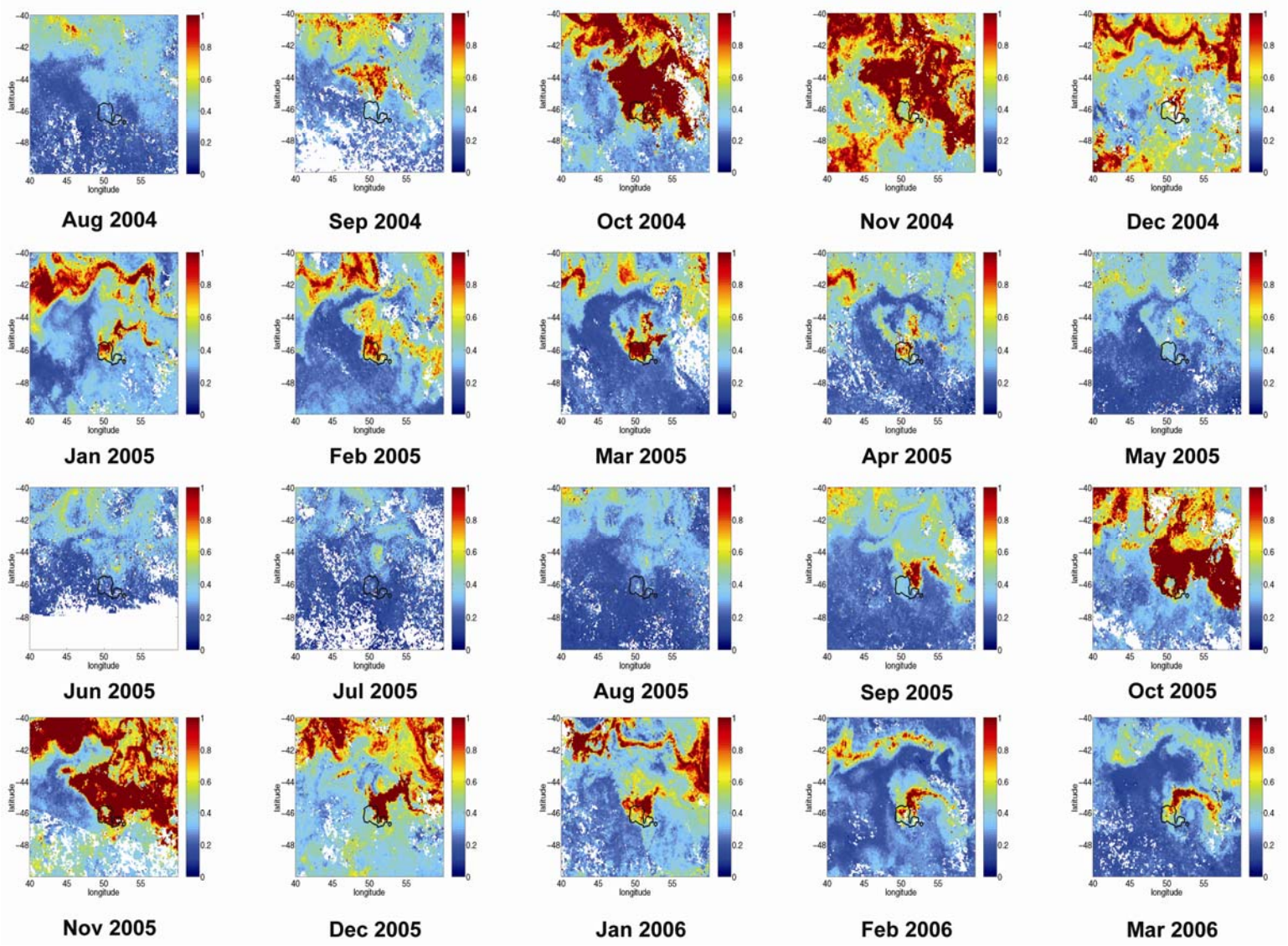

Fig. 4.3 Composite SeaWiFs images of surface chlorophyll in the vicinity of the Crozet Plateau.

Changes in surface chlorophyll are related to changes in particle flux at depth. It is important for this type of study to examine when and where sediment traps were deployed in relation to local patterns of surface chlorophyll in order to effectively relate surface production with material collected at depth. Monthly composite images (Fig. 4.3) lack the necessary temporal and spatial resolution required for this type of analysis. In the absence of information on the spectrum of sinking speeds and detailed hydrography of the area, only a crude estimate of the statistical funnel (Siegel and Deuser, 1997) can be made. Circles were drawn around each of the stations; M2, M5, M6, and M10. The exact co-ordinates of the respective mooring formed the centre of each circle and corresponding areas of 59.8, 299, 777, 1734, and 2930 km^2 (Fig 4.4) were used for the spatial integration of satellite-derived surface chlorophyll. (Fig 4.5). The magnitude and temporal trends of chlorophyll are broadly similar and independent of the area used, with some exceptions (Fig 4.5). There are fewer "rogue" chlorophyll features apparent from the stations south of the plateau, probably because of the quiescent nature of the biomass maxima in the low productivity environment.

Each panel in Fig 4.6 represents one sediment trap mooring. The dashed black line marks the date the sediment trap was deployed, i.e. the start of the collection period. The dashed blue and red lines indicate which surface chlorophyll features may have generated the measured particulate flux based on pre-defined sinking rates. The blue dashed line assumes a sinking rate of 100 m d^{-1}, and the red dashed line 50 m d^{-1}. The thick black line represents the arithmetic mean of the various pixel areas. Therefore the distance between the blue dashed line and the black dashed line represents sinking rates between 100 m d^{-1} and ∞ m d^{-1} and the distance between the red dashed line and the blue dashed line represents sinking rates between 50 and 100 m d^{-1}. The intervals between the lines create a "window" showing which surface chlorophyll features the sediment traps had the potential to sample assuming particle sinking velocity was >50 m d^{-1}.

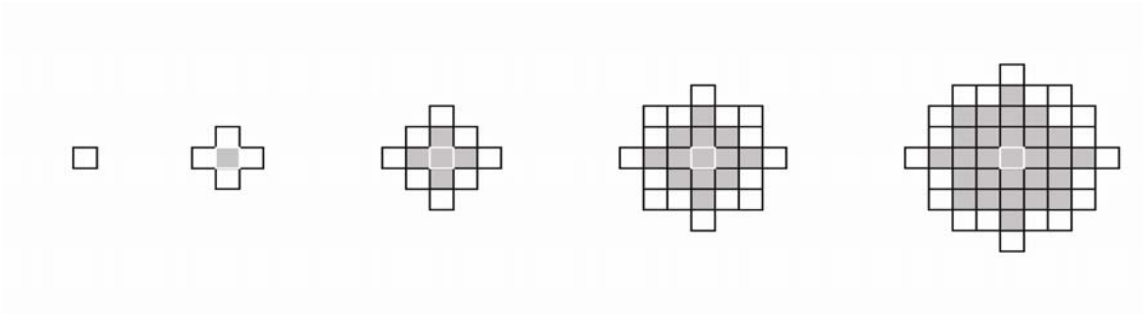

Figure 4.4 Schematic showing how pixels were built up in order to create the various circles over which the satellite-derived surface chlorophyll values were integrated for use in Fig. 4.5

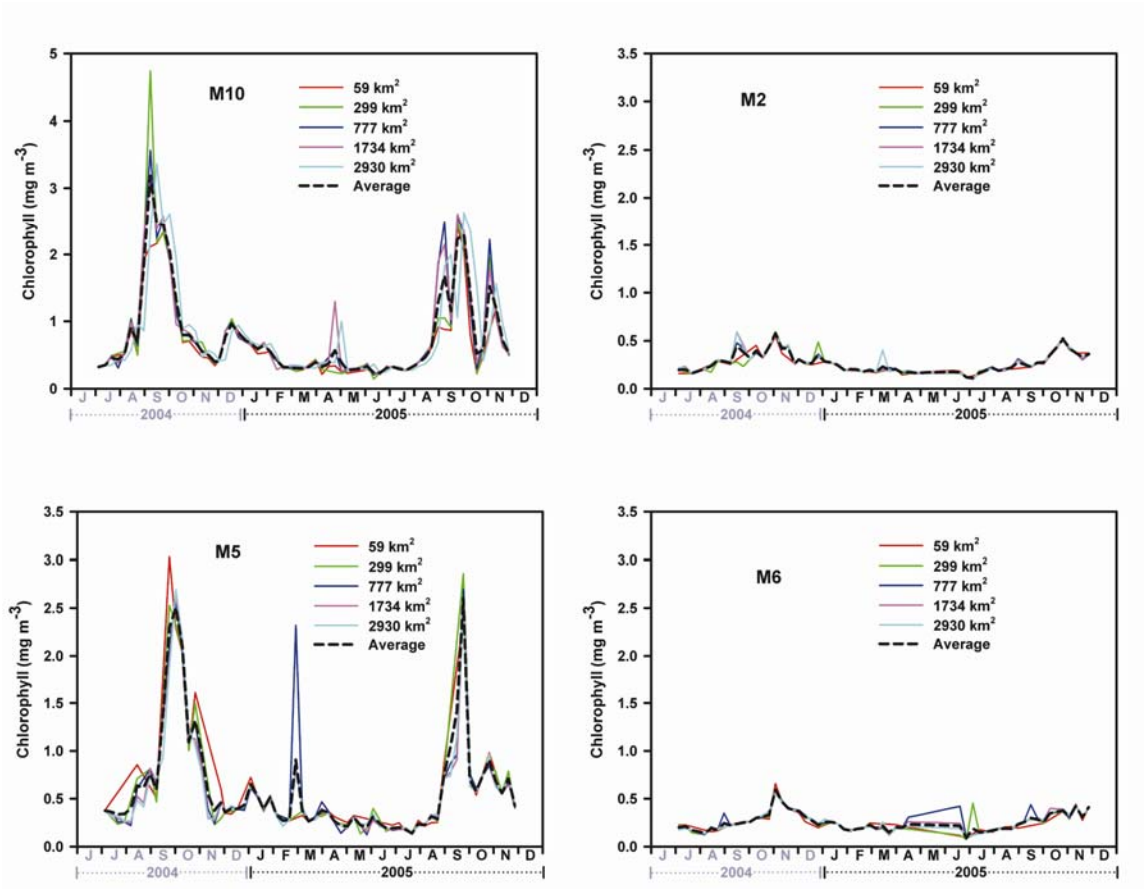

Figure 4.5 Satellite-derived surface chlorophyll for each sediment trap mooring location from June 2004 to December 2005. Different coloured lines correspond to different areas of integration as detailed in the captions and also Fig 4.4.

At M10 the chlorophyll reached a maximum of 3.2 ± 1.1 mg m^{-3} in early October compared to 2.6 ± 0.2 mg m^{-3} estimated 24 days later at M5 (Fig 4.6). Despite this delay in surface biomass maxima the assumed sinking rates indicate the 2000m traps at M5 and M10 may have under-sampled the potential flux. The M5-3000m trap could have sampled surface biomass that originated 10-20 days earlier. At M2 and M6 the peak in surface chlorophyll are 0.57 ± 0.02 and 0.59 ± 0.04 mg m^{-3} respectively, not much greater than background values. Crucially the biomass maxima south of the plateau occurred around 40 days later than that to the north, such that the relative deployment times of M2-2000m, M6-2000m, and M6-3000m had the potential to fully sample this surface feature.

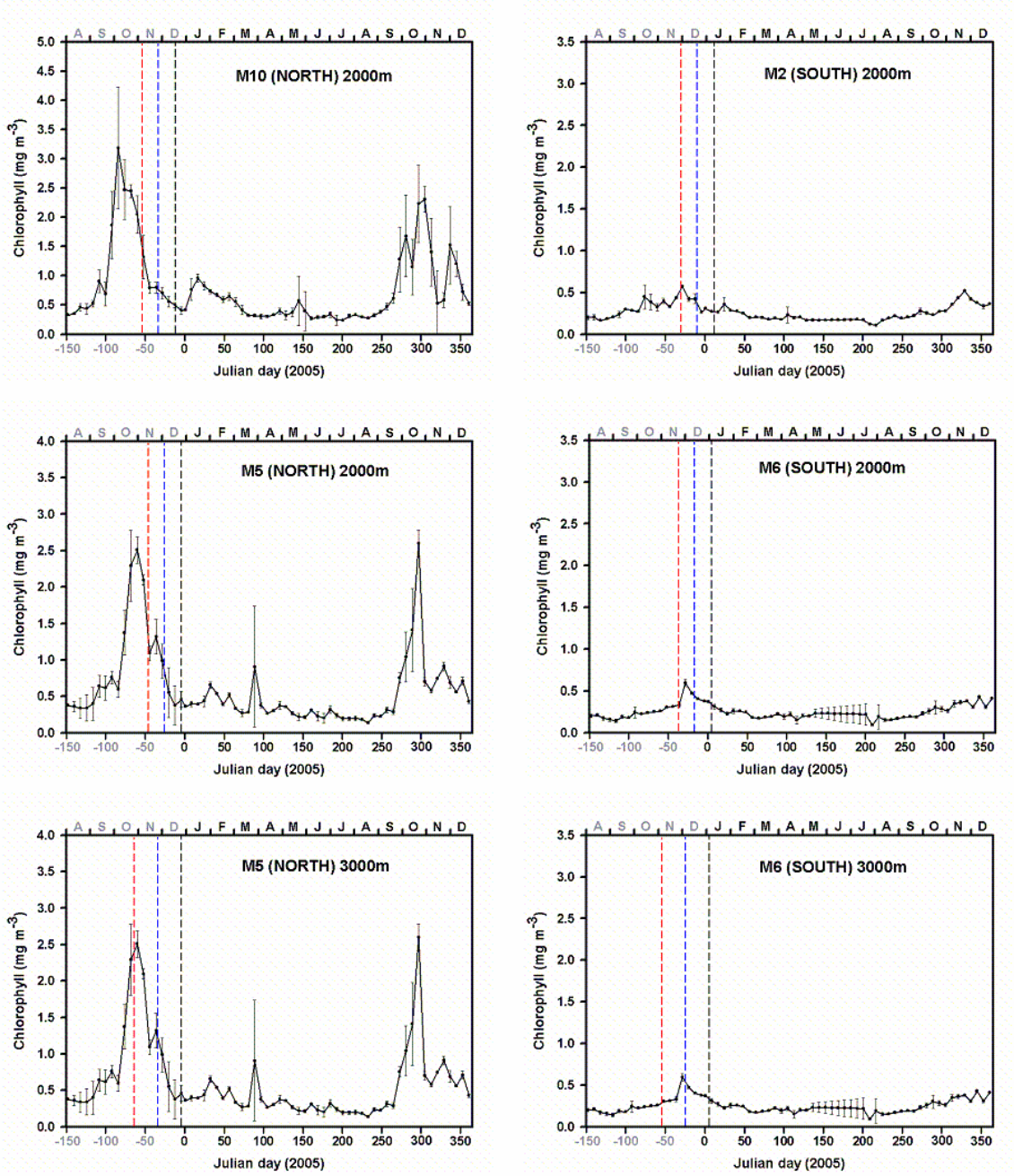

Fig. 4.6 Arithmetic mean and standard deviation of satellite-derived surface chlorophyll data calculated from individual integrations presented in Fig. 4.5. Black-dashed line denotes the time of the sediment trap deployment. Coloured dashed lines denote when the particles are likely to have originated based on assumed sinking speeds of 50 m d^{-1} (blue) and 100 m d^{-1} (red). See text for further details.

4.4.3 Total Mass Flux

Deep-water particle fluxes south of the plateau are generally characterised by a single mass sedimentation event occurring in January (Fig. 4.7). At M2-2000m and M6-3000m this single flux event contributed particle fluxes of 630 and 500 mg m^{-2} d^{-1}, respectively. The flux profiles show that subsequent minor flux events are evident in late February at M2 and in April at M6, although their validity is uncertain (see section 4.3.2). North of the plateau the sedimentation profiles contrast with those of the southern stations and are characterised by total mass fluxes of lower magnitude sustained for a longer period of time. At M10-2000m the largest flux event recorded was 220 mg m^{-2} d^{-1} decreasing exponentially to 22 mg m^{-2} d^{-1} over a period 120 days. A similar profile was observed at M5-3000m although the initial flux measurement was larger and the sedimentation profile persisted for 173 days.

4.4.4 Spatial and seasonal variations in biogeochemical fluxes

4.4.4.1 Organic Carbon

Fig 4.8 shows particulate organic carbon (POC) fluxes at each sediment trap location along with the fraction of total mass that can be accounted for by organic carbon (POC/TM). The organic carbon content of sedimenting material ranges between 0.016 and 0.14, although the higher values coincide with the presence of contaminating fish debris. Particulate fluxes north of the plateau were enriched in POC/TM (0.028 ± 0.014) relative to those south of the plateau (0.016 ± 0.001). The flux of POC follows similar patterns to those previously discussed for total mass flux. The largest POC flux of 11 mg C m^{-2} d^{-1} was observed north of the plateau at M5-3000m. POC flux events of similar magnitude were observed at M2-2000m and M6-3000m but were limited to a short period of time. The M10-2000m, M5-3000m, and M2-2000m deployments also sampled the onset of particulate flux from productivity maximum in 2005. POC/TMF values of 0.05 at M10-2000m and 0.06 at M5-3000m indicate that the early stage of the flux profile is carbon-rich compared to that recorded in 2004 and early 2005. It is possible that the earliest flux measurements obtained in 2004/05 do not represent the

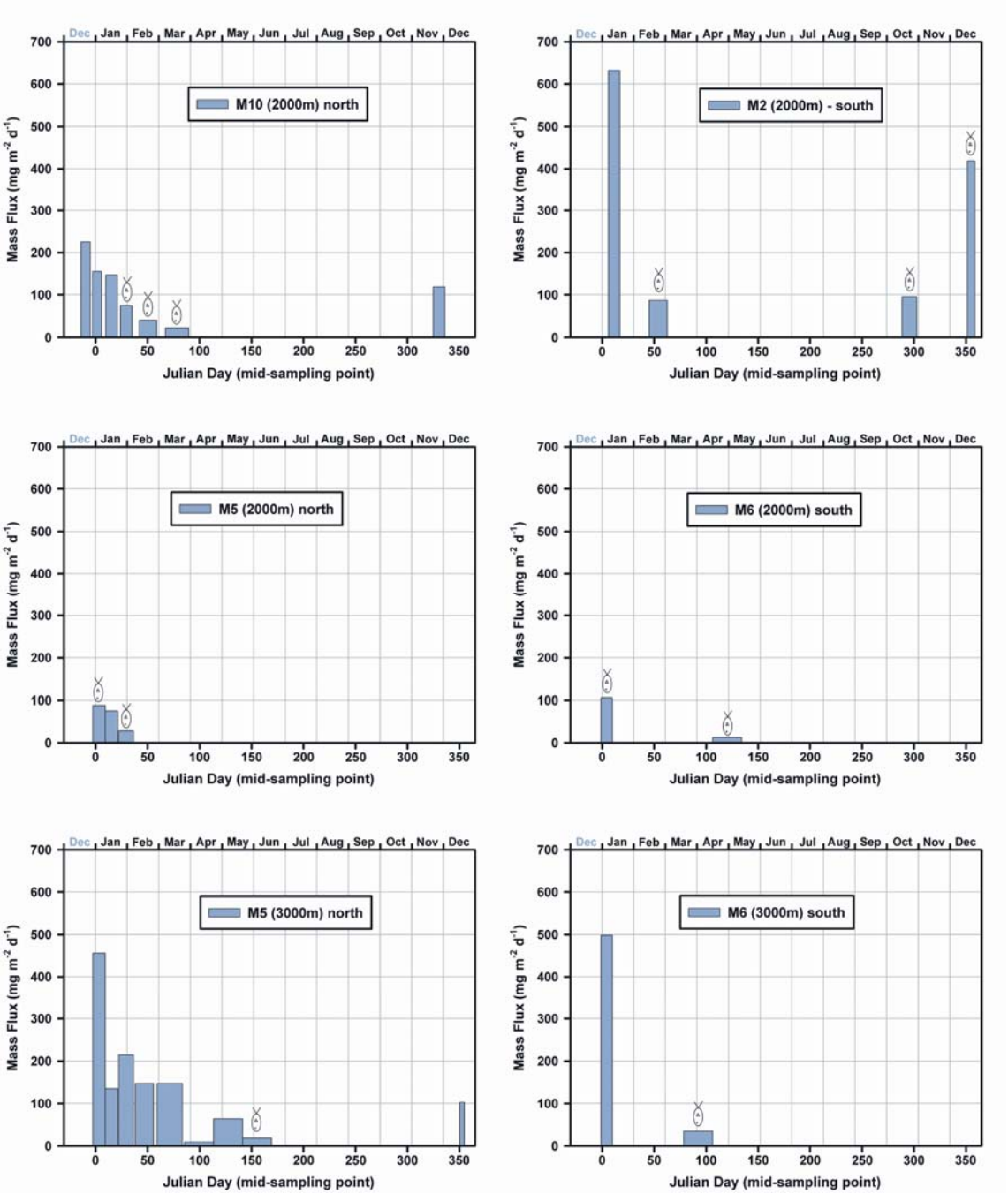

Figure 4.7 Profiles of total mass flux for each sediment trap. Fish icon denotes samples that were contaminated by fish debris. Width of bars represents the length of the sampling intervals such that the area of the bars is proportional to the integrated flux. No bar indicates zero flux.

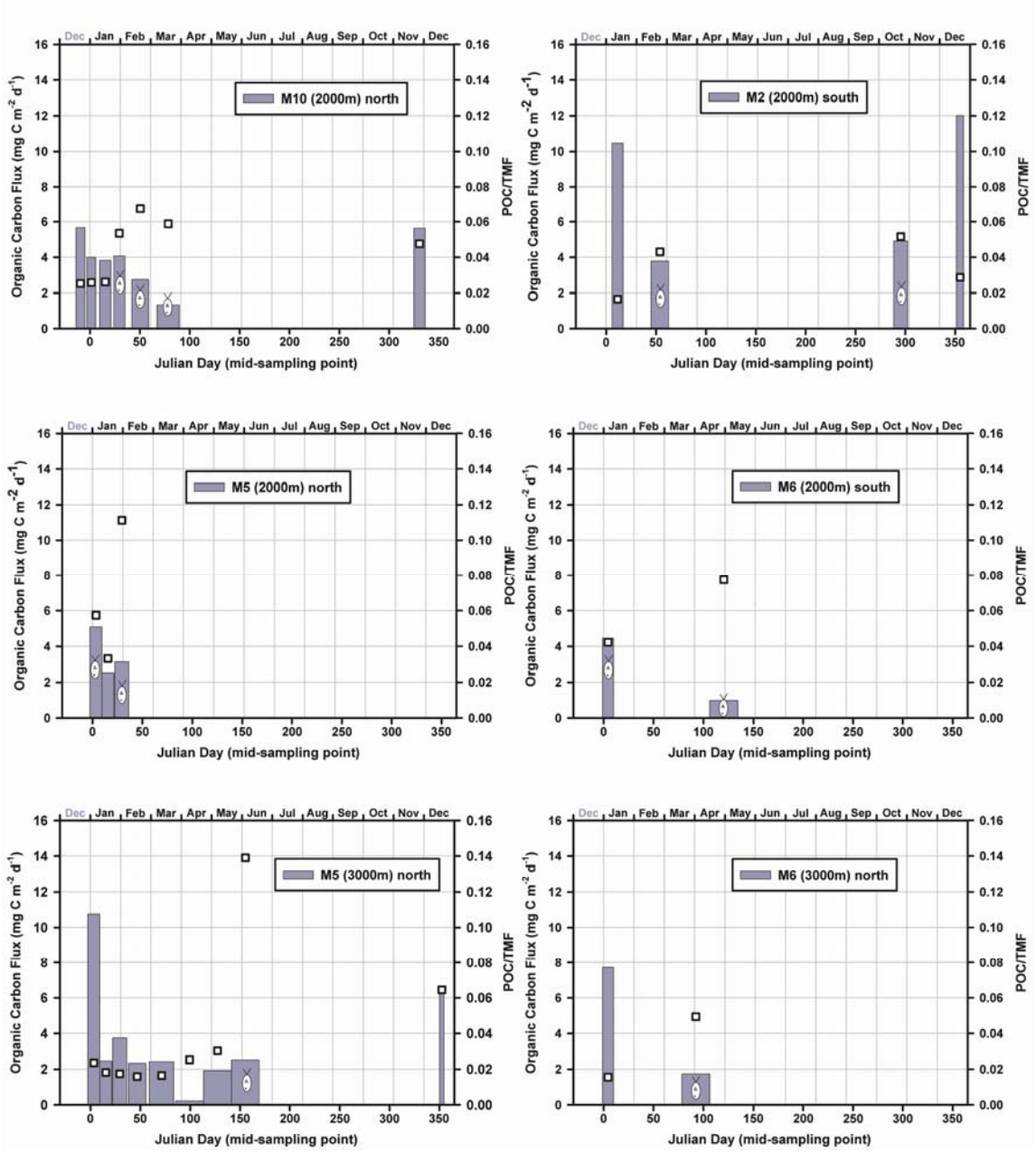

Figure 4.8 Profiles of organic carbon flux for each sediment trap. Fish icon denotes samples that were contaminated by fish debris. Width of bars represents the length of the sampling intervals such that the area of the bars is proportional to the integrated flux. Open white squares are the fraction of total mass flux that can be accounted for by organic carbon (POC/TMF). No bar indicates zero flux.

earliest sedimentation events from the bloom. This could result in an underestimate of POC flux north of the plateau, although aspects of inter-annual variability cannot be eliminated as the source of this difference. In contrast, the Dec-05 flux event observed at M2-2000m was similar to the Jan-05 event in both the fraction POC/TM and the absolute magnitude of POC flux, albeit with a shorter sampling interval.

4.4.4.2 Biogenic Silica

Fig 4.9 shows biogenic silica fluxes at each sediment trap location along with the fraction of total mass that can be accounted for by biogenic silica (BSi/TM). The biogenic silica content of particulate flux ranged between 0.3 and 0.8, indicating that it is the main component of deep-water particulate flux around the plateau, although there are certain times of year when this is not the case. The highest BSi fluxes observed were 440 mg BSi m^{-2} d^{-1} at M2-2000m and 400 mg BSi m^{-2} d^{-1} at M6-3000m, with correspondingly high BSi/TMF values of 0.7 and 0.8 respectively. At the northern stations M10-2000m and M5-3000m both the BSi Flux and the fraction BSi/TM decrease exponentially with time. M10-2000m and M5-3000m sampled the onset of the particulate flux from the 2005 bloom; the BSi fluxes were low and BSi/TM values were also relatively low at 0.45 and 0.35 respectively.

4.4.4.3 Calcium Carbonate

Fig. 4.10 shows calcium carbonate fluxes at each sediment trap location along with the fraction of total mass that can be accounted for by calcium carbonate (Cal/TM). The calcium carbonate content of particulate flux ranges between 0.12 and 0.65. This range indicates that whilst biogenic silica represents the major component of deep-water particle flux in the region, calcium carbonate is an important component of the flux both north and south of the plateau, especially during periods of low total mass flux. At the southern stations, the Cal/TM values that characterise the January flux event are relatively low, 0.14 at M2-2000m and 0.12 M6-3000m. The largest $CaCO_3$ flux of 154 mg m^{-2} d^{-1} was observed north of the plateau at station M5-3000m in early January.

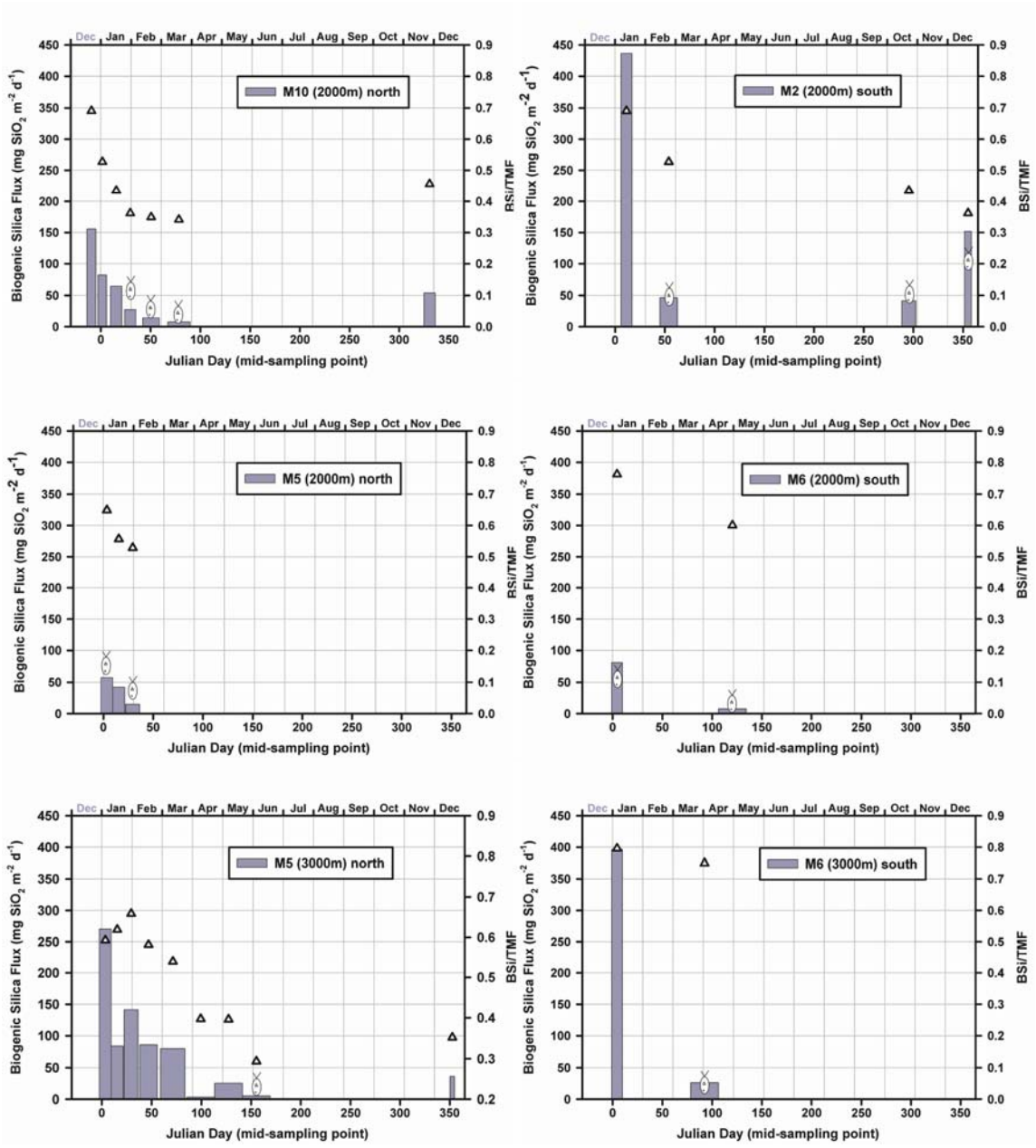

Figure 4.9 Profiles of biogenic silica flux for each sediment trap. Fish icon denotes samples that were contaminated by fish debris. Width of bars represents the length of the sampling intervals such that the area of the bars is proportional to the integrated flux. Open white triangles are the fraction of total mass flux that can be accounted for by biogenic silica (BSI/TMF). No bar indicates zero flux.

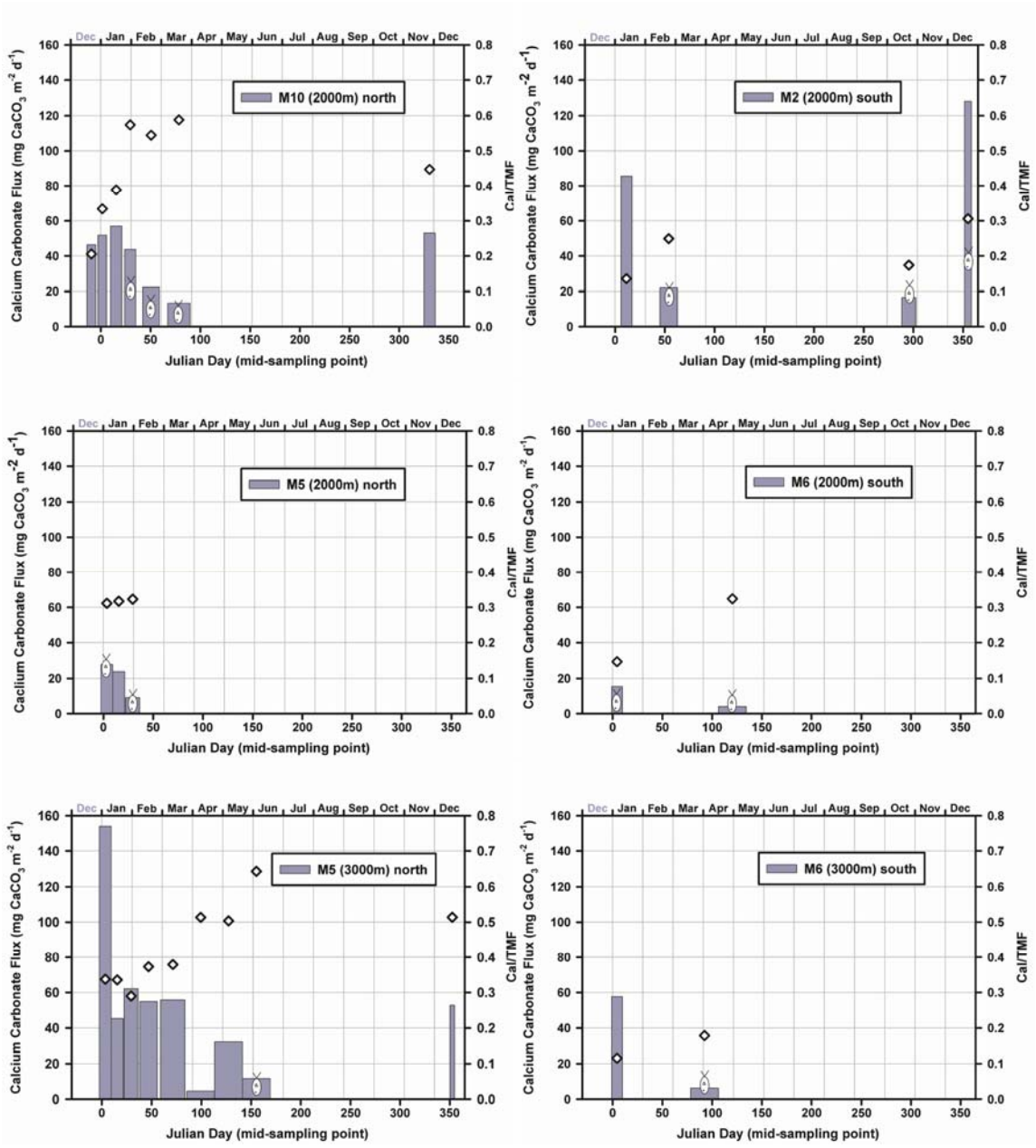

Figure 4.10 Profiles of calcium carbonate flux for each sediment trap. Fish icon denotes samples that were contaminated by fish debris. Width of bars represents the length of the sampling intervals such that the area of the bars is proportional to the integrated flux. Open white diamonds are the fraction of total mass flux that can be accounted for by calcium carbonate (CAL/TMF). No bar indicates zero flux.

4.4.5 Spatial variations in annual geochemical fluxes

The particle fluxes of the three major biogenic components have been normalised to a full annual cycle. Generally this normalisation procedure required minimal numerical manipulation since the deployment period almost represented a complete year. The total sediment trap collection intervals were 352, 357, 363, and 352 days at M2, M5, M6, and M10 respectively. The annual flux budgets for all biogenic components are presented in Fig. 4.11, both including and omitting samples contaminated with fish debris.

The annual budget of organic carbon flux displays the largest discrepancies between inclusion and omission of contaminated fish samples, corroborating the statistical analysis undertaken in section 4.4.4.1. The stations most severely affected are M5-2000m and M2-2000m; the deeper stations were less affected probably due to the depth distribution of the fish *N. coatsi*. Because of the difficulty in interpreting the impact of contaminated samples their contribution, is excluded from further analysis, although it is acknowledged that in some instances this may lend to an underestimate of annual fluxes. The largest annual POC flux was observed north of the plateau at M5-3000m followed by M10-2000m. The 1.7-fold difference between these stations is considered to be due to the deployment time of the sediment trap relative to surface chlorophyll features (see section 4.4.2). The annual POC flux south of the plateau is lower and more consistent than that measured to the north.

The annual flux of biogenic silica exhibits similar trends to those described for organic carbon. The largest BSi flux of 11.5 g SiO_2 m^{-2} yr^{-1} was also observed at M5-3000m whilst the BSi fluxes observed south of the plateau were relatively consistent with each other and also comparable to those measured at M10-2000m. Differences in annual flux budgets between the north and south of the Crozet Plateau are perhaps most obvious with respect to calcium carbonate. It is clear that the deep-water flux of calcite is enhanced north of the plateau, and the range of values obtained suggests this difference can range between a factor of 3.8 and 57.

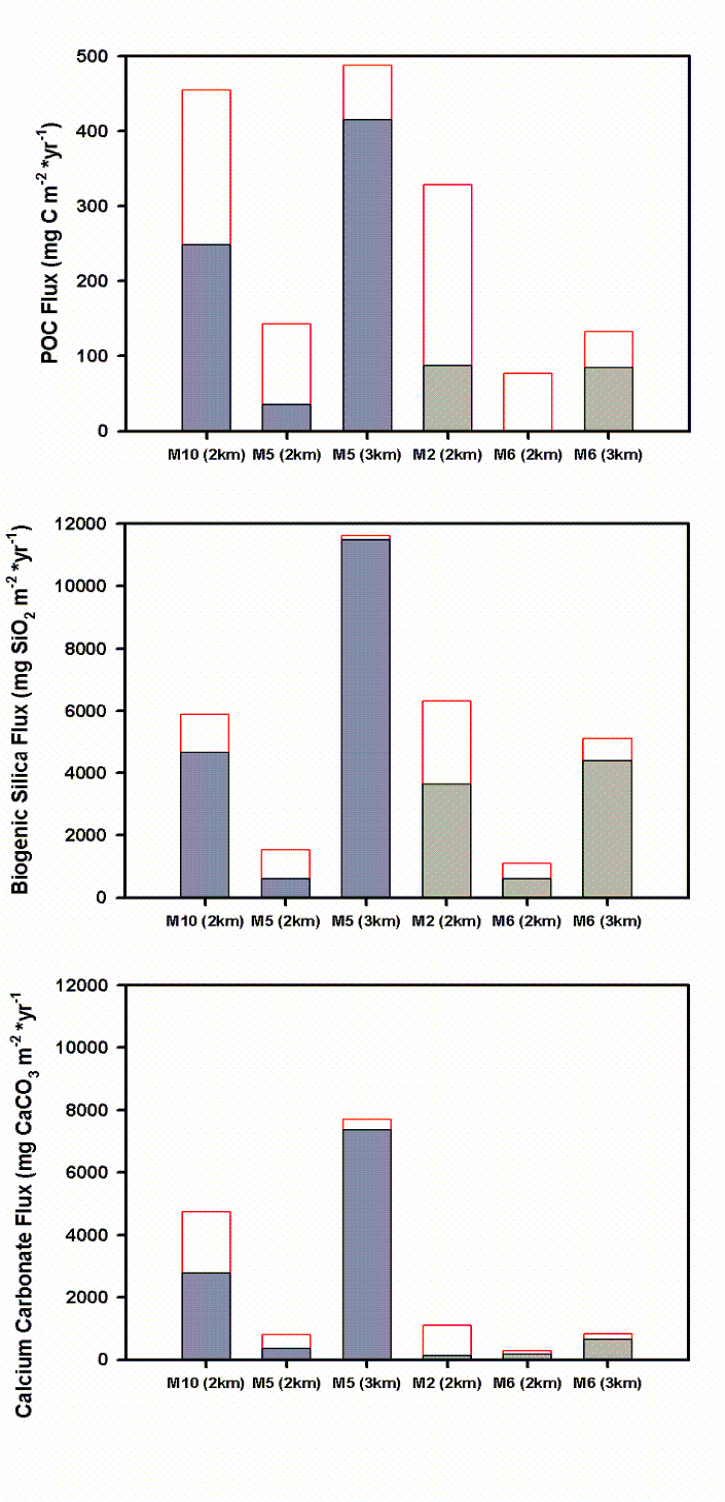

Fig 4.11 Annual fluxes of major biogenic components. Solid bars represent the annual budget excluding samples badly contaminated with fish debris; empty red bars are annual budgets including fish debris.

4.4.6 Molar ratios

Table 4.2 shows the seasonal changes in molar elemental ratios of the deep-water particulate flux at each site as well as the annual weighted means including and excluding contaminated samples. The annual $Si:C_{org}$ ratios are generally lower north of the plateau than they are to the south. Particles exported to 2000m north of the plateau have $Si:C_{org}$ values of 3.7 (M10) and 3.4 (M5). South of the plateau particles exported to 2000m have a higher $Si:C_{org}$ of 8.3 (M2). Si:N ratios are also much lower Both north and south of the plateau the $Si:C_{org}$ values are greater at 3000m reflecting the preferential remineralisation of carbon over silica as particles sink through the water column. There are distinct differences in the ratio of $C_{org}:C_{inorg}$ north and south of the plateau. North of the plateau annual $C_{org}:C_{inorg}$ ratios are <1 and south of the plateau they are >1.

4.4.7 Diatom Fluxes

Table 4.3 and 4.4 document the flux and relative abundance of the most important diatom species recorded in the sediment trap. At the southern sites, M2 and M6, the flux of diatom valves was dominated by *F. kerguelensis* which in all cases accounted for more than 80% of the total diatom frustules present. The largest flux of diatoms (78 x 10^6 valves m^{-2} d^{-1}) was also measured south of the plateau at M2 and corresponded to the largest biogenic silica flux of 7.3 mmol Si m^{-2} d^{-1} (Table 4.4). Centric diatoms generally accounted for the rest of the diatom flux contributing between 5-15%, and the pennate *C. criophilum* between 1-3%. At the northern sites, M10 and M5, fluxes of *F. kerguelensis* were significant but more variable than at the Southern stations and ranged between 0.4-71 x 10^6 valves m^{-2} d^{-1} which represented between 30-85% of total diatom cells enumerated. In contrast to the southern stations the centric diatom *E. antarctica* formed a major component of sinking diatom frustules north of the plateau, ranging between 15 and 70%. *E. antarctica* was in greater abundance during the early part of the flux profiles and also at M10 relative to M5.

Table 4.2 Molar elemental ratios of particles measured in Crozet sediment trap samples. Annual values are presented both including ($\sum_{inc.}$ fish) and excluding ($\sum_{exc.}$ fish) samples heavily contaminated with fish debris, which are marked by red typeset.

Cup #	Open date	Duration	C_{org}:C_{inorg}	C_{org}:N	Si:C_{org}	Si:N	Si:C_{inorg}
	dd/mm/yyyy	days	mole ratio				
M10 (49.50°S; 60.00°E; bottom depth: 2935m)							
2000m							
A1	21/12/2004	12	1.0	3.0	5.5	16.3	5.6
A2	02/1/2005	14	0.6	3.1	4.1	12.9	2.6
A3	16/1/2005	14	0.6	3.5	3.3	11.6	1.9
A4	30/1/2005	21	0.8	3.9	1.4	5.2	1.0
A5	20/2/2005	28	1.0	3.7	1.0	3.8	1.1
A6	20/3/2005	28	0.8	3.4	1.2	4.0	1.0
A17	27/11/2005	11	0.9	3.3	1.9	6.4	1.7
$\Sigma_{inc.}$ fish			**0.8**	**3.4**	**2.6**	**8.9**	**2.1**
$\Sigma_{exc.}$ Fish			**0.7**	**3.2**	**3.8**	**12.1**	**2.8**
M5 (46.00°S; 56.08°E; bottom depth: 4277m)							
2001m							
A1	28/12/2004	12	1.5	4.1	2.3	9.3	3.5
A2	09/01/2005	14	0.9	3.2	3.4	10.7	2.9
A3	23/01/2005	14	2.9	5.1	0.9	4.8	2.7
$\Sigma_{inc.}$ fish			**1.5**	**4.1**	**2.1**	**8.6**	**3.1**
$\Sigma_{exc.}$ Fish			**0.9**	**3.2**	**3.4**	**10.7**	**2.9**
M5 (46.00°S; 56.08°E; bottom depth: 4277m)							
3195m							
B1	28/12/04	12	0.6	2.2	5.0	11.0	2.9
B2	09/01/05	14	0.5	1.8	6.8	12.2	3.1
B3	23/01/05	14	0.5	1.7	7.5	12.5	3.8
B4	06/02/05	21	0.4	1.7	7.3	12.5	2.6
B5	27/02/05	28	0.4	1.6	6.5	10.4	2.4
B6	27/03/05	28	0.4	3.3	3.1	10.4	1.3
B7	24/04/05	28	0.5	3.2	2.6	8.4	1.3
B8	22/05/05	28	1.8	5.1	0.4	2.2	0.8
B19	18/12/05	7	1.0	4.1	1.1	4.5	1.1
$\Sigma_{inc.}$ fish			**0.5**	**2.3**	**4.6**	**10.3**	**2.5**
$\Sigma_{exc.}$ Fish			**0.5**	**2.1**	**5.2**	**10.9**	**2.6**

Table 4.2 ***continued***

Cup #	Open date	Duration	$C_{org}:C_{inorg}$	$C_{org}:N$	$Si:C_{org}$	Si:N	$Si:C_{inorg}$
	dd/mm/yyyy	days	mole ratio				
M2 (47.75°S; 52.86°E; bottom depth: 3856m)							
1973m							
A1	08/01/2005	8	5.7	4.8	8.3	40.0	47.2
A4	13/02/2005	21	7.7	6.0	2.4	14.8	18.8
A14	16/10/2005	14	0.7	5.2	1.7	8.8	1.2
A19	18/12/2005	7	16.0	4.3	2.5	10.8	40.2
$\Sigma_{inc.}$ fish			**2.5**	**5.0**	**3.9**	**19.2**	**9.6**
$\Sigma_{exc.}$ Fish			**5.7**	**4.8**	**8.3**	**40.0**	**47.2**
M6 (49.00°S; 51.50°E; bottom depth: 4221m)							
2007m							
A1	05/01/2005	11	2.4	3.9	3.6	14.1	8.7
A7	01/05/2005	28	2.0	4.7	1.6	7.4	3.1
$\Sigma_{inc.}$ fish			**2.2**	**4.2**	**2.9**	**12.0**	**6.4**
$\Sigma_{exc.}$ Fish		**n.**	**n.d.**	**n.d.**	**n.d.**	**n.d.**	**n.d.**
M6 (49.00°S; 51.50°E; bottom depth: 4221m)							
3160m							
B1	05/01/2005	11	1.1	5.6	10.2	57.2	11.4
B6	03/04/2005	28	2.3	4.1	3.0	12.3	7.0
$\Sigma_{inc.}$ fish			**1.4**	**4.9**	**7.6**	**37.5**	**10.5**
$\Sigma_{exc.}$ Fish			**1.1**	**5.6**	**10.2**	**57.2**	**11.4**

Table 4.3 Individual diatom species as a percentage of total diatom cells enumerated in the sediment trap samples. Red typset denotes samples that were heavily contaminated with fish debris. Shannon's diversity Index (H) and Eveness (EH) is also presented for each sediment trap sample.

Cup #	*Centric*	*Chaetoceros*	*Corethron*	*Dactyliosolen*	*Eucampia*	*Fragilariopsis*	*M. rostratum*	*Rhizosolenia*	*Thalassiothrix*	**H**	**EH**
M10 (49.50°S; 60.00°E; bottom depth: 2935m)											
2000m											
A1	0.1	-	1.1	0.0	71.0	27.7	-	0.03	-	0.66	0.37
A2	1.5	-	0.7	0.04	60.8	36.8	0.04	0.04	-	0.78	0.40
A3	0.8	-	0.2	-	61.8	37.1	-	0.04	-	0.72	0.45
A4	1.0	-	0.6	-	60.6	37.8	-	0.1	-	0.75	0.47
A5	1.0	-	0.1	-	62.1	36.8	-	-	-	0.72	0.52
A6	1.2	-	-	-	40.6	58.2	-	-	-	0.73	0.67
A17	2.4	-	0.1	-	15.8	81.8	-	-	-	0.55	0.40
M5 (46.00°S; 56.08°E; bottom depth: 4277m)											
2001m											
A1	1.2	-	0.3	0.1	59.1	39.1	-	0.1	0.2	0.77	0.40
A2	1.7	-	0.7	0.03	46.7	50.7	0.03	0.1	-	0.82	0.42
A3	2.3	-	0.7	0.1	33.4	63.4	0.05	0.05	0.05	0.80	0.38
M5 (46.00°S; 56.08°E; bottom depth: 4277m)											
3195m											
B1	2.6	-	0.1	-	48.1	49.1	-	-	-	0.81	0.58
B2	2.3	-	0.6	-	49.2	47.9	-	0.05	-	0.82	0.46
B3	6.4	-	0.9	0.04	36.0	56.4	0.1	0.1	0.1	0.93	0.45
B4	6.3	-	0.8	0.2	34.8	57.8	-	0.1	-	0.87	0.45
B5	5.6	-	0.7	0.2	19.3	73.9	0.2	0.1	-	0.77	0.39
B6	3.9	-	-	-	25.2	70.9	-	-	-	0.72	0.65
B7	3.3	-	0.1	0.04	13.0	83.5	-	-	0.1	0.54	0.30
B8	2.3	-	-	-	12.0	85.7	-	-	-	0.47	0.43
B19	3.7	-	-	0.03	10.7	85.5	0.03	-	-	0.50	0.28

Table 4.3 ***continued***

Cup #	*Centric*	*Chaetoceros*	*Corethron*	*Dactyliosolen*	*Eucampia*	*Fragilariopsis*	*M. rostratum*	*Rhizosolenia*	*Thalassiothrix*	**H**	**E_H**
M2 (47.75°S; 52.86°E; bottom depth: 3856m)											
1973m											
A1	15.4	0.2	1.7	0.7	0.5	80.6	0.05	0.2	0.6	0.65	0.30
A4	13.6	0.1	1.7	0.5	-	83.4	-	0.3	0.4	0.57	0.29
A14	9.5	-	1.5	0.1	-	88.4	-	0.2	0.3	0.43	0.24
A19	14.5	-	0.8	0.1	0.8	83.4	-	0.1	0.3	0.54	0.28
M6 (49.00°S; 51.50°E; bottom depth: 4221m)											
2007m											
A1	7.6	0.3	2.2	0.9	0.6	87.2	0.1	0.4	0.6	0.55	0.25
A7	2.3	-	0.8	0.1	0.9	95.8	0.1	-	0.1	0.23	0.12
M6 (49.00°S; 51.50°E; bottom depth: 4221m)											
3160m											
B1	14.2	0.2	3.2	0.9	-	80.8	0.1	0.4	0.3	0.66	0.32
B6	4.8	0.0	0.8	0.3	-	93.8	0.1	0.2	0.1	0.28	0.15

Table 4.4 Fluxes of diatoms into sediment traps (10^6 valves m^{-2} d^{-1}). Red typeset denotes contaminated samples

Cup #	*Centric*	*Chaetoceros*	*Corethron*	*Dactyliosolen*	*Eucampia*	*Fragilariopsis*	*M. rostratum*	*Rhizosolenia*	*Thalassiothrix*	*Total cells*
M10 (49.50°S; 60.00°E; bottom depth: 2935m)										
2000m										
A1	0.030	-	0.282	-	17.550	6.838	-	0.008	-	24.707
A2	0.260	-	0.127	0.007	10.321	6.251	0.007	0.007	-	16.980
A3	0.139	-	0.039	-	10.777	6.466	-	0.007	-	17.429
A4	0.085	-	0.050	-	5.371	3.348	-	0.005	-	8.859
A5	0.036	-	0.004	-	2.227	1.319	-	-	-	3.585
A6	0.033	-	-	-	1.106	1.585	-	-	-	2.724
A17	0.231	-	0.005	-	1.551	8.005	-	-	-	9.793
M5 (46.00°S; 56.08°E; bottom depth: 4277m)										
2001m										
A1	0.02	-	0.01	0.00	1.11	0.73	-	0.00	0.00	1.88
A2	0.04	-	0.02	0.00	0.97	1.06	0.00	0.00	-	2.08
A3	0.01	-	0.00	0.00	0.19	0.36	-	-	-	0.56
M5 (46.00°S; 56.08°E; bottom depth: 4277m)										
3195m										
B1	0.434	-	0.021	-	7.897	8.052	-	-	-	16.403
B2	0.362	-	0.090	-	7.786	7.590	-	0.008	0.004	15.840
B3	1.239	-	0.176	0.009	6.967	10.923	0.017	0.017	0.026	19.374
B4	0.689	-	0.112	0.008	3.610	7.759	-	0.012	0.012	12.203
B5	0.607	-	0.081	0.019	2.101	8.029	0.019	0.009	-	10.864
B6	0.057	-	-	-	0.365	1.027	-	-	-	1.449
B7	0.244	-	0.008	0.003	0.963	6.169	-	-	0.006	7.392
B8	0.038	-	-	-	0.196	1.405	-	-	-	1.639
B19	3.070	-	0.027	0.027	8.809	70.742	0.027	-	-	82.702

Table 4.4 ***continued***

Cup #	*Centric*	*Chaetoceros*	*Corethron*	*Dactyliosolen*	*Eucampia*	*Fragilariopsis*	*M. rostratum*	*Rhizosolenia*	*Thalassiothrix*	*Total cells*
M2 (47.75°S; 52.86°E; bottom depth: 3856m)										
1973m										
A1	12.00	0.17	1.35	0.52	0.39	62.89	0.04	0.14	0.48	77.99
A4	1.20	0.01	0.15	0.04	-	7.36	-	0.03	0.03	8.83
A14	1.43	-	0.23	0.01	-	13.27	-	0.03	0.04	15.02
A19	5.57	-	0.31	0.05	0.31	32.02	-	0.03	0.11	38.39
M6 (49.00°S; 51.50°E; bottom depth: 4221m)										
2007m										
A1	0.785	0.032	0.233	0.096	0.064	9.033	0.013	0.038	0.064	10.358
A7	0.066	-	0.024	0.002	0.026	2.789	0.002	-	0.003	2.913
M6 (49.00°S; 51.50°E; bottom depth: 4221m)										
3160m										
B1	4.109	0.054	0.925	0.249	-	23.356	0.022	0.108	0.097	28.920
B6	0.363	-	0.060	0.026	-	7.161	0.004	0.012	0.010	7.635

4.5 Discussion

From the analysis in section 4.4 the 3000m traps deployed at M5 and M6 provide the most accurate representation of particle fluxes from north and south of the plateau. They are the least affected by the problem of fish contamination, and because of their deployment depth the particles they sampled are likely to have originated from the peak in chlorophyll biomass.

4.5.1 Strength of the biological carbon pump in the PFZ of the Southern Ocean

Deep-water particle fluxes south of the plateau in the HNLC control area are characterised by a short-lived flux event constrained to an 8-10 day period in January 2005 (Fig. 4.7-4.10). In contrast the particle fluxes from the region north of the plateau are sustained for a longer period of time. Despite the brevity of the particle flux events south of the plateau the magnitude of total mass, organic carbon and biogenic silica flux is equal to and greater than the largest fluxes recorded north of the plateau over a similar time period (e.g. 8-10 days). In contrast particle fluxes from the region north of the plateau are sustained for a longer period of time such that annual fluxes of all components reported are greater (Fig 4.11). The 4-fold increase in annual POC fluxes is the first direct evidence to suggest that the addition of iron to an otherwise HNLC system can increase the export of organic carbon to the deep ocean. This corroborates the inferences made from short shallow sediment trap deployments (Salter *et al*., 2007).

4.5.1.1 Comparison of carbon fluxes with Southern Ocean fertilisation experiments

It has been difficult in artificial iron fertilisation experiments in the Southern Ocean to demonstrate an obvious increase in POC flux, although enhanced phytoplankton growth has been observed in every case (de Baar *et al*., 2005). SOIREE took place in February 1999 at 61°S 140°E, and over the 13-day observation period, no measurable changes in POC flux were observed either by using the ^{234}Th method (Charette and Buesseler, 2000), or 2-3 day shallow sediment trap deployments (Nodder *et al*., 2000). EisenEx took place in November 2000 at 48°S 21°E, and 22 days of ^{234}Th measurements showed

no differences between activities IN versus OUT of the fertilised patch (Buesseler *et al*., 2004).

SOFeX took place in January-February 2002 and involved the addition of iron to high Si (60µM) waters south of the PFZ (66°S 172°W) and low Si (2.5µM) waters north of the PFZ (55°S 172°). In the high-Si waters south of the PFZ ^{234}Th measurements (100m) indicated an increase of 7mmol C m^{-2} d^{-1} between the fertilised and control patch, or 225mmol C m^{-2} over the course of the 28-day experiment (Buesseler *et al*., 2004). Elongation of the fertilised patch north of the PFZ rendered any comparative thorium estimates obsolete. Evidence for enhanced POC flux in the low-Si waters north of the PFZ were obtained using an autonomous float to measure particle abundances. This approach provides a lower limit of 120 to 190 mmol C m^{-2} for 100-m POC flux and an upper limit of 760 to 1170 mmol C m^{-2} (50 days) depending which set of assumptions are followed (Bishop *et al*., 2004). There may be further uncertainties associated with these estimates regarding the calibration of the data. ^{234}Th measurements were used to convert particle abundances to carbon export. Since no convincing ^{234}Th measurements were conducted north (low-Si) of the PFZ, Bishop *et al*. (2004) used ^{234}Th data from the high-Si waters south of the PFZ. This calibration seems flawed when considering the central hypothesis of SOFeX was that a lack of dissolved silicate as well as iron would limit both biomass growth and carbon export (Coale *et al*., 2004).

Blain *et al* (2007) are the first to publish estimates of upper-ocean carbon export from a naturally fertilised bloom in the Southern Ocean (Kerguelen Plateau). ^{234}Th estimates suggest a difference of 11 mmol C m^{-2} d^{-1} between the bloom area (A3) and HNLC control area (C11). This is comparable to the SOFeX estimate of 7mmol C m^{-2} d^{-1} (Buesseler, 2004), but when integrated over the much longer time-scale of the natural bloom (≈90 days) the POC export at 100m is substantially larger (1100 mmol C m^{-2}) than the SOFeX estimate (225mmol C m^{-2}). Performing similar calculations with annual deep-flux data from the +Fe region north and HNLC control region south of the Crozet Plateau, normalised to 100m (Martin *et al*., 1987), indicates excess POC export of 565 mmol C m^{-2}, about half the estimate from the Kerguelen Plateau. It is possible that the thorium-derived POC flux estimates from the Kerguelen Plateau could be a slight over-

estimate. ^{234}Th fluxes are unlikely to have been constant for the entire period (90 days) of the bloom and are often observed to increase during the declining phase of a bloom (Savoye *et* al., 2004; Chapter 2). Also estimating 100m POC fluxes from data measured at 3000m with a normalisation procedure that has no observational validity in the Southern Ocean may introduce errors to the Crozet-derived estimates. Alternatively it could be that the observational discrepancy between the two naturally fertilised blooms is systematic since inter-annual variations in POC flux can often vary by a factor of two or more at the same site (e.g. Chapter 5). Despite these considerations estimates of carbon flux from naturally fertilised systems exceed those made from artificial experiments in the Southern Ocean.

4.5.1.2 Comparison of deep-trap carbon fluxes with other CROZEX estimates.

In addition to the deployment of deep-sediment traps, seasonal nutrient deficits (Sanders *et al*., 2007), new production measurements (Lucas *et al*., 2007), dissolved inorganic carbon estimates (Bakker *et al*., 2007), ^{234}Th measurements (Morris *et al*., 2007) and shallow drifting sediment trap deployments (Chapter 3; Salter *et al*., 2007), were all conducted to constrain carbon fluxes from the Crozex bloom. Table 4.5 summarises the various estimates of carbon export (100m) for the regions north and south of the Crozet Plateau. Measurements of new production and DIC deficits seem to be in fairly good agreement. In contrast estimates of export from ^{234}Th deficits, and normalised sediment trap data (both PELAGRA and deep traps) are relatively consistent with each other but approximately half of the new production and DIC measurements. These results support the scenario that a significant fraction of new production (i.e. 50%) may be advected or subducted as DOM (e.g. Toggweiler, 1990; Feely *et al*., 1995; Peltzer *et al*., 1996; Hernes *et al*., 2001).

Table 4.5 Comparison of sediment trap measurements with surface estimates of export production. Deep-sediment trap data have been normalised to 100m using the equation of Martin *et al*., 1987 and various estimates of the exponent *b* from Martin *et al*., 1987, Schlitzer, 2002; and Buesseler *et al*., 2007. ^{234}Th estimates are average thorium-derived carbon fluxes multiplied by bloom lengths of 60 days (north) and 30 days (south) as evidenced from satellite measurements (e.g. Fig 4.6)

Measurement	North g C m^{-2} ssn^{-1}	South g C m^{-2} ssn^{-1}	Reference
New Production (Nutrient Defecit)	30	5	Sanders et al., 2007
New Production (^{15}N Uptake)	20 - 50	5 - 15	Lucas et al., 2007
DIC defecit	30 - 40	15	Bakker et al., 2007
^{234}Th	12	5	Morris et al., 2007
PELAGRA	11-15	-	this study; Chapter 3
Sediment trap	4 - 14	1.5 - 4	this study

Convergence of carbon flux estimates from such a diverse range of techniques is highly improbable due to the different time and space scales over which the various methods integrate. In addition there are a range of methodical and systematic uncertainties that may contribute to the observed differences. Methodical uncertainties include i) remineralisation length scales used to normalise flux data, ii) using average thorium fluxes and integrating over the duration of the bloom, and iii) variations of C:^{234}Th ratios with particle size (Burd *et al*., 2007). Systematic uncertainties include i) decoupling of new and export production through the accumulation of DOM, ii) regeneration of nitrate above the mixed layer (e.g. Yool *et al*., 2007), and iii) applicability of Redfield stoichiometry for new production estimates (Lucas *et al*., 2007).

4.5.1.3 Comparison of deep-trap carbon fluxes with Southern Ocean data

There has only been one other sediment trap study conducted in the Polar Frontal Zone of the Indian Sector (Table 4.6a); Trull *et al*., 2001). Direct comparison of this study with Crozet indicate that depth-normalised (Martin *et al*., 1987) organic carbon fluxes were very similar to those obtained south of the plateau (0.4 and 0.2 g C m^{-2} yr^{-1}), and

significantly lower than those obtained from the iron-replete north (1.4 g C m^{-2} yr^{-1}). This provides a strong indication that the fluxes measured south of the plateau are typical of this particular environment and the elevated fluxes north of the plateau can be directly attributed to processes associated with the presence of iron. A broader comparison with different sectors and hydrographic regions of the Southern Ocean suggest that the organic carbon fluxes measured north of Crozet are slightly above the calculated mean and similar to fluxes originating from productive fronts.

4.5.2 Elemental stoichiometry of exported particles?

The deep sediment trap data highlight some important differences in the elemental stoichiometry of fluxes originating from iron-replete production north of the plateau relative to iron-deplete production to the south.

4.5.2.1 Si:C and Si:N ratios

Annual Si:C and Si:N ratios are larger in the particles exported south of the plateau relative to those exported north (Table 4.6b). Several studies demonstrate that diatoms take up substantially less silicic acid relative to nitrate under high-iron conditions (Hutchins and Bruland, 1998; Takeda, 1998; Brzezinski *et al*., 2002). Particles from both north and south of the plateau have Si:C ratios an order of magnitude higher than 0.13, a value commonly quoted for Fe-replete diatoms (Brzezinski, 1985). Such a large difference is unsurprising when considering the well-documented decoupling between particulate Si and C/N with depth (e.g. Nelson *et al*., 2002; Boyd *et al.,* 2006; Chapter 3). The lower Si:C and Si:N ratios in particles originating from the Fe-replete waters north of the plateau are consistent with these observations.

The decoupling of the silica and carbon/nitrogen cycles with depth imposes an important limitation on the interpretation of elemental molar ratios obtained from sediment trap studies. On one hand particle flux measurements were made at 3000m for both the iron-replete and iron-deplete areas surrounding the Crozet Plateau. However, the perspective that the attenuation of carbon flux with depth is linked to phytoplankton community

Table 4.6a Comparison with Southern Ocean sediment trap data, 1000m fluxes normalized using the equation of Martin *et al*., 1987

Site	Mooring Name	Southern Ocean Zone	Lat	Long	Year	Trap depth m	Corg g C m^{-2} yr^{-1} (1000m)	Corg mmol m^{-2} yr^{-1}	Reference
Atlantic (Polar Front)	PF3*	APF	50 °S	6 °E	1990	3196	12.5	384	Fischer *et al*., 2002
	PF5*	APF	50 °S	6 °E	1992	3219	0.5	14	Fischer *et al*., 2002
	PF7*	APF	50 °S	6 °E	1994	3056	1.0	33	Fischer *et al*., 2002
	PF8*	APF	50 °S	6 °E	1995	3110	1.4	43	Fischer *et al*., 2002
Atlantic (Bouvet Island)	BO1	SIZ	54 °S	3 °W	1991	2194	1.0	43	Fischer *et al*., 2002
	BO2	SIZ	54 °S	3 °W	1992	2183	0.9	38	Fischer *et al*., 2002
	BO5	SIZ	54 °S	3 °W	1995	2251	0.3	11	Fischer *et al*., 2002
Indian (Prydz Bay)	PZB - 1	SIZ	63 °S	73 °E	1998-99	1400	1.2	75	Pilskaln *et al*., 2004
Indian (Prydz Bay)	PZB - 2	SIZ	63 °S	76 °E	2000	3300	1.1	33.3	Pilskaln *et al*., 2004
Indian (Prydz Bay)	ANTARES M3	SIZ	63 °S	70 °E	1999	3500	0.6	16.7	Pilskaln *et al*., 2004
Indian (Chatham Rise)	SAZ 47	SAZ	47 °S	142 °W	1997-98	1060	0.8	63	Trull *et al*., 2001
						2050	1.6	70	Trull *et al*., 2001
						3800	1.8	48	Trull *et al*., 2001
Indian (Chatham Rise)	SAF 51	SAF	51 °S	142 °W	1997-98	3100	1.6	50	Trull *et al*., 2001
Indian (Chatham Rise)	PFZ 54	PFZ	54 °S	142 °W	1997-98	800	0.4	44	Trull *et al*., 2001
						1500	0.4	26	Trull *et al*., 2001
Indian (N Crozet Plateau)	M5	PFZ	46 °S	57 °E	2004-2005	3200	1.4	42.5	This study
Indian (S Crozet Plateau)	M6	PFZ	49 °S	52 °E	2004-2005	3000	0.2	7.1	This study
Pacific (AESOPS 1)	MS - 1	SAZ	53 °S	171 °W	1997	1981	1.8	83	Honjo et al., 2000
Pacific (AESOPS 2)	MS - 2	PFZ	57 °S	175 °W	1997	982	1.6	139	Honjo et al., 2000
Pacific (AESOPS 3)	MS - 3	APF	60 °S	170 °W	1997	1003	2.3	195	Honjo et al., 2000
Pacific (AESOPS 4)	MS - 4	SIZ	63 °S	170 °W	1997	1031	2.3	183	Honjo *et al*., 2000
Pacific (AESOPS 5)	MS - 5	SIZ (RSG)	66 °S	170 °W	1997	937	1.8	158	Honjo *et al*., 2000
Pacific (N Chatham Rise)	NCR	STF	43 °S	179 °E	1996-97	1000	7.5	625	Nodder and Northcote, 2001
Pacific (S Chatham Rise)	SCR	SAZ	45 °S	179 °E	1996-97	1000	1.8	150	Nodder and Northcote, 2001

Table 4.6b Molar ratios for Southern Ocean sediment trap studies, corresponding information can be found in Table 4.6a

Site	Trap depth m	$Si:C_{org}$	Si:N	$C_{org}:N$	$Si:C_{inorg}$	$C_{org}:C_{inorg}$	Reference
Atlantic (Polar Front)	3196	0.4	7.2	18.4	2.0	5.1	Fischer *et al*., 2002
	3219	0.1	0.6	6.7	0.3	3.9	Fischer *et al*., 2002
	3056	0.8	5.4	6.9	6.0	7.8	Fischer *et al*., 2002
	3110	0.9	7.3	8.5	1.4	1.7	Fischer *et al*., 2002
Atlantic (Bouvet Island)	2194	6.9	47.2	6.8	16.7	2.4	Fischer *et al*., 2002
	2183	1.3	9.3	7.4	3.4	2.6	Fischer *et al*., 2002
	2251	7.8	47.3	6.1	52.8	6.8	Fischer *et al*., 2002
Indian (Prydz Bay)	1400	4.1	21.7	5.3	34.4	8.3	Pilskaln *et al*., 2004
Indian (Prydz Bay)	3300	5.1	23.9	4.7	28.4	5.6	Pilskaln *et al*., 2004
Indian (Prydz Bay)	3500	3.1	n.d	n.d	26.0	8.3	Pilskaln *et al*., 2004
Indian (Chatham Rise)	1060	0.4	2.9	7.2	0.5	1.2	Trull *et al*., 2001
	2050	0.6	5.1	7.8	0.5	0.8	Trull *et al*., 2001
	3800	0.6	5.0	7.9	0.4	0.7	Trull *et al*., 2001
Indian (Chatham Rise)	3100	2.1	15.1	7.1	0.8	0.4	Trull *et al*., 2001
Indian (Chatham Rise)	800	3.7	22.3	6.0	3.9	1.1	Trull *et al*., 2001
	1500	4.9	33.5	6.8	4.4	0.9	Trull *et al*., 2001
Indian (N Crozet Plateau)	3200	4.5	10.3	2.3	2.5	0.5	This study
Indian (S Crozet Plateau)	3000	10.2	57.2	5.6	11.4	1.1	This study
Pacific (AESOPS 1)	1981	0.4	2.3	5.8	0.5	1.2	Honjo et al., 2000
Pacific (AESOPS 2)	982	1.8	12.7	7.0	2.1	1.2	Honjo et al., 2000
Pacific (AESOPS 3)	1003	2.3	17.6	7.5	3.6	1.5	Honjo et al., 2000
Pacific (AESOPS 4)	1031	5.1	29.9	5.8	8.7	1.7	Honjo *et al*., 2000
Pacific (AESOPS 5)	937	1.7	12.5	7.4	44.6	26.4	Honjo *et al*., 2000
Pacific (N Chatham Rise)	1000	0.0	0.2	9.7	-	-	Nodder and Northcote, 2001
Pacific (S Chatham Rise)	1000	0.1	0.8	10.5	-	-	Nodder and Northcote, 2001

structure (e.g. Boyd and Newton, 1999) and observations that iron availability induces community structure shifts (e.g. Gall *et al*, 2000) will inevitably act to modify the transmission of surface particulate ratios to depth in relation to iron supply. Furthermore elemental molar ratios in sediment traps are bulk particulate measurements such that the presence of non-silicifying phytoplankton (e.g. *Phaeocystis*) or heavily silicifying zooplankton (radiolarian, silicoflagellates) may act to decrease or increase Si:C/N ratios respectively. Although *Phaeocystis* dominated carbon biomass late in the season north of the plateau (Poulton *et* al., 2007 Seeyave *et al*., 2007), and has been documented to represent an important vector for carbon flux elsewhere in the Southern Ocean (DiTullio *et al*., 2000), taxonomy data from the deep sediment traps indicate they were an insignificant component of particle flux in the Crozet region (section 4.3).

In addition to the sediment trap data Moore *et al* (2007) observed a marked decrease in the net Si:N removal ratio when Fe availability was increased within *in vitro* experiments. Si:N removal ratios from the surface ocean were 2.5 times lower in the iron replete region (Sanders *et al*., 2007). However, absolute magnitudes of $SiOH_4$ removal were equivalent in the +Fe and –Fe regions (1 mol Si m^{-2}) indicating the decrease in the removal ratio was driven by an increase in iron-mediated nitrate removal and subsequent new production (e.g. Sanders *et al*., 2007; table 4.5; e.g. Franck *et al*., 2000). Despite consistency in the absolute drawdown of surface silicate (1 mol Si m^{-2} yr^{-1}) in +Fe and –Fe regions, the deep-water SiO_2 flux was 2-fold higher north of the plateau. This data thus indicates that enhanced atmospheric deposition during the LGM (Petit *et al*., 1999) potentially contributed to the increases in sedimentary opal accumulation (Charles *et* al., 1991; Mortlock *et al*., 1991) which appear to have accompanied higher organic carbon export in the glacial Subantarctic (Francois *et al*., 1997; Kohfeld, *et al*., 2005).

4.5.2.2 C_{org}:C_{inorg} ratios

The ratio of particulate C_{org}:C_{inorg} displayed strong regional variations between the iron-replete regions north of the plateau and the iron-deplete regions to the south. The majority of Southern Ocean particulate fluxes are characterised by C_{org}:C_{inorg} molar

ratios >1 (e.g. Honjo *et al*., 2000; table 4.6b). Unusually for the Southern Ocean the C_{org}:C_{inorg} molar ratio was <1 north of the plateau, and are comparable only to observations in the SAZ and PFZ in the Australian sector (Trull *et al*., 2001; Table 4.6a). The fact that these observations are limited to north of the polar front may represent the demarcation of a carbonate/silica biogeochemical front in the Southern ocean as previously inferred in the Pacific sector by Honjo *et al*., (2000).

The presence of such a biogeochemical front would be consistent with the gradual drawdown of silicic acid from Southern Ocean surface waters as they are transferred northwards into the Polar Frontal zone. Upon complete depletion of $SiOH_4$ calcifying coccolithophores may proliferate in response to non-limiting macro-nutrient concentrations and reduced competition from diatoms. This mechanism seems unlikely to be responsible for the observed differences in C_{org}:C_{inorg} molar ratios observed north and south of the plateau for two reasons i) both traps were deployed in the same water mass and the drawdown of $Si(OH)_4$ was the same and ii) the $CaCO_3$ fluxes appear to be mediated by heterotrophic foraminifera and coccolith-bearing tintinnids. Apparently iron-mediated production north of the plateau increases the abundance and resultant flux of heterotrophic organisms in response to an elevated food supply.

The export of PIC reduces the importance of POC export in terms of its influence on surface water carbon dioxide partial pressure because in seawater each mole of carbonate precipitation induces an ≈0.6 mole increase in aqueous CO_2 concentration (Frankignoulle *et al*., 1994). This effect must be considered when assessing the relative importance of physical and biological contributions to the seasonal cycle of pCO_2 (Metzl *et al*., 1999; Bakker *et al*., 2007). In theory it is possible to calculate the effect of enhanced $CaCO_3$ export by discounting the POC export by 0.6 times the PIC export. However, as discussed previously , the utilisation and comparison of elemental molar ratios determined from sediment traps deployed at different depths and in different regions is severely compromised by variable remineralisation of flux components. Although there are reports of biologically-mediated calcite dissolution above the lysocline (Archer, 1996; Milliman *et al*., 1999), it would be safe to assume that $CaCO_3$ flux dominated by foraminifera is less susceptible to shallow-water

dissolution by merit of fast sinking speeds. Organic carbon fluxes have been normalised to below the mixed layer (150m) using a given remineralisation co-efficient (e.g. Martin *et al*., 1990; Buesseler *et al*., 2007) and the recorded calcite fluxes (3000m) have been assumed to be representative of surface fluxes. Performing these calculations north of the plateau yields an annual organic carbon flux of 186 mmol C m^{-2} yr^{-1} and an inorganic carbon flux of 78 mmol m^{-2} yr^{-1}. Thus if we discount the POC flux by 0.6 times the PIC flux (78*0.6 = 48; 186-48=138) then we reduce the effect of atmospheric CO_2 sequestration by around 25%.

A calculation of this nature has errors too large for it to offer any meaningful quantitative information; it should be taken merely to highlight the following concept. Whilst increased iron-supply to HNLC regions can increase the strength and efficiency of the biological pump through enhanced organic carbon flux, the ecological response to an elevated food supply and the resultant PIC flux mediated by calcifying heterotrophic organisms may serve to counteract any net sequestration of atmospheric CO_2.

4.5.2.3 C:N ratios

The particulate C:N ratios are lower north of the plateau than they are to the south, but in both instances are significantly lower than Redfield values. Generally measurements of C:N ratios in exported particles, particularly at depth, are greater than Redfield values. There is some evidence of particulate C:N values of <6.6 in deep traps (table 4.6b; Honjo *et al*., 2000; Gupta and Kawahata, 2000) and mixed layer export (Kortzinger *et al*., 2001). Furthermore studies of the productive surface ocean have demonstrated substantial deviation from Redfield C:N stoichiometry associated with biological uptake (Karl *et al*., 1991; Banse, 1994; Sambrotto and Langdon, 1994). In these cases substantially more carbon was consumed relative to nitrogen than according to the Redfield ratio, a phenomenon termed “carbon overconsumption” by Toggweiler (1993).

The remarkable aspect of the elemental ratios calculated from the Crozex sediment traps is that every sample has a C:N ratio less than Redfield . Based on this observation, and the fact that similar values were obtained from an independent analysis of the samples (University of Liverpool; Appendix 1) it seems unlikely that the results represent an

analytical/methodical error. Furthermore the method used for the Crozet samples is identical to that developed for sediment trap samples from the North-East Atlantic which exhibit no obvious problems. The unique situation with regards to the Crozet samples is the level of contamination from fish and associated debris. The inclusion of fish-derived nitrogen-rich compounds such as keratin would lower C:N ratios, however all of the fish-debris was removed from the sample prior to analysis and samples with low C:N values do not correspond to contaminated samples.

The solubilisation of particles in sediment traps may also act to modify particulate C:N ratios; there is some evidence from the analysis of trap particles and supernatants (e.g. Kortzinger *et al*., 1994) that carbon-rich fatty acids can be lost to the preservative solution during storage. This however seems an unlikely explanation for the low C:N ratios since most evidence points towards the preferential solubilisation of nitrogen relative to carbon (Hansell and Newton, 1994; Kahler and Bauerfeind, 2000; Antia *et al*., 2006). In addition the analysis of surficial sediments obtained from multi-core deployments supports the observation of sub-Redfield C:N ratios north of the plateau, but interestingly not to the South. The cause of the low Redfield ratios in the particulate material remain unknown, detailed analysis of major compound classes may provide additional insights into the nature of the particulate material.

4.5.3 Species composition of diatom fluxes?

It is clear from the sediment trap taxonomy data that *F. kerguelensis* is an important component of particle flux both north and south of the plateau, whilst the significance of *E. antarctica* appears to be constrained to the regions north of the islands. *E. antarctica* was concluded to be an important vector for both Si and C fluxes based on the shallow sediment trap deployments (Chapter 3). In the northern traps there is a linear correlation between the fluxes of opal and *E. antarctica* frustules, with an r value of 0.90 ($P<0.01$; $n=8$) , which is higher than that for opal and *F. kerguelensis* ($r=0.57$; P-n.s; $n=8$) and opal and total diatom cells ($r=0.83$; $P<0.02$; $n=8$). The relationship with organic carbon

is less clear and likely reflects the scale of decoupling between silica and carbon with depth as discussed in section 4.5.3.1.

4.5.4.1 South

South of the plateau the species flux information derived from the sediment traps is in agreement with the direct sampling of surface community structure (e.g. Poulton *et al*., 2007) which documents the importance of the large diatoms *C. criophilium*, *D. antarcticus* and medium-sized *F. kerguelensis*. The presence of large diatoms in the surface and sediment trap assemblage of the "iron-deplete" HNLC area south of the plateau is not consistent with simple empirical models that predict increasing iron limitation with decreasing surface area to volume ratios (e.g. Timmermans *et al*., 2001, 2004). This apparent paradox serves as a useful template to outline the different ecological strategies employed by diatoms in HNLC regions.

Kinetic uptake specialists

Small diatoms (e.g. *Pseudo-Nitzchia*, *T. nitzschioides*) have large SA/V ratios and correspondingly low half saturation (K_μ) constants for iron and other macronutrients (Sunda and Huntsmann 1997; Timmermans *et al*., 2004). Based on this they may be expected to dominate in the low iron HNLC region south of the plateau. The grazing community of HNLC regions is generally characterised by a dominance of micro-and mesozooplankton (e.g. Seeyave *et al*., 2007) which have growth rates similar to those of small diatoms (Banse, 1982). Consequently a population of small diatoms may be controlled by severe grazing pressure (e.g Boyd and Abraham, 2001) irrespective of possessing a nutrient acquisition advantage (low K_μ) in a low-iron environment (e.g. south of the plateau). This inference is supported by the high grazing rates observed south of the plateau, which in some cases were >90% of primary production (Fielding *et al*., 2007).

Defence specialists

Large diatoms (e.g. *C. criophilium; F. kerguelnsis*) have small SA/V ratios and correspondingly high half saturation constants. Therefore as cell size increases diatom

cells are more susceptible to iron limitation (Sunda and Huntsmann, 1997; Timmermans *et al*., 2004). However, large diatom cells are likely to experience less severe grazing pressure (Smetacek *et al*., 2004; Thingstad *et al*., 2005) since they have robust siliceous frustules which provide an efficient defence (e.g. Hamm *et al*., 1999; Hamm *et al*., 2003) against predation by larger herbivores with correspondingly slower growth rates (Smetacek *et al*., 2004). Subsequently in low iron waters, such as those found to the south of the plateau, large diatoms with slow growth rates can accumulate in the surface over the course of the season.

The situation south of the plateau seems to reflect the notion of the "ecumenical iron hypothesis" (Morel *et al*., 1991) which suggests that the small size class represents a grazer-controlled phytoplankton population within an iron-limited ecosystem (e.g. Price *et al*., 1994) with growth rate limitation of large phytoplankton being the principal cause of the HNLC condition. Thus the "ecological success" of large diatoms south of the plateau is probably attributable to decreased mortality offsetting iron-limited growth rates (e.g. Smetacek *et al*., 2004). In section 4.5.3.1 physiological mechanisms were proposed to account for the observed differences in particulate Si:N ratios (and related $SiOH_4$:NO_3^- drawdown ratios) in the iron-replete north versus the iron-deplete south. It is clear from the sediment trap and surface taxonomy data that ecological factors can also influence nutrient cycling and export. In particular the complete removal of $Si(OH)_4$ and minimal drawdown of NO_3^- (Sanders *et al*., 2007) is consistent with the growth and export of heavily silicified diatoms in the Fe-limited southern region, as previously advocated (e.g. Smetacek *et al*., 2004). The depletion of silicic acid is the most likely candidate to explain the termination of biomass and rapid settling of Si-rich material observed in the sediment traps south of the plateau. The subsequent preferential remineralisation of organic material relative to opal helps to explain the very large Si:C and Si:N ratios measured in the sediment traps.

4.5.4.2 North

The CROZEX process study took place between 13th Nov 2004 and 15th Jan 2005 and an unfortunate consequence of this is that no surface taxonomy data exists to coincide with

the period of enhanced chlorophyll north of the plateau (Fig 4.12). Direct sampling of the surface community structure north of the plateau (yellow area in Fig 4.12) indicates that the small pennate *T. nitzschioides* dominated diatom cell abundance with the prymnesiophyte *Phaeocystis* sp. also present in large numbers (Poulton *et al*., 2007). These taxonomical observations coupled with low concentrations of dissolved iron of <0.4nM (Planquette *et al*., 2007) indicate the system north of the plateau was iron-limited by the time the observations began. The species information acquired from sediment traps can provide a long-term retrospective assessment of the upper-ocean community structure at each site. However, it is recognised that the processes of dissolution and grazing may serve to enrich heavily silicified and deplete lightly-silicified taxa in the traps respectively, potentially complicating any such interpretation.

The sediment trap observations (grey area in Fig 4.12) suggest that when $SiOH_4$ and DFe were presumably present in non-limiting concentrations the diatoms *E. antarctica* and *F. kerguelensis* were responsible for the large accumulation of phytoplankton biomass and subsequent export north of the Crozet Plateau. Interestingly observations from the nearby Kerguelen Plateau (50°S, 75°E) also report a dominance of the chain-forming diatom *E. antarctica* in the iron-mediated bloom area north-west of the plateau (Blain *et al*., 2007). Furthermore, Moore *et al*., (2007) report that medium-sized diatoms, especially *E. antarctica*, responded most favourably to iron-addition experiments. In a similar manner for arguments proposed to explain colony formation in *Phaeocystis* (Thingstad *et al*., 2005; Smetacek, 2004), chain formation in diatoms could be hypothesised to enhance defence by increasing apparent size without incurring a cost in terms of increased iron limitation through a lower SA/V (Moore *et al*., 2007).

This hypothesis could explain the response of the chain forming *Pseudo-Nitzschia* and *F. kerguelensis* to mesoscale iron addition experiments in the Southern Ocean (e.g. Gall *et al*., 2001). *F. kerguelensis* can survive in HNLC conditions as observed south of the plateau with slow growth rates and heavily armoured frustules (e.g. Hamm *et al*., 2003), the addition of iron artificially (e.g. Boyd *et al*., 2002) or naturally (i.e. north of the plateau) can thus cause a disproportionate response of this organism. The key difference between artificial and natural fertilisation experiments, and indeed north vs south of the

Crozet Plateau seems to be the role of *E. antarctica* in community structure and subsequent export. In addition paleoceanographic data seem to indicate an increase of *E. antarctica* frustules in the LGM sedimentary record (Burkle, 1982) which coincides with enhanced iron supply through aeolian deposition (Martin, 1990**).** However the complete absence of *E. antarctica* from artificial fertilisation experiments seems to indicate the species has an island affinity. The formation of winter resting spores and dominance in blooms associated with shallow topography appear to be the principle reasons connecting the species apparent importance in naturally-fertilised Southern Ocean blooms. Whilst the paleoceanographic data can be explained by increased sea-ice during the LGM and the retreating sea-ice acting as a pseudo-neritic environment seeding the water with *E. antarctica* resting spores (Armand *et al*., in press).

The combination of direct observations from the period of the cruise and information inferred from sediment trap assemblages (Fig 4.12) seems to suggest the sequence of events north of the plateau proceeded as follows. The circulation around the Crozet basin advects water over the plateau (Pollard *et al*., 2007) bringing it into contact with the sediments. *E. antartcica* winter resting spores and dissolved iron are thus transported northwards into an area of weak circulation with a residence time of approximately 60 days (Pollard *et al*., 2007). Upon the development of a favourable light climate a large bloom of *E. antarctica* and *F. kerguelensis* occurs north of the plateau with a large drawdown of nitrate (e.g. Sanders *et al*., 2007; Lucas *et al*., 2007) and CO_2 (Bakker *et al*., 2007). The depletion of $Si(OH)_4$ to concentrations of <2µM (Sanders, *unpublished data*) and concomitant reduction of bio-available iron in the declining phase of the bloom (e.g. Planquette *et al*., 2007) both contributed to the termination of the bloom. The resulting flux of particulate matter is heavily enriched in *E. antarctica* and *F. kerguelensis* frustules, with bulk particulate material possessing low Si:C and Si:N ratios relative to flux south of the plateau and elsewhere in the Southern Ocean (Table 4.6b). In the upper ocean the low concentrations of $Si(OH)_4$ and dissolved iron initiate a community shift to small pennate diatoms and *Phaeocystis* (e.g. Poulton *et al*., 2007); neither of which appear to be a significant component of flux leading to the

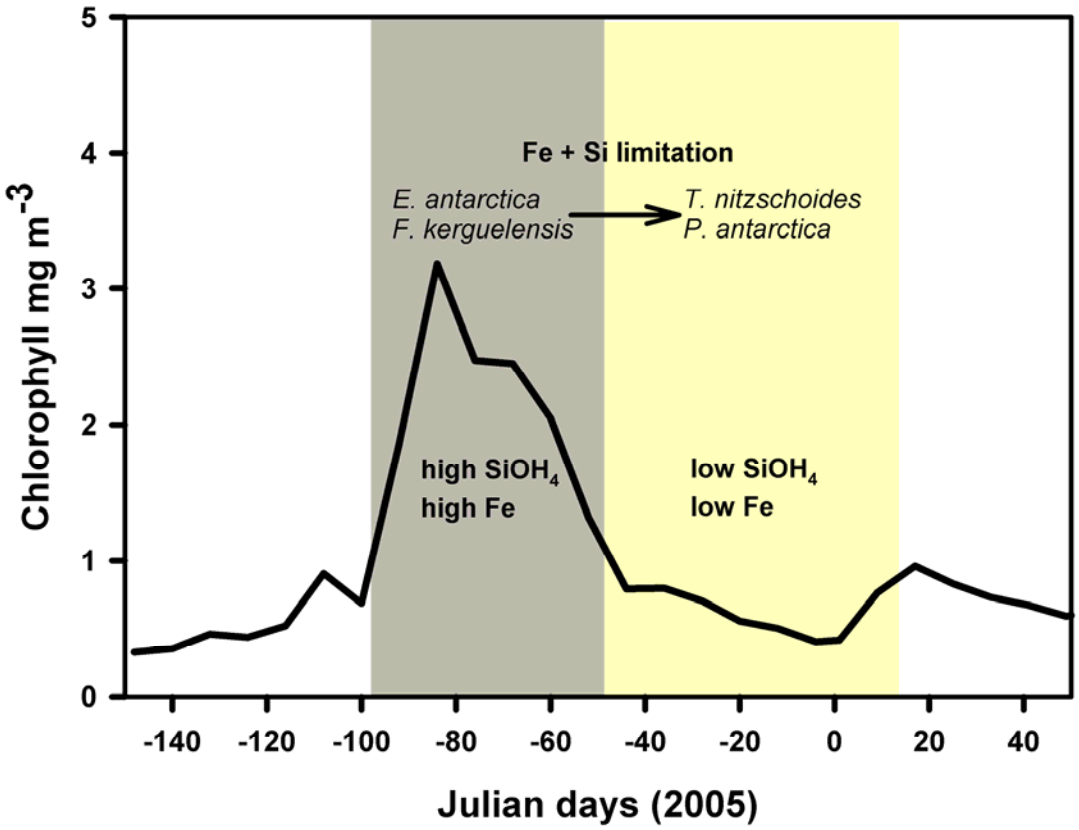

Fig 4.12 Seasonal progression of surface chlorophyll for the bloom area north of the Crozet Plateau as determined from remote-sensing data (e.g. Fig 4.5). Shaded yellow area represents the period of direct observations made by RRS discovery. Shaded grey area represents inferences made about the community structure based on diatom fluxes into the sediment trap.

assumption that they are heavily grazed. There is some evidence of *Phaeocystis* forming large colonies in high iron environments and successfully competing with diatoms even in high $Si(OH)_4$ waters (Smetacek *et al*., 2004) and thus their contribution to the biomass in the initial bloom and resulting particulate ratios measured in sediment traps cannot be discerned from the available observations. The relative importance of the physiological, ecological and biochemical processes in setting particulate Si:C/N ratios remains unclear. It is however obvious that they are a direct or indirect result of iron availability and as such have important implications for modern day and glacial/interglacial nutrient cycling e.g. Sarmiento *et al*., 2004; Martin *et al*., 1990).

4.5.4 Efficiency of the biological carbon pump

Despite consistent demonstrations of increased phytoplankton biomass in response to iron addition experiments (de Baar *et al*., 2005), demonstrating an increase in the strength and efficiency of the biological carbon pump has proved elusive. Here the strength of the biological carbon pump (S_{BP}) is defined as the magnitude of downward carbon flux from the euphotic zone, whilst the efficiency ($E_{BP(Z)}$) is the proportion of primary production (estimated from satellite data) exported to a specific depth (Equation 4.3). Sarmiento and Gruber (2006) define the efficiency of the biological carbon pump according to Equation 4.4.

$$E_{BP(z)} = FC_{org}(z) / IPC_{org} \quad \textbf{(4.3)}$$

$$E_{BP} = ([NO_3^-]_{depth} - [NO_3^-]_{surface}) / [NO_3^-]_{depth} \quad \textbf{(4.4)}$$

where $E_{BP(Z)}$ is the efficiency of the biological carbon pump at depth Z, $FC_{org}(Z)$ is the annual flux of organic carbon at depth Z, and IPC_{org} is the annual euphotic zone integrated primary production. In equation 4.4 E_{BP} is the efficiency of the biological carbon pump below the mixed layer, $[NO_3^-]_{depth}$ is the concentration of nitrate below the mixed layer and $[NO_3^-]_{surface}$ is the concentration of nitrate in the surface after the bloom has subsided, generally summer concentrations. Based on these theoretical constraints and using the Crozex sediment trap data the second tenet of Martin's iron hypothesis is examined.

Section 4.5.1 demonstrates that the strength of the biological carbon pump is greater in the iron-replete area north of the plateau relative to the iron deplete area to the south such that at 3000m fluxes of organic carbon are enhanced by a factor of 4. In order to determine the $E_{BP(Z)}$ then it is necessary to estimate annual integrated primary production. As described in Chapter 3 a strong empirical relationship exists between satellite-derived surface chlorophyll (Venables, 2007) and ^{14}C *in situ* observations of integrated primary production (Seeyave *et al*., 2007). Using this relationship and satellite-derived surface chlorophyll, time-series of integrated production were plotted for each sediment trap station. Summing the calculated integrated production over the

relevant time periods yields estimates of production of 105 g C m^{-2} *yr^{-1} for the bloom north of the plateau and 50 g C m^{-2} *yr^{-1} for the HNLC area to the south. With this estimate of production it is possible to calculate $E_{BP(3000m)}$ values of 0.52% north of the plateau compared to 0.15% south of the plateau. Comparing the POC collected by the traps with the apparent POC export based on seasonal nitrate depletion (assuming a Redfield C:N (Table 4.5; Sanders *et al*., 2007)) suggests that 1.5% of the surface export reached the 3000m trap north of the plateau and 0.5% reached the 3000m trap south of the plateau. Calculating E_{BP} based on the theoretical constraints of Sarmiento and Gruber (2006; Equation 4.4) and nitrate data from the cruise (Sanders *et al*., 2007) indicates that E_{BP} is 20% south of the plateau and 40% to the north. Despite the large uncertainties all three estimates indicate that the presence of iron can increase the efficiency of the biological pump by 2-3 times. Proving the second tenet of Martins "iron-hypothesis" has strong implications for theories regarding the glacial-interglacial cycling of atmospheric pCO_2 and iron fertilisation as potential mitigation strategy for anthropogenically-mediated climate change.

i) Glacial-interglacial CO_2 cycling

The sediment trap results from Crozet suggest that an enhanced supply of iron to the southern ocean during the LGM (Martin, 1990; Petit *et al*., 1999) may have contributed to this observation and the concomitant drawdown of atmospheric CO_2 (Martin, 1990). The important flux of carbon is that which is exported below the ventilation depth since it is this carbon that is removed from atmospheric contact on significant time-scales. The sediment trap data were normalized to the base of the winter mixed layer (Martin *et al*., 1987) as determined by Argo-floats (Venables *et al*., 2007) and multiplied by the approximate bloom area north of the plateau (e.g. Bakker *et al*., 2007). It was then assumed that over this given area the fluxes measured south of the plateau represent the "normal state of play" in the PFZ. Following on from this the difference in carbon flux for the same given area determined from sediment trap deployments to the north can be viewed as the direct effect of iron fertilisation. The result of these calculations suggest that natural iron fertilisation from the Crozet Islands increases POC export below the mixed layer by 0.5 Tg (10^{12}).

It is unclear to what region the measured fluxes apply: an entire circumpolar zone (e.g. the PFZ), the Indian sector, or a more reduced region around the Crozet Plateau, and also whether the fluxes measured in 2004/2005 can be taken as typical. If we assume that results are typical of the circumpolar PFZ then we can extrapolate the results and calculate that iron fertilisation would increase carbon export below the mixed layer to the effect of 0.02 Gt C yr^{-1} (Area of PFZ = $4.89*10^6$ km^2; Moore *et al*., 2000). This compares to the estimated removal of 170 Gt C yr^{-1} calculated (Martin, 1990) to account for the observed 80ppm difference in atmospheric pCO_2. It is clear that changes in export production in larger zones of the Southern Ocean (e.g. Moore *et al*., 2000), changes in sea-ice expanse and subsequent reduction of sea-air CO_2 fluxes (Stephens and Keeling, 2000), Southern Ocean nutrient dynamics (Sigman and Boyle, 2000) and their effect on low-latitude productivity (Matsumoto *et al*., 2002) are needed to explain the observed changes. The results from the Crozex sediment trap study are the first to demonstrate that iron fertilisation increases the deep-water sequestration of organic carbon through the enhanced strength and efficiency of the biological carbon pump.

ii) *Iron fertilisation as a climate mitigation strategy*

Using a dissolved iron input of 600nmol m^{-2} d^{-1} (MLD -100m) (Planquette *et al*., 2007), and a residence time of 100 days (Venables *et al*., 2007) for waters north of the plateau a winter iron reservoir of 6×10^{-5} mol Fe m^{-2} is calculated. Combining this number with the observations of deep-water carbon flux allows results in an Fe_{added}:$C_{sequestered}$ molar ratio of 1.4×10^{-3} at 3000m. This is one order of magnitude higher than similar estimates made during SOFeX (Busseler and Boyd, 2003) , 2 orders of magnitude higher than estimates from KEOPS (Blain *et al*., 2007) and 3 orders of magnitude higher than laboratory-based Fe:C ratios (Sunda and Huntsman, 1995). It is unsurprising that the Fe_{added}:$C_{sequestered}$ ratio is higher since it represents deep-water (3000m) rather than shallow-water (100-200m) sequestration efficiency (Blain *et al*., 2007; Buesseler and Boyd, 2003). It is the flux of organic carbon below the ventilation depth that will act to sequester atmospheric carbon dioxide, and deep observations indicate that the effect of iron in increasing this sequestration is much less efficient than shallow-water observations suggest. It is acknowledged that the uncertainties on the deep sequestration

efficiency are large, but they offer a cautionary note to climate change mitigation strategies based on iron fertilisation of the oceans. Furthermore, commercial enterprises selling carbon credits to global emissions markets view ocean fertilisation as a cheap CO_2 capture mechanism at approximately $1 per tonne of CO_2. The costing is based on laboratory Fe:C ratios (Sunda and Huntsman, 1995), and the observations from CROZEX of carbon sequestration efficiency indicate the real cost may be somewhere in the region of $1000 per tonne of CO_2.

4.6 Conclusions

Natural iron fertilisation has been demonstrated to increase the strength of the biological carbon pump. Comparison of values obtained in this study with those from artificial fertilisation experiments in the Southern Ocean indicates a larger increase in carbon flux results from natural iron fertilisation. Carbon fluxes measured south of the plateau are consistent with previously measured fluxes in similar environments. The carbon fluxes measured to the North are elevated relative to this "background flux" and are above average for the Southern Ocean as a whole. There are large differences in the elemental stoichiometry of particles between the iron-replete north and iron-deplete south. Combined with information regarding dissolved nutrient fields this information is consistent with paleoceanographic evidence suggesting carbon and silica export to the sediments north of the polar front was enhanced during the last glacial maximum, and supports the hypothesis that these changes are related to iron supply. The increased sedimentation of calcifying heterotrophs in response to the iron-mediated bloom north of the plateau lowered the C_{org}:C_{inorg} ratio of settling particles. This effect could potentially lower the sequestration of atmospheric carbon from iron-fertilised productivity due to associated changes in upper ocean carbonate chemistry. Conservative estimates indicate that this reduction of pCO_2 could be as high as 25%.Diatom fluxes recorded in the sediment traps suggest that the chain-forming diatoms *E. antarctica* and *F. kerguelensis* dominated the biomass and subsequent export of the iron-fertilised bloom north of the plateau. It is suggested that the ability of these diatoms to maintain their absolute size and increase their apparent size (chain-formation) represents the optimum compromise

between different ecological strategies of diatoms in the HNLC Southern Ocean. The evidence presented here points towards proof of the second tenet of Martin's hypothesis that the efficiency of the biological carbon pump is enhanced in the presence of non-limiting iron concentrations. The strength of the biological pump in transferring carbon to the deep ocean is perhaps not as high as previous studies suggest. This latter conjecture has important implications for hypotheses regarding glacial-interglacial CO_2 cycling and also the feasibility of iron fertilisation as a climate-change mitigation strategy.

5. SEASONAL AND INTERANNUAL VARIABILITY OF DEEP-WATER PARTICLE FLUXES AND THEIR EFFECT ON THE COMPOSITION OF AMINO ACIDS AND HEXOSAMINES IN THE NE ATLANTIC: IMPLICATIONS FOR THE BALLAST THEORY.

ABSTRACT

Sinking matter collected by deep-moored sediment traps (3000m) which were deployed in the north-east Atlantic (1998-2004) was analysed for the major flux components, organic carbon, calcium carbonate, biogenic silica, and the labile components amino acids and hexosamines. Total mass flux along with the major components showed distinct seasonal and inter-annual variations. Peak fluxes of amino acids and hexosamines closely followed bulk POC and PON fluxes, with the highest amino acid fluxes observed during the summer of 2001. Amino acid content normalised to bulk particulate organic carbon contents (AA-C%) ranged between 10 and 30% and was not related to the mineral composition of sediment trap samples. The fraction of organic carbon that could be accounted for by amino acids may represent both respiration and transformation into uncharacterisable material. The amino acid based degradation index (DI) [Dauwe *et al.*, Linking diagenetic alteration of amino acids and bulk organic matter reactivity. Limnol. Oceanogr. 44 (1999) 1809-1814] was used to quantify the degradation state of sinking particulate organic matter. The least degraded material was observed in the summer of 2001 which was coincident with the highest POC and lithogenic fluxes. A comparison was made with sediment trap samples collected in the Indian Sector of the Southern Ocean. Sinking organic material associated with high silica fluxes in the Southern Ocean was also relatively fresh based on the DI. There were no systematic relationships between the composition of mineral fluxes and the degradation state of organic matter in the sediment trap samples. Disparity between the DI and other molecular proxies (Asp/β-Ala, Glu/γ-Aba, AA-C%) demonstrates that both degradation and source are important factors in explaining the composition of amino acids in sinking particles. Multiple linear regression analysis suggests that mineral fluxes can only explain

between 5.1 and 16.5% of the observed variability in amino acid composition. Asp/Gly mol ratio and Ser + Thr mol% indicated that organic matter was mainly of diatomaceous origin and was independent of the large variations in carbonate and opal composition of the sinking flux. These results are consistent with the selective preservation of diatom cell walls. The lack of any systematic relationships between the molecular composition of labile amino acids and mineral fluxes suggest that the correlations between mineral fluxes and organic carbon fluxes derived in the "ballast-theory" papers are not related to differential protection by carbonate and opal mineral phases.

5.1 Introduction

Identifying the mechanisms of the transfer of particulate organic carbon from the euphotic zone to the deep-ocean in the form of sinking particles is crucial to our understanding of marine biogeochemical cycles. The downward flux of particulate carbon has a direct influence on the partitioning of carbon dioxide between the ocean and the atmosphere. Furthermore, in many marine environments, the primary flux vector is the main energy source to the abyssal ocean, influencing both distribution and species composition of benthic ecosystems (Thurston *et al*., 1998).

The vast majority of our knowledge about deep-water particle fluxes has been obtained through the deployment of moored-sediment traps. Despite uncertainties regarding trapping efficiencies (Scholten *et* al., 2001; Yu *et al*., 2001), swimmer contamination (Gust, 1992) and particle solubilisation (Antia, 2005), the value of sediment traps lies in their ability to "intercept" and store particles for chemical analyses. Syntheses of deep-moored sediment trap observations have been used to advocate the role of mineral fluxes in promoting POC export. Quantitative associations between POC fluxes and "ballast" mineral fluxes (Armstrong *et al*,. 2002), have been used to propose that calcite is more efficient than opal and lithogenic minerals in enhancing POC export (Francois *et al*., 2002; Klass and Archer, 2002). If minerals control the flux of POC to the deep ocean then they must do so by either protecting the organic matter from oxidation (Kiel *et al*., 1994; Mayer,

1999; Hedges *et al*., 2000; Ingalls *et al*., 2003; 2006) and/or by increasing the density and thus the sinking velocity of aggregates (Ittekkot and Haake, 1990; Hamm, 2002; Passow and De La Rocha, 2006). Increasing the sinking velocity of aggregates would reduce the "residence time" of POC in the water column and consequently it's association with bacteria. The preservation of labile organic material in sediments has been observed to occur via sorption to mineral surfaces (Kiel *et al*., 1994) and organic matter preserved over long-timescales is that which is associated with minerals (Hedges and Kiel., 1995; Ingalls *et al*., 2003).

Amino acids are highly labile constituents of all marine phytoplankton and have been used extensively as markers of organic matter source and diagenesis (Wakeham *et al*., 1997; Dauwe and Middelburg, 1998; Keil *et al*., 2000; Lee *et al*., 2000; Ingalls *et al*., 2003; 2006). Changes in amino acid composition with depth are well documented and demonstrate the degradation of cellular organic matter as it sinks through the water column and is incorporated in sediments (Dauwe and Middelburg, 1998; Lundgreen and Duinker, 1998; Gupta and Kawahata, 2000; Lee *et al*., 2000; Ingalls *et al*., 2003; 2006; Unger *et al*., 2005). There is also an additional fraction of organic carbon that is intimately associated with mineral phases since biominerals are deposited on a glycoprotein scaffolding that becomes embedded within the frustules (Lowenstam and Weiner, 1989; Swift and Wheeler, 1991). Analysis of Southern Ocean sediment traps has shown the contribution of amino acids locked into opaline and calcareous biominerals, which only account for between 0.7-4.5 and 0.29-0.54% respectively, of total hydrolysable amino acids in sinking particles (Ingalls *et al*., 2003) It is difficult to conceive that this biomineral-bound fraction can thus account for the observed correlations in deep-sediment traps (e.g. Klaas and Archer, 2002) although it becomes more important within sediments (Ingalls *et al*, 2003). The protective capacity of minerals, if indeed it exists, must in part rely on the adsorption of compounds onto mineral surface reducing the effect of extracellular enzymes and evidence of this in the water column has been previously reported (Tietjen and Wetzel, 2003).

The analysis of sediment trap material for total hydrolysable amino acids (AA) and hexosamines (HA) in the north-east Atlantic is limited to one study (Lundgreen and Duinker, 1998) providing no information on inter-annual variability. The seasonally and annually varying biogenic composition of particles at this site (Lampitt *et al*., 2001) provides a useful template to address questions critical to the ballast hypothesis: i) is the amino acid composition of organic matter related to the co-occuring biomineral phases, and ii) does the extent of organic matter degradation vary seasonally and inter-annually in response to ballast type?

5.2 Study Area

The study area is located in the middle of the Porcupine Abyssal Plain (ca 4850m depth) about 270km southwest of Ireland, at 49^{o}N 16.5^{o}W (Fig. 5.1). The sample location was initially chosen as part of the BENGAL project whose aim was to determine how the seabed community and the geochemistry of the sediments change seasonally in response to a highly seasonal input of organic matter from the overlying water column (Billet and Rice, 2001). Since logistic considerations for benthic sampling were paramount, the site was selected because it is a relatively flat area, remote from the continental slope to the east and the mid-ocean ridge to the west. The site lies in close proximity to 47^{o}N 20^{o}W, in the foothills of the Mid-Atlantic Ridge, which was studied extensively during the JGOFS North Atlantic Bloom Experiment (NABE) (Ducklow and Harris, 1993). Samples were also analysed from deep-sediment traps moored in the Indian Sector of the Southern Ocean as part of the CROZEX project, details of this sampling environment can be found in Chapters 3 and 4.

5.3 Methods

5.3.1 Sediment traps

All traps were large funnels with a baffle at the top (0.5 m^2 surface area) and a narrow opening at the bottom through which the particles fall into individual cups (McLane,

INC. Parflux 21 cup). Deployment schedules were programmed with a sampling resolution that reflected anticipated periods of high and low flux, full details of which can be found in Appendix 4. The 250 mL sample cups were filled with a preservative solution, prepared by adding 100 g of analytical grade NaCL to 19 L of unfiltered deep (>2000m) seawater from the trap deployment location. 1 L of formaldehyde (AnalR® grade, VWR international) was buffered to pH 8.6 with sodium tetraborate and added to the 19 L of hyper-saline seawater, and the solution left to stand for a period of 1 day.

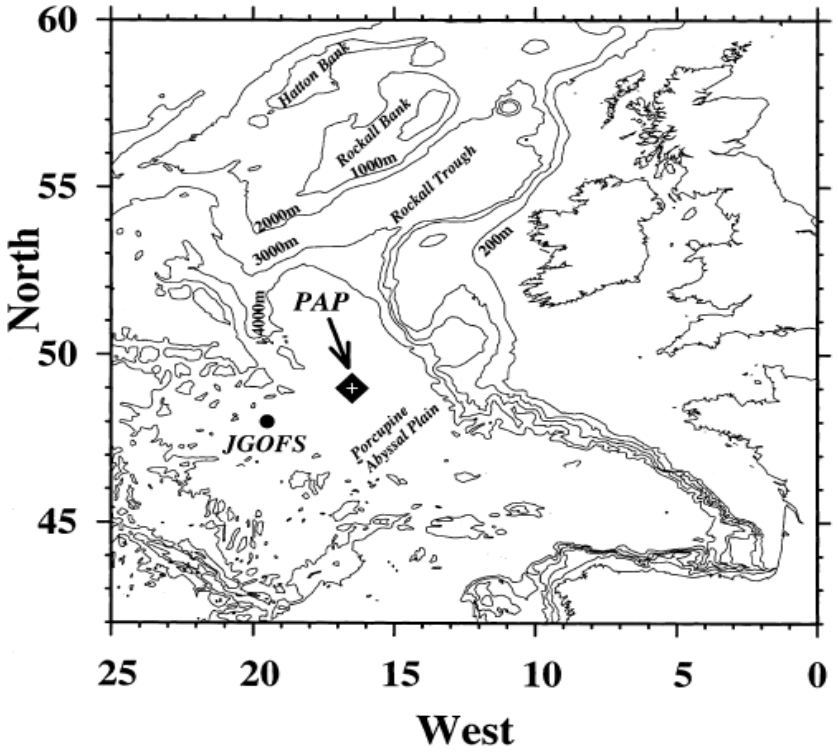

Fig 5.1 Map showing the location of the Porcupine Abyssal Plain (PAP) observatory and JGOFS North Atlantic Bloom Experiment (NABE) and bathymetry. Figure reproduced courtesy of Richard Lampitt.

5.3.2 Swimmers

Prior to chemical analysis of the particulate samples swimmers were removed from the sample with plastic forceps under a dissecting microscope (x50). Swimmers are defined as the zooplankton that have entered the sample cups alive and intact, and therefore do not represent the passive flux from the surface ocean (Michaels *et al*., 1990). The number of swimmers removed from each sample cup can be found in Appendix 4.

5.3.3 Sample splitting and total mass flux

The 250ml samples were split into 8 equal aliquots of equal volume using a rotary splitter (replication error <3% for this methodology; Richard Lampitt, pers. obs.) Depending on sample volume 1-5 these eighths were filtered onto cellulose nitrate filters (47mm, 0.45μm pore size) and the filtrate from 1 aliquot stored in a clean LDPE bottle (60mL). The samples and filters were subsequently rinsed with a 0.56 M ammonium formate solution (pH 7) to remove excess sea-salt and formalin. The sample was carefully removed with a metal spatula as a wet cake of material and transferred to pre-combusted (450^{o}C; 12 hours) glass vials and frozen at -20^{o}C. Frozen samples were freeze-dried over night and homogenised to a fine powder using the flat end of a metal spatula. This material was used to weigh samples for particulate organic carbon (POC), total organic carbon (TOC), biogenic silica (BSi) and total hydrolysable amino acid (THAA) measurements. Total mass flux was determined gravimetrically following the filtration of a 1/8th aliquot onto a pre-weighed cellulose nitrate filter (47mm diameter, 0.45 μM pore size). The filter was rinsed with 0.56M ammonium formate (pH 7) to remove salt and excess formalin and dried at 60^{o}C until a constant weight was achieved.

5.3.4 Chemical analyses

5.3.4.1 Total and organic carbon

TOC was determined using a Carlo-Erba NA-1500 elemental analyser following standardisation with acetanilide. 2-4mg of freeze-dried samples was weighed into pre-combusted (550^{o}C; 12 hours) silver cups which were formed into small capsules with metal spatulas. POC was determined using the same procedure on acidified samples (Nieuwenhuize *et al*., 1994). A 15µl aliquot of 20% HCl was added to the sample in order to remove calcium carbonate. After each aliquot was added the acid was evaporated by gently heating on a hot plate (<60^{o}C). The procedure was repeated until all carbonates were removed as evidenced by the absence of any effervescence upon addition of the acid, and then two more additions of acid were performed to ensure complete removal of inorganic carbon. Samples were subsequently rinsed with a 40 µl aliquot of ultra-pure water and dried on a hotplate at <60^{o}C. This procedure was repeated five times and the samples were then dried overnight at 50^{o}C. Care was taken to note any sample loss from silver cups and samples discarded if this was the case (Full details can be found in Appendix 1).

5.3.4.2 Biogenic silica

Biogenic silica was determined using a wet chemical technique modified from Mortlock and Froelich, (1989). Samples (3-5 mg) were weighed into clean polypropylene tubes. Particulate opal was converted into dissolved silicon using 0.2M sodium hydroxide for 3 hours at 100^{o}C. The extract was separated from the residue via centrifugation and the sediment residue was rinsed with ultrapure water and dried overnight (60^{o}C). The dissolved silicate was converted to the silico-molybdate complex (Strickland and Parsons, 1968) and the absorbance read at 812 nm with a Hitachi U-2000 spectrophotometer. Full details of these methods, including development and validation can be found in Appendix 2.

5.3.4.3 Total hydrolysable amino acids and hexosamines

Hydrochloric acid (3mL 6M) was added to 5-15mg of freeze-dried sediment trap material (e.g. Cowie and Hedges, 1992; Gupta and Kawahata, 2000). Before addition to the sediment, hydrochloric acid was degassed by gently bubbling pure argon through the solution for thirty minutes. The head-space in the vials was displaced by argon and the glass vials sealed and heated at 110^{o}C for 24 hours. The vials were removed from the heat source and allowed to cool for ten minutes. After centrifugation (3000 rpm; 15 mins) 1 ml of the hydrolysate was transferred to an Eppendorf vial and stored at -80^{o}C for analysis. On the day of analysis 250µL of hydrolysate was neutralised with 1M NaOH and diluted with Milli-Q water. 280µL of the neutralised sample and standard was added to a HPLC vial, followed by 15µL of *o*-methyl-threonine and 15µL of boric acid buffer (pH 8.3). For most amino acids detected operational blank values were <2% of sample concentrations. For methionine, valine, and ornithine blank concentrations represented 5.7, 8.5, and 49.8% of sample concentrations. Long-term statistical reproducibility calculated from repeat hydrolysation and analysis of the same sample was better than 10% for total hydrolysable amino acids. Full details can be found in Appendix 3.

Amino acids were analysed by High Performance Liquid Chromatography (HPLC) using pre-column (*o*-phtaldialdehyde (OPA)) derivatisation after acid hydrolysis (Lindroth and Mopper, 1979; Cowie and Hedges, 1992). Amino acids were separated on an Ascentis C_{18}, 15cm x 4.6mm x 3µm reverse-phase column with a mobile phase flow rate of 1ml/min. The analytical column was maintained at a constant temperature of 30^{o}C and fitted with an Alltech guard column. A binary gradient of methanol (eluant A) and 30mM Na-acetate (pH 7) and 2% THF (eluant B) was used to achieve chromatographic resolution. The solvent gradient is shown in Fig 5.2. Amino acids were identified and quantified by comparison to analytical standards (Sigma-Aldrich). All sample and standard peak areas were normalised to the internal standard *o*-methly-threonine (see Appendix 3). The amino acid OPA derivatives were formed online and detected by fluorescence using an excitation wavelength of 360nm and monitoring emission wavelengths at 430nm.

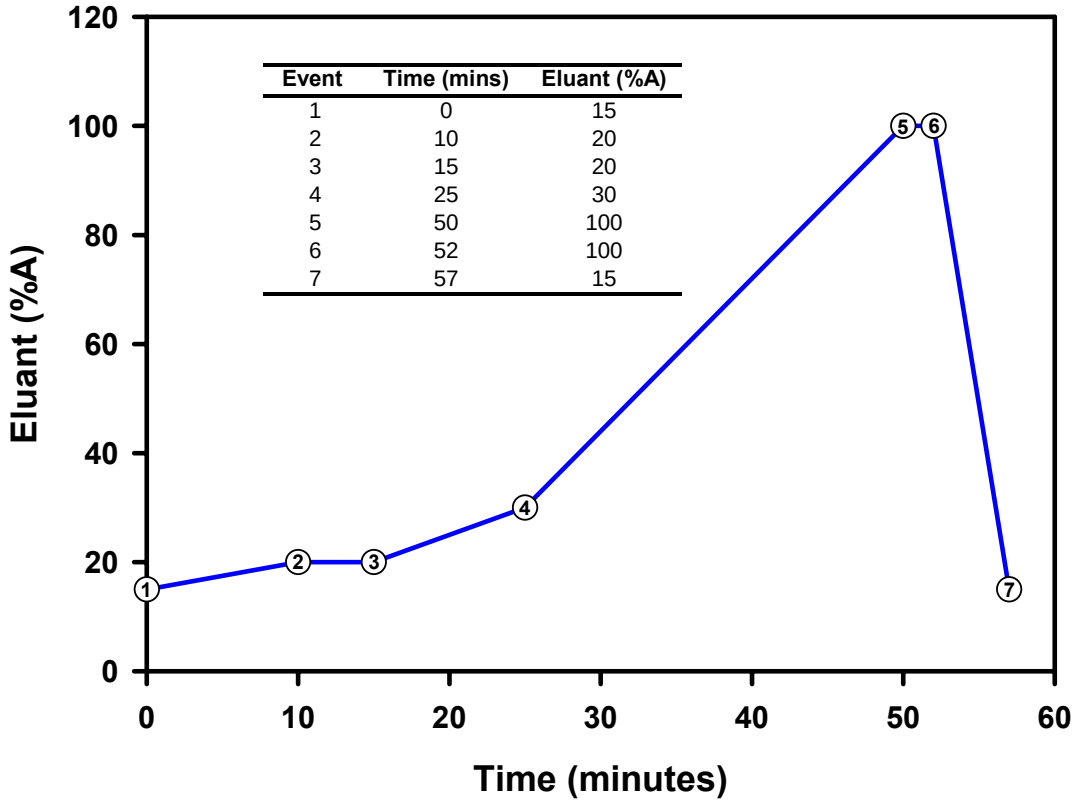

Fig 5.2 Solvent gradient used to separate amino acids and hexosamines

5.4 Results

5.4.1 Total Mass Fluxes at 3000m and 4700m

The 8-yr record of total mass flux at the PAP site for two trap depths (3000 and 4700m) is shown for samples collected from 1998 to June 2005 (Fig 5.3). As discussed previously (Lampitt *et al*, 2001) the magnitude of mass flux at this location exhibits distinct seasonal and inter-annual variability at both depths in the water column. Most years appear to exhibit a bimodal cycle of total mass flux with an initial peak occurring in spring and a second peak in summer, although the presence, timing and duration of these features is variable from year to year. The largest total mass fluxes were recorded during the summer of 2001. The trap at 3000m exhibits a

larger degree of seasonal variability than it's 4700m counterpart. Fig 5.4 shows the mass flux at 3000m and 4700m plotted as a function of time from 01/1998 – 06/2005, the solid red line represents the average total mass flux for the data set calculated from the period of particle flux maxima (Julian day 91-273), which is 99.0 at 3000m. It is clear that most years experience individual flux events that exceed the 8-yr average, but only in 1998 and 2001 are these events sustained for a prolonged period of time. The secondary flux maxima of 2001 represents the largest peak observed in the data set with an integrated value of 29.4 g m^{-2} (duration = 112 days).

The observations at 4700m (100 metres above bottom (m.a.b.)) are broadly similar to the features described at 3000m, although the seasonality is less clearly defined. In most instances the magnitude of the fluxes is equal to or greater than those observed at 3000m with the exception of 2001 (Fig 5.4 and 5.5). Traps set within 1000m of the seabed can be enhanced by re-suspended bottom sediments (e.g. Walsh *et al*., 1988; Lampitt *et al*., 2000; Lampitt *et al*., 2001) and also be subject to different particle origins (e.g.) Waniek *et al*., 2000). The organic composition of samples obtained from traps deployed near the sea-floor has also been noted to vary compared to samples from elsewhere in the water column (Kiriakoulakis *et al*., 2001), possibly related to reprocessing by benthopelagic fauna. For these reasons this chapter will focus on sediment trap samples collected at 3000m.

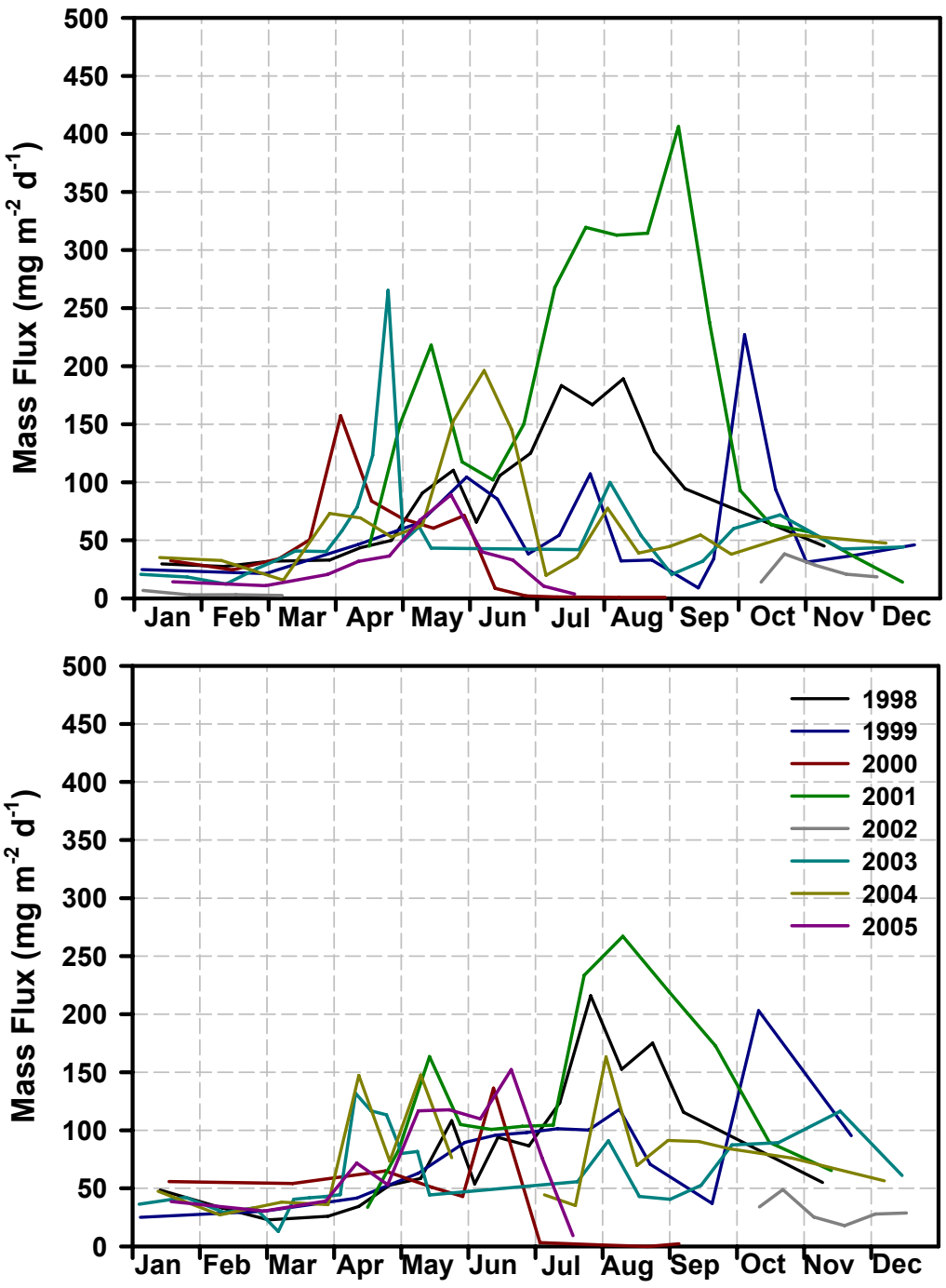

Fig. 5.3 Mass flux for the period 1998-2005 at a) 3000m and b) 4700m water depth

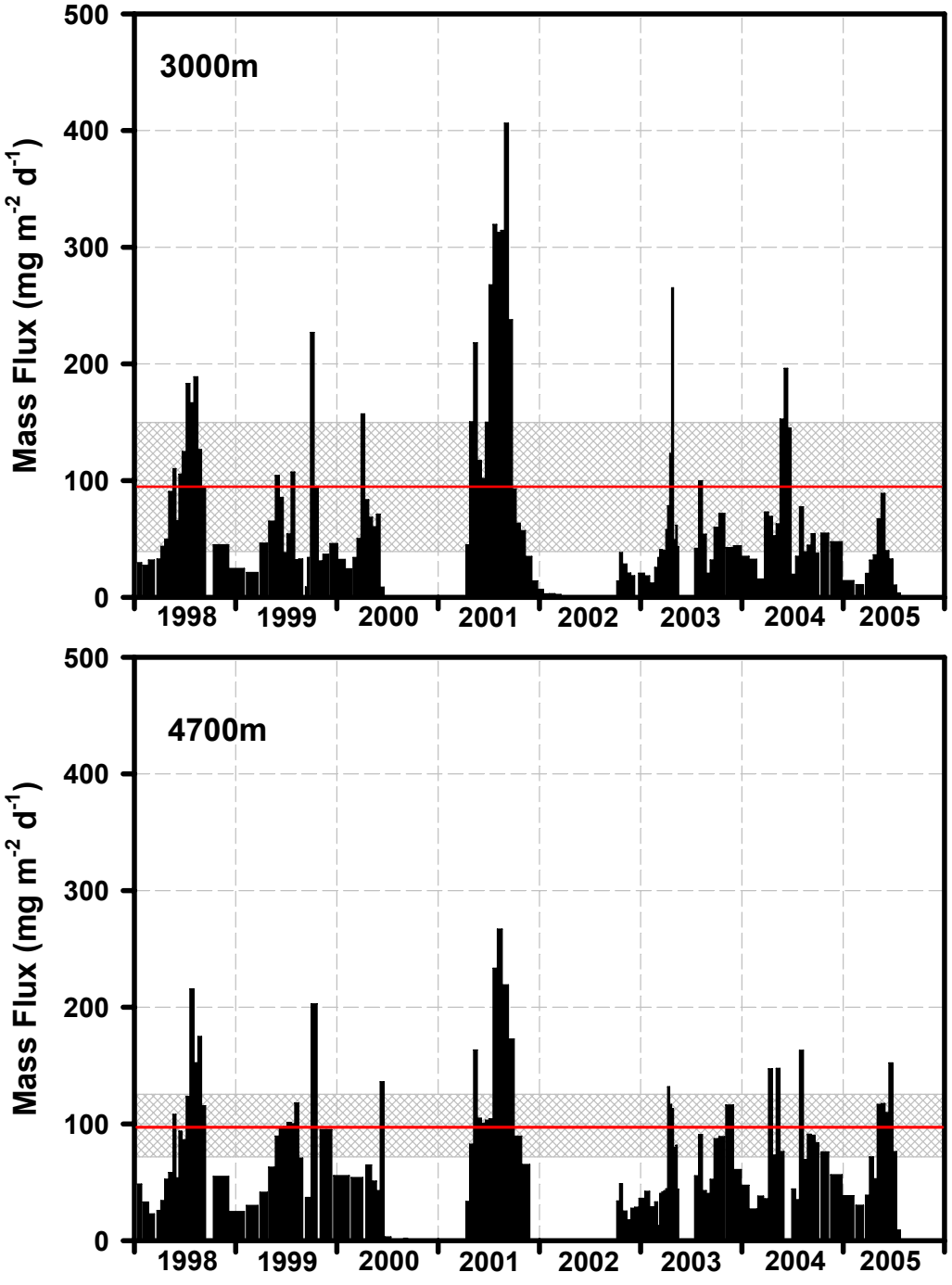

Figure 5.4 Inter-annual variability of mass flux at the PAP site at a) 3000m and b) 4700m. The solid red-line marks the average mass flux calculated from the period of particle flux maxima (Julian day 91-273). The hatched box is ± 1 S.D. of this average.

5.4.3 Organic carbon fluxes at 3000m

The seasonal and inter-annual variability of particulate organic carbon (POC) flux at 3000m is displayed in Figs 5.5 and 5.6. There are less POC data points than there are total mass flux data points because in some instances there was too little material for detailed chemical analysis. The patterns of inter-annual variability presented for total mass flux (Figs 5.3, 5.4) are similar for the POC flux profiles albeit with some differences. From Fig. 5.7 it is clear that POC and total mass flux are well correlated for a large majority of the data set, but when the POC flux is >35 mg C m^{-2} d^{-1} a separate correlation with a much steeper gradient is required to define the relationship between the two parameters. This set of disparate data points are largely the result of the summer 2001 flux event.

The inter-annual variability in the flux of a biogenic component is dependent on both the total mass flux and the contribution of the biogenic component to total particulate mass (TPM). In the case of POC, the contribution towards TPM is quite varied and ranges between 3 and 25%, these variations are consistent with previous studies at the PAP site (Lampitt *et al*., 2001). Grouping together all of the available data from the 3000m sediment trap indicates a marked increase in the relative fraction of POC between July and November (Fig 5.8). The arithmetic mean of POC/TM for this period is 0.10 with a relative standard deviation of 54% compared to a mean of 0.06 and relative standard deviation of 27% for the period between December and June, demonstrating that the period between July and November is characterised by both an elevated and more variable contribution of POC to total particulate mass than the remainder of the year. Examination of Fig. 5.5 implies that the increase in POC flux relative to background values is constrained to the period between April and October, although there is substantial inter-annual variability in the magnitude, timing and duration of individual events occurring within this time-frame. The mean flux of POC within this time-frame is 10 ± 16 mg C m^{-2} d^{-1} (Fig.5.6). The summer flux event during 2001 is the most significant excursion above this calculated average and is sustained for 112 days.

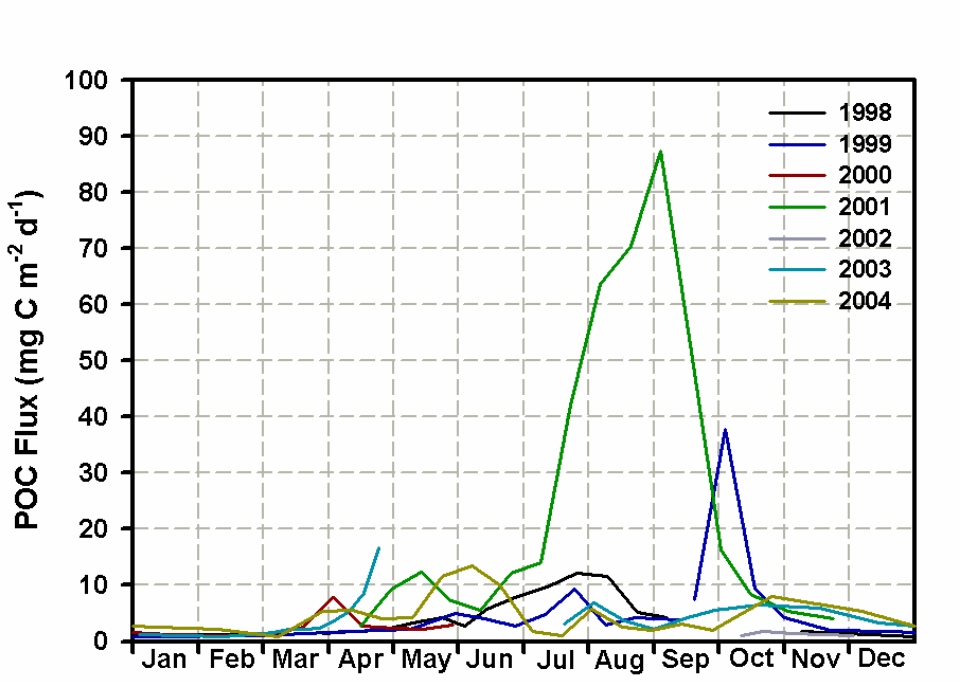

Fig 5.5 Seasonal variability in organic carbon flux at 3000m the PAP site for the period 1998-2004.

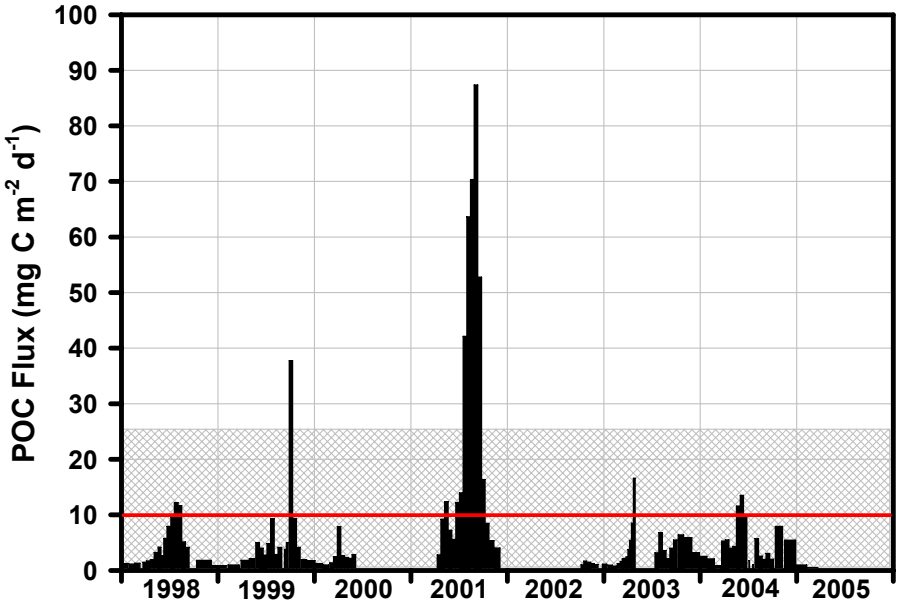

Figure 5.6 Inter-annual variability of POC flux at 3000m. Red line indicates average POC flux (10.6 mg C m^{-2} d^{-1}) calculated between Julian days 91-273. The hatched box is ± 1 S.D. of this average. Time-weighted mean is 10.4 mg C m^{-2} d^{-1}.

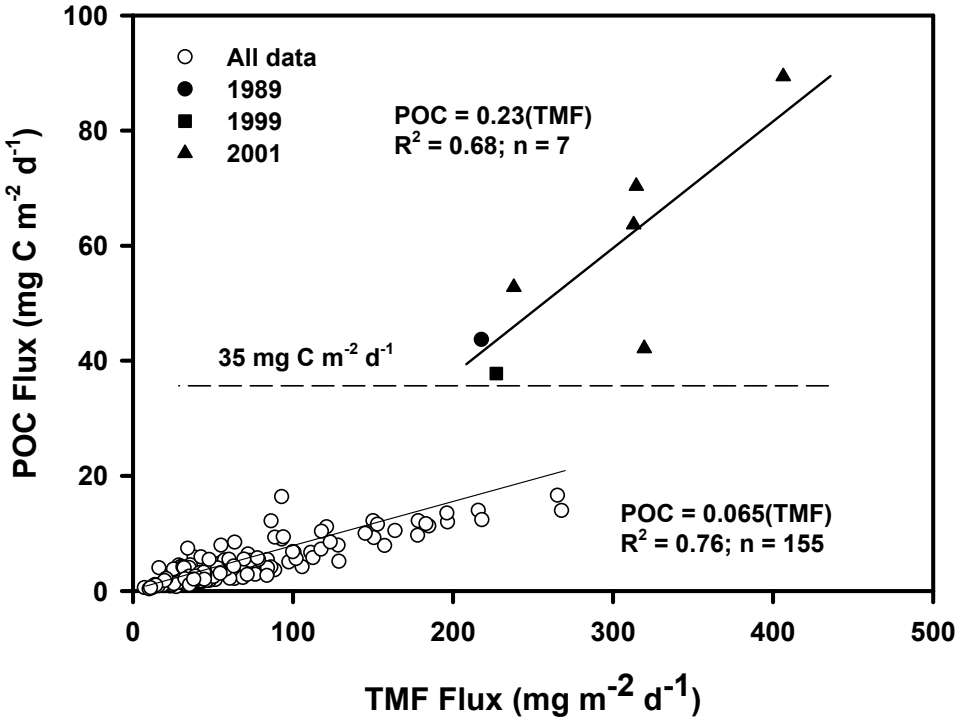

Fig 5.7 Correlation between total mass flux and POC flux at 300om. Each data point represents one cup measurement.

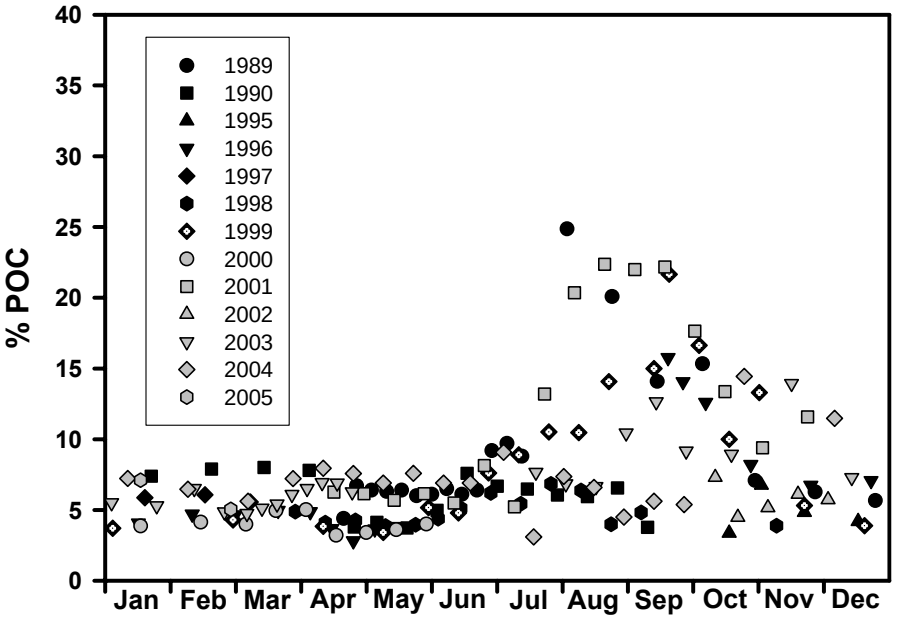

Fig 5.8 Fraction of total mass accounted for by particulate organic carbon. Data 1989-1997 from Lampitt *et al*., 2001.

5.4.3 $CaCO_3$ fluxes at 3000m

Consistent with TM and POC fluxes there is a large range of inter-annual variability present in the $CaCO_3$ flux data (Fig 5.9 and 5.10). The largest flux of $CaCO_3$ observed during the 8-year period was 180 mg m^{-2} d^{-1} which was recorded during the summer 2001 flux event. Unlike for TM and POC flux, $CaCO_3$ flux during 2001 was not greatly different from surrounding years. Based on the 8-year data set presented in Fig 5.9 the rise in $CaCO_3$ flux from "background" levels can occur anytime between the beginning of April and the end of October. The average flux of $CaCO_3$ between April and October for the 8-year record (1998-2005) period is 53 ± 42 mg m^{-2} d^{-1} (n = 46); Fig. 5.10 highlights the periods during the 8-year record when the $CaCO_3$ fluxes are elevated relative to the long-term average. As for POC and TM, the flux events during the summer of 2001 and autumn of 1999 were periods of increased calcium carbonate sedimentation.

The inter-annual variability that is present in the flux of calcium carbonate is also evident in the fraction of $CaCO_3$ that comprises total mass flux (Fig 5.11). The CAL/TM (percentage of total mass that can be accounted for by calcium carbonate) fraction ranges between 11-85% with a mean of 56 ± 17 % (± 1 s.d.). There are no obvious seasonal trends for the fraction of calcium carbonate that comprises the total mass flux. This implies that the increase in $CaCO_3$ sedimentation observed between Apr-Oct is driven primarily by increases in total mass flux rather than an increased weight fraction of $CaCO_3$. A linear regression between total mass flux and $CaCO_3$ flux (Fig 5.12) displays a significant correlation between the two parameters (R^2 = 0.77, $P<0.01$; n = 158).

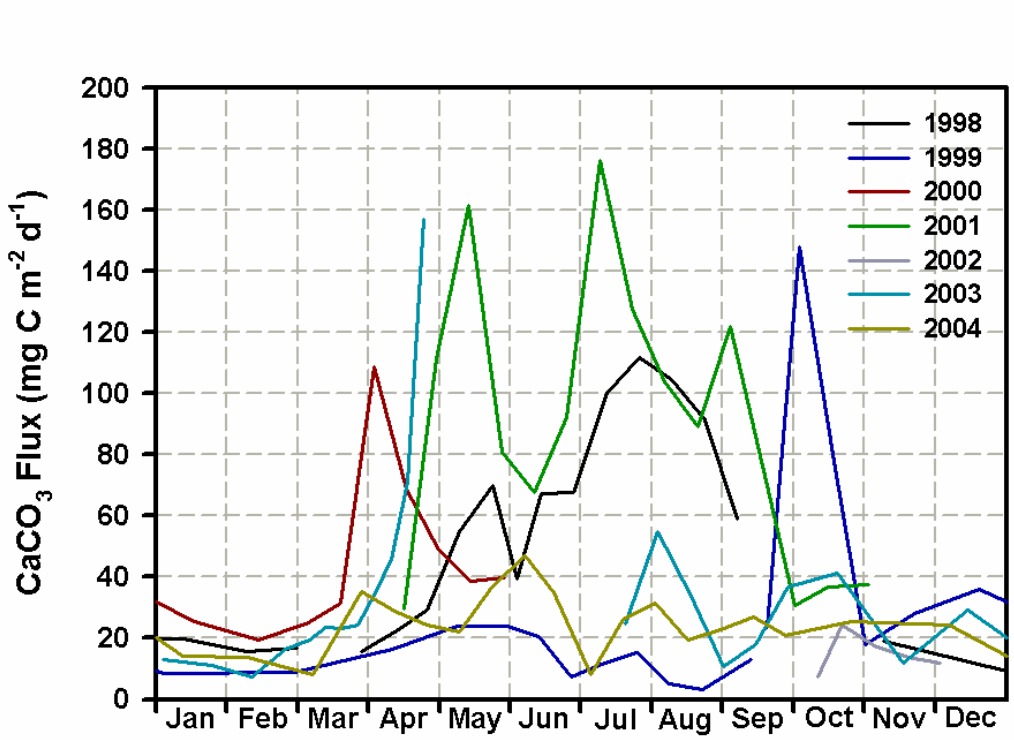

Fig 5.9 Seasonal variability in $CaCO_3$ flux at the PAP site at 3000m for the period 1998-2004.

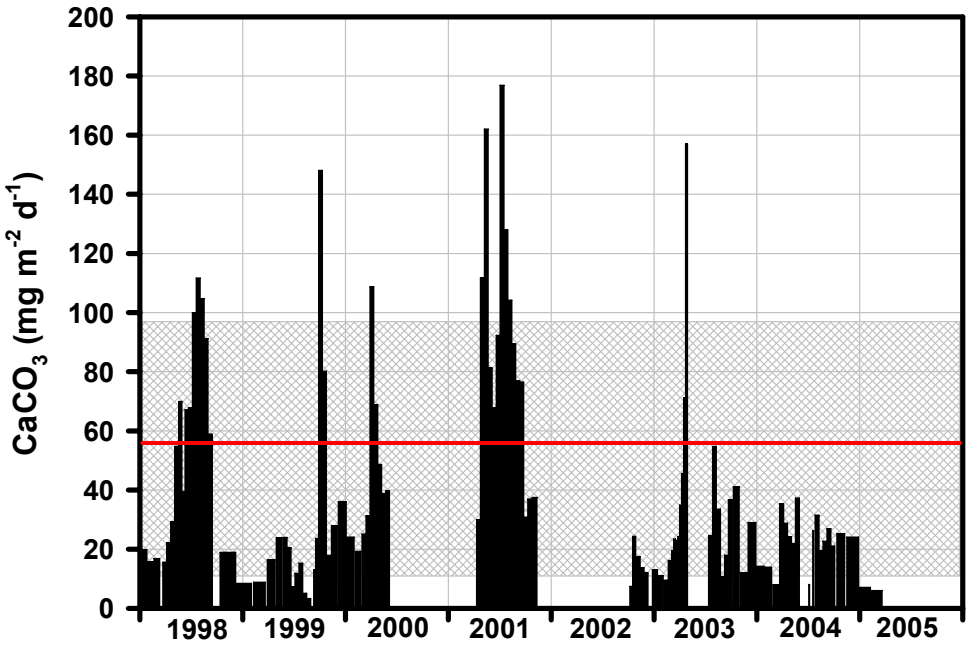

Fig 5.10 Inter-annual variability of $CaCO_3$ flux at 3000m. Red line indicates average $CaCO_3$ flux calculated between Julian days 91-273.

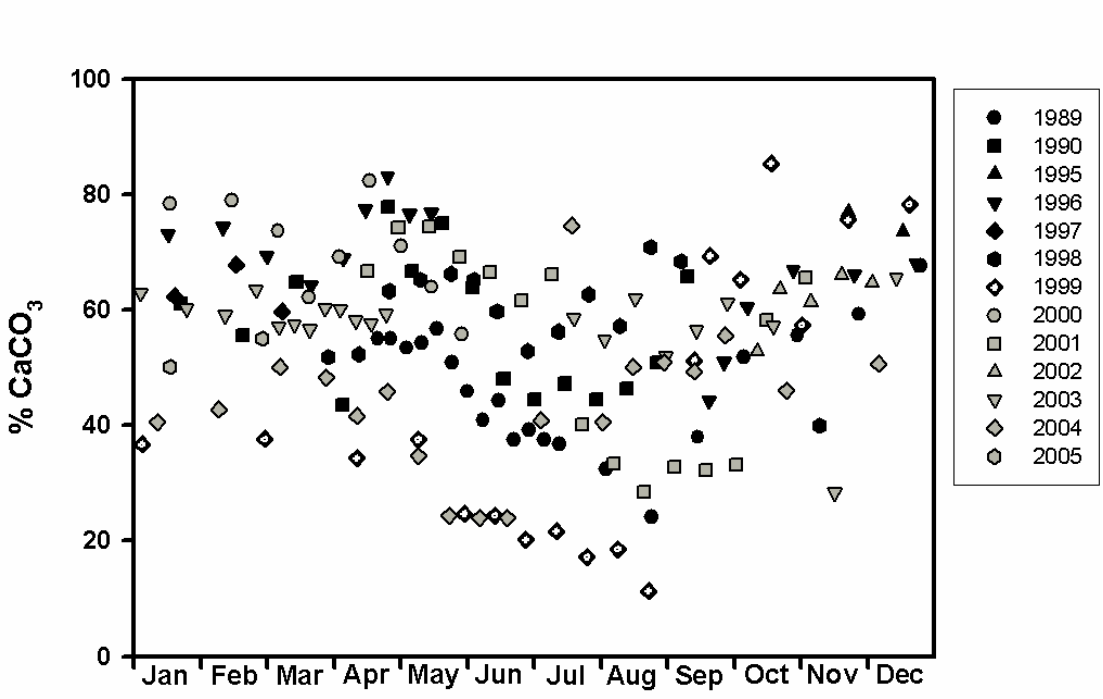

Fig 5.11 Fraction of total mass accounted for by calcium carbonate

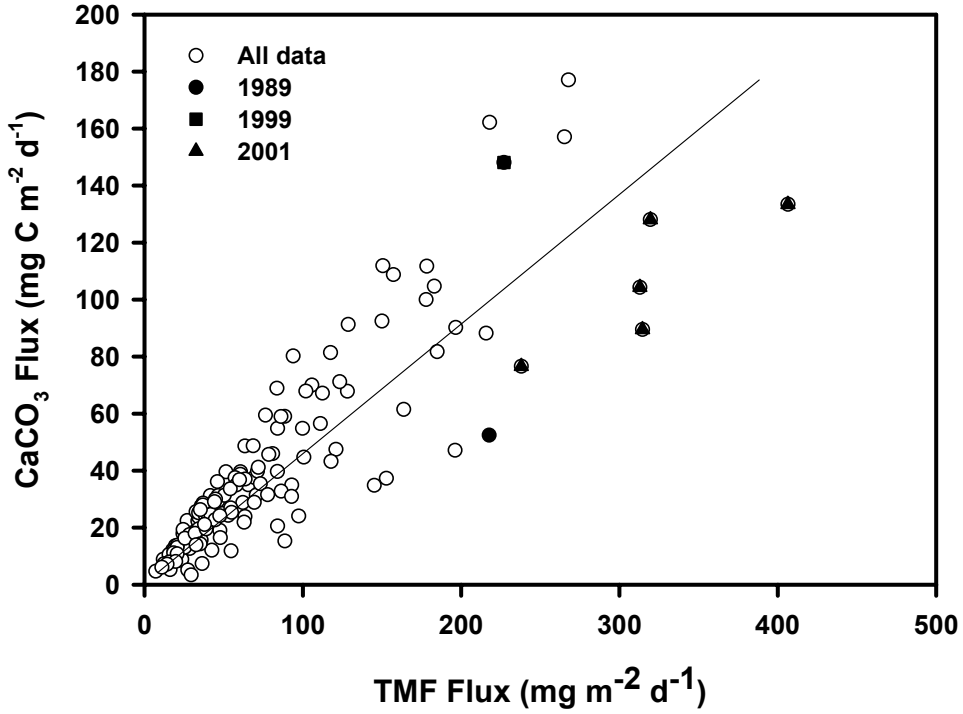

Fig. 5.12 Correlation between $CaCO_3$ and total mass flux

5.4.4 Biogenic Silica Fluxes

There is strong inter-annual variability in the flux of biogenic silica although the trends are somewhat different from the other major biogenic constituents (Fig 5.13 and 5.14). The largest biogenic silica flux event recorded during the 8-year record was 95 mg m^{-2} d^{-1} in June 2004. The summer of 2001 was much less significant in terms of biogenic silica flux than it was for total mass, organic carbon, and calcium carbonate flux. Consistent with POC and $CaCO_3$, the flux of biogenic silica is elevated above background levels between the months of April and October. The average flux of biogenic silica between April and October for the 8-year record (1998-2005) is 19.6 ± 18 mg SiO_2 m^{-2} d^{-1} (n = 70). Fig 5.14 highlights the periods during the 8-year record when the SiO_2 fluxes are elevated relative to the long-term average. Compared to similar plots for POC and CaCO3 short-term excursions above the long-term average are quite numerous. The most notable differences are the elevated fluxes in 1998 and 2004.

The fraction of total mass flux that can be accounted for by biogenic silica ranges from 3-48% (Fig 5.15), with a long term average (1989-2005) of 18 ± 10% (± 1 s.d.). The average SiO_2/TM value between April and October is 20.2 ± 9.6% (n = 103) compared to 12.9 ± 7.9% (n = 63) for the period November to March, which represents a statistically significant difference ($P<0.01$). Although a linear regression (Fig. 5.16) between biogenic silica fluxes total mass fluxes reveals a significant correlation between the two parameters ($R^2 = 0.46$; $p<0.01$; n = 147) it is less significant than the correlation between calcium carbonate and total mass fluxes.

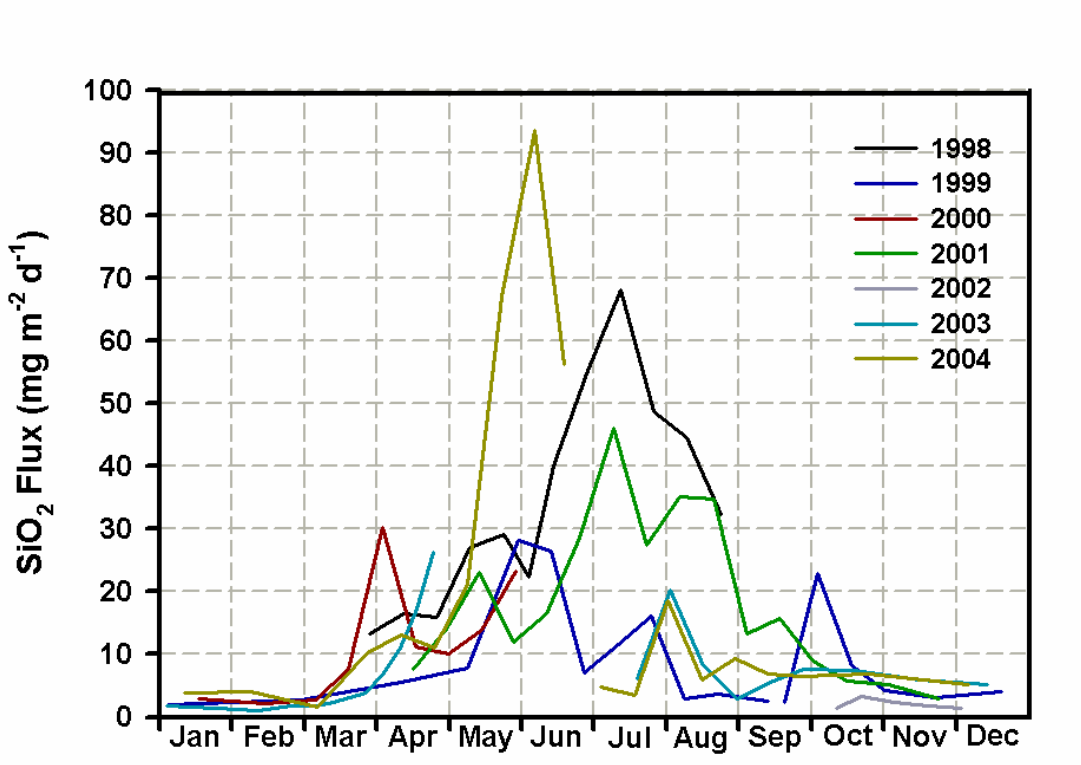

Fig 5.13 Seasonal variability in SiO_2 flux at the PAP site for the period 1998-2004.

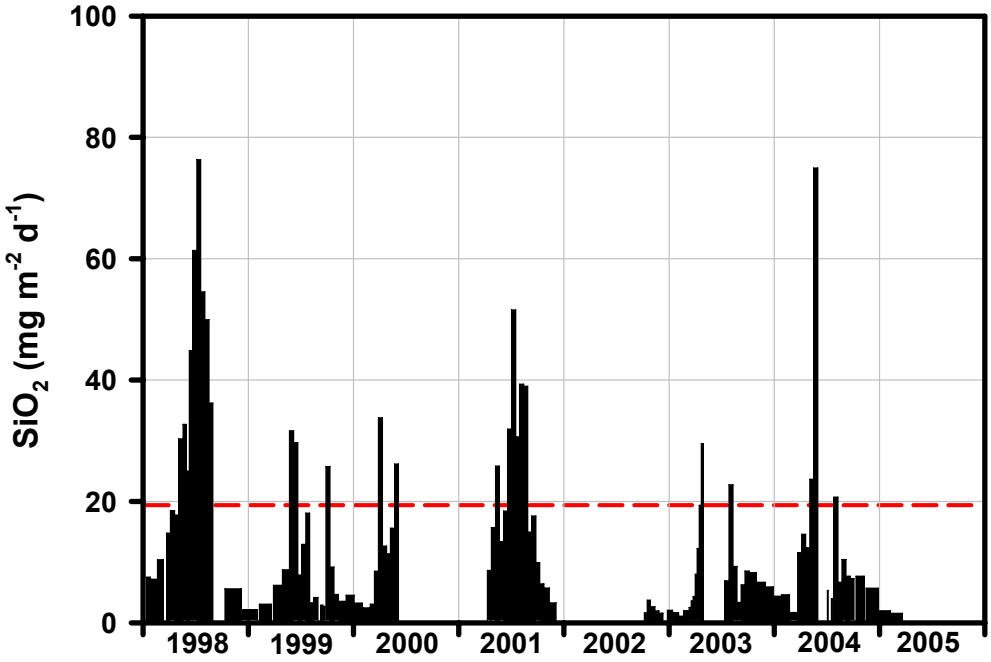

Fig 5.14 Inter-annual variability of SiO_2 flux at 3000m. Red line indicates average $CaCO_3$ flux calculated between Julian days 91-273.

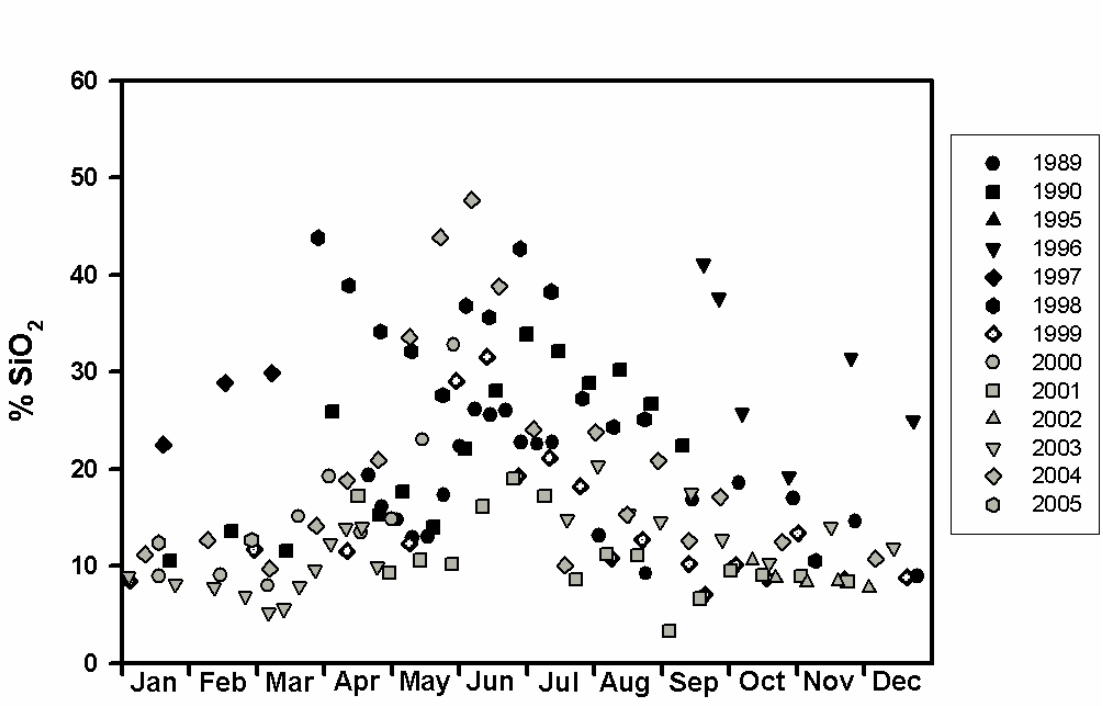

Fig 5.15 Fraction of total mass accounted for by biogenic silica

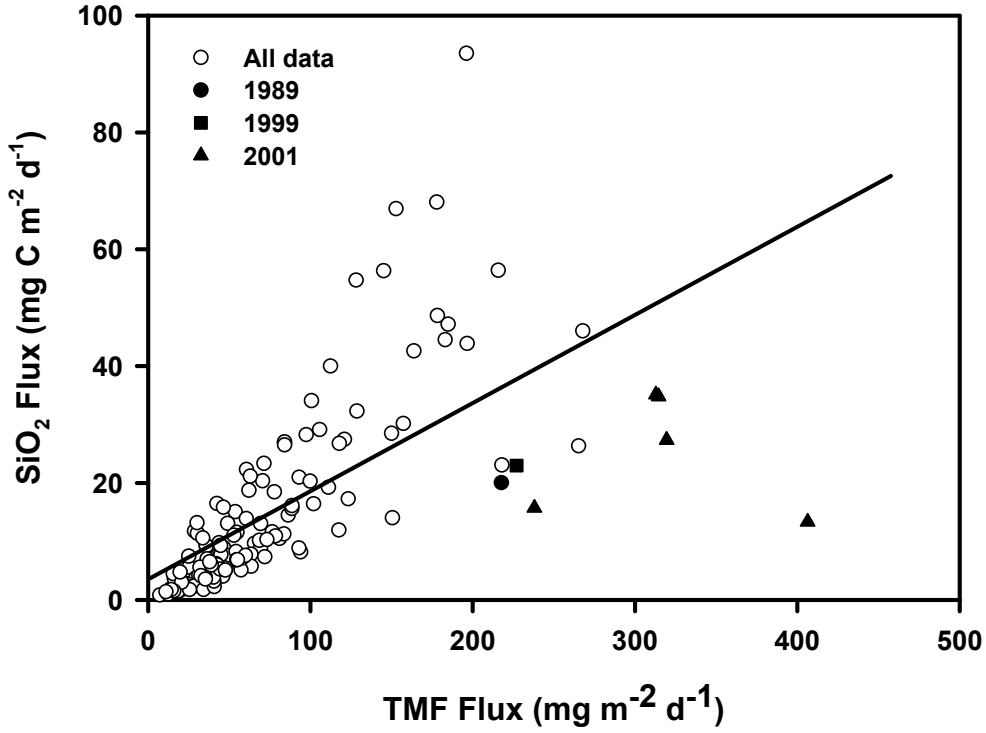

Fig. 5.16 Correlation between SiO_2 and total mass flux

5.4.5 Residual Flux

The residual flux is calculated by difference according to Equation 5.1:

$$(R_{FLUX} = TM - [(POC*S)\text{-}SiO_2\text{-}CaCO_3] \quad (5.1)$$

(where R_{FLUX} is the residual flux, TM is the total mass flux, POC is the organic carbon flux, S is a constant scaling organic carbon to organic matter, SiO_2 is the biogenic silica flux, and $CaCO_3$ is the calcium carbonate flux. Numerous studies use this type of equation to calculate the residual flux and thus infer lithogenic fluxes (e.g. Jickells *et al*., 1998; Klass and Archer 2002). The choice of the scaling factor, S, for converting POC to organic matter affects the calculation of lithogenic fluxes and varies from 1.87 (e.g. Anderson, 1995) to 2.3 (e.g. Conte, *et al*., 2001). Fig 5.17 shows the calculated lithogenic fluxes using both the lowest (1.87) and highest (2.3) conversion factors employed in the literature (Fig 5.17). In some instances calculated lithogenic fluxes are negative, although upon propagation of analytical errors they are within the range of combined errors on the lithogenic flux calculation (Appendix 6). In Fig 5.17 negative lithogenic fluxes are set to equal zero. The summer 2001 flux event was characterised by high lithogenic fluxes, and high fluxes also occurred during 1999.

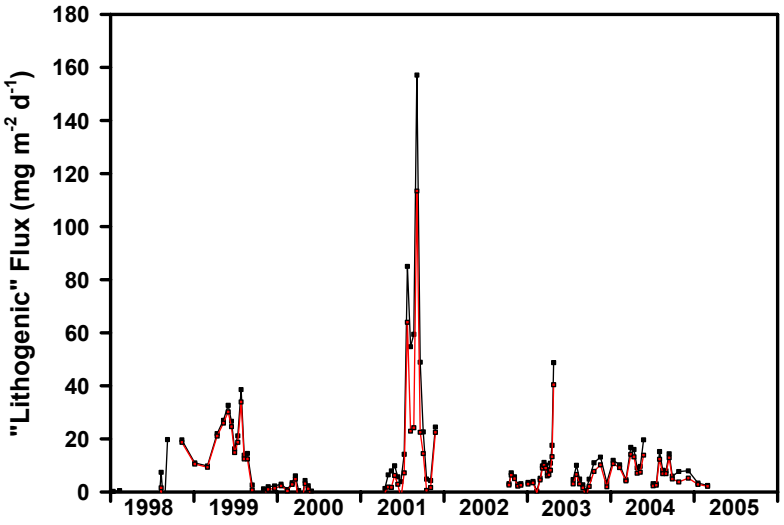

Fig. 5.17 Lithogenic flux calculated by difference according to equation 5.1. The lithogenic flux has been calculated using a POC to POM conversion factor of 1.87 (Anderson, 1995; black line) and 2.3 (Conte *et al*., 2001; red line).

5.4.6 Seasonal Cycles

The seasonal cycle of mass flux at ~3000m depth averaged over the 10-12 year period since 1989 is shown in Fig 5.18. To construct this figure the measured flux for each Julian day was binned into monthly time periods and averaged for each month. The mean and standard deviation for each monthly binned period over the 10-12 years of data recorded were then calculated. As the flux record is discontinuous there are some cases where a particular month (in a particular year) is represented by a low number of Julian days. In order to try and avoid artefacts associated with too few data points, flux data was only included if there was >15 days coverage for a monthly period. A "coverage coefficient" was then calculated for each month using equation 5.2.

$$C_{Coeff} = \Sigma d_{OBS} / (\#Yrs * N) \quad \textbf{(5.2)}$$

where C_{Coeff} is the coverage coefficient, Σd_{OBS} is the sum of total days of observations for a particular month, #Yrs is the number of years of observations for a particular month represented by >15 days coverage, and N is the number of days in the month (i.e. 28, 30, or 31). For all months the C_{Coeff} is >0.88 (Fig 5.18), therefore the ">15 day" filter imposed on the data appears to be a satisfactory constraint for data selection.

Averaging (Fig 5.18) all particle flux data in this way shows a broad flux maximum that starts in March and peaks in June. There is a slight dip in flux during July, and a secondary peak in August which then tails off gradually reaching "background" levels in November/December. The standard deviation of the flux increases significantly in the period June-September, reflecting the extreme inter-annual variability in the timing and duration of the summer period of higher fluxes. In contrast the standard deviation of the flux is at a minimum during November-March, indicating the consistently low mass fluxes recorded every year in the winter and early spring.

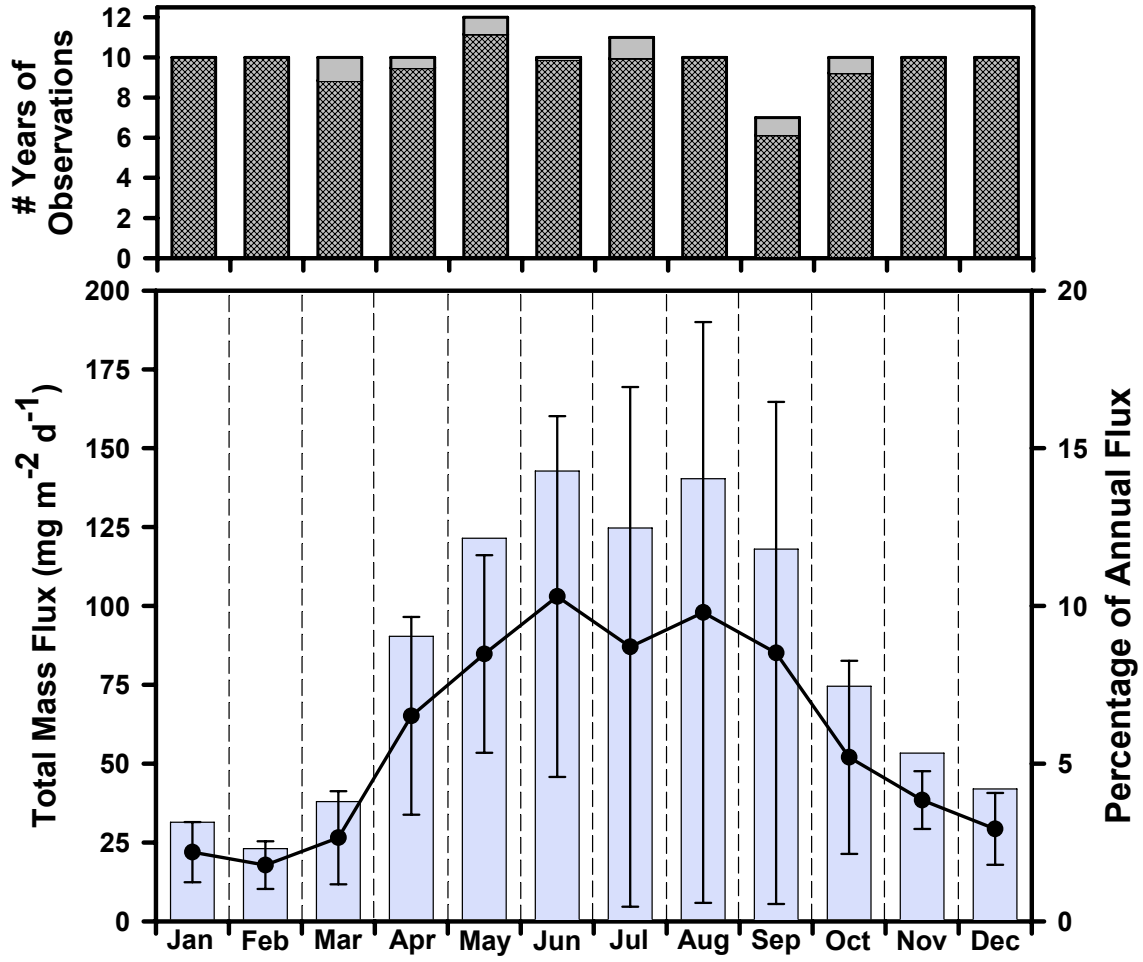

Fig. 5.18 Seasonal cycle of mass flux at 3000m based on averages of all measurements made between 1989 and 2005. In top panel bars represent the number of years for which there is greater than 15 days of flux data per month. Hatched area is the coverage co-efficient as calculated in equation 5.3. In bottom panel light blue bars represent the percentage of annual flux each month contributes. Line plot is the average total mass flux for each individual month with error bars representing ± 1 standard deviation.

5.4.7 Annual Fluxes

Total mass fluxes and major component fluxes have been normalised to a full annual cycle (Fig 5.19). Only sampling years where >70% of the annual mass flux (based on long-term averages described in section 5.4.6; Fig 5.18) were normalised to a full

annual cycle. Total mass fluxes ranged between 19 and 47 g m^{-2} yr^{-1} with the lowest value recorded in 1999 and the highest value in 2001. Excluding 2001, the average total mass flux was 21.3 ± 3.8 g m^{-2} yr^{-1}, whilst the inclusion of this anomalous year increases the average to 25 ± 10.3 g m^{-2} yr^{-1}. Similarly to total mass flux the lowest organic carbon flux of 0.9 g C m^{-2} yr^{-1} was observed in 1990 and the highest value of 6.7 g C m^{-2} yr^{-1} in 2001. The anomalous nature of 2001, and to a lesser extent 1989, is most obvious when examining the annual POC budgets.

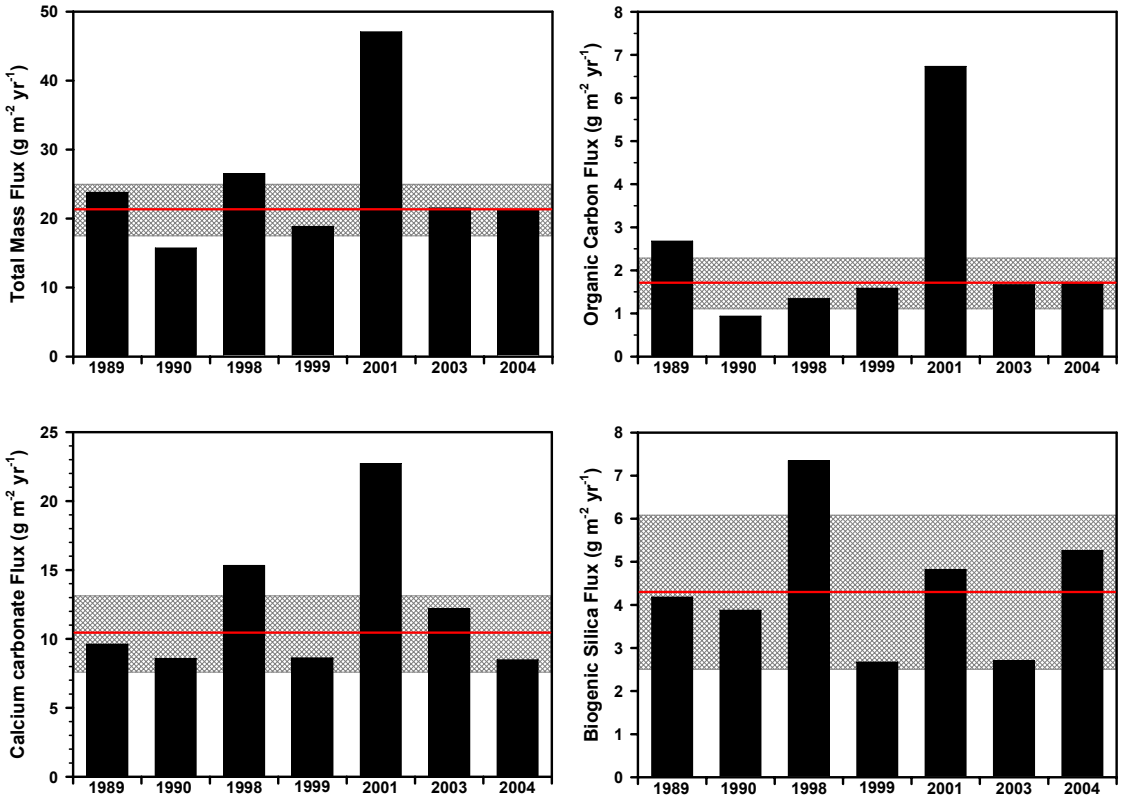

Fig. 5.19 Annually integrated fluxes for all major biogenic components. Data have been normalised according to long-term average deduced from mass flux (Fig 5.17)

The downward flux of organic carbon during 2001 is ≈4-times greater than the long-term average calculated excluding 2001 of 1.7 ± 0.6 g C m^{-2} yr^{-1}. Annual fluxes of calcium carbonate were also highest in 2001 with a sedimentation rate of 22.7 g $CaCO_3$ m^{-2} yr^{-1} compared to the lowest value of 8.5 g $CaCO_3$ m^{-2} yr^{-1} in 2004. It is apparent from the relative standard deviations that the inter-annual variability in

biogenic silica flux is more variable than that of $CaCO_3$. The largest SiO_2 flux of 7.3 g SiO_2 m^{-2} yr^{-1} was recorded in 1998 and the smallest flux of 2.7 g SiO_2 m^{-2} yr^{-1} in 1999. The biogenic silica flux of 4.8 g SiO_2 m^{-2} yr^{-1} in 2001 was close to the long-term average of 4.3 ± 1.8 g m^{-2} yr^{-1}.

5.4.8 Molar ratios

Although organic carbon to nitrogen (C:N) values range from 3 to 16 they are generally well above the canonical Redfield value of 6.6 (Fig 5.20a). The most striking features of the record are the elevated C:N ratios observed during 1999 and the lower values at the beginning of 2000. C:N ratios are very variable and do not appear to exhibit any significant seasonality for the particulate flux data available at 3000m (Fig 5.20a). Annually-integrated C:N ratios have been calculated and are presented in Fig 5.20b. The long term average of annual C:N ratios is 7.6 ± 1.8, although this average is suppressed by two low values in 1989 and 1990 (Fig 5.20b). If one calculates the average excluding 1989 and 1990 then the C:N ratio is 8.4 ± 1.4. There is a strong trend of decreasing C:N ratios from 10.6 in 1998 to 7.4 in 2004 (r^2 = 0.91; p<0.02; n=5).

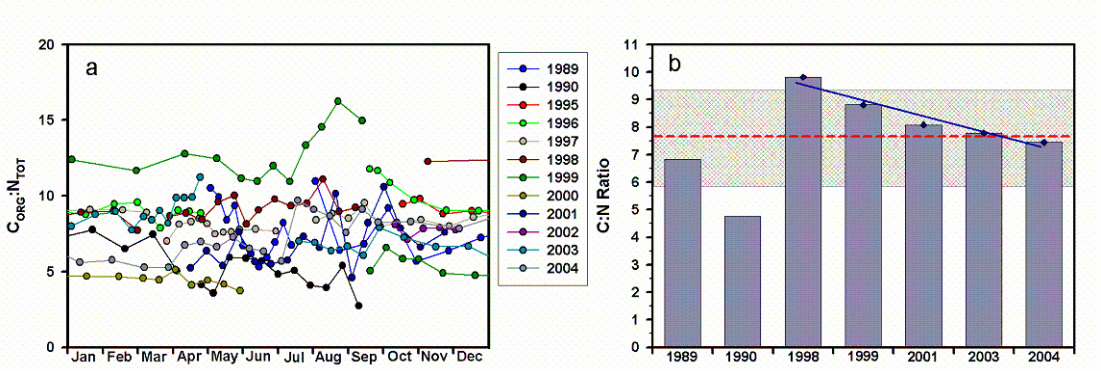

Fig 5.20 (a) Seasonal variation in C:N and (b) annually integrated C:N ratios. C:N ratios are calculated using organic carbon and total nitrogen values, organic nitrogen values were 80-100% of total nitrogen values. Red dashed line is average, hatched box is ± 1σ and dark blue line is the annual trend.

The C_{org}:C_{inorg} (rain) ratio ranges from 0.3 to 10.4 (Fig. 5.21a) with a long-term average of 1.5 ± 0.6 (Fig. 5.21b). Generally the rain ratio is very consistent, and

particularly during the period Jan-Jun. In some years there is a very noticeable increase in the rain ratio during late summer early autumn. This occurs most notably in 1989, 2001, and 1999, and to a lesser extent in 2004. However, upon examination of the annual rain ratio between years (Fig 5.21b) it is clear that the effect of these individual flux events is minimised by the large number of data from the rest of the year. Despite this, 2001 still appears to have a higher rain ratio relative to other years.

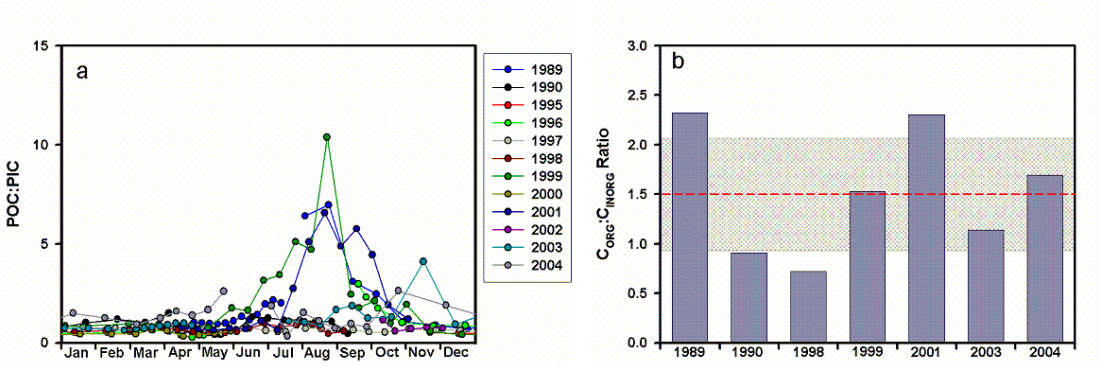

Fig 5.21 (a) Seasonal variation in Corg:Cinorg and (b) annually integrated Corg:Cinorg ratios. Red dashed line is average and the hatched box is ± 1σ

The C_{inorg}:Si ratio ranges from a low of 0.3 to a high of 6.6 (average of 2.4 ± 1.5). and a degree of seasonality with low-values typically found between May and September (Fig 5.22a). Most of the years are characterised by a lowering of the C_{inorg}:Si ratio during the summer months, a feature particularly enhanced during 2001 (Fig 5.22a). The average annual C_{inorg}:Si ratio is 1.8 ± 0.7 (Fig. 5.22b) and is highest during 2001 at 2.8. Based on the data available there is a slight trend of increasing values from 1989 to 2003 although this pattern seems to be reversed during 2004.

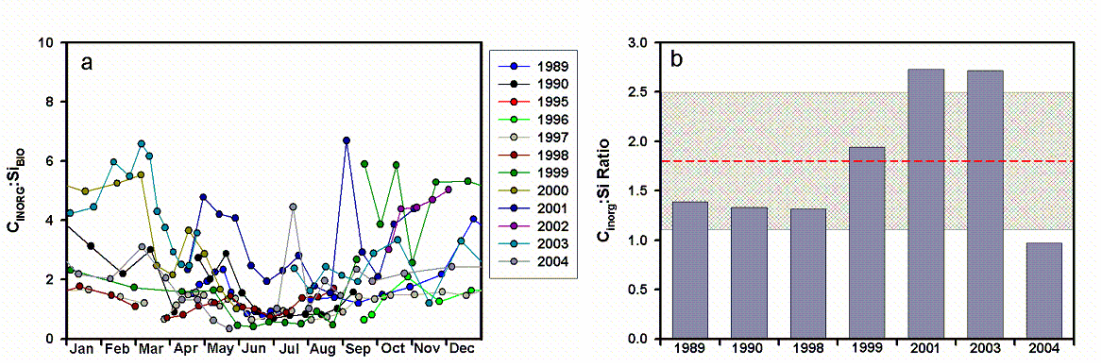

Fig 5.22 (a) Seasonal variation in Corg:Si and (b) annually integrated Cinorg:Si ratios. Red dashed line is average and the hatched box is ± 1σ

5.4.9 Flux and composition of amino acids

During the time period 1998-2004 measured amino acid (AA) fluxes ranged between 0.3 and 19.4 with an average of 2.5 ± 3.5 mg m^{-2} d^{-1} (n = 93, Fig. 5.23). Hexosamine (HA) fluxes (galactosamine + glucosamine) ranged between 0.02 and 1.5 with an average of 0.18 ± 0.27 mg m^{-2} d^{-1} (n = 93, Fig. 5.23). The average fluxes are similar to previous reports in deep-sea sediment trap studies e.g., in the equatorial Pacific (4.5 mg m^{-2} d^{-1} at 1000m and 1.9 gm m^{2} d^{-1} at 3600m; Lee *et al*., 2000), North Atlantic (14 mg m^{-2} d^{-1} at 1000m and 3.3 mg m^{-2} d^{-1} at 3500m; Lundgreen and Duinker, 1998), in the Pacific sector of the Southern Ocean (0.8-2.0 mg m^{-2} d^{-1}; Ingalls *et al*., 2003), and the Brazil coast (0.6-4.0 mg m^{-2} d^{-1}; Jennerjahn *et al*., 1999). The range in amino acid fluxes measured at the PAP site was between 0.3 and 19.4 mg m^{-2} d^{-1} (Fig. 5.23) larger than previously reported but as expected from a large data-set that incorporates both seasonal and inter-annual variability over long-timescales. The large range reported here results predominantly from variations in total mass flux (102% r.s.d) rather than the concentration of AAs in particles (Table 5.1) (50% r.s.d).

The fluxes of POC (Fig. 5.23) and the labile components AA and HA (Fig. 5.23), which contribute 16.5 ± 3.7 and 1 ± 0.4 % to total POC (Table 5.1), respectively, essentially follow the same pattern indicating that the export of bulk POC and both

compound classes is closely linked. Both AA vs POC and HA vs POC fluxes are highly correlated ($r=0.92$, $P<0.001$, $n=93$ for AA vs POC and $r=0.92$, $P<0.001$, $n=93$ for HA vs POC). AA and HA account for 39.2 ± 16.6 and 0.13 ± 0.08 % of total nitrogen. As for carbon, AA-N and HA-N fluxes closely follow ON fluxes ($R=0.98$, $P<0.001$, $n=93$ for AA-N vs TN and $r=0.98$, $P<0.001$, $n=93$ for HA-N vs ON). The content of labile components in particles ranged between 10.5 to 71.3 μg mg^{-1} for AAs and 0.6 to 5.1 μg mg^{-1} for HAs, with respective averages of 27.8 ± 14.1 ($n=93$) and 2.0 ± 1.3 μg mg^{-1}($n=93$) (Table 5.1)

The average AA and HA composition of the sediment trap samples analysed is presented in Fig. 5.24. The general composition of all samples analysed was relatively uniform. The neutral compounds glycine, alanine, and threonine were the most abundant amino acids accounting for 16.4 ± 3.5, 16.1 ± 1.4, and 9.5 ± 1 mol%. Mol% contributions of the non-protein amino acids β-alanine and γ-aminobutyric acid were typically low with averages of 0.4 and 0.5 mol% respectively, very similar to previous reports in sediment trap material (Lundgreen and Duinker, 1998; Gupta and Kawahata, 2000; Lee *et al*., 2000; Ingalls *et al*., 2003).

The amino acid composition of organic matter can be indicative of both its source and extent of degradation. Variation in amino acid composition can be quantitatively assessed using principal components analysis (PCA). Here the PCA-based method of Dauwe *et al*. (1999) is employed to analyse the data set

The "Degradation Index" equation (Dauwe *et al*., 1999) is defined in equation 5.3:

$$[DI = \Sigma_i (var_i - avg\ var_i / std\ var_i) * loading_i] \quad \textbf{(5.3)}$$

where, var_i is the mol % of amino acid *i*, avg var_i and std var_i are the mean and standard deviation of amino acid *i* (mol%) and $loading_i$ is the PCA-derived loading of amino acid *i* (Table 5.2). Dauwe *et al*. (1999) derived these loadings from a PCA of a data set that contained samples of varying degrees of degradation including plankton, particulate matter and sediments. Since the organic composition amongst organisms is so similar, they argue that differences in amino acid composition arise primarily from degradation (Dauwe and Middleburg, 1998; Dauwe *et al*., 1999). In

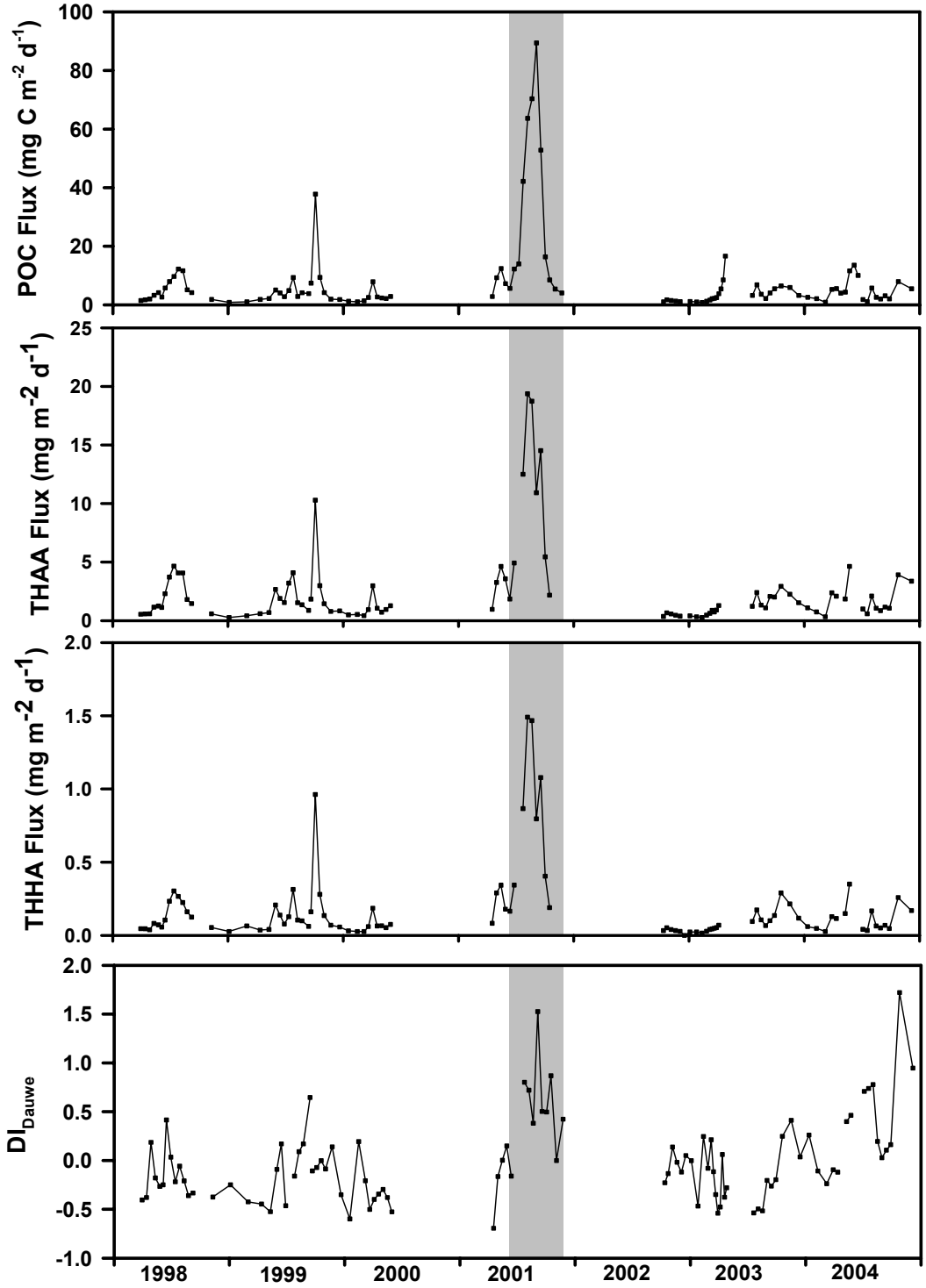
POC Flux (mg C m-2 d-1)
THAA Flux (mg m-2 d-1)
THHA Flux (mg m-2 d-1)
DIDauwe
1998
1999
2000
2001
2002
2003
2004

Fig 5.23 Fluxes of particulate organic carbon, total hydrolysable amino acids (THAA) and hexosamines (THHA). Also shown is the degradation index explained below.

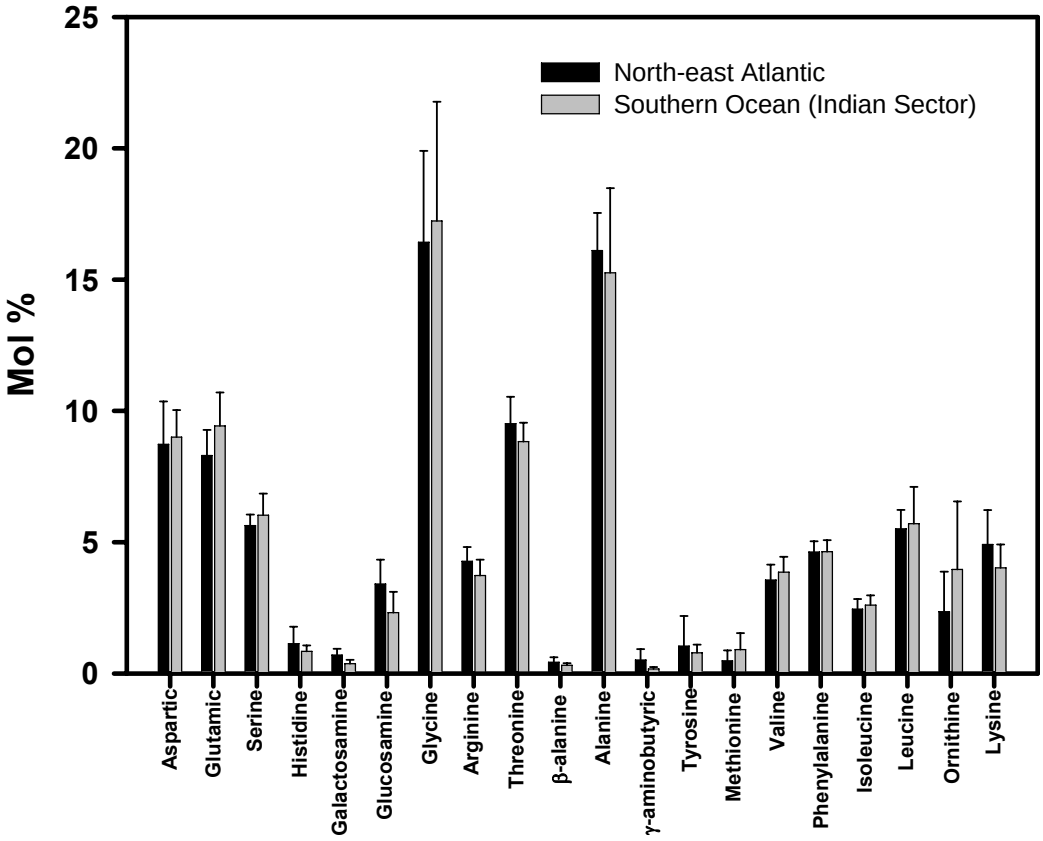

Fig 5.24 Average amino acid (THAA) composition (in mol%) for all samples. Data are not statistically weighted averages but rather averages of all samples collected. Error bars show one standard deviation around this average, not the error in measuring a single sample. These averages are intended to show the ranges of amino acid composition found in the time series trap samples.

Table 5.1 Summary of measured parameters in traps, amino acids are presented as mol%.

Parameter	23aB1	23aB2	23aB3	23aB4	23aB5	23aB6	23aB7	23aB8	23aB9	23aB10	23aB11	23aB12	23aB13
C_{ORG} µg mg^{-1}	48.8	41.0	42.7	38.6	39.5	43.9	51.2	62.0	54.4	68.4	63.7	39.9	48.3
TN µg mg^{-1}	6.6	5.4	5.9	4.7	4.6	6.3	6.6	7.4	6.8	8.4	6.7	5.2	6.1
C_{ORG}:TN	8.7	8.9	8.4	9.6	10.0	8.1	9.1	9.8	9.3	9.5	11.1	9.0	9.2
$CaCO_3$ µg mg^{-1}	518.1	523.2	632.7	651.5	662.0	652.3	597.3	528.9	562.1	626.3	572.0	708.9	684.0
SiO_2 µg mg^{-1}	491.2	436.4	382.8	360.4	309.3	412.7	399.1	478.7	429.0	306.0	272.9	281.6	-
"Lith" µg mg^{-1}	-	-	-	-	-	-	-	-	-	-	-	-	-
Asp	5.5	6.4	8.5	9.1	10.7	5.3	8.9	10.6	9.7	9.2	10.7	9.7	8.5
Glu	6.4	7.3	7.6	7.8	8.1	6.1	7.5	8.3	8.1	8.2	9.4	9.0	8.7
Ser	5.4	5.5	5.6	5.3	5.1	5.4	5.5	6.1	6.3	6.1	5.9	5.7	6.0
His	3.6	2.0	3.1	1.5	1.4	2.6	2.6	1.6	1.3	1.2	1.1	1.2	1.1
Galam	1.0	1.1	0.9	1.1	1.0	0.7	0.5	0.7	0.8	0.7	0.4	0.7	0.8
Gluam	3.8	3.3	2.8	3.0	2.4	2.3	2.2	2.8	3.0	3.0	2.8	4.3	4.1
Gly	27.2	21.1	19.9	15.0	14.7	24.7	17.3	14.8	16.5	15.2	14.7	15.6	18.0
Arg	5.1	5.1	4.8	4.2	3.9	5.3	4.7	3.9	4.0	4.1	3.8	3.9	4.3
Thr	8.2	10.0	9.4	11.2	10.4	8.3	8.8	10.5	10.3	10.7	9.7	9.8	9.0
β-ala	0.8	0.9	0.7	0.7	0.6	0.8	0.4	0.3	0.5	0.3	0.3	0.5	0.5
Ala	13.5	13.6	14.5	14.0	14.7	13.1	15.6	16.6	16.5	17.1	16.5	16.3	16.8
γ-aba	1.4	1.0	2.2	0.7	0.6	1.0	1.7	0.6	0.5	0.6	0.5	0.5	0.5
Tyr	0.8	1.1	1.1	0.9	0.8	0.7	1.0	1.2	0.0	0.6	1.1	0.4	0.3
Met	0.3	0.5	0.6	1.0	0.6	0.7	0.7	0.4	0.6	0.3	0.4	0.4	0.4
Val	1.6	2.4	2.6	3.1	3.6	2.7	3.7	3.5	3.6	3.7	3.4	3.6	3.0
Phe	4.0	4.3	5.0	4.3	4.4	4.0	4.4	4.7	4.7	4.7	4.5	4.3	4.5
Ile	1.2	2.0	2.0	2.3	2.5	1.9	2.6	2.4	2.4	2.5	2.0	2.2	1.9
Leu	4.2	4.4	4.4	4.4	4.6	4.5	5.5	5.4	5.2	5.8	5.2	4.9	5.1
Orn	1.0	1.5	3.0	2.7	3.5	3.0	2.6	1.6	2.3	1.3	3.7	2.4	2.0
Lys	4.9	6.4	1.4	7.8	6.6	6.9	3.9	4.1	4.0	4.7	4.0	4.5	4.6
AA µg mg^{-1}	18.2	13.6	12.7	13.7	11.9	18.7	20.4	29.1	26.2	22.9	22.2	14.1	17.0
HA µg mg^{-1}	1.5	1.1	0.8	1.0	0.7	0.9	0.9	1.8	1.7	1.5	1.2	1.3	1.4
AA-C%	15.3	13.9	12.5	15.1	12.8	17.8	16.9	19.9	20.2	14.2	14.8	14.9	14.8
AA-N%	45.6	40.1	33.7	44.2	38.8	48.9	47.8	57.7	57.7	40.3	49.1	40.5	42.4
DI_{DAUWE}	-0.40	-0.38	0.19	-0.18	-0.27	-0.25	0.42	0.03	-0.22	-0.06	-0.21	-0.36	-0.33

Parameter	25B1	25B2	25B3	25B4	25B5	25B6	25B7	25B8	25B9	25B10	25B11	25B12	25B13
C_{ORG} µg mg^{-1}	38.9	37.1	43.0	38.4	34.2	51.6	47.9	76.1	89.0	105.2	104.7	140.7	150.0
TN µg mg^{-1}	3.7	3.5	4.3	3.5	3.2	5.4	5.1	7.4	9.5	9.2	8.4	10.1	11.7
C_{ORG}:TN	12.3	12.4	11.7	12.8	12.5	11.2	11.0	12.0	10.9	13.3	14.6	16.2	15.0
$CaCO_3$ µg mg^{-1}	399.5	366.7	376.2	343.0	375.6	246.6	244.0	201.6	216.5	172.1	185.7	113.1	512.2
SiO_2 µg mg^{-1}	105.1	84.6	116.7	115.3	123.0	290.3	315.3	192.5	211.3	181.9	108.0	127.0	102.3
"Lith" µg mg^{-1}	393.5	453.3	394.3	439.5	408.1	309.5	292.7	407.7	342.1	382.3	452.5	421.1	28.2
Asp	9.6	9.5	8.7	9.2	9.6	6.6	8.6	9.2	10.2	11.7	9.6	9.3	9.2
Glu	8.3	8.3	8.7	8.1	6.9	7.2	8.0	8.3	9.2	8.4	8.5	8.2	8.5
Ser	5.2	5.0	5.7	5.4	4.9	5.8	5.7	5.3	2.5	5.5	5.2	5.1	5.1
His	1.2	1.1	1.4	1.2	1.1	0.9	0.7	0.8	0.9	0.8	0.8	0.7	0.4
Galam	0.7	0.9	0.7	0.9	0.8	0.6	1.1	0.4	0.3	0.4	0.5	0.5	0.5
Gluam	4.5	4.9	7.8	2.7	2.2	3.8	3.1	2.5	2.0	3.9	3.4	3.7	3.5
Gly	15.3	14.7	15.3	15.4	13.5	19.3	16.5	20.4	16.0	14.5	15.4	14.2	12.4
Arg	3.8	3.9	3.9	4.5	3.8	4.7	3.9	4.3	4.4	3.8	4.0	3.9	3.6
Thr	9.3	10.0	9.7	10.1	8.6	9.1	9.4	8.1	8.4	9.1	9.2	9.3	9.4
β-ala	0.3	0.4	0.3	0.5	0.4	0.3	0.3	0.2	0.2	0.2	0.2	0.2	0.1
Ala	15.7	14.4	14.9	14.4	12.6	16.5	16.8	17.9	20.4	17.9	17.4	17.6	17.2
γ-aba	0.3	0.3	0.3	0.4	0.3	0.4	0.3	0.4	0.2	0.3	0.3	0.4	0.2
Tyr	1.1	0.7	0.5	0.2	0.2	0.3	0.3	0.2	0.1	0.3	0.1	0.5	2.4
Met	0.4	0.5	0.3	0.5	0.4	0.2	0.5	0.2	0.2	0.2	0.2	0.3	0.4
Val	3.6	3.6	3.2	3.7	3.2	3.6	4.0	3.3	4.1	3.8	3.8	4.2	4.1
Phe	4.1	4.4	4.3	4.3	3.9	5.0	5.3	4.7	5.0	5.1	5.1	5.1	5.1
Ile	2.1	2.3	1.9	2.5	2.2	2.5	2.7	2.1	2.7	2.4	2.6	2.6	2.6
Leu	4.6	4.8	4.4	4.7	4.1	5.6	5.4	5.1	6.3	5.8	6.2	6.1	6.3
Orn	5.6	5.9	3.4	5.6	4.6	2.9	2.6	2.0	1.7	2.1	2.1	3.3	4.6
Lys	4.1	4.4	4.7	5.6	4.8	4.7	4.7	4.5	5.1	4.0	5.5	4.9	4.3
AA µg mg^{-1}	12.4	11.5	17.8	12.3	10.9	27.4	22.5	42.5	58.6	46.2	56.1	46.0	34.7
HA µg mg^{-1}	1.1	1.2	2.7	0.8	0.6	2.1	1.6	2.1	2.3	3.5	3.8	3.4	2.4
AA-C%	13.5	13.2	17.5	13.7	13.6	22.5	20.0	23.3	28.1	18.7	22.9	14.1	10.1
AA-N%	50.8	50.2	62.9	54.5	52.5	78.7	66.1	87.4	92.4	73.6	99.5	67.5	43.0
DI_{DAUWE}	-0.37	-0.21	-0.43	-0.30	-0.49	-0.10	0.15	-0.51	-0.05	-0.26	0.13	0.18	0.64

Parameter	26B1	26B2	26B3	26B4	26B5	26B6	26B7	26B8	26B9	26B10	26B11	26B12	26B13
C_{ORG} µg mg^{-1}	146.4	166.4	99.9	133.0	53.1	38.9	38.7	41.4	39.9	49.5	50.2	32.1	34.0
TN µg mg^{-1}	33.8	29.5	20.0	26.6	12.7	9.6	9.6	10.3	10.2	13.0	11.4	9.1	9.0
C_{ORG}:TN	5.0	6.6	5.8	5.8	4.9	4.7	4.7	4.7	4.6	4.5	5.1	4.1	4.4
$CaCO_3$ µg mg^{-1}	693.0	652.3	853.5	573.8	755.9	782.7	741.1	789.1	736.4	621.4	691.7	823.4	709.8
SiO_2 µg mg^{-1}	78.8	113.4	97.8	149.9	95.9	98.7	100.0	100.9	89.3	169.1	215.0	150.8	166.1
"Lith" µg mg^{-1}	-	-	-	-	26.1	29.2	69.8	14.8	82.5	95.5	-	-	45.8
Asp	9.8	9.9	10.6	8.9	9.1	6.9	6.1	5.3	8.4	8.0	8.5	6.7	8.9
Glu	9.7	10.0	9.5	9.4	10.0	7.7	7.1	7.1	8.6	7.5	6.6	6.3	7.0
Ser	5.3	5.2	5.0	5.1	5.4	5.4	5.5	4.8	5.3	5.3	6.0	5.7	6.3
His	0.5	0.7	0.7	0.8	0.8	1.3	1.2	4.0	1.0	0.9	0.8	0.8	0.8
Galam	0.5	0.6	0.6	0.6	0.9	0.8	0.8	0.6	0.9	0.8	0.8	0.6	0.9
Gluam	4.4	4.6	4.7	4.6	4.2	3.2	2.8	2.4	2.5	2.6	2.8	2.9	4.3
Gly	14.3	13.7	13.0	14.5	14.8	19.5	22.2	22.4	15.7	17.2	18.1	20.2	16.3
Arg	3.7	3.7	3.6	4.3	4.4	4.9	5.6	5.5	4.6	4.8	4.5	5.1	4.3
Thr	9.8	10.1	9.9	10.3	10.2	8.7	8.4	7.4	9.9	8.6	9.8	9.3	9.6
β-ala	0.3	0.2	0.2	0.3	0.3	0.6	0.6	0.5	0.5	0.5	0.4	0.4	0.4
Ala	18.2	18.2	17.8	17.1	16.1	14.5	14.4	12.5	14.7	15.0	16.9	15.2	15.9
γ-aba	0.3	0.4	0.4	0.4	0.4	0.6	0.6	3.0	0.5	0.6	0.6	0.6	0.4
Tyr	0.2	0.2	1.5	0.5	0.7	0.5	0.3	0.4	0.4	0.2	0.6	0.7	0.8
Met	0.3	0.6	0.5	0.5	0.6	0.5	0.4	0.2	0.7	0.4	0.4	0.3	0.6
Val	3.6	3.7	3.6	4.1	3.9	3.4	3.3	3.1	3.8	3.1	3.5	3.4	3.2
Phe	4.7	4.5	4.5	4.6	4.5	4.1	4.1	4.0	4.2	4.2	4.8	4.7	4.5
Ile	2.2	2.2	2.1	2.6	2.7	2.3	2.3	2.2	2.7	2.2	2.3	2.5	2.1
Leu	6.1	5.9	5.7	5.7	5.9	5.0	4.9	4.8	5.1	4.7	5.1	5.3	5.1
Orn	1.7	2.3	2.1	1.9	2.2	5.3	4.2	6.6	4.7	2.9	2.7	3.0	3.7
Lys	4.2	3.3	3.9	3.9	5.1	4.9	5.3	3.1	5.9	4.8	4.7	6.3	4.9
AA µg mg^{-1}	53.9	45.3	31.8	46.5	21.4	18.2	15.4	21.7	12.7	18.9	19.0	12.7	10.5
HA µg mg^{-1}	4.7	4.2	3.0	4.3	1.9	1.2	0.9	1.1	0.8	1.2	1.2	0.8	1.0
AA-C%	10.6	11.5	13.6	14.9	17.2	19.7	16.6	22.0	13.5	16.0	16.0	16.8	13.1
AA-N%	23.2	22.3	23.0	25.7	25.1	30.3	25.8	34.9	19.1	22.6	25.3	21.9	17.8
DI_{DAUWE}	-0.11	-0.07	0.00	-0.09	0.14	-0.35	-0.60	0.19	-0.21	-0.50	-0.40	-0.34	-0.30

Parameter	26B14	26B15	27B1	27B2	27B3	27B4	27B5	27B6	27B7	27B8	27B9	27B10	27B11
C_{ORG} µg mg^{-1}	36.0	40.0	62.6	61.5	56.8	61.5	54.9	81.4	52.2	132.0	203.5	223.7	215.0
TN µg mg^{-1}	10.1	12.6	11.0	10.1	10.3	9.6	10.4	14.8	9.5	21.4	31.9	28.0	28.1
C_{ORG}:TN	4.2	3.7	6.6	7.1	6.4	7.5	6.2	6.4	6.4	7.2	7.4	9.3	8.9
$CaCO_3$ µg mg^{-1}	639.6	556.9	666.0	742.3	743.0	691.6	665.1	615.3	660.5	400.5	333.1	284.4	189.5
SiO_2 µg mg^{-1}	257.4	366.7	192.3	104.4	118.5	113.9	180.6	212.7	192.5	96.0	125.7	124.0	36.9
"Lith" µg mg^{-1}	20.1	-	-	11.9	7.8	53.0	28.0	-	26.9	200.1	73.2	77.1	279.1
Asp	8.9	8.3	11.0	10.8	7.9	5.5	12.4	12.2	-	12.3	9.4	9.3	9.5
Glu	6.8	6.7	8.5	9.3	8.1	7.0	9.5	9.0	-	10.5	8.9	9.2	8.9
Ser	6.4	6.2	6.0	5.8	6.0	5.6	5.8	5.4	-	6.0	5.5	5.7	5.2
His	0.9	0.8	0.8	1.0	1.1	2.5	1.3	1.3	-	0.7	0.5	0.3	1.0
Galam	0.8	0.6	1.2	0.9	0.9	0.7	0.9	0.6	-	0.7	0.7	0.7	0.7
Gluam	3.0	2.7	3.6	4.1	3.4	2.3	4.1	3.4	-	3.7	3.3	3.2	2.7
Gly	17.7	18.0	15.6	12.9	15.7	21.9	12.4	12.1	-	12.2	12.0	12.4	10.5
Arg	4.3	4.2	4.7	4.1	4.3	5.1	3.7	3.6	-	3.4	3.2	3.6	3.0
Thr	9.7	9.4	9.6	10.3	9.6	8.1	10.2	10.4	-	12.5	11.2	11.6	8.5
β-ala	0.4	0.3	0.6	0.4	0.5	0.7	0.4	0.3	-	0.4	0.3	0.3	0.4
Ala	16.0	17.1	16.2	17.4	17.5	15.9	16.4	16.6	-	20.1	18.1	18.0	17.1
γ-aba	0.5	0.4	0.4	0.3	0.4	0.6	0.2	0.3	-	0.3	0.4	0.4	0.4
Tyr	0.5	0.6	0.9	0.4	2.4	2.0	0.6	0.6	-	0.1	0.2	0.1	0.0
Met	0.6	0.5	0.2	0.2	0.4	0.2	0.2	0.2	-	0.8	0.8	0.4	2.2
Val	3.4	3.7	2.9	3.5	2.9	2.7	3.6	4.2	-	5.0	4.7	4.6	6.0
Phe	4.5	4.7	4.3	4.8	4.3	4.3	4.7	5.2	-	5.9	5.4	5.3	4.7
Ile	2.3	2.5	2.0	2.4	2.0	1.9	2.3	2.9	-	3.4	3.2	3.2	3.2
Leu	5.0	5.0	5.0	5.7	5.4	5.4	5.5	6.1	-	7.5	6.7	6.9	6.3
Orn	3.4	3.1	1.7	1.2	2.3	2.6	2.1	1.5	-	1.0	3.5	1.4	8.3
Lys	5.0	4.9	4.8	4.5	4.8	4.9	3.7	4.3	-	4.3	2.1	3.3	1.2
AA µg mg^{-1}	15.8	17.8	21.6	21.7	21.2	30.5	18.2	32.8	-	39.1	61.9	59.6	60.3
HA µg mg^{-1}	0.9	1.0	1.8	1.9	1.6	1.5	1.6	2.3	-	2.7	4.8	4.7	4.6
AA-C%	18.2	18.8	14.6	15.0	16.0	21.0	14.1	17.3	-	12.7	13.1	11.4	11.6
AA-N%	25.1	21.7	23.2	28.0	25.7	51.5	23.2	27.3	-	25.8	24.5	33.7	30.8
DI_{DAUWE}	-0.38	-0.53	-0.73	-0.24	-0.02	0.15	-0.29	-0.22	-	0.71	0.48	0.21	1.34

Parameter	27B12	27B13	27B14	28B1	28B2	28B3	28B4	28B5	28B6	28B7	28B8	28B9	28B10
C_{ORG} µg mg^{-1}	133.6	94.0	115.8	73.1	44.8	51.7	61.1	57.3	-	55.0	52.9	65.1	48.6
TN µg mg^{-1}	30.2	21.5	18.0	10.7	7.0	8.2	9.2	8.4	-	8.3	7.6	7.8	7.6
C_{ORG}:TN	5.2	5.1	7.5	8.0	7.5	7.3	7.7	8.0	-	7.7	8.1	9.7	7.5
$CaCO_3$ µg mg^{-1}	321.4	332.1	582.2	528.4	634.9	613.6	660.9	646.3	-	629.2	602.0	771.4	634.2
SiO_2 µg mg^{-1}	106.9	101.2	100.2	117.8	97.2	92.9	94.4	86.2	-	99.7	90.8	86.7	77.5
"Lith" µg mg^{-1}	155.4	9.3	28.4	185.8	164.7	174.6	104.2	135.7	-	144.5	185.5	-7.8	176.5
Asp	8.6	8.7	8.0	8.6	9.8	11.3	9.3	9.3	-	9.6	8.7	9.2	7.7
Glu	9.1	8.9	8.3	8.6	9.1	11.1	9.3	8.7	-	9.5	8.5	9.3	8.4
Ser	5.4	5.7	5.4	6.0	5.8	6.8	5.8	5.9	-	5.5	5.8	6.0	5.8
His	0.6	0.6	0.8	0.2	0.8	0.8	0.6	0.5	-	1.2	0.7	0.8	1.0
Galam	0.6	0.7	0.9	1.1	1.0	1.1	0.8	0.9	-	0.7	0.9	0.7	0.9
Gluam	3.0	3.7	4.0	3.9	3.4	3.4	3.2	3.1	-	2.6	3.0	2.6	2.6
Gly	13.0	14.0	14.3	18.4	16.0	16.1	15.1	15.7	-	15.1	17.9	14.3	17.7
Arg	3.5	3.9	3.9	4.7	4.4	4.8	4.6	4.8	-	4.7	5.0	4.5	5.0
Thr	11.6	11.4	9.8	8.6	9.2	10.6	10.0	9.5	-	9.6	9.3	10.0	9.5
β-ala	0.3	0.3	0.6	0.3	0.4	0.4	0.4	0.4	-	0.4	0.4	0.3	0.4
Ala	17.8	18.6	16.3	15.6	16.0	17.8	15.7	16.0	-	16.2	16.1	15.6	15.3
γ-aba	0.5	0.5	0.4	0.3	0.3	0.4	0.3	0.4	-	0.4	0.4	0.3	0.4
Tyr	0.1	1.8	2.6	2.0	1.5	1.5	1.2	1.4	-	0.9	1.3	0.6	1.0
Met	0.6	0.6	1.0	0.2	0.2	0.3	0.2	0.2	-	0.2	0.2	0.2	0.2
Val	4.8	4.4	4.1	2.9	3.5	3.7	3.8	3.6	-	4.1	3.7	4.1	3.7
Phe	5.1	5.1	5.0	4.3	4.4	5.0	4.8	4.5	-	4.4	4.3	4.9	4.4
Ile	3.3	2.9	2.7	2.1	2.5	2.7	2.9	2.7	-	3.1	2.6	3.2	2.9
Leu	6.7	6.6	5.9	5.6	5.4	6.4	5.6	5.7	-	5.4	5.0	6.0	5.5
Orn	2.3	2.1	2.1	0.9	0.8	0.8	0.8	0.9	-	0.9	0.9	1.1	1.1
Lys	3.1	3.2	4.3	5.6	5.5	6.1	5.8	5.8	-	5.3	5.2	6.2	6.4
AA µg mg^{-1}	61.0	58.7	34.3	26.3	17.6	20.1	22.5	21.1	-	19.6	18.3	21.4	18.4
HA µg mg^{-1}	4.5	4.4	3.0	2.3	1.4	1.4	1.6	1.5	-	1.1	1.2	1.2	1.1
AA-C%	11.8	14.4	11.1	15.2	16.7	16.6	15.8	15.7	-	15.2	14.6	14.1	16.1
AA-N%	27.9	43.4	25.0	36.8	37.1	35.7	36.0	37.6	-	35.0	36.3	40.5	37.1
DI_{DAUWE}	0.32	0.33	0.79	-0.21	-0.13	0.20	0.02	-0.08	-	-0.01	-0.48	0.33	0.02

Parameter	28B11	28B12	28B13	28B14	28B15	31A1	31A2	31A3	31A4	31A5	31A6	31A7	31A8
C_{ORG} µg mg^{-1}	47.5	51.2	54.2	60.9	65.1	76.6	68.4	66.4	104.4	126.4	91.6	89.4	139.4
TN µg mg^{-1}	7.3	7.9	8.2	9.4	9.9	11.1	10.3	10.1	16.0	18.4	11.4	14.1	21.6
C_{ORG}:TN	7.6	7.6	7.7	7.5	7.7	8.1	7.8	7.7	7.6	8.0	9.4	7.4	7.5
$CaCO_3$ µg mg^{-1}	571.0	574.0	566.1	602.3	601.5	585.9	548.9	619.9	520.6	564.1	612.9	571.8	283.3
SiO_2 µg mg^{-1}	58.2	62.5	88.5	107.8	137.8	165.5	227.8	171.5	163.2	195.9	142.3	114.8	157.0
"Lith" µg mg^{-1}	261.6	245.7	220.8	149.8	111.0	72.3	66.1	55.9	76.1	-	34.2	107.9	239.1
Asp	8.2	7.0	9.1	9.6	11.6	11.5	10.5	11.5	6.0	6.8	7.8	7.0	9.8
Glu	8.9	7.9	7.6	7.6	7.7	8.8	8.5	8.6	7.5	7.7	8.3	7.9	8.9
Ser	5.6	6.1	6.0	6.0	5.9	6.7	6.2	6.2	5.3	5.3	5.8	5.2	5.7
His	0.9	0.5	0.5	0.4	0.8	0.9	1.0	1.0	0.8	0.8	0.8	1.3	0.9
Galam	1.3	0.9	1.0	0.9	0.7	0.5	0.5	0.6	0.5	0.5	0.6	0.5	0.8
Gluam	2.4	2.0	2.7	2.5	2.4	3.8	3.6	4.0	3.0	2.3	3.3	4.9	4.5
Gly	15.3	19.2	17.6	17.4	15.9	15.5	16.7	15.9	25.4	24.7	20.0	17.9	13.0
Arg	4.6	5.1	4.8	5.0	4.5	3.9	4.3	4.0	5.1	5.0	4.7	4.6	4.3
Thr	10.3	9.4	9.5	9.7	10.1	9.6	9.0	9.1	7.7	7.8	8.4	8.1	9.9
β-ala	0.4	0.4	0.4	0.4	0.4	0.3	0.4	0.3	0.4	0.4	0.4	0.4	0.4
Ala	15.3	15.2	15.7	15.5	15.7	16.5	16.3	16.2	14.6	14.9	16.3	15.9	16.3
γ-aba	0.3	0.4	0.4	0.4	0.4	0.2	0.3	0.3	0.4	0.4	0.4	0.3	0.2
Tyr	1.2	0.9	1.3	1.5	1.3	0.3	0.5	0.6	0.3	0.3	0.4	0.2	0.1
Met	0.2	0.2	0.2	0.2	0.2	0.2	0.2	0.2	0.3	0.3	0.3	0.6	0.8
Val	3.9	3.8	3.3	3.3	3.5	3.9	3.9	3.8	3.1	3.2	3.0	3.2	3.6
Phe	4.7	4.5	4.8	4.6	4.7	4.2	4.2	4.1	4.2	4.4	4.5	4.4	5.1
Ile	3.1	3.0	2.5	2.5	2.6	2.5	2.5	2.4	2.7	2.6	2.3	2.6	2.8
Leu	6.0	6.0	5.3	5.1	4.9	5.2	4.9	4.9	5.7	5.6	5.7	5.9	6.1
Orn	1.0	1.1	1.0	0.9	0.8	1.0	1.6	1.7	1.2	1.0	1.0	1.0	1.7
Lys	6.3	6.5	6.2	6.6	5.9	4.4	4.7	4.6	5.8	6.1	6.0	5.5	4.9
AA µg mg^{-1}	18.3	21.6	18.4	22.7	22.4	29.2	24.1	24.5	52.5	65.0	33.6	40.8	53.0
HA µg mg^{-1}	1.2	1.1	1.2	1.3	1.2	2.3	1.7	2.0	3.2	3.1	2.3	4.0	5.1
AA-C%	16.5	17.9	14.4	15.8	14.6	16.0	14.8	15.5	20.9	21.4	15.4	19.3	16.3
AA-N%	37.5	42.1	33.8	36.3	33.4	38.7	35.1	35.9	51.8	55.4	45.0	44.7	36.1
DI_{DAUWE}	-0.43	-0.44	-0.19	-0.50	-0.45	-0.63	-0.55	-0.57	-0.16	-0.20	-0.14	0.26	0.39

Parameter	31A9	31A10	31A11	31A12	31A13	31A14	31A15	31A16	31A17	34A1	34A2	34A3	34A4
C_{ORG} µg mg^{-1}	72.9	72.4	64.7	56.1	72.2	79.5	75.8	69.0	75.9	90.8	31.0	73.7	65.9
TN µg mg^{-1}	11.5	12.5	10.4	10.1	8.4	12.8	11.4	11.7	11.4	15.6	5.3	9.7	9.3
C_{ORG}:TN	7.4	6.8	7.2	6.5	10.1	7.3	7.7	6.9	7.7	6.8	6.8	8.9	8.2
$CaCO_3$ µg mg^{-1}	656.2	405.7	427.6	500.7	482.7	415.8	458.2	347.2	244.1	408.2	745.5	405.5	500.5
SiO_2 µg mg^{-1}	133.3	124.8	141.8	108.3	157.7	210.7	234.1	376.0	490.8	269.6	112.6	266.2	171.4
"Lith" µg mg^{-1}	42.8	303.1	281.9	261.8	193.5	190.7	133.4	118.1	90.7	113.3	70.7	158.8	176.4
Asp	8.9	9.6	8.1	8.2	10.6	10.9	-	9.0	9.4	8.1	9.5	9.0	7.6
Glu	9.5	9.8	8.4	8.2	8.1	8.0	-	8.0	9.1	10.3	9.1	8.7	8.6
Ser	5.5	5.6	5.8	6.0	6.4	6.5	-	6.1	6.5	6.3	5.8	5.6	5.4
His	0.9	0.4	0.7	0.6	0.4	0.9	-	0.7	0.8	0.9	1.1	1.0	0.9
Galam	0.7	0.7	1.1	1.2	0.7	0.7	-	0.7	0.7	1.3	0.5	0.4	0.5
Gluam	3.8	2.4	3.1	3.4	2.4	2.5	-	3.8	3.5	1.1	2.7	4.2	3.0
Gly	15.0	12.8	15.9	16.1	14.2	14.0	-	14.0	12.3	12.7	12.9	12.6	20.3
Arg	4.7	4.8	4.8	4.8	4.0	4.2	-	4.0	3.9	4.5	3.9	3.7	4.7
Thr	9.4	10.4	9.2	9.1	10.4	10.4	-	9.9	10.4	10.3	9.2	9.4	8.4
β-ala	0.3	0.4	0.6	0.6	0.3	0.3	-	0.3	0.2	0.1	0.2	0.2	0.4
Ala	16.2	15.2	15.7	15.4	16.2	15.6	-	16.0	16.3	14.5	16.1	16.9	16.0
γ-aba	0.3	0.2	0.3	0.5	0.6	0.6	-	0.4	0.2	0.1	0.3	0.3	0.3
Tyr	0.2	0.4	2.1	2.0	1.4	1.2	-	3.2	1.4	0.7	4.9	4.4	2.9
Met	0.2	0.3	0.2	0.3	0.2	0.2	-	0.2	0.2	0.1	0.1	0.1	0.2
Val	3.5	4.1	3.2	3.1	3.2	3.5	-	3.4	3.9	4.0	3.9	3.9	3.5
Phe	4.7	4.9	4.3	4.3	5.1	4.9	-	4.8	5.0	4.7	4.4	4.6	4.5
Ile	2.9	3.4	2.4	2.3	2.3	2.5	-	2.5	2.9	3.4	2.7	2.7	2.5
Leu	5.9	6.3	5.3	5.0	5.7	5.5	-	5.6	6.3	7.1	5.4	5.8	5.4
Orn	1.7	2.2	2.6	3.0	1.8	1.7	-	1.9	1.2	0.5	0.9	0.8	0.2
Lys	5.6	6.0	6.2	6.1	6.2	6.0	-	5.2	5.9	9.1	6.2	5.8	4.8
AA µg mg^{-1}	34.6	31.2	23.0	21.3	32.5	30.2	-	29.4	30.4	50.6	16.7	27.0	27.2
HA µg mg^{-1}	2.6	1.7	1.5	1.7	1.7	1.7	-	2.4	2.3	2.1	0.9	2.2	1.6
AA-C%	20.2	18.6	15.0	16.2	19.3	16.3	-	18.5	17.4	24.2	23.6	16.1	17.6
AA-N%	45.0	36.8	34.9	31.9	56.6	34.8	-	36.6	38.3	48.0	44.7	39.5	43.7
DI_{DAUWE}	0.08	0.35	0.01	-0.12	0.00	-0.04	-	0.40	0.51	1.04	0.81	0.81	0.12

Parameter	31A5	31A6	31A7	31A8	31A9	38B1	38B2	38B3	38B4	38B5	38B8	38B19	39B1	39B6
C_{ORG} µg mg^{-1}	44.9	56.2	53.8	144.5	114.8	23.6	18.2	17.4	15.9	16.5	139.0	64.5	15.5	49.3
TN µg mg^{-1}	7.6	9.2	8.9	21.0	17.4	7.0	10.3	3.0	8.5	8.5	30.1	18.9	3.2	14.2
C_{ORG}:TN	6.9	7.2	7.1	8.0	7.7	3.9	2.1	6.8	2.2	2.3	5.4	4.0	5.6	4.1
$CaCO_3$ µg mg^{-1}	508.9	493.3	555.5	460.2	506.7	337.5	335.7	289.7	372.9	379.2	644.2	513.8	11.6	17.9
SiO_2 µg mg^{-1}	233.6	140.9	191.8	139.7	119.8	592.7	618.9	658.5	581.5	539.2	293.8	351.3	795.9	749.7
"Lith" µg mg^{-1}	154.1	236.6	129.1	67.7	109.4	20.3	12.6	20.4	17.0	52.0	-	18.8	164.6	143.7
Asp	7.6	7.5	7.6	9.9	7.1	7.3	7.9	8.9	9.1	10.3	10.0	8.2	10.1	9.2
Glu	7.7	7.4	9.5	10.4	8.3	8.7	8.4	10.1	9.0	10.2	11.3	8.2	8.0	11.1
Ser	5.9	5.4	5.7	5.6	5.2	6.7	6.8	6.4	6.4	6.2	4.6	5.3	6.8	5.1
His	1.3	1.8	1.2	1.6	1.5	1.0	0.8	0.6	0.8	1.2	0.7	1.1	0.6	0.7
Galam	0.5	0.5	0.5	0.5	0.4	0.5	0.6	0.3	0.5	0.5	0.3	0.4	0.2	0.1
Gluam	3.0	2.9	2.2	3.7	2.6	2.7	3.4	3.0	2.9	2.2	1.3	1.6	2.5	1.2
Gly	22.5	21.2	19.2	14.9	20.3	18.4	21.2	19.5	18.9	16.8	11.3	24.1	14.8	10.2
Arg	4.9	4.6	4.8	4.3	4.6	4.7	3.8	3.8	3.8	3.8	3.6	4.2	2.5	3.4
Thr	8.1	7.7	8.4	9.8	7.6	9.4	8.8	8.5	8.6	8.4	8.8	7.5	9.9	9.6
β-ala	0.4	0.5	0.4	0.3	0.4	0.2	0.3	0.3	0.4	0.4	0.3	0.4	0.3	0.2
Ala	14.9	14.5	15.3	18.0	15.0	13.7	12.8	12.3	12.3	13.5	20.2	18.5	14.5	19.5
γ-aba	0.4	0.4	0.3	0.2	0.2	0.2	0.3	0.2	0.2	0.2	0.1	0.2	0.1	0.0
Tyr	2.8	3.5	3.0	4.9	3.5	0.9	1.3	0.7	0.7	0.7	0.2	0.9	1.1	0.6
Met	0.2	0.2	0.2	0.9	0.5	1.0	0.8	0.8	0.8	0.8	0.1	0.3	2.2	1.5
Val	3.2	3.1	3.3	3.7	2.9	3.8	3.3	3.6	3.8	3.5	4.9	3.1	4.2	4.5
Phe	4.7	4.2	4.1	5.3	4.6	4.8	5.0	4.9	4.9	4.5	4.8	3.9	3.9	5.0
Ile	2.1	2.1	2.4	2.8	2.5	2.6	2.3	2.5	2.5	2.4	3.4	2.0	2.6	2.9
Leu	4.8	4.6	5.2	6.9	5.9	5.9	5.1	4.9	4.7	5.0	8.1	4.9	4.6	8.1
Orn	0.4	0.3	0.3	0.1	0.1	3.5	3.2	4.6	6.1	5.1	0.8	1.1	9.0	2.3
Lys	4.6	7.6	6.4	6.2	6.7	3.9	4.0	4.1	3.6	4.3	5.4	3.9	2.2	4.7
AA µg mg^{-1}	19.2	21.4	28.1	71.3	70.8	12.3	9.7	9.3	6.4	8.2	96.1	41.1	7.8	28.2
HA µg mg^{-1}	1.1	1.3	1.2	4.7	3.6	0.7	0.7	0.5	0.4	0.4	2.5	1.4	0.4	0.6
AA-C%	18.0	16.2	22.2	21.6	26.5	22.1	22.4	22.6	15.7	21.0	30.0	26.3	21.2	24.9
AA-N%	38.4	36.1	48.0	48.1	61.3	26.6	14.3	46.7	10.5	14.4	45.4	33.5	35.4	28.1
DI_{DAUWE}	-0.06	0.29	0.24	1.77	1.04	0.5	0.4	0.4	0.3	0.4	0.9	-0.7	0.5	1.6

calculating a DI value, mol% threonine, arginine, aspartic acid, glycine and valine have negative loadings (Table 5.2) and are therefore enriched in samples with negative DI values. The more negative the DI, the more degraded the sample. Methionine, phenylalanine, isoleucine, histidine, leucine, and tyrosine have positive loadings (Table 5.2) and are enriched in samples with positive DI values. Thus positive DI values indicate fresh organic matter. These changes in amino acid composition with degradation generally agree with numerous laboratory and field based studies of changes in amino acid composition with degradation (e.g. Lee and Cronin, 1984; Cowie and Hedges, 1996; Nguyen and Harvey, 1997).

Table 5.2 Data matrix of the protein amino acid based degradation index. FC is factor coefficient of Dauwe *et al*., (1999), AVG and STD are the average and standard deviations of protein amino acids from this data set.

Amino Acid	FC	AVG	STD
Threonine	-0.129	9.5	1.0
Arginine	-0.115	4.4	0.6
Aspartic acid	-0.102	8.8	1.6
Glycine	-0.099	16.7	3.5
Valine	-0.044	3.5	0.6
Alanine	-0.043	16.0	1.3
Serine	0.015	5.7	0.4
Glutamic acid	0.065	8.3	1.1
Methionine	0.134	0.4	0.3
Phenylalanine	0.134	4.6	0.4
Isoleucine	0.139	2.5	0.4
Histidine	0.158	1.1	0.6
Leucine	0.169	5.5	0.7
Tyrosine	0.178	1.1	1.1

DI-values ranged from -0.7-1.7 which lie between the range of phytoplankton (DI = 1.0 to1.5) and coastal sediments (DI = -0.4 to 1.0). The most positive DI values are associated with the large POC flux event that occurred during the summer of 2001 and spring and winter flux events during 2004 (Fig 5.23; table 5.1). Aside from the clarity of these two events the DI values are characterised by substantial variability throughout the rest of the record. (Table 5.1).

The enzymatic formation of non-protein amino acids such as β-alanine and γ-aminobutyric acid from protein amino acid precursors such as glutamic and aspartic acid is also a well known criterion of organic matter quality (e.g. Lee and Cronin, 1982, Ittekkot *et al* 1984, Cowie and Hedges, 1994; Dauwe and Middleburg; 1998). Molar ratios of Asp/β-ala and Glu/γ-aba were very variable over the time series record of flux with values of 25.6 ± 13.3 and 22.6 ± 12.2, respectively. For comparison, in the equatorial Pacific Asp/β-ala and Glu/γ-aba (Gupta and Kawahata, 2000) values were 18.5 ± 3.6 and 23.2 ± 5.4. Changes in Asp/β-ala and Glu/γ-aba were positively correlated with each other but neither of the degradation indicators were correlated with DI values.

5.5 Discussion

5.5.1 Contribution of amino acids to POC fluxes

The contribution of amino acid fluxes to organic carbon fluxes measured at the PAP site (3000m) ranges between 10-30% at 3000m (Fig 5.25; Table 5.1). For comparison, at similar trap depths (2000-3000m) in the Southern Ocean, Ingalls *et al*. (2003) report that AA fluxes represented 17-26% of C_{org} fluxes, in the equatorial Pacific, Lee *et al*. (2000) estimate that 24% of C_{org} was in amino acids (3000m). Ittekkot *et al*. (1984) found 13-34% of C_{org} in amino acids in the Sargasso Sea. It may be expected that intrinsically labile organic substances, such as amino acids, are shielded by refractory organic or inorganic matrices, such that systematic trends in amino acid contribution to total carbon should reflect the prevailing biogenic mineral phases. From the inter-annual data set presented here, the amount of organic carbon that can be attributed to amino acids displays no obvious seasonality. Fig. 5.25 shows that AA-C% and AA-N% are highest during 1999, which is co-incident with the time when the highest "residual" contents of particles was recorded (Table 5.2), but not the highest fluxes (Fig. 5.17) However, there are no clear relationships between the prevailing mineral phases and the carbon and nitrogen normalised amino acid concentrations. It is important to consider the fraction of carbon, particularly amino acids that can be characterised by conventional hydrolysis and

chromatographic techniques. The percentage of total particulate matter that can be characterised at the molecular level decreases rapidly through the ocean water columns to become a minor component (25%) at depth (Wakeham *et al*., 1997).

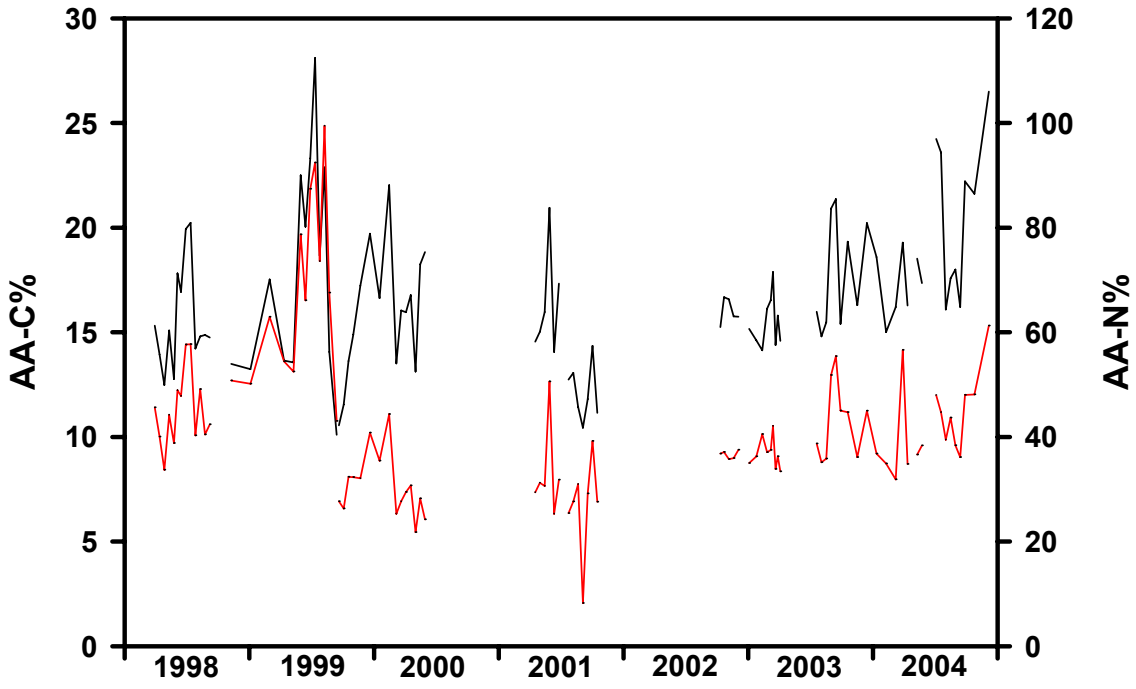

Fig 5.25 Contribution of amino acids to bulk carbon and nitrogen fluxes

Novel ^{13}C NMR studies show that amino acids account for the largest component (40-50%) of POC in deep-sediment trap samples (Equatorial Pacific and Arabian Sea), with "carbohydrates" and "lipids" making up roughly 30 and 20% of the remaining mass (Hedges *et al*., 2001). Assuming this approximate partitioning between major biochemical compound classes can be applied to the north-east Atlantic samples, it suggests that only between 30-60% of potential amino acids present are quantified. It has been suggested previously that labile intermediates released during microbial degradation of biomacromolecules (for example, polysaccharides, lignins, and proteins spontaneously recombine to form chemically complex "geopolymers" (Stevenson, 1994). The products of such abiotic

"humification" reactions may be too structurally complex to chemically analyse (Hedges *et al*., 2001).

5.5.2 Source vs diagenesis

The hydroxyl amino acids Ser and Thr are enriched in diatom cell walls (Hecky *et al*., 1973), the acidic amino acids Asp and Glu are enriched in carbonate skeletons (Degens, 1976) and are preferentially adsorbed onto carbonates (Carter and Mitterer, 1978). The amino acid parameters Asp/Gly and Ser + Thr [mol%]) have been used previously to differentiate diatomaceous from calcareous sources (e.g. Ittekot *et al*., 1984; Wakeham *et al*., 1993; Gupta and Kawahata, 2000). Fig. 5.26 shows this plot for the entire data set from the NE Atlantic, and also data from the Southern Ocean (Crozet deep trap samples) and the equatorial Pacific (Gupta and Kawahata, 2000). Despite the data originating from three very different regimes and incorporating seasonal and inter-annual variability, there is remarkable similarity in the dominance of diatomaceous organic matter irrespective of the relative mineral fractions which range from 11-80% carbonate and 5-75% SiO_2. These observations indicate that organic matter derived from siliceous phytoplankton may contribute more to the organic matter flux than that from calcareous phytoplankton. However, teasing apart the relative effects of organic matter source and alteration complicates any conclusions. It is unclear whether the relationships between these four amino acids are sufficient to represent the provenance of bulk organic carbon groups. The results in Fig 5.26 are consistent with the laboratory experiments of Nguyen and Harvey (1997) and Cowie and Hedges (1996) on the effect of oxic microbial alteration and zooplankton digestion on THAA composition in the diatom *Thalassiosira weissflogii* indicating selective preservation of diatom cell walls.

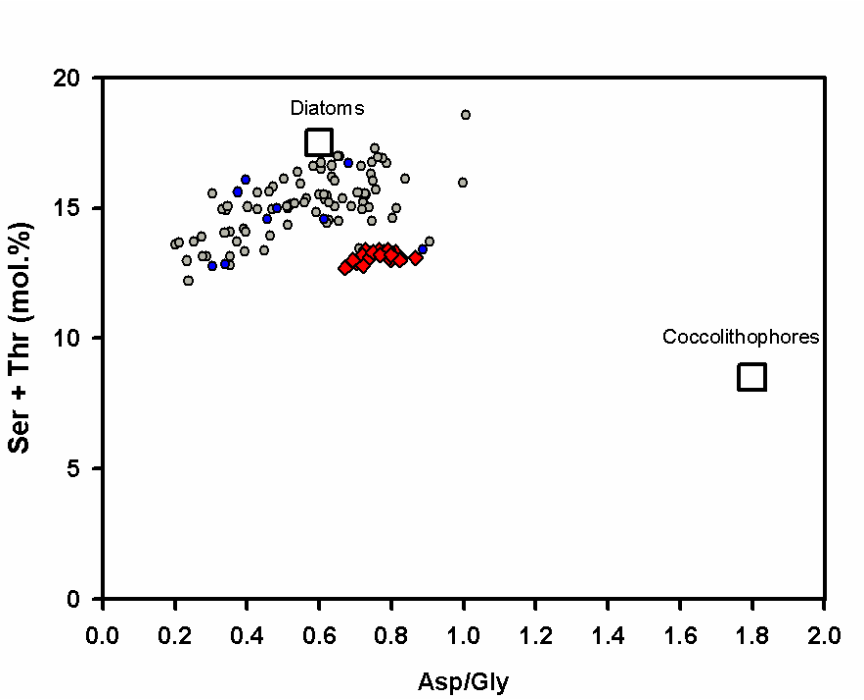

Fig. 5.26 Identification of diatom and coccolithophores dominant organic matter based on the two biogeochemical indicators, following Gupta and Kawahata, 2000 centres of the diatom and coccolithophores boxes are based on data from Muller *et al*.,1986). Grey circles are data from the PAP site, blue circles are data from the Crozet Plateau (this study) and red diamonds are data from the Equatorial Pacific (Gupta and Kawahata, 2000).

Whilst the Asp/β-Ala and Glu/γ-aba ratios exhibit similar patterns over the inter-annual record (Fig 5.27), and support the trends of AA-C% and AA-N% there are instances, i.e. during 1999, when the ratios are decoupled. The ratio of Asp/Glu is relatively constant (1.1 ± 0.2) and likely reflects that both acidic amino acids are enriched in carbonate skeletons (Degens, 1976). Both compounds are subject to similar enzymatic and chemical decarboxylation and deamination reactions (Lee *et al*., 2000). Off the coast of Peru, Lee and Cronin (1982) observed increasing ratios of β-Ala/Asp and absolute increases in β-Ala fluxes that could be due to the decarboxylation of Asp. But γ-aba, from decarboxylation of Glu, did not increase suggesting multiple degradation pathways or rates exist. The variation in mol% of γ-aba was much higher (0.5 ± 0.6) than that of β-ala (0.4 ± 0.2), supporting this notion.

It may also be possible that γ-aba decomposes more quickly than β-ala (Lee *et al*., 2000) explaining the decoupling observed in Fig 5.27, although why this occurs in some years and not others, and the governing mechanisms remain unclear. Additional constraints on interpreting these ratios as diagenetic indicators are that any asparagine and glutamine present in the samples would be converted to their acid counterparts Asp and Glu, although asparagine and glutamine are thought to be minor component of the amino acid spectra in particulate material (Greg Cowie, personal communication).

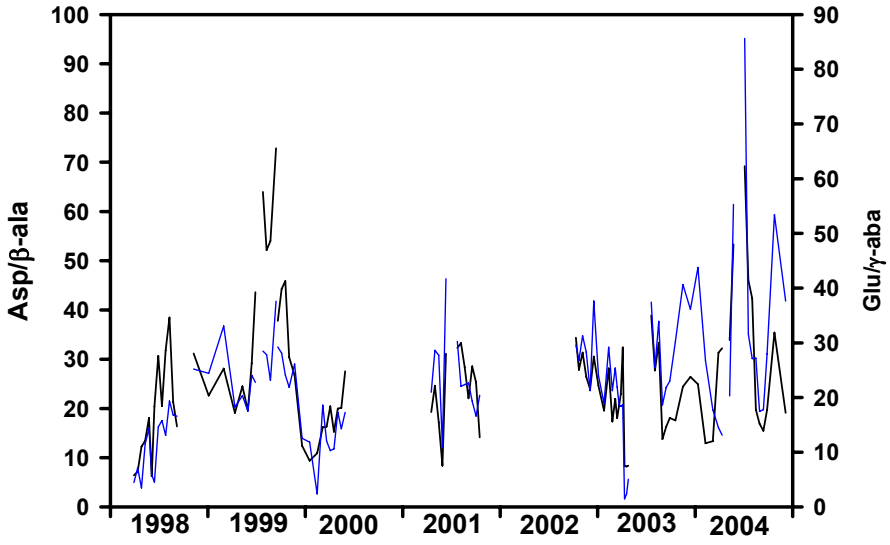

Fig 5.27 Asp/β-ala (black line) and Glu/γ-aba (blue line) as a function of time

5.5.3 Relationship between amino acid composition and the flux of ballast minerals

One of the principal hypotheses instigating this study was that the biogenic composition of particulate flux will affect the degradation state of particulate organic carbon. Global analyses of deep-sediment trap data (Francois *et al*., 2002; Klaas and Archer, 2002) seem to indicate that there are strong quantitative relationships between the flux of biogenic minerals and organic carbon, with particularly strong correlations ($r^2 \approx 0.7$) observed for calcium carbonate (Francois *et al*., 2002; Klass and Archer., 2000).

This study had the benefit of examining the amino acid composition of sediment trap samples from an opal dominated system (Indian Sector of the Southern Ocean) and a carbonate-dominated system (North-East Atlantic). The fraction of organic carbon that can be accounted for by amino acids between these two systems seems to be invariable with respect to the prevailing biogenic mineral phase (Table 5.1). However, the degradation index (Dauwe *et* al., 1999) indicated that the Southern Ocean sediment trap material which was dominated by biogenic silica was relatively fresh in comparison to the majority of the NE Atlantic samples (Table 5.1). In order to test the hypothesis that the flux of minerals to the deep-sea can protect organic matter via association, multiple linear regression analyses between the flux of biogenic minerals and various degradation proxies diagnosed from amino acid compositions, including DI_{Dauwe}, Asp/Bala, Glu/Gaba, AA-C%, AA-N% were conducted. The conclusion from this analysis is that the flux of mineral phases can only explain between 5.1 and 16.5% of the variability. This result suggests that in deep-waters at least, the degradation state of particulate organic carbon cannot be explained by mineral fluxes. There are two possible explanations for this result; 1) amino acid compositions of sedimenting material are incapable of accurately documenting the diagenetic maturity of POM at 3000m, or 2) the quantitative association of POC fluxes and mineral fluxes observed in the deep-ocean (e.g. Klass and Archer, 2002) is not related to minerals protecting the organic matter from degradation.

5.5.3.1. Are THAAs an appropriate tool to assess the degradation state of POM flux in deep-waters?

The general similarity in the amino acid composition of sedimenting material (Fig 5.24) over seasonal and inter-annual timescales indicates a homogenisation of the amino acid pool at 3000m. In the Equatorial Pacific using production rates derived from suspended particles, Lee *et al*. (2000) estimate that about 91% of amino acids produced by phytoplankton are lost in the euphotic zone and over 90% of the amino acids that are exported from the euphotic zone are lost in deeper waters. One may argue that the uniformity of the observed amino acid compositions at 3000m

precludes their use as suitable proxies for the degradation state of organic material. Numerous studies indicate that the largest changes in amino acid content and composition occur in the upper ocean (Lee *et al*., 2000; Ingalls *et al*., 2003, 2006, Unger *et al*., 2005). However, trap studies conducted over multiple sampling depths clearly demonstrate further changes to the content and composition of labile components (e.g. Lee *et al*., 2000; Ingalls *et al*., 2006; Gupta and Kawahata, 2000; Unger *et al*., 2005) that should reflect the protection and increased sinking velocities from association with mineral phases. It may be that at 3000m the changes in amino acid composition in relation to the associated mineral phases are very subtle and cannot be resolved within the accuracy of the method.

5.5.3.2 Implications for the Ballast hypothesis

The mechanisms controlling the large inter-annual and seasonal variability observed in the North-East Atlantic are unclear. The level of production in the upper ocean clearly influences the flux of carbon to the deep-ocean and some studies (e.g. Fischer *et al*., 2000; Waniek *et al*., 2005) attribute inter-annual variability in fluxes to variations in the levels of production. However, comparison of annual fluxes (Fig 5.19) with satellite-derived estimates of productivity (Appendix 5) indicates that differences in production alone are not sufficient to account for deep-water flux variations. This reflects the notion of Boyd and Newton (1995) that whilst observations/models of oceanic productivity may yield input to the biological pump, they cannot, on annual timescales, reliably provide information on the efficiency of the pump in transferring carbon into the deep ocean. From the data-set analysed and presented here, it is also apparent that changes in the flux and composition of ballast minerals in the north-east Atlantic is unable to systematically explain the degradation state of organic carbon through "protective-association" with mineral phases as implied by the "ballast-theory"(Klass and Archer, 2000). Furthermore, the similarity in amino acid composition between sediment trap samples from the carbonate-dominated north-east Atlantic and opal-dominated Southern Ocean do not support hypotheses of differential mineral protection capacities.

Despite the analysis of the entire data set indicating the absence of a mechanistic relationship between mineral fluxes and degradation, there are some isolated exceptions. The summer of 2001 was characterised by high mass, POC, AA, HA fluxes and elevated DI-values which indicate the sedimenting organic matter was relatively fresh relative to other years (Fig. 5.23). The summer flux event in 2001 was also characterised by high residual i.e. lithogenic (Jickells *et al,* 1998) fluxes. For the large majority (95%) of the data POC fluxes were less than 20 mg C m^{-2} d^{-1} and tightly correlated with the total mass flux (Fig 5.7). The data not characterised by this regression all had POC fluxes greater than 35 mg m^{-2} d^{-1} and lithogenic fluxes >50 mg m^{-2} d^{-1}, implying that lithogenic fluxes may have been important in controlling the flux of fresh organic matter from the upper ocean, at least during 1989 and 2001.

Ittekkot and Haake (1990) first suggested that lithogenic matter could act as ballast for sinking particles allowing for a more rapid export to deep waters and reduced degradation during descent. This mechanism has also been shown to be important for high export rates of carbohydrates in the Bay of Bengal (Unger *et al*., 2005). Laboratory studies show that the presence of lithogenic matter can promote the formation and density of marine aggregates (Hamm, 2002). However, in this same study it was demonstrated that aggregate sinking velocity was a function of mineral type and the diatom culture used to form aggregates, some combinations of which actually reduced the sinking velocity. Similar experiments conducted by Passow and De La Rocha (2006) demonstrated that the addition of minerals increase aggregate sinking velocity. These observations may help to explain the ambiguous relationship between "lithogenic" fluxes and the degradation of organic carbon in the study area over the entire data set. The impact of elevated lithogenic fluxes on POC fluxes during discrete sampling events in 1989 and 2001 exert a large effect on the magnitude of POC export on both seasonal (Fig.5.5) and annual time-scales (Fig.5.15). The data could help to further explain observed patterns of enhanced dust sedimentation (Petit *et al*., 1999) and reduced atmospheric pCO_2 (Martin *et al*., 1988)

during the LGM that extend beyond iron fertilisation of the upper ocean (Martin, 1990).

Based on the results of this study the observed correlations between mineral fluxes and POC fluxes are not related to a physical protection mechanism as diagnosed by hydrolysable amino acids and hexosamines. If the results obtained here, which are limited to one locality, are representative of flux mechanisms elsewhere, then alternative explanations for the findings of Klass and Archer, (2002); Francois *et al*., 2002, and Armstrong (2002) need to be sought.

Global silica to POC data from various depths above 3000m show many different opal to POC relationships, with slopes unique to geographic regions (e.g. Ragueneau *et al*., 2000), in contrast the slopes of POC to $CaCO_3$ are similar between geographic regions (De La Rocha and Passow, 2007). It has been suggested (De La Rocha and Passow, 2007) that a large part of the POC formed by diatoms will remain associated with the opal frustule during sinking (e.g. Beaulieu, 2002), whereas coccoliths are only loosely attached to the coccolithophorid cell and can become easily detached through for example viral attack (Castberg *et al*., 2001) and grazing (Schnetzer and Steinberg, 2002). Thus, a large part of POC formed by diatoms will remain associated with opal frustule during sinking, whilst coccoliths shed by coccolithophorids will be less strongly associated with the organic matter of the organism that produced them, leaving it more open to attaining homogenous mineral to POC ratios during aggregation and sinking (De La Rocha and Passow, 2007). As a consequence of how different biominerals find there way into aggregates, it may be expected that the regional variability in the opal to POC ratio observed during production is transferred to the deep-sea whereas any spatial or temporal variability in the carbonate to POC ratio is obscured (Da La Rocha and Passow, 2007).

5.6 Conclusions

This study focuses on the flux and composition of amino acids in relation to the dominant mineral phases that comprise the particulate flux. Sediment trap samples

from the opal-dominated Southern Ocean and carbonate-dominated north-east Atlantic were examined to try and elucidate degradation processes related to the mineral composition of sinking particles. Samples from the north-east Atlantic were collected between 1998 and 2004 and exhibited high seasonal and inter-annual variability in all biogenic components fluxes and associated elemental ratios providing a useful template to test the ballast hypothesis. The fluxes of POC and the labile components, amino acids and hexosamines essentially follow the same pattern indicating that the export of bulk POC and both compound classes is closely linked. The fraction of carbon that could be accounted for by total hydrolysable amino acids varied very little with sample composition, implying that systematic relationships between mineral fluxes and the preservation of labile components of organic matter are not apparent from deep-water particle fluxes. The compositional spectrum of protein amino acids was used to quantify the degradation state of the settling particulate material. Based on this parameter, the least degraded material was found in association with high POC and lithogenic fluxes observed in 2001. However, disagreement between the various amino acid degradation proxies suggests that both degradation and source are important factors in explaining the composition of amino acids in sinking particles. Multiple linear regression analysis reveals that mineral fluxes can only explain a very small amount of the variability in amino acid composition. Specific amino acids seem to infer that diatomaceous organic matter is more important than calcareous organic matter, but whether these provenance markers are representative of bulk organic matter remains unclear. Given the apparent importance of mineral type to the amount of carbon exported (Klass and Archer, 2002), it was hypothesised that the degradation of organic matter was governed by mineral fluxes, based on this study this does not seem to be the case. However, despite the large spatial and temporal gradients in the data-set, the homogenisation of amino acid composition at 3000m suggests that this sampling depth may be inappropriate to elucidate processes relating to the ballast-theory. A similar study of contrasting flux regimes conducted over multiple-depth horizons in the upper 1000m of the water column may prove to be more insightful.

6 Conclusions and Future Directions

6.1 Conclusions

The first part of this study documents the design and deployment of a free drifting buoyancy-controlled sediment trap, PELAGRA during post-bloom periods in the north-east Atlantic. PELAGRA addresses the substantial technical challenges in accurately sampling upper-ocean particle flux. It is envisaged that PELAGRA will provide a stream of high quality data on the export of material from the upper ocean and how this is attenuated with depth. The vertical fluxes of ^{234}Th into the traps were less than those estimated from the upper water column budget of the isotope and this is interpreted as a consequence of previous export events that had stripped ^{234}Th from the water column. Alternatively lateral advection of gradients of total ^{234}Th/^{238}U disequilibria may have confounded the Eulerian budgeting approach adopted.

Organic carbon fluxes measured by the traps are compatible with estimates of new production (2003-2006) although the time scales of observation are clearly different and therefore unlikely to agree. A highly successful simultaneous deployment in July 2006 by traps at two different depths provides a direct measurement of the attenuation in flux with depth and a measure of the Martin *b*-value, which at 1.8 is substantially greater than the canonical value of 0.86. This agreed well with estimates of new production in the overlying water column. In common with comparable observations in the Pacific (Buesseler et al 2007), it would seem that there is spatial heterogeneity in the rate of flux attenuation with depth and that these variations must be incorporated into global biogeochemical models as soon as the number of observations increases.

PELAGRA was deployed numerous times in the Indian Sector of the Southern Ocean as part of the CROZEX project, although unfortunately simultaneous multiple-depth deployments were not achieved. Many previous studies have quantified export ratios in which normalised carbon flux values are compared to contemporaneous measurements

of primary production. This can yield over- and under-estimates of export ratios that can only be sensibly interpreted in the context of the temporal decoupling of production and export. In this study retrospective estimates of production were made based on satellite data and empirical observations between chlorophyll and integrated production. Using assumed sinking velocities to represent slow, medium, and fast settling particles a range of export ratios were calculated. Based on this analysis the artefact of temporal decoupling was most prevalent in the highly productive regime north of the Crozet Plateau where large changes in surface biomass occurred over relatively short periods of time.

In the Southern Ocean the PELAGRA traps were deployed at numerous sampling depths and it was important to normalise organic carbon fluxes to a nominal depth to enable full comparison of the data set. Instead of normalising fluxes by a single factor based on an empirical relationship that has no observational validity in the study area, this study had the benefit of employing normalising factors from similar environments derived from recently published work (Buesseler *et al*., 2007). Comparison of these two techniques indicated that the traditional Martin curve under- and over-estimated normalised fluxes at southern (HNLC) and northern (productive) stations respectively.
The measured and depth-normalised organic carbon flux north of the plateau was an order of magnitude larger than fluxes from all other stations. Based on observed production profiles this deployment seems to represent the best estimate of surface export from the fertilised region north of the plateau. Using a simple mass balance approach to account for seasonal depletion of dissolved silicic acid in surface waters and Si fluxes from the euphotic zone, potential surface export (100m) of organic carbon from the bloom area was estimated to be in the order of 11-15 g C m^{-2}. This is higher than previous estimates obtained from mesoscale perturbation experiments, possibly reflecting fundamental differences in methodical approach.

Diatom size correlated well with a range of calculated export $ratios_{(100m)}$ demonstrating the significant role of large diatoms in mediating surface export from a naturally fertilised bloom. The main diatoms involved in export from the surface are medium-

large centric diatoms, particularly *E. antarctica*; although to the south of the plateau the heavily silicified pennate *F. kerguelensis* was most important, reflecting the regional differences in community structure and its effect on the magnitude of carbon export. The role of *E. antarctica* as an agent of downward particle flux from the productive regime north of the plateau was also evident from the analysis of deep-sediment trap material. In the HNLC region to the south, deep-water diatom fluxes were dominated by *F. kerguelensis*. It is clear that the presence if iron in otherwise HNLC waters promotes the production of diatoms that are 1) both present in sufficient numbers and 2) capable of blooming. The importance of *E. antarctica* in the productive regime north of the plateau is related to the regions proximity to the Crozet Islands, where winter resting spores and dissolved iron are advected into the bloom area during the winter.

Carbon fluxes measured south of the plateau are consistent with previously measured fluxes in similar environments. The carbon fluxes measured to the North are elevated relative to the "background flux" and are above average for the Southern Ocean as a whole. Comparison of annually integrated deep-sediment trap fluxes from the productive regime to the north and HNLC regime to the south indicates that natural iron fertilisation can increase the strength of the biological carbon pump by a factor of 4. An assessment of the deep-water carbon fluxes in relation to satellite-derived productivity suggest that the efficiency of the biological pump in transferring organic carbon to the deep-ocean is increased by a factor of 3 in the presence of iron. Assuming that the sediment trap results obtained around Crozet are typical of the circumpolar Polar Frontal Zone, extrapolating them over this area indicates that iron fertilisation increases carbon export below the mixed layer to the effect of 0.02 Gt C yr^{-1}. The lowering of C_{org}:C_{inorg} ratios of settling particles north of the plateau and towards the end of the flux profile is believed to be mediated by enhanced sedimentation of calcifying heterotrophs in response to an increased food source. This effect could potentially lower the sequestration of atmospheric carbon from iron-fertilised productivity due to associated changes in upper ocean carbonate chemistry. An Fe_{added}:$C_{sequestered}$ molar ratio of 1.4×10^{-3} was calculated at 3000m, which is 2 orders of magnitude higher than similar estimates obtained from KEOPS (Blain *et al*.,

2007). It is suggested that these values are representative of deep-water (3000m) rather than shallow-water (100-200m) sequestration efficiency.

The final part of this study focuses on the flux and composition of amino acids in relation to the dominant mineral phases that comprise the particulate flux. Sediment trap samples from the opal-dominated Southern Ocean and carbonate-dominated north-east Atlantic were examined to try and elucidate degradation processes related to the mineral composition of sinking particles and the relative role of opal vs carbonate in C_{org} fluxes. Samples from the north-east Atlantic were collected between 1998 and 2004 and exhibited high seasonal and inter-annual variability in major biogenic component fluxes and associated elemental ratios providing a useful template to test the ballast hypothesis. The fluxes of POC and the labile components, amino acids and hexosamines essentially follow the same pattern indicating that the export of bulk POC and both compound classes is closely linked. The fraction of carbon that could be accounted for by total hydrolysable amino acids varied very little (20-30%) with sample composition (20-30%) implying that systematic relationships between mineral fluxes and the preservation of labile components of organic matter are not apparent from deep-water particle fluxes. The compositional spectrum of protein amino acids was used to quantify the degradation state of the settling particulate material. Based on this parameter, the least degraded material was found in association with high POC and lithogenic fluxes observed in 2001. However, disagreement between the various amino acid degradation proxies suggests that both degradation and source are important factors in explaining the composition of amino acids in sinking particles. Multiple linear regression analysis reveals that mineral fluxes can only explain a very small amount of the variability in amino acid composition. The dominant amino acids present in both North Atlantic and Southern Ocean samples indicate that diatomaceous organic matter is more important than calcareous organic matter, but whether these provenance markers are representative of total organic matter remains unclear due to the combined effect of source and diagenesis on amino acid compositions. Given the apparent importance of mineral type to the amount of carbon exported (Klass and Archer, 2002), it was hypothesised

that the degradation of organic matter was governed by mineral flux, however, based on this study this does not seem to be the case.

6.2 Future directions

The interpretation of sediment trap data is severely hindered by the decoupling of production and export and as such these events are under-sampled and poorly represented in models. In order to understand the relationships between estimates of surface flux based on ^{234}Th measurements, nutrient budgets, and to reconcile with those direct measurements made by PELAGRA, longer periods of observation are required. A dedicated cruise program over a sufficient length of time that accurately samples both increasing and decreasing levels of productivity at a specific site, in unison with a suite of export proxies and direct measurements would be an invaluable study. The availability of well-resolved information on the magnitude and composition of upper ocean biomass is required to successfully interpret export processes, and identify the principal factors mediating variations in flux attenuation with depth. It is also crucial to aim for simultaneous multiple-depth deployments of PELAGRA in the future, with several traps deployed at the same depth horizon in order to fully resolve remineralisation profiles in the upper ocean.

The attenuation of flux with depth is described by the exponent *b* in power-law expressions. This value, which can essentially be considered as a remineralisation co-efficient, represents a composite of all major biochemical compound classes. Different biochemical groups, such as pigments, amino acids, lipids, and carbohydrates are characterised by varying labilities such that the relative proportions of each compound class define the shape of flux attenuation of bulk POC with depth. There are a number of ecological scenarios in which the relative partitioning of carbon between these groups may change. With the improved technology now available to measure particle fluxes in the upper ocean it would be desirable to quantify the flux attenuation of each compound class, as well as specific important

compounds (e.g. chlorophyll a) to examine the effect that they exert on the attenuation of undistinguished particulate organic carbon.

Molecular-level (Mol%) amino acid analysis is a powerful tool in understanding diagenetic effects in organic matter. Mol% analyses of amino acids are perhaps most powerful when combined with methods to tease out statistical changes in average molar composition that can be related to fresh vs degraded material. The statistical compilations of minor changes in mol% provide a generalised measure of relative degradation, however, they do not accurately indicate source, trophic transfer, or provide information about specific organisms responsible for organic matter transformation.
D/L amino acid ratios have emerged as a powerful new tool to track prokaryotic input to detrital organic matter. Combined d-amino acids are thought to derive exclusively from peptidoglycan in modern materials, and as such they are extremely specific tracers of bacterial source. The analysis of amino acid enantiomers in settling particulate material would provide additional information about the heterotrophic remineralisation of organic matter.

Compound specific isotopic signatures of amino acids represent a powerful new approach to understanding the source and transformation of OM in sinking particles. It has long been recognised that major biochemical classes have distinct isotopic fractionations relative to bulk OM. Such fractionations are typically relatively small (1-5 ‰) and reflect the cumulative averaged effect of distinct pathways of cellular biosynthesis. Compound-specific isotopic analysis shows that variability in individual amino acids is dramatically larger. All primary producers and heterotrophic microorganisms synthesise around twenty major protein amino acids, but pathways used for the synthesis of each can vary widely, resulting in unique patterns in their total $\delta^{13}C$ and $\delta^{15}N$-amino acid fractionations. Recent work McClelland *et al*., 2000 has provided the first detailed view of how $\delta^{15}N$ values of individual amino acids behave with trophic transfer. Some amino acids, such as aspartic acid and glutamic acid, display large enrichments with each trophic step, while others such as phenylalanine, serine and threonine, remain essentially unchanged through multiple trophic transfers. The $\delta^{15}N$

values of specific non-enriching amino acids (NE-AA) might provide a fixed record of $\delta^{15}N$ values at the base of the food chain, while the $\delta^{15}N$ differences between selected enriching amino acids (E-AA) represents an internally normalised indicator of trophic history, unaffected by unknown mixture components. The characterisation of amino acid isotopic signatures of primary producers and in sinking POM accurately sampled with new technologies such as PELAGRA would provide invaluable information on the functioning of upper ocean community structures and their effects on surface export processes.

Inter-annual variability in particle fluxes makes it challenging to draw firm conclusions from the analysis of a single year of data. The redeployment of deep-sediment traps around the Crozet Plateau would benefit the interpretation of the effects of iron fertilisation on the functioning of the biological pump. Unfortunately in this study it is possible that part of the downward flux was under-sampled due to the deployment date of the sediment trap samples relative to surface patterns of biomass accumulation. Future studies should consider earlier deployments in order to effectively sample the particle flux profile in its entirety.

Although the deep-water particle flux measured around the Crozet Plateau was dominated by diatoms and biogenic silica, there was evidence of enhanced carbonate fluxes towards the end of the flux profile. In this study it was suggested that these carbonate fluxes are caused by the sedimentation of calcifying heterotrophs (i.e. foraminfera and pteropods) in response to an increased food source. Distinguishing the main agents of calcium carbonate flux in this environment, and others should be a future recommendation of all sediment trap studies. Where possible this analysis would benefit from an assessment of the abundance and calcification rates of foraminfera in order to fully resolve their influence on surface water carbonate chemistry and the sequestration of atmospheric pCO_2 upon iron fertilisation.

APPENDIX 1: TOTAL AND ORGANIC CARBON ANALYSIS

This method described here is based on that of Nieuwenhuize et al., (1994)

A1.1 Overview of chemistry

Measurements of organic carbon and total carbon are made using the Carlo Erba EA-1108 CN elemental analyser. Quantitative partitioning between organic and inorganic forms of carbon is achieved by in-situ acidification with 3.05M HCl (e.g. Nieuwenhuize et al., 1994).

The operation of the elemental analyser is based on the "flash combustion" of the sample introduced into a high temperature column reactor by an autosampler. The combustion column contains stationary phases composed of a porous layer of oxidation catalyst of chromium trioxide (Cr_2O_3) overlying silver cobalt oxide granules (Co_3O_4+Ag) maintained at 1050°C. At these temperatures Verado *et al*., (1990) were able to achieve >99% recovery of carbon from graphite. The sample and container are oxidised in a burst of high purity oxygen. The combustion products, a mixture of CO_2, NOx and H_2O, are then swept through the combustion column by a high purity helium carrier gas into the reduction column. The reduction column, a U-shaped tube packed with metallic copper granules, is maintained at 650^oC, and removes excess oxygen and reduces the nitrogenous oxides to N_2. The N_2, CO_2, and H_2O are then carried through a water absorbing filter containing magnesium perchlorate, $Mg(ClO_4)_2$. The remaining N_2 and CO2 is carried onto a 2m chromatographic column at 54^oC, where detection is by thermal conductivity.

A1.2 Method Validation

The acidification methods measure organic carbon, following acid dissolution of biogenic and abiogenic carbonate minerals. Inorganic carbon is then calculated by subtraction of organic carbon measurements from total carbon values. The main criticism of these methods is the possibility of hydrolysation of organic matter by the acid which may be lost if the particulate residue is separated from the spent acid

(Froelich et al., 1980). Over 40% of the organic carbon in modern sediments can be soluble in acid (Roberts et al., 1973). This problem can be overcome by either analysing the carbon content in both the spent acid and residue (e.g. Froelich, 1980), using an acid vapour procedure to remove inorganic carbon (Hedges and Stern, 1984), or the addition of acid to samples already weighed out into sample cups (e.g. Verado et al., 1990; Nieuwenhuize et al., 1994). These procedures provide significant improvements in accuracy. However, the first method requires relatively large samples (50-200mg) which is not generally possible for sediment trap samples. Moreover, Froelich's procedure demands a dissolved and solid phase carbon analyser. Vapour phase methods do not have these restrictions, but can fail to remove all traces of carbonate from calcareous oozes (e.g. Hedges and Stern, 1984), and carbonate associated with complicated organic matrices. In-situ acidification methods have the advantage that they eliminate reweighing procedures, avoid losses of acid-soluble organic carbon, and consume a small amount of material for analysis.

A1.3 Comparative Measurements

Total carbon measurements were made on samples previously analysed and published (Lampitt *et al*., 2001) and the results are shown in Fig. A1.1a. Generally the agreement between the measurements is very good. The vertical error bars are ± 1 S.D. of triplicate measurements from this study. An additional comparison was made by independently estimating total carbon using the coulometer. Fig. A1.1b shows the relationship between estimates made using the CHN and coulometer for a sample subset. A subset of samples were also analysed independently for particulate organic carbon at the University of Liverpool, these results are compared with the ones obtained during this study and presented in Figure A1.2. There is some disagreement between the nitrogen values, this is likely related to different methods of acidification employed in the two separate studies.

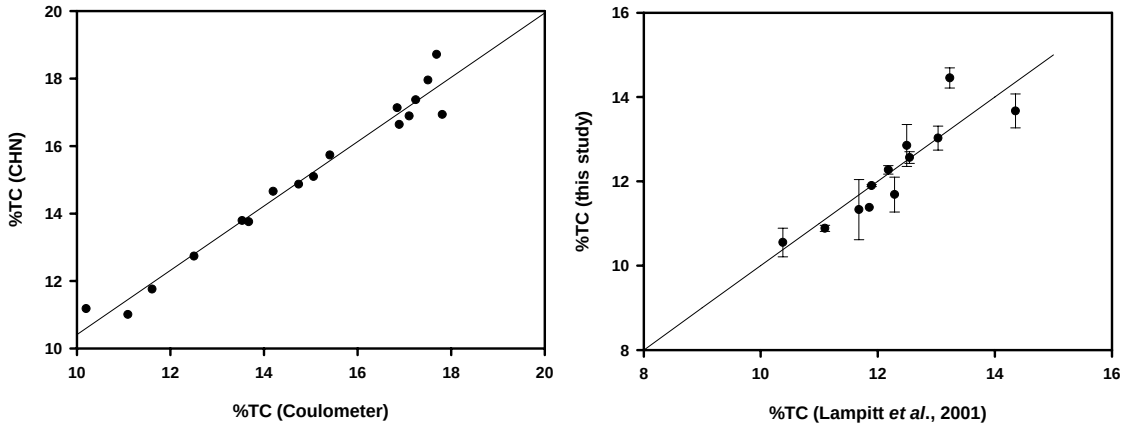

Fig. A1.1 Comparison of total carbon measurements obtained during this study with those obtained using a coulometer (A1.1a) and previous CHN analyser measurements (A1.1b)

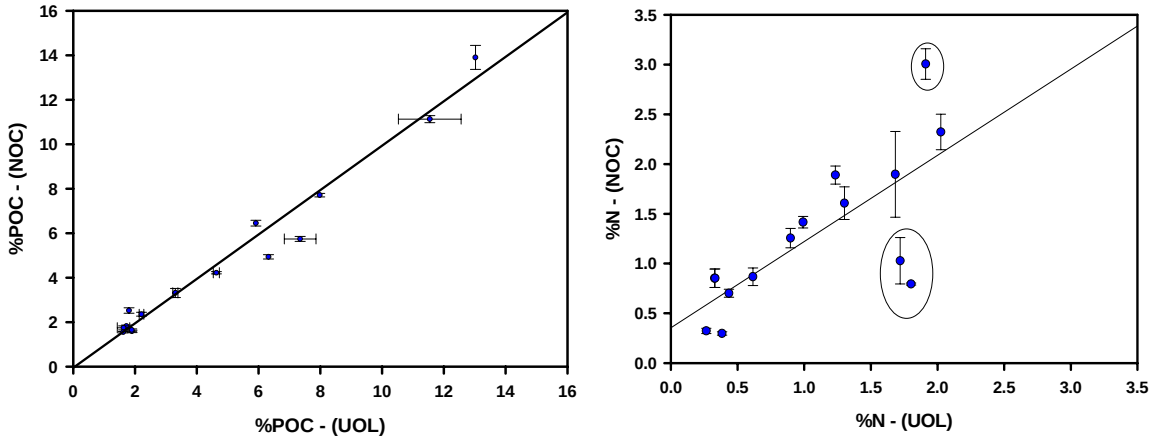

Fig A1.2 Comparison of organic carbon measurements compiled during this study, %POC – (NOC) and those analysed independently at the University of Liverpool %POC – (UOL).

A1.4 Reagents

3.05M HCl: Add 15ml of 12.2M HCl to 45ml of Milli-Q water and leave to cool

A1.5 Procedure

A1.5.1 Freeze-dried sediment

1) Samples should be freeze-dried overnight to remove any excess water

2) Samples are then crushed in a plastic medicine cup using the base of a polypropylene sample tube and the flat end of a clean metal spatula.

3) Silver cups combusted in the furnace at 550^{o}C overnight.

4) For each sample weigh approximately 3-5mg of sediment into six, pre-combusted, pre-weighed, silver cups. Holding the rim of the cup with curved forceps, tap it on the rim of a glass Petri-dish to shake down the contents.

5) Reserve three cups for organic carbon and three cups for total carbon analysis.

6) For the cups reserved for total carbon analysis – Hold the cup with curved forceps and pinch together with metal forceps a few millimetres from the top and twist 90^{0}. Fold over the twisted silver and place the cup into a metallic screw press. Use the base of the screw press to gently hit the pin pressing the silver cup into a sealed capsule. Drop the cup a few times onto a glass plate to check that it is correctly sealed. If any of the sediment escapes then discard the sample.

7) For the organic carbon samples add 15µl of 3.05M HCl to each cup, the degree of effervescence will depend on the carbonate content of the sample. After completion of the reaction, evidenced by termination of effervescence (i.e. carbon dioxide escape), a further 15µl of 3.05M HCl should be added. After the reactions have completed place the sample on a hot plate for 15 minutes at 60^{o}C.

8) Step 7 (i.e. two acid additions followed by evaporation of acid) should be repeated until no further effervescence is detected. To confirm complete removal of organic carbon add an additional 20µl of 3.05M HCl. Dry the sample on a hot plate at 50^{o}C for thirty minutes. Note: The acidification procedure must be performed very carefully to avoid sample loss and to ascertain the complete saturation of the sample

with HCl. If any material is lost from the sample cup, the sample should be discarded.

9) To each sample add 20µl of Milli-Q water and evaporate on a hot-plate at 70^{o}C for thirty minutes. Repeat this procedure three more times to rinse the sample of excess acid.

10) Place the samples in an oven at 70^{o}C overnight to dry. Ensure the samples are covered with foil to prevent in material falling into the sample cups. This drying procedure was chosen to achieve minimal loss of volatile organic compounds, while removing hydrochloric acids that may otherwise enter the CHN analyser and accumulate in the combustion tube.

11) Repeat step 6. The samples are know ready for analysis (see running the elemental analyser)

A1.5.2 Filtered samples

12) Sample aliquots are filtered onto pre-weighed, pre-combusted 25mm GF/F filters.

13) Samples are rinsed with ammonium formate, followed by Milli-Q.

14) Samples and filters are dried in an oven at 60^{0}C overnight

15) The samples and filters are weighed to determine the mass of sample on the filter.

16) The samples for organic carbon analysis are placed onto labelled trays inside a plastic desiccator. The base of the desiccator is filled with concentrated Sulphurous acid. These operations should be performed inside a fume cupboard.

17) The plastic desiccator is then vacuum sealed and left for 48 hours. The vacuum seal should be checked at 12, 24, and 36 hours if possible.

18) The samples should be removed from the vacuum desiccator and placed directly into an oven to at 60^{0}C overnight. This drying procedure removes excess acid from the samples (e.g. step 10).

19) The acidified sample and filter should be placed onto a 30mm aluminium foil disk (available from elemental microanalysis ltd). The aluminium foil disk and filter is folded in half like a pancake. The excess foil disk is then folded over to seal the "pancake" shape. From one end roll the "pancake" as tightly as possible into a cigar

shape. Care is needed not to tear the foil. The cigar-shaped foil and filter is then placed into the screw press (c.f. step 6) and converted into a small capsule that can be accommodated by the CHN analyser.

A1.6 Running the elemental analyser

At the start of each analytical run there is a defined set of procedures that should be followed to ensure that the elemental analyser is correctly calibrated and running efficiently.

a) Two bypass runs are initially made to check that the combustion tube is allowing the correct flow of gases and that it is not contaminated by previous analyses.

b) A silver pellet containing a small amount (0.5mg) of the standard (Cyclohexanone-2, 4-dinitrophenylhydrazone) is run as a "bypass". The carbon and nitrogen in the sample is detected, and the column retention times for each element are calculated. The new values are then entered if they are different to when they were previously calculated (to account for slight drifts in the retention times).

c) Two blank samples (pre-combusted silver cups; 500^{o}C, 12 hours) are analysed to determine the quantities of carbon and nitrogen in the silver cups.

d) Two standard samples are run as unknowns, permitting the analysers software to calculate the K-factor for carbon and nitrogen. This is a constant multiplier applied to the area of an unknown sample and is calculated according to equation A.1.1:

$$K = (S_{C\%} \times S_W) / (S_C - B_C) \qquad \textbf{(A1.1)}$$

where, $S_{C\%}$ is the theoretical composition of the analytical standard (51.79% for carbon and 20.14% for nitrogen), S_W is the weight of the standard, and S_C and B_C are the carbon (or nitrogen i.e. S_N and B_N) areas of the standard and blank samples respectively. This takes into account the values associated with a blank sample and reduces the areas of the unknown samples accordingly.

e) Two analytical standards are run as standards (software option) and the K-factor determined in step b is used to calculate the percentage composition of both carbon and nitrogen in the standards by transposing Equation A1.1. These values are then

compared with the theoretical composition of the standard and if they are within ±0.5% (i.e. 51.29-52.19% for carbon) sample analysis is permitted.

f) The procedure is identical if filters rather than freeze-dried sediment are used. The blank should consist of an acidified filter for organic carbon analyses and a pre-combusted filter for total carbon. In both cases the 30mm aluminium foil discs will have been pre-combusted at 400^{o}C for 12 hours)

g) Sets of 9-12 samples are "capped" with analytical standards to monitor the performance of the elemental analyser. The schematic in Fig. A1.2 Shows how this is achieved.

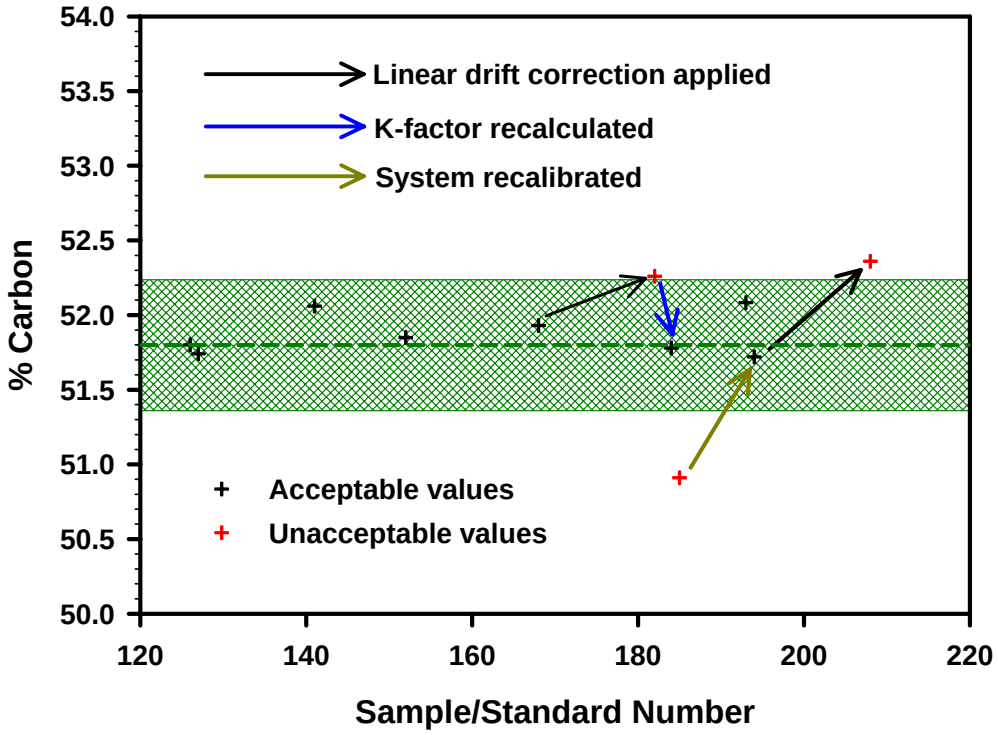

Fig. A1.2 Schematic of standard positions within an analytical run and the appropriate corrections.

If after a set of samples the analytical standard is out of the acceptable range another standard should be run. If second standard displays consistent high/or low percent composition then the K-factor can be recalculated manually, i.e. the aim of the exercise is to determine the numerical value of the K-factor required to obtain the

theoretical composition of the standard. This can be calculated manually using equation A.1.1. The new K-factor is then entered into the software, and another two standards run which use the new k-factor to calculate the composition of the analytical standard. If these values are within the accepted range then analysis can continue.

Second to the problem of adjusting the K-factor is applying a correction to the samples analysed prior to the unacceptable standard value. In this scenario and based on the information available one must assume linear drift theory, that is that value of the standard (i.e. performance of the machine) has drifted linearly with fixed increments between the two analytical standards that "cap" the sample set. Based on this assumption it is possible to isolate the samples that are outside of the acceptable range and apply a correction according to the equations described below (carbon given as an example).

$$A = (S_C \times F_C) / X \quad \textbf{(A1.2)}$$

where A is the adjusted sample area, S_C is the carbon (or nitrogen) area of the standard closest to the theoretical maximum (when using Cyclohexanone-2, 4-dinitrophenylhydrazone) this is 51.79% C and 20.14% N), F_C is the area of the sample to be corrected, and X is the average carbon (or nitrogen) area of the standards analysed before and after sample(s) F. Using the adjusted areas (A), absolute values (mg) of carbon and nitrogen can be calculated by the following:

$$M_C = (W \times A) / S_C \quad \textbf{(A1.3)}$$

where M_C is mg of carbon (or nitrogen) in the sample, W is mg of carbon (or nitrogen) in the standard closest to the theoretical maximum, A is the adjusted area for the sample, and S_C is the carbon (or nitrogen) area of the standard closest to the theoretical maximum. The corrected percentage composition can therefore be recalculated according to

$$\%C_{CORR.} = (M_C / M_{SAM}) \times 100 \quad \textbf{(A1.4)}$$

where $\%C_{CORR}$ is the corrected composition data, and M_{SAM} is the total mass of the sample concerned.

Occasionally the drift is severe and an entire recalibration of the instrument is warranted. This may be cause by obstruction of carrier gases by residual ash, a shift in retention times, or some unknown cause. In this instance steps a-e should be carried out.

A1.7 Calculations

C_{TOTAL}	Total carbon in sample (mg)
C_{ORG}	Organic carbon in sample (mg)
C_{INORG}	Inorganic carbon in sample (mg)
$CaCO_3$	Calcium carbonate in sample (mg)

$C_{INORG} = C_{TOTAL} - C_{ORG}$

$CaCO_3 = 8.33(C_{INORG})$

APPENDIX 2: BIOGENIC SILICA ANALYSIS

The method is based on the modified wet-alkaline extraction technique of Mortlock and Froelich (1989) as reviewed in the inter-laboratory comparison of Conley *et al* (1998).

A.2.1 Overview of Chemistry

This method is based on the dissolution of biogenic opal and subsequent measurement of dissolved silicon in solution. The solubility of biogenic opal increases significantly with increasing temperature and the strength of alkaline solution. This method uses a strong alkaline solution (0.2M NaOH) held at 100^0C for a period of 3 hours. Once in solution, the concentration of dissolved silicon is measured by reacting the sample solution with molybdate to form a silicomolybdate complex. The resulting yellow solution is reduced using a metol and oxalic acid solution to generate strongly coloured blue compound. The reducing solution also decomposes phosphomolybdate and arsenomolybdate eliminating interference from any phosphate or arsenate content of the sample.

A.2.2 Method Validation

A representative sediment trap sample (XXVIIB8) was analysed using the differential extraction method (e.g. Eggiman *et al*., 1980; DeMaster, 1981) to determine the length of time necessary for complete dissolution of biogenic opal. Duplicate samples were extracted with 0.2M NaOH at 100^oC and sampled periodically between 0-8 hours with higher temporal resolution during the beginning of the extraction period (Fig. A2.1). It was deduced from this analysis that using 0.2M NaOH a digestion period of 3 hours was optimal. Selected analyses of residues confirm that the large majority of biogenic silica is solubilised with this treatment.

In order to test the accuracy and long-term reproducibility of the method three of the samples used in the inter-laboratory calibration experiment organised by Conley *et al*.

(1998) were analysed alongside five of the sample batches. The reproducibility of samples was better than 10% for each of the Conley samples analysed. Generally the results were very close to the overall mean calculated by Conley *et al*. (1998) (Fig. A2.2). The method employed here seems to slightly overestimate SiO_2 concentrations relative to the overall mean reported by Conley *et al*. (1998). For low and high $\%SiO_2$ samples (S1 and S2) the results from this method fall within the upper section of laboratory spread, whereas for the intermediate sample this method appears to overestimate $\%SiO_2$.

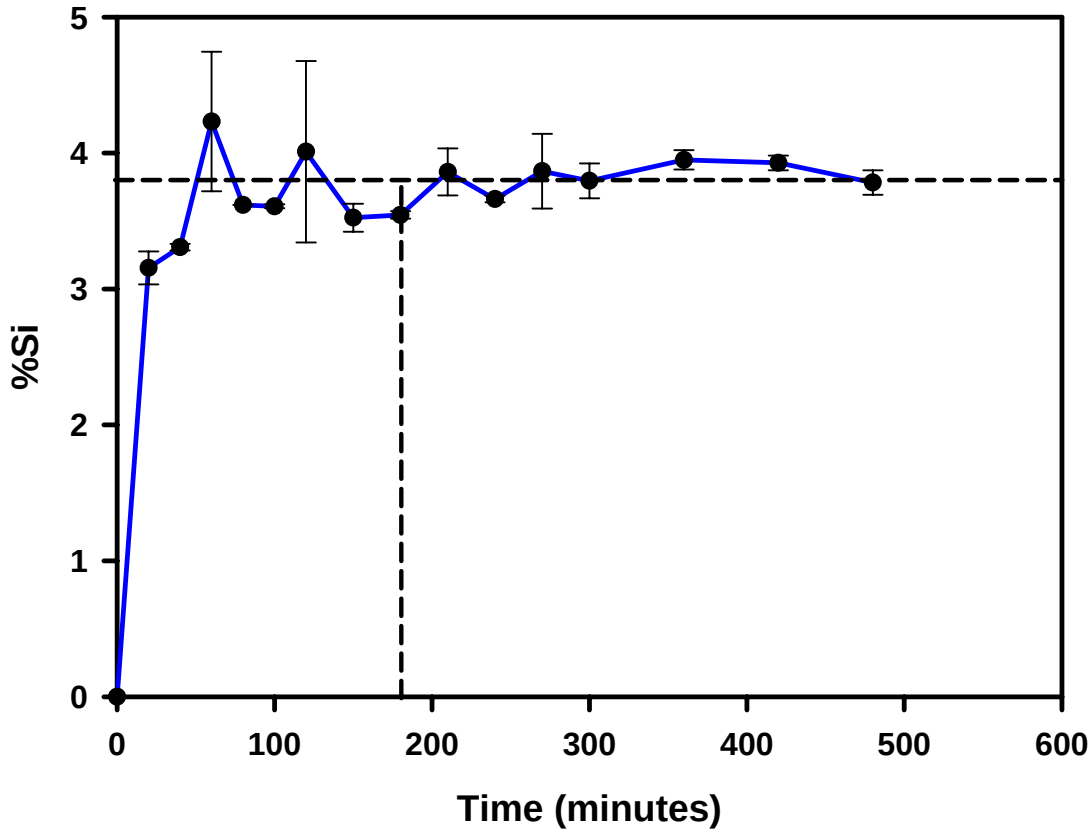

Fig. A2.1 Differential extraction of representative sample (XXVIIB8), range bars are from duplicate analyses.

The use of an appropriate concentration of digestion solution during analysis is imperative to ensure complete dissolution of biogenic silica whilst minimising the

extraction of silica from lithogenic silicates. Since the methods here were developed to analyse sediment trap samples from the north-east Atlantic and Southern Ocean, a strong base was selected (0.2M NaOH) to ensure complete dissolution of opal-rich particles. In order to examine whether the digestion conditions leached a significant amount of lithogenic silicate, samples from the Conley *et al*. (1998) inter-laboratory experiment were analysed for dissolved aluminium and dissolved silicon using the ICP-AES.

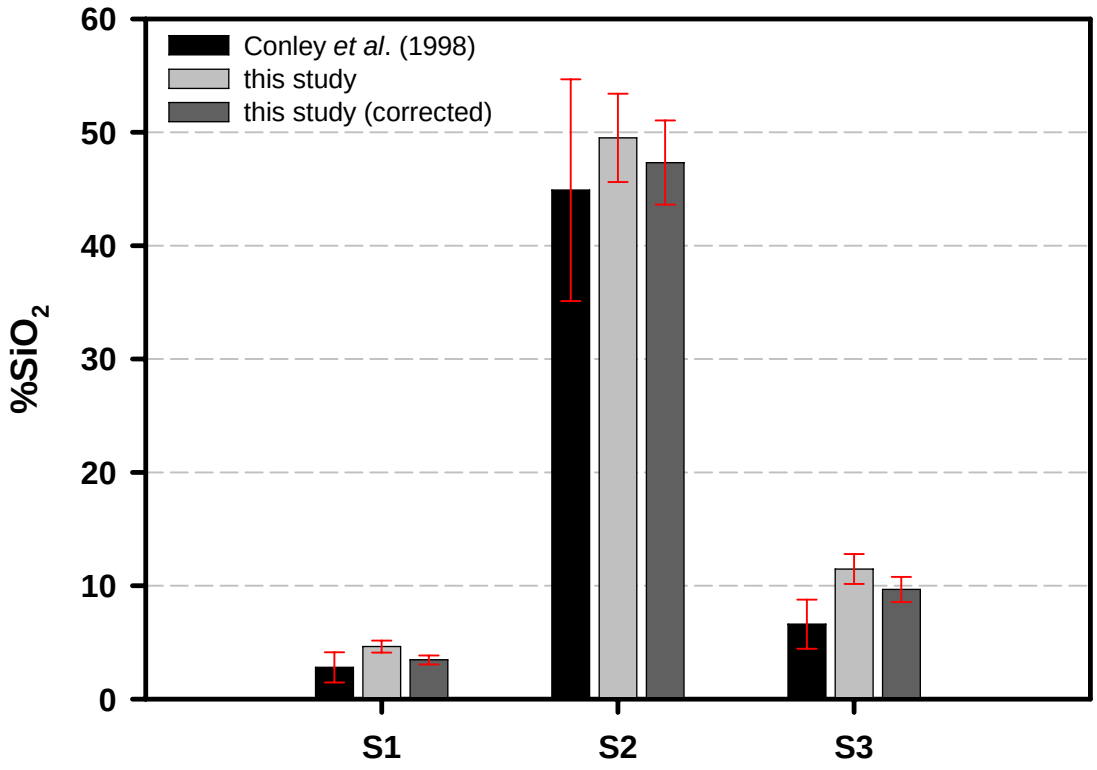

Fig. A2.2 Comparison of means determined by the inter-laboratory comparison of Conley *et al*. (1998) with those obtained during this study. Error bars on the Conley *et al*. (1998) data is ±1 standard deviation of the mean as determined independently by 27 laboratories. Error bars on the data from this study is the mean from replicate analyses (n=5).

Dissolved Si:Al molar ratios varied amongst the samples, they were 4.0 ± 0.2, 23.4 ± 0.6, and 6.4 ± 0.4 for samples S1, S2, and S3 respectively. Assuming an aluminosilicate Si:Al ratio of 1:1 the samples were corrected for lithogenic silica solubilised during the digestion period. The result of this mineral correction was to reduce the biogenic silica content in the Conley *et al.* (1998) samples by 25.4, 4.4, and 15.7% for S1, S2 and S3 respectively. Figure A.2.2 shows the corrected values plotted against the uncorrected values and the averages obtained from the comparison exercise. The corrected values are within the laboratory spread when error bars are considered, but the averages are still slightly higher. If the average from the inter-laboratory experiment is close to the absolute concentration of biogenic silica then the results obtained by the method in this study may be considered to be a very slight over-estimate.

It was decided that a mineral correction would not be necessary for the sediment trap samples analysed in this study. In order to verify this decision a similar exercise to that described above was conducted on deep-sea sediment cores obtained from north of the Crozet Plateau (M10) which have a significant lithogenic component in surficial sediments (Marsh *et al*., 2007). The Si:Al ratios were very high in the digest solution (84.4-98.7) and thus corrected values were not significantly different from the non-corrected values.

As further confirmation the biogenic silica content of sediments determined via this method were compared with independent estimates for a set of sediment samples collected in the vicinity of the Crozet Plateau (Marsh *et al*., 2007). A three-component mixing model can be applied to the Crozet sediments (Francois *et al*., 1993) where the total sediment composition is equal to the sum of the lithogenic, carbonate and biogenic silica phases. Biogenic silica content was thus estimated by difference (i.e., 100 – carbonate% - lithogenic %). The lithogenic component was measured from elemental analysis of sediments subjected to combined Aqua Regia, HF, and $HClO_4$ total digestion. The accuracy of this analysis was assessed through analysis of certified reference materials (MAG-1) and was better than 3% for all

elements measured (Marsh *et al*., 2007). $CaCO_3$ was estimated from excess calcium data, after correction for the lithogenic bound elemental contribution according to equation A2.1

$$Ca_{XS} = Ca_{bulk} - (Ti^*(Ca/Ti)_{end\ member}) \quad \textbf{(A2.1)}$$

where Ca_{XS} is the excess calcium, Ca_{bulk}, is the bulk calcium concentration in sediments subjected to total digestion, Ti* is the bulk titanium concentration, and $(Ca/Ti)_{end\ member}$ is the ratio of calcium to titanium in the lithogenic end member. $CaCO_3$ was also independently determined by coulometry and there is close agreement between the two methods ($r^2 = 0.85$) demonstrating that the assumptions used are largely valid (Marsh *et al*., 2007) Comparison of biogenic silica determined using the 0.2M NaOH digestion with that inferred by difference according to the methods described above is presented in Fig. A2.3. There is excellent agreement between the two independent estimates providing additional confidence in the methods employed during this study.

In order to confirm that the first digest had solubilised the majority of particulate biogenic silica in the sample, selected residues were analysed a second time under identical conditions. The recovery efficiency from the 1st extraction (Ex_{Eff}) is calculated per equation A.2.3. The arithmetic mean of the recovery is calculated as 89.4 ± 4.0% for the entire data set (n=78), individual values can be found in Table A2.1. The samples from the Southern Ocean contained numerous radiolarian and large diatoms which can be resistant to experimental dissolution (e.g. Mortlock and Froelich, 1989) due to heavy silicification of frustules. The high Ex_{Eff} values from the Southern Ocean sediment traps (Table A.2.1) confirm that the selected treatment is capable of almost complete dissolution of biosliceous frustules of varying morphology. It is also considered that a fraction of the Si solubilised in the second extract may originate from alumino-silicates and thus values have not been corrected for Ex_{Eff}.

$$Ex_{Eff} = (\%Si\ 1^{st}\ Extract) / (\%Si\ 1^{st}\ Extract + \%Si\ 2^{nd}\ Extract) \quad \textbf{(A2.2)}$$

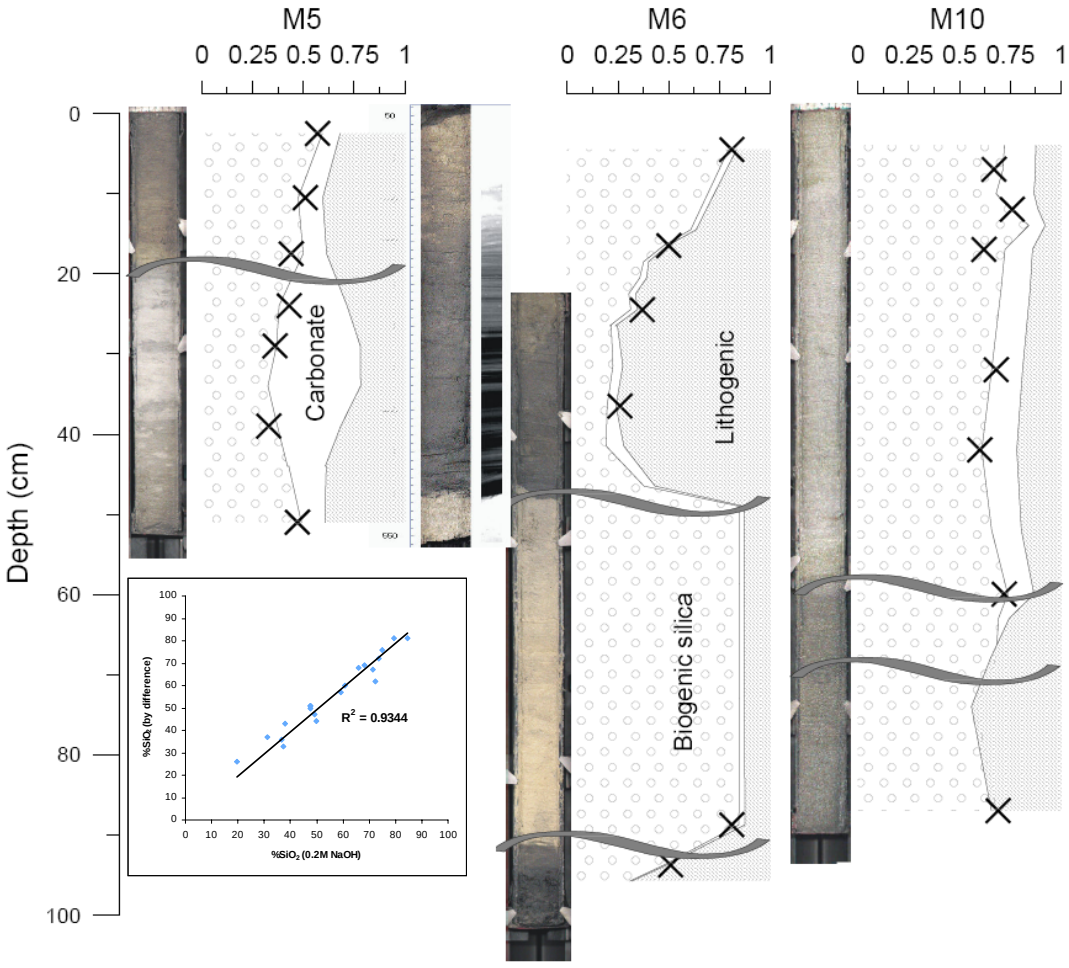

Fig. A2.3 Comparison of biogenic silica values determined by the methods employed during this study and those described in text. Inlay shows the correlation between the two sets of estimates, with the intercept forced through zero (r^2 = 0.93, n = 20, P<0.001). Modified from Marsh *et al*., 2007.

Table A2.1 Extraction efficiency of the biogenic silica method

Sample Code	1st Extract $\%SiO_2$	2nd Extract $\%SiO_2$	Ex_{EFF} %
25 B1b	9.7	0.9	91.7
25 B2c	8.8	1.1	88.7
25 B3c	12.0	1.2	90.7
25 B4c	14.2	1.7	89.5
25 B5a	12.5	1.4	90.1
25 B6a	29.6	2.2	93.0
25 B7b	31.5	2.3	93.3
25 B8a	21.4	1.3	94.2
25 B9a	20.2	1.7	92.2
25 B10a	19.3	1.4	93.3
25 B11a	11.4	1.0	91.9
25 B12b	13.3	1.3	90.8
25 B13a	10.0	1.1	89.7
27 B1a	18.0	1.5	92.4
27 B2b	9.7	1.0	90.8
27 B3b	9.8	1.0	90.4
27 B4a	10.2	1.0	90.8
27 B5c	17.0	1.6	91.5
27 B6b	18.9	1.8	91.4
27 B7b	17.3	1.8	90.8
27 B8a	8.9	0.9	90.6
27 B9b	10.8	1.1	90.7
27 B10b	11.6	0.8	93.3
27 B11a	3.5	0.7	82.3
27 B12a	6.8	0.6	92.0
27 B13a	10.4	0.9	91.9
27 B14c	10.7	0.7	94.0
27 B15a	8.9	0.8	92.2
28 B1b	11.0	1.1	90.6
28 B2b	8.4	1.3	86.2
28 B3b	8.5	1.3	86.4
28 B4a	8.3	1.2	87.3
28 B5a	7.7	1.3	85.9
28 B7a	9.3	1.3	87.5
28 B8c	8.2	1.2	87.5
28 B9a	7.7	1.1	87.2
28 B10c	7.0	1.3	84.7
28 B11c	5.2	1.5	77.9
28 B12a	5.5	1.3	80.8
28 B13a	7.9	1.5	84.3
28 B14b	9.6	1.3	87.7
28 B15a	12.1	1.2	90.8
28 B16b	13.9	1.0	93.6
28 B17b	14.8	1.5	90.6
28 B18a	10.8	1.5	87.9

Table A2.1 continued

Sample Code	1st Extract $\%SiO_2$	2nd Extract $\%SiO_2$	Ex_{EFF} %
31 A1a	14.2	1.8	88.6
31 A2a	21.5	2.1	91.0
31 A3b	15.9	2.0	88.8
31 A4c	13.6	1.9	87.8
31 A5c	16.8	2.6	86.7
31 A6c	12.8	1.7	88.2
31 A7a	10.0	1.4	88.1
31 A8b	14.0	2.8	83.3
31 A9c	11.8	2.1	84.9
36 A1a	71.4	4.9	93.6
36 A2a	52.5	8.8	85.7
36 A3b	44.7	7.6	85.4
36 A4a	38.1	8.0	82.7
36 A5a	34.4	7.5	82.1
36 A6a	34.7	8.9	79.5
37 A19a	54.9	7.4	88.1
37 A20a	55.6	9.2	85.8
38 A1a	67.1	2.9	95.9
38 A2a	51.7	3.6	93.5
38 A3a	51.6	3.9	93.0
38 B1a	61.4	4.0	93.9
38 B2a	62.2	3.6	94.5
38 B3a	65.2	4.2	94.0
38 B4a	59.0	5.5	91.5
38 B5a	53.5	7.1	88.3
38 B6a	39.7	5.8	87.2
38 B7a	40.0	6.7	85.6
38 B8a	31.0	2.4	92.7
38 B19a	35.4	4.9	87.8
39 B1a	79.4	3.0	96.4
39 B6a	74.7	1.7	97.8

A.2.3 Reagents

A.2.3.1 Extraction Reagents

1) 0.2M NaOH – Dissolve 3.6g of sodium hydroxide pellets in 450ml of Milli-Q water. Note, it is difficult to obtain an exact weight with pellets so they should be

weighed as accurately as possible to 3.6g and the volume of Milli-Q adjusted to provide an accurate concentration of 0.2M. Store in a polyethylene bottle.

A.2.3.2 Stock Reagents

2) Molybdate reagent – Dissolve 16g of analytical reagent quality ammonium paramolybdate $(NH_4)_6Mo_7O_{24}.H_2O$ in 1000ml of Milli-Q water. Store the solution in a tightly capped polyethylene bottle out of direct sunlight. The solution is stable indefinitely but if a white precipitate forms or the solution turns faintly blue it should be discarded.

3) Metol-sulphite reduction reagent – In a glass conical flask dissolve 3g of anhydrous sodium sulphite (Na_2SO_3) in 200ml of MQ water. Add 5g of metol (paramethylaminophenol sulphate), use 50ml of Milli-Q water to rinse the weighing boat and internal neck of conical flask; ultrasonicate until dissolved (10-15 minutes). Store the solution in an amber ground glass stoppered bottle in a refridgerator. The solution is stable for 1-2 weeks but should be made fresh for analysis where possible.

4) Oxalic acid reagent – Dissolve 30g of analytical quality oxalic acid dihydrate $[(COOH)_2.2H_2O]$ in 500ml of Milli-Q and store in polyethylene. Stable indefinitely.

5) Sulphuric acid reagent – In a large glass beaker, slowly add 300ml of concentrated (sp. gr. 1.82) analytical reagent quality sulphuric acid into 770ml of Milli-Q. Allow to cool to room temperature and store in polyethylene.

6) Hydrochloric acid reagent – Add 48ml of concentrated (12.2M) HCl to 925ml of Milli-Q and store in polyethylene.

A.2.3.3 Working Reagents

7) Molybdate working solution – Mix molybdate stock reagent. HCl stock reagent, and Milli-Q in volume proportions of 1:1:5. The mixture should be prepared for immediate use and fresh for each analysis. It is stable for 6-12 hours. Store in polyethylene out of direct sunlight.

8) Reducing working solution – Mix equal volumes of metol-sulphite stock reagent, oxalic acid stock reagent, and sulphuric acid stock reagent, adding the sulphuric acid

last. The solution is stable for 4-6 hours, but should be prepared immediately before use.

A.2.3.4 Standard solutions

9) Working standards (0.2M NaOH) – Add primary standard (35.6mM silica; see table A.2.2 for details) to acid cleaned 25ml polyethylene volumetric flasks and fill to line with Milli-Q. Mix thoroughly and transfer to clean wide-necked polyethylene flasks. Add 2.75ml of 2M NaOH to each standard so that they are matrix matched with the sample solutions. The standard solutions are stable for 3 months. Wide-necked polyethylene flasks should be tightly capped and sealed with parafilm to minimise evaporative concentration effects over time.

Table A2.2 Volumes of silica standard solution used in preparation of experimental standards

Initial standard concentration	Volume of 1000 µg/ml silica standard	Volume of Milli-Q water added	Volume of 2M NaOH added	Final Standard Concentration
0mM	0ml	25ml	2.75ml	0mM
1.43mM	1ml	24ml	2.75ml	1.29mM
2.85mM	2ml	23ml	2.75ml	2.57mM
4.27mM	3ml	22ml	2.75ml	3.85mM
5.70mM	4ml	21ml	2.75ml	5.14mM
7.12mM	5ml	20ml	2.75ml	6.41mM

A.3.4 Calibration

For each set of samples analysed a separate calibration should be performed. This takes into account any variations arising from the preparation of reagents and in the performance of the spectrophotometer. An example calibration graph is provided in Fig. A2.4.

A.3.5 Cleaning

All equipment was rinsed three times with deionised water, three times with Milli-Q water, soaked in 10% HCl overnight, and rinsed three times with Milli-Q water and air-dried.

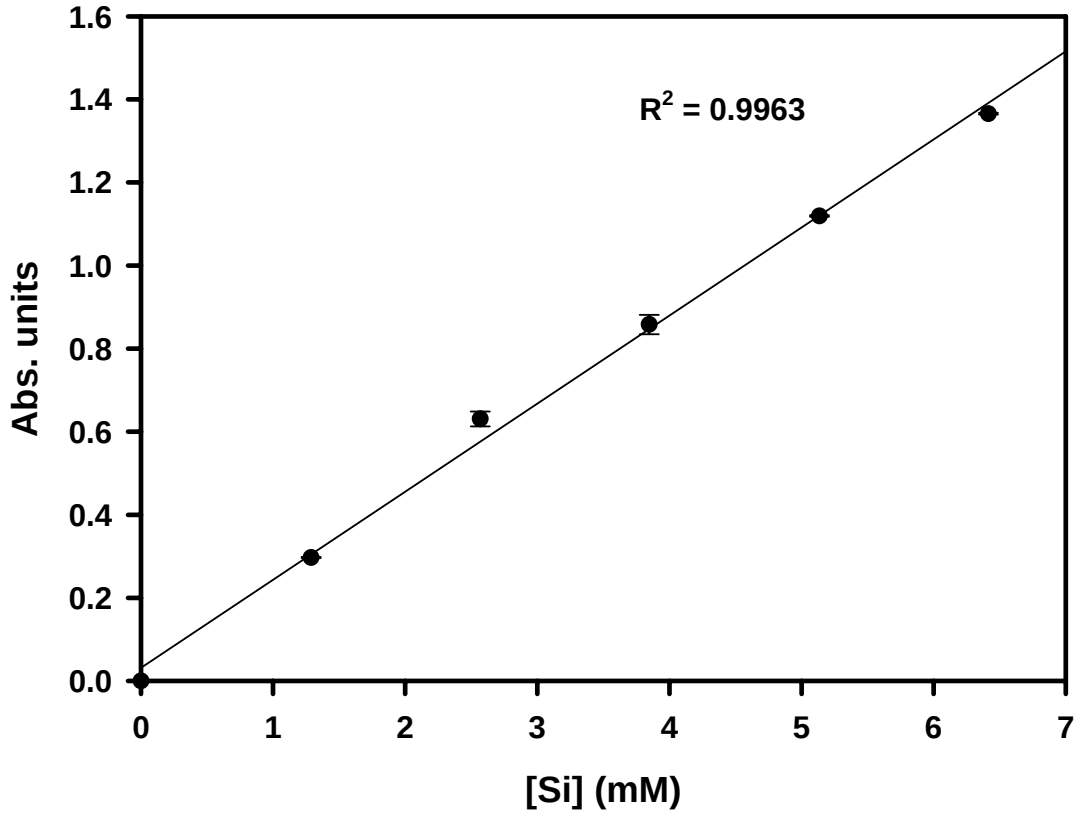

Fig A2.4 Example calibration graph. Each calibration point represents triplicate readings from duplicate measurements and thus combines systematic errors from the spectrophotometric output and pipetting errors.

A3.6 Extraction Procedure

1) Samples should be freeze-dried overnight to remove any excess water

2) Samples are then crushed in a plastic medicine cup using the base of a polypropylene sample tube and the flat end of a clean metal spatula. Agate pestle and mortar traditionally used for crushing sediment samples should not be used since they have high Si contents and may contribute to the final Si concentration.

3) Carefully weigh out 3-5mg of sediment into the interior rim of a cap belonging to the polypropylene sample tube, if any material falls into the outer rim discard the sample. Leaving the cap on a firm surface, invert the sample tube and tightly screw

to the cap. Re-invert the sample tube and gently tap with a spatula to accumulate the sediment in the base of the sample tube.

4) Remove lids from the sample tubes keeping note of which lids belong to which tubes. Add 8ml of 0.2M NaOH to each sample tube (40 at a time) and attach the correct lid tightly.

5) Invert each sample tube using the 8ml of 0.2M NaOH to rinse the side of the tube and the cap.

6) Place the sample tubes into a heated (70^{o}C) ultrasonic bath for two minutes, during which time invert the sample tubes sequentially

7) Place the sample tubes into a pre-heated constant temperature water bath at 100^{o}C for 3 hours

8) After 1 and 2 hours repeat step 6.

9) After 3 hours remove samples and centrifuge at 3700rpm for 15 minutes.

10) Pipette 4ml of the supernatant into a clean labelled polypropylene tube and store for subsequent analysis.

11) Carefully decant of remaining supernatant and dry the residue in an oven at 60^{o}C overnight. This residue is used in the second extraction of selected samples

12) Repeat steps 4-10 for the selected residues upon which a second extraction is to be carried out.

A3.7 Analysis

1) Place the sample solutions in an ultrasonic bath for 10 minutes to re-dissolve any precipitates.

2) Prepare a rack of clean labelled polypropylene tubes in identical positions to sample tubes containing supernatant of extract solution.

3) Pipette 7ml of molybdate working solution into each analysis tube

4) Working at 30 second intervals add 100µl of the sample or standard solution to each tube, followed by two aliquots of 100µl Milli-Q to rinse the pipette tip, flick to mix.

5) Leave each cup for exactly 20 minutes to react. The time for formation of the silicomolybdate complex is critical and must be the same (within 30s, Fanning and Pilson, 1973) for each analysis carried out. By addressing the tubes at 30 second intervals these times can be accurately controlled.
6) Working at 30 second intervals, pipette 3.0ml of the reducing working solution to each tube, flick to mix (see Fig A.2.5 for an example of time control of this stage).
7) Leave the solutions to stand to complete the reaction of the silicomolybdate complex with the reducing working solution. The blue colour takes about three hours to develop. Solutions are stable for up to 12 hours
8) Read the absorbances using a 1cm sipper cell with a sipper time of 9 seconds. This permits triplicate absorbance readings from each sample tube.
9) Absorbances are measured against Milli-Q in a spectrophotometer (Hitachi U-2000) set at 810nm.

A3.8 Blanks

Milli-Q Blank – The Milli-Q blank is composed of Milli-Q plus the colour forming reagents and should be analysed with each batch of silica determinations to ensure there is no contamination. Provided high quality analytical grade chemicals are used the blank should have absorbances near zero. Absorbances for Milli-Q blanks were typically less than 0.003 and constantly less than 0.010 and are insignificant for the sample concentrations presented here. The variation in the Milli-Q blank is probably related to the quality of the water purification system. Dissolved Si is only weakly charged and thus minor contamination of water systems can occur as the Milli-Q pack ages.
Operational Blank – This is the alakaline extraction solution and is treated identical to the sample solutions with the omission of the sediment sample. The absorbances were less than 0.010 and were used to correct sample absorbances.
Zero standard – This acts as a zero calibration and as a check on the operational blank. The absorbance results from any silica in NaOH and is used to construct the calibration curve

D10	**C10**	**B10**	**A10**
19:30	14:30	09:30	04:30
39:30	34:30	29:30	24:30
D9	**C9**	**B9**	**A9**
19:00	14:00	09:00	04:00
39:00	34:00	29:00	24:00
D8	**C8**	**B8**	**A8**
18:30	13:30	08:30	03:30
38:30	33:30	28:30	23:30
D7	**C7**	**B7**	**A7**
18:00	13:00	08:00	03:00
38:00	33:00	28:00	23:00
D6	**C6**	**B6**	**A6**
17:30	12:30	07:30	02:30
37:30	32:30	27:30	22:30
D5	**C5**	**B5**	**A5**
17:00	12:00	07:00	02:00
37:00	32:00	27:00	22:00
D4	**C4**	**B4**	**A4**
16:30	11:30	06:30	01:30
36:30	31:30	26:30	21:30
D3	**C3**	**B3**	**A3**
16:00	11:00	06:00	01:00
36:00	31:00	26:00	21:00
D2	**C2**	**B2**	**A2**
15:30	10:30	05:30	00:30
35:30	30:30	25:30	20:30
D1	**C1**	**B1**	**A1**
15:00	10:00	05:00	00:00
35:00	30:00	25:00	20:00

Fig A2.5 Example of the how accurate time control of colour-forming reagents and reducing solutions was maintained. The times in blue type-set document the addition of the sample to the molybdate solution, whilst those in red-type set document the addition of the reducing solution.

A.3.9 Calculations

C_{STD} Silicon concentration of working standard (mM)

A_{STD} Absorbance of the standard (average of triplicates: absorbance units)

1/G where G is the gradient of the linear regression through the standard curve: a plot of A_{STD} vs C_{STD} for all the standards (units of mM Abs^{-1}). The linear regression should yield a correlation coefficient (r^2) >0.99 (e.g. Fig A.2.4).

C_S	Silicon concentration of the sample
As	Absorbance of sample (average of triplicate measurements; absorbance units)
A_O	Absorbance of the operational blank (average of two pairs of triplicate measurements; absorbance units)
V_{ml}	Volume of alkaline extract solution (ml)
Si_{Mol}	Moles of Si in extraction fluid
Si_{Mass}	Mass of silicon (mg)
M	Sample mass (mg)
%Si	Percentage of elemental silicon in sample
%SiO_2	Percentage of biogenic silica in sample
%$SiO_2.nH_2O$	Percentage of biogenic opal in sample

$C_S = 1/G[A_S - A_O]$

$Si_{mol} = C_S[V_{ml} \times 10^{-6}]$

$Si_{Mass} = Si_{Mol}[2.809 \times 10^{4}]$

$\%Si = (Si_{Mass} / M)*100$

$\%SiO_2 = (\%Si)*2.14$

$\%SiO_2.nH_2O = (\%Si)*2.4$

The calculation of biogenic opal ($SiO_2.nH_2O$) relies on the assumption that diatomaceous opal has a relatively constant water content of 10%; e.g. Mortlock and Froelich (1989). This calculation may induce errors for the Southern Ocean sediment trap samples where a portion of the biogenic opal is comprised of silicoflagellates and radiolarian. All data is thus presented as biogenic silica (SiO_2).

APPENDIX 3: ANALYSIS OF TOTAL HYDROLYSABLE AMINO ACIDS AND HEXOSAMINES

This method is based on that of Lindroth and Mopper (1979) and Cowie and Hedges (1992).

A3.1 Overview of the chemistry

Amino acids were separated using reverse-phase high performance liquid chromatography. In reverse-phased chromatography, a relatively non-polar stationary phase is used, with a polar mobile phase, and compounds are separated based on their hydrophobic character. The most common bonded phase used in reverse-phase HPLC are *n*-octyldecyl (C_{18}) or *n*-decyl (C_8) chains.

In the presence of a reducing agent, such as 2-mercaptoethanol, OPA reacts in an alkaline medium with primary amines, to form highly fluorescent thioalkyl-substituted isoindoles. The poor fluorescence of the lysine and ornithine derivatives is considered to be a drawback of the OPA-derivatisation technique. The instability of some OPA-derivatives rules out the use of a traditional autoinjector, derivatives need to be formed immediately prior to injection. Venema *et al*, (1983) have described a continuous flow system in which the sample is mixed with OPA and led through the loop of the injection valve under the control of a microprocessor. As a result of the wide range of polarities of the amino acid derivatives, gradient elution is preferred over isocratic elution. In this method a binary gradient elution profile is employed, the polar solvent is H_2O buffered with sodium acetate and tetrahydrofuran added as an organic modifier. The second eluant is HPLC grade methanol. Hydrophobic amino acids such as valine are thus retained on the column for longer and elute towards the end of the chromatographic run.

A3.1.1 Apparatus

High performance liquid chromatography was carried out using binary gradient high pressure pumps (Shimadzu, -10AD_{VP}) equipped with an autosampler (SIL-10AD_{VP}) and a fluorescence detector (RF-10A_{XL}). The system was computer operated (LC

Solutions) via a system controller (Shimadzu, SCL-10A$_{VP}$). Separations were performed using a silica-bound *n*-octyldecyl (C_{18}) stationary phase (15cm x 4.6mm, 3µm, Ascentis) fitted with an Alltech pre-column and maintained at a constant temperature of 30°C using a Shimadzu column oven (CTO-10AS$_{VP}$). The solvents were eluted at a flow rate of 1 ml min^{-1}. OPA derivatisation was performed online immediately prior to column injection, 20µl of OPA reagent was added to 300µl of the sample solution, 40µl of which was injected onto the column. Spectra and chromatograms were analysed using LC Solutions Post-Run Analysis software.

A3.2 Method Validation

A3.2.1 Sample Preparation

The preparation of sediment trap samples involved filtering the sample onto a cellulose nitrate filter (47 mm, 0.45 µm) to separate the particulate phase from the preservative solution. As the preservative solution is 95% seawater by volume, then it contains dissolved salts which can precipitate onto the sample during the drying procedure. These salts need to be rinsed away as they can generate large gravimetric errors which propagate through to the calculations of sample concentrations. The standard sediment trap protocol is to rinse samples with ammonium formate (0.56 mol L^{-1}) as it has the same osmotic pressure as seawater and thus prevents cell lysis and the consequent loss of intracellular organic carbon that may result from using Milli-Q water. However, amino acid chromatography is detrimented by the presence of ammonia and related compounds which cause a large broad peak and obscure the resolution of many individual amino acid compounds.

The effect of rinsing the samples with Milli-Q water and 0.56 mol L^{-1} ammonium formate was tested and the results are presented in Figures A3.1-A3.3. Figure A3.1 shows total hydrolysable amino acids (THAAs) for two samples, 23aC9 and 23aC13, both of which were rinsed with ammonium formate and Milli-Q water and ran in duplicate. There is a small decrease in THAAs for sample 23aC9 from 13.08 to 11.41 µg mg^{-1}, however for sample 23aC13 the difference was neglible decreasing

from 9.43 μg mg^{-1} using the ammonium formate rinse to 9.32 μg mg^{-1} with the Milli-Q water rinse. For both of these examples the change in measured THAA's is within the standard deviation for the individual sample analysis. The larger decrease in THAAs observed for 23aC9 is most likely caused by a larger relative standard deviation for this sample (8.79%) compared to 23aC13 (3.77%).

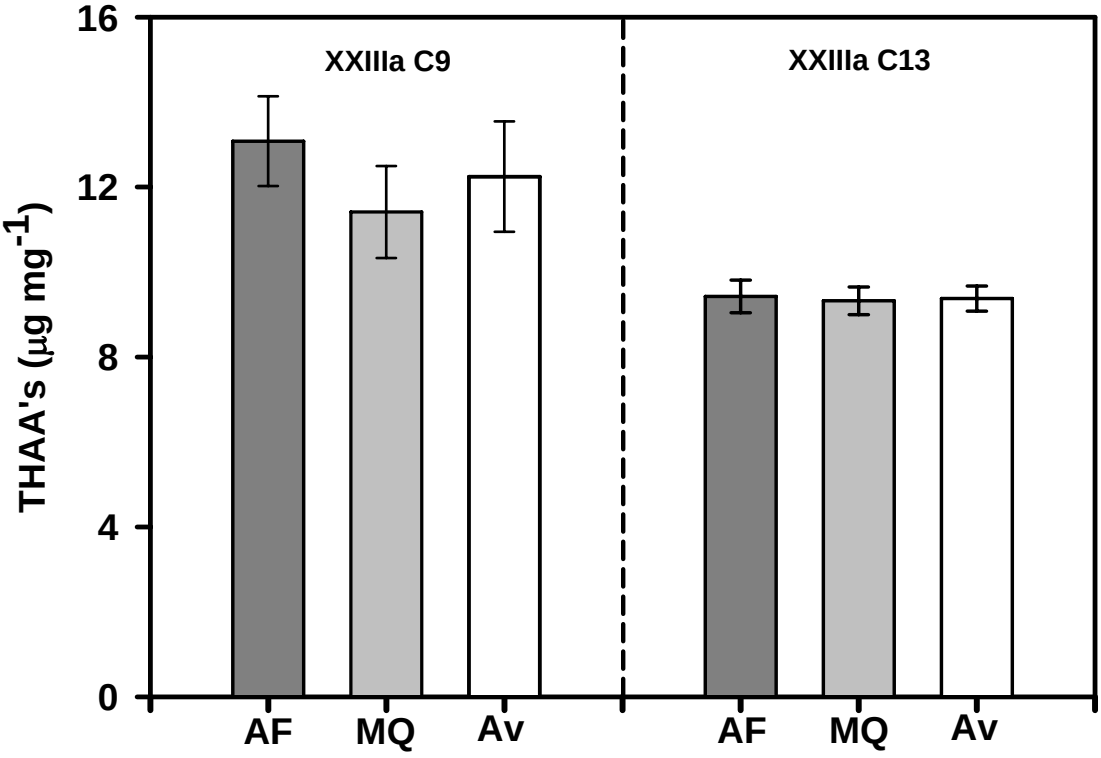

Fig. A3.1 Effect of rinsing sediment trap samples with Milli-Q water and 0.56 M ammonium formate.

In addition to examining the absolute concentrations of THAAs, the mole percentage contribution of individual amino acids under different rinse protocols was also assessed (Fig. A3.2). For the majority of the amino acids there were no significant differences in their mole percentages and all fell within the error associated with replicates of the same sample. However, for the amino acids aspartic acid and glutamic acid, the mole percentage seemed to be a few percent higher using the Milli-Q rinse, whilst for histidine, methionine, and ornithine there seemed to be some

consistency in the observation that their mole percentages were lower using the Milli-Q rinse relative to ammonium formate.

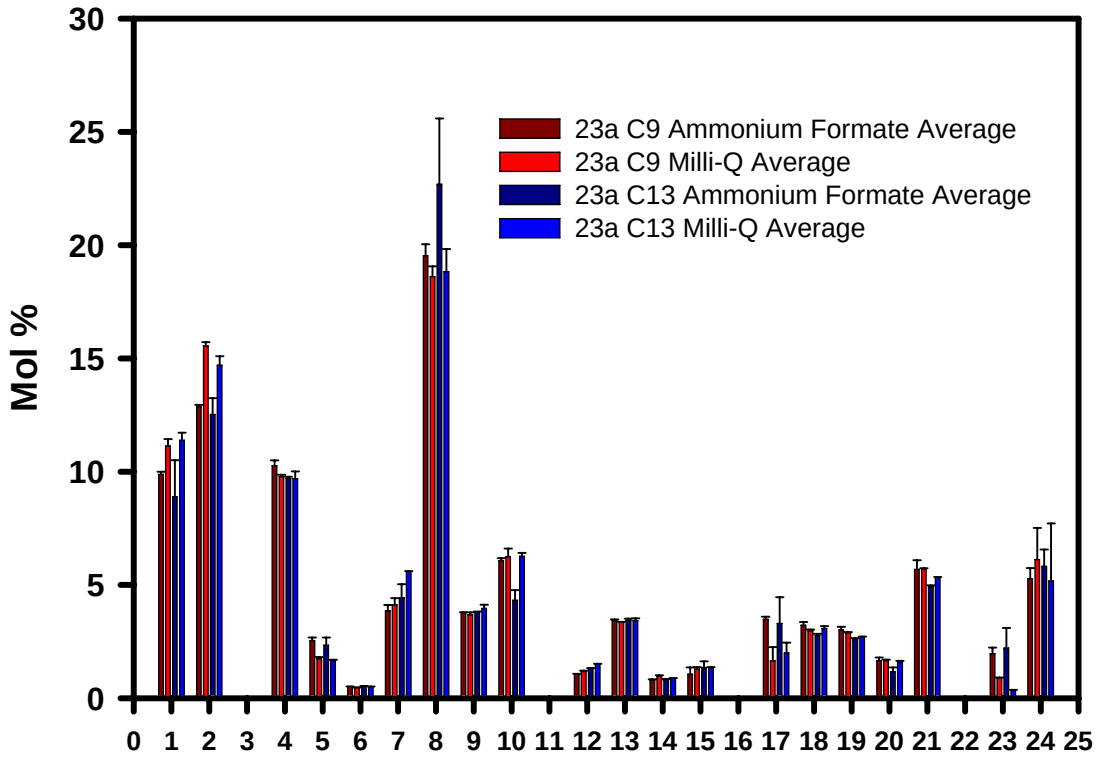

Fig. A3.2 Differences in Mol % of individual amino acids extracted, separated and quantified using reverse phase liquid chromatography. Dark red and dark blue bars are the samples that were rinsed with 0.56M ammonium formate and bright red and bright blue bars are samples that were rinsed with Milli-Q water. 1-Asp, 2-Glu, 3-Aada, 4-Ser, 5-His, 6-Gala, 7-Gluc, 8- Gly, 9-Arg, 10-Thr, 11-Lhom 12-Bala, 13-Ala, 14-Gaba, 15-Tyr, 16-Mthr, 17-Met, 18-Val, 19-Phe, 20-Ile, 21-Leu, 22-Mleu, 23-Orn, 24-Lys.

The chromatographic resolution appeared to be largely unaffected by the use of Milli-Q water over ammonium formate. However, in a region shortly after 35 minutes of the gradient, there seemed to be an increase in the unidentified signal response that occurs just prior to the elution of methionine (Fig A3.3). Although this seems comparable to the broad peak associated with ammonia contamination, it does not

have a major effect on the resolution of methionine. It is clear however that differences in sample preparation can exert minor effects on certain compounds, and that the pre-treatment of sediment trap material prior to analysis should remain consistent, furthermore caution should be exercised when comparing data with that available in the literature.

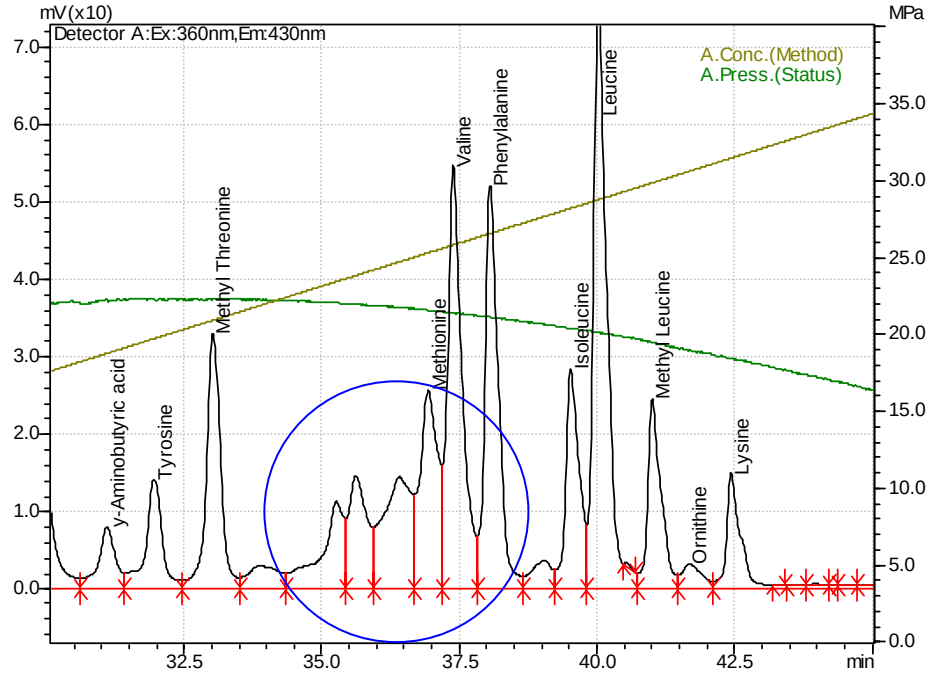

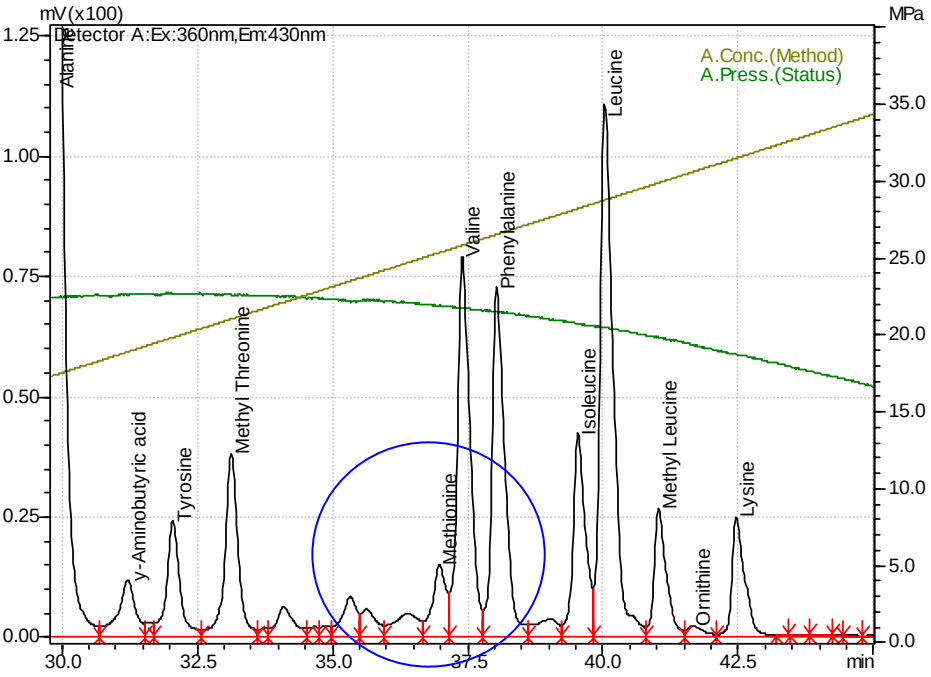

Fig.A3.3 Comparison of chromatograms obtained with Milli-Q (top panel) and ammonium formate (bottom panel) rinses.

A3.2.2 Hydrolysis Procedure

Similar to numerous other studies (e.g. Hashimoto *et* al., 1998; Gupta and Kawahata, 2002; Unger *et al*., 2005) sediment samples were hydrolysed with 6 M HCl at 110^{o}C for 24 hours. Previous work (Lookhart *et al*., 1982; Cowie and Hedges, 1992; Ingalls *et al*., 2003) have extracted amino acids from sediments using high temperature, short-duration hydrolyses (e.g. 150^{o}C, 70-90 minutes). The high-temperature, short-duration hydrolysis method displayed very inconsistent responses during this study and often no amino acids were detectable. This response was attributed to the integrity of the vials used for the hydrolysis which were frequently observed to crack at the higher temperatures. The low-temperature (110^{o}C) long-duration (24 hours) hydrolysis was also prone to random failures although much less numerous. The success of the hydrolysis was improved by degassing the acid using argon prior to addition to the sediment, and also filling the headspace with argon in the vial prior to sealing. Vial seals were improved by tightly wrapping the vial and cap with PTFE tape.

A3.2.3 Internal standard (*o*-methyl threonine)

Peak areas can vary within an analytical run as the solvents and or derivatisation reagent age, and also slight deviations from the optimal pH can cause a reduction or enhancement of peak areas that is not mediated by the absolute concentration of the amino acid. All samples and standard areas were corrected relative to the internal standard *o*-methyl threonine (MTHR). MTHR was added post hydrolysis as an absolute recovery standard prior to injection of the sample/standard onto the analytical column. The reference area of MTHR was statistically-derived by taking the average of all MTHR areas within the analytical run. The criterion was that the coefficient of variation of this average was between 5-10%, and "outlying" MTHR

areas were thus deleted accordingly to satisfy this statistical criterion. The MTHR area of each sample/standard was compared to the pre-determined MTHR reference area and expressed as a fraction which could then be used as a correction factor for the individual amino acids. The effectiveness of this approach can be demonstrated by comparing calibration curves before and after the methyl-threonine correction (e.g. for aspartic acid; Fig.A3.4).

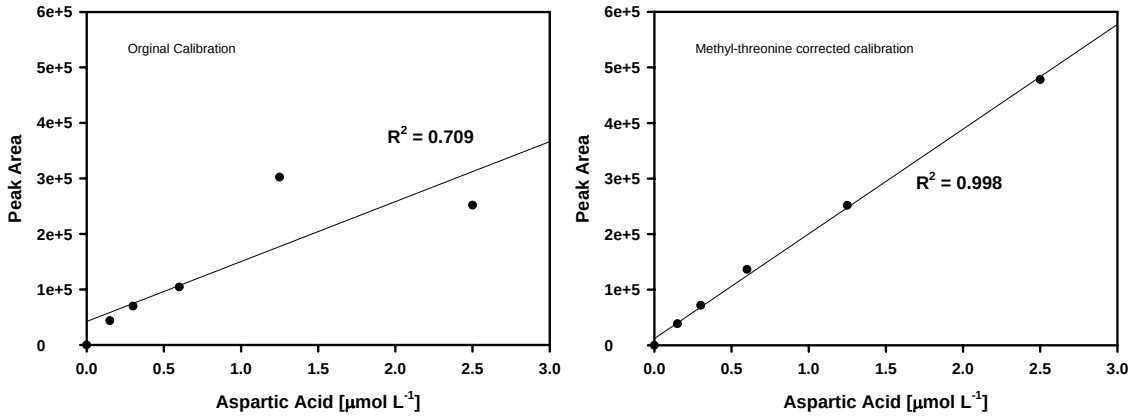

Fig A3.4 Six-point calibration for aspartic acid before and after correction with the internal standard *o*-methyl threonine.

A crucial assumption in using one internal standard to correct for all amino acid concentrations is that all the individual amino acids respond proportionally to variations in the selected internal standard. In addition to the five-point calibration conducted at the start of each analytical run, single mixed standards were also included in the middle and at the end of sample batches. Since the exact concentration of amino acids in the mixed standard is known, then the response of individual amino acids to the methyl-threonine correction can be compared between mixed standards of identical concentrations within the same analytical run. The calculations were performed based on the equations described below:

$\mathbf{A_{[MTHR]MS1}}$ Area of methyl-threonine in mixed standard one

$\mathbf{A_{[MTHR]MS2}}$ Area of methyl-threonine in mixed standard two

$D_{FRAC[MTHR]}$ Fractional difference between methyl-threonine in mixed standards one and two

$A_{[AAi]MS1}$ Area of amino acid *i* in mixed standard one

$A_{[AAi]MS2}$ Area of amino acid *i* in mixed standard two

$D_{FRAC[AAi]}$ Fractional difference between amino acid *i* in mixed standards one and two

RCE Relative correction efficiency of amino acid *i* (%)

Note The concentration of mixed standards one and two are identical

$$D_{FRAC[MTHR]} = A_{[MTHR]MS1} / A_{[MTHR]MS2} \quad \textbf{(A3.1)}$$

$$D_{FRAC[AAi]} = A_{[AAi]MS1} / A_{[AAi]MS2} \quad \textbf{(A3.2)}$$

$$RCE = (\sqrt{[(D_{FRAC[MTHR]} - D_{FRAC[AAi])}^2]}) * 100 \quad \textbf{(A3.3)}$$

These calculations were performed for each amino acid when identical concentrations of mixed standards were available within the same analytical run (n = 25) and the results are presented in Fig. A3.5. For almost all amino acids the relative correction efficiency is between 3 and 10% with the exception of ornithine and lysine. In order to check that the relative correction efficiency did not dominate the compositional variations observed in the samples they were compared to principal components analysis of the data set. One of the outputs from PCA is the contribution (%) of each individual amino acid to the observed variability explained by the first axis. If the relative correction efficiency was responsible for driving the observed compositional variations then one would expect them to be positively correlated with the contribution derived from PCA. It is clear from Fig A3.6 that this is not the case, and in fact amino acids with the largest RCEs such as methionine, ornithine, and lysine actually contribute very little to the variation within the data-set. However, correcting all amino acids with one internal standard may make a small contribution to the observed variability within the data-set.

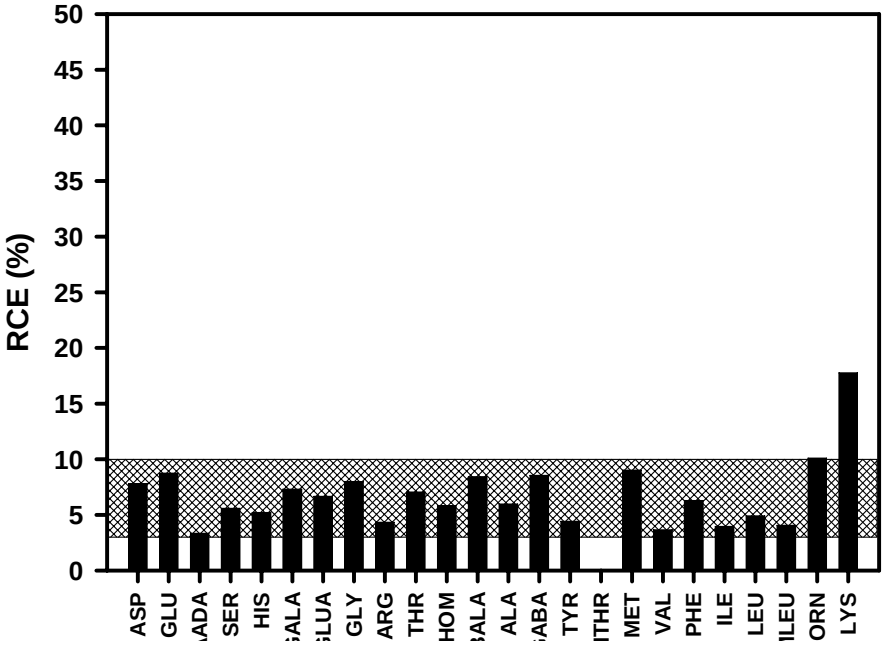

Fig A3.5 Relative correction Efficiency (RCE) for individual amino acids

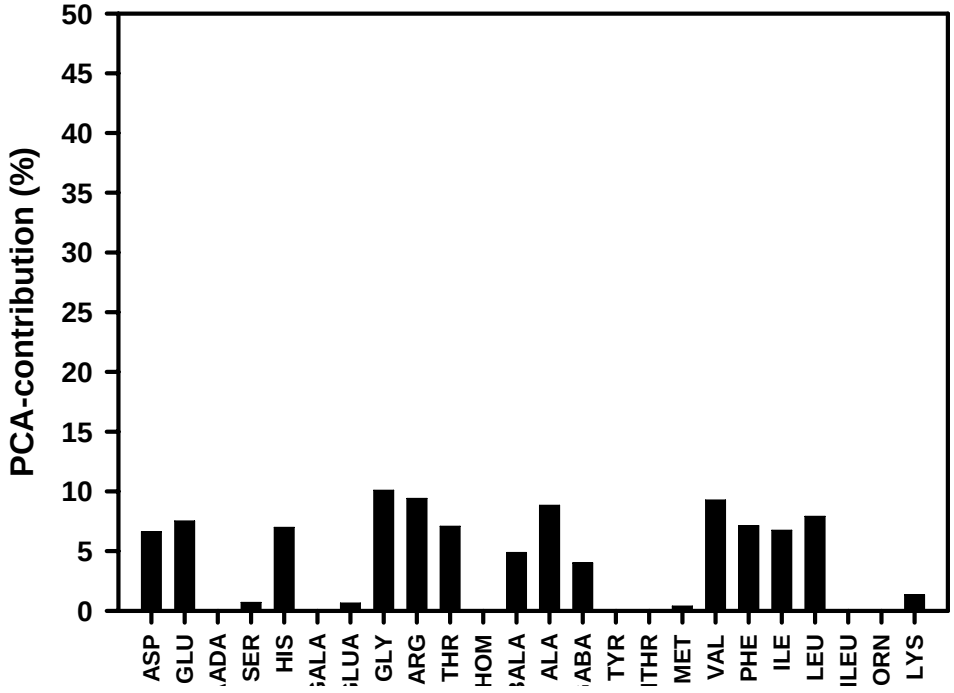

Fig A3.6 Contribution of individual amino acids to the variability of the data-set

A3.2.4 Reproducibility

Repeat injections of standards highlight that the reproducibility of the method is better than 5% for all amino acids, with the exception of ornithine and lysine which are better than 10% Fig. A3.7

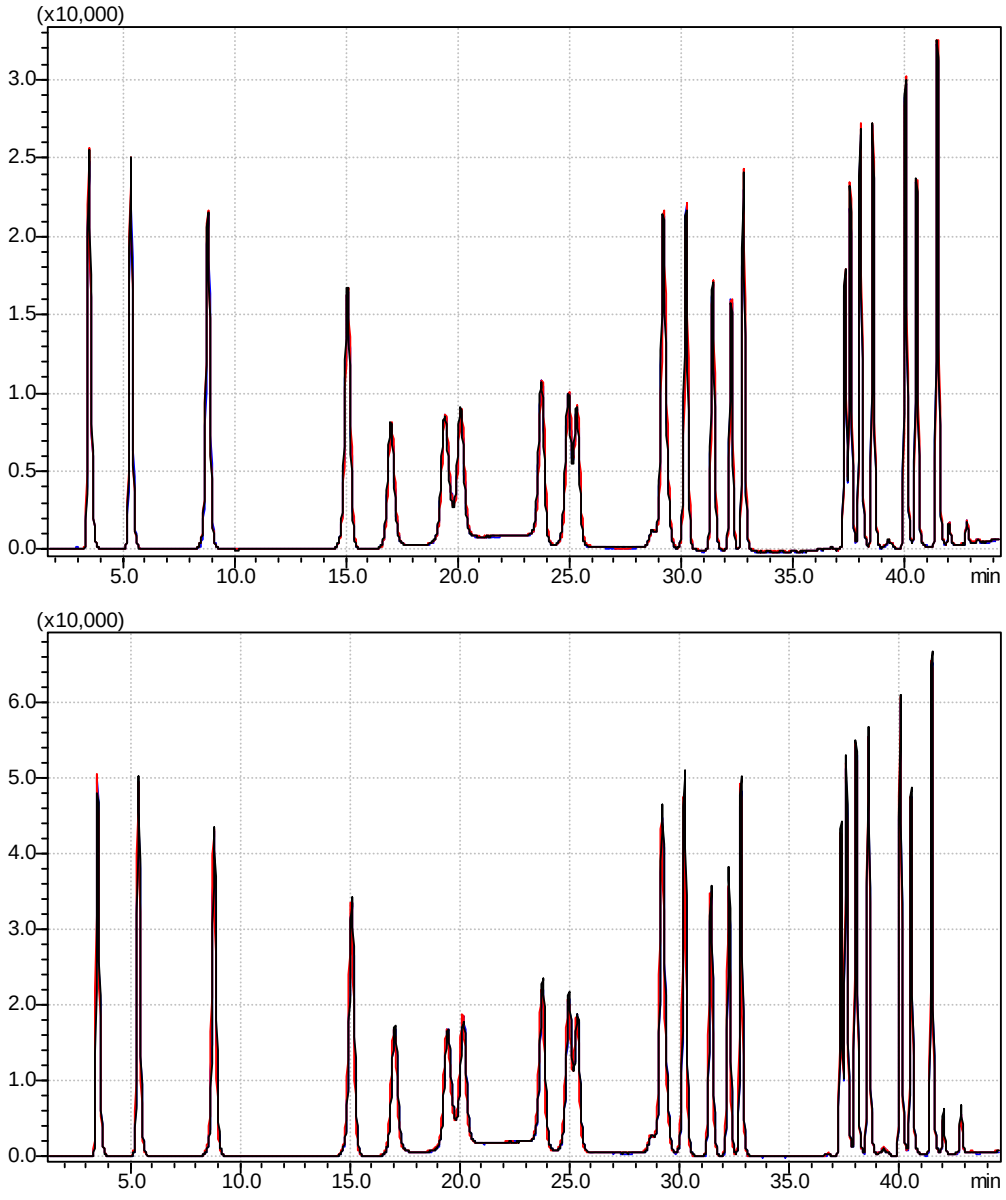

Fig. A3.7 Repeat injections for mixed standard concentrations of 0.3µM (top panel), and 0.6µM bottom (panel). Red, black, and blue chromatogram traces are for individual replicates.

In order to establish long-term statistical reproducibility sample 27B8 was run with each batch of hydrolyses and determined within randomly selected analytical runs. In total 8 samples were analysed in this way. It is important to highlight that this does not report the reproducibility of injecting the same hydrolysate. Each of the 8 samples was weighed out, hydrolysed, and neutralised separately, then calibrated within its analytical run and subjected to the methyl-threonine correction based on the statistical criterion described above. The average amino acid content of 27B8 was 42.2 ± 3.3 μg mg^{-1}, which represents a relative error of <8%, for hexosamines the average content was 3.0 ± 0.4 μg mg^{-1} with a relative error of <13%.

A3.2.5 Blanks, Limit of detection and limit of quantification

An operational blank was included with each batch of hydrolyses and concentrations were typically very low. The operational blank takes into account any amino acids from the vials, acid, sodium hydroxide, and Milli-Q water used in preparation of the samples for analysis. Average operational blank values were highest for ornithine (187nM), glycine (57nM), valine (55nM), threonine (32nM) and serine (25nM), for all other amino acids average blank values were < 20nM. The detection limit was calculated based on 3 times the standard deviation of the blank. These values are presented in Table A3.1 along with the concentrations observed in the samples. The precision at the detection limit is by definition 33%. For accurate quantitative measurements, concentrations should be at least 10 times the detection limit. It is clear from Table A.3.1 that the measured concentrations far exceed the detection limit for all amino acids, with the exception of ornithine. It must be concluded from this that the uncertainty associated with the detection of ornithine is greater than for the other amino acids. This arises from the relatively high blank and low concentration of ornithine, however, since it typically represents <4 mol% of the samples this is not perceived to be a major problem.

Table A3.1 Blank values and limits of detection and quantification

Amino Acid	Blank [nM]	Detection Limit [nM]	Sample [nM]	%Blank
Aspartic acid	10	29	6537	**0.4**
Glutamic acid	9	27	7700	**0.3**
Aminoadipic acid				
Serine	25	76	6439	**1.2**
Histidine	3	10	4309	**0.2**
Galactosamine	2	7	1182	**0.6**
Glucosamine	1	4	4565	**0.1**
Glycine	57	172	32558	**0.5**
Arginine	4	12	6096	**0.2**
Threonine	33	99	9821	**1.0**
L-homoarginine				
b-Alanine	0	1	1012	**0.1**
Alanine	17	52	16136	**0.3**
y-Aminobutyric acid	1	3	1717	**0.2**
Tyrosine	7	22	1002	**2.2**
Methyl-threonine				
Methionine	8	24	415	**5.7**
Valine	55	166	1968	**8.5**
Phenylalanine	8	23	4747	**0.5**
Isoleucine	18	55	1494	**3.7**
Leucine	19	58	4969	**1.2**
Methyl leucine				
Ornithine	187	561	1143	**49.1**
Lysine	64	192	5881	**3.3**

A3.3 Reagents

A3.3.1 Charge-matched standards

1. *1mM Aminoadipic Acid:* 16.16mg of aminoadipic acid (fw =161.6g mol^{-1}) dissolved in 100ml of Milli-Q water and frozen at -20^{o}C
2. *1mM l-homoarginine:* 22.47mg of *l*-homoarginine (fw = 224.7g mol^{-1}) dissolved in 100ml of Milli-Q water and frozen at -20^{o}C
3. *1mM Methyl-leucine:* 14.52mg methyl-leucine (fw = 145.2g mol^{-1}) dissolved in 100ml of Milli-Q water and frozen at -20^{o}C
4. *0.25mM Charge-matched standards:* 10ml of the 1mM stock solutions was added to 30ml Milli-Q water and frozen at -20^{o}C

A3.3.2 Analytical Standards

5. *Primary stock solutions:* Primary standards were made up by dissolving the individual amino acids in Milli-Q according to the quantities summarised in Table A3.2.
6. *Secondary stock solutions:* Secondary stock solutions were made up for all the amino acids which had a primary stock solution concentration of 100mM (Table A3.2). 250µl of 100mM stock solution was added to 9.75ml of Milli-Q water to create the secondary stock solution which was frozen at -20^{o}C.
7. *Mixed Standard:* 100µl of 2.5mM amino acids and 250µl of 1mM amino acids were added to a 100 ml volumetric flask and made up to volume with Milli-Q water to give 2.5µM mixed standard. This mother solution was sequentially diluted to give mixed standards with concentrations of 1.25, 0.63, and 0.31, and 0.16µM. The 0µM standard was pure Milli-Q water.

Table A3.2 Preparation of Mixed Standard

Amino acid	Formula Weight g mol^{-1}	Standard Weight g	Volume ml	Concentration mmol L^{-1}
Alanine	89.1	0.0891	10	100
b-Alanine	*89.1*	*0.0089*	*100*	*1*
y-Aminobutyric acid	*103.1*	*0.0103*	*100*	*1*
Serine	105.1	0.1051	10	100
Valine	117.2	0.1172	10	100
Threonine	119.1	0.1191	10	100
Isoleucine	131.2	0.1312	10	100
Leucine	131.2	0.1312	10	100
Glycine	132.1	0.1321	10	100
Aspartic acid	133.1	0.1331	10	100
Methyl Leucine	*145.2*	*0.0145*	*100*	*1*
Lysine	146.2	0.1462	10	100
Glutamic acid	147.1	0.1471	10	100
Methionine	149.2	0.1492	10	100
Histidine	155.2	0.1552	10	100
Aminoadipic acid	*161.2*	*0.0161*	*100*	*1*
Phenylalanine	165.2	0.1652	10	100
Ornithine	168.6	0.1686	10	100
Arginine	174.2	0.1742	10	100
Tyrosine	181.2	0.1812	10	100
Galactosamine	*215.6*	*0.0216*	*100*	*1*
Glucosamine	*215.6*	*0.0216*	*100*	*1*
L-Homoarginine	*224.7*	*0.0225*	*100*	*1*

A3.3.3 Hydrolysis and HPLC reagents

8. *6.7M HCl:* 27.5ml of concentrated HCl (12.2M) (grade) was added slowly to 22.5ml of Milli-Q water and allowed to cool.
9. *1M NaOH:* 4g of NaOH dissolved in 100ml of Milli-Q
10. *0.1M boric acid buffer:* 0.611g of boric acid and one NaOH pellet were added to ultrasonicated until dissolved in 10ml of Milli-Q water and ultrasonicated until completely dissolved. The boric acid buffer was titrated to pH 8.2 using 1M NaOH.
11. *Derivatisation reagent (OPA):* 137mg of OPA (fluorescing) was dissolved in 5ml of methanol and added to a 25ml volumetric flask. The solution was made to volume with a 0.04M boric acid solution (pH 9.5). 1.25ml aliquots of the OPA

derivatisation reagent were added to HPLC vials which were subsequently frozen at -20°C. **Prior to use 5µl of 2-mercaptoethanol was added to each vial**

12. *0.04M boric acid solution:* 0.25g of boric acid was dissolved in 100ml of Milli-Q water. The solution was titrated to pH 9.5 using 6M NaOH.
13. *Eluant A (Methanol):* HPLC grade Methanol
14. *Eluant B (THF):* 4.080g of Na-Acetate added to a 1 L volumetric flask and dissolved in 250ml of MQ water. 20ml of concentrated tetrahydrofuran added to the flask and made to volume with Milli-Q water. 80µl of 10% acetic acid added. Contents of the flask mixed and left for thirty minutes.

A3.4 Procedure

A3.4.1 Hydrolysis

1. 1-4 (depending on size) 1/8th sediment trap aliquots were filtered onto cellulose nitrate filters (0.4µm, 47mm diameter).
2. Samples were rinsed with Milli-Q water to remove excess salts
3. Wet sediment was carefully scraped from the filter with a clean metal spatula and placed into pre-combusted (500°C, 12 hours) glass vials and frozen at -20°C
4. Sediment was freeze-dried overnight and crushed with a metal spatula.
5. Approximately 10 mg of homogenised sample weighed into a pre-combusted (500°C, 12 hours) 7ml capped glass vial.
6. 100µl of each 0.25mM charge-matched standards, aminoadipic acid (AADA), l-homoarginine (LHOM), methyl-leucine (MLEU) were carefully pipetted into each sample vial.
7. 6.7 M HCl solution purged with argon for 30 minutes (HCl_{purged})
8. 2.7ml of 6.7 M HCl_{purged} pipetted into sample vial.
9. Headspace in the sample vial was displaced by flushing with pure argon for 1 minute.
10. The vial was capped and PTFE tape tightly wrapped between the vial and cap to ensure a proper seal.
11. Sample placed in a sand bath heated to 100°C for a period of 24 hours.

A3.4.2 Neutralisation

12. Samples removed from sand bath and placed in an ice-bath for ten minutes to cool.
13. Sealed vials and samples removed from the ice-bath and centrifuged at 3000rpm for 15 minutes.
14. 1ml of the supernatant hydrolysate was carefully pipetted from the glass sample vial and transferred to a clean labelled Eppendorf tube; stored samples were frozen at -80^{o}C
15. 250µl of 6M HCl hydrolysate was added to 1.5ml of 1 M NaOH, followed by 2ml of Milli-Q (18.2) water to give a total volume of 3.75ml.
16. The neutralised solution was then syringe-filtered into a clean, labelled Eppendorf tube.

A3.4.3 HPLC preparation

17. 270µl of sample, standard, and blank pipetted into a HPLC vial.
18. 10µl of 0.1M boric acid buffer solution (pH – 8.6) was added to each vial
19. 15µl of the internal standard methyl-threonine was added to each vial.
20. The HPLC vials were capped and loaded into the autosampler.

A3.5 Chromatography

The protein amino acids, non-protein amino acids, and hexosamines were analysed by HPLC using a modified method of Cowie and Hedges (1992). An Ascentis C_{18} 15 cm 3µm column equipped with a guard column was eluted at a flow rate of 1 ml min^{-1} at a constant temperature of 30^{o}C. To separate the compounds a binary gradient of methanol (Eluant A) and 30mM sodium acetate (pH 7) and 2% THF (eluant B) was used. The ionic strength, pH, and THF content of eluant B were occasionally modified to maintain resolution as guard column and analytical column aged. The gradient is presented in Fig A3.8. OPA-derivatisation was achieved online and the

amino acids were detected by fluorescence and identified by comparison to retention times of authenticated standards determined from the mixed standard.

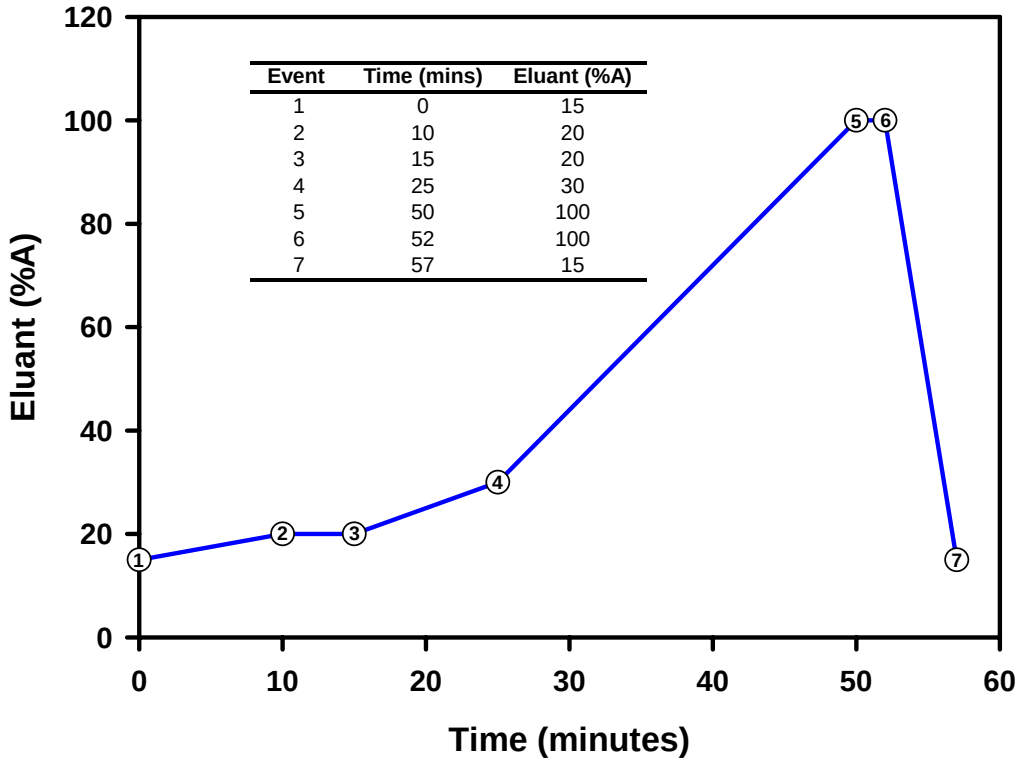

Fig A3.8 Solvent gradient used to separate amino acids and hexosamines

A3.6 Mixed Standard Calibration

At the start of each analytical run a six-point calibration was conducted using the mixed standards (concentrations 0, 0.15, 0.30, 0.6, 1.2, 2.5µM). The areas of individual compounds were corrected by reference to the internal standard methyl-threonine (see Section A3.2.3). Linear regression for all individual amino acids yielded correlation coefficients >0.99. Sample chromatograms for the mixed standard, sample, and blank are shown in Fig. A.3.9

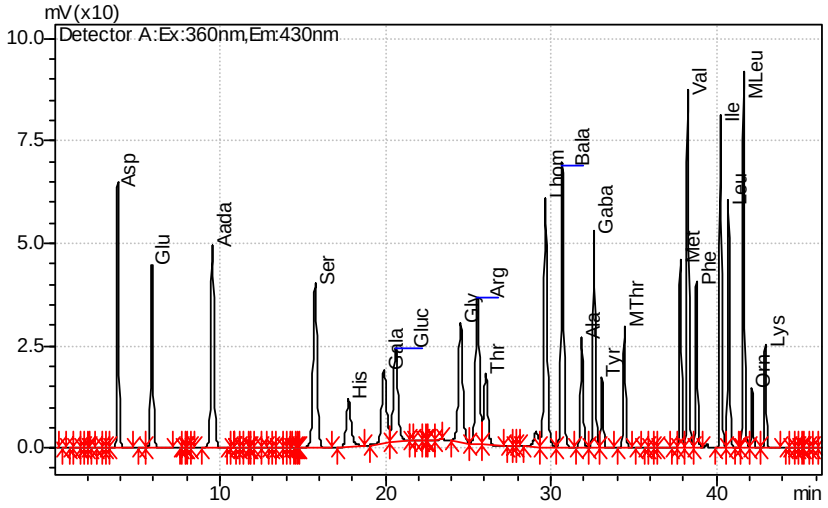
mV(x10)
Detector A:Ex:360nm,Em:430nm
10.0
7.5
5.0
2.5
0.0
Asp
Glu
Aada
Ser
His
Gala
Gluc
Gly
Arg
Thr
Lhom
Bala
Gaba
Ala
Tyr
MThr
Met
Val
Phe
Ile
Leu
MLeu
Orn
Lys
10
20
30
40
min

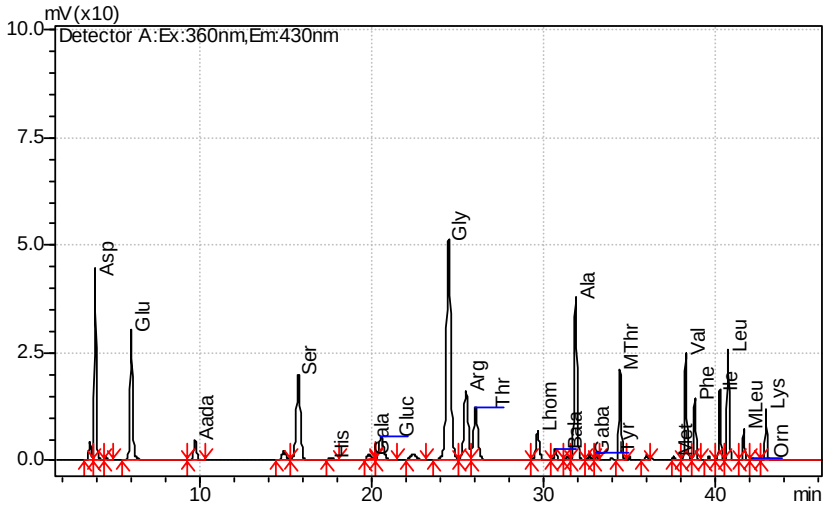
mV(x10)
Detector A:Ex:360nm,Em:430nm
10.0
7.5
5.0
2.5
0.0
Asp
Glu
Aada
Ser
His
Gala
Gluc
Gly
Arg
Thr
Lhom
Bala
Ala
Gaba
Tyr
MThr
Met
Val
Phe
Ile
Leu
MLeu
Orn
Lys
10
20
30
40
min

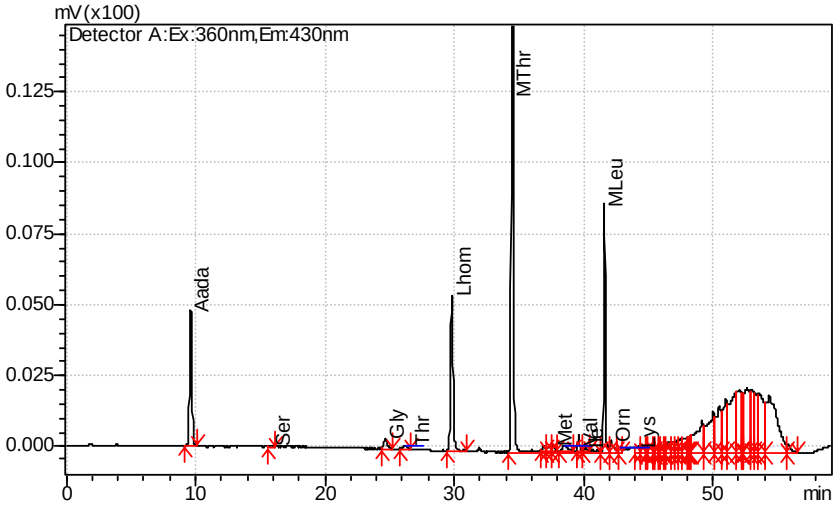
mV(x100)
Detector A:Ex:360nm,Em:430nm
0.125
0.100
0.075
0.050
0.025
0.000
Aada
Ser
Gly
Thr
Lhom
MThr
Met
Val
Ala
Orn
Lys
MLeu
0
10
20
30
40
50
min

Fig A.3.9 Representative chromatograms for a) 2.5µM mixed standard, b) sample, and c) blank.

A3.7 Sample Calculations

$C_{AAi} = ([1/G]_{AAi})\ (A_{AAi})$

$N_{AAi} = (C_{AAi})(V)(D_F)$

$W_{AAi} = [(N_{AAi})(FW_i)] / S_{MASS}$

C_{AAi}	concentration of amino acid *i* (µmol L^{-1} or µM)
$[1/G]_{AAi}$	G is the gradient of amino acid *i* obtained from the linear regression of five point mixed standard calibration (µM A^{-1}; where A is the integrated peak area)
A_{AAi}	the peak area of amino acid *i* (A)
N_{AAi}	number of moles of amino acid *i* (µmol)
V	volume of hydrolysate (L)
D_F	dilution factor prior to loading the sample onto the HPLC (no units)
W_{AAi}	weight of amino acid *i* in sample (µg mg^{-1})
FW_i	formula weight of amino acid *i* in sample (µg $µmol^{-1}$)
S_{MASS}	sample mass (mg)

A3.8 A study of recovery efficiencies

Almost all sediment trap amino acid studies hydrolyse samples with little regard for recovery efficiency. Amino acids, as a compound class, are chemically diverse. Among the primary amino acids, hydroxyl, thiol, and phenyl groups are found in a variety of orientations relative to the amino and carboxyl groups. The amino acids also vary in molecular weight, hydrophobicity and charge. This diversity results in an equally large range of potential losses via physical or chemical processes during extraction and isolation. These processes potentially present serious problems for the accurate quantification of amino acids in environmental samples of varied matrix type

i.e. sediment trap samples. This method builds on the study of Cowie and Hedges (1992) and incorporates charge-matched amino acids as recovery standards to account for selective amino acid losses due to adsorption or chemical reactions, which are typically charge-related, and may be related to sediment composition.

The principal criteria for the selection of compounds as recovery standards were

a) matched charge and similarity of structure to the amino acids they were to represent

b) no known natural sources

c) elution in a chromatographic window

Prior to hydrolysis charge-matched standards were added to the samples so that the recovery efficiency could be calculated. ***Note that all areas in these equations have already been corrected using the internal standard methyl-threonine (see section A3.2.3.)***

$\mathbf{A_{CMS}}$	Peak area of the charge-matched standard in sample (A)
$\mathbf{C_{CMS}}$	Concentration of charge-matched standard in hydrolysate (µmol L^{-1} or µM)
$\mathbf{[1/G]_{CMS}}$	G is the gradient of the charge-matched standard of a linear regression through the five-point mixed standard calibration (µM A^{-1}; where A is the integrated peak area)
$\mathbf{ExC_{CMS}}$	Theoretical concentration of charge-matched standard in hydrolysate (µM)
[CMS]	Concentration of charge-matched standard initially added to sediment sample prior to hydrolysis (µM)
$\mathbf{V_{CMS}}$	Volume of [CMS] added to sediment sample prior to hydrolysis (µL)
$\mathbf{V_{HYD}}$	Volume of mineral acid used to hydrolyse sediment sample (L)
$\mathbf{D_F}$	Dilution factor prior to loading the sample onto the HPLC (no units)
%R	Recovery efficiency (percent)

$A_{CMS} = C_{CMS} / [1/G]_{CMS}$

$ExCMS = (([CMS] * V_{CMS}) / V_{HYD}) / D_F$

$\%R = (A_{CMS} * [1/G]_{CMS}) / ExC_{CMS}$

Based on this technique and the calculations above, recovery efficiencies were calculated for each sample (Fig A3.10.) The recoveries of aminoadipic acid and methyl leucine were more consistent than that of L-homoarginine, possibly related to co-eluting fluorescent derivatives. The neutral amino acids which represent the bulk of the compounds detected had the best recoveries, whilst those of the acidic amino acids (aspartic and glutamic acid) and basics (ornithine and lysine) were 64 and 54% respectively. The method needs to be developed further to take account of these recoveries and incorporate charge-matched internal standards.

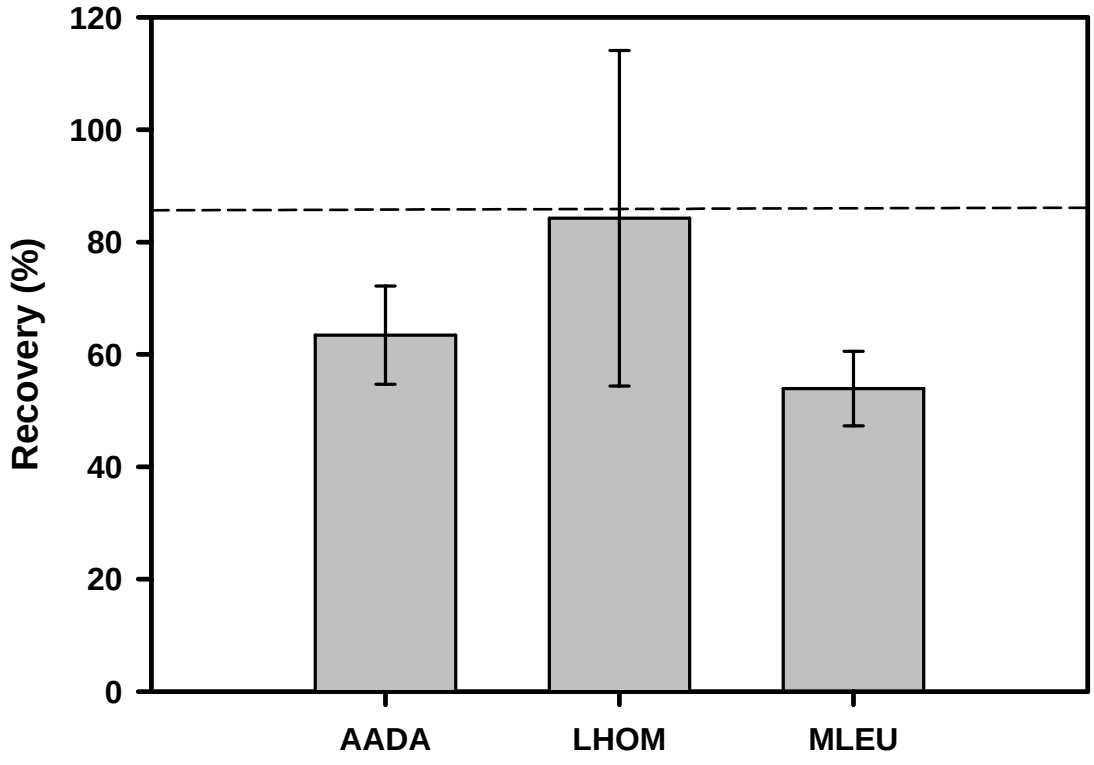

Fig A3.10 Average recovery efficiencies for all sample types (n = 72) for aminoadipic acid (AADA), l-homoarginine (LHOM) and methyl-leucine (MLEU).

In order to embed solutions to these complicated problems into a routine analysis then it is suggested that nine replicates would need to be analysed for each sample;

a) Three replicates would be used to ascertain the natural and/or fluorescent derivatives of unknown compounds that elute at the same retention times of the selected charge-matched standards.

b) Three replicates would require a pre-hydrolysis addition of the selected charge match standards, with normalized values from a) subtracted to remove this source of error. The combination of point a and point b would provide a sample-specific recovery efficiency that could be applied to a particular sample to correct for losses during the hydrolysis procedure.

C) Three replicates with a post-hydrolysis addition of the selected recovery standards to quantify absolute recoveries of individual amino acids by subtracting normalized values obtained from point a.

Given the complexity of samples encountered and the long analytical chromatography required to separate these compounds, each sample can take between 40-80 minutes to analyse depending on selected elution profiles and running conditions. Consequently the proposed scheme is both time consuming and expensive and in many instances is considered to be an impractical solution to the range of analytical problems encountered, particularly during the course of this project.

APPENDIX 4: MOORING DEPLOYMENTS

Information regarding the times and positions of the various moorings analysed during this study is presented in tabulated form below. In addition, and with reference to the Crozex moorings, schematics of Type I and Type II moorings are provided.

Deployment number	**XXV**
Cruise deployed	**D237**
Date	**09/10/1998**
Trap depth	**3000m**

Bottom depth	**4835m**
Latitude	**49°N**
Longitude	**16.43°W**

Sample ID	Cup Number (#)	Open Date At 1200 hours	Julian Day Open	Julian Day Mid-Day	Sampling Interval (days)	pH of Preservative Solution	Swimmers (#)
XXV-B-1	1	11/10/1998	284.5	313.5	56	8.5	78
XXV-B-2	2	06/12/1998	340.5	4.5	56	8.5	33
XXV-B-3	3	31/01/1999	31.5	60.5	56	8.5	18
XXV-B-4	4	28/03/1999	87.5	102.5	28	8.5	28
XXV-B-5	5	25/04/1999	115.5	130.5	28	8.5	46
XXV-B-6	6	23/05/1999	143.5	151.5	14	8.5	28
XXV-B-7	7	06/06/1999	157.5	165.5	14	8.5	12
XXV-B-8	8	20/06/1999	171.5	179.5	14	8.5	16
XXV-B-9	9	04/07/1999	185.5	193.5	14	8.5	7
XXV-B-10	10	18/07/1999	199.5	207.5	14	8.5	9
XXV-B-11	11	01/08/1999	213.5	221.5	14	8.5	10
XXV-B-12	12	15/08/1999	227.5	235.5	14	8.5	3
XXV-B-13	13	29/08/1999	241.5	256.5	28	8	9
					Close		

Deployment number	**XXVI**
Cruise deployed	**C147c**
Date	**10/09/1999**
Trap depth	**3000m**

Bottom depth	**4804m**
Latitude	**48.98°N**
Longitude	**16.43°W**

Sample ID	Cup Number (#)	Open Date At 1200 hours	Julian Day Open	Julian Day Mid-Day	Sampling Interval (days)	pH of Preservative Solution	Swimmers (#)
XXVI-B-1	1	12/09/99	255.5	262.5	14	8.3	4
XXVI-B-2	2	26/09/99	269.5	276.5	14	8.0	1
XXVI-B-3	3	10/10/99	283.5	290.5	14	8.1	1
XXVI-B-4	4	24/10/99	297.5	304.5	14	8.0	4
XXVI-B-5	5	07/11/99	311.5	325.5	28	8.1	2
XXVI-B-6	6	05/12/99	339.5	353.5	28	8.2	1
XXVI-B-7	7	02/01/00	2.5	16.5	28	8.2	2
XXVI-B-8	8	30/01/00	30.5	44.5	28	8.2	1
XXVI-B-9	9	27/02/00	58.5	65.5	14	8.3	2
XXVI-B-10	10	12/03/00	72.5	79.5	14	8.3	4
XXVI-B-11	11	26/03/00	86.5	93.5	14	8.1	-
XXVI-B-12	12	09/04/00	100.5	107.5	14	8.2	6
XXVI-B-13	13	23/04/00	114.5	121.5	14	8.3	1
XXVI-B-14	14	07/05/00	128.5	135.5	14	8.2	-
XXVI-B-15	15	21/05/00	142.5	149.5	14	8.1	4
XXVI-B-16	16	04/06/00	156.5	163.5	14	8.3	-
XXVI-B-17	17	18/06/00	170.5	177.5	14	8.4	-
XXVI-B-18	18	02/07/00	184.5	191.5	14	8.3	-
XXVI-B-19	19	16/07/00	198.5	205.5	14	8.4	-
XXVI-B-20	20	30/07/00	212.5	219.5	14	8.4	-
XXVI-B-21	21	13/08/00	226.5	240.5	28	8.4	-
					Close		

Deployment number	**XXVII**
Cruise deployed	**D251T**
Date	**04/04/2001**
Trap depth	**3000m**

Bottom depth	**4812m**
Latitude	**49°N**
Longitude	**16.46°W**

Sample ID	Cup Number (#)	Open Date At 1200 hours	Julian Day Open	Julian Day Mid-Day	Sampling Interval (days)	pH of Preservative Solution	Swimmers (#)
XXVII-B-1	1	08/04/01	99.5	106.5	14	7.5	125
XXVII-B-2	2	22/04/01	113.5	120.5	14	7.5	34
XXVII-B-3	3	06/05/01	127.5	134.5	14	7.5	35
XXVII-B-4	4	20/05/01	141.5	148.5	14	7.5	55
XXVII-B-5	5	03/06/01	155.5	162.5	14	7.5	36
XXVII-B-6	6	17/06/01	169.5	176.5	14	7.5	10
XXVII-B-7	7	01/07/01	183.5	190.5	14	7.5	87
XXVII-B-8	8	15/07/01	197.5	204.5	14	7.5	129
XXVII-B-9	9	29/07/01	211.5	218.5	14	7.5	44
XXVII-B-10	10	12/08/01	225.5	232.5	14	7.5	79
XXVII-B-11	11	26/08/01	239.5	246.5	14	7.5	47
XXVII-B-12	12	09/09/01	253.5	260.5	14	7.5	61
XXVII-B-13	13	23/09/01	267.5	274.5	14	7.5	27
XXVII-B-14	14	07/10/01	281.5	288.5	14	7	49
XXVII-B-15	15	21/10/01	295.5	306	21	7.5	26
XXVII-B-16	16	11/11/01	316.5	327	21	7.5	40
XXVII-B-17	17	02/12/01	337.5	348	21	7.5	24
XXVII-B-18	18	23/12/01	358.5	4	21	8	24
XXVII-B-19	19	13/01/02	14.5	25	21	7.5	14
XXVII-B-20	20	03/02/02	35.5	46	21	8	11
XXVII-B-21	21	24/02/02	56.5	67	21	8	13
					Close		

Deployment number	**XXVIII**
Cruise deployed	**D266**
Date	**04/10/2002**
Trap depth	**3000m**

Bottom depth	**4845m**
Latitude	**49°N**
Longitude	**16.47°W**

Sample ID	Cup Number (#)	Open Date At 1200 hours	Julian Day Open	Julian Day Mid-Day	Sampling Interval (days)	pH of Preservative Solution	Swimmers (#)
XXVIII-B-1	1	06/10/02	280.5	284	7	8	7
XXVIII-B-2	2	13/10/02	287.5	294.5	14	8	25
XXVIII-B-3	3	27/10/02	301.5	308.5	14	7.5	17
XXVIII-B-4	4	10/11/02	315.5	322.5	14	7.5	20
XXVIII-B-5	5	24/11/02	329.5	336.5	14	7.5	11
XXVIII-B-6	6	08/12/02	343.5	350.5	14	7.5	
XXVIII-B-7	7	22/12/02	357.5	3	21	7.5	21
XXVIII-B-8	8	12/01/03	13.5	24	21	7.5	43
XXVIII-B-9	9	02/02/03	34.5	41.5	14	7.5	17
XXVIII-B-10	10	16/02/03	48.5	55.5	14	7.5	15
XXVIII-B-11	11	02/03/03	62.5	66	7	7.5	16
XXVIII-B-12	12	09/03/03	69.5	73	7	7.5	9
XXVIII-B-13	13	16/03/03	76.5	80	7	7.5	9
XXVIII-B-14	14	23/03/03	83.5	87	7	7.5	9
XXVIII-B-15	15	30/03/03	90.5	94	7	7.5	8
XXVIII-B-16	16	06/04/03	97.5	101	7	7.5	21
XXVIII-B-17	17	13/04/03	104.5	108	7	7.5	3
XXVIII-B-18	18	20/04/03	111.5	115	7	7.5	5
XXVIII-B-19	19	27/04/03	118.5	122	7	7.5	13
XXVIII-B-20	20	04/05/03	125.5	129	7	7.5	17
XXVIII-B-21	21	11/05/03	132.5	134.5	4	7.5	3
					Close		

Deployment number	**XXXI**
Cruise deployed	**P300/1**
Date	**12/07/2003**
Trap depth	**3000m**

Bottom depth	**4805m**
Latitude	**49°N**
Longitude	**16.5°W**

Sample ID	Cup Number (#)	Open Date At 1200 hours	Julian Day Open	Julian Day Mid-Day	Sampling Interval (days)	pH of Preservative Solution	Swimmers (#)
XXXI-A-1	1	13/07/03	194.5	201.5	14	8	7
XXXI-A-2	2	27/07/03	208.5	215.5	14	8	10
XXXI-A-3	3	10/08/03	222.5	229.5	14	8	8
XXXI-A-4	4	24/08/03	236.5	243.5	14	8	5
XXXI-A-5	5	07/09/03	250.5	257.5	14	8	4
XXXI-A-6	6	21/09/03	264.5	271.5	14	8	3
XXXI-A-7	7	05/10/03	278.5	292.5	28	8	3
XXXI-A-8	8	02/11/03	306.5	320.5	28	8	14
XXXI-A-9	9	30/11/03	334.5	348.5	28	8	4
XXXI-A-10	10	28/12/03	362.5	11.5	28	8	4
XXXI-A-11	11	25/01/04	25.5	39.5	28	8	17
XXXI-A-12	12	22/02/04	53.5	67.5	28	8	12
XXXI-A-13	13	21/03/04	81.5	88.5	14	8	9
XXXI-A-14	14	04/04/04	95.5	102.5	14	8	2
XXXI-A-15	15	18/04/04	109.5	116.5	14	7.5	3
XXXI-A-16	16	02/05/04	123.5	130.5	14	8	3
XXXI-A-17	17	16/05/04	137.5	144.5	14	8	4
XXXI-A-18	18	30/05/04	151.5	164	25	8	0
XXXI-A-19	19	24/06/04	176.5	183.5	14		
XXXI-A-20	20	08/07/04	190.5	197.5	14		
XXXI-A-21	21	22/07/04	204.5	211.5	14		
					Close		

Deployment number	**XXXIV**
Cruise deployed	**CD158**
Date	**24/06/2004**
Trap depth	**3000m**

Bottom depth	**4803m**
Latitude	**49°N**
Longitude	**16.5°W**

Sample ID	Cup Number (#)	Open Date At 1200 hours	Julian Day Open	Julian Day Mid-Day	Sampling Interval (days)	pH of Preservative Solution	Swimmers (#)
XXXIV-A-1	1	27/06/04	179.5	186.5	14	7.5	77
XXXIV-A-2	2	11/07/04	193.5	200.5	14	7.5	44
XXXIV-A-3	3	25/07/04	207.5	214.5	14	8	0
XXXIV-A-4	4	08/08/04	221.5	228.5	14	7.8	18
XXXIV-A-5	5	22/08/04	235.5	242.5	14	8	30
XXXIV-A-6	6	05/09/04	249.5	256.5	14	8	26
XXXIV-A-7	7	19/09/04	263.5	270.5	14	7.8	10
XXXIV-A-8	8	03/10/04	277.5	298.5	42	7	27
XXXIV-A-9	9	14/11/04	319.5	340.5	42	7.2	24
XXXIV-A-10	10	26/12/04	361.5	17.5	42	7.2	43
XXXIV-A-11	11	06/02/05	38.5	59.5	42	7.5	39
XXXIV-A-12	12	20/03/05	80.5	87.5	14	8.3	16
XXXIV-A-13	13	03/04/05	94.5	101.5	14	8.3	10
XXXIV-A-14	14	17/04/05	108.5	115.5	14	7.8	10
XXXIV-A-15	15	01/05/05	122.5	129.5	14	7.8	7
XXXIV-A-16	16	15/05/05	136.5	143.5	14	7.2	7
XXXIV-A-17	17	29/05/05	150.5	157.5	14	8	36
XXXIV-A-18	18	12/06/05	164.5	171.5	14	7.4	69
XXXIV-A-19	19	26/06/05	178.5	185.5	14	8	38
XXXIV-A-20	20	10/07/05	192.5	199.5	14	7.8	0
XXXIV-A-21	21	24/07/05	206.5	213.5	14	8.5	0
			220.5		**Close**		

Deployment number	**XXXVI**
Cruise deployed	**D285**
Date	**20/12/2004**
Trap depth	**2000m**

Bottom depth	**2935m**
Latitude	**44.5°S**
Longitude	**50°E**

Sample ID	Cup Number (#)	Open Date At 1200 hours	Julian Day Open	Julian Day Mid-Day	Sampling Interval (days)	pH of Preservative Solution
XXXVI-A-1	1	21/12/2004	356.5	361.5	12	8.0
XXXVI-A-2	2	02/01/05	2.5	8.5	14	8.0
XXXVI-A-3	3	16/1/2005	16.5	22.5	14	8.0
XXXVI-A-4	4	30/1/2005	30.5	40	21	7.0
XXXVI-A-5	5	20/2/2005	51.5	64.5	28	7.5
XXXVI-A-6	6	20/3/2005	79.5	92.5	28	7.5
XXXVI-A-7	7	17/4/2005	107.5	120.5	28	7.0
XXXVI-A-8	8	15/5/2005	135.5	148.5	28	7.5
XXXVI-A-9	9	12/6/2005	163.5	176.5	28	8.0
XXXVI-A-10	10	10/7/2005	191.5	204.5	28	8.5
XXXVI-A-11	11	07/08/05	219.5	232.5	28	8.5
XXXVI-A-12	12	04/09/05	247.5	260.5	28	8.3
XXXVI-A-13	13	02/10/05	275.5	281.5	14	8.3
XXXVI-A-14	14	16/10/2005	289.5	295.5	14	8.5
XXXVI-A-15	15	30/10/2005	303.5	309.5	14	8.3
XXXVI-A-16	16	13/11/2005	317.5	323.5	14	8.3
XXXVI-A-17	17	27/11/2005	331.5	336	11	8.3
XXXVI-A-18	18	11/12/2005	345.5	345	7	8.5
XXXVI-A-19	19	18/12/2005	352.5	352	7	8.5
XXXVI-A-20	20	25/12/2005	359.5	359	7	8.5
XXXVI-A-21	21	01/01/05	1.5	4.5	14	8.5
					Close	

Deployment number	**XXXVII**
Cruise deployed	**D285**
Date	**06/01/2005**
Trap depth	**1973m**

Bottom depth	**3856m**
Latitude	**47.8°S**
Longitude	**52.9°E**

Sample ID	Cup Number (#)	Open Date At 1200 hours	Julian Day Open	Julian Day Mid-Day	Sampling Interval (days)	pH of Preservative Solution
XXXVII-A-1	1	08/01/05	8.5	11.5	8	6
XXXVII-A-2	2	16/01/05	16.5	22.5	14	8
XXXVII-A-3	3	30/01/05	30.5	36.5	14	7.5
XXXVII-A-4	4	13/02/05	44.5	54	21	6.5
XXXVII-A-5	5	06/03/05	65.5	78.5	28	8
XXXVII-A-6	6	03/04/05	93.5	106.5	28	8
XXXVII-A-7	7	01/05/05	121.5	134.5	28	8
XXXVII-A-8	8	29/05/05	149.5	162.5	28	8
XXXVII-A-9	9	26/06/05	177.5	190.5	28	8
XXXVII-A-10	10	24/07/05	205.5	218.5	28	8
XXXVII-A-11	11	21/08/05	233.5	243	21	8
XXXVII-A-12	12	11/09/05	254.5	264	21	8
XXXVII-A-13	13	02/10/05	275.5	281.5	14	8
XXXVII-A-14	14	16/10/05	289.5	295.5	14	6
XXXVII-A-15	15	30/10/05	303.5	309.5	14	7.5
XXXVII-A-16	16	13/11/05	317.5	323.5	14	8
XXXVII-A-17	17	27/11/05	331.5	337.5	14	8
XXXVII-A-18	18	11/12/05	345.5	348	7	8
XXXVII-A-19	19	18/12/05	352.5	355	7	6
XXXVII-A-20	20	25/12/05	359.5	362	1	8
XXXVII-A-21	21	26/12/05	-4.5	8.5	14	
					Close	

Deployment number	**XXXVIII**
Cruise deployed	**D285**
Date	**26/12/2004**
Trap depth	**2001m**

Bottom depth	**4277m**
Latitude	**46°S**
Longitude	**56.1°E**

Sample ID	Cup Number (#)	Open Date At 1200 hours	Julian Day Open	Julian Day Mid-Day	Sampling Interval (days)	pH of Preservative Solution
XXXVIII-A-1	1	28/12/04	363.5	3.5	12	6.5
XXXVIII-A-2	2	09/01/05	9.5	15.5	14	7.5
XXXVIII-A-3	3	23/01/05	23.5	29.5	14	6.5
XXXVIII-A-4	4	06/02/05	37.5	47	21	7.0
XXXVIII-A-5	5	27/02/05	58.5	71.5	28	7.5
XXXVIII-A-6	6	27/03/05	86.5	99.5	28	8.0
XXXVIII-A-7	7	24/04/05	114.5	127.5	28	8.0
XXXVIII-A-8	8	22/05/05	142.5	155.5	28	8.3
XXXVIII-A-9	9	19/06/05	170.5	183.5	28	8.0
XXXVIII-A-10	10	17/07/05	198.5	211.5	28	8.0
XXXVIII-A-11	11	14/08/05	226.5	236	21	8.0
XXXVIII-A-12	12	04/09/05	247.5	257	21	8.3
XXXVIII-A-13	13	25/09/05	268.5	278	21	8.0
XXXVIII-A-14	14	16/10/05	289.5	295.5	14	8.0
XXXVIII-A-15	15	30/10/05	303.5	309.5	14	8.0
XXXVIII-A-16	16	13/11/05	317.5	323.5	14	8.0
XXXVIII-A-17	17	27/11/05	331.5	337.5	14	8.3
XXXVIII-A-18	18	11/12/05	345.5	348	7	8.0
XXXVIII-A-19	19	18/12/05	352.5	352.5	2	7.5
XXXVIII-A-20	20	20/12/05	354.5	357	7	8.0
XXXVIII-A-21	21	27/12/05	-3.5	1.5	14	8.0
					Close	

Deployment number	**XXXVIII**
Cruise deployed	**D285**
Date	**26/12/2004**
Trap depth	**3195m**

Bottom depth	**4277m**
Latitude	**46°S**
Longitude	**56.1°E**

Sample ID	Cup Number (#)	Open Date At 1200 hours	Julian Day Open	Julian Day Mid-Day	Sampling Interval (days)	pH of Preservative Solution
XXXVIII-B-1	1	28/12/04	363.5	3.5	12	8.0
XXXVIII-B-2	2	09/01/05	9.5	15.5	14	8.0
XXXVIII-B-3	3	23/01/05	23.5	29.5	14	8.0
XXXVIII-B-4	4	06/02/05	37.5	47	21	8.0
XXXVIII-B-5	5	27/02/05	58.5	71.5	28	8.0
XXXVIII-B-6	6	27/03/05	86.5	99.5	28	8.0
XXXVIII-B-7	7	24/04/05	114.5	127.5	28	8.0
XXXVIII-B-8	8	22/05/05	142.5	155.5	28	7.0
XXXVIII-B-9	9	19/06/05	170.5	183.5	28	7.5
XXXVIII-B-10	10	17/07/05	198.5	211.5	28	8.0
XXXVIII-B-11	11	14/08/05	226.5	236	21	8.0
XXXVIII-B-12	12	04/09/05	247.5	257	21	-
XXXVIII-B-13	13	25/09/05	268.5	278	21	8.0
XXXVIII-B-14	14	16/10/05	289.5	295.5	14	8.0
XXXVIII-B-15	15	30/10/05	303.5	309.5	14	8.0
XXXVIII-B-16	16	13/11/05	317.5	323.5	14	8.0
XXXVIII-B-17	17	27/11/05	331.5	337.5	14	8.0
XXXVIII-B-18	18	11/12/05	345.5	348	7	8.0
XXXVIII-B-19	19	18/12/05	352.5	352.5	2	7.5
XXXVIII-B-20	20	20/12/05	354.5	357	7	8.0
XXXVIII-B-21	21	27/12/05	-3.5	1.5	14	8.0
					Close	

Deployment number	**XXXIX**
Cruise deployed	**D285**
Date	**03/01/2005**
Trap depth	**2007m**

Bottom depth	**4221m**
Latitude	**49°S**
Longitude	**51.5°E**

Sample ID	Cup Number (#)	Open Date At 1200 hours	Julian Day Open	Julian Day Mid-Day	Sampling Interval (days)	pH of Preservative Solution
XXXIX-A-1	1	05/01/05	5.5	10	11	6.0
XXXIX-A-2	2	16/01/05	16.5	22.5	14	7.0
XXXIX-A-3	3	30/01/05	30.5	36.5	14	7.0
XXXIX-A-4	4	13/02/05	44.5	54	21	7.0
XXXIX-A-5	5	06/03/05	65.5	78.5	28	7.0
XXXIX-A-6	6	03/04/05	93.5	106.5	28	6.0
XXXIX-A-7	7	01/05/05	121.5	134.5	28	7.0
XXXIX-A-8	8	29/05/05	149.5	162.5	28	7.0
XXXIX-A-9	9	26/06/05	177.5	190.5	28	7.0
XXXIX-A-10	10	24/07/05	205.5	218.5	28	7.0
XXXIX-A-11	11	21/08/05	233.5	243	21	7.0
XXXIX-A-12	12	11/09/05	254.5	264	21	7.0
XXXIX-A-13	13	02/10/05	275.5	281.5	14	7.0
XXXIX-A-14	14	16/10/05	289.5	295.5	14	7.0
XXXIX-A-15	15	30/10/05	303.5	309.5	14	7.0
XXXIX-A-16	16	13/11/05	317.5	323.5	14	7.0
XXXIX-A-17	17	27/11/05	331.5	337.5	14	7.0
XXXIX-A-18	18	11/12/05	345.5	348	7	7.0
XXXIX-A-19	19	18/12/05	352.5	355	7	7.0
XXXIX-A-20	20	25/12/05	359.5	362	7	7.0
XXXIX-A-21	21	01/01/06	1.5	1.5	2	6.0

Deployment number	**XXXIX**
Cruise deployed	**D285**
Date	**03/01/2005**
Trap depth	**3160m**

Bottom depth	**4221m**
Latitude	**49°S**
Longitude	**51.5°E**

Sample ID	Cup Number (#)	Open Date At 1200 hours	Julian Day Open	Julian Day Mid-Day	Sampling Interval (days)	pH of Preservative Solution
XXXIX-B-1	1	05/01/05	5.5	10	11	6.0
XXXIX-B-2	2	16/01/05	16.5	22.5	14	7.5
XXXIX-B-3	3	30/01/05	30.5	36.5	14	7.0
XXXIX-B-4	4	13/02/05	44.5	54	21	7.0
XXXIX-B-5	5	06/03/05	65.5	78.5	28	7.0
XXXIX-B-6	6	03/04/05	93.5	106.5	28	6.0
XXXIX-B-7	7	01/05/05	121.5	134.5	28	6.0
XXXIX-B-8	8	29/05/05	149.5	162.5	28	6.5
XXXIX-B-9	9	26/06/05	177.5	190.5	28	7.0
XXXIX-B-10	10	24/07/05	205.5	218.5	28	7.0
XXXIX-B-11	11	21/08/05	233.5	243	21	7.0
XXXIX-B-12	12	11/09/05	254.5	264	21	7.0
XXXIX-B-13	13	02/10/05	275.5	281.5	14	7.0
XXXIX-B-14	14	16/10/05	289.5	295.5	14	7.0
XXXIX-B-15	15	30/10/05	303.5	309.5	14	7.0
XXXIX-B-16	16	13/11/05	317.5	323.5	14	7.0
XXXIX-B-17	17	27/11/05	331.5	337.5	14	7.0
XXXIX-B-18	18	11/12/05	345.5	348	7	7.0
XXXIX-B-19	19	18/12/05	352.5	355	7	7.0
XXXIX-B-20	20	25/12/05	359.5	362	7	7.0
XXXIX-B-21	21	01/01/06	1.5	1.5	2	6.0

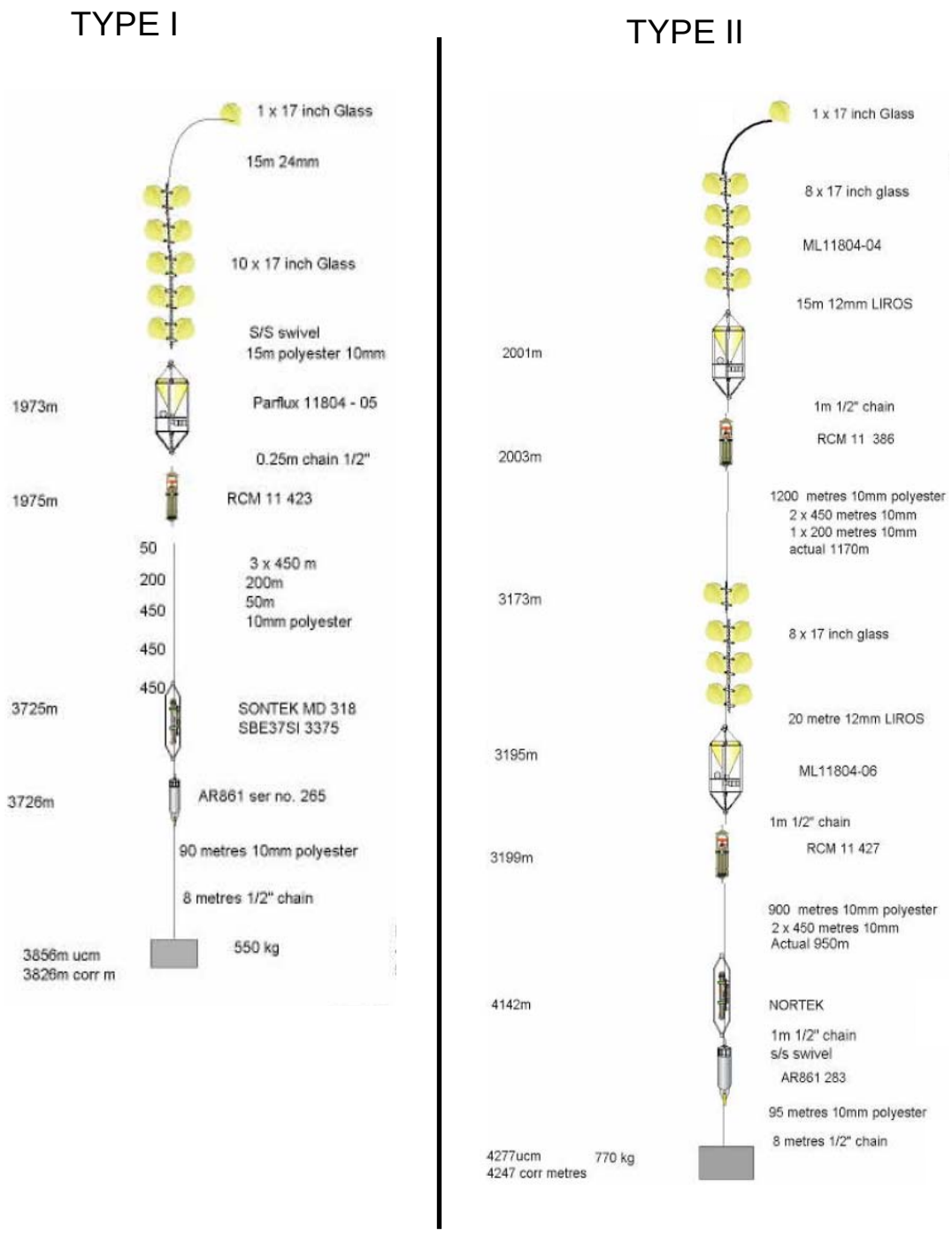

Figure A4.1 Schematic of two different Mooring configurations used during the CROZEX project.

APPENDIX 5: Temporal Variations in Export Efficiency

The inter-annual flux record from the Porcupine Abyssal Plain was compared to satellite estimates of productivity to examine the temporal variation in export efficiency at 3000m in the North-East Atlantic.

A5.1 Methods

A5.1.1 NCEP reanalysis

The NCEP/NCAR (National Centres for Environmental Prediction/ National Centre for Atmospheric Research) Reanalysis Project is an effort to reanalyze historical land and marine surface meteorological data using coupled models. The project uses a state-of-the-art analysis/forecast system to perform data assimilation using past data from 1948 to the present. The model includes parameterizations of all major physical processes, i.e. convection, large scale precipitation, shallow convection, gravity wave drag, radiation with diurnal cycle and interaction with clouds, boundary layer physics, an interactive surface hydrology, and vertical and horizontal diffusion processes. Details of the model dynamics and physics can be found in Kanamitsu (1989) and Kanamitsu et al. (1991). NCEP/NCAR reanalysis products are freely available to download from their website: (http://ingrid.ldeo.columbia.edu/SOURCES/.NOAA/.NCEP-NCAR/.CDAS-1/.DAILY/.).

Since, net heat flux is not available as a product, variables for net upward flux of long-wave radiation, upward latent heat flux, upward sensible heat flux and net flux of short-wave solar radiation were downloaded and net heat flux calculated according to equation A5.1:

Net Heat Flux = A+B+C+D **(A5.1)**

where A is short-wave solar radiation, B is net upward flux of long-wave radiation, C is upward latent heat flux, and D is upward sensible heat flux. Similarly for wind stress, the *u* (zonal momentum) and *v* (meridional momentum) components were downloaded and calculated according to equation A5.2:

$$\text{Wind Stress (N m}^{-2}) = \sqrt{[u^2 + v^2]} \quad \textbf{(A5.2)}$$

where u is the zonal momentum flux and v is the meridional momentum flux.

A5.1.2 Satellite-derived chlorophyll and column production

Primary production was estimated using the model of Smyth *et al*., (2005). The model uses satellite-derived fields of chlorophyll, photosynthetically active radiation (PAR) and sea-surface temperature (SST) to estimate column productivity. Full details of model parameterisation and formulation for Case I waters can be found in Smyth *et al*., (2005). All the chlorophyll data is SeaWIFS 18km data filtered by the NASA level 3 (global composites) processing. For the primary production fields, SeaWiFS 8-day composites of chlorophyll, SeaWiFS monthly composite of PAR and Pathfinder monthly composites of SST are implemented into the model. The vertical structure of bio-physical parameters is unattainable from space using sensors such as SeaWiFS (AVHRR). Therefore it is assumed that the chlorophyll and temperature profiles are invariant with depth.

A5.1.3 Argo Floats

Temperature profiles obtained from Argo floats were used to calculate the mixed layer depth (MLD) at the porcupine abyssal plain. The Argo float profiles are optimally interpolated (Hadfield, personal communication) at 0.5 month resolution. The MLD was identified by examining the 0.2^{o}C temperature deviation from the 10m temperature.

A5.2 Results and Discussion

A5.2.1 Chlorophyll and Primary productivity

Satellite-derived chlorophyll data for the PAP region was used to calculate integrated primary production based on the model of Smyth *et al*., (2005); see Methods section A5.1.3). The chlorophyll data used in the model was averaged over areas of

Table A5.1 Correlation matrix between mean and median estimates of productivity as determined from the model of Smyth *et al*., (2005) for the years 1998-2005. Also presented are the gradients of the correlations.

100km	Gradient	r^2	200km	Gradient	r^2	400km	Gradient	r^2
1998	1.00	1.00	1998	0.99	1.00	1998	1.00	1.00
1999	1.00	1.00	1999	0.98	1.00	1999	1.02	1.00
2000	0.96	0.99	2000	1.00	1.00	2000	0.98	1.00
2001	1.00	0.99	2001	1.02	1.00	2001	1.01	0.99
2002	0.98	0.99	2002	0.98	1.00	2002	0.97	0.99
2003	1.00	1.00	2003	0.97	1.00	2003	0.91	0.99
2004	0.98	0.99	2004	0.99	0.99	2004	0.99	0.99
2005	1.00	0.99	2005	0.97	1.00	2005	0.95	1.00

approximately 8000, 31000, and 126000 km^2, which correspond to circles engulfing the sediment trap location with diameters of 100, 200, and 400km. Both the mean and median chlorophyll values were used to calculate productivity. The different estimates generally exhibit a 1:1 relationship with correspondingly high regressions for all data sets (Table A5.1). The mean values will be used in further analysis since standard deviations are available and thus facilitate the propagation of associated errors. There is generally very good agreement between the estimates of productivity when integrated over different areas with slight discrepancies that are presumably related to mesoscale patchiness (Fig A5.1). In all years the productivity peaks between May and July, in 2001 there was an additional peak in productivity during 2001. The productivity peak in the years 2002, 2004, and 2005 is substantially lower than the other years examined. Annual productivity was calculated from the 400km data set and is presented in Figure A5.2. Based on the output of the model productivity ranges from 140 to 220 g C m^{-2} yr^{-1} and there appears to be a trend of decreasing annual productivity between 1998 and 2005.

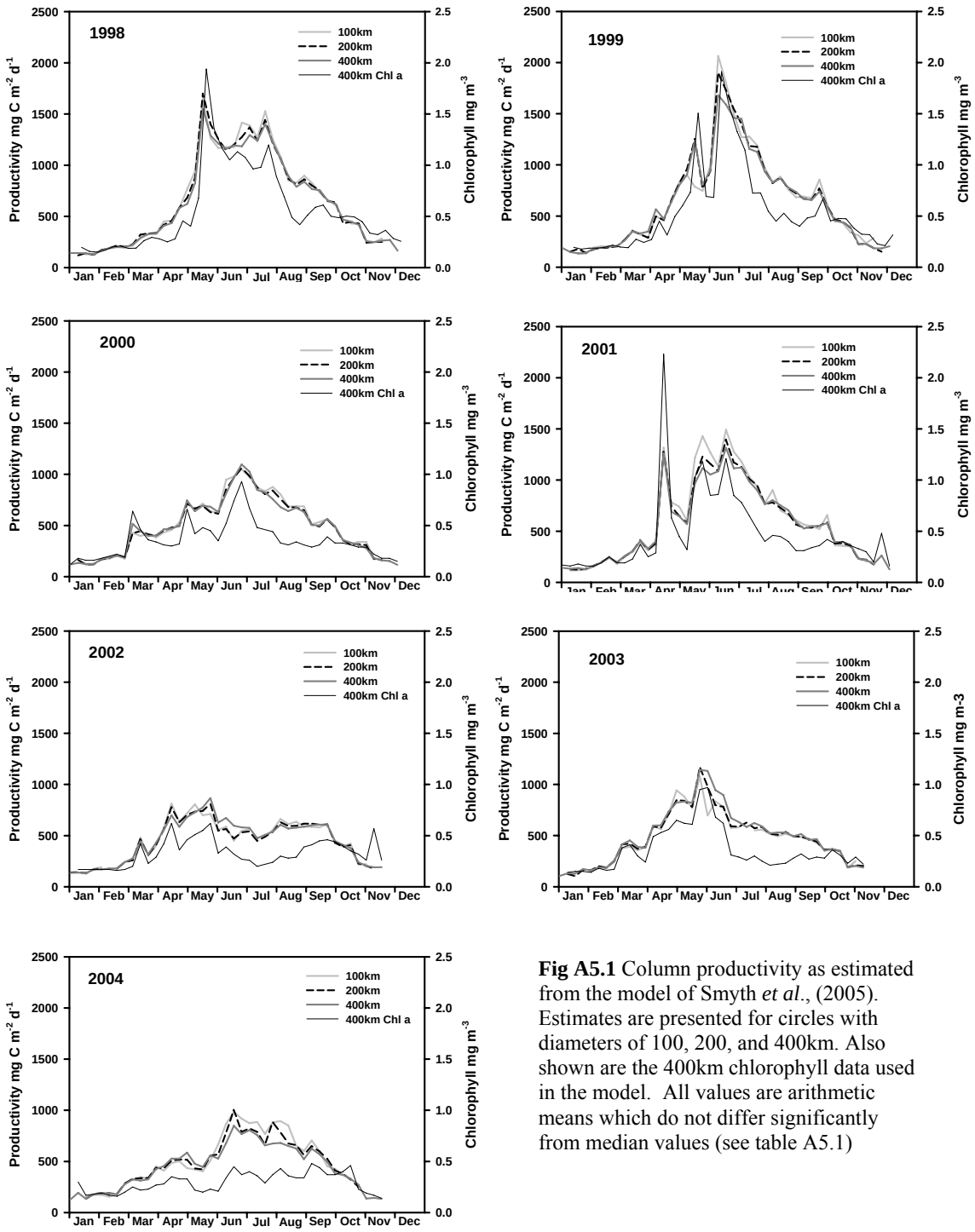

Fig A5.1 Column productivity as estimated from the model of Smyth *et al*., (2005). Estimates are presented for circles with diameters of 100, 200, and 400km. Also shown are the 400km chlorophyll data used in the model. All values are arithmetic means which do not differ significantly from median values (see table A5.1)

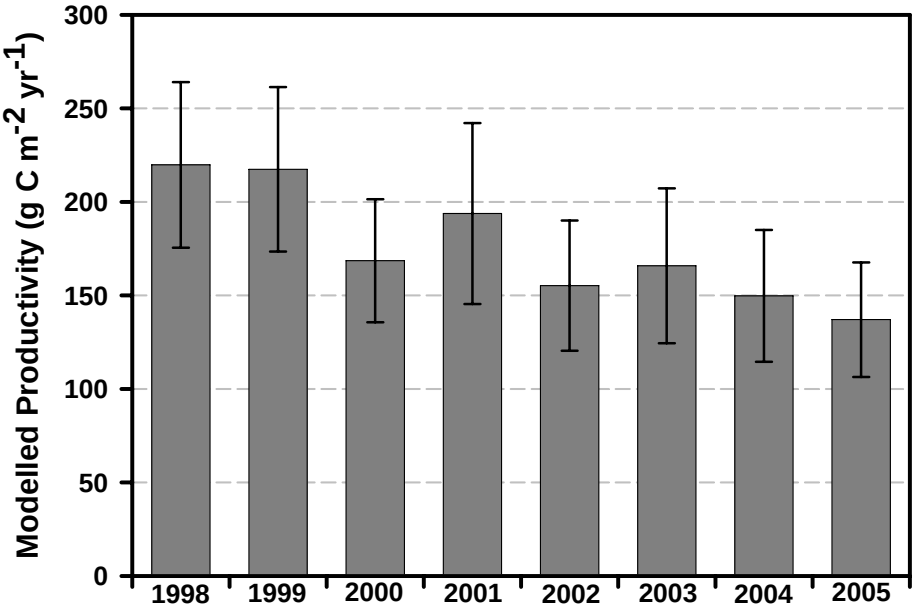

Figure A5.2 Annual estimates of productivity from the model of Smyth *et al*. (2005). Data have been calculated by integrating the model output over a circle with a diameter of 400km radius and the PAP site at its centre. Error bars are propagated standard deviations of the mean.

A5.2.2 Inter-annual flux variability

Data from PAP is compared to previously published particle flux data obtained from the north-east Atlantic (Table A5.2). The organic carbon fluxes determined at the PAP station are in the range of previously reported values. It is clear from Table A5.2 that accurate comparison of particle-flux data from different regions is significantly impeded by large inter-annual variations, such as the fluxes measured during 2001 (Table A5.2). In addition to temporal changes there are also spatial variations to consider, i.e. what region measured fluxes can be considered representative. For example, sediment trap observations of increased fluxes during 1989 relative to 1990 at the PAP site are comparable with flux variations determined at the near-by NABE site (Honjo and Manginini, 1993; Boyd and Newton, 1995) for the same period. In contrast the large flux event observed during 2001 was not

Table A5.2 Sediment trap observations from the North-East Atlantic. Values in blue are the spatial averages on standard deviation of the POMME study, all other averages presented are averages over time.

ID	Water depth (m)	Trap depth (m)	Lat °N	lon °W	Start	End	Days	Mass Flux g m^{-2} yr^{-1}	POC g m^{-2} yr^{-1}	Trap Eff. (%)	$POC_{Corrected}$ g m^{-2} yr^{-1}	POC - 1000m g m^{-2} yr^{-1}	Source
L1	5275	2000	33.1	22	12-Mar-94	14-Mar-95	367	13.3	0.62	52	1.2	1.1	Kuss and Kremling [1999]
	5275	2000	33.1	22	14-Mar-95	16-Mar-96	368	15.8	0.7	52	1.3	1.3	Schulz-Bull *et al*. (unpub.)
	5275	2000	33.1	22	20-Mar-96	23-Mar-97	368	15.2	0.8	52	1.5	1.5	Schulz-Bull et al. (unpub.)
								14.8 ± 1.3	**0.7 ± 0.1**		**1.4 ± 0.2**		
	5275	4000	33.1	22	18-Oct-93	02-Sep-94	319	18.4	0.7	71	0.9	2.2	Kuss and Kremling [1999]
Honjo -34	5172	1159	34	21	03-Apr-89	18-Mar-90	349	19.4	1.0	60	1.7	1.1	Honjo and Manganini [1993]
	5172	1981	34	21	03-Apr-89	18-Mar-90	349	22.4	1.0	90	1.1	1.9	Honjo and Manganini [1993]
	5172	4472	34	21	03-Apr-89	18-Mar-90	349	21.9	0.9	123	0.7	3.1	Honjo and Manganini [1993]
POMME SE	4940	1000	39.5	17.3	14-Feb-01	25-Jun-02	363	15.2	1.2	34	3.5	1.2	Guieu *et al*. [2005]
POMME SW[1]	4786	1000	39.6	18.9	20-Feb-01	25-Aug-02	186	19.2	1.9	27.5	6.9	1.9	Guieu *et al*. [2005]
POMME NE	3760	1000	43.5	17.3	14-Feb-01	25-Jun-02	363	17.7	1.8	32	5.6	1.8	Guieu *et al*. [2005]
POMME quadrangle[2]		1000							**1.6 ± 0.4**		**5.3 ± 1.7**		Guieu *et al*. [2005]
IM3	2245	1000	42.6	10	01-Jul-97	31-Jun-98	365	39.8	4.4	n.d		4.4	Fagel *et al*. [2004]
BOFS-1	4555	3100	47	20	18-Apr-89	22-Apr-90	369	22.1	1.8	80	2.2	4.7	Newton *et al*. [1994]
L2	4481	1000	47	20	28-Mar-92	28-Mar-93	365	11.2	1.2	20	6	1.2	Kuss and Kremling [1999]
	4481	2000	47	20	20-Mar-94	20-Mar-95	365	24.4	0.9	54	1.7	1.6	Kuss and Kremling [1999]
BOFS-1	4555	3100	47	20	18-Apr-89	22-Apr-90	369	22.1	1.8	80	2.2	4.7	Newton et al. [1994]
Honjo-48	4435	1000	48	21	03-Apr-89	02-Apr-90	364	20.7	1.5	41	3.6	1.5	Honjo and Manganini [1993]
	4435	2000	48	21	03-Apr-89	02-Apr-90	364	26.7	1.4	n.d		2.5	Honjo and Manganini [1993]
	4000	3300	48	21	03-Apr-89	02-Apr-90	364	26.2	1.0	n.d		2.8	Honjo and Manganini [1993]
OX3	3260	1440	48.9	13.5	01-Jul-93	01-Jul-94	365	42.5	3.6	n.d		4.9	Antia et al. [1999]
	3260	3260	48.9	13.5	01-Jul-93	01-Jul-94	365	37.8	1.9	n.d		5.2	Antia *et al*. [1999]
PAP[3]	4559	3000	48	19.5	18-Apr-89	31-Dec-90	245	23.8	2.7	n.d		6.9	Lampitt *et al*. [2001]; **this study**
PAP[4]	4570	3000	48	19.5	01-Jan-90	16-Sep-90	252	15.7	0.9	n.d		2.4	Lampitt *et al*. [2001]; **this study**
PAP[5]	4869	3000	49	16.5	01-Jan-98	01-Jan-99	325	26.8	1.3	n.d		3.5	Lampitt *et al*. [2001]; **this study**
PAP	4830-60	3000	49	16.5	01-Jan-99	01-Jan-00	365	18.9	1.6	n.d		4.1	Lampitt *et al*. [2001]; **this study**
PAP	4812	3000	49	16.5	08-Apr-01	01-Jan-01	267	47.1	6.0	n.d		15.5	**this study**
PAP[6]	4805-4845	3000	49	16.5	01-Jan-03	01-Jan-04	308	21.5	1.7	n.d		4.3	**this study**
PAP[7]	4802-4805	3000	49	16.5	01-Jan-04	31-Jan-04	362	21.3	1.7	n.d		4.4	**this study**
								25 ± 10.4	**2.2 ± 1.7**				**this study**
OX2	1500	1050	49.6	12.3	01-Jul-93	01-Jul-94	365	26.5	2.2			2.3	Antia *et al*. [1999]
L3	3070	1000	54	21	29-Jul-95	03-Jul-96	340	27.3	4.4	38	11.7	4.4	Schulz-Bull et al. (unpub.)
	3070	1000	54	21	20-Mar-97	22-Mar-97	367	-	1.2	38	3	1.2	Schulz-Bull et al. (unpub.)
	3070	2200	54	21	20-Mar-94	20-Mar-95	365	18.7	0.6	77	0.7	1.1	Kuss and Kremling [1999]
	3070	2200	54	21	21-Mar-95	22-Mar-96	367	22.8	2.1	77	2.8	4.2	Schulz-Bull et al. (unpub.)
	3070	2200	54	21	20-Mar-96	22-Mar-97	367	15.3	0.7	77	0.8	1.3	Schulz-Bull et al. (unpub.)

apparent from the POMME experiment (Guieu, *et al*., 2005) conducted from Feb 2001 to Feb 2002 in relatively close proximity (Table A5.2). Application of thorium corrections to the POMME data narrow the discrepancy with the PAP data, but sediment traps deployed at different depths can make direct comparisons very challenging (Table A5.2).

Normalisation procedures can be carried out (e.g. Lampitt and Antia, 1997) to compare data from different depths, but heavy reliance is placed on the accuracy of the empirical algorithm used to define carbon flux attenuation with depth. Fig. A5.3 shows all the data from Table A5.2 (without thorium corrections) as a function of depth. The data has been split into different latitude bands (see fig A5.3 legend). Also plotted are the decay curves of Martin *et al*., 1989) and the one obtained from PELAGRA deployments at the PAP site (Chapter 2). It is clear that the large spatial and inter-annual variations in the attenuation of flux with depth that are unlikely to be captured by the use of a single algorithm within one particular region (i.e. NE Atlantic), posing an interesting challenge for regional and global biogeochemical models.

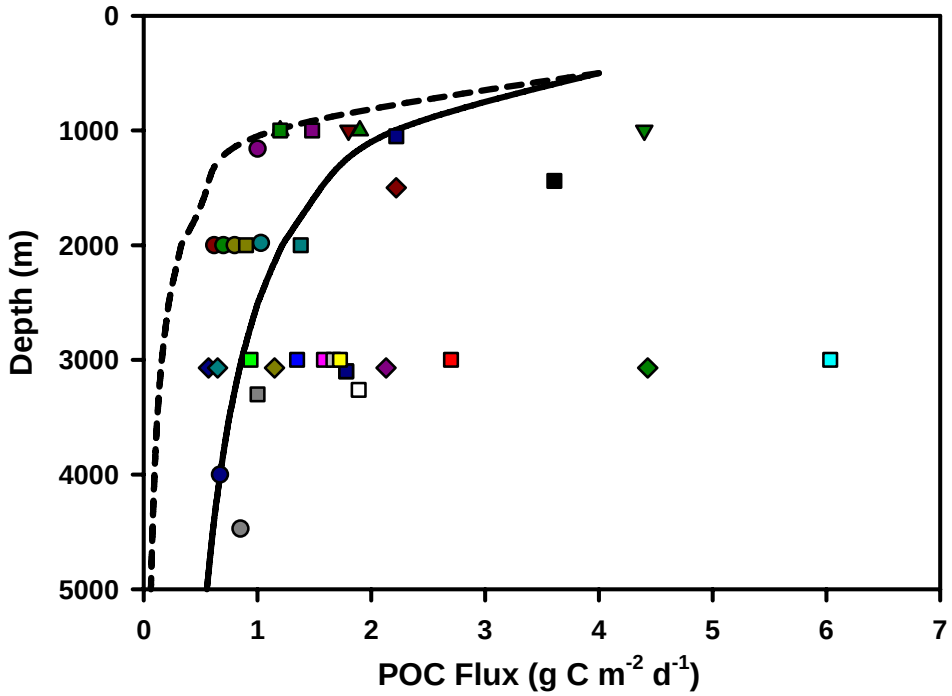

Fig A5.3 All data from Table A5.2 plotted as a function of depth and grouped into different latitude bands: 30-35°N (circles), 35-40°N (triangles), 40-45°N (inverted triangles), 45-50°N (squares), and 50-55°N (diamonds). Different colours represent data from different years.

The inter-annual variability depicted by the PAP data has been documented previously in the north-east Atlantic (Newton *et al*., 1994; Guieu, *et al*., 2005). Waniek *et al*. (2005) recently highlighted that the strong inter-annual variability of the particle flux observed between 1994 and 2001 at station L1 is the result of the variability of phytoplankton biomass and primary production in the euphotic zone of this region. Similarly, using climatological nitrate profiles, Williams *et al*. (2000) demonstrate how changes in wind stress and mixed layer depth (MLD) cycles can affect convective nitrate fluxes to the euphotic zone. This convectively induced variability in nitrate supply should modulate new and export production (Eppley and Peterson, 1979) whenever nitrate is limiting.

Primary production, as diagnosed from the model of Smyth *et al*., (2005) (Fig.A5.1; A5.2) appears unable to explain the large flux variability observed at the PAP site. More precisely, such inter-annual variability can be related to differences observed in the mixed layer depth (MLD). The comparison of production and mixed layer depths, diagnosed from Argo float profiles (Fig A5.4), for the PAP site do not appear to display sufficient differences to account for the observed inter-annual variability in deep-water fluxes during 2001. Further scrutiny of meteorological variables known to influence production such as wind stress (Fig. A5.5) SST (Fig A5.6), and net heat flux (Fig A5.7) do not show major discrepancies in 2001 relative to other years examined, although certain features may help to explain discrete flux events. For example the large POC flux event that occurred in September 1999 (Julian day 276.5;) is unusual compared to the rest of the record, and seems to correspond to a preceding meteorological event characterised by elevated wind stress (Fig. A5.5). Schiebel *et al*. (1995) have previously reported that storms in the NE Atlantic increase foraminferal test production and flux which may help to explain the large $CaCO_3$ flux measured during this event.

Whilst no direct measurements for "lithogenic" fluxes exist, they can be estimated by difference (Jickells *et al*., 1998). The errors associated with the analyses of the individual components, $CaCO_3$, Opal, and organic matter, are small and thus the propagated errors on "lithogenic" fluxes are also small (see Chapter 5 and Appendix 4). Previous work in the Sargasso Sea has demonstrated the calculation of "lithogenic" fluxes by difference to be in excellent agreement with independently determined aluminium fluxes (Jickells *et al*.,1998). The large fluxes or organic carbon observed during 2001, and 1989 are accompanied by large "lithogenic" fluxes. Multiple linear regression analysis with POC flux as the dependant quantitative variable and $CaCO_3$ and Opal fluxes as the explanatory quantitative variables accounts for 30% of the observed variability in the data set. Including "lithogenic" fluxes as a third quantitative variable increases this to 60%.

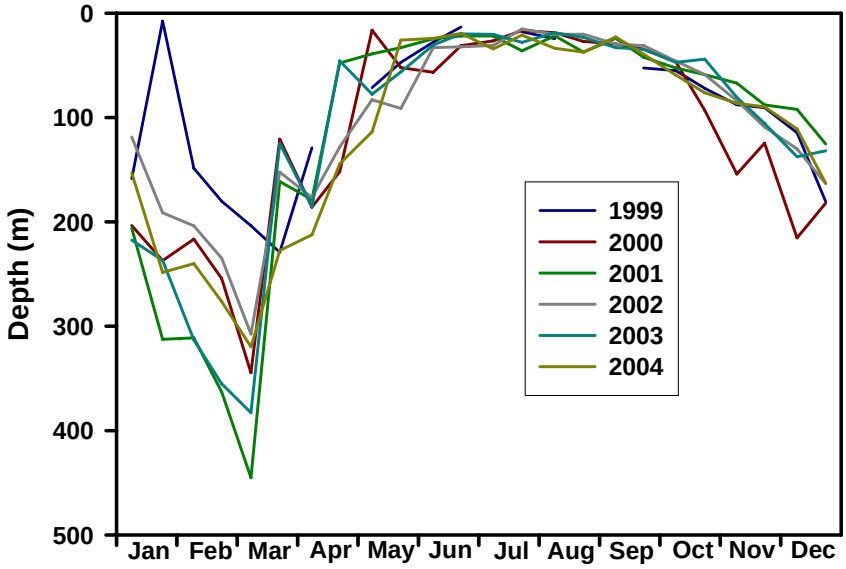

Figure A5.4 Mixed layer depth as diagnosed from Argo Float Profiles (see section A5.1.3)

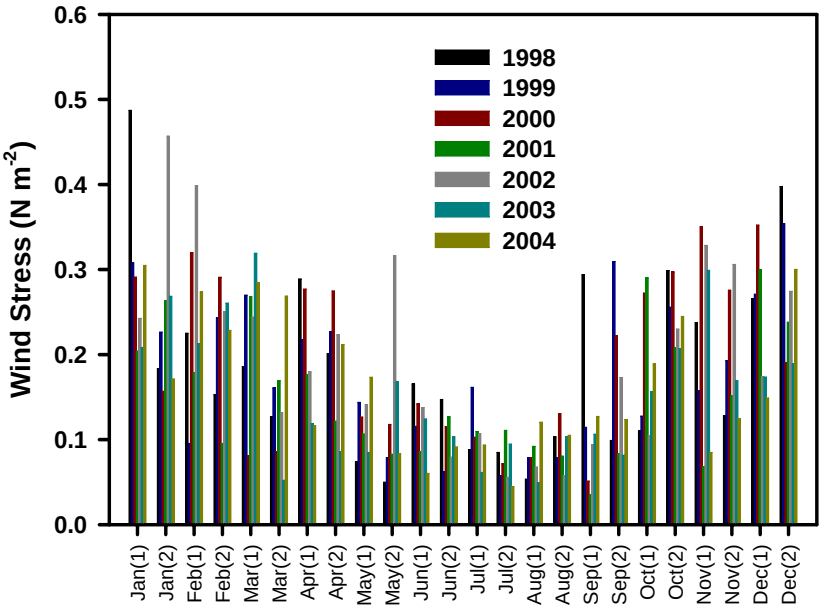

Fig A5.5 Wind stress at the PAP station between 1998-2004. Each bar represents a half-monthly average, e.g. Jan(1) is the average wind stress for the period 01/01 to 15/01.

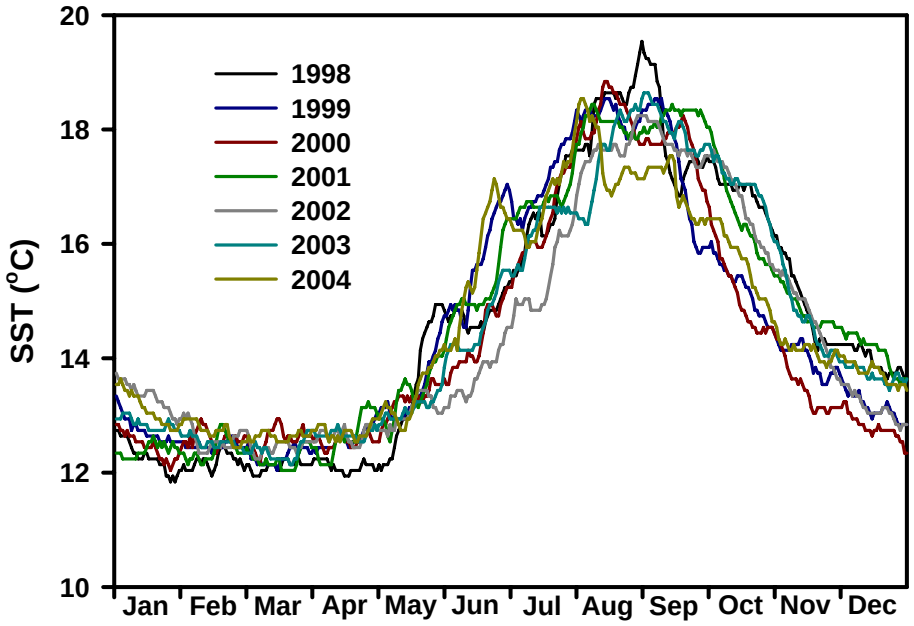

Fig A5.6 Average sea-surface temperature at the PAP station for the period 1998-2004

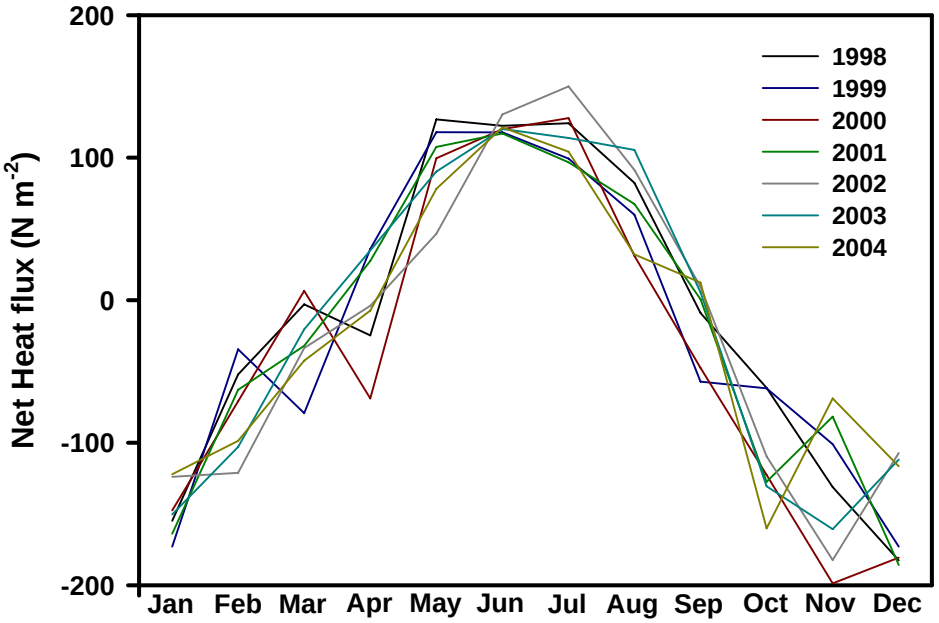

Fig A5.7 Net heat flux at the PAP station for the period 1998-2004

These observations seem to support the notion of Ittekkot (1993) of abiogenic particles enhancing the efficiency of the biological carbon pump, but are not consistent with similar observations in the Sargasso Sea (Jickells *et al*., 1998). Passow and De La Rocha (2006) suggest that it is organic carbon fluxes that drive the sedimentation of otherwise suspended minerals. Several lab studies (Passow and De La Rocha, 2006; Hamm, 2002) clearly demonstrate the potential of lithogenic particles to increase the settling velocity of aggregates, but factors such as community structure and mineralogy complicate interpretation (see Chapter 5). Complimentary to this is the observation that the trophic status of surface waters can give rise characteristic differences in the downward transport of lithogenic material in the eastern subtropical North Atlantic Ocean (Bory and Newton, 2000). There is clearly no simple relationship between the fluxes of POC and "lithogenics", but there is evidence to suggest that high lithogenic fluxes can perturb the efficiency of the biological carbon pump in this region.

A5.2.3 Comparison with primary production estimates: temporal changes in the export ratio

It is known that production and flux are not in balance on short-time scales (e.g. Antia *et al*., 2001; Chapter 2, 3) due to nutrient and particle retention by a seasonally variable food-web (Wassmann, 1998; Boyd and Newton; 1999). However, over annual time-scales comparison of deep-water POC fluxes and primary production should yield fairly reliable estimates of the export efficiency at a particular depth. Process cruise logistics dictate that *in-situ* estimates of integrated primary production at the PAP station generally represent data collected during summer cruises. In addition *in-situ* measurements do not cover the spatial extent necessary for comparison with sediment trap data. Primary production integrated over relevant spatial scales can be estimated from models (results section 5.4.8) and thus provide the means to constrain the export ratio at the sediment trap deployment depth (3000m). There are seven years of reliable annually-integrated POC flux data available from the PAP site (Chapter 5), but only five of these succeed the advent of remote sensing. The $ER_{(3000m)}$ has been calculated for the available data and the

results are presented in Fig. A5.8. The $ER_{(3000m)}$ calculated for 2001 is much higher than the other four years reflecting the observation that the inter-annual variability in PP_{MOD} is much less than the differences in annual POC flux integrals. With the exception of 2001 the $ER_{(3000m)}$ ranges between 0.6 and 1.2%, which is consistent with numerous reports that approximately 1% of carbon produced in the euphotic zone reaches the deep-ocean

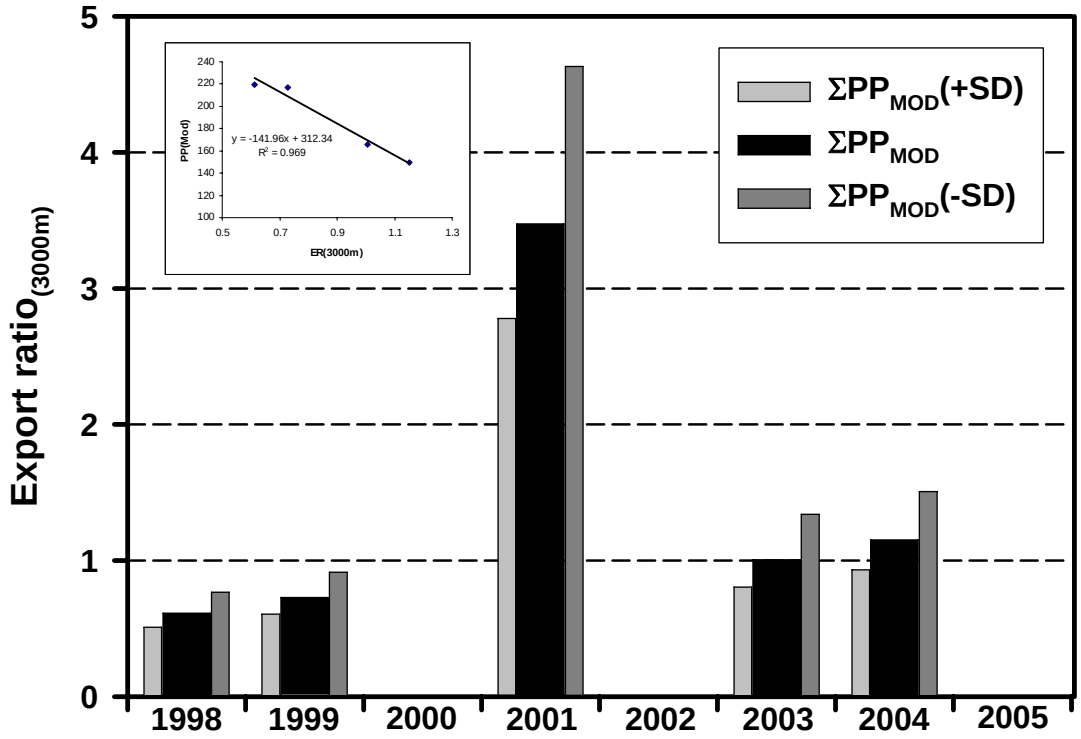

Fig A5.8 Export ratio calculated at 3000m based on annually-integrated sediment trap data and column productivity estimated from the model of Smyth *et al*., 2005. The export ratio has been calculated using the lower (mean – 1 S.D) and upper (mean + 1 S.D) estimates of productivity and the arithmetic mean. The inset panel is the correlation between productivity and the export ratio at 3000m excluding 2001 data.

Within this particular data set there are some subtle differences that suggest that $ER_{(3000m)}$ in 2003 and 2004 is slightly higher than in 1998 and 1999 despite the elevated annual production calculated for the latter two years. Excluding 2001 there

seems to be a negative relationship between PP_{Mod} and $ER_{(3000m)}$. Intuitively one might expect a larger fraction of primary production to be lost at higher levels of production, although empirical evidence does not always support this hypothesis. The HOT and VERTEX datasets (Lohrenz *et al*., 1992 and Pace *at al*., 1992) document a negative relationship derived from spot measurements of PP and POC flux at the base of the euphotic zone. Furthermore, POC profiles from the Southern Ocean (Lam and Bishop, 2007) indicate that surface waters with high biomass are associated with low particle loadings at depth implying conditions of low export. It is easy to rationalise these results in the context of decoupling between production and export over short timescales, however the results presented here demonstrate that such inverse relationships between production and export to the deep ocean can also be observed on annual timescales.

The differences in $ER_{(3000m)}$ presented here reflect the notion of Boyd and Newton (1995) that whilst observations/models of oceanic productivity may yield input to the biological pump, they cannot, on annual timescales, reliably provide information on the efficiency of the pump in transferring carbon into the deep ocean. Boyd and Newton (1995) observed a 1.8-fold difference between 1989 and 1990 in POC flux to deep (3100m) sediment traps despite similar levels of productivity. Comparison of surface taxonomy and size-fractionated productivity between the two years suggests that community structure rather than the magnitude of production dictates the efficiency of the biological carbon pump. In 1989 high densities of large chain-forming diatoms including the genus *Chaetoceros* (size >200µm) were noted in the spring (Decker, 1991), whilst the small diatom *Nanoneis hasleae* (size approx 5µm x 3µm) and autotrophic nanoflagellates dominated the assemblage in 1990 (Savidge *et al*., 1995; Stoecker *et al*., 1994). Unfortunately surface taxonomy data for the PAP site does not exist to facilitate an extension of Boyd and Newtons analysis. Whilst sediment trap data from PAP site support the observations from NABE that annual POC fluxes in 1989 were higher than 1990, comparison with subsequent years suggest they may have been elevated above "background" levels. It is considered that detailed taxonomy of sediment trap samples from the PAP site would yield some

interesting relationships between community structure and the strength and efficiency of the biological carbon pump but presently this data is not available.

APPENDIX 6 Mass Balance Data

Table A6.1 Mass balance data for sediment trap samples. Material is calculated by (POC*1.87)+SiO_2+$CaCO_3$. Analytical errors from triplicate measurements of each component are propagated to derive the error displayed in the table.

Trap	Cup	Material	Error ±%	Trap	Cup	Material	Error ±%
XXVI	1	103.4	2.7	XXVIII	9	96.7	32.5
XXVI	2	106.1	2.2	XXVIII	10	79.2	1.7
XXVI	3	112.4	5.0	XXVIII	11	70.9	2.9
XXVI	4	95.3	4.0	XXVIII	12	72.3	1.5
XXVI	5	93.7	1.8	XXVIII	13	74.3	2.9
XXVI	6	94.0	5.6	XXVIII	14	80.9	3.1
XXVI	7	89.9	7.4	XXVIII	15	84.2	1.2
XXVI	8	95.3	1.7	XXVIII	16	84.6	1.4
XXVI	9	88.7	2.6	XXVIII	17	84.2	0.8
XXVI	10	86.2	2.1	XXVIII	18	80.5	1.0
XXVI	11	97.4	1.9	XXXI	1	87.8	8.9
XXVI	12	101.4	3.4	XXXI	2	88.1	7.1
XXVI	13	91.8	4.9	XXXI	3	89.8	3.3
XXVI	14	93.4	1.9	XXXI	4	86.2	8.6
XXVI	15	95.7	1.4	XXXI	5	97.6	9.3
XXVII	1	95.2	2.8	XXXI	6	91.2	10.8
XXVII	2	94.8	5.7	XXXI	7	84.2	4.5
XXVII	3	95.2	2.0	XXXI	8	68.4	3.9
XXVII	4	90.6	4.4	XXXI	9	91.2	8.1
XXVII	5	92.6	3.6	XXXI	10	65.3	4.7
XXVII	6	95.5	10.1	XXXI	11	67.6	4.5
XXVII	7	92.7	1.9	XXXI	12	70.3	1.6
XXVII	8	73.1	4.8	XXXI	13	75.9	3.7
XXVII	9	82.5	7.1	XXXI	14	75.3	2.8
XXVII	10	81.2	3.5	XXXI	15	81.0	3.1
XXVII	11	73.5	6.1	XXXIV	1	81.9	8.2
XXVII	12	80.1	6.5	XXXIV	2	90.5	6.8
XXVII	13	75.6	12.1	XXXIV	3	78.1	1.4
XXVII	14	92.0	3.0	XXXIV	4	77.7	4.6
XXVII	15	91.8	2.4	XXXIV	5	80.2	3.6
XXVIII	1	76.6	9.5	XXXIV	6	72.5	3.5
XXVIII	2	80.3	1.4	XXXIV	7	82.8	2.2
XXVIII	3	79.0	2.9	XXXIV	8	85.6	2.2
XXVIII	4	85.6	2.2	XXXIV	9	84.7	2.6
XXVIII	5	82.7	4.5	XXXIV	10	75.9	4.6
XXVIII	7	81.8	4.6	XXXIV	11	77.2	11.0
XXVIII	8	77.9	5.1				

Appendix 7 PELAGRA AND SAPS DATA (PAP SAMPLES; CH.2)

CRUISE: Poseidon 300

Table A7.1 PELAGRA and SAPS samples from P300

Sample	C_{ORG} (mg)	N_{ORG} (mg)	C_{ORG} on Filter (mg)	N_{ORG} on Filter (mg)
SAP1(12)	0.30	0.01	0.75	0.03
SAP2(12)	0.38	0.06	0.95	0.14
PEL1(12)	0.28	0.01	0.71	0.03
PEL2(12)	0.38	0.06	0.95	0.14
UNK(12)	0.26	0.01	0.65	0.03

PELAGRA and SAP samples from Poseidon 300 were prepared by punching 12 small (4mm^2) discs into the 25mm GF/F filter. The amount of organic carbon was calculated according to the equations A7.1 – A7.2

Equation A7.1 $C(mm^2) = C_{ANALAYSED} / F_{AREA}$

Equation A7.2 $C_{FILTER} = C(mm^2) \times EF_{AREA}$

$C(mm^2)$ carbon normalised to the filter area (mg mm^{-2})

$C_{ANALYSED}$ The amount of carbon determined from the number of small discs (i.e. 12) removed from the filter (mg) (e.g. Table A7.1)

F_{AREA} The sum area of the filter analysed as small discs (mm^2)

EF_{AREA} The effective filtration area of the total filter (mm^2)

C_{FILTER} Total amount of carbon on the filter (mg)

CRUISE: Charles Darwin 158

Table A7.2 PELAGRA and SAPS data from CD158.

Sample	C_{ORG} (mg)	N_{ORG} (mg)	C_{ORG} on Filter (mg)	N_{ORG} on Filter (mg)
PELAGRA				
56522 A1 (1/4)	0.05	0.01	0.29	0.07
56522 A2 (1/8)	0.09	0.02	0.54	0.10
56522 A3 (1/8)	0.07	0.01	0.41	0.08
56522 B1 (1/8)	0.06	0.01	0.33	0.07
56522 B2 (1/8)	0.15	0.03	0.92	0.19
SAPS				
1A 50M 1/8	0.15	0.02	1.53	0.17
1B 100M 1/8	0.02	0.01	0.22	0.05
1C 150M 1/8	0.03	0.01	0.26	0.06

CRUISE: Discovery 295/296t

Table A7.3 PELAGRA data from D295/296t

Sample	Mass Flux mg m^{-2} d^{-1}	C_{ORG} (mg) In sample	N_{ORG} (mg) In sample
15716 Cup 1	106.36	2.73 ± 0.51	0.50 ± 0.17
15716 Cup 3	86.11	2.14 ± 0.26	0.43 ± 0.04

For the PELAGRA samples collected on D295/296t, the entire filters were analysed rather than removing discs as described above. The standard deviations presented in the table above are based on three replicates.

CRUISE: Discovery 306

Table A7.4

Sample	ug N	ug C	% N	% C
18011 1/8 SAPS 100m	142.40	749.05	0.85	4.48
18211 1/8 SAPS 100m	141.29	769.66	1.55	8.44
D306 18011 1/8 SAPS 100m	119.28	718.52	2.77	16.67
D306 18806 SAPS 100m	102.15	571.93	1.26	7.03
183004 P1 1/32 of 3/4 A 150m	482.62	2899.09	1.05	6.33
183004 P1 1/32 of 3/4 150m	475.76	2858.65	1.05	6.29
183003 P2 B 1/32 250m	369.16	2344.17	0.88	5.58
183003 P2 A 1/32 250m	363.34	2191.95	0.89	5.39
183003 P2 C 1/32 250m	391.06	2300.84	0.97	5.73
183003 P2 D 1/32 250m	288.55	1796.04	0.79	4.89

Entire filter was combusted for SAPS and PELAGRA analysis from D306. Sediment trap material was distributed over severa; filters and the numbers provided are pooled data. A, B, C, D denote sample cups underneath each of the four separate collecting funnels of PELAGRA (c.f Figure 2.1)

APPENDIX 8: PELAGRA CARBON, NITROGEN AND BIOGENIC SILICA DATA (CROZEX SAMPLES; CH.3)

Table A8.1 Raw carbon and nitrogen data for CROZEX PELAGRA samples

Sample	Mass (mg)	C_{ORG} (mg)	N_{ORG} (mg)
P2a	0.36	0.11	0.02
P2b	0.34	0.07	0.02
P3a	2.32	0.44	0.05
P3b	1.99	0.28	0.05
P4a	2.18	0.16	0.02
P4b	2.32	0.17	0.03
P5a-1	3.12	0.27	0.07
P5a-2	11.50	0.35	0.09
P6a-1	5.82	0.43	0.07
P6a-2	7.81	0.59	0.10
P6a-3	8.60	0.64	0.11
P6a-4	8.20	0.72	0.13
P6a-5	18.13	0.56	0.11
P6a-6	5.06	0.33	0.06
P12a	0.89	0.15	0.02
P12b	1.06	0.15	0.02
P13a	0.78	0.09	0.02
P13b	1.12	0.07	0.01

The suffix a and b denotes replicates, where a replicate is a $1/8^{th}$ split of the sediment trap sample. For P5 and P6 there was a lot of material, which was distributed over a number of filters (i.e. a-1 and a-2).

Table A8.2 Raw biogenic silica data for PELAGRA samples. Second digestions were carried out on selected residues and these values are also reported.

	1st Extract		2nd Extract		1st/2nd
Sample	**Si (µg)**	**$SiO_2.nH_2O$ (µg)**	**Si (µg)**	**$SiO_2.nH_2O$ (µg)**	
P2A	30.1	72.2	6.2	15.0	20.7
P2B	-	-	-	-	-
P3A	97.8	234.7	2.9	7.0	3.0
P3B	106.6	255.9	2.8	6.6	2.6
P4A	329.8	791.4	1.7	4.0	0.5
P4B	342.8	822.7	1.1	2.6	0.3
P5A	607.8	1458.6	-	-	-
P5B	570.9	1370.1	-	-	-
P5C	574.6	1378.9	-	-	-
P6A	1179.2	2830.1	-	-	-
P6B	1578.1	3787.5	-	-	-
P6D	1230.2	2952.5	-	-	-
P12A	16.0	38.3	1.1	2.6	6.9
P12B	16.5	39.6	1.1	2.6	6.7
P13A	48.1	115.4	0.7	1.8	1.5
P13B	50.6	121.6	0.4	0.9	0.7

APPENDIX 9 Total carbon, nitrogen, and Organic Carbon measurements

Table A9.1 Summary of Carbon and nitrogen data from fixed trap samples

Sample Code	Total Carbon %	Total Nitrogen %	Organic carbon %
26 B1 A	30.1	3.4	21.5
26 B1 B	30.1	3.4	21.9
26 B1 C	29.7	3.4	21.6
26 B2 A	24.7	3.0	16.6
26 B2 B	24.5	2.9	16.7
26 B2 C	24.2	2.9	16.7
26 B3 A	20.2	2.0	10.5
26 B3 B	20.4	2.0	10.0
26 B3 C	20.1	2.0	9.4
26 B4 A	19.9	2.6	13.1
26 B4 B	20.5	2.7	13.2
26 B4 C	20.1	2.7	13.7
26 B5 A	14.4	1.3	5.1
26 B5 B	14.4	1.3	5.3
26 B5 C	14.3	1.3	5.5
26 B6 A	12.5	0.9	3.9
26 B6 B	13.8	1.0	3.8
26 B6 C	13.5	0.9	4.0
26 B7 A	13.3	1.0	5.4
26 B7 B	13.3	0.9	3.8
26 B7 C	13.2	1.0	3.9
26 B8 A	13.6	1.1	4.0
26 B8 B	13.7	1.0	4.3
26 B8 C	13.5	1.0	4.1
26 B9 A	12.7	1.0	4.3
26 B9 B	12.8	1.1	3.9
26 B9 C	12.9	1.0	3.7
26 B10 A	12.5	1.3	4.9
26 B10 B	12.4	1.3	5.1
26 B10 C	12.4	1.3	4.9
26 B11 A	13.3	1.2	5.1
26 B11 B	13.3	1.1	5.0
26 B11 C	13.4	1.2	5.0
26 B12 A	13.1	1.1	3.5
26 B12 B	13.1	0.9	2.9
26 B12 C	13.1	0.8	3.2
26 B13 A	11.9	0.9	3.3
26 B13 B	11.9	0.9	3.4
26 B13 C	12.0	0.9	3.5
26 B14 A	11.3	1.0	3.5
26 B14 B	11.3	1.0	3.6
26 B14 C	11.2	1.0	3.6
26 B15 A	10.7	1.3	4.2
26 B15 B	10.7	1.3	3.9
26 B15 C	10.7	1.2	3.9

Sample Code	Total Carbon %	Total Nitrogen %	Organic Carbon %
27 B1 A	14.2	1.4	6.1
27 B1 B	14.5	1.5	6.4
27 B1 C	14.1	1.3	-
27 B2 A	15.1	1.1	6.6
27 B2 B	15.0	1.1	5.7
27 B2 C	15.1	1.2	-
27 B3 A	14.7	1.2	5.8
27 B3 B	14.7	1.3	5.6
27 B3 C	14.4	1.2	-
27 B4 A	14.5	1.0	5.8
27 B4 B	14.4	0.9	6.5
27 B4 C	14.5	0.9	-
27 B5 A	13.3	1.1	5.3
27 B5 B	13.3	1.1	5.7
27 B5 C	13.8	1.2	-
27 B6 A	15.8	1.8	7.3
27 B6 B	15.7	1.8	8.9
27 B6 C	15.1	1.6	-
27 B7 A	13.2	1.1	-
27 B7 B	13.1	1.0	5.2
27 B7 C	13.1	1.1	-
27 B8 A	18.4	2.2	13.5
27 B8 B	17.7	2.0	12.9
27 B8 C	17.9	2.1	-
27 B9 A	23.7	3.3	20.6
27 B9 B	24.2	3.5	20.1
27 B9 C	25.2	4.0	-
27 B10 A	26.0	2.6	22.2
27 B10 B	25.8	2.6	22.6
27 B10 C	25.5	2.5	-
27 B11 A	26.0	5.4	21.0
27 B11 B	26.0	5.5	22.0
27 B11 C	25.8	5.5	-
27 B12 A	25.9	2.9	21.7
27 B12 B	26.1	3.3	22.7
27 B12 C	26.1	3.2	-
27 B13 A	21.6	2.0	17.7
27 B13 B	23.1	2.2	17.6
27 B13 C	20.2	1.7	-
27 B14 A	20.3	2.0	13.2
27 B14 B	20.2	1.9	13.5
27 B14 C	20.6	2.1	-
27 B15 A	17.3	1.6	9.6
27 B15 B	17.3	1.7	9.2

Sample Code	Total Carbon %	Total Nitrogen %	Organic carbon %
28 B1a	13.1	1.0	8.1
28 B1b	14.2	1.1	7.2
28 B1c	-	-	6.5
28 B2a	12.2	0.8	4.4
28 B2b	12.0	0.7	4.6
28 B2c	12.1	0.7	4.4
28 B3a	12.6	0.7	5.2
28 B3b	12.2	0.8	5.1
28 B3c	12.8	0.8	5.3
28 B4a	13.8	0.9	6.2
28 B4b	14.3	1.0	6.0
28 B4c	14.0	0.9	6.1
28 B5a	14.1	1.0	5.6
28 B5b	13.2	0.8	5.9
28 B5c	13.2	0.8	5.7
28 B7a	13.1	0.8	6.0
28 B7b	12.8	0.7	5.4
28 B7c	13.2	0.9	5.1
28 B8a	12.7	0.7	4.9
28 B8b	12.1	0.7	5.8
28 B8c	12.7	0.7	5.2
28 B9a	14.0	0.9	5.6
28 B9b	13.4	0.8	7.4
28 B9c	13.4	0.8	-
28 B10a	12.6	0.7	5.0
28 B10b	12.4	0.7	4.7
28 B10c	12.4	0.7	4.8
28 B11a	11.5	0.6	4.6
28 B11b	11.9	0.7	5.0
28 B11c	11.5	0.6	4.6
28 B12a	12.2	0.7	5.2
28 B12b	11.9	0.7	5.1
28 B12c	12.0	0.7	-
28 B13a	12.1	0.7	5.8
28 B13b	12.2	0.7	5.4
28 B13c	12.3	0.7	5.1
28 B14a	13.1	0.8	6.3
28 B14b	13.2	0.8	6.1
28 B14c	13.7	0.9	5.9
28 B15a	13.8	0.8	6.6
28 B15b	13.6	0.7	6.2
28 B15c	13.8	0.8	6.7
28 B16a	13.9	0.8	6.7
28 B16b	14.0	0.9	6.9
28 B16c	13.8	0.7	7.1

Sample Code	Total Carbon %	Total Nitrogen %	Organic Carbon %
28 B17a	13.8	0.9	6.8
28 B17b	13.8	0.9	7.0
28 B17c	13.8	0.7	6.9
28 B18a	13.4	0.8	6.2
28 B18b	13.3	0.5	6.3
28 B18c	13.4	0.7	-
31 A1a	14.8	1.2	6.6
31 A1b	14.8	1.4	8.6
31 A1c	14.5	1.2	7.8
31 A2a	13.4	1.2	6.2
31 A2b	13.7	1.2	7.6
31 A2c	13.2	1.1	6.7
31 A3a	14.3	1.2	6.6
31 A3b	13.9	1.3	6.4
31 A3c	14.0	1.2	7.0
31 A4a	16.7	1.8	9.9
31 A4b	16.4	1.8	9.9
31 A4c	16.9	1.8	11.4
31 A5a	20.1	2.5	11.9
31 A5b	19.4	2.4	13.5
31 A5c	18.7	2.4	12.5
31 A6a	17.6	1.5	7.9
31 A6b	15.6	1.2	10.3
31 A6c	16.4	1.4	9.3
31 A7a	15.9	1.5	9.2
31 A7b	16.0	1.5	8.5
31 A7c	15.5	1.4	9.1
31 A8a	17.4	2.4	13.8
31 A8b	17.7	2.6	13.7
31 A8c	16.9	2.3	14.3
31 A9a	14.7	1.2	7.2
31 A9b	14.5	1.2	7.4
31 A9c	16.3	1.4	7.3
31 A10a	-	-	7.1
31 A10b	12.2	1.6	7.8
31 A10c	12.0	1.4	6.8
31 A11a	12.0	1.4	6.5
31 A11b	11.2	1.2	6.8
31 A11c	11.6	1.3	6.1
31 A12a	11.6	1.2	5.5
31 A12b	11.6	1.3	5.6
31 A12c	11.5	1.2	5.7
31 A13a	13.1	1.6	7.0
31 A13b	12.9	1.6	7.7
31 A13c	12.9	1.6	7.0

Sample Code	Total Carbon %	Total Nitrogen %	Organic Carbon %
31 A14a	13.0	1.4	8.1
31 A14b	12.9	1.4	7.7
31 A14c	12.9	1.3	8.0
31 A15a	13.2	1.3	7.5
31 A15b	13.1	1.3	7.7
31 A15c	12.9	1.1	7.6
31 A16a	11.0	1.2	6.7
31 A16b	11.0	1.2	7.0
31 A16c	11.2	1.3	7.0
31 A17a	10.5	1.2	7.7
31 A17b	10.4	1.1	7.7
31 A17c	10.7	1.3	7.3
31 A18a	-	-	6.9
31 A18b	-	-	7.2
31 A18c	-	-	6.6
31 A19a	-	-	6.9
31 A19b	-	-	6.9
31 A19c	-	-	-
34 A1a	13.3	1.5	8.9
34 A1b	13.6	1.5	9.0
34 A1c	15.0	2.5	9.3
34 A2a	11.9	0.4	3.0
34 A2b	12.2	0.4	2.4
34 A2c	12.0	0.4	3.9
34 A3a	12.2	0.9	7.4
34 A3b	12.1	1.0	7.3
34 A3c	12.4	1.0	-
34 A4a	12.5	0.8	6.3
34 A4b	12.5	0.8	7.2
34 A4c	12.8	1.0	6.3
34 A5a	10.8	0.7	4.8
34 A5b	10.4	0.7	4.6
34 A5c	10.6	0.7	4.1
34 A6a	11.4	0.7	5.3
34 A6b	11.7	0.7	5.9
34 A6c	11.5	0.7	-
34 A7a	11.9	0.8	5.4
34 A7b	12.1	0.7	5.1
34 A7c	12.1	0.8	5.6
34 A8a	20.0	2.0	14.6
34 A8b	19.7	2.0	14.4
34 A8c	20.1	2.1	14.3
34 A9a	17.7	1.7	11.7
34 A9b	17.4	1.7	11.2
34 A9c	17.6	1.7	11.5

Sample Code	Total Carbon %	Total Nitrogen %	Organic Carbon %
34 A10a	13.3	1.0	6.9
34 A10b	12.9	0.8	6.7
34 A10c	13.1	0.9	7.7
34 A11a	10.1	0.6	4.9
34 A11b	12.4	0.7	5.2
34 A11c	12.4	0.7	5.0
36 A1a	5.2	1.0	2.6
36 A1b	4.8	1.0	2.4
36 A1c	5.0	1.0	2.6
36 A2a	6.6	0.9	2.6
36 A2b	6.6	1.0	2.6
36 A2c	6.5	1.0	2.6
36 A3a	7.2	0.9	2.6
36 A3b	7.3	0.9	2.5
36 A3c	7.3	0.9	2.7
36 A4a	12.5	1.6	5.5
36 A4b	12.2	1.6	5.3
36 A4c	12.0	1.6	5.2
36 A5a	13.4	2.1	6.7
36 A5b	13.2	2.1	6.8
36 A5 c	13.2	2.2	6.7
36 A6a	12.8	1.9	5.8
36 A6b	13.0	2.0	6.1
36 A6c	13.0	2.0	5.7
36 A17a	10.7	1.5	4.7
36 A17b	9.7	1.7	4.7
36 A17c	10.0	1.8	4.8
37 A1a	2.8	1.0	1.7
37 A1b	2.9	1.1	1.7
37 A1c	4.1	1.5	1.6
37 A4a	7.4	1.4	4.1
37 A4b	7.3	1.3	4.3
37 A4c	7.1	1.4	4.5
37 A14a	7.2	1.7	5.2
37 A14b	7.1	1.6	5.2
37 A14c	7.4	1.7	5.1
37 A19a	6.5	1.1	2.9
37 A19b	6.6	1.1	2.9
37 A19c	6.5	1.1	2.8
37 A20a	7.1	1.1	3.1
37 A20b	6.4	1.0	2.8
37 A20c	6.5	1.0	2.9
38 A1a	9.4	1.6	5.8
38 A1b	9.2	1.7	5.8
38 A1c	9.8	1.6	5.6
38 A2a	7.3	1.1	3.4
38 A2b	6.9	1.3	3.1
38 A2c	7.2	1.2	3.5

Sample Code	Total Carbon %	Total Nitrogen %	Organic Carbon %
38 A3a	15.9	2.4	11.1
38 A3b	14.8	2.7	11.0
38 A3c	14.4	2.5	11.3
38 B1a	6.3	1.2	2.4
38 B1b	6.3	1.3	2.4
38 B1c	6.6	1.3	2.3
38 B2a	5.9	1.2	1.9
38 B2b	5.9	1.2	1.8
38 B2c	5.8	1.2	1.8
38 B3a	6.0	1.2	3.1
38 B3b	5.4	1.2	1.7
38 B3c	5.0	1.3	1.8
38 B4a	5.8	1.1	1.6
38 B4b	6.0	1.1	1.5
38 B4c	6.3	1.1	1.6
38 B5a	6.0	1.1	1.8
38 B5b	6.3	1.2	1.5
38 B5c	6.3	1.3	1.6
38 B6a	-	-	-
38 B6b	8.8	0.9	2.4
38 B6c	8.6	0.9	2.6
38 B7a	9.4	1.2	2.9
38 B7b	8.9	1.0	3.2
38 B7c	8.9	1.1	2.9
38 B8a	22.0	3.3	14.5
38 B8b	20.8	3.0	13.8
38 B8c	22.0	3.3	13.4
38 B19a	12.5	1.8	6.5
38 B19b	12.5	1.8	6.6
38 B19c	12.9	1.8	6.3
39 A1a	6.0	1.5	4.3
39 A1b	6.0	1.5	4.2
39 A1c	5.9	1.4	4.2
39 A7a	11.5	2.1	7.8
39 A7b	11.7	2.1	7.7
39 A7c	11.7	2.0	-
39 B1a	2.9	1.0	1.5
39 B1b	2.9	1.0	1.6
39 B1c	3.0	0.9	1.5
39 B6a	7.2	1.8	5.0
39 B6b	6.8	1.6	4.9
39 B6c	7.2	1.6	4.9

Appendix 10 Biogenic silica measurements

A10.1

Sample Code	SiO_2 %	Sample Code	SiO_2 %
25 B1a	10.6	26 B2a	10.3
25 B1b	9.7	26 B2b	9.8
25 B1c	11.3	26 B2c	10.3
25 B2a	8.4	26 B3a	8.8
25 B2b	8.3	26 B3b	8.8
25 B2c	8.8	26 B3c	8.5
25 B3a	11.8	26 B4a	13.6
25 B3b	11.2	26 B4b	13.2
25 B3c	12.0	26 B4c	13.3
25 B4a	13.8	26 B5a	8.3
25 B4b	14.2	26 B5b	8.4
25 B4c	-	26 B5c	8.9
25 B5a	12.5	26 B6a	8.8
25 B5b	12.2	26 B6b	8.7
25 B5c	12.2	26 B6c	8.9
25 B6a	29.6	26 B7a	8.8
25 B6b	28.0	26 B7b	9.0
25 B6c	29.5	26 B7c	9.0
25 B7a	31.8	26 B8a	9.1
25 B7b	31.5	26 B8b	8.8
25 B7c	31.3	26 B8c	9.1
25 B8a	21.4	26 B9a	8.0
25 B8b	19.2	26 B9b	8.1
25 B8c	17.2	26 B9c	7.9
25 B9a	20.2	26 B10a	14.2
25 B9b	22.8	26 B10b	15.5
25 B9c	20.4	26 B10c	15.5
25 B10a	9.0	26 B11a	19.7
25 B10b	8.3	26 B11b	19.6
25 B10c	8.2	26 B11c	18.3
25 B11a	5.3	26 B12a	14.4
25 B11b	5.4	26 B12b	12.5
25 B11c	4.4	26 B12c	13.5
25 B12a	5.6	26 B13a	17.1
25 B12b	6.2	26 B13b	14.0
25 B12c	-	26 B13c	13.4
25 B13a	4.7	26 B14a	22.7
25 B13b	4.9	26 B14b	23.9
25 B13c	-	26 B14c	22.4
26 B1a	7.4	26 B15a	32.5
26 B1b	7.0	26 B15b	32.7
26 B1c	6.7	26 B15c	33.1

Sample Code	SiO_2 %	Sample Code	SiO_2 %
27 B1a	18.0	28 B1a	9.9
27 B1b	16.7	28 B1b	11.0
27 B1c	17.0	28 B1c	10.9
27 B2a	9.5	28 B2a	8.9
27 B2b	9.7	28 B2b	8.4
27 B2c	8.9	28 B2c	9.0
27 B3a	10.7	28 B3a	8.4
27 B3b	9.8	28 B3b	8.5
27 B3c	11.3	28 B3c	8.2
27 B4a	10.2	28 B4a	8.3
27 B4b	-	28 B4b	8.5
27 B4c	-	28 B4c	8.7
27 B5a	14.8	28 B5a	7.7
27 B5b	16.9	28 B5b	8.1
27 B5c	17.0	28 B5c	7.6
27 B6a	18.6	28 B7a	9.3
27 B6b	18.9	28 B7b	8.1
27 B6c	19.8	28 B7c	9.5
27 B7a	18.0	28 B8a	8.2
27 B7b	17.3	28 B8b	8.2
27 B7c	16.5	28 B8c	8.2
27 B8a	8.9	28 B9a	7.7
27 B8b	8.8	28 B9b	7.9
27 B8c	8.2	28 B9c	7.8
27 B9a	11.6	28 B10a	6.8
27 B9b	10.8	28 B10b	7.1
27 B9c	11.4	28 B10c	7.0
27 B10a	10.7	28 B11a	5.2
27 B10b	11.6	28 B11b	5.3
27 B10c	11.1	28 B11c	5.2
27 B11a	3.5	28 B12a	5.5
27 B11b	3.2	28 B12b	5.5
27 B11c	3.3	28 B12c	5.8
27 B12a	6.8	28 B13a	7.9
27 B12b	6.9	28 B13b	7.8
27 B12c	6.3	28 B13c	8.2
27 B13a	10.4	28 B14a	9.7
27 B13b	8.5	28 B14b	9.6
27 B13c	9.8	28 B14c	9.9
27 B14a	8.5	28 B15a	12.1
27 B14b	8.0	28 B15b	12.0
27 B14c	10.7	28 B15c	13.2
27 B15a	8.9	28 B16a	14.8
27 B15b	9.1	28 B16b	13.9
27 B15c	8.9	28 B16c	13.4
27 B16a	8.7	28 B17a	13.8
27 B16b	8.2	28 B17b	14.8
27 B16c	8.5	28 B17c	13.9

Sample Code	SiO_2 %	Sample Code	SiO_2 %
28 B18a	10.8	31 A15a	22.1
28 B18b	10.2	31 A15b	20.4
28 B18c	9.1	31 A15c	20.8
31 A1a	14.2	31 A16a	34.5
31 A1b	14.0	31 A16b	35.6
31 A1c	16.1	31 A16c	31.6
31 A2a	21.5	31 A17a	46.1
31 A2b	19.4	31 A17b	44.1
31 A2c	20.1	31 A17c	42.5
31 A3a	14.8	31 A18a	48.1
31 A3b	15.9	31 A18b	47.7
31 A3c	15.2	31 A18c	47.3
31 A4a	16.2	31 A19a	39.0
31 A4b	13.9	31 A19b	40.1
31 A4c	13.6	31 A19c	37.4
31 A5a	18.1	34 A1a	22.0
31 A5b	17.6	34 A1b	26.0
31 A5c	16.8	34 A1c	24.9
31 A6a	13.1	34 A2a	8.4
31 A6b	12.2	34 A2b	8.1
31 A6c	12.8	34 A2c	-
31 A7a	10.0	34 A3a	23.7
31 A7b	10.8	34 A3b	24.2
31 A7c	9.9	34 A3c	23.5
31 A8a	14.0	34 A4a	15.7
31 A8b	14.0	34 A4b	16.0
31 A8c	14.1	34 A4c	14.3
31 A9a	12.1	34 A5a	20.5
31 A9b	11.8	34 A5b	21.3
31 A9c	11.8	34 A5c	20.9
31 A10a	11.5	34 A6a	19.0
31 A10b	11.2	34 A6b	18.8
31 A10c	10.8	34 A6c	20.0
31 A11a	8.4	34 A7a	16.9
31 A11b	7.9	34 A7b	17.2
31 A11c	7.8	34 A7c	17.3
31 A12a	10.3	34 A8a	12.5
31 A12b	9.6	34 A8b	12.2
31 A12c	9.2	34 A8c	12.8
31 A13a	14.1	34 A9a	13.9
31 A13b	14.1	34 A9b	12.8
31 A13c	14.1	34 A9c	12.9
31 A14a	19.5	34 A10a	12.7
31 A14b	19.4	34 A10b	12.9
31 A14c	17.7	34 A10c	11.9

Sample Code	SiO_2 %	Sample Code	SiO_2 %
34 A11a	13.1	38 B1a	61.4
34 A11b	12.5	38 B1b	57.5
34 A11c	12.7	38 B1c	58.9
36 A1a	71.4	38 B2a	62.2
36 A1b	67.8	38 B2b	62.7
36 A1c	67.9	38 B2c	60.8
36 A2a	52.5	38 B3a	65.2
36 A2b	51.2	38 B3b	66.5
36 A2c	54.5	38 B3c	65.9
36 A3a	43.3	38 B4a	59.0
36 A3b	44.7	38 B4b	55.8
36 A3c	42.5	38 B4c	59.7
36 A4a	38.1	38 B5a	53.5
36 A4b	35.7	38 B5b	54.0
36 A4c	34.7	38 B5c	54.3
36 A5a	34.4	38 B6a	-
36 A5b	34.1	38 B6b	39.7
36 A5c	36.3	38 B6c	-
36 A6a	34.7	38 B7a	-
36 A6b	36.1	38 B7b	40.0
36 A6c	31.5	38 B7c	39.2
36 A17a	47.1	38 B8a	31.0
36 A17b	45.4	38 B8b	27.6
36 A17c	44.3	38 B8c	29.6
37 A1a	82.6	38 B19a	35.4
37 A1b	81.2	38 B19b	35.3
37 A1c	80.8	38 B19c	34.7
37 A4a	56.2	39 A1a	76.4
37 A4b	59.8	39 A1b	75.3
37 A4c	59.6	39 A1c	76.8
37 A14a	71.4	39 A7a	61.4
37 A14b	72.9	39 A7b	58.7
37 A14c	72.6	39 A7c	
37 A19a	54.9	39 B1a	79.4
37 A19b	57.6	39 B1b	77.9
37 A19c	58.4	39 B1c	81.4
37 A20a	55.6	39 B6a	74.7
37 A20b	54.7	39 B6b	76.4
37 A20c	54.2	39 B6c	73.8
38 A1a	67.1		
38 A1b	61.9		
38 A1c	65.6		
38 A2a	51.7		
38 A2b	57.9		
38 A2c	57.4		
38 A3a	51.6		
38 A3b	51.8		
38 A3c	55.2		

APPENDIX 11 AMINO ACID DATA
A11.1

Sample Code	Parameter (μg mg^{-1})					
	AA's	HA's	AA-C	HA-C	AA-N	HA-N
23a B1a	18.23	1.53	7.48	0.62	3.00	0.12
23a B1b	-	-	-	-	-	-
23a B2a	15.57	1.15	6.51	0.46	2.52	0.09
23a B2b	11.71	0.96	4.94	0.39	1.81	0.08
23a B3a	15.52	1.04	6.52	0.42	2.51	0.08
23a B3b	9.85	0.60	4.12	0.24	1.47	0.05
23a B4a	13.80	1.01	5.88	0.41	2.10	0.08
23a B4b	13.54	0.93	5.78	0.38	2.06	0.07
23a B5a	11.86	0.68	5.05	0.27	1.79	0.05
23a B5b	-	-	-	-	-	-
23a B6a	18.75	0.94	7.82	0.38	3.08	0.07
23a B6b	-	-	-	-	-	-
23a B7a	22.34	1.00	9.48	0.40	3.53	0.08
23a B7b	18.53	0.86	7.87	0.35	2.79	0.07
23a B8a	23.01	1.38	9.81	0.55	3.39	0.11
23a B8b	35.14	2.25	14.91	0.91	5.14	0.18
23a B9a	19.12	1.28	8.05	0.52	2.87	0.10
23a B9b	33.24	2.12	13.96	0.85	4.98	0.17
23a B10a	22.73	1.45	9.70	0.58	3.35	0.11
23a B10b	23.00	1.54	9.75	0.62	3.42	0.12
23a B11a	21.98	1.47	9.30	0.59	3.24	0.11
23a B11b	22.49	0.98	9.57	0.40	3.34	0.08
23a B12a	-	-	-	-	-	-
23a B12b	14.09	1.25	5.94	0.50	2.10	0.10
23a B13a	19.18	1.55	8.04	0.63	2.96	0.12
23a B13b	14.77	1.33	6.20	0.53	2.21	0.10
25 B1a	12.58	1.24	5.34	0.50	1.92	0.10
25 B1b	12.13	1.02	5.15	0.41	1.84	0.08
25 B2a	-	-	-	-	-	-
25 B2b	11.53	1.16	4.91	0.47	1.75	0.09
25 B3a	16.46	2.89	6.98	1.16	2.48	0.23
25 B3b	19.21	2.57	8.09	1.04	2.93	0.20
25 B4a	12.54	0.80	5.33	0.32	1.94	0.06
25 B4b	12.15	0.73	5.15	0.29	1.88	0.06
25 B5a	11.28	0.66	4.79	0.26	1.74	0.05
25 B5b	10.54	0.64	4.48	0.26	1.62	0.05
25 B6a	-	-	-	-	-	-
25 B6b	27.44	2.13	11.62	0.86	4.25	0.17
25 B7a	24.41	1.48	10.36	0.60	3.70	0.12
25 B7b	20.67	1.82	8.84	0.73	3.04	0.14
25 B8a	44.97	2.14	18.79	0.86	6.93	0.17
25 B8b	39.97	2.14	16.69	0.86	6.04	0.17

Sample Code	Parameter (µg mg^{-1})					
	AA's	HA's	AA-C	HA-C	AA-N	HA-N
25B9a	54.02	2.09	23.18	0.84	8.01	0.16
25B9b	63.21	2.56	26.88	1.03	9.53	0.20
25B10a	-	-	-	-	-	-
25B10b	46.21	3.54	19.62	1.42	6.77	0.28
25B11a	61.09	4.11	26.07	1.65	9.15	0.32
25B11b	51.14	3.55	21.85	1.43	7.55	0.28
25B12a	46.46	3.42	19.93	1.37	6.95	0.27
25b12b	45.59	3.34	19.62	1.34	6.69	0.26
25B13a	37.65	2.40	16.46	0.96	5.48	0.19
25B13b	31.76	2.45	13.86	0.98	4.58	0.19
26B1a	52.94	4.92	22.47	1.98	7.66	0.38
26B1b	54.82	4.52	23.27	1.82	8.03	0.35
26B2a	45.17	4.32	19.17	1.74	6.57	0.34
26B2b	45.51	4.16	19.25	1.67	6.61	0.33
26B3a	30.74	3.22	13.11	1.30	4.42	0.25
26B3b	32.95	2.74	14.13	1.10	4.74	0.21
26B4a	44.90	4.39	19.13	1.77	6.60	0.34
26B4b	48.14	4.24	20.49	1.70	7.11	0.33
26B5a	20.95	1.92	8.93	0.77	3.12	0.15
26B5b	21.93	1.86	9.37	0.75	3.23	0.15
26B6a	16.09	1.22	6.85	0.49	2.45	0.10
26B6b	20.35	1.25	8.49	0.50	3.34	0.10
26B7a	-	-	-	-	-	-
26B7b	15.40	0.94	6.44	0.38	2.49	0.07
26B8a	-	-	-	-	-	-
26B8b	21.69	1.09	9.12	0.44	3.61	0.09
26B9a	12.67	0.75	5.39	0.30	1.95	0.06
26B9b	-	-	-	-	-	-
26B10a	19.03	1.12	8.03	0.45	2.97	0.09
26B10b	18.71	1.26	7.87	0.51	2.89	0.10
26B11a	-	-	-	-	-	-
26B11b	18.96	1.18	8.01	0.47	2.90	0.09
26B12a	-	-	-	-	-	-
26B12b	12.70	0.77	5.38	0.31	1.99	0.06
26B13a	-	-	-	-	-	-
26B13b	10.53	0.96	4.46	0.39	1.60	0.08
26B14a	13.03	0.87	5.49	0.35	1.99	0.07
26B14b	18.55	0.89	7.66	0.36	3.08	0.07
26B15a	17.84	1.04	7.54	0.42	2.72	0.08
26B15b	-	-	-	-	-	-
27B1a	21.55	1.90	9.06	0.77	3.24	0.15
27B1b	21.75	1.79	9.16	0.72	3.24	0.14
27B2a	22.35	1.83	9.52	0.74	3.29	0.14
27B2b	21.03	2.03	8.96	0.81	3.03	0.16
27B3a	19.62	1.47	8.36	0.59	2.91	0.11
27B3b	22.08	1.46	9.47	0.59	3.27	0.11
27B3c	*21.93*	*1.78*	*9.38*	*0.72*	*3.32*	*0.14*

Sample Code	Parameter (µg mg^{-1})					
	AA's	HA's	AA-C	HA-C	AA-N	HA-N
27B4a	30.47	1.52	12.88	0.61	4.86	0.12
27B4b	-	-	-	-	-	-
27B5a	18.83	1.66	8.00	0.67	2.71	0.13
27B5b	17.50	1.58	7.44	0.63	2.54	0.12
27B6a	32.66	2.42	14.01	0.97	4.68	0.19
27B6b	32.99	2.15	14.20	0.87	4.73	0.17
27B8a	36.29	2.52	15.61	1.01	5.03	0.20
27B8b	41.93	2.90	18.01	1.17	5.83	0.23
27B9a	61.98	4.39	26.74	1.76	8.80	0.34
27B9b	-	-	-	-	-	-
27B9c	*61.86*	*5.14*	*26.41*	*2.07*	*8.87*	*0.40*
27B10a	61.39	4.33	26.47	1.74	8.73	0.34
27B10b	53.87	3.72	23.15	1.50	7.63	0.29
27B10c	*62.66*	*5.06*	*26.95*	*2.03*	*9.03*	*0.40*
27B10d	*60.42*	*5.55*	*25.80*	*2.23*	*9.25*	*0.43*
27B11a	45.01	2.63	19.48	1.06	6.57	0.21
27B11b	-	-	-	-	-	-
27B11c	*63.02*	*5.06*	*27.10*	*2.03*	*9.55*	*0.40*
27B11d	*53.32*	*4.07*	*22.74*	*1.64*	*8.02*	*0.32*
27B12a	62.43	4.20	26.85	1.69	9.08	0.33
27B12b	54.66	3.36	23.53	1.35	7.73	0.26
27B12c	*65.94*	*6.03*	*28.20*	*2.42*	*9.58*	*0.47*
27B13a	53.23	4.00	22.97	1.61	7.71	0.31
27B13b	64.14	4.70	27.68	1.89	9.13	0.37
27B14a	34.29	2.98	14.89	1.20	4.97	0.23
28B1a	28.05	2.61	11.77	1.05	4.32	0.20
28B1b	24.57	2.03	10.51	0.82	3.57	0.16
28B2a	18.74	1.43	7.97	0.57	2.78	0.11
28B2b	16.42	1.30	6.98	0.52	2.42	0.10
28B3a	21.49	1.42	9.18	0.57	3.11	0.11
28B3b	18.68	1.39	7.95	0.56	2.75	0.11
28B4a	23.99	1.59	10.26	0.64	3.56	0.12
28B4b	21.03	1.61	9.01	0.65	3.08	0.13
28B5a	20.36	1.38	8.69	0.56	3.04	0.11
28B5b	21.88	1.58	9.35	0.63	3.24	0.12
28B6a	25.79	1.25	10.80	0.50	3.93	0.10
28B6b	31.61	1.49	13.47	0.60	4.72	0.12
28B7a	16.26	1.07	6.91	0.43	2.43	0.08
28B7b	22.87	1.13	9.78	0.45	3.38	0.09
28B8a	19.30	1.27	8.10	0.51	2.97	0.10
28B8b	17.30	1.22	7.36	0.49	2.57	0.10
28B9a	21.42	1.23	9.20	0.49	3.17	0.10
28B9b	-	-	-	-	-	-
28B10a	20.00	1.11	8.50	0.45	3.09	0.09
28B10b	16.84	1.09	7.17	0.44	2.54	0.08
28B11a	19.04	1.24	8.14	0.50	2.89	0.10
28B11b	17.51	1.16	7.57	0.47	2.55	0.09

Sample Code	Parameter (µg mg^{-1})					
	AA's	HA's	AA-C	HA-C	AA-N	HA-N
28B12a	22.85	1.17	9.68	0.47	3.55	0.09
28B12b	20.25	0.98	8.63	0.39	3.06	0.08
28B13a	17.92	1.06	7.63	0.43	2.68	0.08
28B13b	18.79	1.33	7.96	0.53	2.86	0.10
28B14a	22.66	1.32	9.62	0.53	3.42	0.10
28B14b	-	-	-	-	-	-
28B15a	23.06	1.20	9.79	0.48	3.42	0.09
28B15b	21.72	1.21	9.22	0.49	3.21	0.09
31A1a	28.65	2.13	12.00	0.86	4.21	0.17
31A1b	29.73	2.39	12.49	0.96	4.35	0.19
31A2a	26.26	1.86	11.02	0.75	3.98	0.15
31A2b	21.94	1.62	9.23	0.65	3.25	0.13
31A3a	25.46	2.06	10.70	0.83	3.77	0.16
31A3b	23.47	1.88	9.85	0.76	3.48	0.15
31A4a	52.52	3.24	21.83	1.31	8.31	0.25
31A4b	-	-	-	-	-	-
31A5a	64.82	3.22	27.08	1.30	10.13	0.25
31A5b	65.10	3.06	26.96	1.23	10.29	0.24
31A6a	35.55	2.56	14.89	1.03	5.47	0.20
31A6b	31.55	1.98	13.30	0.80	4.82	0.15
31A7A	43.42	4.19	18.22	1.68	6.85	0.33
31A7b	38.18	3.88	16.32	1.56	5.72	0.30
31A8a	51.98	5.34	22.25	2.15	7.72	0.42
31A8b	54.12	4.78	23.18	1.92	7.88	0.37
31A9a	40.06	2.53	17.02	1.02	5.99	0.20
31A9b	29.11	2.77	12.46	1.11	4.37	0.22
31A10a	31.21	1.70	13.46	0.68	4.60	0.13
31A10b	-	-	-	-	-	-
31A11a	24.06	1.37	10.02	0.55	3.98	0.11
31A11b	21.90	1.58	9.38	0.64	3.31	0.12
31A12a	22.44	1.74	9.58	0.70	3.42	0.14
31A12b	20.13	1.65	8.61	0.66	3.04	0.13
31A13a	30.84	1.84	13.21	0.74	4.50	0.14
31A13b	34.10	1.65	14.63	0.66	4.98	0.13
31A14a	30.12	1.75	12.87	0.70	4.45	0.14
31A14b	30.33	1.56	13.01	0.63	4.45	0.12
31A16a	-	-	-	-	-	-
31A16b	29.45	2.36	12.78	0.95	4.28	0.18
31A17a	29.88	2.23	12.93	0.90	4.32	0.17
31A17b	30.94	2.36	13.40	0.95	4.46	0.18
34A1a	55.37	2.37	24.17	0.95	8.21	0.18
34A1b	45.80	1.81	19.86	0.73	6.72	0.14
34A2a	15.11	0.63	6.64	0.25	2.17	0.05
34A2b	18.21	1.26	7.98	0.51	2.58	0.10

Sample Code	Parameter (μg mg^{-1})					
	AA's	HA's	AA-C	HA-C	AA-N	HA-N
34A4a	26.30	1.60	11.31	0.64	3.86	0.12
34A4b	28.15	1.70	11.86	0.68	4.30	0.13
34A5a	18.54	1.01	7.90	0.41	2.76	0.08
34A5b	19.80	1.29	8.27	0.52	3.10	0.10
34A6a	23.94	1.54	10.07	0.62	3.88	0.12
34A6b	18.82	0.99	8.15	0.40	2.74	0.08
34A7a	34.91	1.19	14.74	0.48	5.41	0.09
34A7b	21.23	1.26	9.13	0.51	3.10	0.10
34A8a	65.10	4.90	28.61	1.97	9.03	0.38
34A8b	77.50	4.49	33.87	1.81	11.21	0.35
34A9a	72.89	3.23	31.08	1.30	11.16	0.25
34A9b	68.70	3.88	29.77	1.56	10.20	0.30
38A1a	36.22	1.05	15.61	0.42	5.56	0.08
38A1b	35.23	0.83	15.20	0.33	5.46	0.06
38A2a	20.64	1.16	8.80	0.46	3.22	0.09
38A2b	-	-	-	-	-	-
38A3a	76.90	1.10	33.12	0.44	11.27	0.09
38A3b	77.09	1.45	33.44	0.58	11.62	0.11
38B1a	11.01	0.76	4.66	0.31	1.66	0.06
38B1b	13.52	0.56	5.76	0.22	2.07	0.04
38B2a	10.05	0.60	4.19	0.24	1.54	0.05
38B2b	9.40	0.72	3.99	0.29	1.39	0.06
38B3a	9.42	0.50	3.97	0.20	1.40	0.04
38B3b	9.21	0.46	3.90	0.18	1.38	0.04
38B4a	5.91	0.32	2.50	0.13	0.90	0.03
38B4b	6.97	0.42	0.00	0.00	0.00	0.00
38B5a	8.71	0.33	3.68	0.13	1.31	0.03
38B5b	7.65	0.41	3.24	0.17	1.14	0.03
38B8a	96.14	2.54	41.75	1.02	13.64	0.20
38B8b	-	-	-	-	-	-
38B19a	41.14	1.43	16.96	0.57	6.34	0.11
38B19b	-	-	-	-	-	-
39A1a	26.05	0.52	11.34	0.21	3.62	0.04
39A1b	23.95	0.51	10.39	0.21	3.32	0.04
39A7a	50.80	1.31	22.31	0.53	7.44	0.10
39A7b	52.63	1.07	23.28	0.43	7.39	0.08
39B1a	7.76	0.35	3.28	0.14	1.13	0.03
39B1b	7.75	0.39	3.29	0.16	1.16	0.03
39B6a	28.29	0.63	12.35	0.25	3.97	0.05
39B6b	28.04	0.66	12.19	0.27	3.98	0.05

AA is total hydrolysable amino acids, HA is total hydrolysable hexosamines (glucosamine + galactosamine), AA-C and HA-C is amino acid and hexosamine carbon, AA-N and HA-N is amino acid and hexosamines nitrogen

References

Abraham, E. R., Law, C.S., Boyd, P.W., Lavender, S.J., Maldonado, M.T., Bowie, A.R. (2000). "Importance of in stirring the development of an iron-fertilised phytoplankton bloom." Nature **407**: 727-730.

Abrantes, F., Moita, M.T. (1999). "Water column and recent sediment data on diatoms and coccolithophorids, off Portugal, confirm sediment record of upwelling events." Oceanologica Acta **22**: 67-84.

Adams, J. M., H. Faure, L. Fauredenard, J. M. McGlade and F. I. Woodward (1990). "Increases in terrestrial carbon storage from the last glacial maximum to the present." Nature **348**(6303): 711-714.

Alldredge, A. L. and M. W. Silver (1988). "Characteristics, dynamics and significance of marine snow." Progress in Oceanography **20**(1): 41-82.

Altabet, M. A., R. Francois, D. W. Murray and W. L. Prell (1995). "Climate-related variations in denitrification in the Arabian Sea from sediment $^{15}N/^{14}N$ ratios." Nature **373**(6514): 506-509.

Amiel, D., Cochran, J.K., Hirschberg, D.J. (2002). "$^{234}Th/^{238}U$ disequilibrium as an indicator of the seasonal export flux of particulate organic carbon in the North Water." Deep-Sea Research II **49**(22-23): 5191-5209.

Antia, A. N. (2005). "Solubilization of particles in sediment traps: revising the stoichiometry of mixed layer export." Biogeosciences **2**(2): 189-204.

Antia, A. N., W. Koeve, G. Fischer, T. Blanz, D. Schulz-Bull, J. Scholten, S. Neuer, K. Kremling, J. Kuss, R. Peinert, D. Hebbeln, U. Bathmann, M. Conte, U. Fehner and B. Zeitzschel (2001). "Basin-wide particulate carbon flux in the Atlantic Ocean: Regional export patterns and potential for atmospheric CO_2 sequestration." Global Biogeochemical Cycles **15**(4): 845-862.

Antia, A. N., B. von Bodungen and R. Peinert (1999). "Particle flux across the mid-European continental margin." Deep-Sea Research Part I **46**(12): 1999-2024.

Archer, D. (1996). "A data-driven model of the global calcite lysocline." Global Biogeochemical Cycles **10**(3): 511-526.

Archer, D. and E. Maier-Reimer (1994). "Effect of deep-sea sedimentary calcite preservation on atmospheric CO_2 concentration." Nature **367**(6460): 260-263.

Archer, D., Winguth, A., Lea, D., Mahowald, N. (2000). "What caused the glacial/interglacial atmospheric pCO_2 cycles." Geophysical Reviews **38**(2): 159-189.

Armstrong, R. A., Lee, C., Hedges, J.I., Honjo, S., Wakeham, S.G. (2002). "A new, mechanistic model for organic carbon fluxes in the ocean based on the quantitative association of POC with ballast minerals." Deep-Sea Research II **49**: 219-236.

Azam, F. (1998). "Microbial control of oceanic carbon flux: The plot thickens." Science **280**(5364): 694-696.

Bacon, M. P. (1985). "Seasonality in the flux of natural radionuclides and plutonium in the deep Sargasso Sea." Deep Sea Research Part I **32**.

Bacon, M. P., Cochran, J.K., Hirschberg, D., Hammar, T.R., Fleer, A.P. (1996). "Export flux of carbon at the equator during the EqPac time-series cruises estimated from ^{234}Th measurements." Deep-Sea Research II **43**: 1133-1154.

Bainbridge, R. (1953). "Studies on the inter-relationships of zooplankton and phytoplankton." Journal of the Marine Biological Association of the United Kingdom **32**(2): 385-445.

Baker, E. T., Milburn, H.B., Tennant, D.A. (1988). "Field assessment of sediment trap efficiency under varying flow conditions." Journal of Marine Research **46**: 573-592.

Bakker, D. C. E., Nielsdottir, M.C., Morris, P.J., Venables, H.J., Watson, A.J. (2007). "Quantifying the island mass effect for the marine cycles of carnon and oxygen near the Crozet Plateau in the southern Indian Ocean." Deep-Sea Research II **54**(18-20): 2174-2190.

Bakker, D. C. E., Watson, A.J., Law, C.S. (2001). "Southern Ocean iron enrichment promotes inorganic carbon drawdown." Deep Sea Research Part II **48**(18-20): 2483-2507.

Banse, K. (1982). "Cell volumes, maximal growth-rates of unicellular algae and ciliates, and the role of ciliates in the marine pelagial." Limnology and Oceanography **27**(6): 1059-1071.

Banse, K. (1990). "Does iron really limit phytoplankton production in the offshore Sub-Arctic Pacific." Limnology and Oceanography **35**(3): 772-775.

Banse, K. (1994). "Uptake of inorganic carbon and nitrate by marine plankton and the Redfield Ratio." Global Biogeochemical Cycles **8**(1): 81-84.

Beaulieu, S. E. (2002). "Accumulation and fate of phytodetritus on the sea floor." Oceanography and Marine Biology.

Behrenfeld, M. J., Bale, A.J., Kolber, Z.S., Aiken, J., Falkowski, P. (1996). "Confirmation of iron limitation of phytoplankton photosynthesis in the Equatorial Pacific Ocean." Nature **383**: 508-511.

Behrenfeld, M. J., R. T. O'Malley, D. A. Siegel, C. R. McClain, J. L. Sarmiento, G. C. Feldman, A. J. Milligan, P. G. Falkowski, R. M. Letelier and E. S. Boss (2006). "Climate-driven trends in contemporary ocean productivity." Nature **444**(7120): 752-755.

Berelson, W. M. (2001). "The flux of particulate organic carbon into the ocean interior: A comparison of four U.S. JGOFS regional studies." Oceanography **14**(4): 59-67.

Bidle, K. D. and F. Azam (1999). "Accelerated dissolution of diatom silica by marine bacterial assemblages." Nature **397**(6719): 508-512.

Billett, D. S. M., Rice, A.L. (2001). "The BENGAL programme: an introduction and overview." Progress in Oceanography **50**(1-4): 13-25.

Bird, M. I., J. Lloyd and G. D. Farquhar (1994). "Terrestrial carbon storage at the LGM." Nature **371**(6498): 566-566.

Bishop, J. K. B., T. J. Wood, R. E. Davis and J. T. Sherman (2004). "Robotic observations of enhanced carbon biomass and export at 55 degrees S during SOFeX." Science **304**(5669): 417-420.

Blain, S., B. Queguiner, L. Armand, S. Belviso, B. Bombled, L. Bopp, A. Bowie, C. Brunet, C. Brussaard, F. Carlotti, U. Christaki, A. Corbiere, I. Durand, F. Ebersbach, J. L. Fuda, N. Garcia, L. Gerringa, B. Griffiths, C. Guigue, C. Guillerm, S. Jacquet, C. Jeandel, P. Laan, D. Lefevre, C. Lo Monaco, A. Malits, J. Mosseri, I. Obernosterer, Y. H. Park, M. Picheral, P. Pondaven, T. Remenyi, V. Sandroni, G. Sarthou, N. Savoye, L. Scouarnec, M. Souhaut, D. Thuiller, K. Timmermans, T. Trull, J. Uitz, P. van Beek, M. Veldhuis, D. Vincent, E. Viollier, L. Vong and T. Wagener (2007). "Effect of natural iron fertilization on carbon sequestration in the Southern Ocean." Nature **446**(7139): 1070-U1.

Blain, S., Sedwick, P.N., Griffiths, F.B., Queguiner, B., Bucciarelli, E., Fiala, M., Pondaven, P., Treguer, P. (2002). "Quantification of algal iron requirements in the subantarctic Southern Ocean (Indian Sector)." Deep Sea Research II **49**(16): 3255-3273.

Blain, S., P. Treguer, S. Belviso, E. Bucciarelli, M. Denis, S. Desabre, M. Fiala, V. Martin Jezequel, J. Le Fevre and P. Mayzaud (2001). "A biogeochemical study of the island mass effect in the context of the iron hypothesis: Kerguelen Islands, Southern Ocean." Deep Sea Research Part I: Oceanographic Research Papers **48**(1): 163-187.

Blair, J. D. and J. A. Buesseler (1998). "Competitive forces in the medical group industry: A stakeholder perspective." Health Care Management Review **23**(2): 7-27.

Bory, A. J. M. and P. P. Newton (2000). "Transport of airborne lithogenic material down through the water column in two contrasting regions of the eastern subtropical North Atlantic Ocean." Global Biogeochemical Cycles **14**(1): 297-315.

Boyd, P. and P. Newton (1995). "Evidence of the potential influence of planktonic community structure on the interannual variability of particulate organic carbon flux." Deep-Sea Research Part I-Oceanographic Research Papers **42**(5): 619-639.

Boyd, P. a. D. S. C. (2003). The impact of climate change and feeback processes on the ocean carbon cycle. Ocean Biogeochemistry: The role of the carbon cycle in global change. M. J. R. Fasham, Springer**:** 157-187.

Boyd, P. W. (2002). "The role of iron in the biogeochemistry of the Southern Ocean and Equatorial Pacific: a comparison of *in-situ* iron enrichments." Deep Sea Research Part II: **49**(9-10): 1803-1821.

Boyd, P. W. and E. R. Abraham (2001). "Iron-mediated changes in phytoplankton photosynthetic competence during SOIREE." Deep-Sea Research Part II **48**(11-12): 2529-2550.

Boyd, P. W., *et al* (2000). "Phytoplankton bloom upon mesoscale iron fertilisation of polar Southern Ocean waters." Nature **407**: 695-702.

Boyd, P. W., C. S. Law, C. S. Wong, Y. Nojiri, A. Tsuda, M. Levasseur, S. Takeda, R. Rivkin, P. J. Harrison, R. Strzepek, J. Gower, R. M. McKay, E. Abraham, M. Arychuk, J. Barwell-Clarke, W. Crawford, D. Crawford, M. Hale, K. Harada, K. Johnson, H. Kiyosawa, I. Kudo, A. Marchetti, W. Miller, J. Needoba, J. Nishioka, H. Ogawa, J. Page, M. Robert, H. Saito, A. Sastri, N. Sherry, T. Soutar, N. Sutherland, Y. Taira, F. Whitney, S. K. E. Wong and T. Yoshimura (2004). "The decline and fate of an iron-induced subarctic phytoplankton bloom." Nature **428**(6982): 549-553.

Boyd, P. W. and P. P. Newton (1999). "Does planktonic community structure determine downward particulate organic carbon flux in different oceanic provinces?" Deep-Sea Research Part I **46**(1): 63-91.

Boyd, P. W. and T. W. Trull (2007). "Understanding the export of biogenic particles in oceanic waters: Is there consensus?" Progress in Oceanography **72**(4): 276-312.

Boyd, P. W., A. J. Watson, C. S. Law, E. R. Abraham, T. Trull, R. Murdoch, D. C. E. Bakker, A. R. Bowie, K. O. Buesseler, H. Chang, M. Charette, P. Croot, K. Downing, R. Frew, M. Gall, M. Hadfield, J. Hall, M. Harvey, G. Jameson, J. LaRoche, M. Liddicoat, R. Ling, M. T. Maldonado, R. M. McKay, S. Nodder, S. Pickmere, R. Pridmore, S. Rintoul, K. Safi, P. Sutton, R. Strzepek, K. Tanneberger, S. Turner, A. Waite and J. Zeldis (2000). "A mesoscale phytoplankton bloom in the polar Southern Ocean stimulated by iron fertilization." Nature **407**(6805): 695-702.

Broecker, W. S. (1982). "Ocean chemistry during glacial time." Geochimica Et Cosmochimica Acta **46**(10): 1689-1705.

Broerse, A. T. C., P. Ziveri, J. E. van Hinte and S. Honjo (2000). "Coccolithophore export production, species composition, and coccolith-$CaCO_3$ fluxes in the NE Atlantic (34^oN 21^0W and 48^oN 21^oW)." Deep-Sea Research Part II **47**(9-11): 1877-1905.

Brzezinski, M. A. (1985). "The Si-C-N ratio of marine diatoms - interspecific variability and the effect of some environmental variables." Journal of Phycology **21**(3): 347-357.

Brzezinski, M. A., C. J. Pride, V. M. Franck, D. M. Sigman, J. L. Sarmiento, K. Matsumoto, N. Gruber, G. H. Rau and K. H. Coale (2002). "A switch from $Si(OH)_4$ to NO_3 - depletion in the glacial Southern Ocean." Geophysical Research Letters **29**(12).

Buesseler, K. (1991). "Do upper-ocean sediment traps provide and accurate record of particle flux." Nature **353**: 420-423.

Buesseler, K., Bacon MP, Cochran JK, Livingston HD. (1992). "Carbon and nitrogen export during the JGOFS North Atlantic Bloom Experiment estimated from ^{234}Th:^{238}U disequilibria." Deep-Sea Research I **39**: 1115-1137.

Buesseler, K., Steinberg, DK, Michaels, AF, Johnson, RJ, Andrews, JE, Valdes, JR, Price, JF (2000). "A comparison of the quantity and composition of material caught in a neutrally buoyant versus surface-tethered sediment trap." Deep-Sea Research I **47**: 277-294.

Buesseler, K. O. (1998). "The decoupling of production and particulate export in the surface ocean." Global Biogeochemical Cycles **12**(2): 297-310.

Buesseler, K. O., Andrews, J.A., Hartman, M.C., Belastock, R., Chai, F. (1995). "Regional estimates of the export flux of particulate organic carbon derived from thorium-234 during the JGOFS EqPac program." Deep-Sea Research II **42**: 777-804.

Buesseler, K. O., Andrews, J.E., Pike, S.M., Charette, M.A. (2004). "The effects of iron fertilisation on carbon sequestration in the Southern Ocean." Science **304**: 414-417.

Buesseler, K. O., Antia, A.N., Chen, M., Fowler, S.W., Gardner, W.D., Gustaffson, Ö., Harada, K., Michaels, A.F., Rutgers van der Loeff, M., Sarin, M., Steinberg D.K., Trull T. (2007). "An assessment of the use of sediment traps for estimating upper ocean particle fluxes." Journal of Marine Research ***in press***.

Buesseler, K. O., L. Ball, J. Andrews, J. K. Cochran, D. J. Hirschberg, M. P. Bacon, A. Fleer and M. Brzezinski (2001). "Upper ocean export of particulate organic carbon and biogenic silica in the Southern Ocean along 170 degrees W." Deep-Sea Research Part II **48**(19-20): 4275-4297.

Buesseler, K. O., C. R. Benitez-Nelson, S. B. Moran, A. Burd, M. Charette, J. K. Cochran, L. Coppola, N. S. Fisher, S. W. Fowler, W. Gardner, L. D. Guo, O. Gustafsson, C. Lamborg, P. Masque, J. C. Miquel, U. Passow, P. H. Santschi, N. Savoye, G. Stewart and T. Trull (2006). "An assessment of particulate organic carbon to thorium-234 ratios in the ocean and their impact on the application of Th-234 as a POC flux proxy." Marine Chemistry **100**(3-4): 213-233.

Buesseler, K. O., Benitez-Nelson, C.R., Moran, S.B., Burd, A., Charette, M., Cochran, J.K., Coppola, L., Fisher, N.S., Fowler, S.W., Gardener, W.D., *et al*. (2006). "An assessment of particulate organic carbon to thorium-234 ratios in the ocean and their impact on the application of ^{234}Th as a POC flux proxy." Marine Chemistry **100**(3-4): 213-233.

Buesseler, K. O. and P. W. Boyd (2003). "Will ocean fertilization work?" Science **300**(5616): 67-68.

Buesseler, K. O., C. H. Lamborg, P. W. Boyd, P. J. Lam, T. W. Trull, R. R. Bidigare, J. K. B. Bishop, K. L. Casciotti, F. Dehairs, M. Elskens, M. Honda, D. M. Karl, D. A. Siegel, M. W. Silver, D. K. Steinberg, J. Valdes, B. Van Mooy and S. Wilson (2007). "Revisiting carbon flux through the ocean's twilight zone." Science **316**(5824): 567-570.

Burckle, L. H. (1984). "Ecology and paleoecology of the marine diatom *Eucampia antarctica* (Castr) Mangin." Marine Micropaleontology **9**(1): 77-86.

Burd, A. B., G. A. Jackson and S. B. Moran (2007). "The role of the particle size spectrum in estimating POC fluxes from ^{234}Th/^{238}U disequilibrium." Deep-Sea Research Part I **54**(6): 897-918.

Burd, A. B., Moran, S.B., Jackson, G.A. (2000). "A coupled-adsorption-aggregation model of the POC/^{234}Th ratio of marine particles." Deep-Sea Research I **47**: 103-120.

Butman, C. A., Grant, W.D., Stolzenbach, K.D. (1986). "Predictions of sediment trap biases in turbulent flows: a theoretical analysis based on observations from the literature." Journal of Marine Research **44**: 601-644.

Caldeira, K. and P. B. Duffy (2000). "The role of the Southern Ocean in uptake and storage of anthropogenic carbon dioxide." Science **287**(5453): 620-622.

Carter, P. W. and R. M. Mitterer (1978). "Amino acid composition of organic-matter associated with carbonate and non-carbonate sediments." Geochimica Et Cosmochimica Acta **42**(8): 1231-1238.

Castberg, T., A. Larsen, R. A. Sandaa, C. P. D. Brussaard, J. K. Egge, M. Heldal, R. Thyrhaug, E. J. van Hannen and G. Bratbak (2001). "Microbial population dynamics and diversity during a bloom of the marine coccolithophorid Emiliania huxleyi (Haptophyta)." Marine Ecology-Progress Series **221**: 39-46.

Cavender-Bares, K. K., Mann, E.L., Chisholm, S.W., Ondrusek, M.E., Bidigare, R.R. (1999). "Differential response of equatorial Pacific phytoplankton to iron fertilisation." Limnology and Oceanography **44**: 237-246.

Charette, M., Gonneea, M., Morris, P., Statham, P., Fones, G., Planquette, H., Salter, I, Garabato, A. (2007). "Radium isotopes as tracers of iron sources fuelling a Southern Ocean phytoplankton bloom." Deep-Sea Research II **54**(18-20): 1989-1998.

Charette, M. A., Buesseler, K.O (2000). "Does iron fertilisation lead to rapid carbon export in the Southern Ocean?" Geochemistry, Geophysics, Geosystems (G3) **1**.

Chen, J. H., R. L. Edwards and G. J. Wasserburg (1986). "U-238,U-234 and Th-232 in Seawater." Earth and Planetary Science Letters **80**(3-4): 241-251.

Coale, K. H., K. S. Johnson, F. P. Chavez, K. O. Buesseler, R. T. Barber, M. A. Brzezinski, W. P. Cochlan, F. J. Millero, P. G. Falkowski, J. E. Bauer, R. H. Wanninkhof, R. M. Kudela, M. A. Altabet, B. E. Hales, T. Takahashi, M. R. Landry, R. R. Bidigare, X. J. Wang, Z. Chase, P. G. Strutton, G. E. Friederich, M. Y. Gorbunov, V. P. Lance, A. K. Hilting, M. R. Hiscock, M. Demarest, W. T. Hiscock, K. F. Sullivan, S. J. Tanner, R. M. Gordon, C. N. Hunter, V. A. Elrod, S. E. Fitzwater, J. L. Jones, S. Tozzi, M. Koblizek, A. E. Roberts, J. Herndon, J. Brewster, N. Ladizinsky, G. Smith, D. Cooper, D. Timothy, S. L. Brown, K. E. Selph, C. C. Sheridan, B. S. Twining and Z. I. Johnson (2004). "Southern ocean iron enrichment experiment: Carbon cycling in high- and low-Si waters." Science **304**(5669): 408-414.

Coale, K. H., Kenneth S. Johnson, Steve E. Fitzwater, R. Michael Gordon, Sara Tanner, Francisco P. Chavez, Laurie Ferioli, Carole Sakamoto, Paul Rogers, Frank Millero, Paul Steinberg, Phil Nightingale, David Cooper, William P. Cochlan, Michael R. Landry, John Constantinou, Gretchen Rollwagen, Armando Trasvina, Raphael Kudela (1996). "A massive phytoplankton bloom induced by an ecosystem-scale iron fertilisation experiment in the equatorial Pacific Ocean." Nature **383**: 495-501.

Commission, I. O. (1996). Protocols for the Joint Global Ocean Flux studies: Core Measurements. Joint Global Ocean Flux Study Report (No. 19). I. O. Commision. Paris, Intergovernmental Oceanographic Commission**:** 210pp.

Conley, D. J. (1998). "An interlaboratory comparison for the measurement of biogenic silica in sediments." Marine Chemistry **63**(1-2): 39-48.

Conte, M. H., N. Ralph and E. H. Ross (2001). "Seasonal and interannual variability in deep ocean particle fluxes at the Oceanic Flux Program (OFP)/Bermuda Atlantic Time Series (BATS) site in the western Sargasso Sea near Bermuda." Deep-Sea Research Part II **48**(8-9): 1471-1505.

Cooper, D. J., Watson, A.J., Nightingale, P.D. (1996). "Large decrease in ocean-surface CO_2 fugacity in response to *in situ* iron fertilisation." Nature **383**: 511-513.

Coppola, L., M. Roy-Barman, P. Wassmann, S. Mulsow and C. Jeandel (2002). "Calibration of sediment traps and particulate organic carbon export using ^{234}Th in the Barents Sea." Marine Chemistry **80**(1): 11-26.

Cowie, G. L. and J. I. Hedges (1992). "Improved amino acid quantification in environmental samples - charge-matched recovery standards and reduced analysis time." Marine Chemistry **37**(3-4): 223-238.

Cowie, G. L. and J. I. Hedges (1994). "Biochemical indicators of diagenetic alteration in natural organic matter mixtures." Nature **369**(6478): 304-307.

Cowie, G. L. and J. I. Hedges (1996). "Digestion and alteration of the biochemical constituents of a diatom (*Thalassiosira weissflogii*) ingested by an herbivorous zooplankton (*Calanus pacificus*)." Limnology and Oceanography **41**(4): 581-594.

Crawford, R. M. (1995). "The role of sex in the sedimentation of a marine diatom bloom." Limnology and Oceanography **40**(1): 200-204.

Crowley, T. J. (1995). "Ice-age terrestrial carbon changes revisited." Global Biogeochemical Cycles **9**(3): 377-389.

Dasaro, E. A., D. M. Farmer, J. T. Osse and G. T. Dairiki (1996). "A Lagrangian float." Journal of Atmospheric and Oceanic Technology **13**(6): 1230-1246.

Dauwe, B. and J. J. Middelburg (1998). "Amino acids and hexosamines as indicators of organic matter degradation state in North Sea sediments." Limnology and Oceanography **43**(5): 782-798.

Dauwe, B., J. J. Middelburg, P. M. J. Herman and C. H. R. Heip (1999). "Linking diagenetic alteration of amino acids and bulk organic matter reactivity." Limnology and Oceanography **44**(7): 1809-1814.

De Baar, H. J. W., de Jong, J.T.M., Bakker, D.C.E., Loscher, B.M., Veth, C., Bathmann, U., Smetacek, V. (1995). "Importance of iron for phytoplankton spring blooms and CO_2 drawdown in the Southern Ocean." Nature **373**: 412-415.

De Baar, H. J. W., *et al*. (2005). "Synthesis of iron fertlisation experiments: From the Iron age in the Age of Enlightment." Journal of Geophysical Research **110**(C09S16): 1-24.

De La Rocha, C. L. and U. Passow (2007). "Factors influencing the sinking of POC and the efficiency of the biological carbon pump." Deep-Sea Research Part II
54(5-7): 639-658.

De Master, D. J. (1981). "The supply and accumulation of silica in the marine sediments." Geochimica et Cosmochimica Acta **45**: 1715-1732.

Degens, E. T. (1976). "Molecular mechanisms on carbonate, phosphate, and silica deposition in the living cell." Topics in Current Chemistry **64**: 1-112.

Demaster, D. J. (1981). "The Supply and Accumulation of Silica in the Marine-Environment." Geochimica Et Cosmochimica Acta **45**(10): 1715-1732.

DiTullio, G. R., J. M. Grebmeier, K. R. Arrigo, M. P. Lizotte, D. H. Robinson, A. Leventer, J. B. Barry, M. L. VanWoert and R. B. Dunbar (2000). "Rapid and early export of *Phaeocystis antarctica* blooms in the Ross Sea, Antarctica." Nature **404**(6778): 595-598.

Doney, S. C., K. Lindsay, K. Caldeira, J. M. Campin, H. Drange, J. C. Dutay, M. Follows, Y. Gao, A. Gnanadesikan, N. Gruber, A. Ishida, F. Joos, G. Madec, E. Maier-Reimer, J. C. Marshall, R. J. Matear, P. Monfray, A. Mouchet, R. Najjar, J. C. Orr, G. K. Plattner, J. Sarmiento, R. Schlitzer, R. Slater, I. J. Totterdell, M. F. Weirig, Y. Yamanaka and A. Yool (2004). "Evaluating global ocean carbon models: The importance of realistic physics." Global Biogeochemical Cycles **18**(3).

Ducklow, H. W. and R. P. Harris (1993). "Introduction to the JGOFS North-Atlantic Bloom Experiment." Deep-Sea Research Part II **40**(1-2): 1-8.

Dugdale, R. C. and F. P. Wilkerson (1986). "The use of ^{15}N to measure nitrogen uptake in eutrophic oceans - experimental considerations." Limnology and Oceanography **31**(4): 673-689.

Dunne, J. P., Armstrong, R.A., Gnanadesikan, A., and Sarmiento, J.L. (2005). "Empirical and mechanistic models for the particle export ratio." Global Biogeochemical Cycles **19**(4): Art. No. GB4026.

Duplessy, J. C., M. Arnold, N. J. Shackleton, N. Kallel, L. Labeyrie and A. Juilletleclerc (1988). "Changes in the rate of ventilation of intermediate and deep-water masses in the Pacific-Ocean during the last deglaciation." Chemical Geology **70**(1-2): 108-108.

Dutkiewicz, S., M. Follows, J. Marshall and W. W. Gregg (2001). "Interannual variability of phytoplankton abundances in the North Atlantic." Deep-Sea Research Part II **48**(10): 2323-2344.

Eggimann, D. W., F. T. Manheim and P. R. Betzer (1980). "Dissolution and analysis of amorphous silica in marine sediments." Journal of Sedimentary Petrology **50**(1): 215-225.

Emerson, S., P. Quay, D. Karl, C. Winn, L. Tupas and M. Landry (1997). "Experimental determination of the organic carbon flux from open-ocean surface waters." Nature **389**(6654): 951-954.

Eppley, R. W., and Peterson, B.J (1979). "Particulate organic matter flux and planktonic new production in the deep ocean." Nature **282**: 677-680.

Fagel, N., F. Dehairs, R. Peinert, A. Antia and L. Andre (2004). "Reconstructing export production at the NE Atlantic Margin: potential and limits of the Ba proxy." Marine Geology **204**(1-2): 11-25.

Fairbanks, R. G. (1989). "A 17,000-Year Glacio-Eustatic Sea-Level record - influence of glacial melting rates on the Younger Dryas event and deep-ocean circulation." Nature **342**(6250): 637-642.

Falkowski, P. G. (1997). "Evolution of the nitrogen cycle and its influence on the biological sequestration of CO_2 in the ocean." Nature **387**(6630): 272-275.

Falkowski, P. G., R. T. Barber and V. Smetacek (1998). "Biogeochemical controls and feedbacks on ocean primary production." Science **281**(5374): 200-206.

Feely, R. A., R. Wanninkhof, C. E. Cosca, P. P. Murphy, M. F. Lamb and M. D. Steckley (1995). "CO_2 Distributions in the Equatorial Pacific during the 1991-1992 ENSO event." Deep-Sea Research Part Ii-Topical Studies in Oceanography **42**(2-3): 365-386.

Feldman, G. C., McClain, C.R. (2006). Ocean Color Web, SeaWiFS Reprocessing 5.1, NASA Goddard Space Fligth Center. N. Kuring, Bailey, S.W.

Fielding, S., Pollard, R.T., Read, J., Seeyave, S., Ward, P. (2007). "Community structure and grazing impact of mesozooplankton during late spring / early summer in the vicinity of the Crozet Islands (Southern Ocean)." Deep-Sea Research II **54**(18-20): 2106-2125.

Fischer, G., Gersonde, R., Wefer, G. (2002). "Organic carbon, biogenic silica and diatom fluxes in the marginal winter sea-ice zone and in the Polar Front Region: interannual variations and differences in composition." Deep-Sea Research II **49**: 1721-1745.

Fischer, G., V. Ratmeyer and G. Wefer (2000). "Organic carbon fluxes in the Atlantic and the Southern Ocean: relationship to primary production compiled from satellite radiometer data." Deep-Sea Research Part II **47**(9-11): 1961-1997.

Fowler, S. W. and G. A. Knauer (1986). "Role of Large Particles in the Transport of Elements and Organic-Compounds through the Oceanic Water Column." Progress in Oceanography **16**(3): 147-194.

Franck, V. M., M. A. Brzezinski, K. H. Coale and D. M. Nelson (2000). "Iron and silicic acid concentrations regulate Si uptake north and south of the Polar Frontal Zone in the Pacific Sector of the Southern Ocean." Deep-Sea Research Part Ii-Topical Studies in Oceanography **47**(15-16): 3315-3338.

Francois, R., M. A. Altabet, E. F. Yu, D. M. Sigman, M. P. Bacon, M. Frank, G. Bohrmann, G. Bareille and L. D. Labeyrie (1997). "Contribution of Southern Ocean surface-water stratification to low atmospheric CO_2 concentrations during the last glacial period." Nature **389**(6654): 929-935.

Francois, R., Honjo, S., Krishfield, R., Manganini, S. (2002). "Factors controlling the flux of organic carbon to the bathypelagic zone of the ocean." Global Biogeochemical Cycles **16**(4): 1-19.

Frankignoulle, M. and C. Canon (1994). "Marine calcification as a source of carbon dioxide - positive feedback of increasing atmospheric CO_2." Limnology and Oceanography **39**(2): 458-462.

Frew, R., Bowie, A., Croot, P., Pickmere, S. (2001). "Macronutrient and trace-metal geochemistry of an *in-situ* iron-induced Southern Ocean bloom." Deep Sea Research Part II **48**: 2467-2482.

Frew, R. D., D. A. Hutchins, S. Nodder, S. Sanudo-Wilhelmy, A. Tovar-Sanchez, K. Leblanc, C. E. Hare and P. W. Boyd (2006). "Particulate iron dynamics during FeCycle in subantarctic waters southeast of New Zealand." Global Biogeochemical Cycles **20**(1).

Froelich, P. N. (1980). "Analysis of organic carbon in marine sediment." Limnology and Oceanography **25**: 564-572.

Froneman, P. W., Pakhomov, E.A., Laubscher, R.K. (1997). "Microphytoplankton assemblages in the waters surrounding South Georgia, Antarctica during austral summer 1994." Polar Biology **17**: 515-522.

Gall, M. P., Boyd, P.W., Hall, J., Safi, K.A., Chang, H. (2001b). "Phytoplankton processes. part 1: Community structure during the Southern Ocean Iron Release Experiment (SOIREE)." Deep Sea Research Part II **48**: 2551-2570.

Gall, M. P., Strzepek, R., Maldonado, and P.W. Boyd (2001a). "Phytoplankton processes. part 2: Rates of primary production and factors controlling algal growth during the Southern Ocean Iron Release Experiment (SOIREE)." Deep Sea Research Part II **48**: 2571-2590.

Ganeshram, R. S., T. F. Pedersen, S. E. Calvert and J. W. Murray (1995). "Large changes in oceanic nutrient inventories from glacial to interglacial periods." Nature **376**(6543): 755-758.

Gardner, W. D. (1980). "Sediment trap dynamics and calibration: a laboratory evaluation." Journal of Marine Research **38**: 17-39.

Gardner, W. D. (1985). "The effect of tilt on sediment trap efficiency." Deep-Sea Research **32**: 349-361.

Gardner, W. D. (2000). Sediment trap sampling in surface waters. The Changing Ocean Carbon Cycle: A Midterm Synthesis of the Joint Global Ocean Flux Study. R. B. Hanson, Ducklow, H.W., and Field J.G.**:** 240-281.

Gardner, W. D., M. J. Richardson, C. A. Carlson, D. Hansell and A. V. Mishonov (2003). "Determining true particulate organic carbon: bottles, pumps and methodologies." Deep-Sea Research Part II **50**(3-4): 655-674.

Gervais, F., Riebesell, U., Gorbunov, M.Y. (2002). "Changes in primary productivity and chlorophyll a in response to iron fertilisation in the southern Polar Frontal Zone." Limnology and Oceanography **47**(1324-1335).

Glibert, P. M., F. Lipschultz, J. J. McCarthy and M. A. Altabet (1982). "Isotope dilution models of uptake and remineralization of ammonium by marine plankton." Limnology and Oceanography **27**(4): 639-650.

Goeyens, L., N. Kindermans, M. Abu Yusuf and M. Elskens (1998). "A room temperature procedure for the manual determination of urea in seawater." Estuarine Coastal and Shelf Science **47**(4): 415-418.

Goutx, M., C. Guigue, N. Leblond, A. Desnues, A. Dufour, D. Aritio and C. Guieu (2005). "Particle flux in the northeast Atlantic Ocean during the POMME experiment (2001): Results from mass, carbon, nitrogen, and lipid biomarkers from the drifting sediment traps." Journal of Geophysical Research-Oceans **110**(C7).

Gruber, N. and J. L. Sarmiento (1997). "Global patterns of marine nitrogen fixation and denitrification." Global Biogeochemical Cycles **11**(2): 235-266.

Guieu, C., M. Roy-Barman, N. Leblond, C. Jeandel, M. Souhaut, B. Le Cann, A. Dufour and C. Bournot (2005). "Vertical particle flux in the northeast Atlantic Ocean (POMME experiment)." Journal of Geophysical Research-Oceans **110**(C7).

Guilderson, T. P., R. G. Fairbanks and J. L. Rubenstone (1994). "Tropical temperature variations since 20,000 years ago - modulating interhemispheric climate change." Science **263**(5147): 663-665.

Gupta, L. P. and H. Kawahata (2000). "Amino acid and hexosamine composition and flux of sinking particulate matter in the equatorial Pacific at 175 degrees E longitude." Deep-Sea Research Part I **47**(10): 1937-1960.

Gust, G., Byrne, R.H., Bernstein, R.E., Betzer, P.R., Bowles, W. (1992). "Particle fluxes and moving fluids: experience from synchronous trap collections in the Sargasso Sea." Deep-Sea Research I **41**: 831-857.

Hamm, C. E. (2002). "Interactive aggregation and sedimentation of diatoms and clay-sized lithogenic material." Limnology and Oceanography **47**(6): 1790-1795.

Hamm, C. E., Merkel, R., Springer, O., Jurkojc, P., Maier, C., Prechtel, K., Smetacek, V. (2003). "Architecture and material properties of diatom shells provide effective mechanical protection against grazing." Nature **421**: 841-843.

Hamm, C. E., D. A. Simson, R. Merkel and V. Smetacek (1999). "Colonies of *Phaeocystis globosa* are protected by a thin but tough skin." Marine Ecology Progress Series **187**: 101-111.

Hansell, D. A. and J. A. Newton (1994). "Design and evaluation of a swimmer segregating particle interceptor trap." Limnology and Oceanography **39**(6): 1487-1495.

Harris, J. R. W., E. D. Stutt and C. M. Turley (2001). "Carbon flux in the northwest Mediterranean estimated from microbial production." Deep-Sea Research Part I **48**(12): 2631-2644.

Hart, T. J. (1934). "On the phytoplankton of the Southwest Atlantic and Bellingshausen Sea 1929-1931." Discovery Reports **8**: 1-268.

Hashimoto, S. and Y. Maita (2003). "Fluxes of amino acid and hexosamine in sinking particles in subarctic and arctic coastal regions." Journal of Oceanography **59**(5): 731-738.

Haug, G. H., T. F. Pedersen, D. M. Sigman, S. E. Calvert, B. Nielsen and L. C. Peterson (1998). "Glacial/interglacial variations in production and nitrogen fixation in the Cariaco Basin during the last 580 kyr." Paleoceanography **13**(5): 427-432.

Hays, J. D., J. Imbrie and N. J. Shackleton (1976). "Variations in Earths orbit - pacemaker of ice ages." Science **194**(4270): 1121-1132.

Hecky, R. E., K. Mopper, P. Kilham and E. T. Degens (1973). "Amino acid and sugar composition of diatom cell walls." Marine Biology **19**(4): 323-331.

Hedges, J. I., J. A. Baldock, Y. Gelinas, C. Lee, M. Peterson and S. G. Wakeham (2001). "Evidence for non-selective preservation of organic matter in sinking marine particles." Nature **409**(6822): 801-804.

Hedges, J. I., G. Eglinton, P. G. Hatcher, D. L. Kirchman, C. Arnosti, S. Derenne, R. P. Evershed, I. Kogel-Knabner, J. W. de Leeuw, R. Littke, W. Michaelis and J. Rullkotter (2000). "The molecularly-uncharacterized component of nonliving organic matter in natural environments." Organic Geochemistry **31**(10): 945-958.

Hedges, J. I. and R. G. Keil (1995). "Sedimentary organic matter preservation - an assessment and speculative synthesis." Marine Chemistry **49**(2-3): 81-115.

Hedges, J. I. and J. H. Stern (1984). "Carbon and nitrogen determinations of carbonate-containing solids." Limnology and Oceanography **29**(3): 657-663.

Hernes, P. J., Hedges, J.I., Peterson, L., Wakeham, S.G., Lee, C. (1996). "Neutral carbohydrate geochemistry on particulate material in the central equatorial Pacific." Deep-Sea Research II **43**(4-6): 1181-1204.

Hernes, P. J., M. L. Peterson, J. W. Murray, S. G. Wakeham, C. Lee and J. I. Hedges (2001). "Particulate carbon and nitrogen fluxes and compositions in the central equatorial Pacific." Deep-Sea Research Part I **48**(9): 1999-2023.

Hilton, J., Lishman, J.P., Mackness, S., Heaney, S.I. (1986). "An automated method for the analysis of particulate carbon and nitrogen in natural waters." Hydrobiologica **141**: 269-271.

Hoffmann, L. J., Peeken, I., Lochte, K., Assmy, P., Veldhuis, M. (2006). "Different reactions of Southern Ocean phytoplankton size classes to iron fertilisation." Limnology and Oceanography **51**(3): 1217-1229.

Holeton, C. L., F. Nedelec, R. Sanders, L. Brown, C. M. Moore, D. P. Stevens, K. J. Heywood, P. J. Statham and C. H. Lucas (2005). "Physiological state of phytoplankton communities in the Southwest Atlantic sector of the Southern Ocean, as measured by fast repetition rate fluorometry." Polar Biology **29**(1): 44-52.

Holmes, R. M., A. Aminot, R. Kerouel, B. A. Hooker and B. J. Peterson (1999). "A simple and precise method for measuring ammonium in marine and freshwater ecosystems." Canadian Journal of Fisheries and Aquatic Sciences **56**(10): 1801-1808.

Honda, M., Kawakama, K., Sasaoka, S., Watanabe, D., Dickey, T. (2006). "Quick transport of primary produced organic carbon to the ocean interior." Geophysical Research Letters **33**: L16603.

Honjo, S. (1996). Fluxes of Particulates to the Interior of the Open Oceans. Particle Flux in the Ocean. V. Ittekkot, Schäffer, P., Honjo, S., Depetris, P.J. Tortonto, John Wiley & Sons. **57:** 91-145.

Honjo, S., R. Francois, S. Manganini, J. Dymond and R. Collier (2000). "Particle fluxes to the interior of the Southern Ocean in the Western Pacific sector along 170 degrees W." Deep-Sea Research Part II **47**(15-16): 3521-3548.

Honjo, S. and S. J. Manganini (1993). "Annual Biogenic Particle Fluxes to the Interior of the North-Atlantic Ocean - Studied at 34-Degrees-N 21-Degrees-W and 48-Degrees-N 21-Degrees-W." Deep-Sea Research Part II **40**(1-2): 587-607.

Honjo, S., S. J. Manganini and L. J. Poppe (1982). "Sedimentation of lithogenic particles in the deep ocean." Marine Geology **50**(3): 199-220.

Honjo, S., D. W. Spencer and W. D. Gardner (1992). "A sediment trap intercomparison experiment in the Panama Basin, 1979." Deep-Sea Research Part A **39**(2A): 333-358.

Houghton, J., Jenkins, GJ., Ephraums, JJ. (1990). Climate Change - the IPCC scientific assessment. C. U. Press. Cambridge.

Howard, M. T., A. M. E. Winguth, C. Klaas and E. Maier-Reimer (2006). "Sensitivity of ocean carbon tracer distributions to particulate organic flux parameterizations." Global Biogeochemical Cycles **20**(3).

Hutchins, D. A., Bruland, K.W. (1998). "Iron-limited diatom growth and Si:N uptake ratios in a coastal up-welling regime." Nature **393**: 561-564.

Indermuhle, A., T. F. Stocker, F. Joos, H. Fischer, H. J. Smith, M. Wahlen, B. Deck, D. Mastroianni, J. Tschumi, T. Blunier, R. Meyer and B. Stauffer (1999). "Holocene carbon-cycle dynamics based on CO_2 trapped in ice at Taylor Dome, Antarctica." Nature **398**(6723): 121-126.

Ingalls, A. E., C. Lee, S. G. Wakeham and J. I. Hedges (2003). "The role of biominerals in the sinking flux and preservation of amino acids in the Southern Ocean along 170 degrees W." Deep-Sea Research Part II **50**(3-4): 713-738.

Ingalls, A. E., Z. F. Liu and C. Lee (2006). "Seasonal trends in the pigment and amino acid compositions of sinking particles in biogenic $CaCO_3$ and SiO_2 dominated regions of the Pacific sector of the Southern Ocean along 170 degrees W." Deep-Sea Research Part I **53**(5): 836-859.

Ittekkot, V. (1993). "The abiotically driven biological pump in the ocean and short-term fluctuations in atmospheric CO_2 contents." Global and Planetary Change **8**(1-2): 17-25.

Ittekkot, V., W. G. Deuser and E. T. Degens (1984). "Seasonality in the fluxes of sugars, amino acids, and amino sugars to the deep ocean - Sargasso Sea." Deep-Sea Research Part A **31**(9): 1057-1069.

Jackson, G. A. (1990). "A model of the formation of marine algal flocs by physical coagulation processes." Deep-Sea Research I **37**: 1197-1211.

Jackson, G. A. and A. B. Burd (1998). "Aggregation in the marine environment." Environmental Science & Technology **32**(19): 2805-2814.

Jackson, G. A. and T. Kiorboe (2004). "Zooplankton use of chemodetection to find and eat particles." Marine Ecology-Progress Series **269**: 153-162.

Jenkins, W. J. (1982). "Oxygen utilization rates in North-Atlantic Sub-Tropical Gyre and primary production in oligotrophic systems." Nature **300**(5889): 246-248.

Jennerjahn, T. C., V. Ittekkot, C. E. V. Carvalho, A. R. C. Ovalle, C. E. Rezende and H. Erlenkeuser (1999). "Temporal variability of amino acid, hexosamine, and carbohydrate fluxes on the eastern Brazilian continental margin related to discharge of the Sao Francisco River, Brazil." Geo-Marine Letters **19**(3): 202-208.

Jickells, T. D., Z. S. An, K. K. Andersen, A. R. Baker, G. Bergametti, N. Brooks, J. J. Cao, P. W. Boyd, R. A. Duce, K. A. Hunter, H. Kawahata, N. Kubilay, J. laRoche, P. S. Liss, N. Mahowald, J. M. Prospero, A. J. Ridgwell, I. Tegen and R. Torres (2005). "Global iron connections between desert dust, ocean biogeochemistry, and climate." Science **308**(5718): 67-71.

Jickells, T. D., S. Dorling, W. G. Deuser, T. M. Church, R. Arimoto and J. M. Prospero (1998). "Air-borne dust fluxes to a deep water sediment trap in the Sargasso Sea." Global Biogeochemical Cycles **12**(2): 311-320.

Jin, X., Gruber, N., Dunne, J.P., Sarmiento, J.L., Armstrong, R.A. (2006). "Diagnosing the contribution of phytoplankton functional groups to the production and export of particulate organic carbon, $CaCO_3$, and Opal from global nutrient and alkalinity distributions." Global Biogeocehmical Cycles **19**(4).

Joint, I. R. and A. J. Pomroy (1986). "Photosynthetic characteristics of nanoplankton and picoplankton from the surface mixed layer." Marine Biology **92**(4): 465-474.

Kahler, P. and E. Bauerfeind (2001). "Organic particles in a shallow sediment trap: Substantial loss to the dissolved phase." Limnology and Oceanography **46**(3): 719-723.

Kanamitsu, M. (1989). "Description of the NMC global data assimilation and forecast system." Weather and Forecasting **4**: 335-342.

Kanamitsu, M., Alpert, J.C., Campana, K.A., Caplan, P.M., Deaven, G., Iredell, M., Katz, B., Pan, H.L., Sela, J., White, G.H. (1991). "Recent changes implemented into the global forecast system at NMC." Weather and Forecasting **6**(425-435).

Karl, D. M., J. R. Christian, J. E. Dore, D. V. Hebel, R. M. Letelier, L. M. Tupas and C. D. Winn (1996). "Seasonal and interannual variability in primary production and particle flux at Station ALOHA." Deep-Sea Research Part II **43**(2-3): 539-568.

Karl, D. M., B. D. Tilbrook and G. Tien (1991). "Seasonal coupling of organic-matter production and particle-flux in the Western Bransfield Strait, Antarctica." Deep-Sea Research Part A **38**(8-9): 1097-1126.

Keeling, C. D., T. P. Whorf, M. Wahlen and J. Vanderplicht (1995). "Interannual extremes in the rate of rise of atmospheric carbon-dioxide since 1980." Nature **375**(6533): 666-670.

Keil, R. G., D. B. Montlucon, F. G. Prahl and J. I. Hedges (1994). "Sorptive preservation of labile organic-matter in marine-sediments." Nature **370**(6490): 549-552.

Keil, R. G., Tsamakis, E., Hedges, J.I., (2000). Early diagenesis of particulate amino acids in marine systems. Perspectives in Amino Acid and Protein Geochemistry. G. A. Goodfriend, Collins, M.J., Fogel, M.L., Macko, S.A., Wehmiller, J.F. Oxford, Oxford University Press**:** 69-82.

Kiorboe, T., Andersen, K.P., Dam, H.G. (1990). "Coagulation efficiency and aggregate formation in marine phytoplankton." Marine Biology **107**: 235-245.

Kiorboe, T. and A. W. Visser (1999). "Predator and prey perception in copepods due to hydromechanical signals." Marine Ecology-Progress Series **179**: 81-95.

Kiriakoulakis, K., E. Stutt, S. J. Rowland, A. Vangriesheim, R. S. Lampitt and G. A. Wolff (2001). "Controls on the organic chemical composition of settling particles in the Northeast Atlantic Ocean." Progress in Oceanography **50**(1-4): 65-87.

Klaas, C. and D. E. Archer (2002). "Association of sinking organic matter with various types of mineral ballast in the deep sea: Implications for the rain ratio." Global Biogeochemical Cycles **16**(4).

Knauer, G. A., Karl, D.M., Martin, J.H., Hunter, C.N. (1984). "*In-situ* effects of selected preservatives on total carbon, nitrogen, and metals collected in sediment traps." Journal of Marine Research **42**: 445-462.

Knauer, G. A., J. H. Martin and K. W. Bruland (1979). "Fluxes of particulate carbon, nitrogen, and phosphorus in the upper water column of the Northeast Pacific." Deep-Sea Research **26**(1): 97-108.

Kohfeld, K. E., C. Le Quere, S. P. Harrison and R. F. Anderson (2005). "Role of marine biology in glacial-interglacial CO_2 cycles." Science **308**(5718): 74-78.

Kolber, Z. S., Barber, R.T., Coale, K.H., Fitzwater, S.E., Greene, R.M., Jonson, K.S., Lindley, S., Falkowski, P.G. (1994). "Iron limitation of phytoplankton photosynthesis in the equatorial Pacific Ocean." Nature **371**: 145.

Kopczynska, E. E., Fiala, M., and Jeandel, C. (1998). "Annual and interannual variability in phytoplankton at a permanent station off Kerguelen Islands, Southern Ocean." Polar Biology **20**: 342-351.

Korb, R. E., Whitehouse, M.J., and Ward, P. (2004). "SeaWiFS in the Southern Ocean: spatial and temporal variability in phytoplankton biomass around South Georgia." Deep-Sea Research II **51**: 99-116.

Kortzinger, A., W. Koeve, P. Kahler and L. Mintrop (2001). "C:N ratios in the mixed layer during the productive season in the northeast Atlantic Ocean." Deep-Sea Research Part I-Oceanographic Research Papers **48**(3): 661-688.

Kortzinger, A., D. E. Schulzbull, G. Petrick and J. C. Duinker (1994). "Evidence for Dissolution of Fatty-Acids in Sediment Traps - Impact on Flux Estimates." Journal of Geophysical Research-Oceans **99**(C2): 3407-3415.

Körtzinger, A., Send,S., Lampitt, R.S., Hartman, S., Wallace, D.W.R., Karstensen, J., Villagarcia, M.G., Llinás, O., DeGrandpre, M.D. (Submitted). "The seasonal pCO_2 cycle at 49°N/16.5°W in the northeast Atlantic Ocean and what it tells us about biological productivity." Journal of Geophysical Research **in press**.

Kuss, J. and K. Kremling (1999). "Particulate trace element fluxes in the deep northeast Atlantic Ocean." Deep-Sea Research Part I **46**(1): 149-169.

Lam, P. J. and J. K. B. Bishop (2007). "High biomass, low export regimes in the Southern Ocean." Deep-Sea Research Part II **54**(5-7): 601-638.

Lampitt, R. S. and A. N. Antia (1997). "Particle flux in deep seas: regional characteristics and temporal variability." Deep-Sea Research Part I **44**(8): 1377-1403.

Lampitt, R. S., Bett, B.J., Kiriakoulakis, K., Popova, E.E., Ragueneau, O., Vangreisham, A., Wolff, G.A. (2001). "Material supply to the abyssal seafloor in the northeast Atlantic." Progress in Oceanography **50**(1/4): 27-63.

Lampitt, R. S., P. P. Newton, T. D. Jickells, J. Thomson and P. King (2000). "Near-bottom particle flux in the abyssal northeast Atlantic." Deep-Sea Research Part Ii-Topical Studies in Oceanography **47**(9-11): 2051-2071.

Lampitt, R. S., R. C. T. Raine, D. S. M. Billett and A. L. Rice (1995). "Material supply to the European continental slope: A budget based on benthic oxygen demand and organic supply." Deep-Sea Research Part I-Oceanographic Research Papers **42**(11-12): 1865-&.

Lampitt, R. S., Salter I., de Cuevas B.A., Hartman S., Larkin K., Pebody C. (2008). "Long-term variability of downward particle flux in the deep Northeast Atlantic: causes and trends." Deep Sea Research II **submitted**.

Lancelot, C. (1998). Autoecology of of the marine haptophye *Phaeocystis* sp. Physiological ecology of harmful algal blooms. D. M. Anderson, Cembella, A.D., Hallegraeff, G.M. Berlin, Springer**:** 209-224.

Lange, C. B., Reid, F.M., Vernet, M. (1994). "Temporal distribution of the potentially toxic diatom *Pseudonitzschia australis* at a coastal site in Southern California." Marine Ecology Progress Series **104**: 309-312.

Laws, E. A., P. G. Falkowski, W. O. Smith, H. Ducklow and J. J. McCarthy (2000). "Temperature effects on export production in the open ocean." Global Biogeochemical Cycles **14**(4): 1231-1246.

Lee, C. and C. Cronin (1982). "The vertical flux of particulate organic nitrogen in the Sea - decomposition of amino acids in the Peru Upwelling Area and the Equatorial Atlantic." Journal of Marine Research **40**(1): 227-251.

Lee, C. and C. Cronin (1984). "Particulate amino acids in the sea - effects of primary productivity and biological decomposition." Journal of Marine Research **42**(4): 1075-1097.

Lee, C., S. G. Wakeham and J. I. Hedges (2000). "Composition and flux of particulate amino acids and chloropigments in equatorial Pacific seawater and sediments." Deep-Sea Research Part I **47**(8): 1535-1568.

Lee, C., Wakeham, S.G., Hedges, J.I. (1988). "The measurement of oceanic particle fluxes - are swimmers a problem." Oceanography **1**: 234-236.

Legendre, L., and Le Fevre J (1989). Hydrodynamical singularities as controls of recycled versus export production in oceans. Productivity of the Ocean: Present and Past. W. H. Berger, Smetacek, V.S., and Wefer, G. NY, J. Wiley and Sons**:** 49-63.

Levitus, S., J. I. Antonov, T. P. Boyer and C. Stephens (2000). "Warming of the world ocean." Science **287**(5461): 2225-2229.

Levy, M., Y. Lehahn, J. M. Andre, L. Memery, H. Loisel and E. Heifetz (2005). "Production regimes in the northeast Atlantic: A study based on Sea-viewing Wide Field-of-view Sensor (SeaWiFS) chlorophyll and ocean general circulation model mixed layer depth." Journal of Geophysical Research-Oceans **110**(C7).

Lindroth, P. and K. Mopper (1979). "High-Performance Liquid-Chromatographic determination of sub-picomole amounts of amino acids by precolumn fluorescence derivatization with ortho-Phthaldialdehyde." Analytical Chemistry **51**(11): 1667-1674.

Liu, Z. F., G. Stewart, J. K. Cochran, C. Lee, R. A. Armstrong, D. J. Hirschberg, B. Gasser and J. C. Miquel (2005). "Why do POC concentrations measured using Niskin bottle collections sometimes differ from those using *in-situ* pumps?" Deep-Sea Research Part I **52**(7): 1324-1344.

Lohrenz, S. E., G. A. Knauer, V. L. Asper, M. Tuel, A. F. Michaels and A. H. Knap (1992). "Seasonal variability in primary production and particle-flux in the Northwestern Sargasso Sea - United-States JGOFS Bermuda Atlantic Time-Series Study." Deep-Sea Research Part A **39**(7-8A): 1373-1391.

Lookhart, G. L., B. L. Jones, D. B. Cooper and S. B. Hall (1982). "A method for hydrolyzing and determining the amino acid compositions of picomole quantities of proteins in less than 3 hours." Journal of Biochemical and Biophysical Methods **7**(1): 15-23.

Lowenstam, H. A., Weiner, S. (1989). On Biomineralisation. Oxford, Oxford University Press.

Lucas, M., Seeyave, S., Sanders, R., Moore, C.M., Williamson, R., Stinchcombe, M. (2007). "Nitrogen uptake responses to a naturally Fe-fertilised phytoplankton bloom during the 2004/5 CROZEX study." Deep-Sea Research II **54**(18-20): 2138-2173.

Lundgreen, U. and J. C. Duinker (1998). "Seasonal variability of amino acid flux and composition of particulate matter in the Northeast Atlantic at 47^{o}N 20^{o}W." Marine Chemistry **62**(3-4): 307-323.

Lutz, M., R. Dunbar and K. Caldeira (2002). "Regional variability in the vertical flux of particulate organic carbon in the ocean interior." Global Biogeochemical Cycles **16**(3).

Mari, X., F. Rassoulzadegan, C. P. D. Brussaard and P. Wassmann (2005). "Dynamics of transparent exopolymeric particles (TEP) production by *Phaeocystis globosa* under N- or P-limitation: a controlling factor of the retention/export balance." Harmful Algae **4**(5): 895-914.

Marsh, R., Mills, R., Green, D., Salter, I., Taylor, S. (2007). "Controls on the sediment geochemistry of the Crozet Plateau." Deep-Sea Research II **54**(18-20): 2260-2274.

Marshall, J. and F. Schott (1999). "Open-ocean convection: Observations, theory, and models." Reviews of Geophysics **37**(1): 1-64.

Martin, J. H. (1990). "Glacial-interglacial CO_2 change: The iron hypothesis." Paleoceanography **5**: 1-13.

Martin, J. H., S. E. Fitzwater, R. M. Gordon, C. N. Hunter and S. J. Tanner (1993). "Iron, primary production and carbon nitrogen flux studies during the JGOFS North-Atlantic Bloom Experiment." Deep-Sea Research Part II **40**(1-2): 115-134.

Martin, J. H., K. H. Coale, K. S. Johnson, S. E. Fitzwater, R. M. Gordon, S. J. Tanner, C. N. Hunter, V. A. Elrod, J. L. Nowicki, T. L. Coley, R. T. Barber, S.

Lindley, A. J. Watson, K. Van Scoy, C. S. Law, M. I. Liddicoat, R. Ling, T. Stanton, J. Stockel, C. Collins, A. Anderson, R. Bidigare, M. Ondrusek, M. Latasa, F. J. Millero, K. Lee, W. Yao, J. Z. Zhang, G. Friederich, C. Sakamoto, F. Chavez, K. Buck, Z. Kolber, R. Greene, P. Falkowski, S. W. Chisholm, F. Hoge, R. Swift, J. Yungel, S. Turner, P. Nightingale, A. Hatton, P. Liss, N. W. Tindale (1994). "Testing the iron hypothesis in ecosystems of the equatorial Pacific Ocean." Nature **371**: 123-129.

Martin, J. H., G. A. Knauer, D. M. Karl and W. W. Broenkow (1987). "Vertex - Carbon cycling in the Northeast Pacific." Deep-Sea Research Part A **34**(2): 267-285.

Matsumoto, K., J. L. Sarmiento and M. A. Brzezinski (2002). "Silicic acid leakage from the Southern Ocean: A possible explanation for glacial atmospheric pCO_2." Global Biogeochemical Cycles **16**(3).

Mayer, L. M. (1999). "Surface area control of organic carbon accumulation in continental shelf sediment." Geochimica Et Cosmochimica Acta **58**: 207-215.

McElroy, M. B. (1983). "Marine biological controls on atmospheric CO_2 and climate." Nature **302**(5906): 328-329.

Metzl, N., B. Tilbrook and A. Poisson (1999). "The annual fCO_2 cycle and the air-sea CO_2 flux in the sub-Antarctic Ocean." Tellus Series B-Chemical and Physical Meteorology **51**(4): 849-861.

Michaels, A. F., Silver, M.W., Gowing, M.M., Knauer, G.A. (1990). "Cryptic zooplankton "swimmers" in upper ocean sediment traps." Deep-Sea Research **37**: 1285-1296.

Michaels, N., Bates, R., Buesseler, K.O., Carlson, C.A., Knap, A.H. (1994). "Carbon cycle imbalances in the Sargasso Sea." Nature **372**: 537-540.

Milliman, J. D., P. J. Troy, W. M. Balch, A. K. Adams, Y. H. Li and F. T. Mackenzie (1999). "Biologically mediated dissolution of calcium carbonate above the chemical lysocline?" Deep-Sea Research Part I **46**(10): 1653-1669.

Mitchell, B. G., E. A. Brody, O. Holmhansen, C. McClain and J. Bishop (1991). "Light limitation of phytoplankton biomass and macronutrient utilization in the Southern-Ocean." Limnology and Oceanography **36**(8): 1662-1677.

Moore, C. M., Hickman, A.E., Poluton, A.J., Seeyave, S., Lucas, M. (2007). "Iron-light interactions during the CROZet natural iron bloom and Export experiment (CROZEX) II: taxonomic responses and elemental stoichiometry." Deep-Sea Research II **54**(18-20): 2066-2084.

Moore, C. M., Seeyave, S., Hickman, A.E., Allen, J.T., Lucas, M.I., Planquette, H., Pollard, R.T., Poulton, A.J. (2007). "Iron-light Interactions during the CROZet EXperiment (CROZEX) I : Phytoplankton growth and photophysiology." Deep-Sea Research II **54**(18-20): 2045-2065.

Moore, J. K. and M. R. Abbott (2002). "Surface chlorophyll concentrations in relation to the Antarctic Polar Front: seasonal and spatial patterns from satellite observations." Journal of Marine Systems **37**(1-3): 69-86.

Moore, J. K., M. R. Abbott, J. G. Richman and D. M. Nelson (2000). "The Southern Ocean at the last glacial maximum: A strong sink for atmospheric carbon dioxide." Global Biogeochemical Cycles **14**(1): 455-475.

Moran, S. B., M. A. Charette, S. M. Pike and C. A. Wicklund (1999). "Differences in seawater particulate organic carbon concentration in samples collected using small- and large-volume methods: the importance of DOC adsorption to the filter blank." Marine Chemistry **67**(1-2): 33-42.

Morel, F. M. M., Reuter, J.G., Price, N.P. (1991). "Iron nutrition of phytoplankton and its possible importance in the ecology of ocean regions with high nutrient and low biomass." Oceanography **4**: 56-61.

Morris, P. J., Sanders, R., Turnewitsch, R., Thomalla, S. (2007). "Carbon export from an island induced phytoplankton bloom in the Southern Ocean." Deep-Sea Research II **54**(18-20): 2208-2232.

Mortlock, R. A. and P. N. Froelich (1989). "A simple method for the rapid-determination of biogenic opal in pelagic marine-sediments." Deep-Sea Research Part A **36**(9): 1415-1426.

Muggli, D. L., Lecourt, M., Harrison, P.J. (1996). "Effects of iron and nitrogen source on the sinking rate, physiology and metal composition of an oceanic diatom from the Sub-Arctic Pacific." Marine Ecology Progress Series **132**: 215-227.

Muller, P. J., E. Suess and C. A. Ungerer (1986). "Amino-acids and amino-sugars of surface particulate and sediment trap material from waters of the Scotia Sea." Deep-Sea Research Part A **33**(6): 819-838.

Mulvenna, P. F. and G. Savidge (1992). "A modified manual method for the determination of urea in seawater using diacetylmonoxime reagent." Estuarine Coastal and Shelf Science **34**(5): 429-438.

Murray, J. w., Downs, J.N.,Strom, S., Wei, C.L., Jannasch, H.W. (1989). "Nutrient assimilation, export production, and ^{234}Th scavenging in the eastern equatorial Pacific." Deep-Sea Research **36**: 1471-1489.

Murray, J. W., Young, J., Newton, J., Dunne, J., Chapin, T., Paul, B. (1996). "Export flux of particulate organic carbon from the Central Equatorial Pacific determined using a combined drifting trap ^{234}Th approach." Deep-Sea Research II **43**: 1095-1132.

Nagata, T., H. Fukuda, R. Fukuda and I. Koike (2000). "Bacterioplankton distribution and production in deep Pacific waters: Large-scale geographic variations and possible coupling with sinking particle fluxes." Limnology and Oceanography **45**(2): 426-435.

Nelson, D. M., R. F. Anderson, R. T. Barber, M. A. Brzezinski, K. O. Buesseler, Z. Chase, R. W. Collier, M.-L. Dickson, R. Francois and M. R. Hiscock (2002). "Vertical budgets for organic carbon and biogenic silica in the Pacific sector of the Southern Ocean, 1996-1998." Deep Sea Research Part II **49**(9-10): 1645-1674.

Newton, P. P., R. S. Lampitt, T. D. Jickells, P. King and C. Boutle (1994). "Temporal and spatial variability of biogenic particle fluxes during the JGOFS Northeast Atlantic Process Studies at 47-Degrees-N, 20-Degrees-W." Deep-Sea Research Part I **41**(11-12): 1617-1642.

Nguyen, R. T. and H. R. Harvey (1997). "Protein and amino acid cycling during phytoplankton decomposition in oxic and anoxic waters." Organic Geochemistry **27**(3-4): 115-128.

Nieuwenhuize, J., Y. E. M. Maas and J. J. Middelburg (1994). "Rapid analysis of organic-carbon and nitrogen in particulate materials." Marine Chemistry **45**(3): 217-224.

Nodder, S. D., Charette, M.A., Waite, A.M., Trull, T.W., Boyd, P.W., Zeldis, J., Buesseler, K.O (2001). "Particle transformations and export flux during an *in-situ* iron-stimulated algal bloom in the Southern Ocean." Geophysical Research Letters **28**: 2409-2412.

Nodder, S. D. and L. C. Northcote (2001). "Episodic particulate fluxes at southern temperate mid-latitudes (42-45 degrees S) in the Subtropical Front region, east of New Zealand." Deep-Sea Research Part I **48**(3): 833-864.

Nodder, S. D., Waite, A.M. (2001). "Is Southern Ocean organic carbon and biogenic silica export enhanced by iron-stimulated increases in biological production? Sediment trap results from SOIREE." Deep Sea Research Part II **48**(11-12): 2681-2701.

Pace, M. L., G. A. Knauer, D. M. Karl and J. H. Martin (1987). "Primary production, new production and vertical flux in the Eastern Pacific-Ocean." Nature **325**(6107): 803-804.

Park, Y.-H., R. T. Pollard, J. F. Read and V. Leboucher (2002). "A quasi-synoptic view of the frontal circulation in the Crozet Basin during the Antares-4 cruise." Deep Sea Research Part II **49**(9-10): 1823-1842.

Passow, U. (2002). "Production of transparent exopolymer particles (TEP) by phyto- and bacterioplankton." Marine Ecology-Progress Series **236**: 1-12.

Passow, U. (2004). "Switching perspectives: Do mineral fluxes determine particulate organic carbon fluxes or vice versa?" Geochemistry Geophysics Geosystems **5**.

Passow, U., De La Rocha, C.L. (2006). "Accumulation of mineral ballast on organic aggregates." Global Biogeocehmical Cycles **20**.

Passow, U., J. Dunne, J. W. Murray, L. Balistrieri and A. L. Alldredge (2006). "Organic carbon to 234Th ratios of marine organic matter." Marine Chemistry **100**(3-4): 323-336.

Passow, U., R. F. Shipe, A. Murray, D. K. Pak, M. A. Brzezinski and A. L. Alldredge (2001). "The origin of transparent exopolymer particles (TEP) and their role in the sedimentation of particulate matter." Continental Shelf Research **21**(4): 327-346.

Peltzer, E. T. and N. A. Hayward (1996). "Spatial and temporal variability of total organic carbon along 140 degrees W in the equatorial Pacific Ocean in 1992." Deep-Sea Research Part II **43**(4-6): 1155-1180.

Petit, J. R., J. Jouzel, D. Raynaud, N. I. Barkov, J. M. Barnola, I. Basile, M. Bender, J. Chappellaz, M. Davis, G. Delaygue, M. Delmotte, V. M. Kotlyakov, M. Legrand, V. Y. Lipenkov, C. Lorius, L. Pepin, C. Ritz, E. Saltzman and M. Stievenard (1999). "Climate and atmospheric history of the past 420,000 years from the Vostok ice core, Antarctica." Nature **399**(6735): 429-436.

Pilskaln, C. H., S. J. Manganini, T. W. Trull, L. Armand, W. Howard, V. L. Asper and R. Massom (2004). "Geochemical particle fluxes in the Southern Indian Ocean seasonal ice zone: Prydz Bay region, East Antarctica." Deep-Sea Research Part I **51**(2): 307-332.

Planquette, H. F., Statham, P.J., Fones, G.R., Charette, M.A., Moore, C.M., Salter, I., Nedelec, F.H., Taylor, S.L., French, M., Baker, A.R., Mahowald, N., Jickells, T.D. (2007). "Dissolved Iron in the vicinity of the Crozet Islands, Southern Ocean." Deep-Sea Research **54**(18-20): 1999-2019.

Pollard, R. T., M. I. Lucas and J. F. Read (2002). "Physical controls on biogeochemical zonation in the Southern Ocean." Deep-Sea Research Part II **49**(16): 3289-3305.

Pollard, R. T., Read, J.F. (2001). "Circulation pathways and transports of the Southern Ocean in the vicinity of the Southwest Indian Ridge." Journal of Geophysical Research **C106**: 2881-2898.

Pollard, R. T., Sanders, R., Lucas, M., Statham, P. (2007). "The Crozet Natural Iron Bloom and Export Experiment (CROZEX)." Deep-Sea Research II **54**(18-20): 1905-1914.

Pollard, R. T., Venables, H.J., Read, J.F., Allen, J.T. (2007). "Large scale circulation around the Crozet Plateau controls an annual phytoplankton bloom in the Crozet Basin." Deep-Sea Research II **54**(18-20): 1915-1929.

Poulton, A. J., Moore, C.M., Seeyave, S., Lucas, M.I., Fielding, S., Ward, P. (2007). "Phytoplankton community composition around the Crozet Plateau, with emphasis on diatoms and *Phaeocystis*." Deep-Sea Research II **54**(18-20): 2085-2105.

Price, N. M., B. A. Ahner and F. M. M. Morel (1994). "The Equatorial Pacific-Ocean - grazer-controlled phytoplankton populations in an iron-limited ecosystem." Limnology and Oceanography **39**(3): 520-534.

Priddle, J., Fryxell, G. (1985). Handbook of common plankton diatoms in the Southern Ocean: Centrales except the genus Thalassiosira. N. British Antarctic Survey. Cambridge**:** 158.

Probyn, T. A. (1987). "Ammonium regeneration by microplankton in an upwelling environment." Marine Ecology-Progress Series **37**(1): 53-64.

Queguiner, B. and M. A. Brzezinski (2002). "Biogenic silica production rates and particulate organic matter distribution in the Atlantic sector of the Southern Ocean during austral spring 1992." Deep Sea Research Part II **49**(9-10): 1765-1786.

Ragueneau, O., S. Schultes, K. Bidle, P. Claquin and B. La Moriceau (2006). "Si and C interactions in the world ocean: Importance of ecological processes and implications for the role of diatoms in the biological pump." Global Biogeochemical Cycles **20**(4).

Ragueneau, O., P. Treguer, A. Leynaert, R. F. Anderson, M. A. Brzezinski, D. J. DeMaster, R. C. Dugdale, J. Dymond, G. Fischer, R. Francois, C. Heinze, E. Maier-Reimer, V. Martin-Jezequel, D. M. Nelson and B. Queguiner (2000). "A review of the Si cycle in the modem ocean: recent progress and missing gaps in the application of biogenic opal as a paleoproductivity proxy." Global and Planetary Change **26**(4): 317-365.

Ragueneau, O., E. D. Varela, P. Treguer, B. Queguiner and Y. Delamo (1994). "Phytoplankton dynamics in relation to the biogeochemical cycle of silicon in a coastal ecosystem of Western-Europe." Marine Ecology-Progress Series **106**(1-2): 157-172.

Razouls, C. (1985). "Mesozooplankton biomass data near French-Guyana." Oceanologica Acta **8**(1): 125-129.

Read, J. F., M. I. Lucas, S. E. Holley and R. T. Pollard (2000). "Phytoplankton, nutrients and hydrography in the frontal zone between the Southwest Indian Subtropical gyre and the Southern Ocean." Deep-Sea Research Part I **47**(12): 2341-2368.

Read, J. F., Pollard, R.T., Allen, J.T., Lucas, M.I., Sanders, R. (2007). "Sub-mesoscale structure and the development of an eddy in the Subantarctic Front north of the Crozet Islands." Deep-Sea Research II **54**(18-20): 1930-1948.

Rivkin, R. B. and L. Legendre (2001). "Biogenic carbon cycling in the upper ocean: Effects of microbial respiration." Science **291**(5512): 2398-2400.

Roberts, A. A., J. G. Palacas and I. C. Frost (1973). "Determination of organic carbon in modern carbonate sediments." Journal of Sedimentary Petrology **43**(4): 1157-1159.

Rutgers van der Loeff, M., Sarin, M.M., Baskaran, M., Benitez-Nelson, C., Buesseler, K.O., Charette, M., Dai, M., Gustafsson, Ö., Masque, P., Morris, P.J., Orlandini, K., Rodriguez y Baena, A., Savoye, N. Schmidt, S., Turnewitsch, R., Vöge, I., Waples, J.T., (2006). "A review of present techniques and methodological advances in analyzing ^{234}Th in aquatic systems." Marine Chemistry **100**: 190-212.

Rutgers van der Loeff, M. M., Moore, W.S. (1999). Determination of natural radioactive tracers. Methods of Seawater Analysis. K. Grasshoff, Kremling, K., Ehrhardt, M. Weinheim, Wiley-VCH**:** 365-397.

Sabine, C. L., R. A. Feely, N. Gruber, R. M. Key, K. Lee, J. L. Bullister, R. Wanninkhof, C. S. Wong, D. W. R. Wallace, B. Tilbrook, F. J. Millero, T. H. Peng, A. Kozyr, T. Ono and A. F. Rios (2004). "The oceanic sink for anthropogenic CO_2." Science **305**(5682): 367-371.

Salter, I., Lampitt, R.S., Sanders, R., Poulton, A., Kemp, A.E.S., Boorman, B., Saw, K., Pearce, R. (2007). "Estimating carbon, silica and diatom export from a naturally fertilised phytoplankton bloom in the Southern Ocean using PELAGRA: Anovel drifting sediment trap." Deep Sea Research II **54**(18-20): 2233-2259.

Sambrotto, R. N., G. Savidge, C. Robinson, P. Boyd, T. Takahashi, D. M. Karl, C. Langdon, D. Chipman, J. Marra and L. Codispoti (1993). "Elevated consumption of carbon relative to nitrogen in the surface ocean." Nature **363**(6426): 248-250.

Sanders, R., L. Brown, S. Henson and M. Lucas (2005). "New production in the Irminger Basin during 2002." Journal of Marine Systems **55**(3-4): 291-310.

Sanders, R. and T. Jickells (2000). "Total organic nutrients in Drake Passage." Deep-Sea Research Part I **47**(6): 997-1014.

Sanders, R., Morris, P., Stinchcombe, M., Seeyave, S., Venables, H., Lucas, M., Moore, C.M. (2007). "New production and the *f*-ratio around the Crozet Plateau in the austral summer 2004-5 diagnosed from seasonal changes in inorganic nutrient levels." Deep-Sea Research II **54**(18-20): 2191-2207.

Santschi, P. H., Murray, J.W., Baskaran, M., Benitez-Nelson, C.R., Guo, L.D., Hung, C.C., Lamborg, C., Moran, S.B., Passow, U., Roy-Barman, M. (2006). "Thorium speciation in seawater." Marine Chemistry **100**(3-4): 250-268.

Sarmiento, J., Gruber, N. (2006). Ocean Biogeochemical Dynamics. Princeton, Princeton University Press.

Sarmiento, J. L., N. Gruber, M. A. Brzezinski and J. P. Dunne (2004). "High-latitude controls of thermocline nutrients and low latitude biological productivity." Nature **427**(6969): 56-60.

Sarmiento, J. L., T. M. C. Hughes, R. J. Stouffer and S. Manabe (1998). "Simulated response of the ocean carbon cycle to anthropogenic climate warming." Nature **393**(6682): 245-249.

Savidge, G., P. Boyd, A. Pomroy, D. Harbour and I. Joint (1995). "Phytoplankton production and biomass estimates in the Northeast Atlantic-Ocean, May to June 1990." Deep-Sea Research Part I **42**(5): 599-617.

Savoye, N., C. Benitez-Nelson, A. B. Burd, J. K. Cochran, M. Charette, K. O. Buesseler, G. A. Jackson, M. Roy-Barman, S. Schmidt and M. Elskens (2006). "Th-234 sorption and export models in the water column: A review." Marine Chemistry **100**(3-4): 234-249.

Savoye, N., Buesseler, K.O., Cardinal, D., Dehairs, F. (2004). "^{234}Th deficit and excess in the Southern Ocean during spring 2001: particle export and remineralization." Geophysical Research Letters **21**(12).

Saw, K. A., Boorman, B., Lampitt, R.S., Sanders, R. (2004). "PELAGRA: early development of an autonomous, neutrally bouyant sediment trap." Advances in Technology for Underwater Vehicles: 165-175.

Schiebel, R., B. Hiller and C. Hemleben (1995). "Impacts of storms on recent planktic foraminiferal test production and $CaCO_3$ flux in the North Atlantic at 47 degrees N, 20 degrees W (JGOFS)." Marine Micropaleontology **26**(1-4): 115-129.

Schlitzer, R. (2002). "Carbon export fluxes in the Southern Ocean: results from inverse modeling and comparison with satellite-based estimates." Deep Sea Research Part II **49**(9-10): 1623-1644.

Schnetzer, A. and D. K. Steinberg (2002). "Natural diets of vertically migrating zooplankton in the Sargasso Sea." Marine Biology **141**(2): 403-403.

Scholten, J. C., J. Fietzke, S. Vogler, M. M. R. van der Loeff, A. Mangini, W. Koeve, J. Waniek, P. Stoffers, A. Antia and J. Kuss (2001). "Trapping efficiencies of sediment traps from the deep Eastern North Atlantic: the Th-230 calibration." Deep-Sea Research Part II **48**(10): 2383-2408.

Sedwick, P. N., Di Tullio, G.R. (1997). "Regulation of algal blooms in Antarctic shelf waters by the release of iron from melting sea-ice." Geophysical Research Letters **24**: 2515-2518.

Seeyave, S., Lucas, M.I., Moore, C.M., Poulton, A.J. (2007). "Phytoplankton productivity and community structure in the vicinity of the Crozet Plateau during the austral summer 2004/2005." Deep Sea Research II **54**(18-20): 2020-2044.

Sherr, E. B. and B. F. Sherr (1996). "Temporal offset in oceanic production and respiration processes implied by seasonal changes in atmospheric oxygen: The role of heterotrophic microbes." Aquatic Microbial Ecology **11**(1): 91-100.

Sigman, D. M. and E. A. Boyle (2000). "Glacial/interglacial variations in atmospheric carbon dioxide." Nature **407**(6806): 859-869.

Sigman, D. M., D. C. McCorkle and W. R. Martin (1998). "The calcite lysocline as a constraint on glacial/interglacial low-latitude production changes." Global Biogeochemical Cycles **12**(3): 409-427.

Sigmon, D. E., D. M. Nelson and M. A. Brzezinski (2002). "The Si cycle in the Pacific sector of the Southern Ocean: seasonal diatom production in the surface layer and export to the deep sea." Deep Sea Research Part II **49**(9-10): 1747-1763.

Simon, M., H. P. Grossart, B. Schweitzer and H. Ploug (2002). "Microbial ecology of organic aggregates in aquatic ecosystems." Aquatic Microbial Ecology **28**(2): 175-211.

Smetacek, V., Assmy, P., Henjes, J. (2004). "The role of grazing in structuring Southern Ocean pelagic ecosystems and biogeochemical cycles." Antarctic Science **16**(4): 541-558.

Smyth, T. J., G. H. Tilstone and S. B. Groom (2005). "Integration of radiative transfer into satellite models of ocean primary production." Journal of Geophysical Research-Oceans **110**(C10).

Stanley, R. H. R., K. O. Buesseler, S. J. Manganini, D. K. Steinberg and J. R. Valdes (2004). "A comparison of major and minor elemental fluxes collected in neutrally buoyant and surface-tethered sediment traps." Deep-Sea Research Part I **51**(10): 1387-1395.

Staresinic, N., G. T. Rowe, D. Shaughnessey and A. J. Williams (1978). "Measurement of vertical flux of particulate organic-matter with a free-drifting sediment trap." Limnology and Oceanography **23**(3): 559-563.

Staresinic, N., K. Vonbrockel, N. Smodlaka and C. H. Clifford (1982). "A comparison of moored and free-drifting sediment traps of two different designs." Journal of Marine Research **40**(1): 273-292.

Stephens, B. B. and R. F. Keeling (2000). "The influence of Antarctic sea ice on glacial-interglacial CO_2 variations." Nature **404**(6774): 171-174.

Stevenson, F. J. (1994). Humus Chemistry. New York, Wiley.

Stoecker, D. K., M. E. Sieracki, P. G. Verity, A. E. Michaels, E. Haugen, P. H. Burkill and E. S. Edwards (1994). "Nanoplankton and protozoan microzooplankton during the JGOFS North-Atlantic Bloom Experiment - 1989 and 1990." Journal of the Marine Biological Association of the United Kingdom **74**(2): 427-443.

Strickland, J. D. H., and Parsons, T.R. (1968). Inorganic micronutrients in seawater. A Practical Handbook of Seawater Analysis. J. C. Stevenson. Ottawa, Fisheries Reasearch Board of Canada. **Bulletin 167:** 45-137.

Sunda, W. G. and S. A. Huntsman (1995). "Iron uptake and growth limitation in oceanic and coastal phytoplankton." Marine Chemistry **50**(1-4): 189-206.

Sunda, W. G. and S. A. Huntsman (1997). "Interrelated influence of iron, light and cell size on marine phytoplankton growth." Nature **390**(6658): 389-392.

Sverdrup, H. U. (1953). "On the conditions of the vernal blooming of phytoplankton." Journal du counseil international pour l'exploration de la mer **18**: 287-295.

Swift, D. M., Wheeler, P. (1991). "Evidence of an organic matrix from diatoms biosilica." Journal of Phycology **28**: 202-209.

Takahashi, T., S. C. Sutherland, C. Sweeney, A. Poisson, N. Metzl, B. Tilbrook, N. Bates, R. Wanninkhof, R. A. Feely, C. Sabine, J. Olafsson and Y. Nojiri (2002). "Global sea-air CO_2 flux based on climatological surface ocean pCO_2, and seasonal biological and temperature effects." Deep-Sea Research Part II **49**(9-10): 1601-1622.

Takeda, S. (1998). "Influence of iron availability on nutrient consumption ratios of diatoms in oceanic waters." Nature **393**: 774-777.

Thingstad, T. F., L. Ovreas, J. K. Egge, T. Lovdal and M. Heldal (2005). "Use of non-limiting substrates to increase size; a generic strategy to simultaneously optimize uptake and minimize predation in pelagic osmotrophs?" Ecology Letters **8**(7): 675-682.

Thomalla, S., R. Turnewitsch, M. Lucas and A. Poulton (2006). "Particulate organic carbon export from the North and South Atlantic gyres: The Th-234/U-238 disequilibrium approach." Deep-Sea Research Part II **53**(14-16): 1629-1648.

Tietjen, T. and R. G. Wetzel (2003). "Extracellular enzyme-clay mineral complexes: Enzyme adsorption, alteration of enzyme activity, and protection from photodegradation." Aquatic Ecology **37**(4): 331-339.

Timmermans, K. R., L. J. A. Gerringa, H. J. W. de Baar, B. van der Wagt, M. J. W. Veldhuis, J. T. M. de Jong, P. L. Croot and M. Boye (2001). "Growth rates of large and small Southern Ocean diatoms in relation to availability of iron in natural seawater." Limnology and Oceanography **46**(2): 260-266.

Timmermans, K. R., B. van der Wagt and H. J. W. de Baar (2004). "Growth rates, half-saturation constants, and silicate, nitrate, and phosphate depletion in relation to iron availability of four large, open-ocean diatoms from the Southern Ocean." Limnology and Oceanography **49**(6): 2141-2151.

Toggweiler, J. R. (1990). "U.S. JGOFS News." 2 **1**.

Toggweiler, J. R. (1993). "Oceanography - carbon overconsumption." Nature **363**(6426): 210-211.

Tomas, C. R. (1997). Reprint of: Identifying Marine Diatoms and Dinoflagellates. San Diego, Academic Press.

Treguer, P., Legendre, L., Rivkin, R.T., Ragueneau, O., Dittert, N. (2003). Water column biogeochemistry below the euphotic zone. Ocean Biogeochemistry: The role of the ocean carbon cycle in global change. M. J. R. Fasham, Springer**:** 145-153.

Trull, T. W. and L. Armand (2001). "Insights into Southern Ocean carbon export from the delta C-13 of particles and dissolved inorganic carbon during the SOIREE iron release experiment." Deep-Sea Research Part II **48**(11-12): 2655-2680.

Trull, T. W., S. G. Bray, S. J. Manganini, S. Honjo and R. Francois (2001). "Moored sediment trap measurements of carbon export in the Subantarctic and Polar Frontal Zones of the Southern Ocean, south of Australia." Journal of Geophysical Research-Oceans **106**(C12): 31489-31509.

Tsuda, A., S. Takeda, H. Saito, J. Nishioka, Y. Nojiri, I. Kudo, H. Kiyosawa, A. Shiomoto, K. Imai, T. Ono, A. Shimamoto, D. Tsumune, T. Yoshimura, T. Aono, A. Hinuma, M. Kinugasa, K. Suzuki, Y. Sohrin, Y. Noiri, H. Tani, Y. Deguchi, N. Tsurushima, H. Ogawa, K. Fukami, K. Kuma and T. Saino (2003). "A mesoscale iron enrichment in the western Subarctic Pacific induces a large centric diatom bloom." Science **300**(5621): 958-961.

Tsunogai, S. and M. Minagawa (1976). "Th-234, Pb-210 and Po-210 in surface and deep waters of Pacific as tracers of particulate materials." Transactions-American Geophysical Union **57**(4): 255-255.

Turner, J. T. (2002). "Zooplankton fecal pellets, marine snow and sinking phytoplankton blooms." Aquatic Microbial Ecology **27**(1): 57-102.

Turnewitsch, R. and B. M. Springer (2001). "Do bottom mixed layers influence Th-234 dynamics in the abyssal near-bottom water column?" Deep-Sea Research Part I **48**(5): 1279-1307.

Turnewitsch, R., B. M. Springer, K. Kiriakoulakis, J. C. Vilas, J. Aristegui, G. Wolff, F. Peine, S. Werk, G. Graf and J. J. Waniek (2007). "Determination of particulate organic carbon (POC) in seawater: The relative methodological importance of artificial gains and losses in two glass-fiber-filter-based techniques." Marine Chemistry **105**(3-4): 208-228.

Unger, D., V. Ittekkot, P. Schafer and J. Tiemann (2005). "Biogeochemistry of particulate organic matter from the Bay of Bengal as discernible from hydrolysable neutral carbohydrates and amino acids." Marine Chemistry **96**(1-2): 155-184.

Valdes, J. R., Price, J.F. (2000). "A neutrally bouyant, upper ocean sediment trap." Journal of Atmospheric and Oceanic Technology **17**: 62-68.

Van Cappellen, P., S. Dixit and J. van Beusekom (2002). "Biogenic silica dissolution in the oceans: Reconciling experimental and field-based dissolution rates." Global Biogeochemical Cycles **16**(4).

Venables, H. J., Pollard, R.T., Popova, E.E. (2007). "Physical conditions controlling the early development of a regular phytoplankton bloom north of the Crozet Plateau, Southern Ocean, described using remotely sensed data." Deep-Sea Research II **54**(18-20): 1949-1965.

Venema, K., W. Leever, J. O. Bakker, G. Haayer and J. Korf (1983). "Automated precolumn derivatization device to determine neurotransmitter and other amino-acids by reversed-phase High-Performance Liquid-Chromatography." Journal of Chromatography **260**(2): 371-376.

Verado, D. J., Froelich, P.N., McIntyre, A. (1990). "Determination of organic carbon and nitrogen in marine sediments using the Carlo-Erba NA-1500 analyser." Deep Sea Research I **37**: 157-165.

Verity, P. G. (2000). "Grazing experiments and model simulations of the role of zooplankton in *Phaeocystis* foodwebs." Journal of Sea Research **43**: 317-343.

Verity, P. G., Smetacek, V. (1996). "Organism life cycles, predation, and the structure of marine pelagic ecosystems." Marine Ecology Progress Series **130**: 277-293.

Waite, A., Bienfang, P.K., Harrison, P.J. (1992). "Spring bloom sedimentation in a Sub-Arctic ecosystem I: nutrients and sinking." Marine Biology **114**: 119-129.

Waite, A., Fisher, A., Thompson, P.A., Harrison, P.J. (1997). "Sinking rate vs volume relationships illuminate sinking control mechanisms in marine diatoms." Marine Ecology Progress Series **157**: 97-108.

Waite, A. M., Hill, P.S. (2006). "Flocculation and phytoplankton cell size can alter 234Th-based estimates of the vertical flux of particulate organic carbon in the sea." Marine Chemistry **100**(3-4): 366-375.

Waite, A. M. and S. D. Nodder (2001). "The effect of in situ iron addition on the sinking rates and export flux of Southern Ocean diatoms." Deep Sea Research Part II **48**(11-12): 2635-2654.

Wakeham, S. G., C. Lee, J. I. Hedges, P. J. Hernes and M. L. Peterson (1997). "Molecular indicators of diagenetic status in marine organic matter." Geochimica Et Cosmochimica Acta **61**(24): 5363-5369.

Wakeham, S. G., Lee, C. (1993). Production, transport, and alteration of particulate organic matter in the marine water column. Organic Geochemistry. M. H. Engel, Macko, S.A. New York, Plenum Press**:** 145-165.

Walsh, I., K. Fischer, D. Murray and J. Dymond (1988). "Evidence for resuspension of rebound particles from near-bottom sediment traps." Deep-Sea Research Part A **35**(1): 59-70.

Waniek, J., W. Koeve and R. D. Prien (2000). "Trajectories of sinking particles and the catchment areas above sediment traps in the northeast Atlantic." Journal of Marine Research **58**(6): 983-1006.

Waniek, J. J., D. E. Schulz-Bull, J. Kuss and T. Blanz (2005). "Long time series of deep water particle flux in three biogeochemical provinces of the northeast Atlantic." Journal of Marine Systems **56**(3-4): 391-415.

Wassmann, P. (1994). "Significance of sedimentation for the termination of *Phaeocystis* blooms." Journal of Marine Systems **5**(1): 81-100.

Wassmann, P. (1998). "Retention versus export food chains: processes controlling sinking loss from marine pelagic systems." Hydrobiologia **363**: 29-57.

Watson, A. J., D. C. E. Bakker, A. J. Ridgwell, P. W. Boyd and C. S. Law (2000). "Effect of iron supply on Southern Ocean CO_2 uptake and implications for glacial atmospheric CO_2." Nature **407**(6805): 730-733.

Watson, A. J., Law, C.S., van Scoy, K.A., Millero, F.J., Yao, W., Friederich, G.E., Liddicoat, M.I., Wanninkhof, R.H., Barber, R.T., Coale, K.H. (1994). "Minimal effect of iron fertilization on sea-surface carbon dioxide concentrations." Nature **371**: 143-145.

Williams, R. G., Follows, M.J. (2003). Physical transport of nutrients and the maintenence of biological production. Ocean Biogeochemistry: The role of the ocean carbon cycle in global change. M. J. R. Fasham, Springer**:** 19-95.

Williams, R. G., A. J. McLaren and M. J. Follows (2000). "Estimating the convective supply of nitrate and implied variability in export production over the North Atlantic." Global Biogeochemical Cycles **14**(4): 1299-1313.

Yool, A., A. P. Martin, C. Fernandez and D. R. Clark (2007). "The significance of nitrification for oceanic new production." Nature **447**(7147): 999-1002.

Yu, E. F., R. Francois, M. P. Bacon, S. Honjo, A. P. Fleer, S. J. Manganini, M. M. R. van der Loeff and V. Ittekot (2001). "Trapping efficiency of bottom-tethered sediment traps estimated from the intercepted fluxes of Th-230 and Pa-231." Deep-Sea Research Part I **48**(3): 865-889.

Zubkov, M. V., Holland, R.J., Burkill, P.H., Croudace, I.W., Warwick, P.E. (2007). "Microbial abundance, activity and iron uptake in the vicinity of the Crozet Isles in November 2004 - January 2005." Deep-Sea Research II **54**(18-20): 2126-2137.